Investigating the role of astrocytes in Parkinson's disease pathogenesis in *GBA-N370S* iPSC-derived neural cultures



Naroa Ibarra Aizpurua

University College

Department of Physiology, Anatomy and Genetics

University of Oxford

A thesis submitted for the degree of

Doctor of Philosophy

Trinity 2024

To my parents and James

Abstract

Parkinson's disease (PD), the second most common neurodegenerative disease, is characterized by the loss of dopaminergic neurons (DAn) in the substantia nigra. However, the research available indicates that other cells found in the midbrain, such as astrocytes, are also involved in the disease pathogenesis, although their role has not been fully elucidated yet. Moreover, it is still to be determined whether the neuroinflammation found in PD patients has a causative effect in disease onset or is in turn a consequence of neurodegeneration. Similarly, the currently available data regarding the effects of α-synuclein in human astrocytes remains inconclusive. Therefore, the aim of this thesis was to investigate the role of astrocytes in PD pathogenesis, focusing on cells carrying the PD-associated *GBA-N370S* mutation. In addition, the response of astrocytes to a range of inflammatory cytokines and α-synuclein pre-formed fibrils (PFFs) was extensively investigated, as well as the impact of reactive astrocytes on DAn.

To generate a representative in vitro model of midbrain cells, induced pluripotent stem cells (iPSC) obtained from healthy donors and PD patients carrying the *GBA-N370S* mutation were derived into dopaminergic neurons (iDAn) and midbrain-specific astrocytes (iASTROs). An in-depth characterization of iASTROs demonstrated their regional and astrocytic identity and their functional maturity. Overall, throughout the experiments conducted in this thesis, very few cell-autonomous alterations were observed in *GBA-N370S* iASTROs, and no significant genotypic differences were observed regarding the response of iASTROs to inflammatory cytokines and PFFs. Nonetheless, *GBA-N370S* iASTROs displayed differences in calcium signalling and a higher production of reactive oxygen species. Additionally, a direct iDAn-iASTRO co-culture was established, optimized, and used to investigate the effects of the *GBA-N370S* mutation on iDAn-iASTRO homeostasis. Whereas control and *GBA-N370S* iASTROs presented similar neurosupportive characteristics, *GBA-N370S* iDAn elicited a different response in iASTROs compared to control iDAn.

Furthermore, bulk RNAseq data of control iASTROs treated with inflammatory cytokines and PFFs for 24h revealed very extensive transcriptomic changes in response to inflammatory cytokines but not PFFs, a finding that was verified with subsequent immunocytochemistry and RT-qPCR experiments conducted after 24h and 7 days of treatment. Various genes related to

calcium signalling and homeostasis, as well as vitamin D metabolism, were upregulated in iASTROs after exposure to TNFα+IFNγ. Further in vitro experiments showed the timescale and magnitude of the increases in calcium signalling in reactive control and *GBA-N370S* iASTROs, but partial blockage of endoplasmic reticulum calcium release did not result in changes in iASTROs reactivity. Moreover, even if *CYP27B1* and *VDR* expression and nuclear translocation were elevated in reactive iASTROs, vitamin D supplementation in iDAn did not result in changes in cell viability.

Lastly, to investigate if iASTROs treated with inflammatory cytokines presented neurotoxic or neuroprotective characteristics, experiments in iDAn-iASTRO co-cultures were conducted. Pre-treatment of iASTROs with TNFα+IFNγ before the co-cultures did not affect their neurosupportive capacity, whereas some of the data suggests that when treating and maintaining the co-cultures with cytokines, control and *GBA-N370S* iASTROs became neurotoxic and/or lost neurosupportive functions. In the case of co-cultures treated with TNFα+IFNγ, this neurotoxic activity was potentiated with the addition of PFFs, suggesting that PFFs modulate the reactive response of iASTROs to inflammatory cytokines.

Acknowledgements

This thesis would not have been possible without the continuous support and help from many people, who deserve to be thanked and acknowledged.

First, I would like to thank Dr Nora Bengoa-Vergniory for all the supervision, guidance, support, and help provided throughout these years. I have been extremely lucky to have one of the best and most knowledgeable scientists as my supervisor, while also being one of the most humble and helpful people I know. I will never be able to thank you enough.

Thank you also Prof Richard Wade-Martins for welcoming me into your lab, for facilitating my research throughout all these years, and for always providing all the help I asked for. I would also like to thank to my supervisor, Dr Sally Cowley, for always providing such helpful insight and knowledge regarding glia and inflammation, for always making time in your busy schedule for our meetings, and for being so generous as to look at my thesis draft during your holiday.

To Dr Becky Carlisle, thank you for inviting me into your team and always giving me support and guidance in the lab. Dr Peter Kilfeather and Dr Benjamin Vallin, thank you for all your help in the RNAseq analysis.

I would also like to thank all the members of the Wade-Martins lab, past and present, that have not only been my colleagues but have also become some of my best friends. Dr Maria Claudia Caiazza, thank you for always been there for me, scientifically and personally. Rachel Héon-Roberts, thank you for being the kindest friend I could have asked for and always listening to my rambles. Dr Kaitlyn Cramb, thank you for all our therapy session in Uni parks, for all the support you always give me, and for being my concert pal. Martha Lavelle, Féodora Bertherat, Dr Marta Madureira, Dr William McGuiness, Katrina Savoy, Dr Sandor Szunyogh, thank you for being my friends and lab mates.

Thank you to the Oxford-Radcliffe scholarship and the Oxford MRC-DTP for the financial support that has made my DPhil possible. I would also like to thank the graduate community of University College and all the Senior officers and Staff members, for giving me a community out of the lab.

To Taylor Swift, Lana del Rey, Maisie Peters, Noah Kahan and many other artists and podcast hosts, thank you for providing me with the entertainment needed during those long TC, lab and analysis hours, and for helping me keep anxiety at bay.

In addition, I would like to thank my parents, Elisabet and Iñaki, because I would never be where I am without their unconditional support throughout my education, for always prioritizing and facilitating my choices, and always encouraging me to study abroad. Mum, thank you for always reminding me to prioritize my happiness and showing me that my worth as a person is not measured by my grades or achievements. To Iker, my brother, thank you for always being an exceptional role model and reminding me that I can achieve what I want without letting stress and anxiety overtake me.

To my partner James, thank you for making the last two years of this DPhil project the best two years of my life, for being patient when I had to prioritize work, for always showing me how proud of me you are, and for being the sunshine and rock of my life.

And lastly, to myself, Naroa, thank you for learning to slow down when needed, for accepting yourself as you are, for treating yourself with love and care, and for choosing your own happiness. Congratulations, you did it.

Declaration

I declare that all the work presented in this thesis is the result of my own work, except for the α-synuclein pre-formed fibril (PFF) preparation, which was done by Dr Nora Bengoa-Vergniory, and the comparison between the bulk RNAseq data generated in this thesis and the human sc-RNAseq data generated by Agarwal et al., (2020), which was conducted by Dr Benjamin Vallin.

Table of Contents

Chapter 1 - Introduction 18
1.1. Parkinson's disease 18
1.1.1. Pathophysiology of Parkinson's disease 18
1.1.1.1. Preferential vulnerability of DAn 20
1.1.1.2. α-synuclein 21
1.1.2. Clinical presentation of Parkinson's disease 22
1.1.3. Aetiology of Parkinson's disease 24
1.1.3.1. Non-genetic risk factors 24
1.1.3.2. Genetic risk factors 25
1.1.4. GBA in PD 26
1.1.5. Lipid dysregulation in PD 28
1.1.6. Vitamin D in PD 28
1.2. Astrocytes in Parkinson's disease 29
1.2.1. Astrocytes 30
1.2.2. Calcium signalling in astrocytes 31
1.2.3. Evidence of astrocyte involvement in Parkinson's disease pathogenesis 33
1.2.3.1. α-synuclein in astrocytes 35
1.2.3. iPSC-derived astrocyte models to study astrocyte involvement in Parkinson's disease 36
1.3. Neuroinflammation in PD 38
1.3.1. Evidence of neuroinflammation in PD patients 38
1.3.2. Adaptive immune responses in PD 39
1.3.3. Innate immune responses in PD 40
1.3.3.1. Microglial contribution to neuroinflammation 40
1.3.3.2. Astrocytic contribution to neuroinflammation 42
1.3.4. What came first: neuroinflammation or neurodegeneration? 43
1.3.5. Anti-inflammatory therapeutic strategies 44
1.4. Hypotheses and thesis aims 45
Chapter 2 - Materials and methods 46
2.1. Cell culture 47
2.1.1. Human induced pluripotent stem cell lines 48
2.1.2. Human induced pluripotent stem cell thawing, maintenance and passaging 48
2.1.2.1. Thawing iPSCs 48
2.1.2.2. Single cell passaging of iPSCs 49
2.1.3. Human midbrain astrocyte differentiation and cryopreservation 49

2.1.4. Human dopaminergic neuron differentiation and cryopreservation of mFPPs 53
2.1.5. Human iPSC-derived midbrain astrocyte and dopaminergic neuron co-culture 58
2.2. Preparation of α-synuclein pre-formed fibrils (prepared by Dr Nora Bengoa-Vergniory) 59
2.3. Molecular Biology Techniques 60
2.3.1. RNA extraction and cDNA synthesis 60
2.3.2. Real-time quantitative polymerase chain reaction 60
2.4. Immunocytochemistry 60
2.5. BODIPY staining 63
2.6. High-content image acquisition and analysis 63
2.7. Glutamate uptake assay 64
2.8. Fura-2 calcium imaging 64
2.8.1. ATP-induced calcium release imaging 64
2.8.2. Store Operated Calcium Entry (SOCE) imaging 65
2.9. GCase Assays 66
2.9.1. MDW-941 immunofluorescent labelling 66
2.9.2. 4-MUG GCase activity assay 66
2.10. DCFDA/ H_2DCFDA cellular reactive oxygen species detection assay 67
2.11. Statistical analysis 67
2.12. Bulk RNA sequencing and data processing 68
2.12.1. Comparison with online datasets 69
2.12.1.1. sc-RNAseq dataset (analysis performed by Dr Benjamin Vallin) 69
2.12.1.2. Bulk RNAseq datasets 70
Chapter 3 - Investigating cell autonomous and non-autonomous dysfunction caused by the *GBA-N370S* mutation in iPSC-derived ventral midbrain astrocytes 71
3.1. Introduction and aims 71
3.2. Generation and characterization of mature control and *GBA-N370S* iPSC-derived ventral midbrain astrocytes 72
3.3. Functional characterization of control and *GBA-N370S* iASTROs 81
3.4. Assessing the β-glucocerebrosidase activity of control and *GBA-N370S* iASTROs and iDAn 83
3.5. Establishment and optimization of a direct iDAn-iASTRO co-culture system 85
3.6. Studying the effects of the *GBA-N370S* mutation on iDAn-iASTRO homeostasis 88
3.7. Discussion 95
Chapter 4 - Studying the reactive response of control and *GBA-N370S* iASTROs to inflammatory stimuli and α-synuclein pre-formed fibrils 102
4.1. Introduction and aims 102

4.2. Bulk RNA sequencing of control iASTROs treated with different combinations of inflammatory cytokines and α-synuclein PFFs 103
4.2.1. Initial data quality assessment 105
4.2.2. Differential gene expression analysis summary 106
4.2.3. Gene set enrichment analysis overview 110
4.2.4. In-depth analysis of DEGs and enriched GO:BP terms 111
4.2.4.1. Comparisons between treatments with inflammatory cytokines and the untreated control 112
4.2.4.2. Comparison between α-synuclein PFF-treated and untreated iASTROs 117
4.2.4.3. Comparisons between different treatments 118
4.2.4.4. Calcium dysregulation in iASTROs treated with TNFα+IFNγ 124
4.2.5. RNAseq experiment results summary 126
4.3. In vitro study of the inflammatory response of control and *GBA-N370S* iASTROs to different inflammatory stimuli over time 129
4.3.1. RT-qPCR analysis of relative gene expression 130
4.3.2. Immunocytochemistry analysis of inflammatory markers and cellular morphology 133
4.3.3. Reactive oxygen species generation 138
4.3.4. Lipid homeostasis and lipid droplet formation 140
4.3.5. Relative gene expression of growth factors 143
4.4. In vitro study of the inflammatory response of control and *GBA-N370S* iASTROs to α-synuclein PFFs, with or without TNFα+IFNγ 146
4.4.1. RT-qPCR analysis of relative gene expression 146
4.4.2. Immunocytochemistry analysis of inflammatory markers and cellular morphology 149
4.4.3. Reactive oxygen species generation 154
4.4.4. Lipid homeostasis and droplet formation 155
4.5. Discussion 157
4.5.1. Astrogliosis in iASTROs treated with inflammatory cytokines 157
4.5.2. Effects of α-synuclein PFFs on iASTROs 163
4.5.3. Concluding remarks 167
Chapter 5 - Exploring calcium homeostasis and vitamin D metabolism in reactive iASTROs 168
5.1. Introduction and aims 168
5.2. Calcium homeostasis in reactive control and *GBA-N370S* iASTROs 169
5.2.1. Relative gene expression of calcium channels in reactive iASTROs 169
5.2.2. Store Operated Calcium Entry in reactive iASTROs 171
5.2.3. ATP-induced ER calcium release in reactive iASTROs 174
5.3. Vitamin D metabolism in reactive iASTROs 177

5.3.1. *CYP27B1* and *VDR* expression in iASTROs after treatment with inflammatory cytokines and α-synuclein PFFs 178
5.3.2. VDR nuclear translocation in reactive iASTROs 180
5.3.3. Blockage of VDR nuclear translocation with MeTC7 and the effects on iASTRO reactivity 182
5.3.4. Vitamin D supplementation in iDAn and its effects on cell survival 185
5.4. Discussion 187
5.4.1. Calcium signalling and homeostasis in reactive iASTROs 188
5.4.2. Vitamin D metabolism and signalling in reactive iASTROs 192
Chapter 6 - Investigating the effect of reactive iASTROs on iDAn 196
6.1. Introduction and aims 196
6.2. Effect of pre-treated reactive control and *GBA-N370S* iASTROs on iDAn 197
6.3. Effect of inflammatory iASTROs on iDAn when treating the co-cultures directly 205
6.3.1. Co-cultures with control iASTROs – batch #1 of experiments 205
6.3.1.1. Treatment with TNFα and the Liddelow factors 206
6.3.1.2. Treatment with IFNγ and TNFα+IFNγ 209
6.3.1. Co-cultures with control and *GBA-N370S* iASTROs – batch #2 of experiments 213
6.3.2.1. Treatment with TNFα and the Liddelow factors 213
6.3.2.2. Treatment with IFNγ and TNFα+IFNγ 218
6.4. Exploration of the effects of α-synuclein PFF treatment, alone or in combination with TNFα+IFNγ, in direct iDAn-iASTRO co-cultures 223
6.5. Discussion 229
Chapter 7 – Discussion 239
7.1. Main findings and discussion 239
7.1.1. Control and *GBA-N370S* iASTROs are a representative human model of midbrain astrocytes, capable of supporting DAn 239
7.1.2. The *GBA-N370S* mutation has a very small impact on iASTRO function 241
7.1.3. Control and *GBA-N370S* iASTROs undergo vast transcriptional and cellular changes in response to inflammatory cytokines but not α-synuclein PFFs 241
7.1.4. Calcium signalling pathways and vitamin D metabolism and signalling at altered in reactive control and *GBA-N370S* iASTROs 246
7.1.5. In direct co-culture, reactive control and *GBA-N370S* iASTROs may lose neurosupportive properties and become neurotoxic, and this effect is potentiated in the presence of α-synuclein PFFs 247
7.2. Conclusions 250
S. Appendix 251
S.1. Effects of partially blocking ATP-induced ER calcium release with 2-APB in reactive iASTROs 251

S.1 1. Relative gene expression of calcium channels in reactive iASTROs after treatment with 2-APB 253
S.1.2. Effects of 2-APB treatment on iASTRO reactivity 255
S.2. Studying the potential of MeTC7 to act as a blocker of VDR nuclear translocation 261
References 263

List of Figures

Figure 1.1. Simplified diagram of the ATP-induced ER calcium release signalling pathway 32
Figure 1.2. Simplified diagram of store operated calcium entry (SOCE) 33
Figure 2.1. Schematic diagram of the human iPSC-derived midbrain astrocyte differentiation protocol 51
Figure 2.2. Schematic diagram of the iPSC-derived dopaminergic neuron differentiation protocol 56
Figure 2.3. Schematic diagram of iASTRO and iDAn differentiation and co-culture set up 59
Figure 2.4. Example electron microscope images of PFFs 59
Figure 3.1. Representative images of iASTROs at day 30, 60 and 100 of the differentiation protocol, stained for astrocytic, midbrain, progenitor cell, and neuronal markers 75
Figure 3.2. Morphological analysis and Foxa2 and Pax6 expression analysis at day 30, 60 and 100 of the iASTRO differentiation protocol 76
Figure 3.3. RT-qPCR analysis of different markers at day 30, 60 and 100 of the iASTRO differentiation protocol shows an increase in expression of astrocytic markers and a decrease in proliferation and progenitor cell markers 77
Figure 3.4. The relative gene expression of astrocytic and neuronal markers of mature iDAn and iASTROs correlates with their cellular identity 78
Figure 3.5. RNAseq comparison with a human post-mortem scRNAseq dataset and bulk RNAseq datasets of iPSC-derived neural models demonstrates the midbrain and astrocytic identity of iASTROs 80
Figure 3.6. At day 100, iASTROs display ATP-induced calcium release from the ER and glutamate uptake from the media 82
Figure 3.7. *GBA-N370S* iASTROs do not have reduced GCase activity compared to control iASTROs, whereas *GBA-N370S* iDAn have reduced GCase activity compared to control iDAn 84
Figure 3.8. A media composed of 50% DAn MAT media and 50% Astro MAT media is the most optimal for the survival of both iDAn and iASTROs in direct co-culture 87
Figure 3.9. Studying the effect of the *GBA-N370S* mutation in the iDAn-iASTRO co-cultures 89
Figure 3.10. Both control and *GBA-N370S* iASTROs support the growth and survival of control and *GBA-N370S* iDAn, but iASTROs respond differently to *GBA-N370S* iDAn compared to control iDAn 90
Figure 3.11. Ki67 expression analysis in iDAn-iASTRO co-cultures suggests that the increase in the number of iDAn in the presence of iASTROs is not due to an increase in the proliferation of iDAn 92
Figure 3.12. Both control and *GBA-N370S* iASTROs support the formation of synapses 94
Figure 4.1. RNAseq analysis of control iASTROs treated for 24h with different combinations of inflammatory cytokines and α-synuclein PFFs shows sample clustering according to treatment 106
Figure 4.2. Volcano plots displaying the statistical significance of the differentially expressed genes between different treatment conditions show very extensive gene expression changes in response to inflammatory cytokines but not α-synuclein PFFs 109

Figure 4.3. Analysis of the main genes and pathways activated and suppressed in iASTROs treated with different combinations of inflammatory cytokines and α-synuclein PFFs compared to untreated iASTROs 116
Figure 4.4. Gene set enrichment analysis of iASTROs treated with α-synuclein PFFs, without or with TNFα+IFNγ 118
Figure 4.5. Analysis of the main genes and pathways activated and suppressed in iASTROs treated with different combinations of inflammatory cytokines and α-synuclein PFFs compared to iASTROs with other treatments 124
Figure 4.6. iASTROs treated with TNFα+IFNγ have activated pathways related to calcium transport and homeostasis 126
Figure 4.7. Normalized counts of the genes of interest to be further explored in vitro 129
Figure 4.8. Relative gene expression analysis by RT-qPCR shows that 24h and 7 days after treatment with TNFα+IFNγ or the Liddelow factors, the expression profile of control and *GBA-N370S* iASTROs does not resemble either the A1 or A2 astrocyte profile 133
Figure 4.9. Representative immunocytochemistry images of control (top panel) and GBA-N370S (bottom panel) iASTROs treated with different combinations of inflammatory cytokines for 72h 135
Figure 4.10. Control and *GBA-N370S* iASTROs treated with TNFα, TNFα+IFNγ or the Liddelow factors have an increase in the expression and nuclear translocation of NFκB 24h after treatment, and this decreases with time 137
Figure 4.11. ROS levels are increased over time in control and *GBA-N370S* iASTROS in response to TNFα+IFNγ but not the Liddelow factors 139
Figure 4.12. Control and *GBA-N370S* iASTROs present changes in the relative gene expression of some lipid metabolism related genes in response to TNFα+IFNγ, but this does not result in changes in the number or size of lipid droplets 143
Figure 4.13. Relative gene expression of some growth factors is increased in control and *GBA-N370S* iASTROs in response to TNFα+IFNγ or the Liddelow factors 145
Figure 4.14. Relative gene expression analysis by RT-qPCR shows that iASTROs do not undergo an inflammatory response after 24h or 7-day treatment with α-synuclein PFFs 149
Figure 4.15. Representative immunocytochemistry images of control (top panel) and *GBA-N370S* (bottom panel) iASTROs treated with inflammatory cytokines and α-synuclein PFFs 151
Figure 4.16. Control and *GBA-N370S* iASTROs do not undergo reactive astrogliosis in response to α-synuclein PFFs alone 24h, 72h and 7 days after treatment 153
Figure 4.17. ROS levels are increased over time in control and *GBA-N370S* iASTROS in response to TNFα+IFNγ with or without α-synuclein PFFs, but not in cells treated with α-synuclein PFFs alone 154
Figure 4.18. Control and *GBA-N370S* iASTROs present changes in the relative gene expression of some lipid metabolism related genes in response to α-synuclein PFFs and TNFα+IFNγ, but this does not result in changes in the number or size of lipid droplets 157

Figure 5.1. Relative gene expression of some calcium channels is increased in control and *GBA-N370S* iASTROs in response to TNFα+IFNγ, and to a lesser extent to the Liddelow factors .171
Figure 5.2. Store operated calcium entry (SOCE) is increased in iASTROs treated with TNFα+IFNγ, with bigger changes in *GBA-N370S* iASTROs 173
Figure 5.3. ATP-induced calcium release from the ER is increased over time in some, but not all, lines of control and *GBA-N370S* iASTROs treated with TNFα+IFNγ and the Liddelow factors 176
Figure 5.4. *CYP27B1* and *VDR* expression are increased in control and *GBA-N370S* iASTROs treated with TNFα+IFNγ but not α-synuclein PFFs alone, and the increase is bigger in *GBA-N370S* iASTROs 179
Figure 5.5. Control and *GBA-N370S* iASTROs have increased VDR nuclear translocation after 7-day treatment with TNFα+IFNγ but not the Liddelow factors 181
Figure 5.6. Representative immunocytochemistry images of control (top panel) and *GBA-N370S* (bottom panel) iASTROs treated for 72h with MeTC7 and TNFα+IFNγ.....183
Figure 5.7. The VDR blocker MeTC7 does not affect the reactive response of iASTROs to TNFα+IFNγ 184
Figure 5.8. Representative immunocytochemistry images of (A) control and (B) *GBA-N370S* iDAn treated for 7 days with increasing concentrations of vitamin D.....186
Figure 5.9. Vitamin D supplementation to iDAn does not affect their viability and survival 187
Figure 6.1. Experimental design and immunocytochemistry images of iDAn co-cultured with iASTROs treated for 24h with TNFα+IFNγ prior to the co-culture.....199
Figure 6.2. 24h treatment of iASTROs with TNFα+IFNγ prior to the co-culture does not affect their ability to support iDAn.....201
Figure 6.3. iASTROs treated for 24h with TNFα+IFNγ maintain their reactivity after co-culture establishment with iDAn, but the reactivity decreases over time in the co-cultures 204
Figure 6.4. Representative immunocytochemistry images of control (top panel) and *GBA-N370S* (bottom panel) iDAn in mono-culture or in co-culture with control iASTROs, untreated or treated for 14 days with TNFα or the Liddelow factors 207
Figure 6.5. In direct co-culture, control iASTROs treated with Liddelow factors or TNFα alone become more neurosupportive to iDAn.....208
Figure 6.6. Representative immunocytochemistry images of control (top panel) and *GBA-N370S* (bottom panel) iDAn in mono-culture or in co-culture with control iASTROs, untreated or treated for 14 days with IFNγ or TNFα+IFNγ.....211
Figure 6.7. In direct co-culture, control iASTROs treated with IFNγ alone or TNFα+IFNγ become more neurosupportive to iDAn but this is accompanied with increased death of non-iDAn cells 212
Figure 6.8. Representative immunocytochemistry images of control (top panel) and *GBA-N370S* (bottom panel) iDAn in mono-culture or in co-culture with control (top panel) or *GBA-N370S* (bottom panel) iASTROs, untreated or treated for 21 days with TNFα or the Liddelow 215

Figure 6.9. In direct co-culture, reactive control and *GBA-N370S* iASTROs treated with the Liddelow factors or TNFα alone lose their neurosupportive capacities to iDAn 217
Figure 6.10. Representative immunocytochemistry images of control and *GBA-N370S* iDAn in mono-culture or in co-culture with control or *GBA-N370S* iASTROs, untreated or treated for 21 days with IFNγ or TNFα+ IFNγ 220
Figure 6.11. In direct co-cultures, reactive control and *GBA-N370S* iASTROs treated with IFNγ alone or TNFα+IFNγ lose their neurosupportive functions and become neurotoxic to iDAn 222
Figure 6.12. Representative immunocytochemistry images of control iDAn in mono-culture or in co-culture with control iASTROs, untreated or treated for (A) 7 days or (B) 21 days with α-synuclein PFFs with or without TNFα+IFNγ 226
Figure 6.13. In control and *GBA-N370S* iDAn mono-cultures or in co-cultures with control and *GBA-N370S* iASTROs, α-synuclein PFFs alone do not affect the viability of either cell type, but when combining them with TNFα+IFNγ, iASTROs become reactive and neurotoxic..... 228

Figure S.1. The ITPR blocker 2-APB reduces the amount of calcium released from the ER in response to ATP in iASTROs..... 252
Figure S.2. The ITPR blocker 2-APB does not alter the expression changes of various calcium channels in iASTROs, with or without combined treatment with TNFα+IFNγ 254
Figure S.3. Representative immunocytochemistry images of control (top panel) and GBA-N370S (bottom panel) iASTROs treated for 72h with different cytokines..... 256
Figure S.4. The ITPR blocker 2-APB does not affect the reactive response of iASTROs to TNFα+IFNγ 258
Figure S.5. The ITPR blocker 2-APB does not alter the gene expression changes of iASTROs, with or without combined treatment with TNFα+IFNγ 260
Figure S.6. Addition of vitamin D to iASTROs increases the nuclear translocation of VDR, and this is partially blocked with MeTC7, without affecting the cellular viability..... 262

List of Tables

Table 2.1. Kits used..... 46
Table 2.2. Reagents and drugs used 46
Table 2.3. Cell culture medias, reagents, and growth factors used..... 47
Table 2.4. Details of the iPSC lines used 48
Table 2.5. Composition of basal medias used for iASTRO differentiation 50
Table 2.6. Specific composition of the medias used for iASTRO differentiation 50
Table 2.7. Composition of basal medias used for DAn differentiation..... 54
Table 2.8. Specific composition of the medias used for DAn differentiation 54

Table 2.9. Primers used for qRT-PCR 61
Table 2.10. Primary antibodies used for immunocytochemistry 62
Table 2.11. Secondary antibodies used for immunocytochemistry 63
Table 2.12. Human iPSC-derived cell model bulk RNAseq datasets used for the comparison 70
Table 3.1. Media compositions tested in the iDAn-iASTRO co-cultures 87
Table 4.1. Number of DEGs, upregulated and downregulated genes 108
Table 4.2. Number of activated and suppressed GO:BP terms 111

List of Abbreviations

2-APB	2-Aminoethoxydiphenyl borate
4-MUG	4-Methylumbelliferyl β-D-glucopyranoside
AD	Alzheimer's Disease
AK	Adenylate cyclase
ATP	Adenosine triphosphate
BCA	Bicinchoninic acid
BDNF	Brain-derived neurotrophic factor
BMP4	Bone morphogenetic protein 4
bp	Base pair
BP	Biological process
BSA	Bovine serum albumin
C1q	Complement component 1q
C3	Complement component 3
CBE	Conduritol B epoxide
CC3	Cleaved caspase 3
cDNA	Complementary DNA
CNS	Central nervous system
DAn	Dopaminergic Neuron
db-cAMP	Dibutyryl cyclic adenosine monophosphate
DEG	Differentially expressed gene
DL-TBOA	DL-threo-beta-Benzyloxyaspartate
DMEM	Dulbecco's modified eagle medium
DMSO	Dimethyl sulfoxide
EGF	Epidermal growth factor
ER	Endoplasmic reticulum
FGF2	Fibroblast growth factor 2
FGF8α	Fibroblast growth factor 8α
GD	Gaucher's disease
GDNF	Glial cell line-derived neurotrophic factor
GFAP	Glial fibrillary acidic protein
GLAST	Glutamate-aspartate transporter (GLAST/EAAT1)
GO	Gene ontology
GSEA	Gene set enrichment analysis

GWAS	Gebine-wide association studies
HBSS	Hank's balanced salt solution
iASTRO	Induced pluripotent stem cell derived midbrain astrocyte
ICC	Immunocytochemistry
IFN-γ	Interferon γ
IL1α	Interleukin 1α
iPSC	Induced pluripotent stem cell
ITPR	Inositol 1,4,5-triphosphate receptor
LB	Lewy body
LIF	Leukemia inhibitory factor
LN	Lewy neurite
MANF	Mesencephalic astrocyte-derived neurotrophic factor
MAP2	Microtubule-associated protein 2
mRNA	Messenger RNA
NFκB	Nuclear factor kappa-light-chain-enhancer of activated B cells
ORAI1	Calcium release-activated calcium channel protein 1
PBS	Phosphate-buffered saline
PCR	Polymerase chain reaction
PD	Parkinson's disease
PFFs	Pre-formed fibrils
RNAseq	RNA sequencing
sc-RNAseq	Single cell RNAseq
RT-qPCR	Quantitative reverse transcription polymerase chain reaction
S100B	S100 calcium-binding protein B
SEM	Standard error of the mean
SHH	Sonic Hedgehog
SNpc	Substantia nigra pars compacta
SOCE	Store operated calcium entry
STIM1	Stromal interaction molecule 1
TBS	Tris-buffered saline
TGFβ3	Transforming growth factor β3
TH	Tyrosine hydroxylase
TNFα	Tumor necrosis factor α
VDR	Vitamin D receptor
α-syn	α-synuclein

Chapter 1 - Introduction

1.1. Parkinson's disease

Parkinson's disease (PD) is named after James Parkinson, who, in 1817, first described PD as a specific syndrome in "An Essay on the Shaking Palsy" (Parkinson, 2002). PD is currently described as a progressive neurodegenerative movement disorder. In 2019, global PD cases were estimated to be 8.5 million, which makes it the second most common neurodegenerative disease after Alzheimer's disease (AD) (Ou et al., 2021). This number is projected to double, or more than double, by 2040, mostly due to the aging population and increased life expectancy (Dorsey et al., 2018). The continuous increase in the number of PD cases has also caused a big economic burden; for instance, in 2010, the annual spend in Europe on PD was approximately €13.9bn (Gustavsson et al., 2011). PD incidence increases with age, although it is estimated that 5-10% of patients are affected before the age of 50 (Dodel et al., 2021). Nevertheless, this percentage, as well as the overall number of diagnosed PD cases, is believed to be an underestimation, and would increase with earlier and better diagnostic techniques. The incidence of PD differs amongst different populations, as it is affected by sex, country of residence and ethnicity. For example, males have a higher risk of developing PD than females (Ou et al., 2021; Willis et al., 2022). Moreover, the prevalence is higher in North America and Europe than in Africa, Latin America and Asia (Ben-Shlomo et al., 2024). Additionally, studies conducted in ethnically diverse locations indicate that the incidence of PD is higher in European White people than in Asian or Black people (Wright Willis et al., 2010). There is also a correlation between PD prevalence and the gross domestic product (GDP) per capita: the higher the GDP per capita of a country, the higher the prevalence of PD (Dorsey et al., 2018).

1.1.1. Pathophysiology of Parkinson's disease

Histologically, PD is characterized by the selective loss of dopaminergic neurons (DAn) in the substantia nigra pars compacta (SNpc) of the midbrain amongst other features (Hayes, 2019). Neuronal loss is also observed in other regions such as the basal nucleus of Meynert, the locus ceruleus and the dorsal motor nucleus of the vagus (Kalia & Lang, 2015).

Another main neuropathological hallmark of PD is Lewy Pathology, characterized by the presence of intracellular proteinaceous inclusions called Lewy bodies (LBs) in DAn of the SNpc. LBs have also been found in other regions of the central nervous system (CNS), such as the olfactory bulb (Sengoku et al., 2008) and the cerebellum (Kakita et al., 1994), and in glial cells (Fares et al., 2021). One of the main components of LBs is α-synuclein (Spillantini et al., 1997), but over 90 other molecules have also been identified to be constituents of LBs, such as lipids, membranous fragments, and proteins involved in the ubiquitin-proteasome system. The interaction of α-synuclein with these structures and molecules is believed to have a role in α-synuclein misfolding, aggregation, and inclusion formation (Shahmoradian et al., 2019). The structure, morphology, and composition of LBs varies amongst brain regions and patients (Kuusisto et al., 2003), but there is no clear understanding of how different LBs might reflect different disease states. Lewy neurites (LNs), also found in PD, are similar in composition to LBs, but are located in neuronal processes as opposed to cell bodies (Wakabayashi et al., 2013). In 2003, Braak and colleagues proposed that LB pathology could be classified into six stages based on their analyses of post-mortem brain tissue of individuals with PD (Braak et al., 2003). According to this hypothesis, in the early stages, LB pathology is detected in the olfactory bulb, and lower brainstem, and as pathology worsens it progresses to the higher brainstem, to the SNpc and the amygdala, and lastly, to the neocortex (Braak et al., 2003). These findings led on to the development of the "Braak Hypothesis", which suggests that α-synuclein pathology might originate from the olfactory bulb, the brainstem, or even the gut given the connectivity of the involved brain regions (Hawkes et al., 2007). The initial spread of α-synuclein pathology in non-motor regions might explain some of the prodromal PD symptoms (discussed in Section 1.1.2.). However, subsequent studies have shown that, in approximately 50% of PD cases, disease progression does not follow Braak staging (Kalaitzakis et al., 2008). Lewy pathology is also one of the hallmarks of other neurodegenerative diseases, most notably Dementia with Lewy bodies (DLB) (Sezgin et al., 2019) and Multiple system atrophy (MSA) (Poewe et al., 2022).

Lastly, another hallmark of PD is neuroinflammation, as demonstrated by multiple neurohistological and neuroimaging studies, as well as studies examining the cerebrospinal fluid (CSF) and blood of PD patients (Tansey et al., 2022). Further information regarding the role of inflammation in PD is provided in Section 1.3.

1.1.1.1. Preferential vulnerability of DAn

The preferential vulnerability of DAn of the SNpc in PD can be explained by numerous cell autonomous factors. Firstly, dopamine metabolism might increase the susceptibility of DAn, as its metabolism by monoamine oxidase (MAO) can lead to oxidative stress if the turnover is very high (Graves et al., 2020). At the same time, oxidative stress can cause the oxidation of dopamine, which results in aggregation of α-synuclein as well as lysosomal impairments (Burbulla et al., 2017). Furthermore, DAn have a very long, highly branched and poorly myelinated axonal tree (Braak & Del Tredici, 2004) that participates in 1-2 million synapses (Bolam & Pissadaki, 2012). This extensive axonal arbour has a very high bioenergetic demand due to its vesicle trafficking (Bolam & Pissadaki, 2012) and proteostatic burden caused by the need to produce, transport and degrade axonal proteins, as well as the transport of mitochondria across the axon (Misgeld & Schwarz, 2017). Other vulnerable neuronal populations in PD (e.g. adrenergic neurons in the locus ceruleus) also have vast axonal arborization, which explains their specific vulnerability in PD (Gonzalez-Rodriguez et al., 2020). In addition, DAn have broad action potentials and autonomous pacemaking activity, with slow and rhythmic (1-4 Hz) spikes. These spikes are accompanied by large intracellular calcium oscillations that are reliant on the opening of L-type (Ca_v1) calcium channels in the plasma membrane (Guzman et al., 2009), but DAn have low intrinsic calcium buffering capacity (Foehring et al., 2009). Consequently, most of the calcium gets taken up by the endoplasmic reticulum (ER) and the mitochondria. In the latter, calcium positively regulates the activity of proteins and enzymes involved in oxidative phosphorylation (Rossi et al., 2019). Thus, calcium fluctuations in DAn act as anticipatory bioenergetic signals by stimulating ATP production and help meet the high energetic demands of these cells. However, extensive calcium-induced oxidative phosphorylation results in an increase in generation of reactive oxygen species (ROS) and mitochondrial oxidative stress in DAn (Guzman et al., 2018). Furthermore, DAn are more susceptible to oxidative stress because they express low levels of antioxidant enzymes (Guo et al., 2018).

1.1.1.2. α-synuclein

α-synuclein is encoded by the *SNCA* gene, located in chromosome 4 (4q21-22) (Chen et al., 2022). α-synuclein is an intrinsically disordered protein with 140 amino acids, consisting of a lysine-rich amphipathic N-terminal domain, a hydrophobic non-amyloid-component (NAC) and an acidic C-terminal binding domain. Binding of the N-terminal to lipid membranes results in acquisition of a partial α-helical conformation (Mehra et al., 2019). On the other hand, the NAC region is responsible for the aggregation of α-synuclein (Giasson et al., 2001), whereas most posttranslational modifications (PTMs) occur in the C-terminal (Oueslati et al., 2010). α-synuclein undergoes extensive PTMs such as phosphorylation, nitration, ubiquitination, acetylation and truncation. Of these, phosphorylation of serine 129 (pS129) has been the one most consistently related to PD pathology (Anderson et al., 2006), although its exact function and effects on aggregation are still unclear.

Despite decades of research, the physiological function of α-synuclein is not fully understood yet. Its cellular location, the presynaptic region, provided initial clues to its function; α-synuclein is now thought to be involved in synaptic plasticity and various stages in the process of synaptic vesicle assembly, trafficking and release (Rocha et al., 2018; Sharma & Burré, 2023). α-synuclein is also found in the nucleus, and even if the roles of nuclear α-synuclein are less known, recent studies have suggested that it participates in histone methylation (Nakamura et al., 2024) and DNA repair (Schaser et al., 2019). Furthermore, α-synuclein is considered a biomarker of PD, as it is present in the CSF, blood, saliva, skin, and the enteric nervous system. However, because α-synuclein is also expressed by other cell types in the body, its levels in different fluids and regions of the body might not be a direct reflection of its levels in the CNS (Ganguly et al., 2021).

Under normal physiological conditions, α-synuclein is found in its monomeric form or as a tetramer, which are believed to exist in equilibrium (Bartels et al., 2011). However, α-synuclein has a propensity to aggregate, and thus, it can exist in different aggregated forms (or α-synuclein species), such as oligomers, protofibrils and fibrils, all of which have been identified in PD brains. Various factors contribute to the aggregation of α-synuclein, including genetic mutations, PTMs, and interactions with lipid membranes. All these shift the equilibrium of monomeric α-synuclein conformational states in favour of β-like conformers, which have a propensity to associate (Mehra et al., 2019). Consequently, misfolded α-synuclein forms

oligomers that are stabilized by the interactions between β-sheets, and then into higher molecular weight protofibrils that further polymerize into highly ordered cross-β-sheet amyloid fibrils that are protease-resistant (Conway et al., 2000). However, even if initially α-synuclein fibrils were believed to be the most toxic species, there is also substantial evidence regarding the toxicity of oligomers and their contribution to PD pathology (Bengoa-Vergniory et al., 2017). Similarly, in recent years, the prion-like behaviour of α-synuclein has gained a lot of attention. The hypothesis that α-synuclein pathology might spread in a prion-like manner came from the observations that grafted healthy neuronal cells in the brain of PD patients eventually presented LB inclusions (Li et al., 2008), and the spatio-temporal spreading of Lewy pathology described in the Braak hypothesis also supports this idea. Therefore, many studies now use α-synuclein pre-formed fibrils (PFFs), which act as "seeds", to recapitulate the prion like spreading of α-synuclein in animal models and cultured cells (Stoll & Sortwell, 2022). For PFFs to induce the formation of aggregates that resemble LBs, the presence of endogenous α-synuclein in the cells is required.

Lastly, many studies have tried to elucidate the mechanisms by which α-synuclein and its different conformations cause neuronal dysfunction and neurotoxicity, as this will help understand some of the mechanisms underlying neuronal degeneration and help identify new therapeutic targets. One of the main mechanisms by which α-synuclein exerts neurotoxicity is by causing mitochondrial dysfunction, which can happen through various mechanisms, such as impaired mitophagy (L. Chen et al., 2015), mitochondrial fragmentation (Plotegher et al., 2014), and altering mitochondrial protein import (Di Maio et al., 2016). Furthermore, defects in autophagy and lysosomal function have also been observed, such as blockage of chaperon-mediated autophagy (CMA) (Martinez-Vicente et al., 2008), and defective macroautophagy (Tanik et al., 2013). Other affected neuronal cellular pathways include ER stress (Colla et al., 2012), disruptions to the synaptic vesicle cycle (Choi et al., 2013), and damage to lipid membranes (Chaudhary et al., 2016).

1.1.2. Clinical presentation of Parkinson's disease

The main clinical hallmark of PD is a combination of motor symptoms including bradykinesia (slowness of movement), resting tremor (4-6 Hz, slower than classic essential tremor), rigidity

(muscle inflexibility or stiffness), and postural instability (Tysnes & Storstein, 2017). The former three are considered the three cardinal motor symptoms of PD and are generally referred to as Parkinsonism. These motor impairments develop due to the loss of DAn of the SNpc that project to the dorsal putamen of the striatum, as they have an important role in motor control (Kalia & Lang, 2015). Moreover, PD patients present a range of different non-motor symptoms, such as cognitive decline, anxiety, apathy, depression, sleep disturbances (e.g. rapid eye movement sleep behaviour disorder (RBD), insomnia), hyposmia or anosmia (partial or complete loss of sense of smell), and gastrointestinal issues (e.g. constipation, bloating, nausea), which can be as debilitating as the motor symptoms (Hayes, 2019; Tolosa et al., 2021). For years, only motor impairments were used in the clinical diagnostic criteria for PD, but recently revised criteria by The Movement Disorders Society (MDS) have also added "supportive criteria" that include non-motor symptoms such as olfactory loss, as well as "absolute exclusion criteria" or "red flags", such as cerebellar abnormalities and early bulbar dysfunction, to reduce misdiagnosis (Postuma et al., 2015). Nevertheless, one of the main challenges in PD research remains the fact that, by the time first motor symptoms are detected, around 30-50% of DAn in the SNpc have been lost (Fearnley & Lees, 1991; Grosch et al., 2016). On the contrary, some of the non-motor symptoms often appear prior to the clinical diagnosis, during the prodromal phase of PD (Postuma & Berg, 2019). Therefore, researchers have focused on the detection of these prodromal markers, such as RBD (Friederich et al., 2019), and olfactory loss (Siderowf et al., 2012) for early detection of PD, as well as blood-based biomarkers (Tönges et al., 2022).

Despite decades of research, there is still no cure for PD, and the treatments available are solely symptomatic, meaning that they are only used to manage the symptoms of the disease (Elsworth, 2020). The main treatments available are either pharmacological or neurosurgical. The most common treatment remains the use of drugs that enhance the dopamine concentrations in the brain or stimulate dopamine receptors (receptor agonists) (Connolly & Lang, 2014). Examples of the most widespread drugs include levodopa (L-Dopa, the immediate precursor of dopamine), MAO-B inhibitors (e.g. selegiline), dopamine agonists (e.g. apomorphine) and amantadine (Kalia & Lang, 2015). In addition, a well stablished neurosurgical treatment to reduce PD motor symptoms is deep brain stimulation (DBS) in the subthalamic nucleus or globus pallidus internus, but patients need to be selected carefully to

ensure that they will tolerate and respond to the surgery, and it is usually limited to late-stage patients (Malek, 2019). All things considered, one of the main ongoing goals of PD research is to find disease-modifying drugs that slow or halt the neurodegenerative process.

1.1.3. Aetiology of Parkinson's disease

PD is a multifactorial disease, with the interplay between aging, genetics, and environmental factors underlying disease onset and pathogenesis. Nevertheless, in most PD cases, the causal determinants of the disease remain unknown. PD has generally been classified as sporadic/idiopathic (without a known cause, ~90% of cases) or familial/genetic (with a known genetic cause, ~10% of cases) (Pang et al., 2019).

1.1.3.1. Non-genetic risk factors

Age is the biggest risk factor for PD, and thus, disease prevalence increases significantly with age (Pringsheim et al., 2014; Reeve et al., 2014). Studies have shown that, every decade, in healthy individuals without neurological diseases the number of neurons in the SN decreases about 7-9.8% (Ma et al., 1999). However, aging alone is not a sufficient cause of PD, as most people do not develop PD even in old age, and environmental factors are believed to play a big part in PD development. The main non-genetic risk factors for PD include pesticides, traumatic brain injury, rural living and agricultural occupation, anxiety or depression, and β-blockers (Noyce et al., 2012; Pang et al., 2019). The first evidence of the effect of environmental toxins in PD development came from the observation that a group of drug users exposed to MPTP (1-methyl-4-phenyl-1,2,5,6-tetrahydropyridine, contaminant found in synthetic heroin) developed parkinsonism (Langston et al., 1983). MPTP has a similar structure to paraquat, found in pesticides, and research has shown that farmers exposed to paraquat have increased risk of developing PD (Tanner et al., 2009). Similar observations have been made with the pesticide rotenone (Tanner et al., 2011). Consequently, MPTP and rotenone are used in various animal and cell studies to model PD development. On the other hand, protective or preventative factors have also been identified, and these include caffeine consumption, tobacco smoking (not recommended for many other reasons (Samet, 2013)) and physical activity (Ascherio & Schwarzschild, 2016).

1.1.3.2. Genetic risk factors

In the last 25 years, several mutations in specific genes have been identified as the cause of monogenic familial forms of PD. Even if Mendelian inheritance of monogenic mutations constitutes a small percentage of total PD cases, these mutations are very useful in helping to understand the pathological mechanisms that underly PD and the specific cellular processes that might be altered throughout the disease. Genetic variants linked to PD vary in the frequency, risk of developing PD, and average age of onset (Day & Mullin, 2021). Around 20 genes have been linked to monogenic PD, and these can either be autosomal dominant or recessive (Delamarre & Meissner, 2017). Originally, loci associated with familial PD were named *PARK* loci and the genes *PARK* genes, followed by a number that indicated the order in which they had been discovered (Day & Mullin, 2021). However, this nomenclature has been discarded by most, and nowadays full gene names are preferably used.

The first gene linked to PD was *SNCA*, which encodes α-synuclein (Polymeropoulos et al., 1997). Missense mutations and multiplication mutations (mostly duplications and triplications) have been identified in the *SNCA* loci (Pang et al., 2019). The latter indicate that excessive expression of wild-type (WT) α-synuclein is sufficient to cause PD, and there is also a dose-dependence, as triplications are linked with earlier onset and worse disease progression (Ibáñez et al., 2004). Missense mutations generally occur in the N-terminal of the protein and increase its propensity to misfold and aggregate (Delamarre & Meissner, 2017). Furthermore, biallelic mutations in *PRKN* (also known as *Parkin*), *PINK-1* (encoding PTEN-induced kinase 1), and *PARK7* (also known as *DJ-1*) are also associated with monogenic PD. All these genes are involved in mitochondrial function, and thus, mutations in these genes result in altered mitophagy, mitochondrial oxidative stress, and apoptosis (Xiong et al., 2009). Additionally, autosomal dominant mutations in *VPS35* (encoding vacuolar protein sorting 35) have been linked to changes in lysosomal and mitochondrial function, as well as neurotransmission (Sassone et al., 2021). Mutations in *LRRK2* (encoding leucine-rich repeat kinase 2) and *GBA1* (encoding β-glucocerebrosidase, which I will explore in more detail in this work) have variable penetrance, and thus, even if they are more common than other monogenic risk variants, they confer less risk to develop PD (Day & Mullin, 2021). Over 100 mutations in *LRRK2* have been identified to date, which account for ~4% of familial PD cases.

Due to their higher frequency, the best studied mutations are *G2019S* and *R1441G/C/H* (Bardien et al., 2011). *LRRK2* mutations are associated with alterations in lysosomal function, synaptic vesicle trafficking, and neuroinflammation (Taylor & Alessi, 2020). Other genes involved in monogenic PD include: *PLA2G6* (encoding calcium-independent phospholipase A2), *ATP13A2* (encoding ATPase cation transporting 13A2), *FBXO7* (encoding F-box only protein 7), *DNAJC6* (encoding auxilin), *SYNJ1* (encoding synaptojanin 1) and *VPS13C* (encoding vacuolar protein sorting 13 homolog C), amongst others (Day & Mullin, 2021).

As for sporadic PD cases, the development of new tools and technologies to examine the genome of thousands of patients has enabled to get a better picture of the genetic architecture driving PD in cases without an identified monogenic cause. The evidence from large-scale genome-wide association studies (GWAS) and meta-analyses suggests that the genetic heritability of PD has been underestimated for many years, and instead of the widely reported estimation of 1-5% heritability, genetic variation might contribute as much as 16-36% to the risk of developing PD (Elsworth, 2020). In a recent meta-analysis, 90 variants were found to be associated with disease risk (Nalls et al., 2019). Some of these variants occur in loci that are involved in familial PD, such as *SNCA*, *LRRK2* and *GBA1*. In addition, a recent GWAS study identified various genome-wide determinants of motor impairment progression and mortality in PD, and loci in or proximal to *APOE, TBXAS1, MORN1, ASNS, PDE5A* and *XPO1* were identified as relevant (Tan et al., 2024).

1.1.4. GBA in PD

Mutations in the *GBA1* gene are one of the most common genetic risk factors in PD. The first association between *GBA1* genetic variants and PD came from the observation that individuals with Gaucher disease (GD, caused by homozygous mutations in *GBA1*) had a higher risk of developing PD (Neudorfer et al., 1996). Since then, over 100 genetic *GBA1* variants have been associated with PD, and even if the pathogenicity of a lot of these is unclear, the better characterized ones have been classified into “severe” (e.g. *L444P*) or “mild” (e.g. *N370S*) variants depending on the risk of developing PD that they confer (Gegg et al., 2022). Overall, PD patients carrying *GBA1* mutations present similar LB pathology (Parkkinen et al., 2011) to

sporadic PD patients, but they have an earlier onset of the disease, more cognitive dysfunction (Zhang et al., 2015), and increased non-motor symptoms (Brockmann et al., 2011).

The *GBA1* gene encodes the lysosomal enzyme β-glucocerebrosidase (GCase), which catalyses the final reaction in glycosphingolipid and ganglioside metabolism by breaking down glucosylceramide into glucose and ceramide, and glucosylsphingosine into glucose and sphingosine. Mutations in *GBA1* that reduce its enzymatic activity result in accumulation of its substrates (Smith & Schapira, 2022). However, studies conducted in *GBA*-PD patients have reported conflicting results regarding the presence, or absence, of increased glucosylceramide and glucosylsphingosine levels in *GBA*-PD patients compared to sporadic PD patients (Gegg et al., 2022).

Using patient, animal and cell models, it has been widely reported that numerous *GBA1* variants result in decreased GCase activity (Bogetofte et al., 2023; Gegg et al., 2012; Polinski et al., 2021). This provides a direct link between *GBA1* mutations and α-synuclein pathology. Indeed, studies have shown that pharmacological inhibition of GCase with conduritol-β-epoxide (CBE) results in accumulation of α-synuclein aggregates (Rocha et al., 2015). Furthermore, glucosylceramide, one of the main substrates for GCase, can interact with α-synuclein and induce conformational changes that result in toxic aggregate formation (Mazzulli et al., 2011). Therefore, if GCase activity is reduced, levels of glucosylceramide will increase, which will cause elevated α-synuclein aggregation. Furthermore, there are many other proposed mechanisms by which *GBA1* mutations cause cellular dysfunction related to PD. For instance, mutations in *GBA1* might prevent normal GCase folding, resulting in GCase retention in the ER and subsequent ER stress (Fernandes et al., 2016). Moreover, reduced GCase activity has been associated with mitochondrial disfunction, as demonstrated by elevated oxidative stress, reduced ATP levels and mitochondrial membrane potential (Cleeter et al., 2013). Changes in calcium homeostasis have also been reported in iPSC-derived *GBA* DAn (Beccano-Kelly et al., 2023; Schöndorf et al., 2014). Lastly, changes in lipid homeostasis have been linked to *GBA*-PD; even if results in patients are unclear, elevated glucosylceramide and glucosylsphingosine levels have been observed in animal models of GCase disfunction (Farfel-Becker et al., 2014; Ikuno et al., 2019) and iPSC-derived models (Fernandes et al., 2016; Schöndorf et al., 2014).

1.1.5. Lipid dysregulation in PD

Multiple studies have shown that PD patients present alterations in their brain and plasma lipid composition and lipid metabolism (Fanning et al., 2020; Galper et al., 2022; Sinclair et al., 2021), although the correlations between specific lipid levels, such as cholesterol, and disease risk and progression are still unclear (Alrouji et al., 2023). Lipid metabolism dysfunctions and lipidome alterations have particularly gained attention in PD cases involving mutations in *GBA* due to the involvement of GCase in lipid metabolism (L. Smith & Schapira, 2022), as discussed above. Indeed, some studies in patients with *GBA1* mutations found that these patients have altered lipid profiles (Guedes et al., 2017; Macías-García et al., 2021). Furthermore, mutations in other genes involved in lipid metabolism, such as *PLA2G6* (encoding calcium-independent phospholipase A2) (Sina et al., 2009), *SCARB2* (encoding lysosomal integral membrane protein 2, LIMP-2) (Nalls et al., 2019) and *SMPD1* (encoding sphingomyelin phosphodiesterase 1) (Dagan et al., 2015), have also been associated with increased PD risk.

In addition, the physiological interaction between lipids and α-synuclein has prompted many to research how different lipids and lipid membranes might influence α-synuclein misfolding and aggregation, and how α-synuclein in turn impacts lipid membranes (Mori et al., 2020). It has been shown that α-synuclein binding might disrupt the integrity of lipid membranes, causing leakage (Fecchio et al., 2013). Similarly, α-synuclein has been associated with various enzymes in lipid metabolic pathways and is thought to modulate their activity. For instance, α-synuclein is involved in fatty acid uptake (Golovko et al., 2007) and acyl-CoA activation (Sánchez Campos et al., 2018). Additionally, LBs contain high levels of lipids, membrane fragments and membranous organelles (Shahmoradian et al., 2019).

1.1.6. Vitamin D in PD

In recent years, the use of vitamin D supplementation has gained a lot of interest as a potential therapeutic strategy for PD, based on two main facts: a) the widely reported vitamin D deficiency in PD patients (Knekt et al., 2010; Xia & Zhou, 2024), and b) the neuroprotective effect of vitamin D (Pignolo et al., 2022). The term vitamin D is used to refer to a group of secosteroids that in humans are taken in the diet or synthetized in the skin during exposure to sunlight. There are two main forms of vitamin D, vitamin D2 (1,25-dihydroxyvitamin D2)

and vitamin D3 (1,25-dihydroxyvitamin D3), which are derived from 25-hydroxyvitamin (Pignolo et al., 2022). The CNS contains the enzyme 25-hydroxyvitamin D 1-alpha-hydroxylase (CYP27B1), which hydroxylates the 25-hydroxyvitamin D that crosses the blood brain barrier (BBB) into its active forms vitamin D2 and D3 (Eyles et al., 2005). Vitamin D is a multitargeting hormone with various genomic and non-genomic effects. In the CNS, it binds to either the nuclear receptor VDR (vitamin D receptor) or MARRS (membrane-associated rapid response steroid binding receptor). VDR activates the expression of various genes, some of them neuroprotective, such as *GDNF* and *BDNF* (Hafiz, 2024). In addition, vitamin D elevates the expression of *NR4A2* (encoding nurr1) and *CDKN1C* (encoding cyclin-dependent kinase inhibitor 1C), which promote the differentiation and maturation of DAn (Cui et al., 2010). Moreover, this vitamin has been postulated to regulate calcium homeostasis and prevent mitochondrial dysfunction and ROS generation (Berridge, 2017).

Based on these findings, researchers have explored the potential of vitamin D supplementation to reduce some PD symptoms. Different clinical studies have provided different outcomes (Detopoulou et al., 2023), with some claiming that vitamin D supplementation improves PD symptoms (Suzuki et al., 2013), whereas others have reported no improvements (Luthra et al., 2018). Additionally, a recent clinical study showed that co-administration of probiotics and vitamin D reduced serum levels of pro-inflammatory cytokines and decreased gastrointestinal problems and disease severity in PD patients (Zali et al., 2024).

1.2. Astrocytes in Parkinson's disease

DAn of the SNpc are one of the cellular populations most greatly affected in PD, and, consequently, for many years these were the only cells investigated by the PD research community. However, in the CNS neurons do not exist in isolation, they are surrounded by glial cells, namely astrocytes, microglia and oligodendrocytes, amongst others (He & Duan, 2023). Multiple studies demonstrated that glial cells are also involved in PD (summary of initial findings reviewed in (Kuter et al., 2020)), which shifted the neuron-centric view of the field to a broader, more inclusive perspective, where it is accepted that different glial cells and their interactions with neurons have important implications for PD. In the 21st century, many PD

researchers have positioned their interest in astrocytes, but, even if the number of published papers increases yearly, the specific role astrocytes play in the progression of PD is not understood yet.

1.2.1. Astrocytes

Astrocytes are the most abundant type of glial cell in the CNS (von Bartheld et al., 2016). The name astrocyte originates from *astron* (Greek word for star), which refers to their star-shaped morphology (Parpura & Verkhratsky, 2012). During CNS development, neurogenesis precedes astrogenesis, and although astrocyte progenitors are generated during embryonic development, most of the migration and maturation of astrocytes occurs during the first few postnatal weeks, when synapse formation happens (Markey et al., 2023). As will be discussed later, this poses a great challenge when trying to recapitulate astrocyte development in vitro. Extensive research in rodents, flies, and mammals has been done to understand the specific molecular cues involved in the regional patterning, differentiation, migration and maturation of astrocytes (Takouda et al., 2017).

Initially, astrocytes were classified into two main categories based on their morphology: protoplasmic (located in the grey matter) and fibrous (located in the white matter). However, it is now widely accepted that astrocytes are a very heterogeneous cell type, presenting transcriptomic, morphological and functional diversity depending on various factors such as the species, brain region, developmental state, age, and disease stage (Hasel et al., 2023). The regional and sub-regional heterogeneity of astrocytes is highly dependent on the specific astrocyte-neuron interactions, as well as the metabolic demands of the neurons in the region (Hasel et al., 2017). Furthermore, developmental patterning and the region-specific molecular cues astrocyte progenitor cells receive also play a role in the cellular heterogeneity (Markey et al., 2023). Astrocytes also undergo multiple changes due to normal aging, including changes in morphology, increase in GFAP expression, and acquisition of a more prominent pro-inflammatory phenotype (Palmer & Ousman, 2018).

For many years, astrocytes were thought to be passive cells in the CNS, a hypothesis that was rapidly discarded when research revealed the broad array of essential functions these cells carry out, such as: synaptogenesis and regulation of synaptic transmission (including

glutamate uptake), metabolic and structural support to neurons, maintaining water and ion homeostasis, regulating the permeability of the BBB, producing neurotrophic factors (e.g. BDNF), and responding to pathogenic stimuli and disease (Jiwaji & Hardingham, 2022). Regarding the specific interaction between astrocytes and DAn, astrocytes participate in clearance of synaptic dopamine by uptake through the Na^+-dependent dopamine transporter (DAT) and subsequent metabolism by MAO-B (Prunell & Olivera-Bravo, 2022). In addition, dopamine acts on the astrocytic dopamine receptors D1R and D2R to induce calcium oscillations (Xin et al., 2019) and promote the release of neurotrophic factors such as BDNF, GDNF and FGF2 (Li et al., 2006; Ohta et al., 2010). Moreover, astrocytes provide antioxidant support to DAn, partially by the dopamine-activated expression of Nrf-2 (nuclear factor erythroid 2-related factor 2) (Miyazaki et al., 2011).

1.2.2. Calcium signalling in astrocytes

Contrary to neurons, astrocytes do not fire action potentials, but they are electrically dynamic, have a hyperpolarized membrane, and express a broad array of potassium, sodium and calcium channels (McNeill et al., 2021). Moreover, one of the main characteristics of astrocytes is their complex and extensive intracellular calcium signalling, which can occur spontaneously or through activation of specific receptors (Ahrens et al., 2024). Indeed, astrocytes express a wide range of ionotropic and metabotropic receptors, which recognize different neurotransmitters at the synapse that subsequently activate intracellular calcium signals (Verkhratsky et al., 2019). Calcium signalling in astrocytes participates in various cellular functions, such as regulation of cerebral blood flow, regulation of synaptic transmission, and perception of the environment and the neuronal activity to adapt their activity accordingly (Lim et al., 2021a).

One of the main pathways leading to astrocytic calcium signalling is through activation of G protein-coupled receptors (GPCRs), followed by hydrolysis of phosphatidylinositol 4,5-biphosphate (PIP_2) by the enzyme phospholipase C (PLC), which produces diacylglycerol (DAG) and inositol 1,4,5-trisphosphate (IP_3). IP_3 then binds to its receptors in the ER (ITPR or IP3R), causing calcium release from the ER (McNeill et al., 2021) (Figure 1.1). When ER calcium stores are depleted, a process called store operated calcium entry (SOCE) is activated: reduced ER

calcium levels are sensed by STIM1/2 proteins (stromal interaction molecule 1/2) in the ER membrane, which then bind to ORAI1/2/3 channels (calcium release-activated calcium channel protein 1/2/3) located in the plasma membrane, causing them to open and allowing calcium flow into the cytoplasm from the extracellular space (Verkhratsky & Parpura, 2014) (Figure 1.2).

Calcium signals in astrocytes vary depending on the brain region and the neuronal activity, and also the subcellular compartments (Semyanov et al., 2020). Moreover, astrocytic calcium signals undergo significant changes after acute and chronic insults to the CNS, including neurodegenerative diseases, and reactive astrocytes have been shown to exhibit altered calcium activity (Bancroft & Srinivasan, 2022). These aberrant calcium signals negatively impact DAn survival, potentially due to glutamate excitotoxicity (Ibáñez et al., 2019). Even if calcium dysregulation has been described in astrocytes carrying PD mutations (Ramos-Gonzalez et al., 2021; Sonninen et al., 2020), it is not well understood how this impacts astrocyte function and neuron-astrocyte cross-talk in PD.

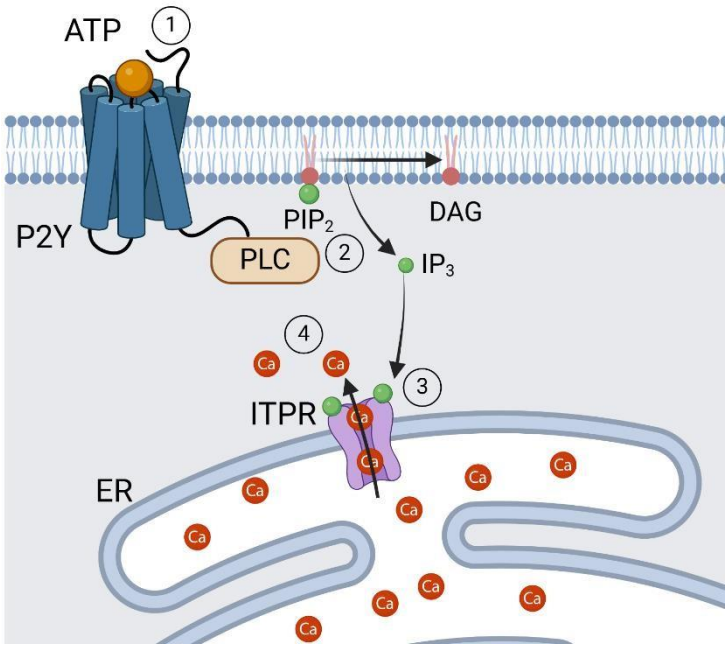


Figure 1.1. Simplified diagram of the ATP-induced ER calcium release signalling pathway
(1) Adenosine triphosphate (ATP) binds to P2Y receptors, which are purinergic G protein-coupled receptors (GPCRs) in the plasma membrane. This activates the receptor, which in turn activates phospholipase C (PLC). (2) PLC cleaved phosphatidylinositol 4,5-bisphophate (PIP_2) into diacylglycerol (DAG) and inositol 1,4,5-triphosphate (IP_3). (3) IP_3 binds to inositol 1,4,5-triphosphate receptors (ITPR or IP3R) in the endoplasmic reticulum membrane (ER), (4) which causes them to open and to release ER calcium into the cytoplasm. Created with BioRender.

.

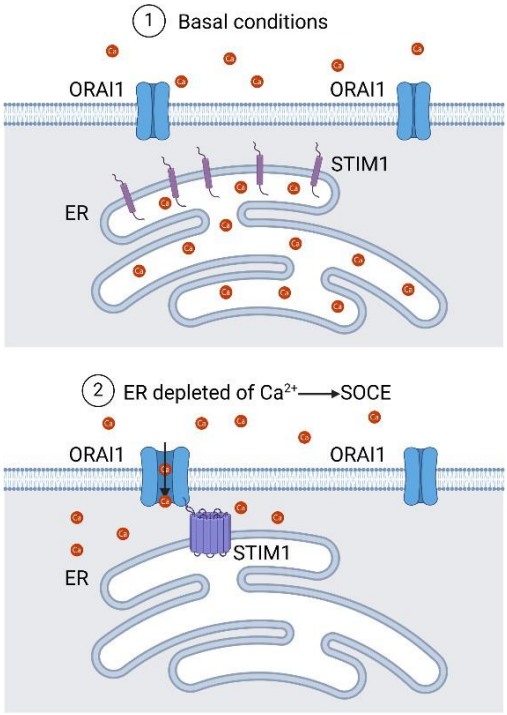


Figure 1.2. Simplified diagram of store operated calcium entry (SOCE)
(1) Under basal conditions, stromal interaction protein 1 (STIM1) in the endoplasmic reticulum (ER) membrane remain in a quiescent conformation, and calcium release-activated calcium channel protein 1 (ORAI1) located on the plasma membrane remain closed. (2) When ER calcium stores are depleted, STIM1 undergoes a morphological change, oligomerizes, and locates to ER-plasma membrane contact regions, where it binds to ORAI1, causing it to open and thus for extracellular calcium to enter through ORAI1 into the cytoplasm. Created with BioRender.

1.2.3. Evidence of astrocyte involvement in Parkinson's disease pathogenesis

At the end of the 20th century, some studies indicated that there was increased astroglial reactivity in PD patients and neurotoxin-induced PD models (Forno et al., 1992). Nevertheless, the first concrete evidence for the involvement of astrocytes in PD came from histological studies of PD post-mortem brains, which showed that astrocytes contained intracellular α-synuclein inclusions (Braak et al., 2007; Wakabayashi et al., 2000). In general, the distribution of astroglial inclusions correlated with the presence of LBs in neurons and degeneration of DAn in the SNpc; in the cases where astrocytes with α-synuclein inclusions were present in regions without neuronal LB pathology, these astrocytes were located close to axonal terminals, which were believed to be the source of astrocytic α-synuclein (Braak et al., 2007). Moreover, astrocytes are thought to be involved in the increased BBB permeability observed in PD patients (Miyazaki & Asanuma, 2020), as well as in the excitotoxicity described in PD, due to impaired astrocytic glutamate uptake (Zhang et al., 2016).

Furthermore, many of the genes associated with monogenic PD, such as *GBA1, PARK7* and *PINK1*, are expressed in astrocytes in similar levels to neurons and participate in different astrocytic functions (Booth et al., 2017). Based on this, multiple studies have investigated the cell autonomous and non-cell autonomous dysfunctions that these mutations might induce in astrocytes. For instance, DJ-1 (encoded by *PARK7*) deficiency in astrocytes reduces their neuroprotective functions (Lev et al., 2013) and causes mitochondrial dysfunction (Larsen et al., 2011). Similarly, Parkin (encoded by *PARK2*) deficient astrocytes have higher levels of cytokines, present increased ER stress, and have less neurotrophic activity (Singh et al., 2018). *ATP13A2* mutations in astrocytes result in impaired α-synuclein uptake and degradation, and subsequent increase in neuronal α-synuclein pathology (Tsunemi et al., 2020). Moreover, astrocytes carrying the *LRRK2-G2019S* mutation exhibit impaired autophagy and macroautophagy, increased α-synuclein accumulation, morphological atrophy, decreased mitochondrial function, increased inflammatory response, as well as neurotoxicity to DAn (de Rus Jacquet et al., 2021, de Rus Jacquet et al., 2023; di Domenico et al., 2019; Ramos-Gonzalez et al., 2021). Lastly, *GBA-D409V* astrocytes display a reduction in lysosomal function and the expression of inflammatory cytokines in unstimulated conditions (Sanyal et al., 2020), whereas GD astrocytes homozygous for *GBA-N370S* display higher levels of α-synuclein accumulation (Aflaki et al., 2020).

Deleterious effects of astrocytes in PD can be due to loss of homeostatic function, a neurotoxic gain-of-function, or both. As detailed in section 1.1.1.1., DAn are particularly vulnerable to age and oxidative stress, and thus, they heavily rely on astrocytic metabolic and antioxidant support. Throughout the course of the disease, astrocytes may switch from a neuroprotective phenotype to prevent or compensate neuronal damage, to a neurotoxic one accompanied with the loss of homeostatic function and neurotoxicity, thus contributing to disease progression (Sanchez et al., 2021). Indeed, it is thought that, initially, astrocytes increase expression of neurotrophic factors, but the expression decreases throughout the course of PD (Rangasamy et al., 2010). In addition, a study in a MPTP model showed that ventral tegmental area (VTA) astrocytes were more neuroprotective to SNpc DAn than SNpc astrocytes (Kostuk et al., 2019), suggesting that SNpc-specific astrocytes might be less capable of protecting DAn in PD than astrocytes from other brain regions.

Lastly, neuroinflammatory or reactive astrocytes are also thought to play an important role in PD pathogenesis, and the data available supporting this hypothesis will be presented in section 1.3.5.2.

Based on all these observations, astrocytes have been proposed to be therapeutic targets in PD, with therapeutic strategies aimed at either promoting the neurosupportive or neuroprotective activity of astrocytes, particularly their antioxidative and neurotrophic functions, or inhibiting their neurotoxic functions (Miyazaki & Asanuma, 2020; Sanchez et al., 2021).

1.2.3.1. α-synuclein in astrocytes

Astrocyte express little to no α-synuclein (expression levels vary on the model and report) (Zhang et al., 2016; Aflaki et al., 2020), but in PD patients, α-synuclein inclusions are found in astrocytes (Braak et al., 2007; Wakabayashi et al., 2000). This suggests that astrocytes have the capacity to engulf extracellular α-synuclein or α-synuclein that is transferred from other cells, particularly neurons. Moreover, in mice, astrocyte-specific expression of mutant *A53T* α-synuclein is sufficient to cause neurodegeneration (Gu et al., 2010), further demonstrating the involvement of astrocytes in α-synuclein pathology. Nonetheless, the specific function endogenous α-synuclein has in astrocytes is not known yet.

α-synuclein can be transferred from neurons to astrocytes (Cavaliere et al., 2017; Lee et al., 2010) and between astrocytes (Cavaliere et al., 2017; Loria et al., 2017; Rostami et al., 2017). Furthermore, in a less efficient manner (Loria et al., 2017), excessive astrocytic α-synuclein can also be transferred to neurons, which leads to neuronal death (Cavaliere et al., 2017). α-synuclein uptake and transport between different cell types can occur through various mechanisms. α-synuclein can be taken up by endocytosis (Filippini et al., 2021; Lee et al., 2010; Lindström et al., 2017), macropinocytosis (Bayati et al., 2022), transferred by direct contact (Cavaliere et al., 2017), tunnelling nanotubes (Rostami et al., 2017, Rostami et al., 2020), and exosomes (Meng et al., 2020).

Moreover, excessive α-synuclein uptake by astrocytes can surpass the lysosomal degradation capacity of the cell, resulting in the formation of α-synuclein inclusions and subsequent mitochondrial dysfunction and ER swelling (Braidy et al., 2013; Lindström et al., 2017; Rostami

et al., 2017). Additionally, astrocytes exposed to monomeric, oligomeric or fibrillar α-synuclein were shown to be toxic to hippocampal neurons (Chavarría et al., 2018). Lastly, some studies have shown that exposure to high levels of α-synuclein induces neuroinflammation in astrocytes (Lee et al., 2010) (discussed in more detail in section 1.3.2.2).

A widespread hypothesis is that, in the initial stages of PD, astrocytic uptake of α-synuclein and subsequent degradation is a neuroprotective mechanism to decrease the neuronal α-synuclein burden, since astrocytes uptake and degrade α-synuclein more efficiently than neurons (Loria et al., 2017; Tsunemi et al., 2020). However, α-synuclein overload might surpass the astrocytic capacity to degrade α-synuclein, which might result in lysosomal impairments, α-synuclein accumulation and aggregation, and subsequent cellular disfunction, with or without acquisition of an inflammatory phenotype.

1.2.3. iPSC-derived astrocyte models to study astrocyte involvement in Parkinson's disease

One of the main challenges in the study of neurodegenerative diseases such as PD is that disease-susceptible cells cannot be taken from patients for in vitro study. Consequently, studies in humans are limited to neurohistological examination of post-mortem brain tissue, neuroimaging studies, or analysis of different bodily fluids. However, the information about disease progression that can be obtained with these methods is very limited, and neurohistological studies only show the very end stage of the disease. The inaccessibility to neural cells from live humans has prompted researchers to develop different experimental models of PD, which can be broadly classified into two categories: animal models (rodents, non-human primates, and non-mammalian species) and in vitro cell culture models (Chia et al., 2020). For many years, rodent models of PD and rodent primary cell cultures were the preferred system to study astrocyte involvement in PD, in which the disease was modelled with neurotoxins, α-synuclein overexpression, injection or exposure, and expression of specific mutations associated with monogenic PD. However, the use of rodent models to study PD presents various limitations and are not always translatable to humans, especially considering that age is the most important risk factor in PD, and the numerous years needed to develop PD cannot be replicated in rodents or cell cultures (Dawson et al., 2018).

Moreover, there is a vast body of evidence showing the profound differences between rodent and human astrocytes. For instance, human astrocytes are approximately 20 times larger and morphologically more complex, each human astrocyte interacts with about 10 times more synapses, they present distinct calcium responses and vast transcriptional changes compared to rodent astrocytes (Oberheim et al., 2009; Zhang et al., 2016). There are also species differences in the astrocyte to neuron ratio (Oberheim et al., 2009). All things considered, new in vitro representative human models of PD were urgently needed to study the cellular and inter-cellular mechanisms driving PD pathogenesis.

In 2007, Yamanaka and colleagues developed human induced pluripotent stem cells (iPSCs) from adult human fibroblasts by overexpressing four transcription factors, Oct3/4, c-Myc, Sox2 and Klf4 (Takahashi et al., 2007) (also achieved by another group (Yu et al., 2007)). These iPSCs can then be differentiated into any human cell type. One of the main advantages of this technology is that all cells obtained from iPSCs will maintain the genetic architecture of the donor, and thus, using iPSCs derived from familial PD patients, astrocytes, neurons, or other cell types of interest carrying specific disease-associated mutations can be obtained (Caiazza et al., 2020). In recent years, the body of research using iPSC-derived neural models has increased significantly in the field of PD research.

Protocols to differentiate iPSCs into astrocytes are designed to recapitulate astrogenesis during CNS development. The main challenge, however, is that astrocytes develop much later than neurons, at the end stages of embryogenesis and the first few post-natal weeks (Markey et al., 2023). Consequently, the first protocol to obtain iPSC-derived astrocytes was 6 months long (Chambers et al., 2009). Since then, various protocols have been developed to try and optimize the process and reduce the length. These protocols either involve the formation of neural rosettes/embryoid bodies (Leventoux et al., 2020; Peteri et al., 2021), or are based on a cell monolayer (Giordano et al., 2023; TCW et al., 2017). Additionally, protocols differ in the morphogens and growth factors used, and the number of days each one is applied for, whereas other protocols rely on commercially available astrocyte differentiation medias with unknown composition (TCW et al., 2017). Moreover, even if some protocols use serum, such as foetal bovine serum (FBS) (Santos et al., 2022; Voulgaris et al., 2022), this induces a reactive phenotype in astrocytes (Perriot et al., 2018). Furthermore, although it is widely known that astrocytes present profound regional and sub-regional differences, very few protocols have

been developed to obtain region-specific astrocytes (Clarke et al., 2020; Crompton et al., 2021; Nam et al., 2024; Peteri et al., 2021). Lastly, available protocols vary significantly in their length; while some take over 180 days to generate mature astrocytes (Krencik & Zhang, 2011; Nonaka et al., 2024), protocols based on the inducible expression of growth factors take as little as 7 days (Canals et al., 2018).

In the context of PD, most of the studies conducted using patient iPSC-derived astrocytes have focused on cells carrying the *LRRK2-G2019S* mutation (Booth et al., 2019; de Rus Jacquet et al., 2021, 2023; di Domenico et al., 2019; Ramos-Gonzalez et al., 2021; Streubel-Gallasch et al., 2021). Moreover, most of these studies did not use astrocytes that were patterned towards the midbrain, since they lacked regional specificity. Data on iPSC-derived astrocytes carrying *GBA1* mutations is very scarce, and mostly focuses on GD cells (Aflaki et al., 2020). Recently, Yarkova and colleagues developed a protocol to obtain *GBA-N370S* iPSC-derived astrocytes, but no experiments were conducted with these cells besides a very basic characterization (Yarkova et al., 2023).

1.3. Neuroinflammation in PD

The role neuroinflammation may have in PD onset and progression has only recently gained the interest of the research community. The main biological role of neuroinflammation is to defend the CNS from pathogenic stimuli, but it has also been observed in patients suffering from different neurodegenerative diseases, including PD, AD, Huntington's disease, and amyotrophic lateral sclerosis (ALS) (Farooqui, 2022). Age is the greatest risk factor for developing PD, and it is believed that the aging immune system plays an important role in disease progression. In PD, neuroinflammation is driven by both adaptive and innate/intrinsic immune responses, which are described in more detail below.

1.3.1. Evidence of neuroinflammation in PD patients

The first evidence of the presence of neuroinflammation in individuals with PD came in 1988, when a study in post-mortem PD brain tissue showed that there was an elevated number of reactive microglia in the SNpc (McGeer et al., 1988). Subsequent neurohistological studies

have corroborated these findings by demonstrating that the SNpc of individuals with PD contains a higher number of reactive microglia (Doorn et al., 2014). On the other hand, neurohistological evidence of astrogliosis in PD patients is not as conclusive (Tong et al., 2015), probably because most studies relied on GFAP immunostaining, which does not detect all astrocytes and might result in an underestimation of the extend of astrogliosis (Messing & Brenner, 2020). Additionally, the presence of reactive microglia and astrocytes in PD brains has been validated using advanced neuroimaging studies, particularly positron emission tomography (PET) imaging studies. Furthermore, inflammatory markers, including inflammatory cytokines and immune cell surface markers, have been detected in the blood and CSF of PD patients. In most studies, an increase of these markers has been reported, providing further evidence for the elevated inflammatory state in PD (Lai et al., 2022). This observation implies that the adaptive immune system and peripheral immune cells are also activated in PD, and it also provides potential biomarkers for detecting prodromal PD and monitoring inflammation and disease progression in patients (Eidson et al., 2017). On another note, GWAS studies of sporadic PD patients have revealed that variants in *HLA* (human leukocyte antigen) genes are associated with increased PD risk (Hamza et al., 2010; Nalls et al., 2019). Lastly, sc-RNAseq studies in post-mortem PD brain tissue have shown enrichment of activated and reactive microglia and astrocytes (Smajić et al., 2022).

1.3.2. Adaptive immune responses in PD

The evidence currently available shows that PD is not a disease contained to the CNS but a multisystem disease, with involvement of the peripheral immune system, the gut, and the enteric nervous system. T cells are the main cells of the adaptive immune system, and under normal circumstances, they are rarely found in the CNS. However, numerous studies in post-mortem PD brains and animal models of PD have shown increased T cell infiltration in the brain, changes in the surface characteristics of circulating T cells, and an overall decrease in the total T cell population (Baird et al., 2019). Both CD4+ and CD8+ T cells have been found in the SNpc of PD patients and have been postulated to have a role in PD, but whether they have an immunosuppressive role or in turn potentiate inflammation and disease progression highly depends on the specific subtype of T cells (Xu et al., 2023). Furthermore, increased BBB permeability in PD might result in increased infiltration of peripheral cells such as T cells (Khor

et al., 2024). However, it must be mentioned that not all studies have found BBB dysfunction in individuals with PD (Fujita et al., 2021).

Activated microglia and astrocytes release pro-inflammatory cytokines (e.g. TNFα, IL-1β and IL-6) and chemokines (e.g. CXCL9, CXCL10) that promote the differentiation of T cells into cytotoxic cells, their recruitment, and their activation, leading to T cell-mediated release of pro-inflammatory cytokines (Jurcau et al., 2023). Furthermore, microglia and astrocytes can also recruit and activate CD4+ T cells by presenting numerous peptides, such as α-synuclein peptides, in MHC class II proteins (Gu et al., 2024). Additionally, studies in rodents and primary cultures have shown that exposure to excess α-synuclein or expression of mutant *A53T-SNCA* promotes the activation, infiltration and recruitment of T cells (Choe et al., 2024; Karikari et al., 2022), and these infiltrating activated T cells have been linked to neuronal death (Gate et al., 2021). The ability of T cells to recognize α-synuclein has also been demonstrated in patients (Sulzer et al., 2017), and α-synuclein-specific T cells are abundant prior to the clinical diagnosis of PD motor symptoms (Lindestam Arlehamn et al., 2020). Similarly, a study in humans found that CD8+ T cell infiltration was increased in the early stages of PD when α-synuclein aggregation was still absent and there was no DAn death (Galiano-Landeira et al., 2020). This data suggests that neuroinflammation precedes neuronal death and the appearance of clinical PD symptoms. α-synuclein-specific T cells may have important implications for therapy, as studies have revealed that they can have immunosuppressive effects and are neuroprotective in MPTP mouse models of PD (Park et al., 2023). However, CD4+ T cells have also been shown to increase IL-10 and IFNγ production in a mouse model of α-synuclein overexpression (Williams et al., 2021).

1.3.3. Innate immune responses in PD

1.3.3.1. Microglial contribution to neuroinflammation

Microglia are the resident macrophages of the CNS, and contrary to neurons and other glial cells, they are derived from primitive macrophages in the embryonic yolk sac, and then penetrate the CNS during embryogenesis (Thion et al., 2018). Under normal physiological conditions, homeostatic microglia carry out their normal functions such as synaptic pruning, and scan the environment for potential pathological signals. When a pathological trigger is detected, microglia transit to an activated or reactive state and migrate to the site of injury

(Ho, 2019). Multiple different microglial activation states exist, which depend on the specific brain region, the inflammatory trigger and the pathological state (Hanisch & Kettenmann, 2007). As mentioned above, there is a large body of evidence for the presence of reactive microglia in PD patients (Doorn et al., 2014; Gerhard et al., 2006), as well as in toxin-based rodent models of PD (Smeyne et al., 2016). In addition, microglia are one of the main sources of the elevated levels of pro-inflammatory cytokines found in the blood and CSF of PD patients (Tansey et al., 2022).

Extracellular α-synuclein is recognized by microglia and triggers their activation (Su et al., 2008), which can occur through different mechanisms. Like other immune cells, microglia express pattern recognition receptors (PRRs) that recognize pathogen- and danger associated molecular patterns (PAMPs and DAMPs). An important type of microglial PRRs in PD are toll-like receptors (TLRs), since they recognize α-synuclein, and especial attention has been given to TLR2 and TLR4 (Yang et al., 2020). Various models have shown that activation of TLR2 by α-synuclein in microglia leads to activation of multiple signalling pathways, and release of pro-inflammatory cytokines such as TNFα (Daniele et al., 2015; Kim et al., 2013). Similarly, α-synuclein binding to TLR4 activates microglia and promotes the release of inflammatory cytokines and ROS (Hughes et al., 2019), although some findings claim that α-synuclein binding to TLR4 promotes its clearance and the survival of DAn (Stefanova et al., 2011). Moreover, α-synuclein activates the NOD-like receptor pyrin domain-containing protein 3 (NLRP3) inflammasome in microglia, which results in release of pro-inflammatory cytokines like IL-1β and IL-18 (Pike et al., 2021). Microglia also participate in the clearance of extracellular α-synuclein via phagocytosis (Stefanova et al., 2011), but some reports indicate that α-synuclein might impair the phagocytic activity of microglia and thus impede the degradation of α-synuclein aggregates (Choi et al., 2015; Haenseler et al., 2017). Lastly, microglia act as antigen presenting cells (APCs) by processing antigenic peptides in endosomes that are then presented in MHC class II proteins to recruit CD4+ T cells (Gu et al., 2024). α-synuclein promotes the expression of MHC class II proteins in microglia, which then present processes α-synuclein to CD4+ T cells, causing their recruitment, activation and subsequent aggravation of the inflammatory response (Harms et al., 2013).

1.3.3.2. Astrocytic contribution to neuroinflammation

Microglia are the first line of defence in the CNS, as they usually are the first responders to pathogenic triggers and inflammatory stimuli. Inflammatory cytokines released by activated microglia then act on astrocytes to induce astrogliosis, which act as amplifiers of inflammation (Yang et al., 2020). However, evidence shows that astrocytes can also directly respond to pathological triggers by acquiring a reactive phenotype. Indeed, research has revealed that astrocytes undergo vast transcriptional, morphological and functional changes in response to acute insults, such as stroke, infections and spinal cord injury, and chronic neurodegenerative diseases like AD, PD, and ALS (Lawrence et al., 2023). This response and the specific reactive phenotype astrocytes acquire highly depends on various factors, such as the pathological trigger, the disease stage, the brain region, and age (Escartin et al., 2021). In 2012, Zamanian and colleagues showed that ischemic stroke induced the acquisition of a neuroprotective reactive phenotype in astrocytes, termed A2, whereas exposure to lipopolysaccharides (LPS) induced the transition into a neurotoxic reactive phenotype, termed A1 (Zamanian et al., 2012). Later, these A1 astrocytes were shown to be activated by microglia via the release of 3 inflammatory cytokines, TNFα, IL-1α and complement component 1q (C1q), and they were detected in the SNpc of PD patients by complement component 3 (C3) staining (Liddelow et al., 2017). A1 astrocytes are also thought to arise due to normal aging (Clarke et al., 2018). Nevertheless, in recent years, this binary classification of reactive astrocytes has been discarded in favour of the hypothesis that astrocytes exist in a continuous and very dynamic reactive state (Barbar et al., 2020; Spreng et al., 2022).

In addition, various studies have shown that astrocytes recognize and bind α-synuclein, which in turn induces astrogliosis and disrupts normal astrocytic function (Chavarría et al., 2018; Gu et al., 2010; Lee et al., 2010; Rannikko et al., 2015). The α-synuclein-induced astrogliosis was shown to be dependent on TLR4 and independent of TLR2 (Rannikko et al., 2015). On the contrary, other studies have not observed any prominent inflammatory response in astrocytes after exposure to α-synuclein (Russ et al., 2021; Sanyal et al., 2020), instead, astrocytes acquired an antigen presenting phenotype when treated with α-synuclein fibrils (Russ et al., 2021). Indeed, similar to microglia, astrocytes act like APCs and express MHC class II proteins to present processed antigenic peptides and promote the differentiation and recruitment of T cells (Gu et al., 2024). In post-mortem PD brains, MHC class II proteins were found to be

highly co-localized with GFAP staining and were surrounded by CD4+ T cells (Rostami et al., 2020). On another note, astrocytes carrying PD-related mutations, such as *LRRK2-G2019S*, have been shown to release more pro-inflammatory cytokines upon inflammatory stimuli (Sonninen et al., 2020). Lastly, during CNS inflammation reactive astrocytes produce vascular endothelial growth factor A (VEGF-A), which promotes BBB permeability (Argaw et al., 2012), and thus, extravasation of adaptive immune cells.

1.3.4. What came first: neuroinflammation or neurodegeneration?

After demonstrating that neuroinflammation is a key hallmark of PD, the main question that was posed in the field, and is yet to be answered, was: does neuroinflammation precede neurodegeneration, acting as a driver of neurodegeneration, or in turn, does neurodegeneration drive neuroinflammation? The latter option also poses the question of whether neuroinflammation resulting from neurodegeneration is a neuroprotective or neurotoxic mechanism, and whether this changes throughout the course of the disease.

Some evidence indicates that, in the initial stages of PD, activated microglia are neuroprotective and promote neuronal survival. This is carried out by release of anti-inflammatory cytokines, activation of trans-repression pathways through various nuclear receptors, and by neuron-microglia crosstalk, which conversely reduce the inflammatory response of microglia (Le et al., 2016). However, sustained inflammatory signals and exposure to α-synuclein override these neuroprotective microglial mechanisms and result in acquisition of a pro-inflammatory phenotype (Ho, 2019). Furthermore, in the context of PD and other neurodegenerative diseases, astrocytes are often referred to as a "double-edged sword" (Ding et al., 2021), as they present both neurotrophic/neuroprotective and neurotoxic phenotypes which are highly context dependent. It is not understood yet how these different properties of astrocytes change throughout the progression of PD. As for T cells, it is believed that the balance between the pro-inflammatory Th1 and Th17 cells and anti-inflammatory Th2 and Treg cells changes throughout the course of the disease, with a higher activation of Treg cells in the early phases of the disease, and a higher ratio of pro-inflammatory T cells in later stages of the disease (Xu et al., 2023).

The main challenge when investigating the involvement of neuroinflammation in PD onset and progression is the difficulty of studying this process in individuals with PD. Since neuroinflammation is often present before the clinical diagnosis of the disease, information regarding the inflammatory state of PD patients in the prodromal phase is lacking. Furthermore, more longitudinal studies are needed to monitor the progression of inflammation throughout PD and how this relates to the activation of each population of immune cells, as well as α-synuclein aggregation and DAn degeneration.

1.3.5. Anti-inflammatory therapeutic strategies

Multiple studies have set out to investigate the therapeutic potential of molecules with an immunomodulatory or anti-inflammatory effect to treat PD patients (Jurcau et al., 2023). Various candidates have already been tested, or are currently being tested, in animal models and clinical trials. Unfortunately, the outcome of most trials in human patients have been negative or inconclusive so far (Tansey et al., 2022).

One of the first anti-inflammatory disease-modifying approaches studied was the use of non-steroidal anti-inflammatory drugs (NSAIDS) such as ibuprofen, an inhibitor of cyclooxygenase 1 and 2 (COX-1/2), which has been shown to be neuroprotective in in vitro and in MPTP mouse models (Teismann & Ferger, 2001), although its effectiveness in human patients is still unclear (Rees et al., 2011; Singh et al., 2021). Molecules targeting the NLRP3 inflammasome have also been tested, such as MCC950, which in MPTP mouse models reduces DAn neurodegeneration and improves behavioural dysfunctions (Huang et al., 2021). In addition, inhibitors of the signalling pathways involving NFκB have been widely explored using cell culture and PD animal models (Dolatshahi et al., 2021). Similarly, blocking receptors involved in activation of neuroinflammation is a very promising strategy, including the use of antibodies specific for TNFR1 (Dong et al., 2016) and TLR2 (Kim et al., 2018). Lastly, treatment strategies targeting the gut-brain-axis, with a special focus on re-equilibrating gut dysbiosis, have also been tested. This can be achieved by making changes to the diet, using pre- and probiotics, as well as through stool transplants (Brown & Goldman, 2020).

1.4. Hypotheses and thesis aims

Based on the findings published to date, the starting hypotheses for the work conducted in this thesis were:

- *GBA-N370S* iASTROs will present one or more cellular dysfunctions, the most probable being: morphological atrophy/less mature morphology, changes in ATP-induced ER-calcium release, and decreased GCase activity.
- If *GBA-N370S* iASTROs do have cellular alterations compared to control iASTROs, they will be less neurosupportive to control and *GBA-N370S* iDAn, whereas *GBA-N370S*, but not control, iDAn will cause cellular stress in control and *GBA-N370S* iASTROs.
- Control and *GBA-N370S* iASTROs will undergo astrogliosis in response to inflammatory cytokines and α-synuclein pre-formed fibrils, and the combination of cytokines and α-synuclein will potentiate their inflammatory effect.
- Reactive control and *GBA-N370S* iASTROs will be neurotoxic and/or less neurosupportive to control and *GBA-N370S* iDAn.

To investigate these hypotheses, the aims of this thesis are:

- To generate and characterize mature control and *GBA-N370S* iPSC-derived midbrain astrocytes (iASTROs) (Chapter 3)
- To evaluate if there is any cell autonomous or non-cell autonomous dysfunction in *GBA-N370S* iASTROs (Chapter 3)
- To investigate the inflammatory response of control and *GBA-N370S* iASTROs to inflammatory cytokines and α-synuclein pre-formed fibrils (Chapter 4)
- To explore intracellular mechanisms altered in inflammatory iASTROs (Chapter 5)
- To study the effect of inflammatory iASTROs on control and *GBA-N370S* iPSC-derived dopaminergic neurons, with or without the addition of α-synuclein pre-formed fibrils (Chapter 6)

Chapter 2 - Materials and methods

Table 2.1. Kits used

Name	Company	Catalog #
RNeasy Mini Kit (250)	Qiagen	74106
High-Capacity RNA-to-cDNA™ Kit	Applied Biosystems	4387406
Glutamate Assay Kit	Abcam	ab83389
Fura-2 QBT Calcium Kit (explorer)	Molecular Devices	R8197
Fast SYBR™ Green Master Mix	Life Technologies Ltd	4385618
NucBlue™ Fixed Cell ReadyProbes™ Reagent (DAPI)	Life Technologies Ltd	R37606
NucBlue™ Live ReadyProbes™ Reagent (Hoechst 33342)	Life Technologies Ltd	R37605
Pierce™ Chromogenic Endotoxin Quant Kit	Life Technologies Ltd	A39552
Silicone Sylgard 184 Kit	Dow	63416.5S

Table 2.2. Reagents and drugs used

Drug/Reagent	Company	Catalog #
DL-TBOA	Bio-Techne (R&D Systems)	1223/10
2-APB	Tocris	1224/10
TNFα	Peprotech	AF-300-01A
IFN-γ	BioLegend Inc	570204
C1q	Sigma-Aldrich	C1740
IL1α	Peprotech	200-01A
MeTC7	Cambridge Bioscience Ltd	CAY37338
1α,25-Dihydroxyvitamin D3	Insight Biotechnology Ltd	sc-202877B
H_2DCFDA (H_2-DCF, DCF)	Life Technologies Ltd	D399
ATP	Sigma-Aldrich	A26209
CBE	Sigma-Aldrich	C5424
4-MUG	Sigma-Aldrich	M3633
BODIPY™ 493/503	Life Technologies Ltd	D3922
Thapsigargin	Enzo	BML-PE180
Taurocholic acid sodium salthydrate	Sigma-Aldrich	T4009

2.1. Cell culture

Table 2.3. Cell culture medias, reagents, and growth factors used

Product name	Company	Catalog #
2-Mercaptoethanol	Life Technologies Ltd	21985023
Advanced DMEM/F-12	Life Technologies Ltd	12634028
Ascorbic Acid	Sigma-Aldrich	A4544
B-27™ Supplement without Vitamin A	Life Technologies Ltd	12587010
BDNF	Peprotech	450-02
BMP4	Peprotech	AF-120-05ET
CELLBANKER® 2	AMS Biotechnolology	11914
CHIR-99021	Tocris	4423/10
DAPT	Abcam	ab120633
db-cAMP	Sigma-Aldrich	D0627
EGF	Peprotech	AF-100-15
FGF8α	Cambridge Bioscience Ltd	Z03172
GDNF	Peprotech	450-10
Geltrex	Life Technologies Ltd	A1413302
GlutaMAX™ Supplement	Life Technologies Ltd	35050061
hESC-qualified Matrigel	Corning	354277
Knockout™ DMEM	Life Technologies Ltd	10829018
Knockout™ Serum Replacement	Life Technologies Ltd	10828010
L-Glutamine	Thermo Fisher Scientific	25030024
LDN-193189	Sigma-Aldrich	SML0559
LIF	Peprotech	300-05
MEM non-essential amino acids (NEAA)	Life Technologies Ltd	11140050
Mitomycin C	Abcam	ab120797
mTeSR™1 Complete Medium Kit	STEMCELL Technologies	85850
N2 Supplement	Life Technologies Ltd	17502048
Neurobasal™ Medium	Life Technologies Ltd	21103049
PBS, pH7.4	Life Technologies Ltd	10010023
Penicillin-Streptomycin (Pen-Strep)	Life Technologies Ltd	15140122
Purmorphamine	Tocris	4551/10
RevitaCell™ Supplement	Life Technologies Ltd	A2644501
ROCK inhibitor (Y27632)	APExBIO	A3008-APE
SB-431542	APExBIO	A8249-APE
SHH-C24II	R&D Systems	1845-SH
Solution 18	ChemoMetec A/S	910-3018
StemPro™ Accutase™	Life Technologies Ltd	A1110501
TGFβ3	Peprotech	100-36E

All cells were maintained at 37°C and 5.0% CO_2. All cell culture medias used were prepared fresh daily, filtered through a 0.22 µm PES membrane filter, and warmed up in a 37°C bead bath, unless stated otherwise.

2.1.1. Human induced pluripotent stem cell lines

The iPSC lines used were obtained from the Oxford Parkinson's Disease Centre (OPDC)-StemBANCC consortium cell repository. iPSCs were derived from human skin biopsy fibroblasts from patients that had provided informed consent (Ethics committee: National Health Service, Health Research Authority, NRES Committee South Central, Berkshire, UK, REC 10/H0505/71). The control iPSC lines used in this project were obtained from healthy individuals without a history of PD or dementia, and the *GBA-N370S* iPSC lines used were obtained from PD patients harbouring the *GBA-N370S* mutation. Details of the donors can be found in Table 2.4.

Table 2.4. Details of the iPSC lines used

Genotype	Patient ID	Clone	Abbreviation	Reprogramming Method	Age	Sex
Healthy Controls	SFC065-03	03	65	Cytotune 2 (SeV)	65	Male
	SFC67-03	01	67	Cytotune 2 (SeV)	72	Male
	SFC156-03	01	156	Cytotune 2 (SeV)	75	Male
	SFC840-03	03	840	Cytotune 2 (SeV)	67	Female
	SFC856-03	04	856	Cytotune 2 (SeV)	78	Female
GBA-N370S	MK071	03	71	RV	81	Female
	MK082	26	82	RV	51	Male
	MK088	01	88	RV	46	Male
	SFC848-03	02	848	Cytotune 1	68	Male
	SFC871-03	09	871	Cytotune 2 (SeV)	70	Female

2.1.2. Human induced pluripotent stem cell thawing, maintenance and passaging

2.1.2.1. Thawing iPSCs

iPSC cryovials were stored in liquid nitrogen storage tanks at -196°C and transported in dry ice. Prior to thawing the cells, the required number of wells of 6-well plates were coated with 1 mL hESC-qualified Matrigel™ for at least 1h at 37°C. Cryovials were thawed in the bead bath at 37°C until only a small piece of frozen media was left. The cells were gently transferred to a 15 mL Falcon tube with 10 mL Knockout DMEM at RT, and centrifuged at 400 RCF for 5 min. Afterwards, the supernatant was removed, and the cells were resuspended in mTeSR™ medium supplemented with 1% penicillin-streptomycin (Pen-Strep) and 10 µM ROCK inhibitor

(Y-27632) and plated in the pre-coated 6-well plates. After 24h, the media was replaced with fresh mTeSR™ medium supplemented with 1% Pen-Strep. A full media change of 2 mL was done daily, until 90-100% confluency was reached, at which point cells were passaged.

2.1.2.2. Single cell passaging of iPSCs

When iPSCs reached a confluency of 90-100%, they were passaged using single cell passaging in a 1:2, 1:3 or 1:4 ratio depending on the requirements and growth rate of each line. Before passaging, the required number of wells of 6-well plates were coated with 1 mL hESC-qualified Matrigel™ for at least 1h at 37°C. In the cells to be passaged, the media was removed, 0.5 mL of Accutase at RT was added to each well and cells were incubated at 37°C for 3-5 min until they started detaching. Immediately after, cells were gently dissociated to obtain a single cell suspension, transferred to a 15 mL Falcon tube with warm 10 mL Knockout™ DMEM and centrifuged at 400 RCF for 5 min. At the end of the centrifugation, the supernatant was removed, and cells were resuspended in mTeSR™ medium supplemented with 1% penicillin-streptomycin (Pen-Strep) and 10 µM ROCK inhibitor (Y-27632) and plated in the pre-coated 6-well plates in the appropriate ratio. After 24h, the media was replaced with fresh mTeSR™ medium supplemented with 1% Pen-Strep. A full media change of 2 mL was done daily, until 90-100% confluency was reached, at which point cells were passaged again. This process was repeated until the necessary number of wells was obtained for each line in order to start the differentiation protocols into dopaminergic neurons or astrocytes.

2.1.3. Human midbrain astrocyte differentiation and cryopreservation

iPSCs were differentiated into ventral midbrain astrocytes (iASTROs) following a previously described protocol (Crompton et al., 2021), with minor modifications, illustrated in Figure 2.1. The basal media compositions are described in Table 2.5., and the detailed media constituents for each stage of the protocol are described in Table 2.6.

iPSCs were grown in 6-well plates as described in section 2.1.2. When a confluency of 80-90% was obtained in all the lines, mTeSR™ media was replaced with Day 0-10 media, 4 mL per well. The next day, the media was fully replaced with 4 mL of Day 0-10 media, and the following day a half media change was done by removing 2 mL of media from each well and adding 2

mL of fresh media. A full or half media change was done on alternate days, until day 3-4, when the vmNPCs reached a confluency where they started growing on top of each other. At this point, cells were single cell passaged in a 1:2 ratio, in a process similar to that described in section 2.1.2.2.

Table 2.5. Composition of basal medias used for iASTRO differentiation

Media Name	Composition	Concentration
NNB	Neurobasal™ Medium	96.5% (v/v)
	N2 Supplement	0.5% (v/v)
	B-27™ Supplement without Vitamin A	1% (v/v)
	L-Glutamine	1% (v/v)
	Penicillin-Streptomycin (Pen-Strep)	1% (v/v)
ASTRO media	Advanced DMEM/F-12	95.6% (v/v)
	MEM non-essential amino acids (NEAA)	1% (v/v)
	GlutaMAX™ Supplement	1% (v/v)
	N2 Supplement	1% (v/v)
	B-27™ Supplement without Vitamin A	0.4% (v/v)
	Penicillin-Streptomycin (Pen-Strep)	1% (v/v)

Table 2.6. Specific composition of the medias used for iASTRO differentiation

Media Name	Media Composition	Concentration
Day 0-10	NNB	100% (v/v)
	LDN-193189	100 nM
	SB-431542	10 μM
	SHH-C24II	200 ng/mL
	CHIR-99021	800 nM
Day 11-29	NNB	100% (v/v)
	GDNF	20 ng/mL
	BDNF	20 ng/mL
	Ascorbic Acid	200 μM
APC	ASTRO Media	100% (v/v)
	EGF	20 ng/mL
	hLIF	20 ng/mL
MAT	ASTRO Media	100% (v/v)
	BMP4	20 ng/mL
	hLIF	20 ng/mL

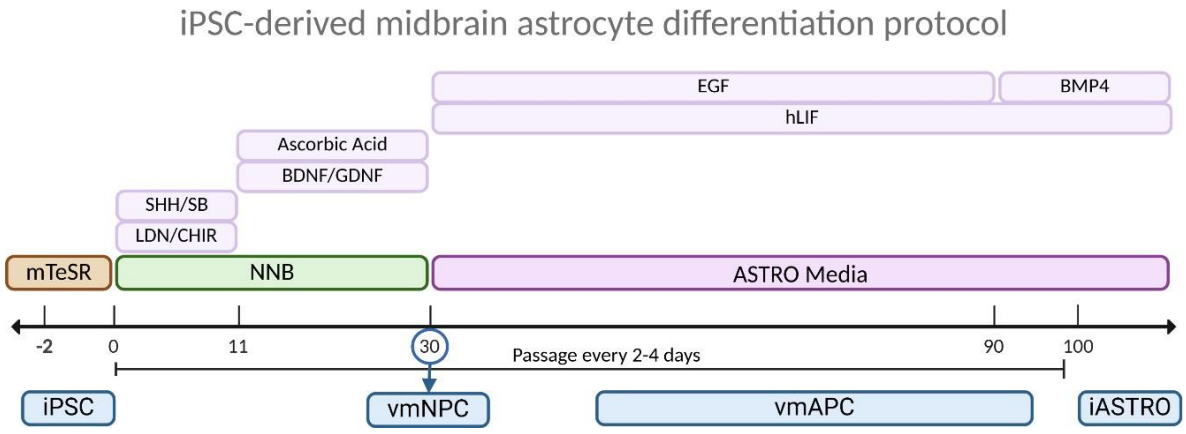


Figure 2.1. Schematic diagram of the human iPSC-derived midbrain astrocyte differentiation protocol
The NNB and ASTRO media compositions are detailed in Table 2.5, and the specific concentration of each molecule and growth factor is outlined in Table 2.6. iPSC = induced pluripotent stem cell. vmNPC = ventral midbrain neural progenitor cell. vmAPC = ventral midbrain astrocyte progenitor cell. iASTRO = mature iPSC-derived ventral midbrain astrocyte. Protocol modified from Crompton et al., 2021. Created with BioRender.

Briefly, prior to passaging, the required number of wells of 6-well plates were coated with 1 mL Geltrex for at least 1 h at 37°C. Media was removed from the vmNPCs, followed by a wash with sterile, pre-warmed PBS (pH 7.4). Next, 0.5 mL of Accutase at RT was added to each well and cells were incubated at 37°C for 5 min or longer, until vmNPCs started dissociating. At that point, cells were gently triturated to obtain a single cell suspension, transferred to a 15 mL Falcon tube with warm 10 mL Neurobasal™ medium and centrifuged at 400 RCF for 5 min. After the centrifugation, the supernatant was removed, and vmNPCs were resuspended in Day 0-10 media supplemented with 1x Revitacell™ Supplement and plated in the pre-coated 6-well plates at a final volume of 4 mL per well. After 24h, the media was fully replaced with fresh Day 0-10 media without Revitacell™ Supplement, and a half media change was done the day after. This feeding schedule was followed until cells needed to be passaged again. On Day 11, the media was fully replaced with 4 mL of Day 11-30 media, and on day 12 a half media change was done. vmNPCs were passaged as required when they reached full confluency. This feeding and cell passaging regime was followed until day 30. After day 20, vmNPCs were passaged at a higher ratio, 1:3 or 1:4 depending on the proliferation patterns of each line. At this stage, only 2 wells of a 6-well plate were kept for each line, discarding the spare cells that are not needed, as cell banking happens in later stages.

On day 30 of the protocol, differentiation and expansion into vmAPCs was started. The media was fully replaced with 2mL/well of APC media. A full media change was done the next day, and afterwards a full media change was done every 2-3 days. When vmAPCs reached a 90-100% confluency, they were single cell passaged as described above, with the exception that cells were resuspended and plated in APC media supplemented with 10 µM ROCK inhibitor (Y-27632). The passaging ratio depended on the growing speed of each line, and a ratio of 1:2-1:8 could be used, and only the required number of wells was kept after each passage. 24h after passaging, the media was replaced with fresh APC media without ROCK inhibitor. vmAPCs were fed every 2-4 days, and passaged as required, until day 90 of the protocol.

After day 50, vmAPCs could be frozen down for future use. For cryopreservation of vmAPCs, cells were incubated with Accutase, disassociated and pelleted as described above. Cell pellets were carefully resuspended in CELLBANKER® 2 cryopreservation solution and transferred into 2 mL cryovials. 1 mL of cryopreservation solution was used per fully confluent well of vmAPCs and transferred into a single cryovial. Cryovials were placed into a CoolCell Freezing container, stored at -80°C for at least 24h, and then transferred to a liquid nitrogen tank and stored for future use. Cryopreserved vmAPCs were thawed when required in a process similar to that described in section 2.1.2.1. Briefly, cryovials were thawed in the bead bath at 37°C until only a small piece of frozen media was left. vmAPCs were immediately transferred to a 15 mL Falcon tube with 10 mL Neurobasal™ medium at RT, and centrifuged at 400 RCF for 5 min. Next, the supernatant was removed, and the cells were resuspended in APC media supplemented with 10 µM ROCK inhibitor (Y-27632) and plated in pre-coated 6-well plates. The next day, the media was replaced with fresh APC media without ROCK inhibitor, and the normal expansion and differentiation protocol was followed from then onwards.

After day 90, mature iASTROs can be generated from vmAPCs. To achieve this, the media in vmAPCs was fully replaced with MAT media. A full media change was done every 3 days, and cells were passaged if required. However, at this stage, many lines proliferated very slowly, and did not require any passaging. After 7 days in MAT media, iASTROs were considered fully mature and could be plated in their final assay plate layout or used for co-cultures with DAn (section 2.1.5). To obtain the required number of iASTROs for subsequent experiments, from day 70-75 onwards, all vmAPCs and iASTROs were kept after every passage. If cells continued to rapidly proliferate after day 90, they were discarded and not used for experiments.

The day before iASTRO replating, the required format and number of plates for iASTRO mono-cultures were pre-coated with Geltrex and incubated at 37°C. The volume of Geltrex used was: 25 µL/well in half-area 96 well-plates, 250 µL/well in 24 well-plates, and 1 mL/well in 6 well-plates. On replating day, Geltrex was removed from all the plates and replaced with equal volumes of MAT media supplemented with 10 µM of ROCK inhibitor (Y-27632). iASTROs were then incubated with 0.5 mL of Accutase at RT until cells started dissociating. Immediately after, the cells were gently triturated to obtain a single cell suspension, and transferred to a 50 mL Falcon tube with warm 30 mL Neurobasal™ medium. 18 wells of 6-well plates of a single line were combined in 1 Falcon. Cells were centrifuged at 400 RCF for 5 min, the supernatant was removed, and iASTROs were resuspended in 1 mL of MAT media supplemented with 10 µM ROCK inhibitor (Y-27632). Multiple Falcons were used for each line, and these were all combined after resuspension. A 20 µL aliquot of the cell suspension was diluted in 180 µL of sterile PBS (pH 7.4). 20 µL of the diluted suspension were then mixed with 1 µL of Solution 18 and counted on a Chemometec NucleoCounter NC250 using NC-Slide A8^{TM} chamber slides. The iASTRO suspension was further diluted as required in MAT media supplemented with 10 µM ROCK inhibitor (Y-27632), and cells were plated into the final plate layout. The cell densities for mono-culture experiments used were as follows: $6x10^3$ cells/well in half-area 96-well plates, $1.5x10^5$ cells/well in 24-well plates, and $5x10^5$ in 6-well plates. The final media volumes were as follows: 50 µL/well in half-area 96-well plates, 500 µL/well in 24-well plates, and 2 mL/well in 6-well plates. The day after, the media was fully replaced with MAT media without ROCK inhibitor, and 48h later cells were ready for harvesting, treatments, or assays, as required.

The same day in which iASTROs were replated into the final assay layout for mono-culture experiments, iASTROs were also used to establish DAn-iASTRO co-cultures, and this process is detailed in section 2.1.5.

2.1.4. Human dopaminergic neuron differentiation and cryopreservation of mFPPs

iPSCs were differentiated into DAns following a previously described protocol (Fedele et al., 2017), with minor modifications, illustrated in Figure 2.3. The basal media compositions are

described in Table 2.7., and the detailed media constituents for each stage of the protocol are described in Table 2.8.

Table 2.7. Composition of basal medias used for DAn differentiation

Media Name	Composition	Concentration
KO DMEM KSR	Knockout™ DMEM	82% (v/v)
	Knockout™ Serum Replacement	15% (v/v)
	L-Glutamine	1% (v/v)
	MEM non-essential amino acids (NEAA)	1% (v/v)
	2-Mercaptoethanol	0.02% (v/v)
	Penicillin-Streptomycin (Pen-Strep)	1% (v/v)
NNB	Neurobasal™ Medium	96.5% (v/v)
	N2 Supplement	0.5% (v/v)
	B-27™ Supplement without Vitamin A	1% (v/v)
	L-Glutamine	1% (v/v)
	Penicillin-Streptomycin (Pen-Strep)	1% (v/v)
NB	Neurobasal™ Medium	96% (v/v)
	B-27™ Supplement without Vitamin A	2% (v/v)
	L-Glutamine	1% (v/v)
	Penicillin-Streptomycin (Pen-Strep)	1% (v/v)

Table 2.8. Specific composition of the medias used for DAn differentiation

Media Name	Days in Protocol	Media Composition	Concentration
Day 0	0	KO DMEM KSR	100% (v/v)
		LDN-193189	100 nM
		SB-431542	10 μM
Day 1-2	1-2	KO DMEM KSR	100% (v/v)
		LDN-193189	100 nM
		SB-431542	10 μM
		SHH-C24II	100 ng/mL
		Purmorphamine	2 μM
		FGF8α	100 ng/mL
Day 3-4	3-4	KO DMEM KSR	100% (v/v)
		LDN-193189	100 nM
		SB-431542	10 μM
		SHH-C24II	100 ng/mL
		Purmorphamine	2 μM
		FGF8α	100 ng/mL
		CHIR-99021	3 μM
Day 5-6	5-6	KO DMEM KSR	75% (v/v)

		NNB	25% (v/v)
		LDN-193189	100 nM
		SHH-C24II	100 ng/mL
		Purmorphamine	2 μM
		FGF8α	100 ng/mL
		CHIR-99021	3 μM
Day 7-8	7-8	KO DMEM KSR	50% (v/v)
		NNB	50% (v/v)
		LDN-193189	100 nM
		CHIR-99021	3 μM
Day 9-10	9-10	KO DMEM KSR	25% (v/v)
		NNB	75% (v/v)
		LDN-193189	100 nM
		CHIR-99021	3 μM
Expansion (Exp)	10+1 - 10+22	KO DMEM KSR	25% (v/v)
		NNB	75% (v/v)
		LDN-193189	100 nM
		CHIR-99021	3 μM
Day 11-12	11-12	NB	100% (v/v)
		GDNF	20 ng/mL
		BDNF	20 ng/mL
		Ascorbic Acid	200 μM
		DAPT	10 μM
		TGFβ3	1 ng/mL
		db-cAMP	500 μM
		CHIR-99021	3 μM
DAn maturation	13+	NB	100% (v/v)
		GDNF	20 ng/mL
		BDNF	20 ng/mL
		Ascorbic Acid	200 μM
		DAPT	10 μM
		TGFβ3	1 ng/mL
		db-cAMP	500 μM

Briefly, iPSCs were grown in 6-well plates as described in section 2.1.2., until a confluency of 90-100% was obtained in all the lines. At this point, Day 0, mTeSR™ media was replaced with 4 mL per well of Day 0 media. On day 1, a full media change was done with 4 mL of Day 1-2 media, and on Day 2 a half media change was done by removing 2 mL of media from each well

and adding 2 mL of fresh media. This feeding schedule, alternating full and half media changes of the medias specified in Table 2.8., was followed until Day 10+1, at which point the expansion of midbrain floor plate progenitors (mFPPs) was started.

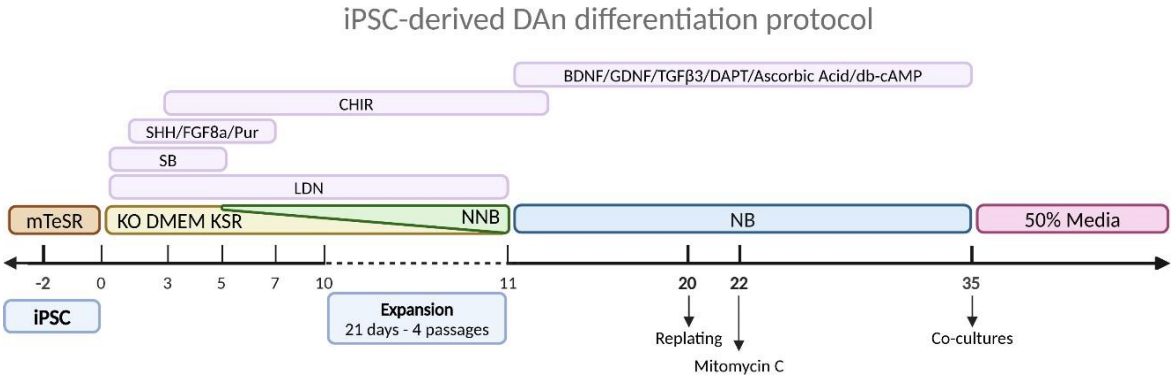


Figure 2.2. Schematic diagram of the iPSC-derived dopaminergic neuron differentiation protocol
Protocol modified from Fedele et al., 2017. Created with BioRender.

On Day 10+1, cells were single passaged in a 1:2 ratio using Accutase, in a process similar to that described in 2.1.2.2. Before passaging, the required number of wells of 6-well plates were coated with 1 mL Geltrex for at least 1h at 37°C. In the cells to be passaged, the media was removed, and mFPPs were washed with sterile, pre-warmed PBS (pH 7.4). Then, 0.5 mL of Accutase at RT was added to each well and cells were incubated at 37°C for 5 min until they started dissociating. Immediately after, mFPPs were gently triturated to obtain a single cell suspension, transferred to a 15 mL Falcon tube with warm 10 mL Neurobasal™ medium and centrifuged at 400 RCF for 5 min. At the end of the centrifugation, the supernatant was removed, and cells were resuspended in expansion media supplemented with 10 µM ROCK inhibitor (Y-27632) and plated in the pre-coated 6-well plates at a final volume of 4 mL per well. The next day, the media was fully replaced with fresh expansion media.

mFPPs were single cell passaged on days 10+1, 10+8 and 10+15, with a full media change the day after passaging, and then following the schedule of full and half feeds on alternate days. On day 10+21, the required number of wells per line were single passaged as described above, and the rest were frozen down for future use. mFPPs to be frozen were incubated with Accutase, disassociated and spun down as described above. After aspirating the supernatant, cells were resuspended in CELLBANKER® 2 cryopreservation solution, transferred into 2 mL cryovials, placed into a CoolCell Freezing container, and stored at -80°C. After at least 24h,

cells were transported to a liquid nitrogen tank and stored until future use. For the cryopreservation, 4-6 wells of each line were combined, resuspended in 3-5 mL of CELLBANKER® 2 cryopreservation solution depending on the cell densities, and distributed evenly in cryovials, adding 1 mL of cell suspension per cryovial.

Frozen mFPPs were thawed when required, in a process similar to that described in section 2.1.2.1. Briefly, cryovials were thawed in the bead bath at 37°C until only a small piece of frozen media was left. mFPPs were immediately transferred to a 15 mL Falcon tube with 10 mL Neurobasal™ medium at RT, and centrifuged at 400 RCF for 5 min. Next, the supernatant was removed, and the cells were resuspended in expansion media supplemented with 10 µM ROCK inhibitor (Y-27632) and plated in the pre-coated 6-well plates at a final volume of 4 mL per well. After 24h, the media was fully replaced with fresh expansion media, and a half media change was done the following day. After this, the DAn differentiation protocol was followed from day 11 onwards (explained next).

On day 10+22, the last day of expansion, a full media change was done with expansion media, and afterwards the DAn differentiation protocol was continued from day 11 onwards, with a full or half media change on alternate days. On day 20, cells were plated for terminal differentiation into their final assay layout. The day before, the required format and number of plates were pre-coated with Geltrex and incubated at 37°C. The volume of Geltrex used was: 25 µL/well in half-area 96-well plates, 250 µL/well in 24-well plates, and 1 mL/well in 6-well plates.

On day 20, Geltrex was removed from all the plates and replaced with equal volumes of DAn maturation media supplemented with 10 µM ROCK inhibitor (Y-27632). Then, the maturing DAns were washed with sterile, pre-warmed PBS (pH 7.4), and incubated with 0.5 mL of Accutase at 37°C for 5 min until cells started dissociating. Immediately after, the cells were gently triturated to obtain a single cell suspension, transferred to a 15 mL Falcon tube with warm 10 mL Neurobasal™ medium and centrifuged at 400 RCF for 5 min. At the end of the centrifugation, the supernatant was removed, and cells were resuspended in 1 mL of DAn maturation media supplemented with 10 µM ROCK inhibitor (Y-27632). A 20 µL aliquot of the cell suspension was diluted in 480 µL of sterile PBS (pH 7.4). 20 µL of the diluted suspension were then mixed with 1 µL of Solution 18 and counted on a Chemometec NucleoCounter NC250 using NC-Slide A8™ chamber slides. The cell suspension was further diluted as required

in DAn maturation media supplemented with 10 µM ROCK inhibitor (Y-27632), and cells were plated into the final plate layout. The cell densities used were as follows: $4x10^4$ cells/well in half-area 96-well plates, $3.5x10^5$ cells/well in 24-well plates, and $2.5x10^6$ in 6-well plates. The final media volumes were as follows: 50 µL/well in half-area 96-well plates, 500 µL/well in 24-well plates, and 2 mL/well in 6-well plates. After seeding, cells were incubated for 48h at 37°C and 5.0% CO_2

On day 22, the media was removed, and cells were incubated for 1h at 37°C with NB media (Table 2.7.) supplemented with 1 µg/mL Mitomycin C to induce apoptosis in proliferating cells. After, media was removed, replaced with NB media to wash any remaining Mitomycin C, and this was replaced with fresh DAn maturation media. After day 24, a half media change was done on Mondays, Wednesdays and Fridays, until the cells were used for assays or to set-up co-cultures with iASTROs.

2.1.5. Human iPSC-derived midbrain astrocyte and dopaminergic neuron co-culture

Figure 2.3. illustrates the direct co-culture set-up. Mature DIV 97-100 iASTROs were plated on top of DIV 35 DAns cultured in half-area 96-well plates. On the day of co-culture, all media was removed from DAns and 25 µL DAn maturation media were added to each well. Then, iASTROs were lifted, spun down, resuspended in MAT media supplemented with 10 µM ROCK inhibitor (Y-27632) and counted as described in section 2.1.3. iASTROs were diluted to obtain a cell suspension of $3.2x10^5$ cells/mL, and 25 µL of this iASTRO suspension were added to the desired wells containing DAns, so that the final iASTRO concentration was $8x10^3$ cells/well. In the wells where no iASTROs were added, 25 µL of MAT media supplemented with 10 µM ROCK inhibitor (Y-27632) were added to DAns. 48h after replating, a full media change was done, or cells were treated, using a 50% media (50% DAn maturation media + 50% astrocyte MAT media) in both cases.

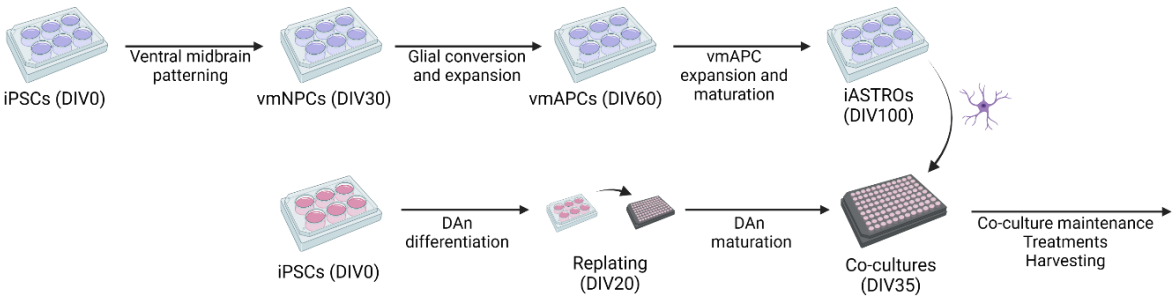


Figure 2.3. Schematic diagram of iASTRO and iDAn differentiation and co-culture set up
Created with BioRender.

2.2. Preparation of α-synuclein pre-formed fibrils (prepared by Dr Nora Bengoa-Vergniory)

Monomeric human α-synuclein was acquired from rpeptide. Endotoxin removal columns were used to remove endotoxin from monomeric α-synuclein, and the Pierce™ Chromogenic Endotoxin Quant Kit was used to ensure complete endotoxin removal. Next, 5 mg/mL α-synuclein monomers were shaken at 37°C and 250 r.p.m. for 7 days to induce aggregation and formation of pre-formed fibrils (PFFs). PFFs were observed in an electron microscope to check correct size and morphology (Figure 2.4.).

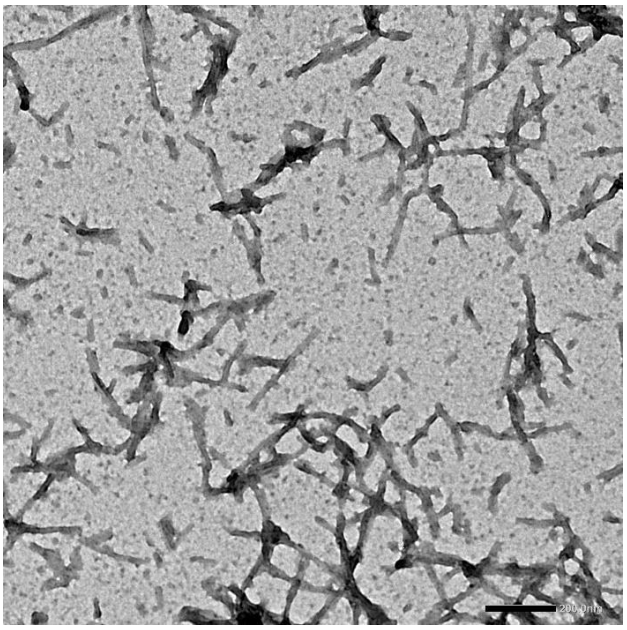


Figure 2.4. Example electron microscope images of PFFs
Scale bar = 250 nm

2.3. Molecular Biology Techniques

2.3.1. RNA extraction and cDNA synthesis

iASTROs and DAns plated on 24-well plates were used for RNA extraction. On the timepoint of interest, the media was removed, the cells were washed with PBS, and 350 µL of RLT buffer (included in the RNeasy Mini Kit) with 10 µL/mL 2-mercaptoethanol were added to each well. The samples were frozen and stored at -80°C until use. On the day of RNA extraction, the samples were thawed and 350 µL of 70% ethanol was added to each well. From this point onwards, the RNA extraction was continued following the instructions and reagents provided in the RNeasy Mini Kit. The resultant RNA samples were quantified, and the purity was assessed using the DeNovix DS-11 Series spectrophotometer/fluorometer. cDNA was synthesized from 200-500 ng RNA depending on the lowest sample yield in each experiment) using the High-Capacity RNA-to-cDNA™ Kit, following the manufacturer's instructions. Thermocycler setting for cDNA synthesis were as follows: 60 min at 37°C, 5 min at 95°C, hold at 4°C. Afterwards, cDNA samples were diluted 1:5-1:7 in DNase/RNase free water.

2.3.2. Real-time quantitative polymerase chain reaction

qRT-PCR was performed using the FAST SYBR Green master mix, following the manufacturer's instructions. Forward and reverse primers for the genes of interest were designed and ordered from Integrated DNA Technologies (IDT), and their efficiency was tested (Livak & Schmittgen, 2001). The primers used in this thesis are listed in Table 2.9. *GAPDH* was used as the housekeeping gene, as it presented the most homogeneous expression across samples and treatment conditions (compared to *ACTB* and *B2M*, data not shown). 96-well plate qPCR plates were read in the StepOnePlus™ System, and 384-well plate qPCR plates were read in the QuantStudio™ 5 System, both from Applied Biosystems. Gene expression changes were calculated using the ΔΔCt method, using *GAPDH* as the housekeeping gene.

2.4. Immunocytochemistry

Cells cultured in half-area 96-well plates were fixed in 4% paraformaldehyde for 5 min (for synaptic marker staining) or 10 min (for every other marker) at RT and washed with PBS (pH

7.4). Fixed cells were permeabilised and blocked in PBS with 0.1% Triton X-100 and 10% normal donkey serum for 1h at RT. Next, cells were incubated overnight at 4°C with the primary antibodies diluted in tris-buffered saline with 0.05% Tween®20 (TBS-T). The primary antibodies used and their dilution are detailed in Table 2.10. The next day, cells were washed 3 times with TBS-T, and incubated with the secondary antibodies (in Table 2.11.) and NucBlue™ Fixed Cell ReadyProbes™ Reagent (DAPI) diluted in TBS-T for 1h at RT. Cells were then washed 3 times with TBS-T and stored at 4°C in PBS with 0.02% sodium azide (pH 7.4) until imaging.

Table 2.9. Primers used for qRT-PCR

Gene	Forward Primer (5'-3')	Reverse Primer (5'-3')
B4GALT5	GAAGATGACGACCTCTGGAACAG	GCCGTTCTTTTGACTTCCTCAGC
BDNF	GGCGGCAGACAAAAAGACTG	CACTGGGAGTTCCAATGCCT
C3	TACAACGTGGAGGCCACATC	ACGGGAGGCACAAAGTCAAA
CCL2	CAGCCACCTTCATTCCCCAA	GACACTTGCTGCTGGTGATTC
CCL5 (RANTES)	CCTGCTGCTTTGCCTACATTGC	ACACACTTGGCGGTTCTTTCGG
CD44	CTGCCGCTTTGCAGGTGTA	CATTGTGGGCAAGGTGCTATT
CYP27B1	TGGCCCAGATCCTAACACATTT	GTCCGGGTCTTGGGTCTAACT
DHCR24	CAGGAGAACCACTTCGTGGAAG	CCACATGCTTAAAGAACCACGGC
ELOVL1	GTCTACAACTTCTCACTGGTGGC	AAGTGCCTCAGGGCTGTTGGAA
FASN	CTTCCGAGATTCCATCCTACGC	TGGCAGTCAGGCTCACAAACG
FGF2	AGCGGCTGTACTGCAAAAACGG	CCTTTGATAGACACAACTCCTCTC
FOXA2	GGGAGCGGTGAAGATGGA	TCATGTTGCTCACGGAGGAGTA
GAPDH	TCATCATCTCTGCCCCCTCT	TCATGGATGACCTTGGCCAG
GBA	GTTGCACAACTTCAGCCTCC	ACCGCTCCATTGGTCTTGAG
GDNF	AGTGACAAAGTAGGGCAGGC	TGGAGCCGGAGTCAGATACA
GFAP	AGAAGCTCCAGGATGAAACC	AGCGACTCAATCTTCCTCTC
HLA-DPB1	GTGCAGACACAACTACGAGCTG	CCTGGGTAGAAATCCGTCACGT
HLA-DRB1	GAGCAAGATGCTGAGTGGAGTC	CTGTTGGCTGAAGTCCAGAGTG
HMGCR	GACGTGAACCTATGCTGGTCAG	GGTATCTGTTTCAGCCACTAAGG
IL6	GGTACATCCTCGACGGCATCT	GTGCCTCTTTGCTGCTTTCAC
ITPR1	GTGACAGGAAACATGCAGACTCG	CAGCAGTTGCACAAAGACAGGC
ITPR2	GGTTGGAGACTATCAGCTCGCT	GCATCATTGGGCTGAACTGGTG
ITPR3	GGGGTAATCATCGACACCTTC	GTTATCAAACTTGTCCCTCTCCA
KI67	GAAAGAGTGGCAACCTGCCTTC	GCACCAAGTTTTACTACATCTGCC
LDLR	CCCAGCGAAGATGCGAAGATAT	GGTGAAGAAGAGGTAGGCGATG
MANF	CAGCCACCAAAATCATCAATGAGG	TCCACTGTGCTCAGGTCGATCT

MAP2	CGAAGCGCCAATGGATTCC	TGAACTATCCTTGCAGACACCT
NFKB1	GCAGCACTACTTCTTGACCACC	TCTGCTCCTGAGCATTGACGTC
ORAI1	GTCACCTACCCGGACTGGAT	TGGAGGCTTTAAGCTTGGCG
PAX6	TCCGTTGGAACTGATGGAGT	GTTGGTATCCGGGGACTTC
RNF145	AATCGGGGCATGACAGAAGG	AGCACGGAAGTGTTTCCACA
S100A10	ATGAAGGACCTGGACCAGTG	GCAGATTCCTTAAGCGACCC
S100B	GGGAGACAAGCACAAGCTGAA	CATTCGCCGTCTCCATCATTG
SLC1A3 (GLAST)	GGTTGCTGCAAGCACTCATCAC	CACGCCATTGTTCTCTTCCAGG
SOX2	TACAGCATGTCCTACTCGCAG	GAGGAAGAGGTAACCACAGGG
STIM1	CACTCTTTGGCACCTTCCACGT	CTGTCACCTCGCTCAGTGCTTG
TGFB1	CGACTCGCCAGAGTGGTTAT	GTGAACCCGTTGATGTCCA
TH	CGAGCTGTGAAGGTGTTTGA	CACGAAGTACTCCAGGTGG
VCAM1	GATTCTGTGCCCACAGTAAGGC	TGGTCACAGAGCCACCTTCTTG
VDR	CGCATCATTGCCATACTGCTGG	CCACCATCATTCACACGAACTGG

Table 2.10. Primary antibodies used for immunocytochemistry

Marker	Host Species	Catalog #	Dilution	Company
GFAP	Chicken	ab4674	1:500	Abcam
S100B	Mouse	SAB4200671	1:250	Sigma-Aldrich
TH	Rabbit	AB152	1:500	Millipore
TH	Sheep	AB1542	1:500	Millipore
MAP2	Chicken	ab92434	1:1000	Abcam
Homer1	Rabbit	160003	1:500	Synaptic Systems
α-synuclein (4D6)	Mouse	ab2434	1:1000	Abcam
NF-κB p65 (D14E12)	Rabbit	8242	1:400	Cell Signaling
Tuj1 (β-tubulin III)	Mouse	801202	1:500	BioLegend
Foxa2	Goat	AF2400	1:250	R&D Systems
Pax6	Rabbit	ab195045	1:500	Abcam
C3d	Rabbit	A006302-2	1:500	Agilent
GLAST	Rabbit	20785-1-AP	1:500	Proteintech
Nestin	Mouse	sc-23927	1:250	Santa Cruz Biotechnology
Ki67	Rabbit	ab15580	1:500	Abcam
VDR	Mouse	sc-13133	1:200	Santa Cruz Biotechnology
Cleaved Caspase-3 (Asp175)	Rabbit	9661S	1:500	Cell Signaling
α-synuclein (phosphoserine 129) [EP1536Y]	Rabbit	ab51253	1:500	Abcam

2.5. BODIPY staining

At the timepoint of interest, treated iASTROs in half-area 96-well plates were incubated with 7.5 µM BODIPY™ 493/503 for 15 min at 37°C. After, cells were washed twice with PBS, and fixed and stained with S100B and DAPI following the protocol described in Section 2.4.

Table 2.11. Secondary antibodies used for immunocytochemistry

Host Species	Target Species	Fluorophore	Catalog #	Dilution	Company
Donkey	Mouse	AlexaFluor 488	A21202	1:1000	Life Technologies
	Mouse	AlexaFluor 555	A31570	1:1000	Life Technologies
	Mouse	AlexaFluor 647	A31571	1:1000	Life Technologies
	Rabbit	AlexaFluor 555	A31572	1:1000	Life Technologies
	Rabbit	AlexaFluor 647	A31573	1:1000	Life Technologies
	Goat	AlexaFluor 488	A21467	1:1000	Life Technologies
	Sheep	AlexaFluor 555	A21436	1:1000	Life Technologies
	Sheep	AlexaFluor 647	A21448	1:1000	Life Technologies
	Chicken	AlexaFluor 488	703-545-155	1:1000	Jackson ImmunoResearch
	Chicken	AlexaFluor 555	A78949	1:1000	Life Technologies

2.6. High-content image acquisition and analysis

Half-area 96-well plates were imaged on a PerkinElmer Opera Phenix high-content screening system. Laser power and exposure time for each channel were adapted according to the marker of interest in each experiment. In iASTRO mono-cultures, the 20x water objective was used in most experiments, except when looking at BODIPY or α-synuclein, in which case the 40x water objective was used. For co-cultures, the 20x water objective was used in most experiments, except when looking at α-synuclein markers (40x water objective) or synaptic markers (63x objective). 10-12 fields of view were imaged per well, and 4-5 Z-stack planes were imaged in iASTRO mono-cultures and 6-8 Z-stack planes in co-cultures.

Images were analysed with the Harmony high-content analysis software, using customised analysis pipelines.

2.7. Glutamate uptake assay

iASTROs grown in half-area 96-well plates were used for this assay. 72h after replating and 48h after a full media change, the media was removed and the cells were incubated in warm HBSS (with $CaCl_2$ and $MgCl_2$) for 30 min at 37°C. Next, cells were incubated in warm HBSS (with $CaCl_2$ and $MgCl_2$) with 100 µM glutamate for 2h at 37°C. After the incubation, the supernatants were collected, frozen and stored at -20°C. As a negative control, iASTROs were treated with 100 µM of the EAAT inhibitor DL-TBOA during the 30 min pre-incubation with HBSS and during the 2h incubation with HBSS and 100 µM glutamate.

To correct for any glutamate iASTROs might release, supernatant from cells incubated for 2h with HBSS (with $CaCl_2$ and $MgCl_2$) without any glutamate was used. HBSS (with $CaCl_2$ and $MgCl_2$) collected from wells without any cells was used as a blank, and HBSS (with $CaCl_2$ and $MgCl_2$) with 100 µM glutamate collected from wells without cells was used to determine the maximum concentration of glutamate initially present in the supernatants.

The concentration of glutamate in the supernatants was determined using the Glutamate Assay Kit (Abcam), following the manufacturer's instructions. The glutamate standards were prepared by serial dilution of the glutamate standard provided in the kit. After correcting for the value of the blanks, the glutamate concentration of each sample was determined from the standard curve obtained, and this value was subtracted from the concentration measured in the wells with glutamate but without cells. From this, the percentage of glutamate taken up by the cells could be measured.

2.8. Fura-2 calcium imaging

2.8.1. ATP-induced calcium release imaging

iASTROs plated on half-area 96-well plates were used for Fura-2 AM calcium imaging, using the Fura-2 QBT Calcium Explorer Kit. Fura-2 AM provided in the kit (Component A) was diluted to a 5 mM solution in HBSS (without $CaCl_2$ and $MgCl_2$) supplemented with 20 mM HEPES buffer (pH 7.4). This Fura-2 AM solution was diluted 1:1 to a 2.5 mM solution in astrocyte MAT media, and warmed up. After removing all the media from iASTROs, 50 µL/well of the 2.5 mM Fura-2 AM solution were added, and cells were incubated for 1.5 h at 37°C. After the incubation, the plates were read using a FlexStation 3 Multi-Mode Microplate Reader (Molecular Devices),

which was programmed to read each column every 4 s for a total of 180 s and to inject 100 µM ATP at 30 s. ATP was prepared in a 3x solution (300 µM) in HBSS (without $CaCl_2$ and $MgCl_2$) supplemented with 20 mM HEPES buffer (pH 7.4). This way, 25 µL of 300 µM ATP solution were added to each well that already had 50 µL of Fura-2 AM solution, thus diluting ATP to a final working concentration of 100 µM.

In the experiments using the calcium channel blocker 2-APB, 25 µM 2-APB were added to the 2.5 mM Fura-2 AM solution, and this was used for the iASTROs previously treated with 2-APB. Equal volumes of DMSO were added to the wells without 2-APB. 2-APB or DMSO were kept throughout the entire experiment and reading of the plate.

For the analysis, the 340/380 nm absorbance ratio measured at each timepoint by the FlexStation was used. The first 8 reads (from 0 s to 28 s, the last timepoint before the injection of ATP) were averaged to obtain the baseline value. This was subtracted to the values of all timepoints, to obtain a normalized response trace for each well. The peak amplitude of the trace, the time of peak amplitude, and the area under the curve (AUC) were calculated using the GraphPad Prism software (v10.0.3), using a baseline of 0 and excluding peaks with less than 10 consecutive timepoints. Non-responding wells and wells with a delayed response (considered when the peak amplitude was 45 s after the injection of ATP) were excluded from the analysis.

2.8.2. Store Operated Calcium Entry (SOCE) imaging

SOCE was studied in iASTROs using Fura-2 AM, in a process similar to that described in section 2.8.1., but with some modifications. This protocol was developed by Dr Maria Claudia Caiazza and adapted to iASTROs by me. iASTROs in half-area 96-well plates were incubated in the 2.5 mM Fura-2 AM dilution (see section 2.8.1.) supplemented with 100 nM Thapsigargin for 1.5 h at 37°C. After, cells were washed 3 times with HBSS (without $CaCl_2$ and $MgCl_2$) supplemented with 20 mM HEPES buffer (pH 7.4), and then 50 µL of HBSS (without $CaCl_2$ and $MgCl_2$) supplemented with 20 mM HEPES buffer (pH 7.4) were added to each well. Plates were read in the FlexStation 3 Multi-Mode Microplate Reader as described in section 2.8.1., however, at 30 s, 25 µL of 7.5 mM $CaCl_2$ were injected into the wells, to obtain a final working

concentration of 2.5 mM $CaCl_2$. The analysis was done as detailed in section 2.8.1., with the same exclusion criteria for non-responding or late-responding wells.

2.9. GCase Assays

2.9.1. MDW-941 immunofluorescent labelling

iASTROs plated in half-area 96-well plates were incubated overnight at 37°C in MAT media with 5 nM MDW-941. The next day, 30 min before imaging, the media was fully replaced with MAT media with 2 drops/mL NucBlue™ Live ReadyProbes™ Reagent (Hoechst 33342). Cells were imaged at 37°C and 5.0% CO_2 in the PerkinElmer Opera Phenix high-content screening system, using the 20x water objective. Images were analysed using the Harmony high-content analysis software, using customised analysis pipelines. As a negative control, 1 mM CBE was added to the control wells 1 h prior to the addition of MDW-941.

2.9.2. 4-MUG GCase activity assay

iASTRO and DAn mono-cultures plated in half-area 96-well plates were washed twice with PBS (pH7.4), snap frozen in dry ice, and stored at -80°C until use. To assay the plates, 35 µL CB^{++} buffer (citrate phosphate buffer (pH 5.4) + 0.25% Triton X-100 + 0.25% (w/v) Taurocholic acid) were added to each well. Plates were freeze/thawed (in dry ice and in an incubator at 37°C) 5 times to lyse the cells. At this point, a few wells per biological replicate were used to quantify the protein concentration using the bicinchoninic acid assay (BCA). Next, 7 µL 6 mM CBE in CB^{++} buffer were added to one well per biological replicate 10 min before the addition of 4-MUG, and 7 µL CB^{++} buffer were added to the rest of the wells. 14 µL of 3.4 mg/mL 4-MUG (diluted in CB^{++} buffer) were added to all the wells, and incubated for 1 h at 37°C. Immediately after, 14 µL 2M glycine-sodium hydroxide buffer (pH 10.4) were added. Fluorescence (excitation = 360 nm, emission = 440 nm) was measured using a PHERAstar® FSX Microplate reader (BMG Labtech). Raw data was normalized to protein concentration.

2.10. DCFDA/ H_2DCFDA cellular reactive oxygen species detection assay

iASTRO mono-cultures grown in half-area 96-well plates were used for this assay. At the timepoint of interest, media was removed, and cells were incubated for 30 min at 37°C with 20 µM H_2DCFDA in MAT media. At the end of the incubation, cells were washed 3 times with PBS (pH 7.4) and 50 µL PBS (pH 7.4) were added to each well. Plates were immediately read in a PHERAstar® FSX Microplate reader (BMG Labtech), by measuring the fluorescence (excitation = 494 nm, emission = 522 nm) emitted by the H_2DCFDA cleavage product 2',7'-dichlorofluorescein (DCF). When finishing the measurement, the plates were fixed and stained for DAPI (as described in section 2.3.) and imaged and analysed as described in section 2.5, in order to quantify the total number of healthy nuclei in each well. The total number of healthy nuclei in each well was used to normalize the fluorescence readout from each well.

2.11. Statistical analysis

This section details the statistical analysis performed in all experiments except for the analysis and graphic presentation corresponding to the RNA sequencing data, which is detailed in section 2.12.

All data are represented as mean ± SEM (standard error of the mean), unless stated otherwise. All graphs were produced using the GraphPad Prism v10.0.3 software, which was also used to perform the statistical analyses. Unless stated otherwise, each data point represents one cell line, averaged across technical replicates and multiple differentiations, details of which can be found in each figure legend. When normalized values are shown, these are normalized to the average of the control lines in the control/untreated condition, as specified in the figure legends. The number of lines used per genotype, as well as the number of differentiations used, are specified in the figure legends.

The details of the specific statistical tests and post-hoc tests for multiple comparisons used in each experiment can be found in the figure legends. p-values >0.05 were considered not significant (ns). *p≤0.05, **p≤0.01, ***p≤0.001, ****p≤0.0001 for all tests.

2.12. Bulk RNA sequencing and data processing

3 control iASTRO lines were used for this experiment. On DIV100, cells were seeded in 24-well plates as described in section 2.1.3., and treated for 24h with the corresponding treatment. 2 replica plates were prepared and treated; one was used for the RNA sequencing experiment, and the other one was used for RT-qPCR to validate the hits of interest from the RNAseq results and to test the primers to be used in follow up experiments. A single technical replicate was used for each cell line and treatment condition for the subsequent RNA extraction and RNA sequencing, due to the considerable number of unique samples.

RNA was extracted as described in section 2.3.1. Quality control of the RNA samples was conducted by Novogene using an Agilent 5400 prior to RNA-sequencing. All samples except one passed RNA integrity and concentration test. However, the sample that failed QC was still included in the experiment, as its concentration was not too low. Afterwards, Novogene proceeded with the library preparation, quality control and sequencing. Briefly, mRNA was purified using poly-T oligo-attached magnetic beads, and fragmented. Next, the first strand cDNA was synthetized using random hexamer primers, and then the second strand cDNA was synthetized. This was followed by end repair, A-tailing, adapter ligation, size selection, amplification and purification. Afterwards, the libraries were checked with Qubit, RT-PCR and a bioanalyzer, and sequenced using the NovaSeq 6000 (PE150) platform.

Raw data was provided and downloaded in FASTQ files. All the subsequent data processing and analysis was conducted using R (v4.3.2) using RStudio (2023.12.1). First, reads were aligned to a reference human transcriptome (Ensembl GRCh38 release 97) and quantified using *Salmon* (Patro et al., 2017) by Dr Peter Kilfeather. The quant.fz files generated with Salmon were imported using *tximeta* (Love et al., 2020), followed by transcript-to-gene mapping. Next, genes that had a total sum of less than 30 counts across all 21 samples, and genes that had 0 counts in 75% or more of the samples, were filtered out. Differential gene expression analysis was performed using DESeq2 (v1.42.1) (Love et al., 2014).

For sample clustering and visualization, the count data matrix was transformed using the *vst* function. Next, principal component analysis (PCA) and plotting was done with the plotPCA function, based on the top 1,000 most variable genes. Heatmap of the sample-to-sample Euclidean distances was performed using the *dist* function in the transposed transformed count matrix, and visualized using *pheatmap*.

Gene set enrichment analysis (GSEA) was performed using *clusterProfiler* (v4.10.1) (Wu et al., 2021; Yu et al., 2012). The Gene Ontology: Biological Process (GO:BP) terms were included in the analysis. The p-value adjustment method used was Benjamini-Hochberg (BH), and the padj cutoff was set to 0.05. In each comparison, all DEGs (padj<0.05) were used in the analysis, without a Log2FoldChange cut off. Fast GSEA was done using the fgsea (v1.30.0) package, focusing on the Hallmark pathways (Liberzon et al., 2015).

2.12.1. Comparison with online datasets

2.12.1.1. sc-RNAseq dataset (analysis performed by Dr Benjamin Vallin)

For iPSC-astrocytes, adaptor trimming was performed with TrimGalore software and sequencing reads were aligned onto a decoy-aware human reference transcriptome (GENCODE v44) with Salmon software (Patro et al., 2017). Transcript-level count data was then summarized to gene-level with the R package tximport (Soneson et al., 2016). For downstream analysis, we considered only the three untreated samples and the protein-coding genes with at least 10 counts in each sample. For post-mortem human brain tissues, we downloaded sample-specific UMI-barcode matrices prefiltered for lowly expressed genes and poor-quality nuclei from the Gene Expression Omnibus (accession code GSE140231). Cell type annotations were kindly shared by the authors of the original publication (PMID: 328268) in personal correspondence. Pseudobulk profiles were then generated for each combination of donor ID and cell type using the python libraries *scanpy* and *decoupler*.

Raw counts for iPSC-astrocytes and selected human brain pseudobulk profiles (either substantia nigra and cortical astrocytes or substantia nigra cell types) were combined in a single matrix, keeping only the genes detected in both datasets. We then applied regularized log transformation to produce homoskedastic count data on the log2 scale and normalized for library size with the R package DESeq2 (Love et al., 2014). The batch effect associated with the dataset ID (Ibarra-Aizpurua or Agarwal) was removed from the transformed data using the R package *limma*. The batch-corrected count matrix was used to produce a heatmap of the sample-to-sample Euclidean distances or a principal component plot based on the 1,000 most variable genes using the R packages *stats* and *pheatmap* or DESeq2.

2.12.1.2. Bulk RNAseq datasets

Raw FASTQ files from different bulk RNA sequencing experiments of iPSC-derived neural models were downloaded from the NCBI SRA repository. The details of the datasets used can be found in Table 2.12. The raw counts were aligned as described in section 2.12., and imported into R (v4.3.2) using *tximeta* (Love et al., 2020), together with the data from the 3 untreated iASTRO samples. Gene filtering and differential gene expression analysis was performed as described above. PCA plot and heatmap of the sample-to-sample distances were done as described in section 2.12.

Table 2.12. Human iPSC-derived cell model bulk RNAseq datasets used for the comparison

Region	Cell Type	Publication	SRA	Abbreviation
Midbrain	Astrocyte	Di Domenico et al., 2019	SRR7406476	i-vmAstro-1
Midbrain	Astrocyte	Di Domenico et al., 2019	SRR7406477	i-vmAstro-2
NA	iPSC	Di Domenico et al., 2019	SRR7406472	iPSC-1
NA	iPSC	Di Domenico et al., 2019	SRR7406473	iPSC-2
Midbrain	DAn	Krauskopf et al., 2022	SRR17898578	i-vmDAn-1
Midbrain	DAn	Semeano et al., 2022	SRR17199498	i-vmDAn-2
Cortex	Astrocyte	Hedegaard et al., 2020	SRR11646512	i-ctxAstro-1
Cortex	Astrocyte	Hedegaard et al., 2020	SRR11646518	i-ctxAstro-2

Chapter 3 - Investigating cell autonomous and non-autonomous dysfunction caused by the *GBA-N370S* mutation in iPSC-derived ventral midbrain astrocytes

3.1. Introduction and aims

One of the most susceptible cells in PD are dopaminergic neurons (DAn) of the substantia nigra pars compacta (SNpc), and hence, most of the research in the field of PD has been carried out in these cells, trying to elucidate the cell autonomous processes that might be impaired throughout the course of the disease that then result in DAn death. However, studies in human post-mortem brain tissue provided evidence of alterations in glial cells in PD patients. Although neurohistological studies are somewhat inconclusive regarding the presence and levels of astrogliosis in PD brains (Tong et al., 2015), the fact that astrocytes in PD contain α-synuclein inclusions has been widely demonstrated (Braak et al., 2007; Wakabayashi et al., 2000), even if astrocytes express little endogenous α-synuclein (Zhang et al., 2016).

Moreover, many of the genes associated with monogenic PD, such as *PARK7, PINK1* and *GBA1*, are expressed at similar, or higher, levels in astrocytes compared to neurons and partake in different astrocytic functions (Booth et al., 2017). This prompted researchers to investigate how different PD-related mutations might affect astrocyte function and their interaction with DAn. Mutations in *GBA1* are one of the most common genetic risk factors in PD, and out of the identified 100+ variants, the *N370S* variant is one of the most prevalent ones (Gegg et al., 2022). Even if multiple cellular dysfunctions caused by the *GBA-N370S* mutation have been described in DAn (Bogetofte et al., 2023; Fernandes et al., 2016; Schöndorf et al., 2014), how this mutation affects astrocytic activity is not fully understood yet, as one of the most extensive studies used Gaucher's disease astrocytes homozygous for *GBA-N370S* (Aflaki et al., 2020).

Lastly, one of the main challenges of investigating PD pathophysiology is the lack of representative human models of the disease. Rodent PD-models and primary cell cultures have been extensively used to study astrocyte involvement in PD, but due to the vast differences between murine and human astrocytes (Oberheim et al., 2009; Y. Zhang et al.,

2016), findings made in rodent models are not fully translatable to humans. With the development of the induced-pluripotent stem cell technology (Takahashi et al., 2007), it is now possible to generate human cells in vitro, including neurons and astrocytes, that maintain the same genetic architecture as the human donor. Various protocols to obtain iPSC-derived astrocytes have been developed, which greatly differ on the length. Moreover, very few protocols are designed to obtain regionally specific astrocytes, but, considering the vast regional differences in human astrocytes (Hasel et al., 2023), it is important to consider this when developing a model to study a disease that most greatly affects a very particular brain region, such as the midbrain in the case of PD.

The aims of this chapter are:

- To generate and characterize mature iPSC-derived ventral midbrain astrocytes (iASTROs).
- To explore the functional maturity of iASTROs and whether the *GBA-N370S* mutation affects the functional maturity of iASTROs.
- To study if the *GBA-N370S* mutation affects the GCase activity in iASTROs.
- To establish a direct co-culture system of iDAn and iASTROs.
- To investigate if the *GBA-N370S* mutation in iDAn and/or iASTROs alters the cellular homeostasis between both cell types.

3.2. Generation and characterization of mature control and *GBA-N370S* iPSC-derived ventral midbrain astrocytes

To generate iPSC-derived ventral midbrain-specific astrocytes, I used a protocol developed by one of our collaborators, Dr Lucy Crompton, which was later published in 2021 (Crompton et al., 2021). The protocol was slightly modified to better comply with the other standard operating procedures used in our tissue culture lab. The diagram detailing the differentiation protocol can be found in Figure 2.1.

During the first 30 days of the differentiation protocol, cells are exposed to specific factors to induce neuronal and ventral midbrain induction and expansion, resulting in the formation of ventral midbrain neural progenitor cells (vmNPCs). After day 30, vmNPCs are exposed to EGF

and hLIF to support cell proliferation and induce their differentiation into ventral midbrain astrocyte progenitor cells (vmAPCs), a process that takes 2 months. After day 90, vmAPCs can be exposed to BMP4 and hLIF to induce their maturation and thus generation of ventral midbrain astrocytes (iASTROs).

In this project, I differentiated 5 control iPSC lines and 5 iPSC lines harbouring the *GBA-N370S* mutation into iASTROs. However, not all the lines were used in all differentiations, as some lines failed to differentiate into iASTROs, and this varied from differentiation to differentiation. Initially, the aim of the project was to also use a *GBA-N370S* iPSC line and its isogenic control. I tried 2 different pairs of *GBA-N370S* iPSC lines with their corresponding isogenic controls that were generated and characterized by other groups (3026 and 3026-iso, characterized in (Chen et al., 2022), and PD4-2 and PD4-2 GC1, characterized in Schöndorf et al., (2014). However, neither one of the lines survived QC when differentiated into iASTROs or iPSC-derived dopaminergic neurons (iDAn) with our protocols. Therefore, as no other isogenic controls were available, I decided to move forward without the use of isogenic controls. For one differentiation, 2 control iASTRO lines differentiated by Dr Lucy Crompton were used, which were kindly given to validate some of the observations presented in chapter 5.

Based on the different stages of the iASTRO differentiation protocol explained above, I chose to use cells at day 30, 60 and 100 of the differentiation protocol to characterize iASTROs and observe how cells differentiated from vmNPCs into vmAPCs, and finally into mature, midbrain iASTROs. To achieve this, I stained cells at day 30, 60 and 100 of the differentiation protocol with the astrocytic markers S100B, GFAP and GLAST/EAAT1, the neuronal markers Tuj1/β-tubulin III and MAP2, the DAn marker TH, the midbrain marker Foxa2, and the NPC makers Pax6 and Nestin (Figure 3.1). At day 30, expression of S100B, GFAP and GLAST was very low, or corresponded to the background signal, at day 60 expression increased, and by day 100 all cells were positive for these 3 markers, which also revealed the distinct astrocytic morphology of iASTROs (Figure 3.1 A-C). Expression of nestin was maintained throughout the entire differentiation protocol (Figure 3.1 C); indeed, even if it has been considered a marker of neural progenitor cells, nestin is also expressed in mature astrocytes (Potokar et al., 2020), and other iPSC-derived astrocyte models have reported a higher nestin expression in mature astrocytes than in NPCs (Spreng et al., 2022). Therefore, the nestin staining was used to study the cell morphology throughout the differentiation protocol (Figure 3.2 A-C). Whereas the cell

area increased throughout the differentiation protocol (Figure 3.2 A), the cell roundness decreased, and the length/width ratio increased (Figure 3.2 B-C), corresponding with the acquisition of a more complex cellular morphology resembling mature astrocytes. At day 30, most cells were positive for Pax6, but the ratio of Pax6 positive cells decreased by day 60 and more so by day 100 (Figure 3.1 B and 3.2 D), as the cells became more mature. At day 30 and 60, almost all cells in the culture were positive for Foxa2, but by day 100, the proportion decreased to around 75% of the total iASTROs (Figure 3.1 A and 3.2 E). At day 30, a few cells in the culture stained positive for TH, Tuj1 and MAP2, but by day 60 and 100 only a background signal was detected (Figure 3.1 A-C), indicating that no NPCs were present in vmAPC and iASTRO cultures.

Next, I sought to investigate the expression of a number of astrocytic, NPC, neuronal and midbrain markers by RT-qPCR. Expression of the astrocytic markers *GFAP*, *S100B* and *CD44* increased throughout the differentiation protocol (Figure 3.3. Ai-iii). A big variability in the relative gene expression was observed between the lines, especially at day 100, due to the line-to-line and differentiation-to-differentiation differences, as well as the heterogeneity of astrocytes in general. On the other hand, expression of the proliferation marker *Ki67* and the neural cell progenitor maker *SOX2* significantly decreased from day 30 to day 100 (Figure 3.3. Aiv-v), indicating that iASTROs lost their proliferative capacity over time, as they differentiated and matured. Lastly, expression of the DAn marker *TH* significantly decreased by day 100, demonstrating the astroglial identity of the cultures and the lack of DAn.

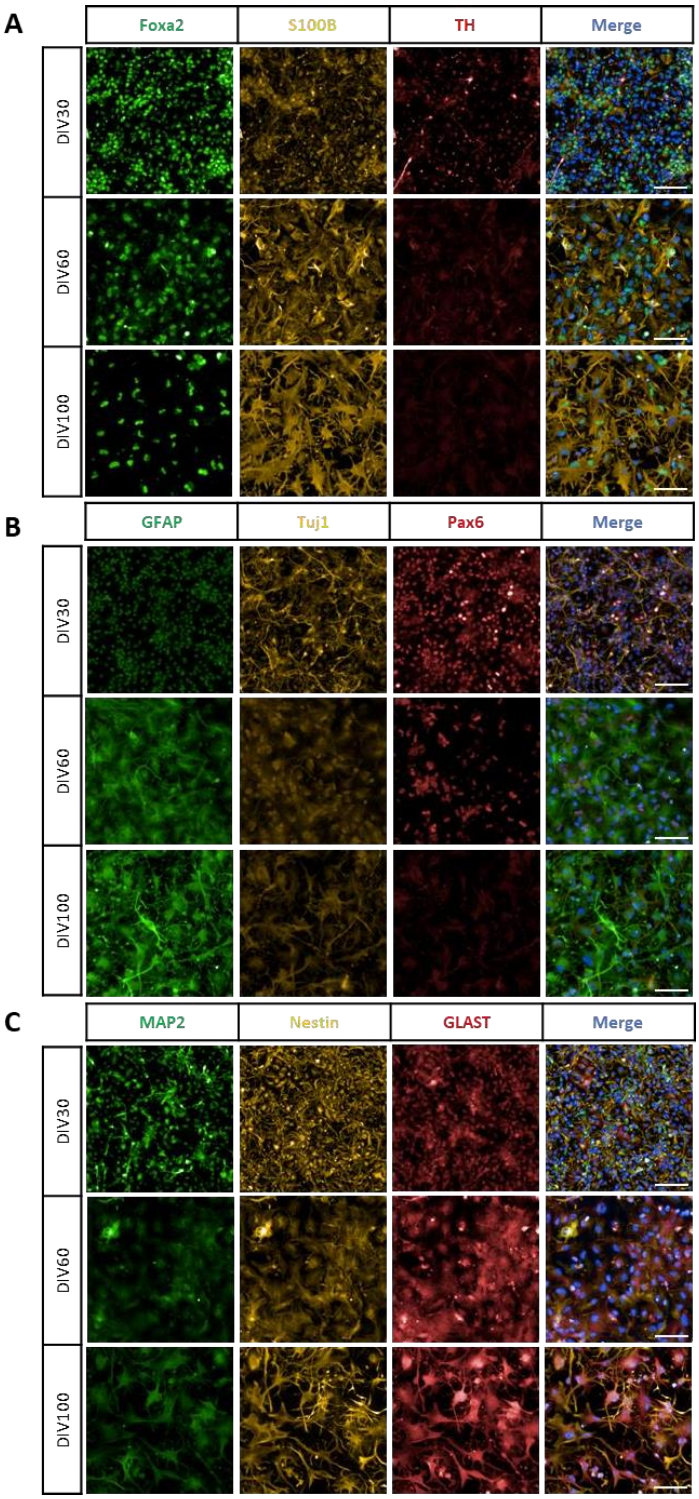


Figure 3.1. Representative images of iASTROs at day 30, 60 and 100 of the differentiation protocol, stained for astrocytic, midbrain, progenitor cell, and neuronal markers

Representative images of cells at day 30, 60 and 100 of the iASTRO differentiation protocol, (A) stained for Foxa2 (midbrain marker - green), S100B (astrocytic marker - yellow) and TH (dopaminergic neuron marker – red); (B) stained for GFAP (astrocytic marker - green), Tuj1 (neuronal marker - yellow) and Pax6 (neural progenitor cell marker– red); (C) stained for MAP2 (neuronal marker - green), Nestin (neural progenitor cell marker - yellow) and GLAST (astrocyte marker – red). All images are from the same control line in the same differentiation. Scale bar: 100 µm.

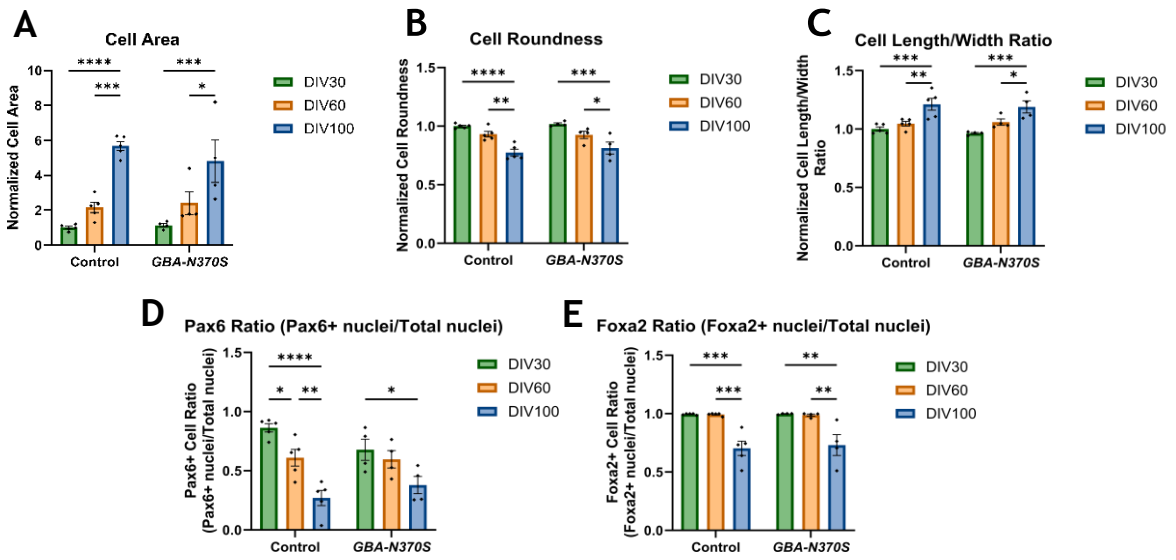


Figure 3.2. Morphological analysis and Foxa2 and Pax6 expression analysis at day 30, 60 and 100 of the iASTRO differentiation protocol

Quantification of the (A) cell area, (B) cell roundness and (C) cell length/width ratio of iASTROs at day 30, 60 and 100 of the iASTRO differentiation protocol. The Nestin stain shown in Figure 3.1C was used for the morphological analysis. (D) Quantification of the ratio of Pax6+ cells at day 30, 60 and 100 of the iASTRO differentiation protocol, calculated by dividing the number of Pax6+ nuclei by the total number of nuclei. The Pax6 staining shown in Figure 3.1B was used for this analysis. (E) Quantification of the ratio of Foxa2+ cells at day 30, 60 and 100 of the iASTRO differentiation protocol, calculated by dividing the number of Foxa2+ nuclei by the total number of nuclei. The Foxa2 staining shown in Figure 3.1A was used for this analysis. To obtain normalized values, calculated values were normalized to the average value of control cells at day 30. N = 5 control and 4 *GBA-N370S* lines, 2-6 differentiations. Each data point represents 1 iASTRO line averaged across differentiations. Mean ± SEM. The statistical analysis performed was two-way ANOVA with Tukey's multiple comparison test. *p<0.05, **p<0.01, ***p<0.001, ****p<0.0001.

I then explored whether there were changes in the relative gene expression of the genes of interest at day 100 between control and *GBA-N370S* iASTROs. The mean relative expression of *GFAP*, *S100B* and *CD44* was lower in *GBA-N370S* iASTROs, but due to the high variability between different control lines, the differences between both genotypes were not statistically significant (Figure 3.3 Bi-iii). *SOX2* expression was similar between both genotypes (Figure 3.3 Bv), and while the mean relative expression of *Ki67* was higher in *GBA-N370S* iASTROs, the difference was not statistically significant due to the variability between the lines (Figure 3.3 iv). Any differences observed in the relative expression of *TH* are not reliable, as the Ct values were above 31 (Figure 3.3 Bvi).

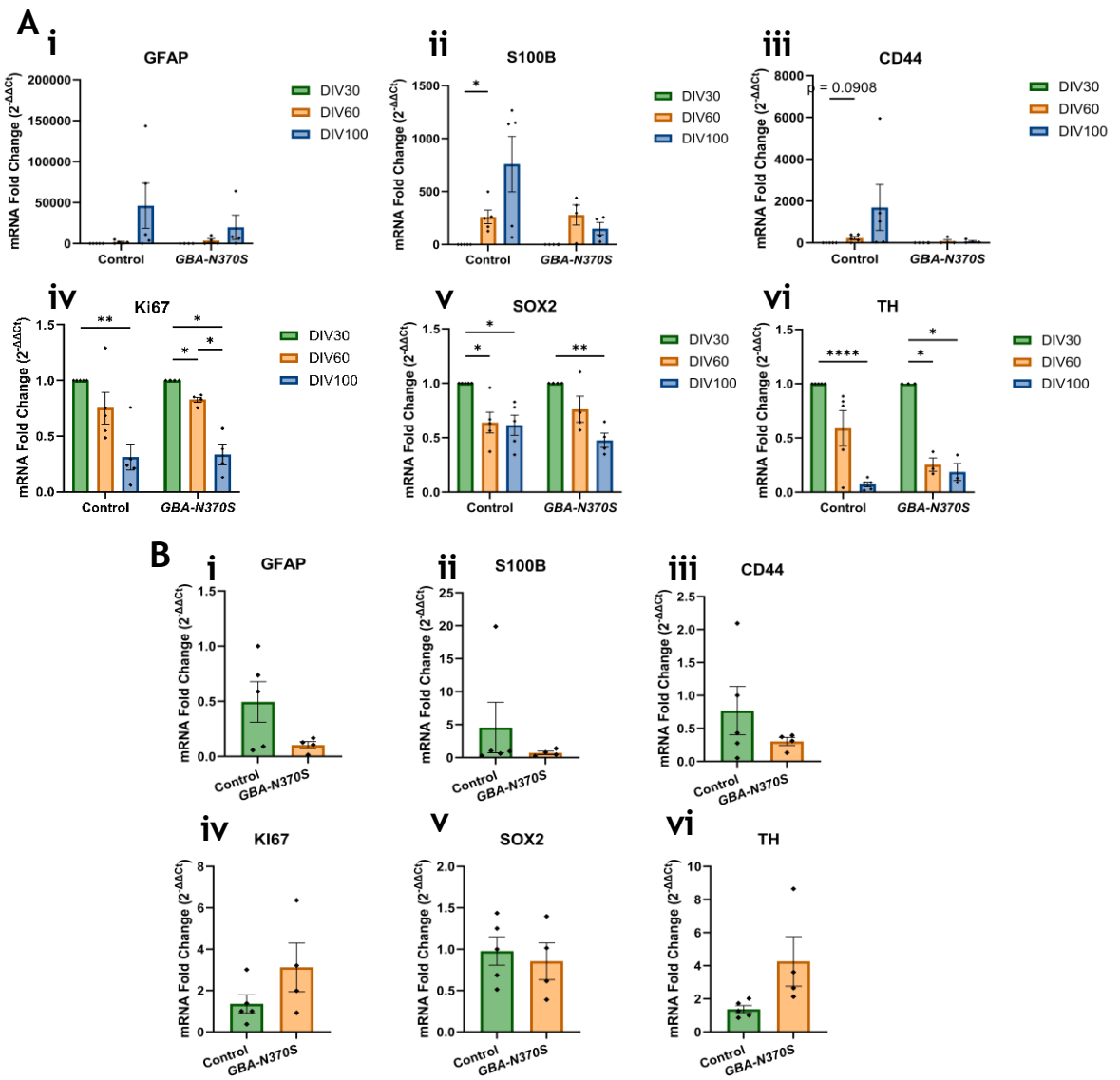


Figure 3.3. RT-qPCR analysis of different markers at day 30, 60 and 100 of the iASTRO differentiation protocol shows an increase in expression of astrocytic markers and a decrease in proliferation and progenitor cell markers

(A) Relative gene expression analysis by RT-qPCR of the astrocytic markers (i) GFAP, (ii) S100B and (iii) CD44, (iv) the proliferation marker Ki67, (v) the progenitor cell marker SOX2, and (vi) the dopaminergic neuron maker TH at day 30, 60 and 100 of the iASTRO differentiation protocol. In each differentiation, to calculate ΔΔCt for each gene, the ΔCt of each line at day 30 was subtracted to the ΔCt of that line at all timepoints (for the gene of interest). Each data point represents 1 iASTRO line averaged across differentiations. N = 5 control and 4 *GBA-N370S* lines, 2-3 differentiations. Mean ± SEM. The statistical analysis performed was two-way ANOVA with Tukey's multiple comparison test. *p<0.05, **p<0.01, ***p<0.001, ****p<0.0001. (B) Comparison of the relative gene expression of the astrocytic markers (i) GFAP, (ii) S100B and (iii) CD44, (iv) the proliferation marker Ki67, (v) the progenitor cell marker SOX2, and (vi) the dopaminergic neuron maker TH between control and *GBA-N370S* iASTROs at D100 of the differentiation protocol. In each differentiation, to calculate ΔΔCt for each gene, the ΔCt of one control line was subtracted to the ΔCt of all lines (for the gene of interest). Each data point represents 1 iASTRO line averaged across differentiations. N = 5 control and 4 *GBA-N370S* lines, 2-3 differentiations. Mean ± SEM. The statistical analysis performed was unpaired t test with Welch's correction.

After demonstrating that iASTROs expressed astrocytic markers, I further validated their astrocytic identity by comparing the expression of astrocytic and neuronal markers between iASTROs and iDAn. iDAn were obtained following a modified protocol based on the one developed by Kriks et al., (2011) and modified by Fedele et al., (2017). iDAn derived from 4 control and 4 *GBA-N370S* lines were used throughout the thesis, as some of the lines failed to differentiate into iDAn. 3 lines of each genotype were used in each differentiation. The expression of *S100B* and *GFAP* was higher in control and *GBA-N370S* iASTROs than in iDAn of the same genotype, but the differences were not statistically significant due to the variability between the iASTRO lines (Figure 3.4 A-B). The expression of the β-glucocerebrosidase encoding gene *GBA1* did not differ between both cell types and genotypes (Figure 3.4 C). As for neuronal markers, control and *GBA-N370S* iDAn had a higher expression of *TH*, *MAP2* and the α-synuclein encoding gene *SNCA* (Figure 3.4 D-F). The expression prolife of each cell type matched their cellular identity, while no differences were observed due to the *GBA-N370S* mutation in either cell type.

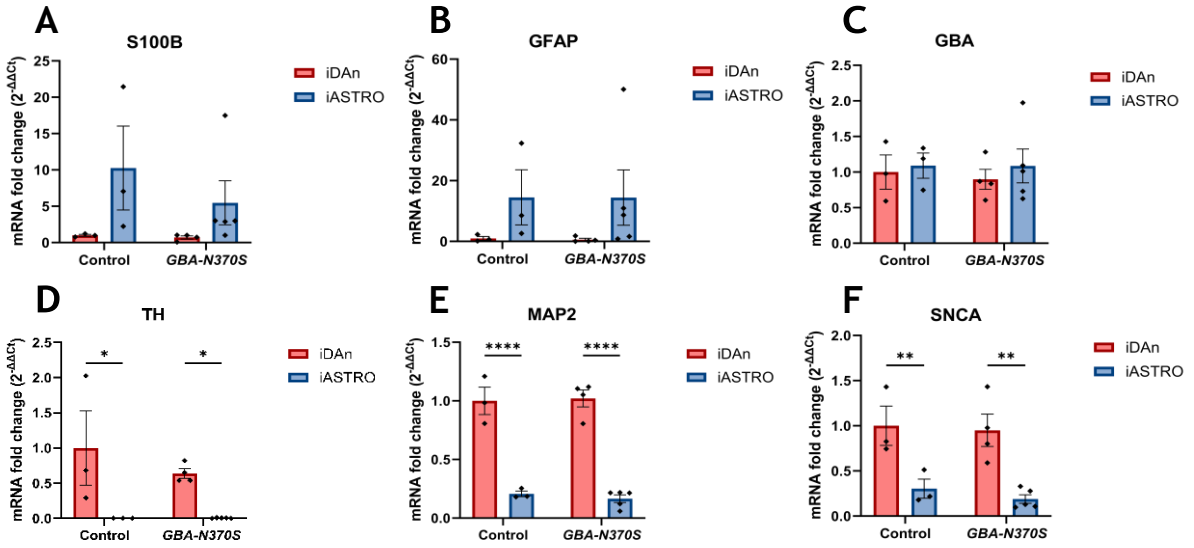


Figure 3.4. The relative gene expression of astrocytic and neuronal markers of mature iDAn and iASTROs correlates with their cellular identity

(A-F) Relative gene expression analysis by RT-qPCR of the astrocytic markers (A) S100B and (B) GFAP, (C) the β-glucocerebrosidase encoding gene GBA1, (D) the DAn marker TH, (E) the neuronal marker MAP2, and (F) the α-synuclein encoding gene SNCA in DIV35 control and *GBA-N370S* iDAn and DIV100 control and *GBA-N370S* iASTROs. To calculate ΔΔCt for each gene, the average ΔCt of control iDAn was subtracted to the ΔCt of all iDAn and iASTRO lines (for the gene of interest). Each data point represents 1 line averaged across differentiations. N = 3 control and 3 *GBA-N370S* lines for iDAn (2 differentiations), and 3 control and 5 *GBA-N370S* lines for iASTROs (1-2 differentiations). Mean ± SEM. The statistical analysis performed was two-way ANOVA with Fisher's LSD test. *p<0.05, **p<0.01, ***p<0.001, ****p<0.0001.

Lastly, I used transcriptomic data obtained from 3 lines of control iASTROs (data collected in the RNAseq experiment presented in chapter 4), to compare the transcriptomic profile of iASTROs with a) human scRNAseq transcriptomic data obtained from the cortex and substantia nigra of control and PD patients, and b) different bulk RNAseq transcriptomic data from iPSC, iDAn and iPSC-derived cortical and midbrain astrocytes published in different studies. Details on the analysis and the accession numbers of the databases used can be found in Section 2.12.1. Firstly, iASTROs cluster closer together with human substantia nigra (SN) astrocytes than with cortical (CTX) astrocytes, proving their regional identity (Figure 3.5 A). Moreover, when comparing iASTROs with the different cell types of the SN, iASTROs cluster closely with astrocytes, microglia, and oligodendrocyte precursor cells (OPCs) (Figure 3.5 B). The 3 control iASTRO lines used for this experiment cluster more closely together than the astrocytes obtained from different human donors. On the other hand, comparisons with other bulk RNAseq datasets show that iASTROs cluster the closest to iPSC-derived midbrain astrocytes, followed by iPSC-derived cortical astrocytes, whereas iPSC-derived DAn and iPSCs each form their own clusters (Figure 3.5 C). Overall, this data validates the midbrain and astrocytic identity of iASTROs.

Collectively, these results demonstrate that the differentiation protocol used to obtain iASTROs produces cells with a morphology and expression profile that resembles mature astrocytes, and the expression of Foxa2 indicates that most cells in the culture maintain a regional ventral midbrain identity.

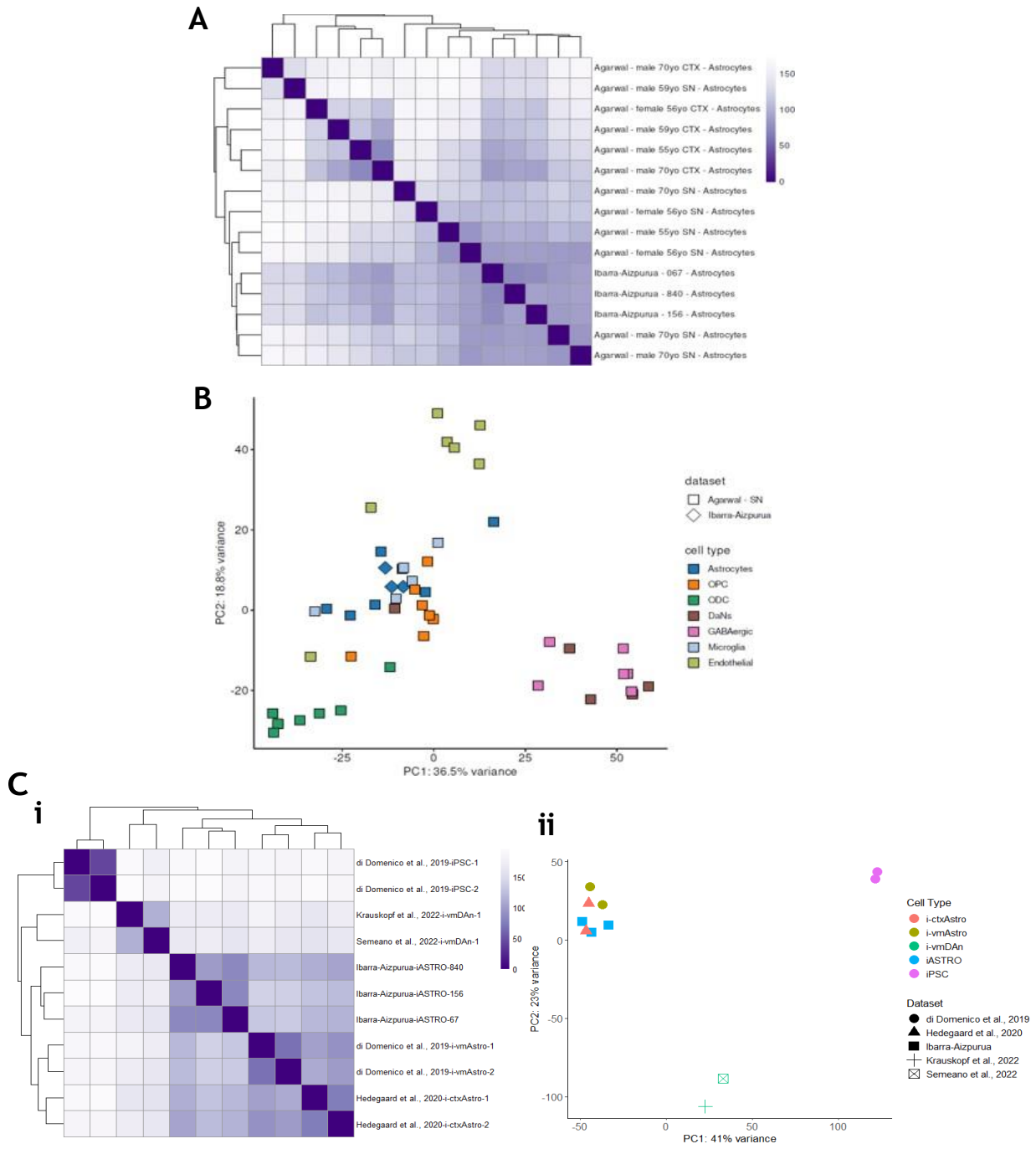


Figure 3.5. RNAseq comparison with a human post-mortem scRNAseq dataset and bulk RNAseq datasets of iPSC-derived neural models demonstrates the midbrain and astrocytic identity of iASTROs

(A) Heatmap showing sample-to-sample distances of bulk RNAseq data of 3 control iASTROs and human scRNAseq data of substantia nigra (SN) and cortex (CTX) astrocytes (B) PCA plot of bulk RNAseq data of 3 control iASTROs and scRNAseq data of different human SN cell types. For A and B, the scRNAseq dataset was obtained from the Agarwal et al., 2020 paper, accession code GSE140231. (C) (i) Heatmap and (ii) PCA plot showing sample-to-sample distances of bulk RNAseq data of 3 control iASTROs, iPSC-derived midbrain astrocytes (i-vmAtro-1/2), iPSC-derived cortical astrocytes (i-ctxAtro-1/2), iPSC-derived midbrain DAn (i-vmDAn-1/2), and iPSCs. Details on the datasets, publications and accession numbers can be found on Table 1.12.

3.3. Functional characterization of control and *GBA-N370S* iASTROs

After demonstrating that control and *GBA-N370S* iASTROs exhibit a cellular morphology and gene expression profile that resembles mature astrocytes, I sought to explore whether they also showed functional properties similar to those described in other in vitro astrocyte models.

Ca^{2+} is an essential second messenger in astrocytes and plays a critical role in multiple cellular signalling pathways (Ahrens et al., 2024). There are various ways in which astrocytes elevate their cytoplasmic [Ca^{2+}]; one of these mechanisms is the binding of ATP to its purinergic P2Y receptors in the plasma membrane, which results in the formation of inositol 1,4,5-triphosphate (IP3), its binding to the ITPR receptors in the ER, and the release of calcium from the ER into the cytosol (Lim et al., 2021b). Indeed, many studies using iPSC-derived astrocytes have used ATP application and subsequent elevation in cytoplasmic [Ca^{2+}] to demonstrate the functional maturity of their astrocyte model (Aflaki et al., 2020; Barbar et al., 2020; Nonaka et al., 2024; Ramos-Gonzalez et al., 2021). I therefore investigated the increases in cytoplasmic [Ca^{2+}] following ATP application in cells at day 30, 60 and 100 of the iASTRO differentiation protocol. Cells were first loaded with the ratiometric calcium sensor Fura-2 AM for 1.5h, and afterwards, 100 µM ATP were used to induce the calcium release from the ER, which results in an increase in the Fura-2 AM 340/380 nm fluorescence ratio. At day 30, vmNPCs did not respond to ATP, by day 60 there was a small response, and by day 100 mature iASTROs presented the characteristic increase in cytoplasmic calcium, as observed in the Fura-2 AM trace peak (Figure 3.6 A). Although both iASTRO genotypes had an increase in cytoplasmic calcium in response to ATP, the increase was bigger in control iASTROs, which could be easily observed in the Fura-2 traces (Figure 3.6 A) and quantified by measuring the area under the curve (AUC) (Figure 3.6 B) and the peak amplitude for the Fura-2 trace peak (Figure 3.6 C). This suggests that *GBA-N370S* iASTROs might be slightly less mature than control iASTROs, at least regarding calcium signalling and homeostasis. Nevertheless, this data shows that both control and *GBA-N370S* iASTROs express purinergic receptors and ER calcium channels required for Ca^{2+} signalling.

Another essential function of astrocytes is to help maintain glutamate homeostasis in the CNS, especially at the synapse, and this is mainly regulated by excessive glutamate uptake by glutamate transporters at the synapse (Mahmoud et al., 2019). Therefore, monitoring the

uptake of glutamate from the extracellular media is another assay frequently used to prove the functionality of iPSC-derived astrocytes (Aflaki et al., 2020; Sonninen et al., 2020; Yeon et al., 2023). After checking that iASTROs expressed the glutamate transporter GLAST/EAAT1 (Figure 3.1 C), I investigated whether iASTROs were capable of taking up glutamate from the media. Thus, day 100 iASTROs were incubated with 100 µM glutamate for 2h, and then the glutamate left in the media was quantified in order to calculate the percentage taken by the cells. 100 µM of the glutamate transporter inhibitor DL-TBOA were added to the cells as a negative control. Both control and *GBA-N370S* iASTROs took up glutamate from the media (~35% of the glutamate added to the media), without any significant differences between the genotypes, and this uptake was completely inhibited in the presence of DL-TBOA (Figure 3.6 D). Thus, this data shows that iASTROs express functional glutamate transporters and carry out the essential astrocytic function of glutamate uptake.

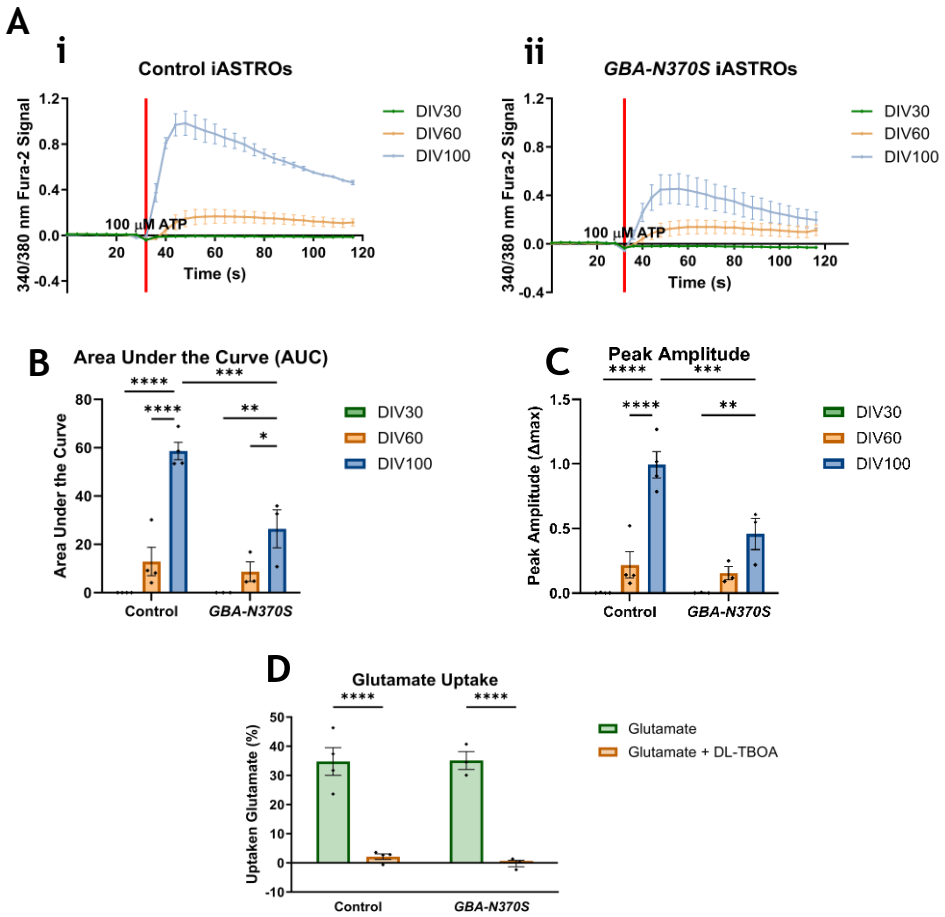


Figure 3.6. At day 100, iASTROs display ATP-induced calcium release from the ER and glutamate uptake from the media

(A) Traces showing the average of the Fura-2 AM ratio in response to 100 µM ATP addition (red line) in (i) control and (ii) *GBA-N370S* iASTROs at day 30, 60 and 100 of the differentiation protocol. (B) Area under the curve (AUC) and (C) peak amplitude analysis of the traces shown in A. Each data point

represents 1 iASTRO line averaged across differentiations. N = 4 control and 3 *GBA-N370S* lines, 2-7 differentiations. Mean ± SEM. The statistical analysis performed was two-way ANOVA with Tukey's multiple comparison test. *p<0.05, **p<0.01, ***p<0.001, ****p<0.0001. (D) Percentage of the glutamate taken from the medium in control and *GBA-N370S* iASTROs at DIV100. The glutamate transporter blocker DL-TBOA (100 µM) was used as a negative control. Each data point represents 1 iASTRO line averaged across differentiations. N = 3 control and 3 *GBA-N370S* lines, 2 differentiations. Mean ± SEM. The statistical analysis performed was two-way ANOVA with Fisher's LSD test. *p<0.05, **p<0.01, ***p<0.001, ****p<0.0001.

3.4. Assessing the β-glucocerebrosidase activity of control and *GBA-N370S* iASTROs and iDAn

Over 300 mutations have been found in the *GBA1* gene, some result in gain-of-function whereas others cause loss-of-function of β-glucocerebrosidase (GCase) (Smith & Schapira, 2022). It has been extensively shown that the *N370S* mutation, one of the most prevalent *GBA1* mutations associated with PD (Zheng & Fan, 2022), results in a reduction in the enzymatic activity of GCase in iDAn (Bogetofte et al., 2023; Fernandes et al., 2016; Grigor'eva et al., 2023; Rosety et al., 2023; Schöndorf et al., 2014; Woodard et al., 2014). A decreased GCase activity was also observed in iPSC-derived astrocytes harbouring the *GBA-N370S* mutation, which was accompanied by a reduction in GCase protein expression (Aflaki et al., 2020). In this thesis, no differences in the expression of *GBA1* at the transcript level were observed in *GBA-N370S* iASTROs and iDAn (Figure 3.4 C), which was expected as the mutation does not reduce transcript expression (Grigor'eva et al., 2023), so I next sought to further evaluate the GCase activity in both cell types. When measuring the GCase activity using the 4-MUG assay, no differences were observed between control and *GBA-N370S* iASTROs (Figure 3.7 Ai), whereas a statistically significant decrease was observed in *GBA-N370S* iDAn (Figure 3.7 Aii). The GCase inhibitor conduritol-β-epoxide (CBE, 1 mM) was used as a positive control. When comparing the total 4-MU fluorescence measured in the 4-MUG assay, normalized to total protein content, a higher value was measured in iASTROs as compared to iDAn, but without any differences in *GBA-N370S* iASTROs (Figure 3.7 B). In this case, the reduction observed in *GBA-N370S* iDAn did not reach statistical significance due to the high variability between different iASTRO lines. To further validate the findings in iASTROs, I used MDW-941, which is a BODIPY-tagged 8-deoxy-8-azidocyclophellitol that covalently binds to the GCase active site, thus inhibiting its function whilst fluorescently labelling the enzyme (Witte et al.,

2010). Both control and *GBA-N370S* iASTROs were labelled with MDW-941, and its signal was almost abolished with 1 mM CBE (Figure 3.7 C). The number and relative intensity of MDW-941 spots did not differ between both genotypes (Figure 3.7 Di-ii), whereas a slight reduction was observed in the corrected spot intensity (Figure 3.7 Diii). Collectively, this data shows that the *GBA-N370S* mutation does not affect the level of enzymatic activity of GCase in iASTROs but causes a reduction in iDAn.

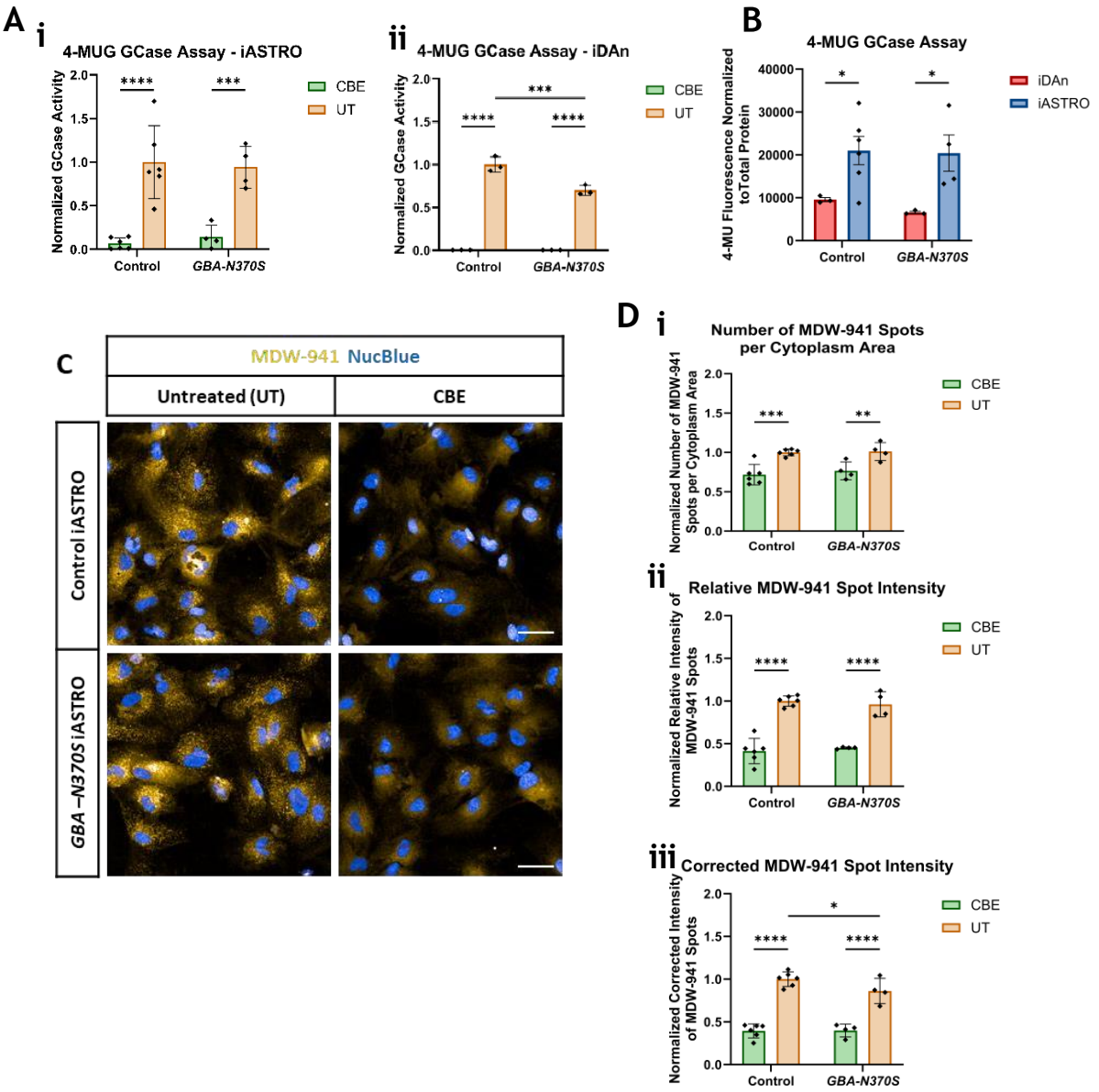


Figure 3.7. *GBA-N370S* iASTROs do not have reduced GCase activity compared to control iASTROs, whereas *GBA-N370S* iDAn have reduced GCase activity compared to control iDAn

(A) Quantification of the GCase activity measured with the 4-MUG assay in control and *GBA-N370S* (i) iASTROs and (ii) iDAn. For each cell type, values were normalized to the average of control cells without CBE (1 mM). (B) Quantification of the total fluorescence measured in the 4-MUG assay, normalized to the total amount of protein, in control and *GBA-N370S* iASTROs and iDAn. Same dataset as in (A). Each data point represents 1 line averaged across differentiations. N = 3 control and 3 *GBA-N370S* lines for

iDAn (2 differentiations), and 6 control and 4 *GBA-N370S* lines for iASTROs (2-4 differentiations). Mean ± SEM. The statistical analysis performed was two-way ANOVA with Fisher's LSD test. *p<0.05, **p<0.01, ***p<0.001, ****p<0.0001. (C) Representative images of MDW-941 (yellow)-loaded live control and *GBA-N370S* iASTROs (also stained for NucBlue) with or without CBE (1 mM). Scale bar: 50 µm. (D) Quantification of (i) the number of MDW-941 spots per area of cytoplasm, (ii) the relative intensity of MDW-941 spots and (iii) the corrected intensity of MDW-941 spots in control and *GBA-N370S* iASTROs, with or without the GCase inhibitor CBE (1 mM). To obtain normalized values, measured values were normalized to the average value of untreated control iASTROs. Each data point represents 1 iASTRO line averaged across differentiations. N = 6 control and 4 *GBA-N370S* lines, 1-5 differentiations. Mean ± SEM. The statistical analysis performed was two-way ANOVA with Fisher's LSD test. *p<0.05, **p<0.01, ***p<0.001, ****p<0.0001.

3.5. Establishment and optimization of a direct iDAn-iASTRO co-culture system

After exploring if the *GBA-N370S* mutation caused any changes in the cell autonomous functions of iASTROs, the next aim was to investigate if this mutation resulted in any alterations in the non-cell autonomous functions of iDAn and iASTROs, and whether this changed the homeostasis between both cell types. Thus, the first step was to develop and optimize a direct co-culture system of iDAn and iASTROs.

In recent years, with neuron-astrocyte interactions capturing the interest of the neuroscience community, multiple cell culture platforms have been developed for iPSC-derived neuron-astrocyte co-cultures, such as transwell systems (Aflaki et al., 2020; Cheng et al., 2020; Yeon et al., 2023), microfluidic chambers (Hyvärinen et al., 2019), coverslips without cell-to-cell contact (Tsunemi et al., 2020), three-dimensional (3D) bioprinting (Whitehouse et al., 2023) and direct co-culture (Barbar et al., 2020; Cheng et al., 2020; de Rus Jacquet, 2019; di Domenico et al., 2019). Based on the protocols of these studies, I decided to follow a direct co-culture approach, where iASTROs were added on top of iDAn on day 35 of the iDAn differentiation protocol (Figure 2.3).

For many years, it was claimed that glial cells outnumbered neurons 10 to 1, but with improved cell counting techniques this ratio is now known to be closer to 1:1, although the specific ratio reported varies between studies and between brain regions (von Bartheld et al., 2016). Similarly, the neuron/astrocyte cell number ratio used in published studies using direct co-cultures also differs: 1:1 (Cheng et al., 2020), 5:2 (di Domenico et al., 2019), 10:3 (Barbar et al., 2020). In this project, on day 20 of the iDAn differentiation protocol, iDAn were plated

at a density of $4x10^4$ cells/well in half-area 96-well plates. However, following mitomycin treatment and after 2 additional weeks in mono-culture, the number of viable iDAn decreased by the time iASTROs were added to the culture. Since the number of surviving iDAn at the time of co-culture varied between lines and differentiations, I decided to add iASTROs at a density where the entire surface of the well would be covered by them. I found that a density of $8x10^3$ cells/well was sufficient to cover the entirety of the well, so this was the density of iASTROs chosen for the co-culture experiments.

Published studies using direct iPSC-derived DAn-astrocyte co-cultures used a DAn maturation media (Barbar et al., 2020; Cheng et al., 2020), Neurobasal™ medium supplemented with 2% B-27 (di Domenico et al., 2019), or Neurobasal™ medium supplemented with 0.5% FBS (de Rus Jacquet, 2019) in the co-cultures. However, I decided to explore multiple media compositions that also included growth factors and supplements of the astrocyte maturation media. Thus, 5 different media conditions were tested in the co-cultures for 10 days (Table 3.1), and afterwards the co-cultures were stained for TH and GFAP to quantify the number of iDAn and iASTROs in each condition (Figure 3.8 A). In one of the conditions, DAPT was removed from the 50% media, based on the findings that blocking the Notch-1 signalling pathway with the γ-secretase inhibitor DAPT negatively affects astrocyte proliferation and reactivity (Qian et al., 2019; Zhang et al., 2015), as well as promote the reprogramming of astrocytes into neurons (Alizadeh et al., 2024; Tan et al., 2022). Indeed, other iDAn-iASTRO co-culture studies also removed DAPT from the co-culture media (Supakul et al., 2024).

Quantification of the ratio of TH-positive and GFAP-positive cells in the co-cultures showed that the highest ratio of TH-positive cells was obtained with DAn maturation media, and the lowest with Astro maturation media (Figure 3.8 B). On the contrary, the highest ratio of GFAP-positive cells was obtained with the Astro maturation media, and the lowest with the DAn maturation media. The 50%, 75% and 50% without DAPT conditions yielded similar results, but since less variability was observed with the 50% media, I decided to use this media for all subsequent co-culture experiments.

Table 3.1. Media compositions tested in the iDAn-iASTRO co-cultures

Media	Composition
DAn MAT	NB media supplemented with BDNF, GDNF, TGFβ3, DAPT, Ascorbic Acid, and cAMP
Astro MAT	ASTRO media supplemented with hLIF and BMP4
50%	50% DAn MAT + 50% Astro MAT
75%	75% DAn MAT + 25% Astro MAT
50% w/o DAPT	50% DAn MAT + 50% Astro MAT minus DAPT

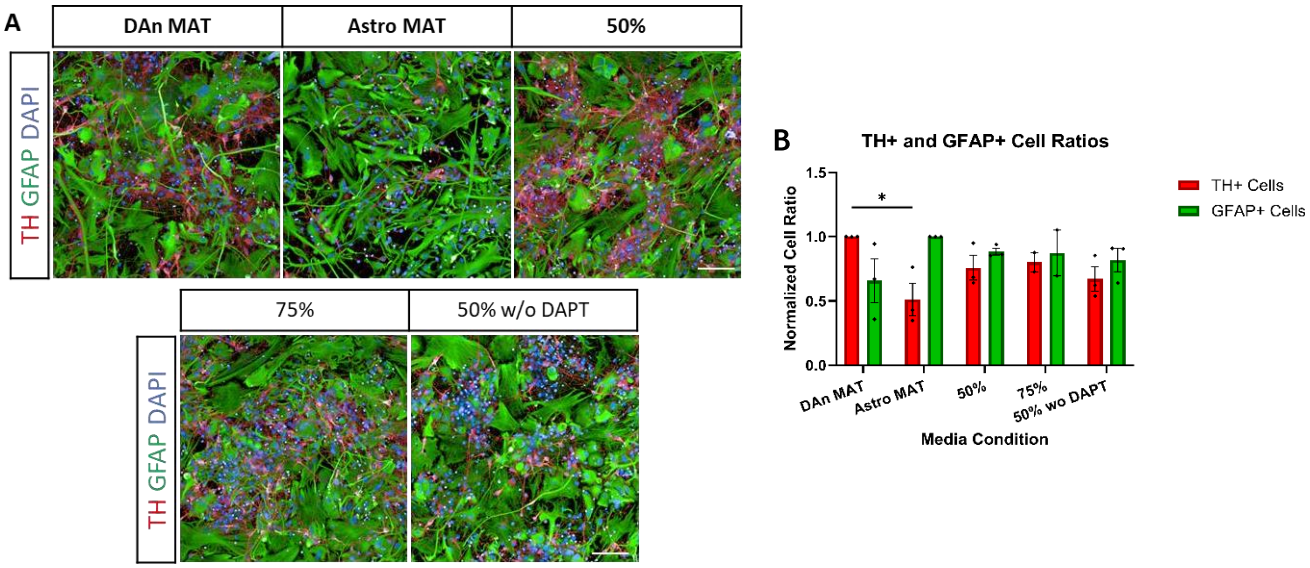


Figure 3.8. A media composed of 50% DAn MAT media and 50% Astro MAT media is the most optimal for the survival of both iDAn and iASTROs in direct co-culture

(A) Representative immunocytochemistry images of iDAn-iASTRO co-cultures treated with the indicated media condition for 10 days, stained for the dopaminergic neuron marker TH (red) and the astrocytic marker GFAP (green). Scale bar: 100 µm. (B) Quantification of the ratio of TH+ cells and GFAP+ cells in the co-cultures treated with the indicated media for 10 days. The ratios were obtained by dividing the number of TH+ or GFAP+ cells by the total number of cells. Then, the TH ratios were normalized to the TH ratio obtained in the DAn MAT condition, and the GFAP+ ratios were normalized to the ratio obtained in the Astro MAT condition. Each data point represents the average of 1 differentiation. N = 6 lines for iDAn (3 differentiations), and 5 lines for iASTROs (1-3 differentiations). Mean ± SEM. The statistical analysis performed was two-way ANOVA with Tukey's multiple comparison test. *p<0.05.

3.6. Studying the effects of the *GBA-N370S* mutation on iDAn-iASTRO homeostasis

Next, I wanted to explore how the *GBA-N370S* mutation in iDAn and/or iASTROs would affect the interaction between both cell types, particularly the survival of iDAn, the formation of synapses, and the reactivity of iASTROs. Hence, 6 different iDAn culture conditions were established (Figure 3.9 A), where either control or *GBA-N370S* iDAn were in mono-culture or in co-culture with control or *GBA-N370S* iASTROs. All these culture conditions were maintained in the 50% media for 10, 20 or 30 days, and then stained for the neuronal marker MAP2, the DAn marker TH and the astrocytic marker S100B (Figure 3.9 B). The number of MAP2-positive neurons increased in the presence of both control and *GBA-N370S* iASTROs compared to iDAn, and this increase was the most significant after 30 days in co-culture (Figure 3.10 A). Moreover, after 20 and 30 days in co-culture, the number of MAP2-positive neurons was significantly lower in co-cultures with *GBA-N370S* iDAn compared to the co-culture conditions with control iDAn (Figure 3.10 A). A decrease in the number of MAP2-positive cells in *GBA-N370S* iDAn mono-cultures was also observed compared to control iDAn mono-cultures at all timepoints, but no statistical significance was reached at any of the timepoints (Figure 3.10 A). Similar results were obtained when quantifying the number of TH-positive dopaminergic neurons, with an increase in the number of TH-positive cells in the presence of both control and *GBA-N370S* iASTROs compared to the mono-cultures, and this increase was most significant after 30 days (Figure 3.10 B). As with MAP2-positive neurons, after 20 days in co-culture, the number of TH-positive cells was lower in co-cultures with *GBA-N370S* iDAn compared to the conditions with control iDAn (Figure 3.10 B). On the other hand, no differences in the number of S100B-positive cells (i.e. astrocytes) were observed between all 4 co-culture conditions at any of the timepoints (Figure 3.10 C). Although there was a trend towards an increase in the cell area of astrocytes in the presence of *GBA-N370S* iDAn compared to control iDAn, these observations were not statistically significant (Figure 3.10 D). Lastly, after 20 and 30 days in co-culture, an increase in the cytoplasmic S100B intensity was observed in both control and *GBA-N370S* iASTROs co-cultured with *GBA-N370S* iDAn compared to control iDAn (Figure 3.10 E). Collectively, these results show that both control and *GBA-N370S* iASTROs support neuronal survival in co-culture with iDAn, without any differences due to the iASTRO genotype, whereas *GBA-N370S* iDAn are more vulnerable than

control iDAn. Moreover, the increase in S100B intensity observed in iASTROs co-cultured with *GBA-N370S* iDAn suggests astrocytes may undergo a different reactive response in the presence of PD iDAn.

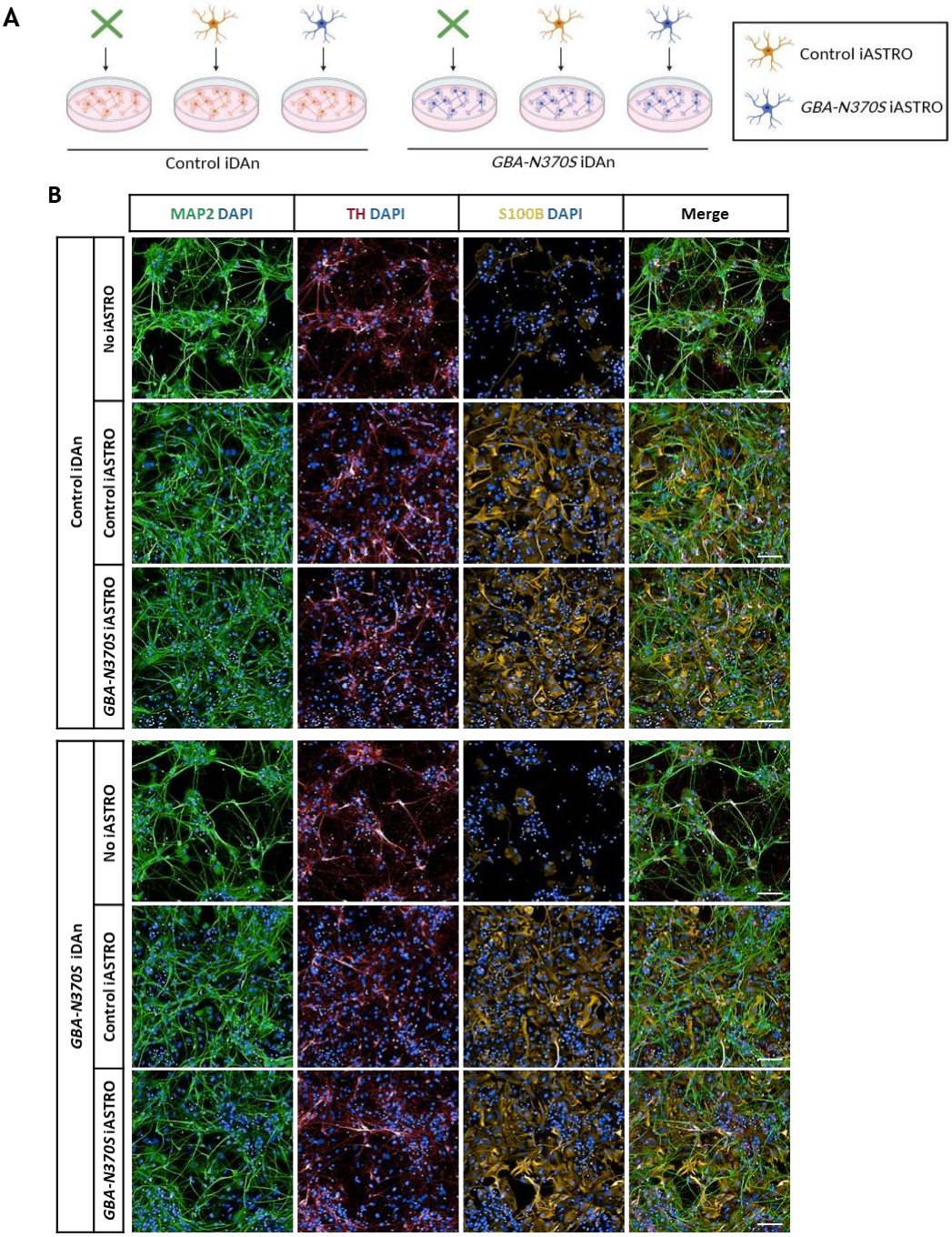


Figure 3.9. Studying the effect of the *GBA-N370S* mutation in the iDAn-iASTRO co-cultures
(A) Diagram of the 6 different iDAn culture conditions analysed depending on the presence/absence of iASTROs and the genotype of both cell types. (B) Representative immunocytochemistry images of control (top panel) and *GBA-N370S* (bottom panel) iDAn at DIV45, either in mono-culture or after 10 days of co-culture with control or *GBA-N370S* iASTROs, stained for MAP2 (green), TH (red) and S100B (yellow). Scale bar: 100 µm.

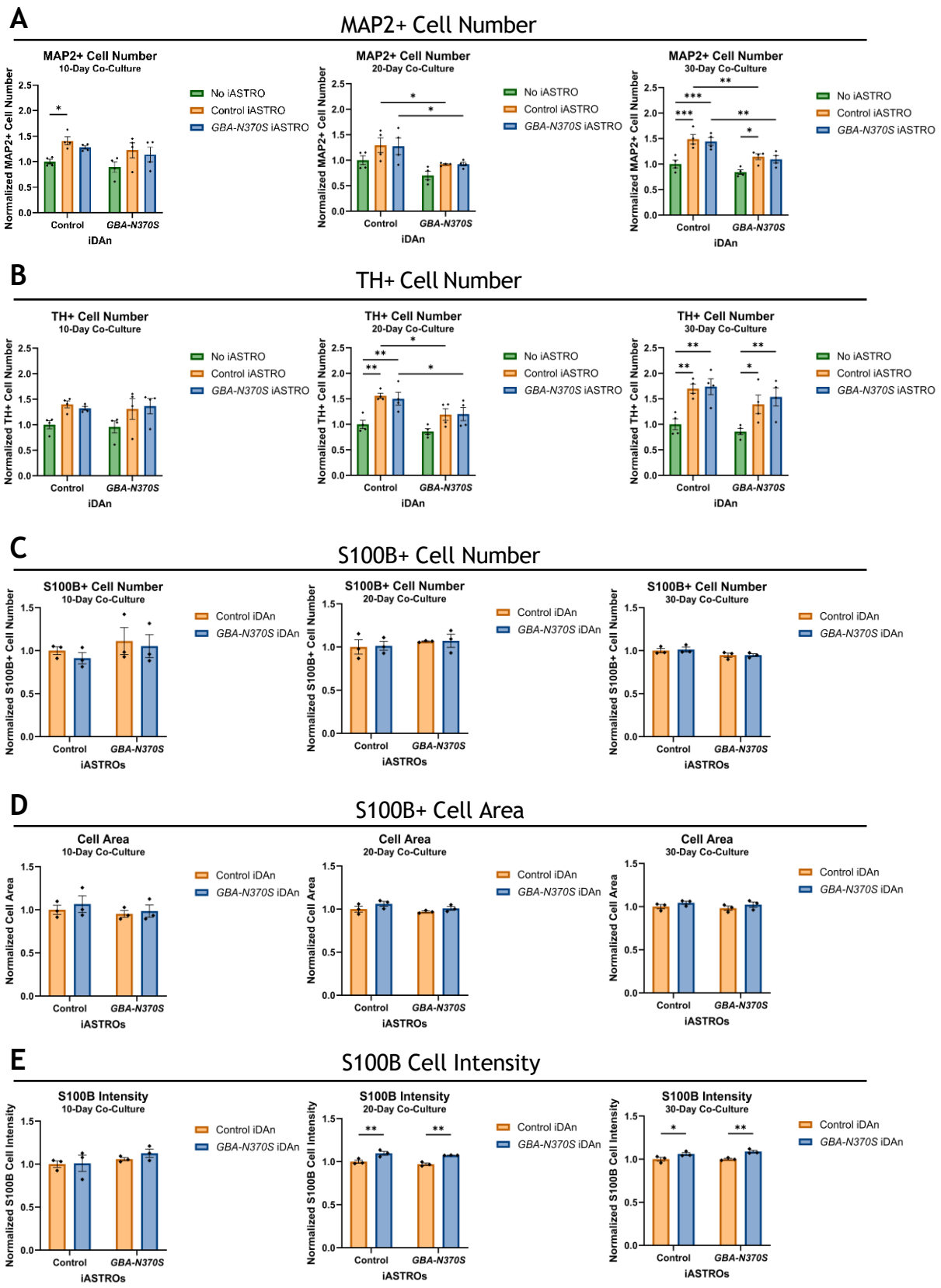


Figure 3.10. Both control and *GBA-N370S* iASTROs support the growth and survival of control and *GBA-N370S* iDAn, but iASTROs respond differently to *GBA-N370S* iDAn compared to control iDAn

Quantifications are based on the stainings shown in Figure 3.10. (A-B) Quantification of the number of (A) MAP2+ and (B) TH+ cells in iDAn mono-culture or co-culture with control or *GBA-N370S* iASTROs

for 10, 20 and 30 days. Each data point represents 1 iDAn line, averaged in each differentiation to all the conditions either in mono-culture or co-cultured with 2 lines of iASTROs of each genotype, and then averaged across differentiations. For each differentiation, values were normalized to the average of control iDAn in mono-culture. N = 3 control and 3 *GBA-N370S* lines for iDAn (3 differentiations), and N = 3 control and 3 *GBA-N370S* lines for iASTROs (1-3 differentiations). Mean ± SEM. The statistical analysis performed was two-way ANOVA with Tukey's multiple comparison test. *p<0.05, **p<0.01, ***p<0.001. (C-E) Quantification of (C) the number of S100B+ cells, (D) the cell area of S100B+ cells and (E) the S100B intensity of S100B+ cells in control and *GBA-N370S* iASTROs in co-culture with control or *GBA-N370S* iDAn for 10, 20 or 30 days. Each data point represents 1 iASTRO line, co-cultured with 3 iDAn lines of the same genotype in each differentiation, averaged per differentiation, and then averaged across differentiations. Values were normalized to the average of control iASTROs co-cultured with control iDAn. N = 3 control and 3 *GBA-N370S* lines for iDAn (3 differentiations), and N = 3 control and 3 *GBA-N370S* lines for iASTROs (1-3 differentiations per line). Mean ± SEM. The statistical analysis performed was two-way ANOVA with Fisher's LSD test. *p<0.05, **p<0.01.

To investigate whether the increase in the number of MAP2- and TH-positive neurons in the co-cultures with iASTROs was not due to increases in cell proliferation, I studied the expression of the proliferation marker Ki67 in all the culture conditions (Figure 3.9 A) after 10, 20 and 30 days. Immunocytochemistry images show that very few cells in the iDAn-iASTRO co-cultures are Ki67-positive, while almost none are in iDAn mono-culture (Figure 3.11 A). Indeed, the total percentage of Ki67-positive cells in iDAn mono-cultures was below 2% at all timepoints studied, and even if a higher percentage was observed in the co-cultures, the percentage decreased over time (Figure 3.11 B). When analysing Ki67-positive cells amongst the MAP2-positive cell population, a higher percentage was observed in all co-culture conditions (Figure 3.11 C). However, this percentage was below 2% after 10 days and decreased to less than 0.5% by 30 days in co-culture (Figure 3.11 C), and these percentages of proliferative cells amongst the MAP2-positive population are not high enough to account for the higher cell numbers described in Figure 3.10 A-B. As for iASTROs, no differences were observed in the percentage of Ki67-positive cells amongst the S100B-positive population between iASTRO genotypes and co-culture conditions (Figure 3.11 D), and similar to MAP2-positive cells, the percentage of Ki67-positive cells decreased over time.

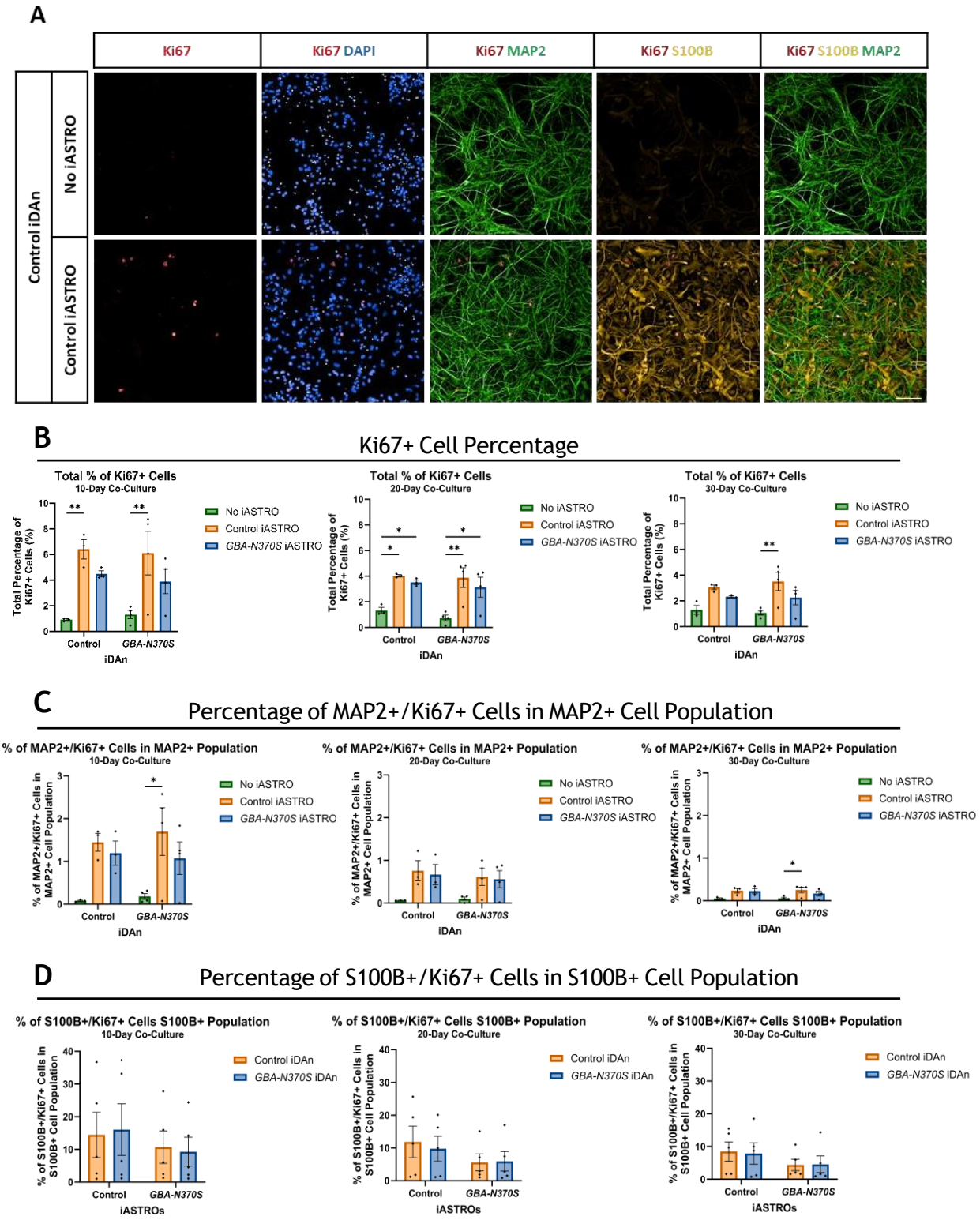


Figure 3.11. Ki67 expression analysis in iDAn-iASTRO co-cultures suggests that the increase in the number of iDAn in the presence of iASTROs is not due to an increase in the proliferation of iDAn

(A) Representative immunocytochemistry images of control iDAn in mono-culture or co-culture with control iASTROs for 10 days, stained for the proliferation marker Ki67 (red), MAP2 (green) and S100B (yellow). Scale bar: 100 µm. (B) Quantification of the percentage of Ki67+ cells (calculated by dividing

the number of Ki67+ cells by the total number of cells and multiplying by 100) in control and *GBA-N370S* iDAn mono-cultures or co-cultured with control or *GBA-N370S* iASTROs for 10, 20 or 30 days. (C) Quantification of the percentage of MAP2+ cells that are Ki67+ (calculated by dividing the number of Ki67+/MAP2+ cells by the total number of MAP2+ cells and multiplying by 100), in control and *GBA-N370S* iDAn mono-cultures or co-cultured with control or *GBA-N370S* iASTROs for 10, 20 or 30 days. Each data point represents 1 iDAn line, averaged in each differentiation to all the conditions either in mono-culture or co-cultured with 2 lines of iASTROs of each genotype, and then averaged across differentiations. N = 3 control and 3 *GBA-N370S* lines for iDAn (4 differentiations), and N = 5 control and 5 *GBA-N370S* lines for iASTROs (1-3 differentiations). Mean ± SEM. The statistical analysis performed was two-way ANOVA with Tukey's multiple comparison test. *p<0.05, **p<0.01. (D) Quantification of the percentage of S100B+ cells that are Ki67+ (calculated by dividing the number of Ki67+/S100B+ cells by the total number of S100B+ cells and multiplying by 100), in control and *GBA-N370S* iASTROs in co-culture with control or *GBA-N370S* iDAn for 10, 20 or 30 days. Each data point represents 1 iASTRO line, co-cultured with 3 iDAn lines of the same genotype in each differentiation, averaged per differentiation, and then averaged across differentiations. N = 5 control and 5 *GBA-N370S* lines for iASTRO (1-3 differentiations), and N = 3 control and 3 *GBA-N370S* lines for iDAn (4 differentiations). Mean ± SEM. The statistical analysis performed was two-way ANOVA with Fisher's LSD test.

Additionally, I investigated whether iASTROs supported the formation of synapses and whether this essential astrocytic function (Tan et al., 2021) was impaired in *GBA-N370S* iASTROs. The same culture conditions illustrated in Figure 3.9 A were maintained for 10, 20 or 30 days and then stained for MAP2, the pre-synaptic protein α-synuclein and the post-synaptic protein Homer1 (Figure 3.12 A). Partial or complete overlapping of α-synuclein and Homer1 puncta in close proximity to MAP2 neurite staining represents a synapse. The number of synapses per MAP2 area were quantified, and a significant increase was observed in the presence of both control and *GBA-N370S* iASTROs at all timepoints compared to iDAn mono-cultures (Figure 3.12 B), thus suggesting that iASTROs support the development of synapses and this function does not appear to be reduced due to the *GBA-N370S* mutation.

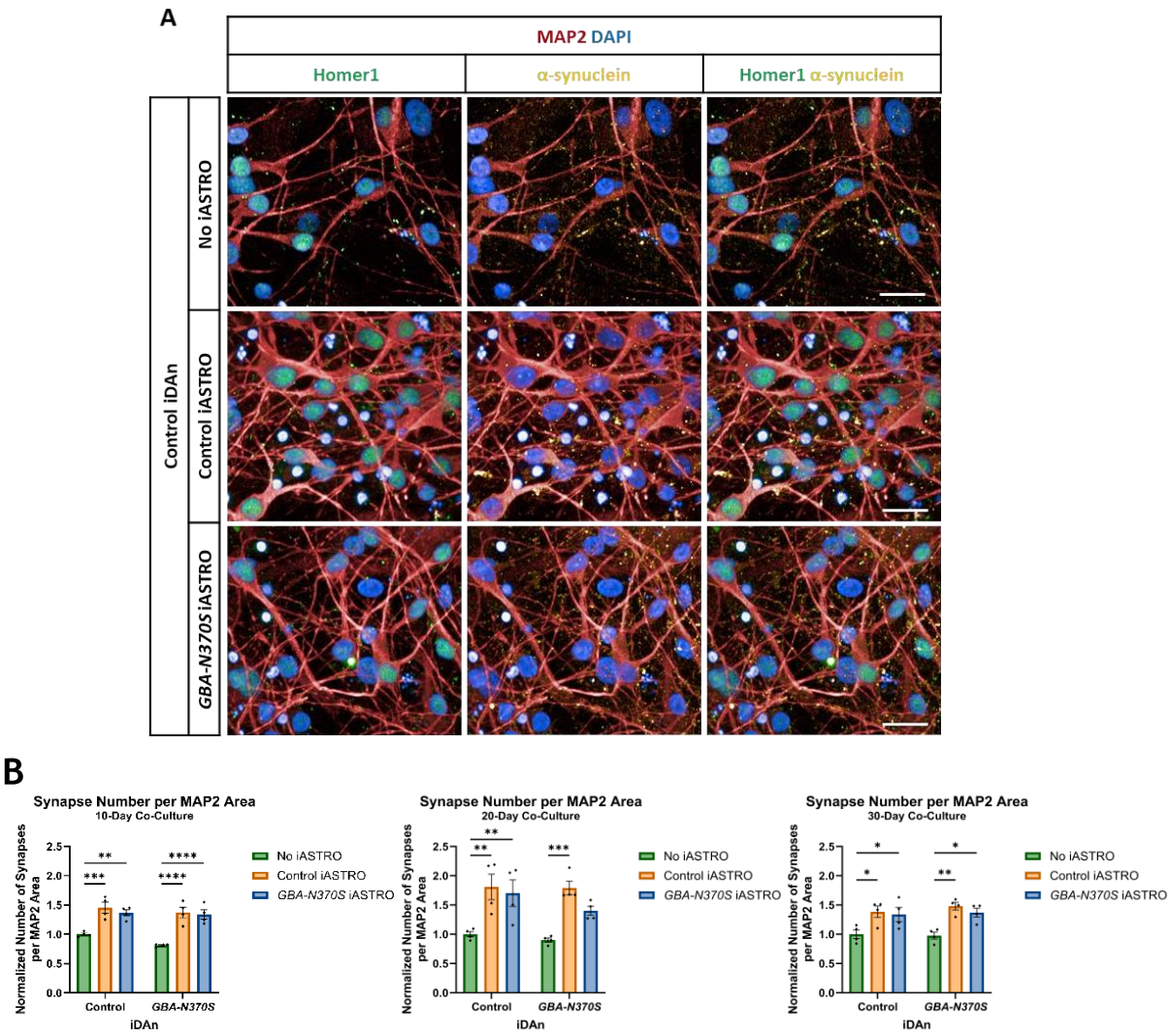


Figure 3.12. Both control and *GBA-N370S* iASTROs support the formation of synapses

(A) Representative immunocytochemistry images of control iDAn in mono-culture or in co-culture for 20 days with control or *GBA-N370S* iASTROs, strained for MAP2 (red), Homer1 (green) and α-synuclein (yellow). Scale bar: 25 µm. (B) Quantification of the number of synapses per MAP2 area in control and *GBA-N370S* iDAn mono-cultures or in co-cultures with control and *GBA-N370S* iASTROs for 10, 20 or 30 days. Each data point represents 1 iDAn line, averaged in each differentiation to all the conditions either in mono-culture or co-cultured with 2 lines of iASTROs of each genotype, and then averaged across differentiations. For each differentiation, values were normalized to the average of control iDAn in mono-culture. N = 3 control and 3 *GBA-N370S* lines for iDAn (3 differentiations), and N = 3 control and 3 *GBA-N370S* lines for iASTROs (1-3 differentiations). Mean ± SEM. The statistical analysis performed was two-way ANOVA with Tukey's multiple comparison test. *p<0.05, **p<0.01, ***p<0.001, ****p<0.0001.

3.7. Discussion

The two main aims of this chapter were: first, to differentiate and characterize control and *GBA-N370S* iPSC-derived ventral midbrain-specific astrocytes (iASTROs), and secondly, to investigate whether the *GBA-N370S* mutation caused any alterations in the cell-autonomous and non-cell autonomous functions of iASTROs. To obtain midbrain-specific iASTROs, I followed a protocol developed by our collaborator Dr Crompton, which was published in 2021 (Crompton et al., 2021). This protocol was chosen because it was designed to generate ventral midbrain-specific astrocytes and thus study astrocytes in the context of PD. Since the goal of this project was not to develop or optimize an iASTRO differentiation protocol, no steps were taken towards this end, and any modifications done to the original protocol were to adjust the cell maintenance and passage methods to the standard operating procedures used in our lab.

Throughout this chapter and the rest of the thesis, in multiple experiments there is a disparity in the number of iASTRO lines used per genotype and the number of differentiations per line. This inconsistency comes from the high line-to-line and differentiation-to-differentiation variability of iASTROs. Indeed, not every iPSC line used in this project differentiated into mature iASTROs in every single differentiation, for yet unknown reasons. Thus, lines that had a high proliferative capacity after day 90 and/or had a morphology that suggested a reverted differentiation with neural progenitor cell morphology were discarded and not used for the experiments of that differentiation. The variability observed could partially be due to the length of the protocol, as the longer it is the higher the chance for differences to occur, but it could also be due to the innate heterogeneity of astroglia in the human brain. In fact, astrocytes are the most heterogeneous cell type in the CNS, and they present transcriptomic, morphological and functional differences depending on the brain region, developmental stage, aging, and pathogenic state, amongst other factors (Hasel et al., 2023). Studies in iPSC-derived astrocytes have shown how their transcriptome and functional properties differ depending on the specific regional identity they acquire during the differentiation process (Bradley et al., 2019).

The differences observed in astrocytes across different brain regions highlights the importance of using an astrocytic cell model that most closely resembles the astrocytes of the brain region of interest. In the case of PD, this would the substantia nigra, and thus, ventral midbrain astrocytes. The specific properties of glial cells in the midbrain have been explored for years

(Garcia-Abreu et al., 1995). Indeed, studies have shown that ventral midbrain-specific iPSC-derived astrocytes are more neurosupportive and neuroprotective to iDAn than iPSC-derived astrocytes without a regional specification (Yeon et al., 2023), as well as the differences between iPSC-derived astrocytes with midbrain or forebrain patterning (Nam et al., 2024). Moreover, the secretory profile of iPSC-derived astrocytes reflects their regional identity (Clarke et al., 2020; Crompton et al., 2023). Nevertheless, many studies using iPSC-derived astrocytes have failed to specify or characterize their regional identity (Aflaki et al., 2020; Cheng et al., 2020; di Domenico et al., 2019; Nonaka et al., 2024; Ramos-Gonzalez et al., 2021), which raises doubts about the validity of their model to answer the specific disease questions they pose. For example, in a few studies, midbrain specific iPSC-derived neurons were co-cultured with iPSC-derived astrocytes without any regional specification (di Domenico et al., 2019; Du et al., 2018; Tsunemi et al., 2020), making the findings of these studies less translatable than if human midbrain-specific astrocytes were used. A current hot topic in the field of PD is to investigate what makes DAn of the substantia nigra the most vulnerable neuronal population in PD. This could be due to intrinsic characteristics of DAn, but also due to the region-specific environment they are surrounded with and the cells they interact with, such as midbrain-specific astrocytes. Therefore, if the interaction between DAn and astrocytes in PD is to be analysed, this should be done using midbrain-specific astrocytes.

Staining of cells at different points of the iASTRO differentiation protocol with the midbrain marker Foxa2 showed that at day 30 and 60 almost every cell in the culture was Foxa2-positive, whereas by day 100 the ratio was reduced to about 0.75. This reduction in Foxa2-positive cells is related to the transcriptomic data collected by RNAseq and RT-qPCR, which shows that Foxa2 is lowly expressed in these cells (data not shown). However, due to the role of Foxa2 in organ development and cellular differentiation (Liu et al., 2024), it might be expressed at lower levels in mature, non-proliferative cells and thus be harder to detect (Ásgrímsdóttir & Arenas, 2020). Others using midbrain specific iPSC-derived astrocytes have also reported this decrease in Foxa2 expression at later stages of the differentiation (Booth et al., 2019). To further validate the regional specificity and astrocytic identity of iASTROs, comparison of bulk RNAseq iASTRO transcriptomic data with bulk RNAseq data from different iPSC-derived cell models and human scRNAseq data demonstrated that iASTROs most closely clustered with iPSC-derived

midbrain-specific astrocytes and human midbrain astrocytes, providing strong proof that our iASTROs are a valid and useful in vitro model of human midbrain astrocytes.

Further characterization of iASTROs by immunocytochemistry and RT-qPCR showed that as cells differentiate and become mature expression of astrocytic markers goes up, whereas expression of progenitor cell and proliferation markers goes down. In addition, comparison with iDAn showed that iASTROs express negligible amounts of neuronal markers. Furthermore, immunocytochemical examination of iASTROs showed that cells acquired a complex astrocytic morphology, but it also highlighted the morphological heterogeneity between different lines and between different cells of the same line, without significant differences between control and *GBA-N370S* iASTROs. This observation directly correlates to the heterogeneity of astrocytes described above, and it is not unique to our iASTRO model but to all studies using this model, as the morphology of these cells greatly differs between studies, the lines within a study, and the cells within a line. A detailed comparison of all the iASTRO morphologies published would take a whole chapter by itself, but to end this topic, it is important to bear in mind to what extent this heterogeneity will affect the reproducibility and translatability of the published studies.

As a final note on iASTRO characterization, staining iASTROs for GFAP showed a big variability in the intensity between cells, with a few iASTROs staining very brightly whereas most cells in the culture had very low signal. This pattern of GFAP immunostaining has also been observed by others (Perriot et al., 2018). Although GFAP has widely been used as an astrocytic marker for over 50 years, research has shown that its expression is not detected in all astrocytes (Messing & Brenner, 2020), and neither can it be used to identify fine processes and the more complex morphologies of astrocytes (Bushong et al., 2002). Thus, for most of our iDAn-iASTRO co-culture experiments, S100B was chosen as the astrocytic marker, as most cells were stained homogenously.

Functional characterization of iASTROs showed that ATP-induced calcium release from the ER was higher in day 100 iASTROs than at earlier timepoints in the differentiation process, and this release was lower in *GBA-N370S* iASTROs. Similar observations have been made in *LRRK2-G2019S* iASTROs by others (Ramos-Gonzalez et al., 2021; Sonninen et al., 2020), as well as *GBA-N370S* iDAn (Beccano-Kelly et al., 2023). On the other hand, both control and *GBA-N370S* iASTROs showed similar capacity to take up glutamate, demonstrating their functional

maturity but indicating that this process is not affected by the *GBA-N370S* mutation. Similarly, Sonninen and colleagues also showed that the glutamate uptake capacity of iASTROs is not diminished due to the *LRRK2-G2019S* or *GBA-N370S* mutation (Sonninen et al., 2020).

On another note, reduced GCase enzymatic activity due to the *GBA-N370S* mutation has been widely demonstrated in multiple models, such as mice (Taguchi et al., 2017), human fibroblasts (Sanchez-Martinez et al., 2016), human iDAn (Bogetofte et al., 2023; Fernandes et al., 2016; Grigor'eva et al., 2023; Rosety et al., 2023; Schöndorf et al., 2014; Woodard et al., 2014), human blood samples (Alcalay et al., 2015), and iASTROs (Aflaki et al., 2020). Indeed, our results indicate that *GBA-N370S* iDAn have reduced GCase activity compared to control iDAn. On the contrary, I did not detect a significant reduction in GCase activity in *GBA-N370S* iASTROs, which does not correlate with the reduction in *GBA-N370S* iASTROs reported by Aflaki and colleagues (Aflaki et al., 2020). However, in this study they also showed a big reduction in the expression levels of the GCase protein, whereas I did not observe changes in its expression at the transcript level, which could explain the differences observed in the enzymatic activity between both studies. To further validate our findings, GCase protein levels would have to be quantified in control and *GBA-N370S* iASTROs to see if there are differences at the protein level depending on the genotype. Furthermore, even if previous transcriptomic studies have revealed that *GBA1* is more highly expressed in astrocytes than in neurons (Zhang et al., 2016), I observed similar expression levels.

In addition, in this chapter I showed how a direct iDAn-iASTRO co-culture was successfully established and optimized, which allowed to maintain both cell types for at least 30 days. With the interest in the role of astrocytes in PD and other neurological diseases increasing, multiple co-culture platforms have been developed to study the interactions between DAn and astrocytes (Aflaki et al., 2020; Barbar et al., 2020; Cheng et al., 2020; de Rus Jacquet, 2019; di Domenico et al., 2019; Hyvärinen et al., 2019; Tsunemi et al., 2020; Whitehouse et al., 2023; Yeon et al., 2023). I opted to use a direct co-culture system, where iASTROs were added on top of iDAn in 96-well plates, because I wanted both cell populations to be in direct contact. Additionally, I showed that a media composed of 50% iDAn maturation media and 50% iASTRO maturation media was the most optimal for the maintenance of both cell types without compromising the survival of either cell type. Other studies using direct iPSC-derived DAn-astrocyte co-cultures relied on basic medias or DAn maturation medias without the addition

of any factors for astrocytic support (Barbar et al., 2020; Cheng et al., 2020; de Rus Jacquet, 2019; di Domenico et al., 2019), but according to our findings, these media conditions are not the most optimal for astrocytic survival, and this may have had an impact on astrocytic activity and, hence, the conclusions drawn in these studies.

Next, I set out to investigate how the *GBA-N370S* mutation in either cell type would affect the interaction between both cell types. Particularly, I was interested in studying if *GBA-N370S* iASTROs were less neurosupportive to iDAn than control iASTROs, and whether *GBA-N370S* iDAn caused cellular alterations in control iASTROs. The cell-autonomous dysfunctions in *GBA-N370S* iDAn have been widely reported, with multiple studies showing that, in the context of PD *GBA-N370S* iDAn present lipidomic alterations (Rosety et al., 2023), calcium dysregulation (Beccano-Kelly et al., 2023), altered mitochondrial function and stress (Beccano-Kelly et al., 2023), reduced dopamine synthesis and release (Woodard et al., 2014), increase in α-synuclein content (Fiore et al., 2022; Woodard et al., 2014) and release (Fernandes et al., 2016; Papadopoulos et al., 2018), autophagy and ER stress (Fernandes et al., 2016; Schöndorf et al., 2014), and impaired neuritogenesis (Bogetofte et al., 2023). However, it is not known if and how these alterations might affect astrocytes, and whether astrocytes are able to rescue some of these disease phenotypes.

As expected, I saw an increase in the number of TH- and MAP2-positive neurons when iDAn were in the presence of control or *GBA-N370S* iASTROs as opposed to in mono-culture, and this observation was also accompanied by an increase in the number of synapses in the co-cultures. The higher number of neurons in the co-cultures does not seem to be caused by an increase in iDAn proliferation, as very little increases in MAP2/Ki67-positive cells were detected in the co-cultures. Therefore, these results demonstrate the neurosupportive activity of the iASTROs used in this study, but the data suggests that this essential function of astrocytes to support neurons is not affected by the *GBA-N370S* mutation. The neurosupportive activity of iPSC-derived astrocytes in direct co-culture has been reported by others and used to validate the model (Barbar et al., 2020; Li et al., 2018; TCW et al., 2017). On the contrary, a study using control iPSC-derived DAn and astrocytes did not observe an increase in TH- and Tuj1-positive neurons when DAn were in co-culture with astrocytes (Cheng et al., 2020). However, this could be explained by the fact that all cultures were maintained in iDAn maturation media, which is optimized to support the growth and survival of iDAn in

mono-culture and might mask any additional support provided by astrocytes. As for other PD-related mutations, di Domenico and colleagues showed that *LRRK2-G2019S* iASTROs were less supportive to control and *LRRK2-G2019S* iDAn than control iASTROs, and their data suggests that *LRRK2-G2019S* iASTROs induce a neurodegenerative phenotype in control iDAn (di Domenico et al., 2019). Similar observations were done by another study using *LRRK2-G2019S* iPSC-derived astrocytes (de Rus Jacquet et al., 2021). These results are in line with the findings that *LRRK2-G2019S* iASTROs have altered calcium signalling, mitochondrial dysfunction, morphological atrophy, increased reactivity, and impaired extracellular vesicle biogenesis (de Rus Jacquet et al., 2021; Pons-Espinal et al., 2024; Ramos-Gonzalez et al., 2021), which might directly affect neuron-astrocyte crosstalk. Therefore, *LRRK2-G2019S* iASTROs might undergo more cellular alterations and thus are less neurosupportive than control or *GBA-N370S* iASTROs. However, more studies using iPSC lines harbouring different PD-related mutations are needed to draw better conclusions on the effects of each mutation on the neurosupportive, neurotrophic and neuroprotective function of astrocytes in PD.

As for iASTROs in co-cultures, I observed an increase in the cytoplasmic S100B intensity in control and *GBA-N370S* iASTROs co-cultured with *GBA-N370S* iDAn compared to control iDAn, suggesting that iASTROs undergo slightly different cellular processes and reactive responses when interacting with *GBA-N370S* iDAn. To further study this potential effect of *GBA-N370S* iDAn on iASTROs, I conducted an experiment where control and *GBA-N370S* iASTROs were fed with neuron conditioned media (NCM) taken from control or *GBA-N370S* iDAn for 72h, 7, 14 or 21 days. This experiment was only conducted in 1 differentiation, and no effects in the reactivity of iASTROs were observed depending on the iDAn genotype the NCM was derived from (data not shown). However, to get more conclusive results, this experiment should be repeated in at least 2 independent differentiations. Additionally, transwell systems where iASTRO and iDAn are not in direct contact could also be used to investigate whether the factors secreted by *GBA-N370S* iDAn are sufficient to induce the increase in S100B intensity in iASTROs or whether direct cell-to-cell contact between both cell populations is needed. As for the mechanism, there are multiple ways by which *GBA-N370S* iDAn could induce a reactive response in iASTROs, such as the increase in α-synuclein content (Fiore et al., 2022; Woodard et al., 2014) and release (Fernandes et al., 2016; Papadopoulos et al., 2018), which would be transferred and taken up by iASTROs and induce a reactive response for example. Moreover,

other cellular alterations described in *GBA-N370S* iDAn by different studies (Beccano-Kelly et al., 2023; Bogetofte et al., 2023; Fernandes et al., 2016; Grigor'eva et al., 2023; Schöndorf et al., 2014) could be detected by iASTROs, causing them to adapt and react accordingly.

Very little data is available on the effect of PD iDAn on astrocytes. In the aforementioned study by di Domenico and colleagues, they did not present properly controlled experiments comparing the effects of control or *LRRK2-G2019S* iDAn on iASTROs in co-culture (di Domenico et al., 2019). Thus, more studies are needed using multiple mixed genotype co-culture conditions to determine the effect of iDAn carrying PD-related mutations on astrocytes.

In conclusion, in this chapter I generated and characterized mature and functional control and *GBA-N370S* iPSC-derived midbrain specific astrocytes. Little cell autonomous differences were observed in iASTROs due to the *GBA-N370S* mutation, except a smaller release in ER-calcium after ATP application. Moreover, after developing a direct iASTRO-iDAn co-culture system, I showed how both control and *GBA-N370S* iASTROs supported neuronal survival and health in a similar way, whereas iASTROs underwent different responses in the presence of iDAn carrying the *GBA-N370S* mutation.

Chapter 4 - Studying the reactive response of control and *GBA-N370S* iASTROs to inflammatory stimuli and α-synuclein pre-formed fibrils

4.1. Introduction and aims

Neuroinflammation is now considered one of the main hallmarks of PD, and it is believed to play an important role in disease onset and progression. However, it is not well understood whether neuroinflammation has protective or deleterious effects in PD pathogenesis, or how this might change throughout the course of the disease. Inflammation in PD occurs by both adaptive and innate immune responses, which are driven by peripheral immune cells (e.g. T cells) and CNS immune cells (microglia and astrocytes), respectively (Jurcau et al., 2023).

Although microglia are the main resident immune cells of the CNS, astrocytes are also capable of responding to different inflammatory and pathogenic stimuli. When doing so, astrocytes undergo vast transcriptional, morphological and functional changes in a process normally referred to as astrogliosis. This response highly depends on the specific trigger, the brain region, age, and the disease state, amongst other factors (Escartin et al., 2021). A study in 2012 proposed a binary categorization to classify reactive astrocytes into A1 (neurotoxic) or A2 (neuroprotective) (Zamanian et al., 2012), and later, a paper showed that a combination of 3 cytokines released by reactive microglia (TNFα, IL-1α and C1q) induced the acquisition of the A1 phenotype in astrocytes (Liddelow et al., 2017). However, emerging data shows that this classification is oversimplistic and does not illustrate the very complex and dynamic reactive phenotypes astrocytes can acquire (Escartin et al., 2021).

On the other hand, there is evidence showing that exposure to WT or mutant α-synuclein species can induce astrogliosis and also result in dysfunction of various astrocytic cellular processes (Lee et al., 2010; Lindström et al., 2017; Rannikko et al., 2015). However, most of these studies have been conducted in rodents or primary cell cultures, and the current data available on human iPSC-derived astrocytes is scarce and inconclusive, as some report inflammatory changes after exposure to α-synuclein species whereas others do not (Russ et al., 2021; Sanyal et al., 2020). Similarly, little information is available regarding the effects *GBA1* mutations have on astrocyte reactivity and their response to α-synuclein. Mutations in

GBA1 and resulting alterations in GCase activity have been linked to neuroinflammation, partially due to the impact of GCase dysfunction in lipid homeostasis (Bo et al., 2022), but studies in human in vitro models are lacking.

The aims of this chapter are:

- To characterize the acute response of control iASTROs to different combinations of inflammatory cytokines and α-synuclein PFFs through transcriptomic analysis.
- To validate the hits of interest from the RNAseq data in vitro.
- To study the inflammatory response of control and *GBA-N370S* iASTROs to different combinations of inflammatory cytokine treatments over time.
- To study the response of control and *GBA-N370S* iASTROs to α-synuclein PFFs, with or without inflammatory cytokines, over time.

4.2. Bulk RNA sequencing of control iASTROs treated with different combinations of inflammatory cytokines and α-synuclein PFFs

Preliminary experiments not shown in this thesis (immunocytochemistry and RT-qPCR of inflammatory markers in iASTROs treated with inflammatory cytokines) demonstrated the capacity of iASTROs to respond to inflammatory cytokines. This observation was followed up by an in-depth transcriptomic analysis using bulk RNAseq to explore the acute transcriptional changes that occur in iASTROs treated with a range of inflammatory cytokines, α-synuclein PFFs, and a combination of cytokines and PFFs. 3 control iASTROs lines (67, 156, 840) at DIV100 were used in this experiment after verifying their astrocytic identity and functional maturity. Only control iASTROs were chosen for this study for two main reasons: the large number of samples required, and, to provide an overview of the astrocytic response to the treatments, regardless of the genotype, that would enable more relevant comparisons with published datasets. iASTROs were subjected to the different treatments for 24h prior to RNA extraction and subsequent sequencing, and this timepoint was chosen based on other published studies, as were the treatments and concentrations used.

I decided to investigate the response of iASTROs to multiple inflammatory cytokines and a combination of these cytokines, because it is now accepted that astrocytes undergo dynamic and context dependent cellular changes that vary greatly due to multiple factors, including the specific cytokines they are stimulated with (Escartin et al., 2021). Most studies exploring the inflammatory response of iPSC-derived astrocytes have used TNFα, found to be elevated in the CSF of PD patients (Mogi et al., 1994), alone or in combination with other inflammatory cytokines to induce astrogliosis (Ma et al., 2022; Perriot et al., 2018; Russ et al., 2021; Smith et al., 2022; Spreng et al., 2022). Additionally, numerous studies have used the combination of TNFα+IL-1α+C1q, described by Liddelow and colleagues (Liddelow et al., 2017), to induce astrocyte reactivity (Barbar et al., 2020; Labib et al., 2022; Leng et al., 2022). On the other hand, the response of iPSC-derived astrocytes to IFNγ, which has been found to be increased in the nigrostriatal region of PD patients (Mogi et al., 2007) and is released by infiltrating cytotoxic T cells (Contaldi et al., 2022), has been less explored. Moreover, the combined treatment of TNFα and IFNγ was used to explore the interaction between these two cytokines and determine whether in iASTROs they acted on an additive or synergistic manner, as previously reported in other models (Barcia et al., 2011; Spreng et al., 2022; Woznicki et al., 2021). Lastly, due to the lack of data regarding the effect of α-synuclein PFFs, alone or in combination with inflammatory cytokines, on astrocyte reactivity, these treatments were also included in the experiments.

DIV100 iASTROs were treated for 24h with: TNFα (30 ng/mL) (T), IFNγ (50 ng/mL) (IF), TNFα (30 ng/mL) + IFNγ (50 ng/mL) (TIF), the Liddelow factors (30 ng/mL TNFα + 3 ng/mL IL-1α + 400 ng/mL C1q) (LID), α-synuclein PFFs (10 µg/mL) (PFF), and TNFα (30 ng/mL) + IFNγ (50 ng/mL) + α-synuclein PFFs (10 µg/mL) (PTIF). An untreated control was also included (C). RNA was then extracted and sent for QC analysis and sequencing to Novogene (details can be found in section 2.12). A replica 24-well plate was prepared and treated in the exact same way in parallel, which was frozen and stored at -80°C. This plate was later used to validate the hits of interest and the primers used for subsequent RT-qPCR experiments.

Raw reads obtained from Novogene were aligned to a reference human transcriptome (Ensembl GRCh38 release 97), quantified using Salmon (Patro et al., 2017), and the quant.fz files generated were imported into R (v4.3.2) using tximeta (Love et al., 2020). Next, genes that had a total sum of less than 30 counts across all 21 samples and genes that had 0 counts

in 75% or more of the samples, were filtered out prior to doing the differential gene expression analysis. This pre-filtering resulted in a total of 17,459 genes, which were used for differential gene expression analysis with DESeq2 (Love et al., 2014).

4.2.1. Initial data quality assessment

After running DESeq2, a data quality assessment was done to ensure the quality of the data, the overall effect of the treatments, and the variability between the biological replicates (i.e. the 3 different iASTRO lines). Principal component analysis (PCA) of the top 500 most variable genes across treatments and cell lines showed that most of the variance (60%) came from the treatment, and 18% of the variance came from the cell lines (Figure 4.1 A). In each line, the variation resulting from the treatment was very similar, and, across treatments, the variation resulting from the lines was very similar. This demonstrated that the response of iASTROs to each of the treatments was very consistent across all 3 lines. Clustering in the PCA plot showed very little variability between untreated cells and PFF-treated cells, as well as between cells treated with TNFα+IFNγ and TNFα+IFNγ+PFFs. Cells treated with TNFα alone or the Liddelow factors also clustered closely together. Lastly, IFNγ-treated cells clustered separately from all other treatments, and caused bigger transcriptional changes than TNFα alone or the Liddelow factors. The sample-to-sample distance heatmap showed a similar clustering (Figure 4.1 B).

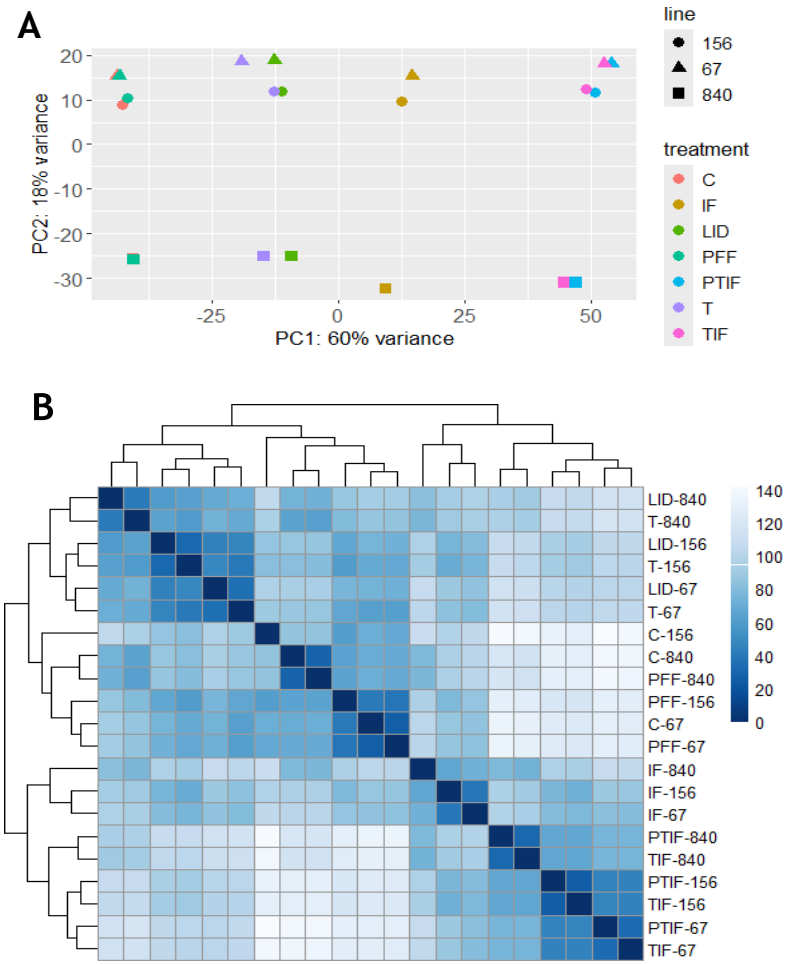


Figure 4.1. RNAseq analysis of control iASTROs treated for 24h with different combinations of inflammatory cytokines and α-synuclein PFFs shows sample clustering according to treatment
(A) PCA plot and (B) heatmap showing sample-to-sample distances of 3 control iASTRO lines (156, 67, 840), untreated (C) or treated for 24h with 50 ng/mL IFNγ (IF), the Liddelow factors (30 ng/mL TNFα + 3 ng/mL IL-1α + 400 ng/mL C1q, LID), 10 µg/mL α-synuclein PFFs (PFF), 10 µg/mL α-synuclein PFFs + 30 ng/mL TNFα + 50 ng/mL IFNγ (PTIF), 30 ng/mL TNFα (T) or 30 ng/mL TNFα + 50 ng/mL IFNγ (TIF).

4.2.2. Differential gene expression analysis summary

Next, I examined the differentially expressed genes (DEGs) in each of the treatment conditions compared to the untreated control, as well as the DEGs between different treatments. Results are summarised in the volcano plots depicted in Figure 4.2. and Table 4.1. Overall, a slightly higher number of upregulated genes were observed in each comparison, and the magnitude of differential expression (Log_2FoldChange) of upregulated genes was greater than downregulated genes.

Compared to untreated iASTROs (Figure 4.2. A), cells treated with TNFα+IFNγ+PFFs had the highest number of DEGs, 8,446 (Figure 4.1. Avi), closely followed by iASTROs treated with TNFα+IFNγ (8,280 DEGs) (Figure 4.1. Av). In IFNγ-treated iASTROs, the number of DEGs was 4,818 (Figure 4.1. Ai). After treatment with the Liddelow factors, the number of DEGs was 4,793 (Figure 4.1. Aiii), and a smaller number, 3,804 DEGs, were observed in iASTROs treated with TNFα alone (Figure 4.1. Aii). Lastly, the smallest number of DEGs was detected in cells treated with PFFs alone, with only 17 DEGs (Figure 4.1. Aiv). Similarly, when comparing cells treated with TNFα+IFNγ+PFFs with those treated with TNFα+IFNγ, there were only 7 DEGs (Figure 4.1. F). These quantifications further validate the observations in Figure 4.1. that PFFs, either alone or in combination with TNFα+IFNγ, do not cause big transcriptional changes in iASTROs after 24h of treatment.

Regarding DEGs between iASTROs treated with different cytokine treatments, there were 4,450 DEGs in cells treated with IFNγ alone compared to TNFα alone (Figure 4.2. Bi). There were few DEGs, 258, in cells treated with the Liddelow factors compared to TNFα alone (Figure 4.2. Bii), whereas 6,685 DEGs were observed in iASTROs treated with TNFα+IFNγ compared to TNFα alone (Figure 4.2. Biii). Comparing to iASTROs treated with the Liddelow factors, there were 4,946 DEGs in iASTROs treated with IFNγ (Figure 4.2. Ci) and 6,857 in cells treated with TNFα+IFNγ (Figure 4.2 Cii). Moreover, there were 4,960 DEGs in iASTROs treated with TNFα+IFNγ versus IFNγ alone (Figure 4.2. D). Lastly, a similar number of DEGs were observed between iASTROs treated with TNFα+IFNγ or TNFα+IFNγ+PFFs and PFFs, 8,137 and 8,271 DEGs respectively (Figure 4.2. Ei-ii). Overall, these results show vast changes in gene expression in iASTROs treated for 24h with inflammatory cytokines, especially the combined treatment of TNFα and IFNγ, but very little effect after exposure to α-synuclein PFFs. Furthermore, these observations indicate that TNFα and IFNγ act synergistically as opposed to additively.

Table 4.1. Number of DEGs, upregulated and downregulated genes

Comparison	DEGs	Log_2FoldChange>0	Log_2FoldChange<0	Log_2FoldChange>1.5	Log_2FoldChange<-1.5
Control vs TNFα	3,804	1,936	1,868	582	434
Control vs Liddelow Factors	4,793	2,445	2,348	756	601
Control vs IFNγ	4,818	2,461	2,357	744	593
Control vs TNFα+IFNγ	8,280	4,235	4,045	1,675	1,411
Control vs α-synuclein PFFs	17	6	11	5	2
Control vs TNFα+IFNγ+PFFs	8,446	4,282	4,164	1,683	1,540
TNFα vs Liddelow Factors	258	183	75	88	19
TNFα vs IFNγ	4,450	2,378	2,072	711	645
TNFα vs TNFα+IFNγ	6,685	3,610	3,075	1,312	843
Liddelow Factors vs IFNγ	4,946	2,602	2,344	749	760
Liddelow Factors vs TNFα+IFNγ	6,857	3,680	3,177	1,273	923
IFNγ vs TNFα+IFNγ	4,960	2,709	2,251	900	494
PFFs vs TNFα+IFNγ+PFFs	8,271	4,204	4,067	1,685	1,487
PFFs vs TNFα+IFNγ	8,137	4,193	3,944	1,659	1,349
TNFα+IFNγ vs TNFα+IFNγ+PFFs	7	1	6	0	5

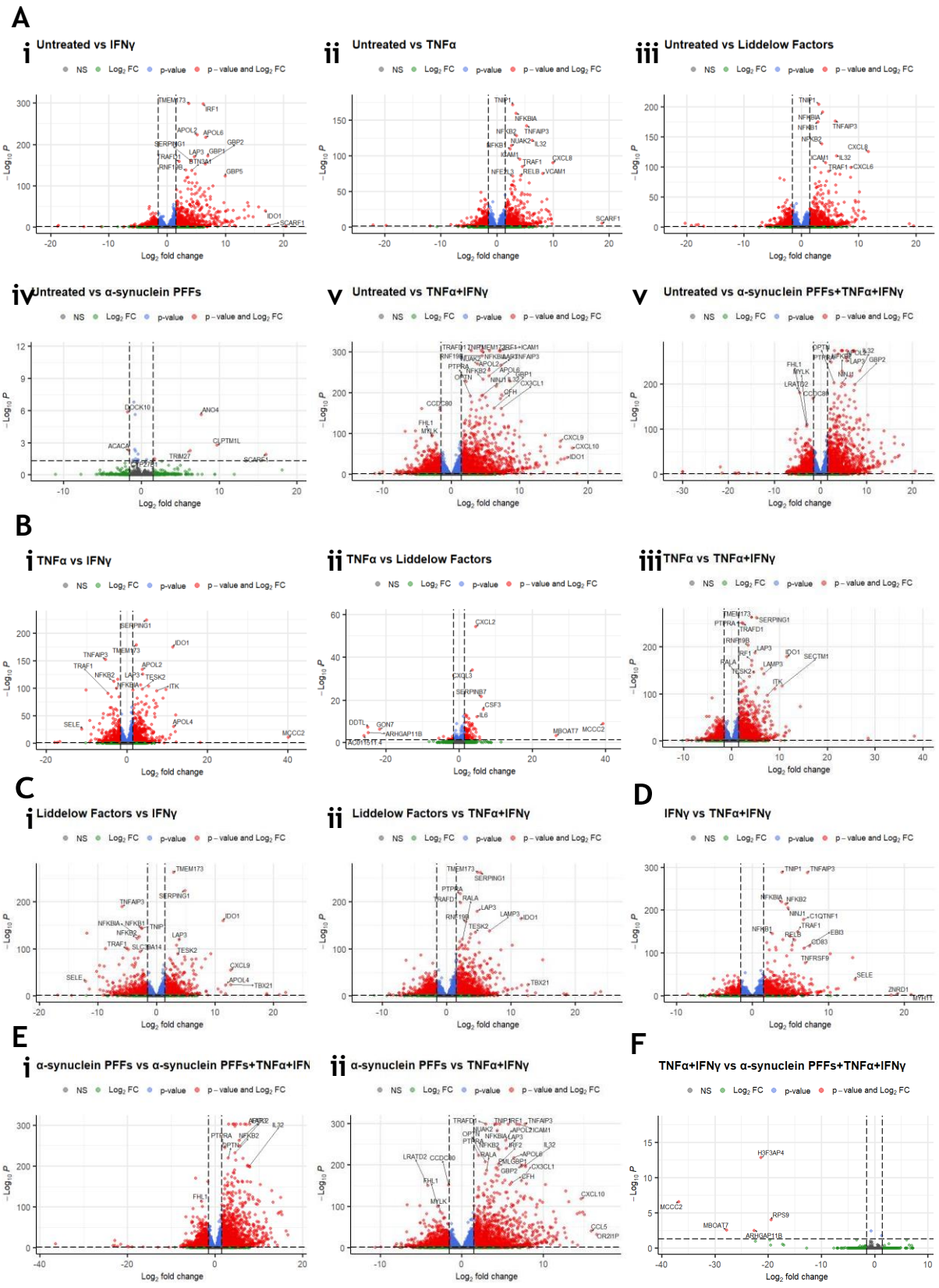


Figure 4.2. Volcano plots displaying the statistical significance of the differentially expressed genes between different treatment conditions show very extensive gene expression changes in response to inflammatory cytokines but not α-synuclein PFFs

(A) Volcano plots showing the DEGs in iASTROs treated with (i) IFNγ, (ii) TNFα, (iii), the Liddelow factors (TNFα + IL-1α + C1q), (iv) α-synuclein PFFs, (v) TNFα + IFNγ, and (vi) α-synuclein PFFs + TNFα + IFNγ compared to untreated iASTROs. (B) Volcano plots showing the DEGs in iASTROs treated with (i) IFNγ, (ii) the Liddelow factors (TNFα + IL-1α + C1q), and (iii) TNFα + IFNγ compared to iASTROs treated with TNFα. (C) Volcano plots showing the DEGs in iASTROs treated with (i) IFNγ and (ii) TNFα + IFNγ compared to iASTROs treated with the Liddelow factors (TNFα + IL-1α + C1q). (D) Volcano plots showing the DEGs in iASTROs treated with TNFα + IFNγ compared to iASTROs treated with IFNγ. (E) Volcano plots showing the DEGs in iASTROs treated with (i) α-synuclein PFFs + TNFα + IFNγ, and (ii) TNFα + IFNγ compared to iASTROs treated with α-synuclein PFFs. (F) Volcano plots showing the DEGs in iASTROs treated with α-synuclein PFFs + TNFα + IFNγ compared to iASTROs treated with TNFα + IFNγ. Each dot represents one gene. Grey dots represent not differentially expressed genes; green dots represent genes with a Log_2FoldChange<-1.5 or >1.5 but a padj>0.05, blue dots represent genes with a padj<0.05 but a Log_2FoldChange>-1.5 and <1.5; red dots represent genes with a Log_2FoldChange<-1.5 or >1.5 and padj<0.05. All treatment concentrations are as follows: 30 ng/mL TNFα, 50 ng/mL IFNγ, the Liddelow factors (30 ng/mL TNFα + 3 ng/mL IL-1α + 400 ng/mL C1q), 10 µg/mL α-synuclein PFFs, 10 µg/mL α-synuclein PFFs + 30 ng/mL TNFα + 50 ng/mL IFNγ, and 30 ng/mL TNFα + 50 ng/mL IFNγ.

4.2.3. Gene set enrichment analysis overview

Next, gene set enrichment analysis (GSEA) was performed to identify the terms over-represented in the genes upregulated or downregulated in iASTROs in response to the different treatments. The Gene Ontology: Biological Process (GO:BP) gene sets were used in the analysis, only using gene sets bigger than 3 and smaller than 500. The p-value adjustment method used was Benjamini-Hochberg (BH), and the padj cutoff was set to 0.05. In each comparison, all DEGs (padj<0.05) were used in the analysis, without a Log_2FoldChange cut off. Table 4.2. summarizes the number of activated and suppressed GO:BP terms in each comparison, and Figures 4.3 and 4.5 provide an overview of the top 15 activated and suppressed terms in each comparison. Overall, the number of activated GO:BP terms was much higher than the number of suppressed terms (excepting Liddelow Factors vs IFNγ). In some comparisons (TNFα vs Liddelow Factors and TNFα+IFNγ vs TNFα+IFNγ+PFFs), due to the low number of DEGs, no significantly suppressed or activated GO:BP terms were found.

As expected, the highest number of activated terms was observed when comparing iASTROs treated with TNFα+IFNγ+PFFs with untreated iASTROs, closely followed by the comparison with TNFα+IFNγ-treated iASTROs. On the other hand, when compared to untreated iASTROs, there was a higher number of both activated and suppressed terms in iASTROs treated with

the Liddelow factors or TNFα alone than with IFNγ alone. Lastly, there were only 2 activated terms in PFF-treated iASTROs compared to the untreated cells, and the p values were relatively high (padj = 0.034). As for the comparisons between different treatments, following the pattern of the number of DEGs, a much higher number of activated and suppressed terms were observed in the TNFα vs TNFα+IFNγ comparison than in the TNFα vs IFNγ comparison. Similar observations were done comparing iASTROs treated with the Liddelow factors compared to those treated with TNFα+IFNγ or IFNγ. Lasty, the number of activated terms in iASTROs treated with TNFα+IFNγ and TNFα+IFNγ+PFFs compared to iASTROs treated with PFFs alone was quite similar.

Table 4.2. Number of activated and suppressed GO:BP terms

Comparison	Activated GO:BP Terms	Suppressed GO:BP Terms
Control vs TNFα	559	93
Control vs Liddelow Factors	623	71
Control vs IFNγ	437	51
Control vs TNFα+IFNγ	680	90
Control vs α-synuclein PFFs	2	0
Control vs TNFα+IFNγ+PFFs	729	31
TNFα vs Liddelow Factors	0	0
TNFα vs IFNγ	51	22
TNFα vs TNFα+IFNγ	368	115
Liddelow Factors vs IFNγ	32	68
Liddelow Factors vs TNFα+IFNγ	274	125
IFNγ vs TNFα+IFNγ	392	98
PFFs vs TNFα+IFNγ+PFFs	732	34
PFFs vs TNFα+IFNγ	714	72
TNFα+IFNγ vs TNFα+IFNγ+PFFs	0	0

4.2.4. In-depth analysis of DEGs and enriched GO:BP terms

After having an overview of the degree of transcriptional changes in response to each treatment, I performed an in-depth analysis of the DEGs and the GO:BP terms enriched in each comparison. Due to the large number of DEGs and enriched GO:BP terms, only the most significant and relevant observations will be discussed here.

4.2.4.1. Comparisons between treatments with inflammatory cytokines and the untreated control

Compared to untreated cells, the top upregulated genes after treatment with inflammatory cytokines were genes associated with inflammation (Figure 4.3 A-Ei), such as genes encoding: chemoattracting chemokines (*CXCL1, CXCL2, CXCL3, CXCL5, CXCL8, CXCL9, CXCL10, CXCL11, CCL5*), proteins involved in antigen processing and presentation (*IFI30* (gamma-interferon-inducible lysosomal thiol reductase), *CTSS* (cathepsin S)), cell adhesion molecules (*SELE* (E-selectin), *VCAM1* (vascular cell adhesion protein 1)), proteins involved in extracellular matrix remodelling (*MMP9* (matrix metalloproteinase 9)), transcription factors regulating the expression of immune-related genes (*TBX21* (T-box transcription factor 21)), and proteins involved in lymphocyte activation (*SLAMF8* (SLAM family member 8)). These genes were upregulated to different extents depending on the treatment, and the degree of differential expression in cells treated with TNFα+IFNγ was much greater than the sum in cells treated with TNFα alone and IFNγ alone. All the main activated GO:BP terms in cells treated with inflammatory cytokines were also terms involved in the immune response, including terms related to response to cytokines, cytokine production, lymphocyte activation, chemotaxis, etc. (Figure 4.3. A-Eii). Moreover, even if GO:BP terms related to antigen processing and presentation were activated in iASTROs after exposure to cytokines, the genes related in this process (e.g. *TAP1/2, IFI30*, most *HLA* genes) had much higher expression in treatments that included IFNγ.

On the other hand, greater variability was observed regarding the genes and GO:BP terms downregulated in reactive iASTROs. Nonetheless, a number of suppressed GO:BP terms were related to development, such as “muscle tissue development” and “central nervous system development”, and included downregulated genes such as *NOTCH3* (neurogenic locus notch homolog protein 3), *PDGFRB* (platelet-derived growth factor receptor beta) and *KDR* (kinase insert domain receptor/vascular endothelial growth factor receptor 2 (VEGFR-2)). Moreover, there were various suppressed terms related to synaptic signalling or synapse assembly (Figure 4.3 Aii, Dii, Eii), and these terms included the downregulated genes *NTRK2* (tropomyosin receptor kinase B (TrkB)), *DMPK* (myotonin-protein kinase), *CLSTN2* (calsyntenin 2), *NLGN1/2/3* (neuroligin-1/2/3), *CUX2* (cut like homeobox 2) and *EPHB3* (ephrin B3), amongst others. Additionally, GO:BP terms related with neuron morphogenesis and

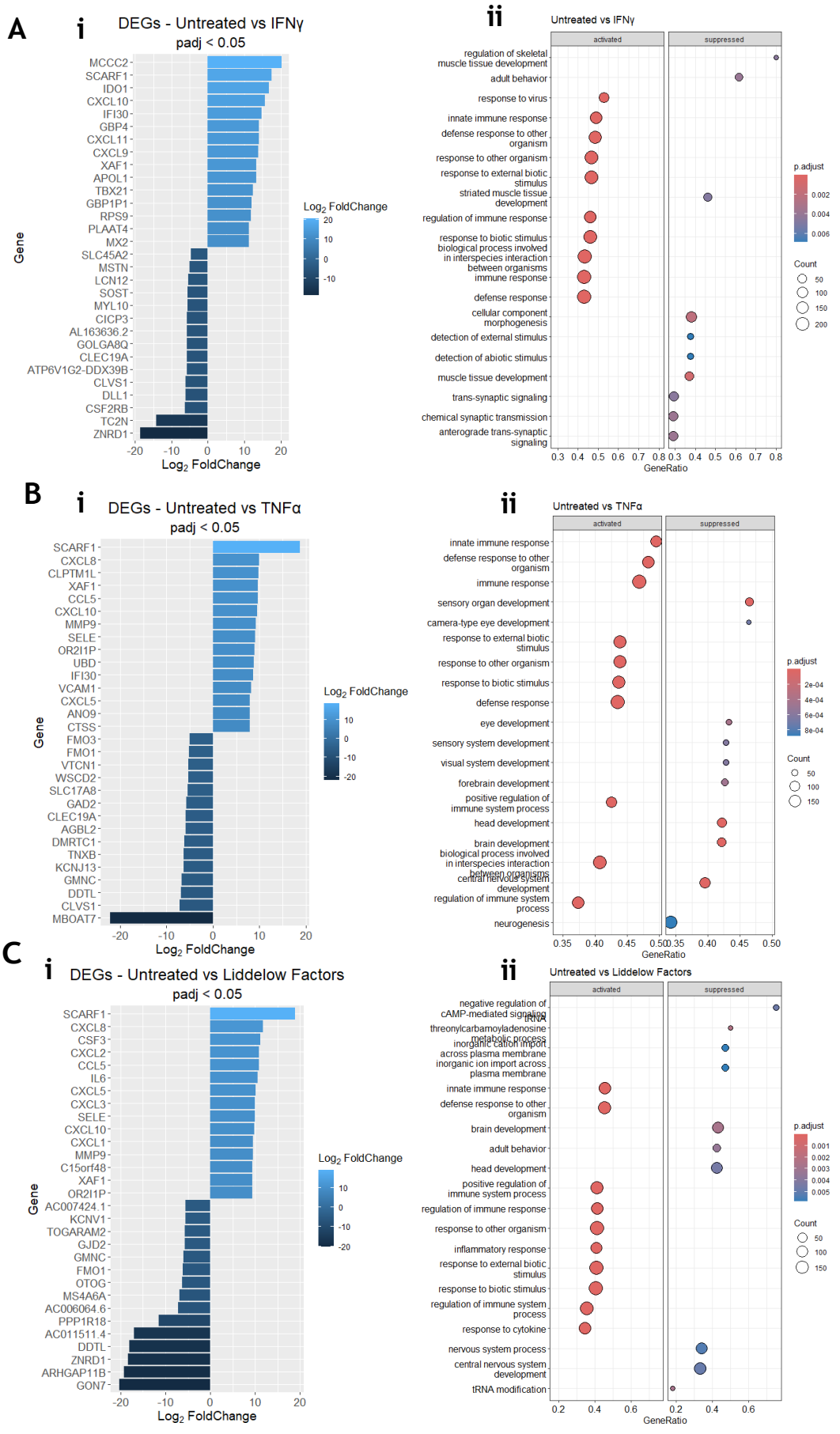
differentiation (e.g. “neuron projection morphogenesis”) were suppressed in reactive iASTROs, and included the genes: *PAX6* (paired box protein Pax-6), *ANK3* (ankyrin-3), *SMO* (smoothened), *NFIB* (nuclear factor 1 B-type), and *EFNB3* (ephrin-B3), amongst others. Similarly, there were suppressed terms related to behaviour, learning and memory, especially in cells treated with TNFα+IFNγ and TNFα+IFNγ+PFFs (Figure 4.3 Aii, Cii, Dii, Eii).

The upregulation of genes and GO:BP terms related to inflammation and the immune response after treatment with inflammatory cytokines was expected (Labib et al., 2022; Spreng et al., 2022), and these observations do not provide significant contributions to the current understanding of the cellular changes that occur during early stages of astrogliosis, nor do they indicate whether reactive iASTROs acquire a neurotoxic or neuroprotective phenotype. Thus, I explored other cellular functions and pathways that might be altered, albeit to a lesser extent, in reactive iASTROs in response to the different treatments. For instance, there were multiple enriched GO:BP terms related to apoptosis and cell death, especially in cells treated with TNFα+IFNγ and TNFα+IFNγ+PFFs. Some of the upregulated genes included in these terms were *LGALS9* (galectin-9), *RIPK1/2* (receptor-interacting serine/threonine-protein kinases 1 and 2), *CD274* (programmed death-ligand 1, PD-L1), *EBF4* (early B-cell factor 4), *FAS* (Fas receptor), and multiple caspase protein-encoding genes (*CASP1, CASP4, CASP7, CASP8, CASP10*). Furthermore, GO:BP terms related to nitric oxide production and oxidative stress were enriched in reactive iASTROs, as were multiple genes encoding proteins with antioxidant function, such as *GPX1* and *GPX4* (glutathione peroxidase 1 and 4), *SOD2* (superoxide dismutase 2), various metallothionein 1 genes (*MT1E, MT1F, MT1M*), *MT2A* (metallothionein 2A), and *PDIA6* (protein disulfide isomerase family A, member 6), amongst others.

In addition, numerous GO:BP terms related to mitosis and chromosome segregation were suppressed in iASTROs treated with TNFα+IFNγ and TNFα+IFNγ+PFFs, whereas they were enriched in iASTROs treated with TNFα and the Liddelow factors. These terms included the genes: *AURKB* (aurora kinase B, AIM-1), *NDC80* (kinetochore protein NDC80 homolog), *CDC20* (cell division cycle protein 20 homolog), *PLK1* (serine/threonine-protein kinase PLK1, polo like kinase 1), and *BIRC5* (baculoviral inhibitor of apoptosis repeat-containing 5, Survivin), amongst others. Overall, all these genes had a relatively low expression in all samples, indicating that

iASTROs have a low proliferative capacity in unstimulated conditions, which are slightly increased or decreased depending on the inflammatory stimuli.

Furthermore, one of the top upregulated genes after treatment with IFNγ was *APOL1*, which encodes apolipoprotein L1, a minor component of high-density lipoprotein (HDL) cholesterol. Numerous other lipoprotein-coding genes, such as *APOL2, APOL3, APOL6* were also upregulated to different extends in response to all treatments with inflammatory cytokines. Expression of other lipid homeostasis-related genes were also dysregulated in reactive iASTROs, including *PTGES* (prostaglandin E synthase), *COX2* (prostaglandin-endoperoxide synthase 2), *FADS2/3* (fatty acid desaturase 2 and 3), *LSS* (lanosterol synthase), and *CYP7B1* (25-hydroxycholesterol 7-alpha-hydroxylase), amongst others. On the contrary, some other genes related with lipid metabolism and homeostasis were downregulated after the treatments, including the genes *CYP46A1* (cholesterol 24-hydroxylase), *FABP7* (fatty acid binding protein 7), and *LPL* (lipoprotein lipase).


A
i
DEGs - Untreated vs IFNγ
padj < 0.05
Gene
Log2 FoldChange
ii
Untreated vs IFNγ
activated
suppressed
GeneRatio
p.adjust
Count
B
i
DEGs - Untreated vs TNFα
padj < 0.05
ii
Untreated vs TNFα
C
i
DEGs - Untreated vs Liddelow Factors
padj < 0.05
ii
Untreated vs Liddelow Factors

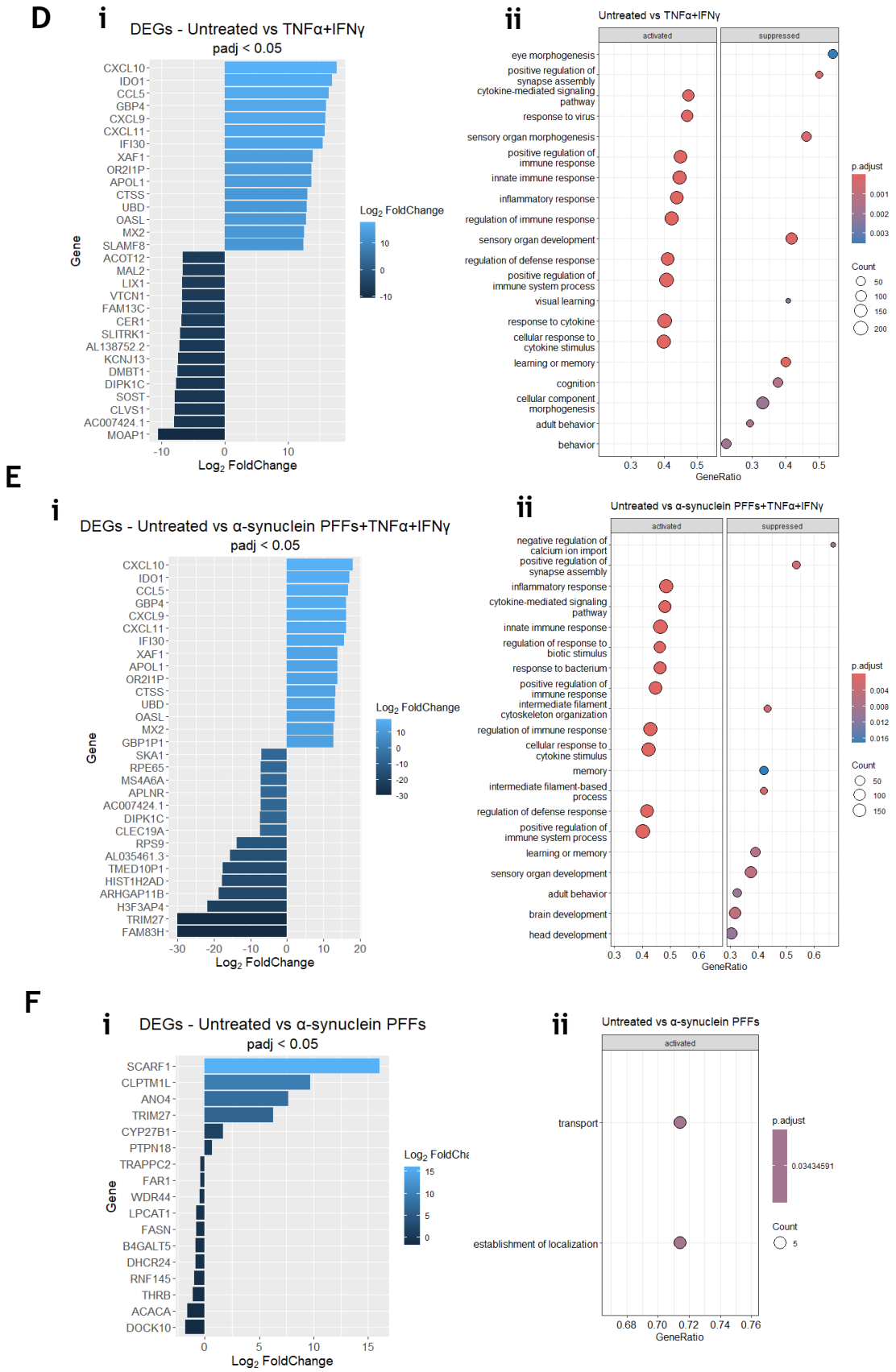


Figure 4.3. Analysis of the main genes and pathways activated and suppressed in iASTROs treated with different combinations of inflammatory cytokines and α-synuclein PFFs compared to untreated iASTROs

Analysis of (i) the top 15 and bottom 15 differentially expressed genes and (ii) the top 10 activated and top 10 suppressed gene ontology biological process terms in control iASTROs treated for 24h with (A) 50 ng/mL IFNγ, (B) 30 ng/mL TNFα, (C) the Liddelow factors (30 ng/mL TNFα + 3 ng/mL IL-1α + 400 ng/mL C1q), (D) 30 ng/mL TNFα + 50 ng/mL IFNγ, (E) 10 µg/mL α-synuclein PFFs + 30 ng/mL TNFα + 50 ng/mL IFNγ and (F) 10 µg/mL α-synuclein PFFs, compared untreated iASTROs. In F, less DEGs and pathways are shown because only those were statistically significant.

4.2.4.2. Comparison between α-synuclein PFF-treated and untreated iASTROs

As mentioned above, α-synuclein PFFs did not trigger major transcriptional changes in iASTROs after 24h of treatment (Figure 4.3. Fi). The 2 most interesting genes upregulated in PFF-treated iASTROs were *CYP27B1* (cytochrome P450 family 27 subfamily B member 1) and *PTPN18* (tyrosine-protein phosphatase non-receptor type 18). On the other hand, most downregulated genes were involved in lipid homeostasis. Of these, the expression of *DHCR24* and *FASN* was lowest in iASTROs treated with PFFs alone and TNFα+IFNγ+PFFs. *RNF145* (ring finger protein 145) was also significantly downregulated in PFF-treated iASTROs, which was one of the few downregulated genes in iASTROs treated with TNFα+IFNγ+PFFs compared to cells treated with TNFα+IFNγ. RNF145 is a E3 ubiquitin ligase, and one of its targets is HMGCR (HMG-CoA reductase) (Jiang et al., 2018), a rate-limiting enzyme in cholesterol homeostasis.

Moreover, only 2 activated GO:BP terms were found in iASTROs treated with PFFs alone, and these were “transport” and “establishment of localization” (Figure 4.3. Fii). Due to the low number of DEGs in PFF-treated iASTROS compared to untreated cells, I decided to use fast gene set enrichment analysis (fgsea), since this analysis takes into account all genes and is not limited to DEGs. Therefore, I used the normalized counts of all the genes in the untreated condition and in iASTROs treated with PFFs alone, and I focused on the hallmark pathways (Liberzon et al., 2015). The top gene sets with the highest positive NES in PFF-treated iASTROs were “Oxidative Phosphorylation”, “Myc Targets V1” and “DNA Repair”, and the ones with the lowest negative NES were “Mitotic Spindle”, “UV Response” and “Cholesterol Homeostasis”. The genes that were most highly downregulated in PFF-treated iASTROs in the “Cholesterol Homeostasis” gene set included *FASN*, *LDLR* (low density lipoprotein receptor) and *HMGCR*.

The same analysis was carried out to explore the gene sets enriched in iASTROs treated with TNFα+IFNγ+PFFs versus TNFα+IFNγ, as no enriched GO:BP terms were found. In this case, the gene sets with the highest positive NES were “Complement”, “Oxidative Phosphorylation” and

"IL6 JAK STAT3 Signaling", and the ones with the lowest negative NES were "Apical Junction", "E2F Targets", and "Myc Targets V2". "Cholesterol Homeostasis" also had a negative NES, but this was not statistically significant. Overall, these results show that treating iASTROs for 24h with α-synuclein PFFs caused very few changes in gene expression, and most of the changes were related to lipid homeostasis.

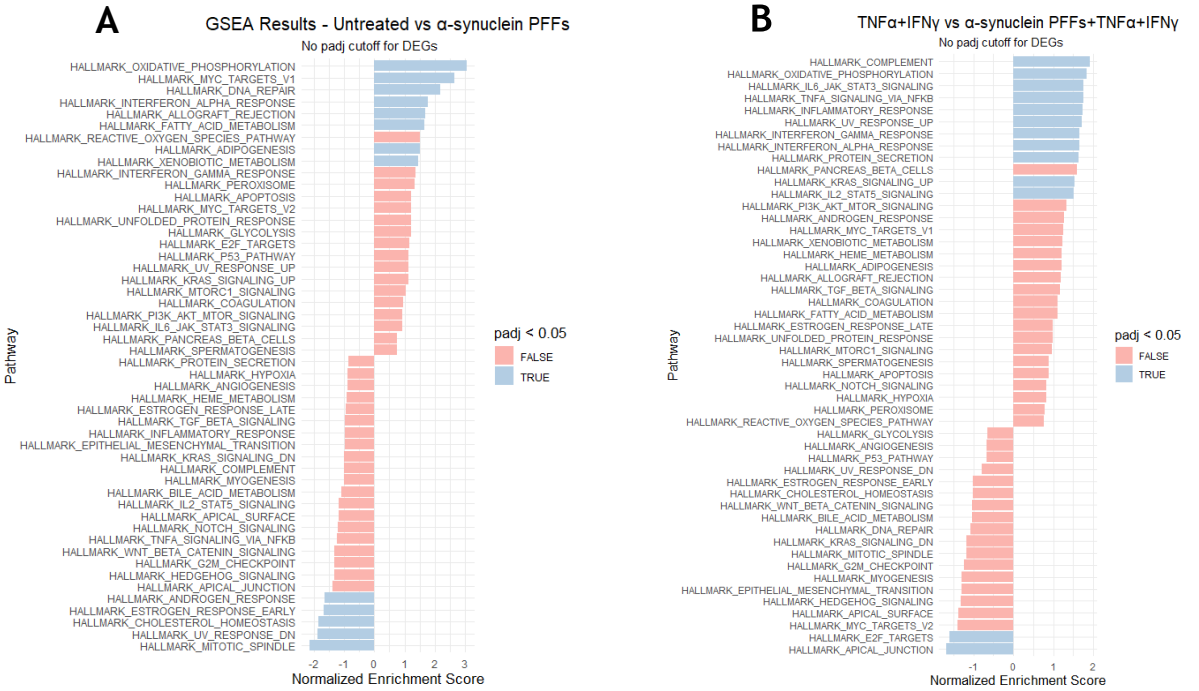


Figure 4.4. Gene set enrichment analysis of iASTROs treated with α-synuclein PFFs, without or with TNFα+IFNγ

(A) Gene set enrichment analysis of iASTROs treated for 24h with 10 µg/mL α-synuclein PFFs, compared to untreated iASTROs. (B) Gene set enrichment analysis of iASTROs treated for 24h with 10 µg/mL α-synuclein PFFs + 30 ng/mL TNFα + 50 ng/mL IFNγ, compared to iASTROs treated with 30 ng/mL TNFα + 50 ng/mL IFNγ. All genes were used in these analyses.

4.2.4.3. Comparisons between different treatments

I next explored the DEGs and enriched GO:BP terms between iASTROs exposed to different treatments. There was a significant overlap in the top upregulated DEGs and enriched GO:BP terms in iASTROs treated with TNFα+IFNγ or IFNγ alone compared to cells treated with the Liddelow factors or TNFα alone. First, when comparing iASTROs treated with TNFα or IFNγ alone, some of the top upregulated genes in IFNγ-treated cells were *CXCL9*, *IDO1*, *TBX21*, *APOL4* (apolipoprotein 4), *HGF* (hepatocyte growth factor), *SECTM1* (secreted and

transmembrane protein 1), *IRF8* (interferon regulatory factor 8), and *SLC17A8* (vesicular glutamate transporter 3, VGLUT3) (Figure 4.5 Ai). Genes downregulated in IFNγ-treated cells included: genes encoding cytokines and chemokines (*TNF, IL1A*, *CXCL8*), *MOGAT2* (2-acylglycerol O-acyltransferase 2), *MMP9*, *SLCO2B1* (solute carrier organic anion transporter family member 2B1), and *SELE* (selectin E) (Figure 4.5 Ai). Furthermore, the main enriched GO:BP terms in IFNγ-treated iASTROs were related to the immune response, antigen processing and presentation, and cytotoxicity, whereas the suppressed terms were related to the inflammatory response, development and morphogenesis, IL-6 production, and extracellular matrix organization (Figure 4.5 Aii).

When comparing iASTROs treated with TNFα+IFNγ or TNFα alone, the main DEGs upregulated in cells treated with TNFα+IFNγ were similar to those described above in the IFNγ vs TNFα comparison, such as *CXCL9, TBX21, IDO1, APOL4, IRF8, HGF, SECTM1* and *CD7* (Figure 4.5 Bi). Some of the top downregulated genes in iASTROs treated with TNFα+IFNγ compared to TNFα included *GABRA6* (gamma-aminobutyric acid receptor subunit alpha-6), *SOST* (sclerostin), and *CHRNA9* (neuronal acetylcholine receptor subunit alpha-9) (Figure 4.5 Bi). Furthermore, the main activated GO:BP terms in iASTROs after treatment with TNFα+IFNγ compared to TNFα were related to the immune response, antigen processing and presentation, cytotoxicity, and calcium transport and homeostasis (Figure 4.5 Bii). On the contrary, most of the suppressed GO:BP terms were related to mitosis and cell division, as well as learning, behaviour and synapse assembly (Figure 4.5 Bii). The bigger transcriptional changes in the TNFα+IFNγ vs TNFα comparison, as opposed to the IFNγ vs TNFα comparison, show how these two cytokines act synergistically.

Additionally, the top upregulated DEGs in cells treated with IFNγ compared to the Liddelow factors included the *CXCL9, TBX21, APOL4, IDO1, IRF8, SECTM1, CD7* and *DES* (Figure 4.5 Ci). The top downregulated genes in IFNγ-treated cells included multiple chemokines (*CXCL6, CXCL5, CXCL1, CXCL3, CXCL2* and *CXCL8*), *SCLO2B1*, *SELE*, *TNFAIP6* (TNF-stimulated gene 6 protein), and *CSF3* (granulocyte colony-stimulating factor/G-CSF) (Figure 4.5 Ci). Moreover, the main activated GO:BP terms in iASTROs treated with IFNγ included multiple terms related to antigen processing and presentation, as well as the immune response (Figure 4.5 Cii). The suppressed included terms related to the inflammatory response, extracellular structure organization, angiogenesis, chemotaxis, and IL-6 production (Figure 4.5 Cii).

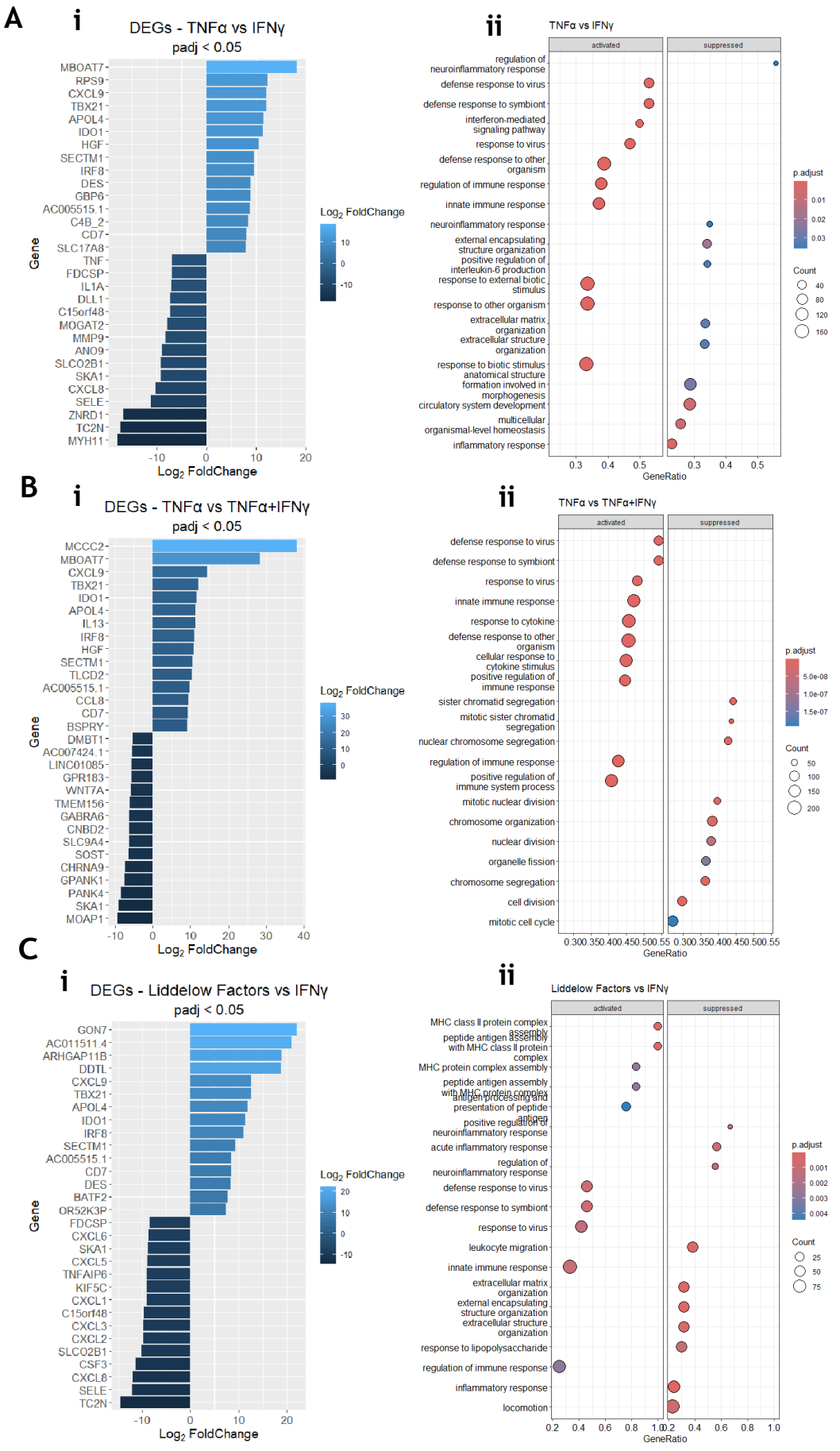
Furthermore, the main upregulated genes after treatment with TNFα+IFNγ compared to the Liddelow factors included *CXCL9, TBX21, IDO1, APOL4, IRF8, SECTM1*, *CD7*, and *IL13* (interleukin 13) (Figure 4.5 Di). On the other hand, some of the main downregulated genes were *CXCL13, SERPINB7* (serpin family B member 7), *CSF3, MGAT4C* (MGAT4 family member C), *CHRNA9*, and *HPD* (4-hydroxyphenylpyruvate dioxygenase) (Figure 4.5 Di). In addition, the main activated GO:BP terms in iASTROs treated with TNFα+IFNγ compared to the Liddelow factors were all related to the immune response, antigen processing and presentation, cytotoxicity, and calcium homeostasis and transport, whereas those suppressed were all related to mitosis (Figure 4.5 Dii).

When comparing iASTROs treated with TNFα+IFNγ to cells treated with IFNγ alone, the top upregulated genes were *SELE, TNF, IL13, ADCY4* (adenylyl cyclase type 4), *CXCL8, ANO9, FDCSP*, *TNFRSF4* (TNF receptor superfamily, member 4), and *CDH22* (cadherin 22) (Figure 4.5 Ei). On the other hand, the main downregulated genes were *GDF10* (growth differentiation factor 10), *FABP7*, *CYP19A1* (aromatase/oestrogen synthase), and *HLA-DRA* (HLA class II histocompatibility antigen, DR alpha chain) (Figure 4.5 Ei). Moreover, the main activated GO:BP terms in cells treated with TNFα+IFNγ were terms related to the immune response, calcium transport and homeostasis, extracellular structure organization, interleukin production, and lipid localization, whereas the main suppressed terms were related to mitosis (Figure 4.5 Eii).

Moreover, iASTROs treated with TNFα+IFNγ+PFFs presented very similar transcriptional changes to cells treated with PFFs as they did to untreated cells, and most of the top upregulated genes were the same (*CXCL5, CXCL9, GBP4, CXCL10, IDO1, CXCL11, OR2I1P, CTSS*, and *IFI30*) (Figure 4.5 Fi). Some of the top downregulated genes included *MS4A6A* (membrane spanning 4-domains A6A), *FAM220A* (family with sequence similarity 220 member A), and *DIPK1C* (divergent protein kinase domain 1C). Moreover, the main activated GO:BP terms in iASTROs treated with TNFα+IFNγ+PFFs were related to the immune response, antigen processing and presentation, lipid localization and transport, and interleukin production, whereas the top suppressed terms included terms related to muscle and CNS development, synapse assembly, and membrane permeability (Figure 4.5 Fii).

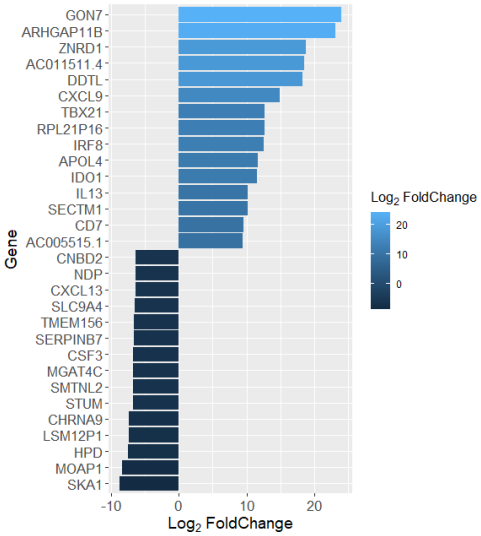
On another note, most of the genes upregulated in iASTROs treated with the Liddelow factors compared to iASTROS treated with TNFα alone were also upregulated in cells treated with the Liddelow factors compared to the rest of the treatments. Some of these genes included: *CSF3, MMP12* (matrix metallopeptidase 12), *SERPINB7, CXCL1* and *CXCL2, PTGS2* (cyclooxygenase-2), and *SP6* (Sp6 Transcription Factor). Since these genes were only, or mostly, upregulated in iASTROs treated with the Liddelow factors, this indicates that IL-1α and/or C1q were driving the upregulated expression of these genes. On the other hand, genes downregulated in iASTROs treated with the Liddelow factors compared to those treated with TNFα alone included *SLCO2A1* (solute carrier organic anion transporter family member 2A1), and *CYP27B1*.

Lastly, there were very few DEGs between iASTROs treated with TNFα+IFNγ or TNFα+IFNγ+PFFs, and most of these genes presented low expression across all samples and/or different expression patterns across all 3 cell lines. However, it is important to highlight *RNF145*, which was downregulated in cells treated with TNFα+IFNγ+PFFs and was also downregulated in iASTROs treated with PFFs alone compared to untreated cells (Figure 4.3 Fi).

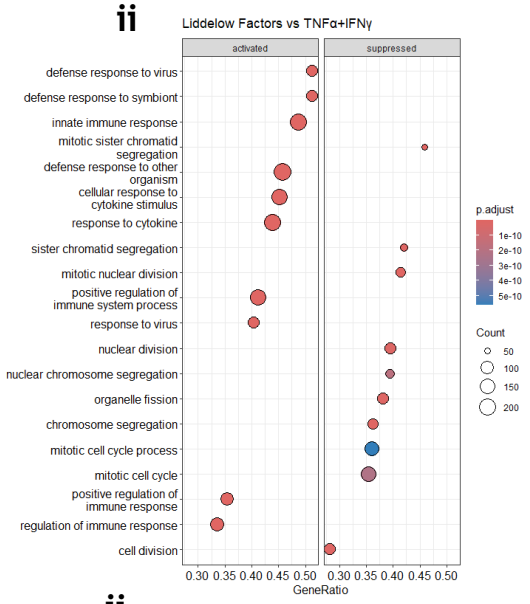

A
i
DEGs - TNFα vs IFNγ
padj < 0.05
MBOAT7
RPS9
CXCL9
TBX21
APOL4
IDO1
HGF
SECTM1
IRF8
DES
GBP6
AC005515.1
C4B_2
CD7
SLC17A8
TNF
FDCSP
IL1A
DLL1
C15orf48
MOGAT2
MMP9
ANO9
SLCO2B1
SKA1
CXCL8
SELE
ZNRD1
TC2N
MYH11
Gene
-10 0 10 20
Log2 FoldChange
Log2 FoldChange
10
0
-10
ii
TNFα vs IFNγ
activated
suppressed
regulation of neuroinflammatory response
defense response to virus
defense response to symbiont
interferon-mediated signaling pathway
response to virus
defense response to other organism
regulation of immune response
innate immune response
neuroinflammatory response
external encapsulating structure organization
positive regulation of interleukin-6 production
response to external biotic stimulus
response to other organism
extracellular matrix organization
extracellular structure organization
response to biotic stimulus
anatomical structure formation involved in morphogenesis
circulatory system development
multicellular organismal-level homeostasis
inflammatory response
0.3 0.4 0.5
0.3 0.4 0.5
GeneRatio
p.adjust
0.01
0.02
0.03
Count
40
80
120
160
B
i
DEGs - TNFα vs TNFα+IFNγ
padj < 0.05
MCCC2
MBOAT7
CXCL9
TBX21
IDO1
APOL4
IL13
IRF8
HGF
SECTM1
TLCD2
AC005515.1
CCL8
CD7
BSPRY
DMBT1
AC007424.1
LINC01085
GPR183
WNT7A
TMEM156
GABRA6
CNBD2
SLC9A4
SOST
CHRNA9
GPANK1
PANK4
SKA1
MOAP1
Gene
-10 0 10 20 30 40
Log2 FoldChange
Log2 FoldChange
30
20
10
0
ii
TNFα vs TNFα+IFNγ
activated
suppressed
defense response to virus
defense response to symbiont
response to virus
innate immune response
response to cytokine
defense response to other organism
cellular response to cytokine stimulus
positive regulation of immune response
sister chromatid segregation
mitotic sister chromatid segregation
nuclear chromosome segregation
regulation of immune response
positive regulation of immune system process
mitotic nuclear division
chromosome organization
nuclear division
organelle fission
chromosome segregation
cell division
mitotic cell cycle
0.300.350.400.450.500.55 0.300.350.400.450.500.55
GeneRatio
p.adjust
5.0e-08
1.0e-07
1.5e-07
Count
50
100
150
200
C
i
DEGs - Liddelow Factors vs IFNγ
padj < 0.05
GON7
AC011511.4
ARHGAP11B
DDTL
CXCL9
TBX21
APOL4
IDO1
IRF8
SECTM1
AC005515.1
CD7
DES
BATF2
OR52K3P
FDCSP
CXCL6
SKA1
CXCL5
TNFAIP6
KIF5C
CXCL1
C15orf48
CXCL3
CXCL2
SLCO2B1
CSF3
CXCL8
SELE
TC2N
Gene
-10 0 10 20
Log2 FoldChange
Log2 FoldChange
20
10
0
-10
ii
Liddelow Factors vs IFNγ
activated
suppressed
MHC class II protein complex assembly
peptide antigen assembly with MHC class II protein complex
MHC protein complex assembly
peptide antigen assembly with MHC protein complex
antigen processing and presentation of peptide antigen
positive regulation of neuroinflammatory response
acute inflammatory response
regulation of neuroinflammatory response
defense response to virus
defense response to symbiont
response to virus
leukocyte migration
innate immune response
extracellular matrix organization
external encapsulating structure organization
extracellular structure organization
response to lipopolysaccharide
regulation of immune response
inflammatory response
locomotion
0.2 0.4 0.6 0.8 1.0
0.2 0.4 0.6 0.8 1.0
GeneRatio
p.adjust
0.001
0.002
0.003
0.004
Count
25
50
75

D

i

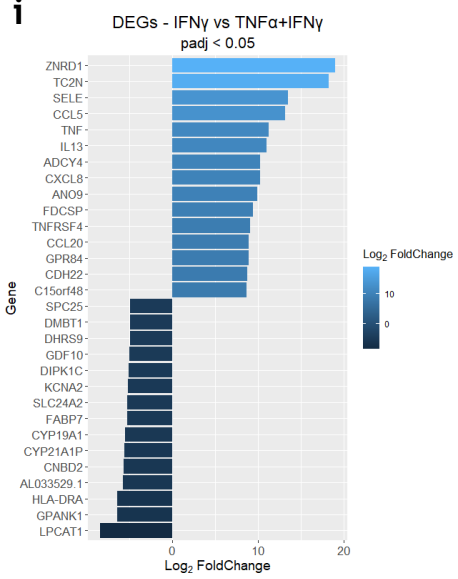


ii

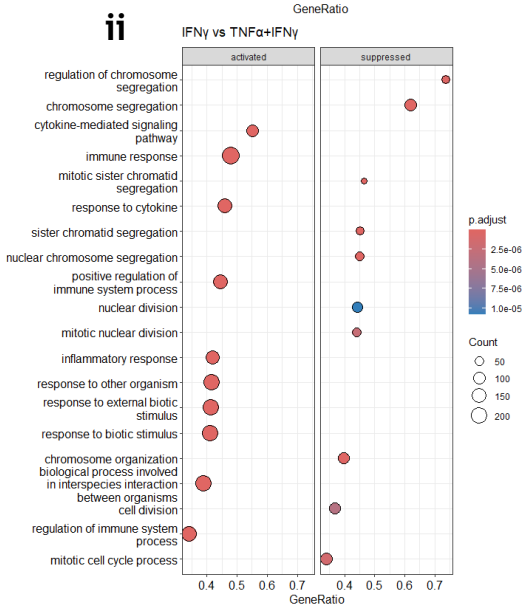


E

i

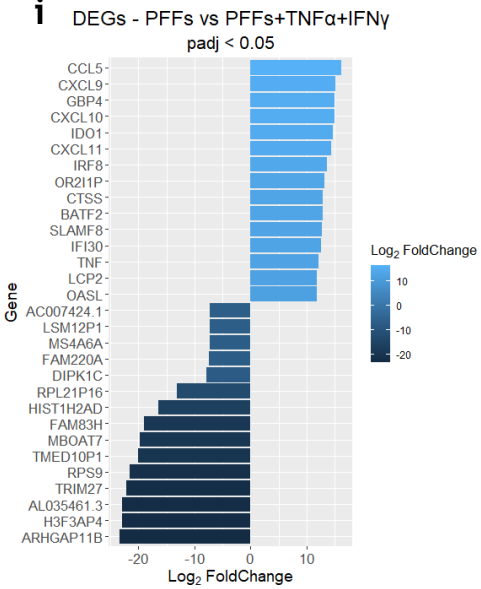


ii



F

i



ii

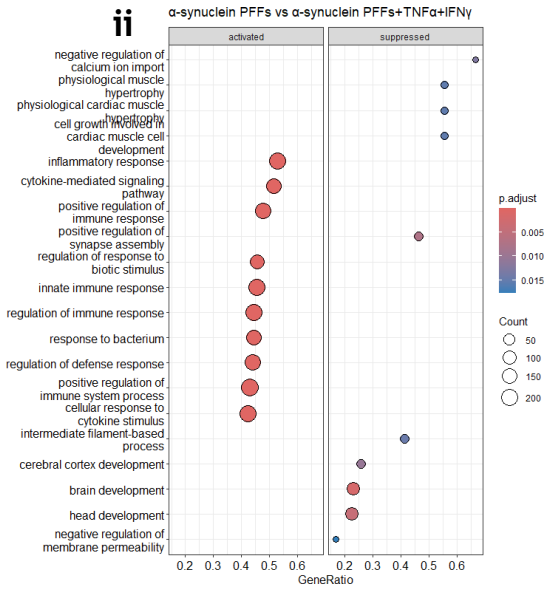


Figure 4.5. Analysis of the main genes and pathways activated and suppressed in iASTROs treated with different combinations of inflammatory cytokines and α-synuclein PFFs compared to iASTROs with other treatments

Analysis of (i) the top 15 and bottom 15 differentially expressed genes and (ii) the top 10 activated and top 10 suppressed gene ontology biological process terms in control iASTROs treated for 24h with (A) IFNγ compared to TNFα, (B) TNFα + IFNγ compared to TNFα, (C) IFNγ compared to the Liddelow factors (TNFα + IL-1α + C1q), (D) TNFα + IFNγ compared to the Liddelow factors (TNFα + IL-1α + C1q), (E) TNFα + IFNγ compared to IFNγ, and (F) α-synuclein TNFα+IFNγ+PFFs compared to α-synuclein PFFs alone. All treatment concentrations are as follows: 30 ng/mL TNFα, 50 ng/mL IFNγ, the Liddelow factors (30 ng/mL TNFα + 3 ng/mL IL-1α + 400 ng/mL C1q), 10 µg/mL α-synuclein PFFs, 10 µg/mL α-synuclein PFFs + 30 ng/mL TNFα + 50 ng/mL IFNγ, and 30 ng/mL TNFα + 50 ng/mL IFNγ.

4.2.4.4. Calcium dysregulation in iASTROs treated with TNFα+IFNγ

As discussed above, there were multiple activated GO:BP terms related to calcium homeostasis and transport in iASTROs treated with TNFα+IFNγ compared to untreated cells (Figure 4.6 Ai), cells treated with the Liddelow factors (Figure 4.6 Aii) or cells treated with TNFα or IFNγ alone. When examining the DEGs included in these terms (Figure 4.6 B), there were genes encoding different ATP-gated P2X cation channels (*P2RX2, P2RX4*, and *P2RX7*), as well as the inositol 1,4,5-trisphosphate receptor, type 3 (*ITPR3*), all of which are involved in ATP-induced ER calcium release. In addition, *ORAI1* (calcium release-activated calcium channel protein 1) and *STIMATE* (STIM activating enhancer) were also upregulated, and they encode proteins involved in store operated calcium entry (SOCE). Additionally, iASTROs treated with TNFα+IFNγ had upregulated expression of a few genes encoding voltage-gated calcium channels (*CACNA1A1, CACNA1I, CACNB1, CACNG6*). Other interesting genes upregulated in iASTROs after treatment with TNFα+IFNγ that are directly involved in calcium transport included: *ATP2A3* (sarcoplasmic/endoplasmic reticulum calcium ATPase 3), *BDKRB1* (bradykinin receptor B1), *EDNRB* (endothelin receptor type B), *GJA4* (Gap junction alpha-4 protein), *HPCA* (hippocalcin), *MCUB* (mitochondrial calcium uniporter dominant negative subunit beta), *PLCH* (phospholipase C eta 1), *SLC8A3* (solute carrier family 8 member A3), *SLC8B1* (solute carrier family 8 member B1), and *TRPC3* (short transient receptor potential channel 3). Moreover, two genes related to vitamin D metabolism, *CYP27B1* and *VDR*, were also included in a couple of the GO:BP terms related to calcium homeostasis. *CYP27B1* was already discussed in Section 4.2.4.2., as *CYP27B1* was one of the few genes upregulated in iASTROs treated with PFFs alone.

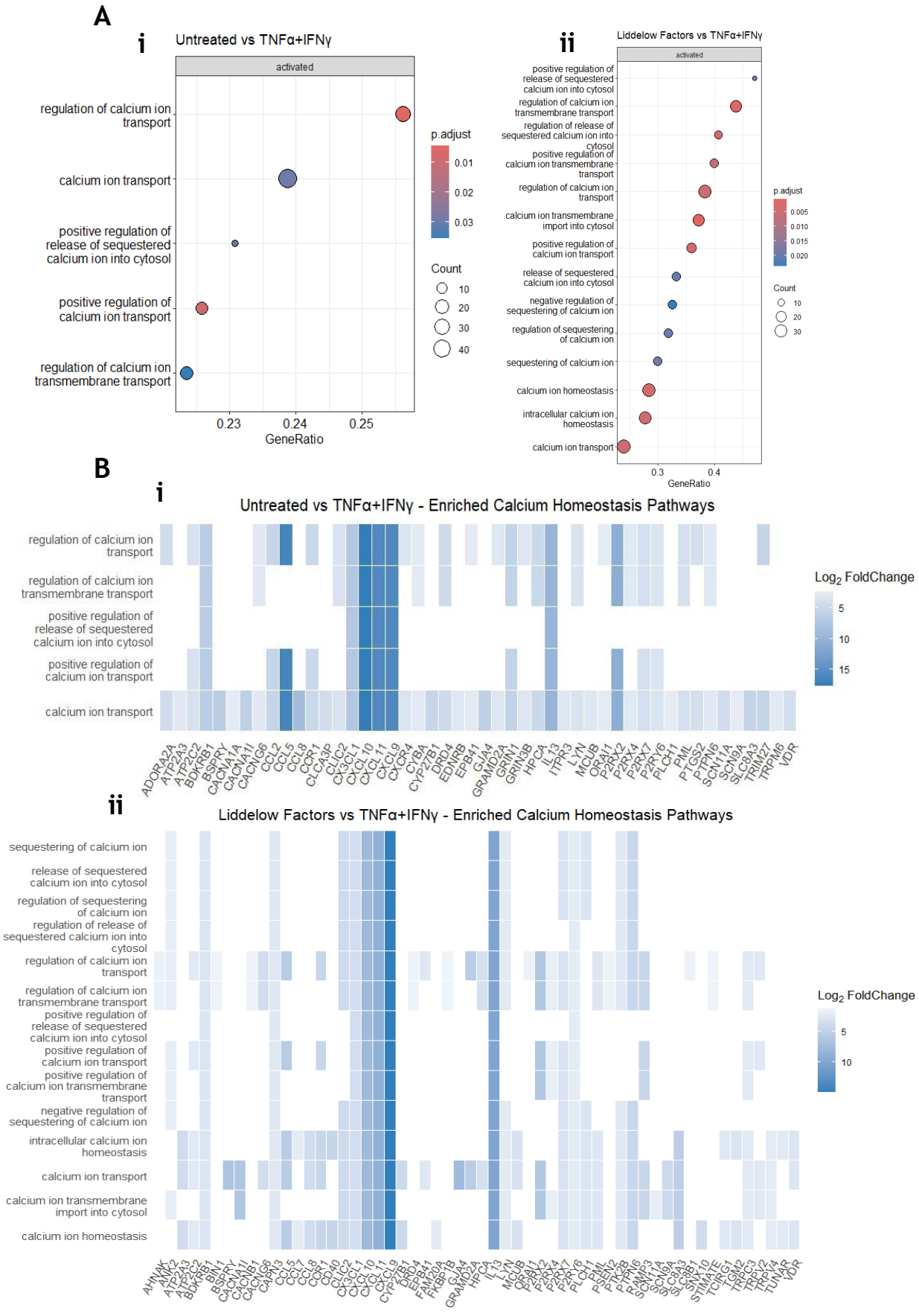

A
i
Untreated vs TNFα+IFNγ
activated
regulation of calcium ion transport
calcium ion transport
positive regulation of release of sequestered calcium ion into cytosol
positive regulation of calcium ion transport
regulation of calcium ion transmembrane transport
0.23
0.24
0.25
GeneRatio
p.adjust
0.01
0.02
0.03
Count
10
20
30
40
ii
Liddelow Factors vs TNFα+IFNγ
activated
positive regulation of release of sequestered calcium ion into cytosol
regulation of calcium ion transmembrane transport
regulation of release of sequestered calcium ion into cytosol
positive regulation of calcium ion transmembrane transport
regulation of calcium ion transport
calcium ion transmembrane import into cytosol
positive regulation of calcium ion transport
release of sequestered calcium ion into cytosol
negative regulation of sequestering of calcium ion
regulation of sequestering of calcium ion
sequestering of calcium ion
calcium ion homeostasis
intracellular calcium ion homeostasis
calcium ion transport
0.3
0.4
GeneRatio
p.adjust
0.005
0.010
0.015
0.020
Count
10
20
30
B
i
Untreated vs TNFα+IFNγ - Enriched Calcium Homeostasis Pathways
regulation of calcium ion transport
regulation of calcium ion transmembrane transport
positive regulation of release of sequestered calcium ion into cytosol
positive regulation of calcium ion transport
calcium ion transport
ADORA2A ATP2A3 ATP2C2 BDKRB1 BSPRY CACNA1A CACNA1I CACNG6 CCL2 CCL5 CCL8 CCR1 CLCA3P CLIC2 CX3CL1 CXCL10 CXCL11 CXCL9 CXCR4 CYBA CYP27B1 DRD4 EDNRB EPB41 GJA4 GRAMD2A GRIN1 GRIN3B HPCA IL13 ITPR3 LYN MCUB ORAI1 P2RX2 P2RX4 P2RX7 P2RY6 PLCH1 PML PTGS2 PTPN6 SCN1A SCN9A SLC8A3 TRIM27 TRPM6 VDR
Log2 FoldChange
5
10
15
ii
Liddelow Factors vs TNFα+IFNγ - Enriched Calcium Homeostasis Pathways
sequestering of calcium ion
release of sequestered calcium ion into cytosol
regulation of sequestering of calcium ion
regulation of release of sequestered calcium ion into cytosol
regulation of calcium ion transport
regulation of calcium ion transmembrane transport
positive regulation of release of sequestered calcium ion into cytosol
positive regulation of calcium ion transport
positive regulation of calcium ion transmembrane transport
negative regulation of sequestering of calcium ion
intracellular calcium ion homeostasis
calcium ion transport
calcium ion transmembrane import into cytosol
calcium ion homeostasis
AHNAK ANK2 ATP2A3 ATP2C2 BDKRB1 BIN1 BSPRY CACNA1I CACNB1 CACNG6 CASP3 CCL5 CCL8 CCR1 CD40 CLIC2 CX3CL1 CXCL10 CXCL11 CXCL9 CYP27B1 DRD4 EPB41 FAM20A FKBP1B GJA4 GRAMD2A HPCA IL13 LYN MCUB ORAI1 P2RX4 P2RX7 P2RY6 PLCH1 PML PSEN2 PTPN6 PTPRB RAMP3 SCN1A SCN9A SLC8A3 SLC8B1 SNX10 STIM1 TCIRG1 TGM2 TRPC3 TRPV2 TRPV4 TUNAR VDR
Log2 FoldChange
5
10

Figure 4.6. iASTROs treated with TNFα+IFNγ have activated pathways related to calcium transport and homeostasis
(A) Gene ontology biological process terms related to calcium transport and homeostasis activated in iASTROs treated for 24h with 30 ng/mL TNFα + 50 ng/mL IFNγ compared to (i) untreated iASTROs or (ii) iASTROs treated with the Liddelow factors (30 ng/mL TNFα + 3 ng/mL IL-1α + 400 ng/mL C1q). (B) Heatplots showing the differentially expressed genes involved in the biological process terms related to calcium transport and homeostasis activated in iASTROs treated for 24h with 30 ng/mL TNFα + 50 ng/mL IFNγ compared to (i) untreated iASTROs or (ii) iASTROs treated with the Liddelow factors (30 ng/mL TNFα + 3 ng/mL IL-1α + 400 ng/mL C1q).

Based on these findings, I decided to further explore the changes in calcium homeostasis in reactive iASTROs, focusing on ATP-induced ER-calcium release and SOCE, and the potential of the former to alter astrocyte reactivity. In addition, I chose to investigate vitamin D metabolism in reactive iASTROs and the potential of vitamin D to enhance DAn survival. These results are presented in Chapter 5.

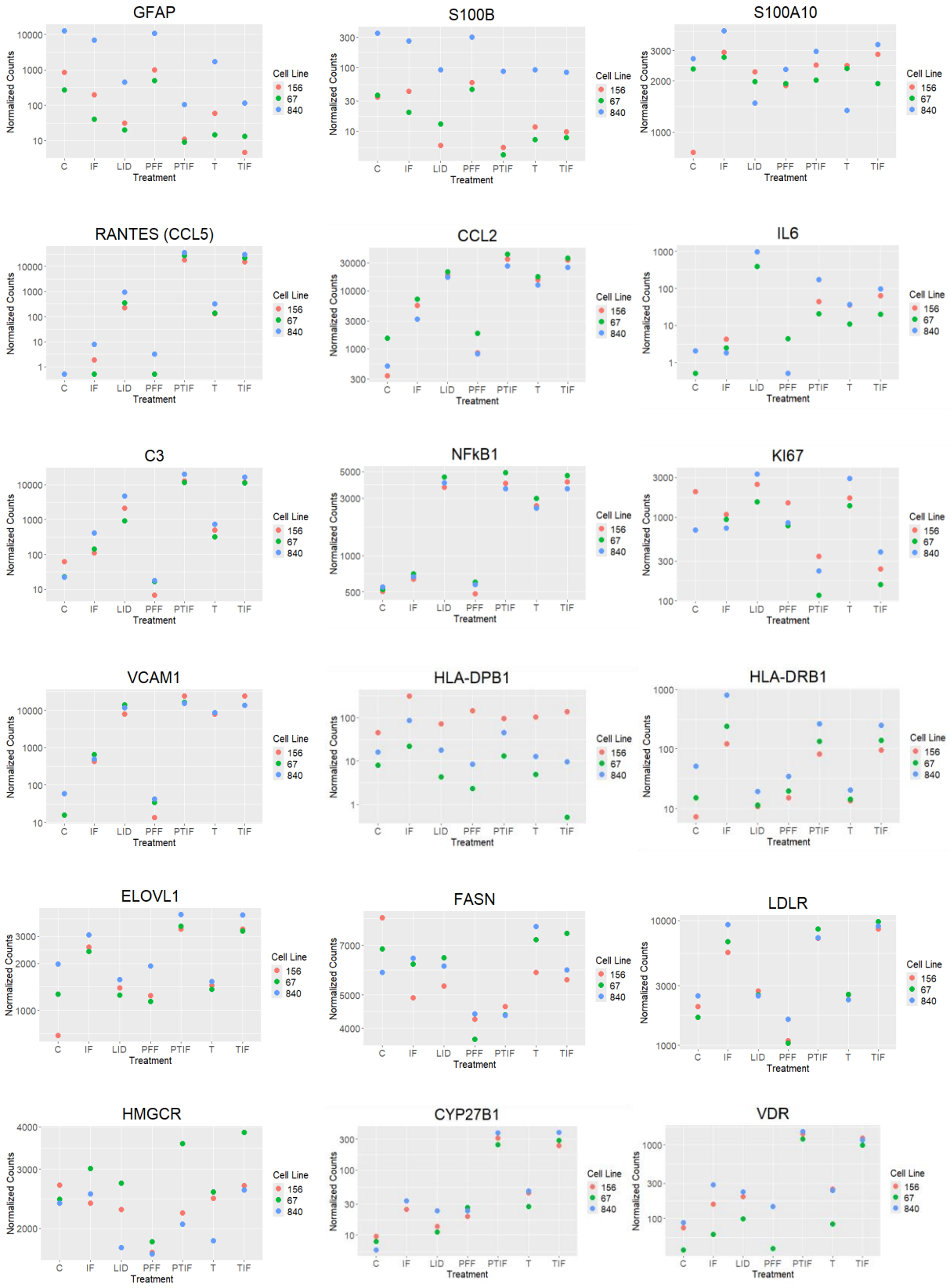
The expression of various genes of interest were explored across all samples in the RNAseq data (Figure 4.7). The expression of these genes was also studied in subsequent RT-qPCR experiments, to a) explore the changes in their expression levels after 7 days, and b) to verify that iASTROs responded similarly to the treatments in the RNAseq experiment and subsequent in vitro experiments.

4.2.5. RNAseq experiment results summary

These are the main findings from the RNAseq experiment of iASTROs treated for 24h with different combinations of inflammatory cytokines and α-synuclein PFFs:

- iASTROs underwent important transcriptional changes in response to inflammatory cytokines but not α-synuclein PFFs.
- Upon inflammatory stimulation, iASTROs did not acquire either an A1 or A2 reactive phenotype.
- When combined, TNFα and IFNγ acted synergistically.
- Most, but not all, of the transcriptional changes in iASTROs treated with the Liddelow factors (TNFα+IL-1α+C1q) were driven by TNFα.

- IFNγ was the main activator of the signalling pathways leading to antigen processing and presentation.
- The combined treatment of TNFα+IFNγ, with or without PFFs, activated pathways related to cytotoxicity and apoptosis.
- TNFα and the Liddelow factors induced an increase in cell proliferation pathways, whereas TNFα+IFNγ, with or without PFFs, suppressed these pathways.
- The combined treatment of TNFα+IFNγ, with or without PFFs, promoted the activation of pathways related to calcium homeostasis and transport.
- Genes related to vitamin D metabolism (*CYP27B1* and *VDR*) were upregulated after all treatments with inflammatory cytokines, and *CYP27B1* was one of the few genes upregulated after treatment with PFFs alone.
- Most of the downregulated genes after treatment with PFFs alone were involved in lipid metabolism, whereas iASTROs treated with inflammatory cytokines mostly presented upregulation of genes related to lipid homeostasis.


GFAP
S100B
S100A10
RANTES (CCL5)
CCL2
IL6
C3
NFkB1
KI67
VCAM1
HLA-DPB1
HLA-DRB1
ELOVL1
FASN
LDLR
HMGCR
CYP27B1
VDR
Normalized Counts
Treatment
C IF LID PFF PTIF T TIF
Cell Line
156
67
840

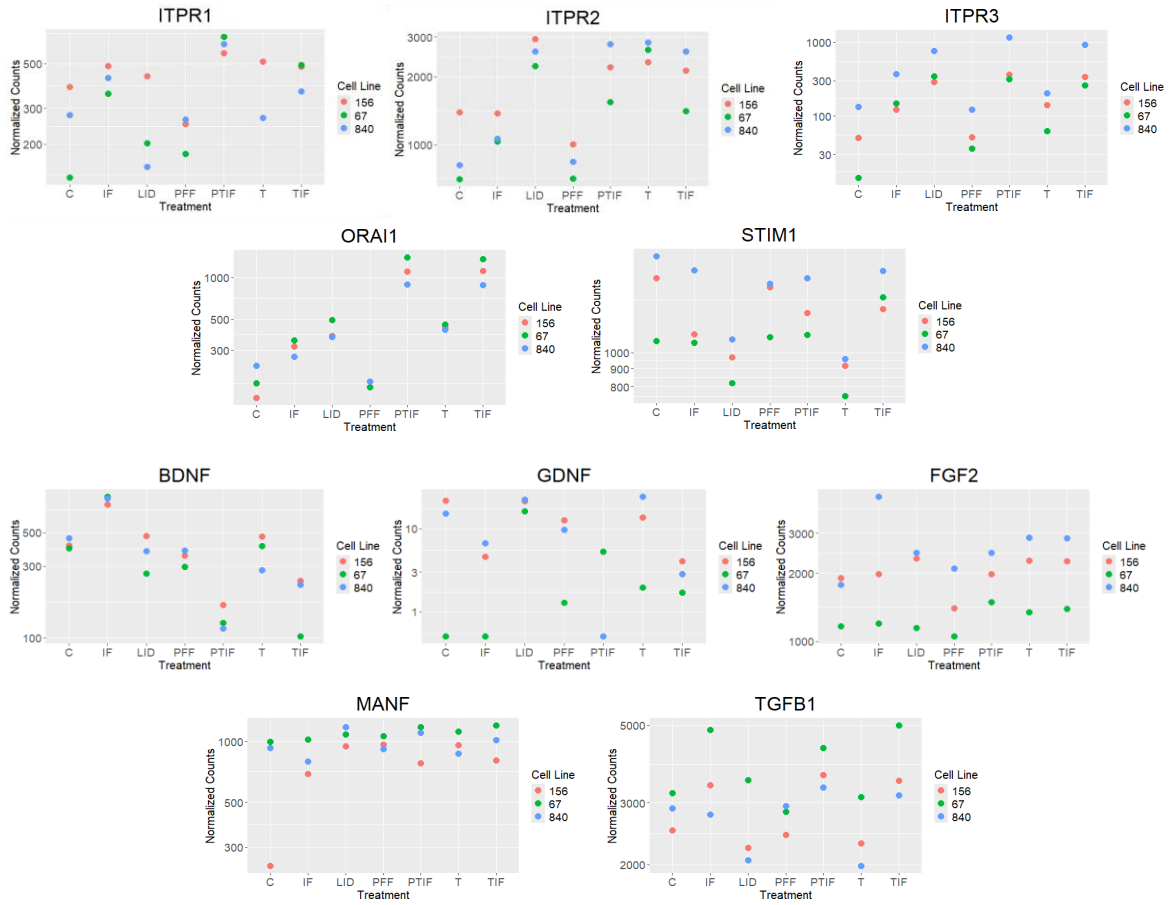


Figure 4.7. Normalized counts of the genes of interest to be further explored in vitro

RNAseq analysis of the normalized counts of a number of genes of interest in control iASTROs untreated (C) or treated for 24h with 50 ng/mL IFNγ (IF), the Liddelow factors (30 ng/mL TNFα + 3 ng/mL IL-1α + 400 ng/mL C1q, LID), 10 µg/mL α-synuclein PFFs (PFF), 10 µg/mL α-synuclein PFFs + 30 ng/mL TNFα + 50 ng/mL IFNγ (PTIF), 30 ng/mL TNFα (T) or 30 ng/mL TNFα + 50 ng/mL IFNγ (TIF). Each dot colour represents a different control iASTRO line. The y-axis is in a Log_{10} scale.

4.3. In vitro study of the inflammatory response of control and *GBA-N370S* iASTROs to different inflammatory stimuli over time

After exploring the transcriptomic changes by RNAseq of control iASTROs treated for 24h with different combinations of inflammatory cytokines and α-synuclein PFFs, I decided to expand this analysis by studying the reactive response of both control and *GBA-N370S* iASTROs in vitro at multiple timepoints. I first focused on the response of iASTROs to inflammatory stimuli, and section 4.4 will expand on the response to α-synuclein PFFs, with or without inflammatory stimuli.

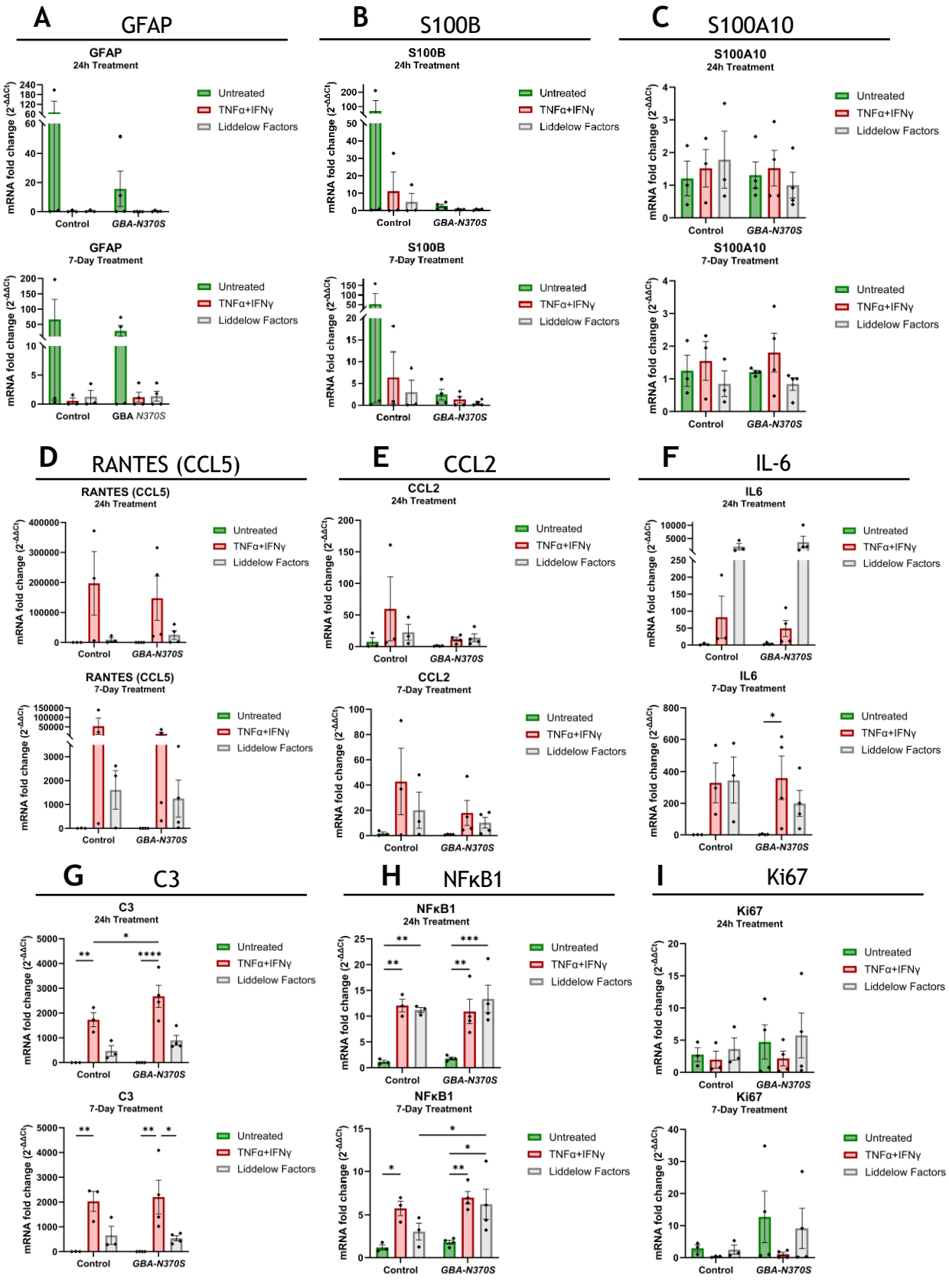
4.3.1. RT-qPCR analysis of relative gene expression

First, I used RT-qPCR to investigate the relative changes in gene expression of some genes of interest related to inflammation and the immune response, which were also explored in the RNAseq experiment (Figure 4.7), in control and *GBA-N370S* iASTROs treated for 24h or 7 days with 30 ng/mL TNFα + 50 ng/mL IFNγ or the Liddelow factors (30 ng/mL TNFα + 3 ng/mL IL-1α + 400 ng/mL C1q). Unless stated otherwise, at the 24h timepoint all genes followed a similar expression pattern in treated iASTROs to that observed by RNAseq, which validates the findings in the RNAseq experiment. The variability in the graphs reflects the line-to-line variability, as well as the difference in the degree of inflammatory response of each line (Figure 4.8). Due to this variability, many of the observations discussed here (and in the next sections) reflect trends.

Expression of *GFAP* and *S100B* was lower after 24h of treatment with both TNFα+IFNγ and the Liddelow factors, and this reduction was maintained 7 days after treatment (Figure 4.8. A-B). No changes were observed in the expression of *S100A10* (Figure 4.8. C). On the contrary, a very big increase in *CCL5* (*RANTES*) expression was observed following TNFα+IFNγ treatment but less so treatment with the Liddelow factors, and decreased over time (Figure 4.8 D). A similar expression pattern was observed with *CCL2*, albeit with a much lower increase in expression (Figure 4.8 E). After 24h, the increase in *IL-6* expression was greater in cells treated with the Liddelow factors than TNFα+IFNγ, but by day 7 the increase in expression relative to the untreated condition was the same with both treatments (Figure 4.8 F). Moreover, there was an increase in *C3* expression after both treatments, which was bigger with TNFα+IFNγ, and remained similar 7 days after treatment (Figure 4.8 G). At the 24h timepoint *C3* expression was higher in *GBA-N370S* iASTROs than in control cells, especially in cells treated with TNFα+IFNγ. Additionally, there was a similar increase in *NFκB1* expression in response to both treatments, and the increase was smaller 7 days after treatment (Figure 4.8 H). Moreover, there was a decrease in the relative expression of *Ki67* with TNFα+IFNγ but not the Liddelow factors, which decreased over time (Figure 4.8. I). Lastly, *VCAM1* expression was elevated after TNFα+IFNγ treatment and less so with the Liddelow factors, and the increase was lower 7 days after treatment (Figure 4.8 J).

As mentioned above, GO:BP terms related to MCH proteins and antigen presentation were activated in response to treatment with inflammatory cytokines, especially treatments that included IFNγ (Figures 4.3 and 4.5). Although there are multiple *HLA* genes, I investigated the expression of two: *HLA-DRB1*, the one most highly associated with PD (E. Yu et al., 2021), and *HLA-DPB1*, found to be reduced in TNFα-treated iPSC-derived astrocytes (Russ et al., 2021). 24h after treatment, *HLA-DPB1* expression was slightly lower in cells treated with the Liddelow factors, and after 7 there was an increase in cells treated with TNFα+IFNγ (Figure 4.8 K). On the contrary, *HLA-DRB1* expression was higher in TNFα+IFNγ treated cells 24h after treatment, and more so at 7 days, but no differences were observed in cells treated with the Liddelow factors (Figure 4.8 L). These results correlate with the findings of the RNAseq experiment, showing that increases in *HLA* gene expression are mostly dependent on IFNγ.

Collectively, these results validate some of the findings done in the RNAseq experiment, and they show how the expression of most inflammation-related genes undergo an initial increase and then decrease over time, except for *HLA* genes.


A
GFAP
GFAP
24h Treatment
GFAP
7-Day Treatment
B
S100B
S100B
24h Treatment
S100B
7-Day Treatment
C
S100A10
S100A10
24h Treatment
S100A10
7-Day Treatment
D
RANTES (CCL5)
RANTES (CCL5)
24h Treatment
RANTES (CCL5)
7-Day Treatment
E
CCL2
CCL2
24h Treatment
CCL2
7-Day Treatment
F
IL-6
IL6
24h Treatment
IL6
7-Day Treatment
G
C3
C3
24h Treatment
C3
7-Day Treatment
H
NFκB1
NFκB1
24h Treatment
NFκB1
7-Day Treatment
I
Ki67
Ki67
24h Treatment
Ki67
7-Day Treatment
mRNA fold change (2-ΔΔCt)
Untreated
TNFα+IFNγ
Liddelow Factors
Control
GBA-N370S
GBA N370S

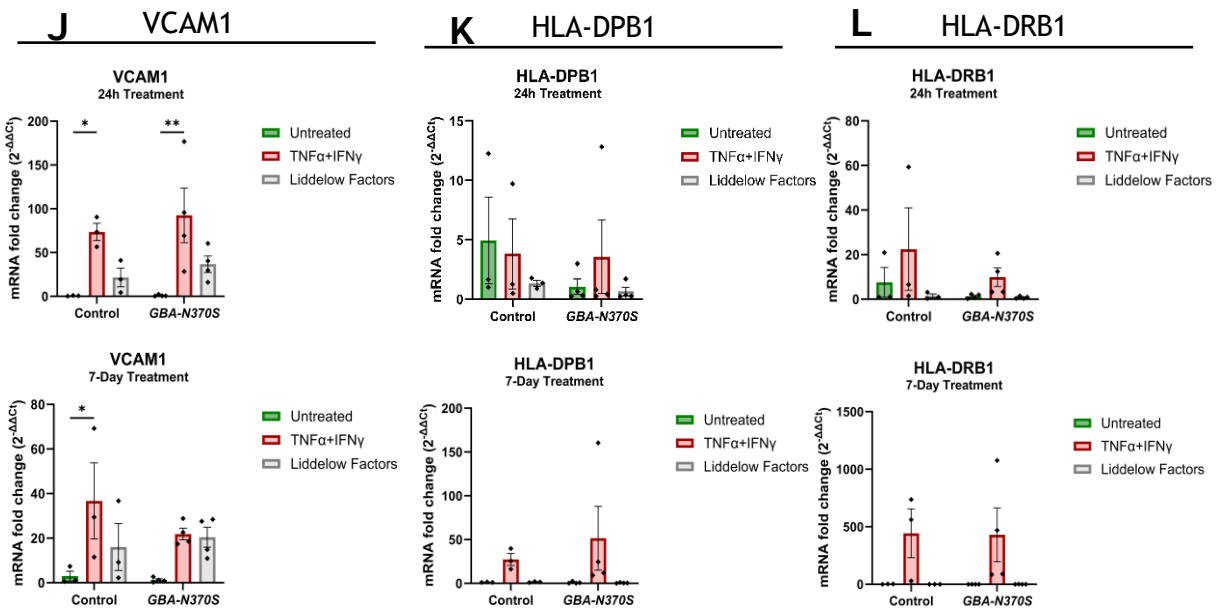


Figure 4.8. Relative gene expression analysis by RT-qPCR shows that 24h and 7 days after treatment with TNFα+IFNγ or the Liddelow factors, the expression profile of control and *GBA-N370S* iASTROs does not resemble either the A1 or A2 astrocyte profile

(A-L) Relative gene expression analysis by RT-qPCR of (A) GFAP, (B) S100B, (C) S100A10, (D) RANTES (CCL5), (E) CCL2, (F) IL-6, (G) C3, (H) NFκB1, (I) Ki67, (J) VCAM1, (K) HLA-DPB1, and (L) HLA-DRB1 in control and *GBA-N370S* iASTROs treated for 24h or 7 days with 30 ng/mL TNFα + 50 ng/mL IFNγ or the Liddelow factors (30 ng/mL TNFα + 3 ng/mL IL-1α + 400 ng/mL C1q). In each differentiation, to calculate ΔΔCt for each gene, the ΔCt of one untreated control iASTRO line was subtracted to the ΔCt of all the lines (for the gene of interest). Each data point represents 1 iASTRO line averaged across differentiations. N = 3 control and 4 *GBA-N370S* lines, 1-4 differentiations. Mean ± SEM. The statistical analysis performed was two-way ANOVA with Tukey's multiple comparison test. *p<0.05, **p<0.01, ***p<0.001, ****p<0.0001.

4.3.2. Immunocytochemistry analysis of inflammatory markers and cellular morphology

Next, I used immunocytochemistry to analyse the cellular morphology, expression of S100B, GFAP, C3 and NFκB1, as well as the nuclear translocation of the latter, in control and *GBA-N370S* iASTROs treated for 24h, 72h or 7 days with 30 ng/mL TNFα, 50 ng/mL IFNγ, 30 ng/mL TNFα + 50 ng/mL IFNγ or the Liddelow factors (30 ng/mL TNFα + 3 ng/mL IL-1α + 400 ng/mL C1q) (Figure 4.9).

24h after treatment, there was a small increase in total live cell number in control and *GBA-N370S* iASTROs treated with IFNγ and TNFα+IFNγ, but by 7 days, there was a decrease in control iASTROs treated with TNFα, TNFα+IFNγ and the Liddelow factors, and in *GBA-N370S* iASTROs treated with TNFα+IFNγ and the Liddelow factors (Figure 4.10 A). Moreover, there

was a trend for an increase in the cell area in control and *GBA-N370S* iASTROs treated with TNFα+IFNγ for 72h and 7 days, and the increase was also notable in cells treated with TNFα alone or the Liddelow factors, especially in control iASTROs (Figure 4.10 B). After 7 days of treatment, cells treated with TNFα or the Liddelow factors presented a trend towards a reduction in cellular roundness, indicating morphological changes (Figure 4.10 C).

The cellular GFAP intensity was very variable between lines, especially because only a few cells in the culture stained very intensely for GFAP. Nevertheless, 72h and 7 days after treatment, there was a tendency towards a decrease in GFAP intensity in control and *GBA-N370S* iASTROs treated with TNFα, TNFα+IFNγ and the Liddelow factors, and to a lesser extent IFNγ (Figure 4.10 D). These results correlate with the decrease in *GFAP* expression shown in Figures 4.7 and 4.8 A. In addition, there was a slight decrease in S100B intensity 72h after treatment with TNFα and TNFα+IFNγ in both iASTRO genotypes, but 7 days after treatment there was an increase in control iASTROs treated with IFNγ and TNFα+IFNγ, and *GBA-N370S* iASTROs treated with IFNγ, but a decrease in intensity could still be observed in *GBA-N370S* iASTROs treated with TNFα alone (Figure 4.10 E). On the other hand, 24h after treatment there was a significant increase in cytoplasmic C3 intensity in both control and *GBA-N370S* iASTROs treated with TNFα+IFNγ. By 72h, the increase was smaller, and at this time a similar increase was observed in cells treated with the Liddelow factors. By 7 days, only a slight increase could be observed in control iASTROs treated with TNFα and TNFα+IFNγ, and a higher increase in those exposed to the Liddelow factors, but a very small increase in *GBA-N370S* iASTROs (Figure 4.10 F).

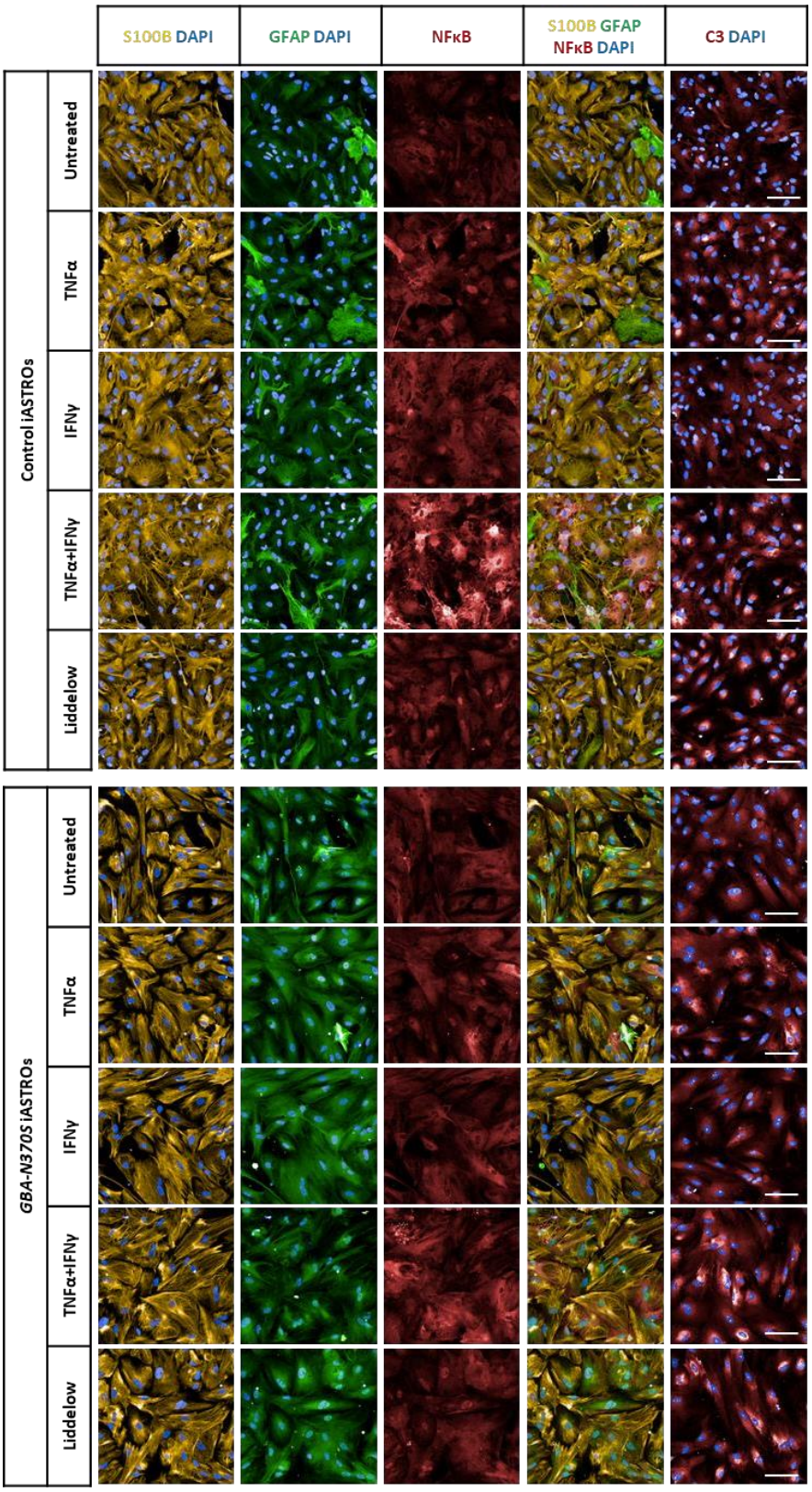
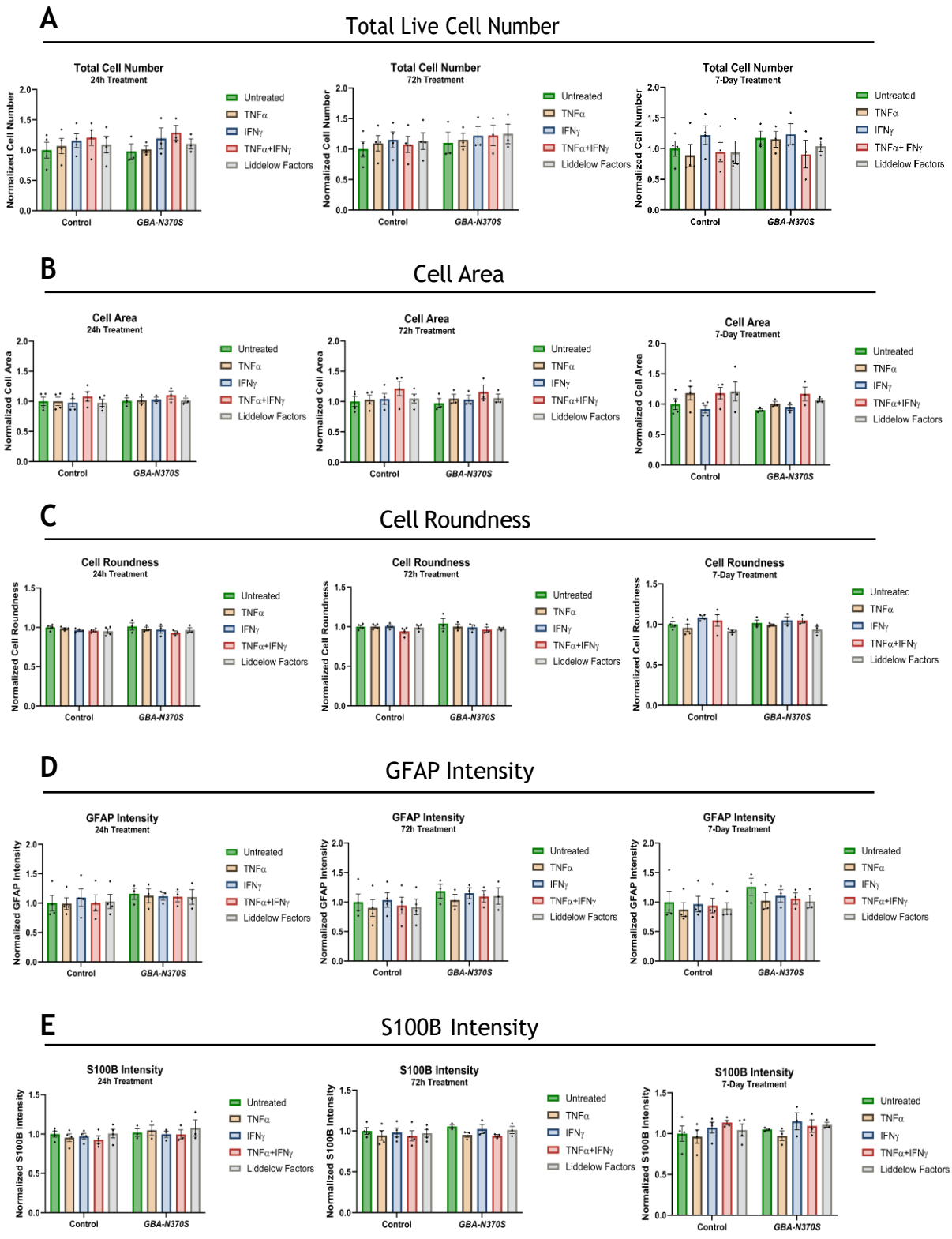


Figure 4.9. Representative immunocytochemistry images of control (top panel) and *GBA-N370S* (bottom panel) iASTROs treated with different combinations of inflammatory cytokines for 72h

30 ng/mL TNFα, 50 ng/mL IFNγ, 30 ng/mL TNFα + 50 ng/mL IFNγ or the Liddelow factors (30 ng/mL TNFα + 3 ng/mL IL-1α + 400 ng/mL C1q. Cells were stained for S100B (yellow), GFAP (green), NFκB (red, third and fourth columns) and C3 (red, fifth column). Scale bar: 100 µm.


A
Total Live Cell Number
Total Cell Number
24h Treatment
Total Cell Number
72h Treatment
Total Cell Number
7-Day Treatment
Normalized Cell Number
Control
GBA-N370S
Untreated
TNFα
IFNγ
TNFα+IFNγ
Liddelow Factors
B
Cell Area
Cell Area
24h Treatment
Cell Area
72h Treatment
Cell Area
7-Day Treatment
Normalized Cell Area
C
Cell Roundness
Cell Roundness
24h Treatment
Cell Roundness
72h Treatment
Cell Roundness
7-Day Treatment
Normalized Cell Roundness
D
GFAP Intensity
GFAP Intensity
24h Treatment
GFAP Intensity
72h Treatment
GFAP Intensity
7-Day Treatment
Normalized GFAP Intensity
E
S100B Intensity
S100B Intensity
24h Treatment
S100B Intensity
72h Treatment
S100B Intensity
7-Day Treatment
Normalized S100B Intensity

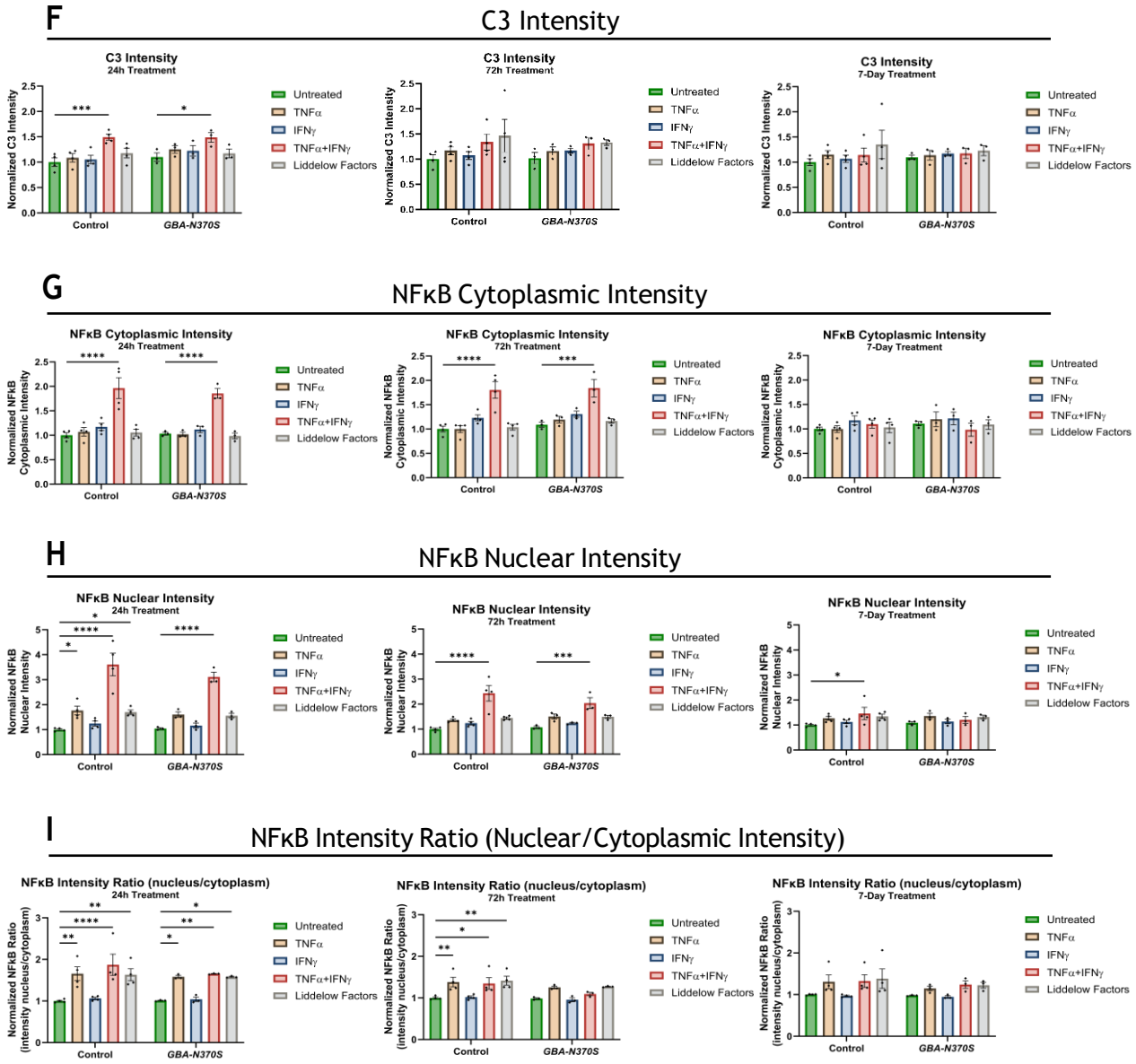


Figure 4.10. Control and *GBA-N370S* iASTROs treated with TNFα, TNFα+IFNγ or the Liddelow factors have an increase in the expression and nuclear translocation of NFκB 24h after treatment, and this decreases with time

(A-I) Quantification of (A) the total live cell number, (B) the cell area, (C) the cell roundness, (D) the cytoplasmic intensity of GFAP, (E) the cytoplasmic intensity of S100B, (F) the cytoplasmic intensity of C3, (G) the cytoplasmic intensity of NFκB, (H) the nuclear intensity of NFκB and (I) the NFκB intensity ratio (calculated by dividing the mean intensity in the nucleus by the mean intensity in the cytoplasm) in control and *GBA-N370S* iASTROs treated for 24h, 72h or 7 days with 30 ng/mL TNFα, 50 ng/mL IFNγ, 30 ng/mL TNFα + 50 ng/mL IFNγ, or the Liddelow factors (30 ng/mL TNFα + 3 ng/mL IL-1α + 400 ng/mL C1q). To obtain normalized values, in each timepoint, measured values were normalized to the average value of untreated control iASTROs. Each data point represents 1 iASTRO line averaged across differentiations. N = 3 control and 3 *GBA-N370S* lines, 3 differentiations. Mean ± SEM. The statistical analysis performed was two-way ANOVA with Dunnett's multiple comparison test to compare all treatment conditions to the untreated condition in each genotype, and two-way ANOVA with Šídák's multiple comparison test to compare both genotypes in each treatment condition. *p<0.05, **p<0.01, ***p<0.001, ****p<0.0001.

Lastly, there was an increase in cytoplasmic NFκB intensity in both genotypes 24h after exposure to TNFα+IFNγ, which was maintained after 72h after but abolished by 7 days (Figure 4.10 G). A small increase in intensity was also detected in cells exposed to IFNγ for 72h (Figure 4.10 G). On the other hand, the nuclear NFκB intensity increased significantly in both cell populations treated for 24h with TNFα and the Liddelow factors, and more so TNFα+IFNγ. 72h after treatment, the increase in nuclear NFκB intensity was lower in all treatments, but still higher in TNFα+IFNγ treated cells, whereas the increase was almost abolished by 7 days (Figure 4.10 H). Finally, a similar increase in NFκB intensity ratio (intensity in the nucleus/intensity in the cytoplasm, indicative of nuclear translocation) was observed in control and *GBA-N370S* iASTROs treated for 24h with TNFα, TNFα+IFNγ and the Liddelow factors, and this increase was lower after 72h and more so 7 days (Figure 4.10 I).

All in all, these results complement the findings done by RT-qPCR and show a higher reactive response in the earlier timepoints after acute treatment with inflammatory cytokines, especially TNFα+IFNγ.

4.3.3. Reactive oxygen species generation

As mentioned in section 4.2.4.1., the RNAseq study in reactive astrocytes showed an increase in GO:BP terms related to reactive oxygen and nitrogen species (ROS and RNS) production, whereas there was also an increase in genes encoding enzymes with antioxidant function (e.g. *SOD2, GPX1/4*). Oxidative stress is believed to be one of the drivers of neurodegeneration in PD (Trist et al., 2019), since DAn of the SNpc are more susceptible to damage caused by oxidative stress (Guo et al., 2018; Taylor et al., 2013). In the CNS, astrocytes have a crucial role in the production of antioxidants as well as the detoxification of RNS and ROS, but this astrocytic function might be impaired in PD (Rizor et al., 2019). Thus, I investigated whether the generation of ROS species in iASTROs changed after treatment with inflammatory cytokines. To this end, control and *GBA-N370S* iASTROs were treated for 24h, 72h, 7 days and 14 days with 30 ng/mL TNFα + 50 ng/mL IFNγ or the Liddelow factors (30 ng/mL TNFα + 3 ng/mL IL-1α + 400 ng/mL C1q), and the formation of ROS was measured using the DCFDA/H_2DCFDA assay (most commonly used assay for ROS detection (Wardman, 2023)) and normalizing for total cell count. 24h after treatment, ROS levels were slightly decreased in

TNFα+IFNγ treated cells in both genotypes compared to untreated cells, and *GBA-N370S* iASTROs appeared to have higher ROS levels at baseline (Figure 4.11 A, not statistically significant). 72h after treatment, there was no difference in ROS levels across conditions in control iASTROs, whereas there was an increase in *GBA-N370S* iASTROs treated with TNFα+IFNγ (Figure 4.11 B, not statistically significant). By 7 days, there was a significant increase in ROS levels in cells treated with TNFα+IFNγ but not the Liddelow factors compared to untreated cells, and this increase was higher in *GBA-N370S* iASTROS (Figure 4.11 C), and this increase was even bigger after 14 days (Figure 4.11 D). Overall, these results show that ROS levels increased in iASTROs treated with TNFα+IFNγ but not the Liddelow factors, and this increase happened gradually a few days after treatment. Moreover, this data suggests that the *GBA-N370S* mutation might negatively affect the detoxifying capacity of iASTROs upon inflammatory stimuli, or that it causes the cells to produce more ROS.

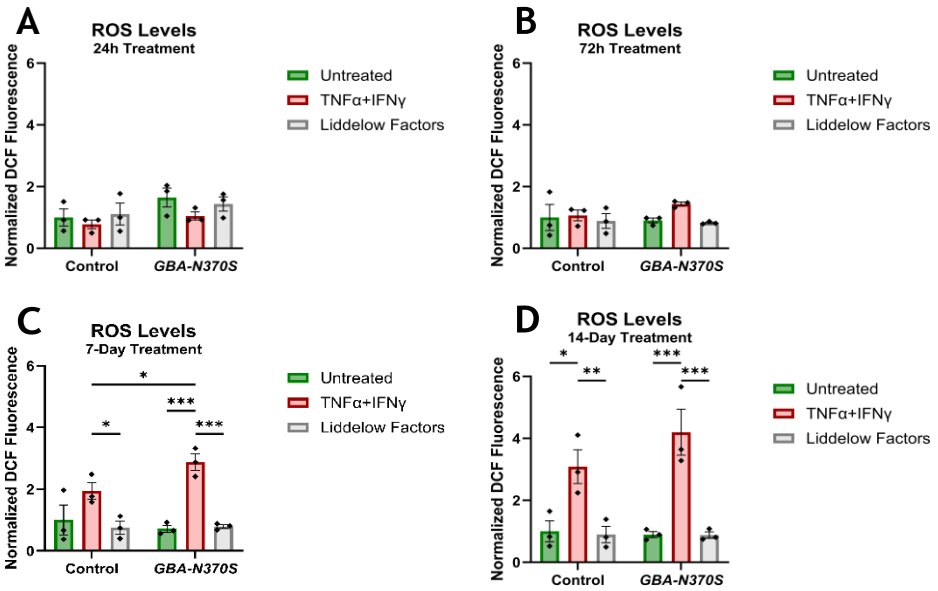


Figure 4.11. ROS levels are increased over time in control and *GBA-N370S* iASTROS in response to TNFα+IFNγ but not the Liddelow factors

(A-D) Quantification of the ROS levels in control and *GBA-N370S* iASTROs treated for (A) 24h, (B) 72h, (C) 7 days or (D) 14 days with 30 ng/mL TNFα + 50 ng/mL IFNγ or the Liddelow factors (30 ng/mL TNFα + 3 ng/mL IL-1α + 400 ng/mL C1q). The DCF fluorescence measured was normalized to the total number of nuclei, and afterwards, in each differentiation the values were normalized to the average of untreated control iASTROs. Each data point represents 1 iASTRO line averaged across differentiations. N = 3 control and 3 *GBA-N370S* lines, 3 differentiations. Mean ± SEM. The statistical analysis performed was two-way ANOVA with Tukey's multiple comparison test. *p<0.05, **p<0.01, ***p<0.001.

4.3.4. Lipid homeostasis and lipid droplet formation

Emerging data has shown that alterations in lipid and cholesterol homeostasis are associated with PD (Xicoy et al., 2019), and reduced neutral lipid content has been observed in substantia nigra astrocytes of PD patients (Brekk et al., 2020), indicating that there is lipid dyshomeostasis in these cells. Based on the fact that multiple genes related to lipid homeostasis and metabolism, including cholesterol metabolism, were dysregulated in reactive iASTROs in the RNAseq experiment, I investigated the expression of a few lipid homeostasis-related genes (identified as hits in the RNAseq experiment) by RT-qPCR in iASTROs treated for 24h or 7 days with 30 ng/mL TNFα + 50 ng/mL IFNγ or the Liddelow factors (30 ng/mL TNFα + 3 ng/mL IL-1α + 400 ng/mL C1q).

I first analysed the expression of *ELOVL1*, which has been related to neurotoxic reactive astrocytes (Guttenplan et al., 2021). Similar to the RNAseq results (Figure 4.7), even if there was a small increase in *ELOVL1* expression in control and *GBA-N370S* iASTROs treated with TNFα+IFNγ for 24h or 7 days compared to untreated cells (not statistically significant), there was no increase in cells treated with the Liddelow factors (Figure 4.12 A). Next, 24h after treatment with TNFα+IFNγ, there was a slight increase in *HMGCR* expression in both iASTRO genotypes compared to untreated cells, which did not reach statistical significance, but by 7 days there was a decrease in cells treated with TNFα+IFNγ and the Liddelow factors (Figure 4.12 B). Lastly, in both control and *GBA-N370S* iASTROs treated with TNFα+IFNγ for 24h, there was a significant increase in the expression of *LDLR* compared to untreated iASTROs or cells treated with the Liddelow factors, but this increase was completely abolished by 7 days (Figure 4.12. C).

I next investigated the content of lipid droplets in iASTROs using BODIPY 493/503, a fluorescent nonpolar lipid probe that stains neutral lipids, which form the centre of lipid droplets (Olzmann & Carvalho, 2019). Control and *GBA-N370S* iASTROs were incubated with BODIPY 493/503 72h and 7 days after treatment with TNFα+IFNγ or the Liddelow factors (Figure 4.12 D), and the number and area of BODIPY spots were quantified. There were no differences in the number and area of BODIPY spots after either treatment in both iASTRO populations (Figure 4.12 E-F). In the RNAseq experiment, genes encoding 2 of the main enzymes involved in the synthesis of neutral lipids, acyl-coenzyme A:cholesterol acyltransferase 1 and 2 (ACAT1 and ACAT2), were slightly downregulated in iASTROs treated

with TNFα+IFNγ and TNFα+IFNγ+PFFs, whereas no differences were observed in genes encoding 2 of the other important enzymes, diacylglycerol acyltransferase 1 and 2 (DGAT1 and DGAT2) (Olzmann & Carvalho, 2019), which might explain why after 24h and 7 days of treatment there were no changes in lipid droplet content and size in reactive iASTROs.

Overall, these results do not show extensive changes in lipid content and homeostasis in iASTROs treated with TNFα+IFNγ or the Liddelow factors. However, the experiments performed in this only scratch the surface of all the lipidomic studies that could be done to study lipid metabolism and content in astrocytes and only look at the first 7 days after an acute inflammatory insult.

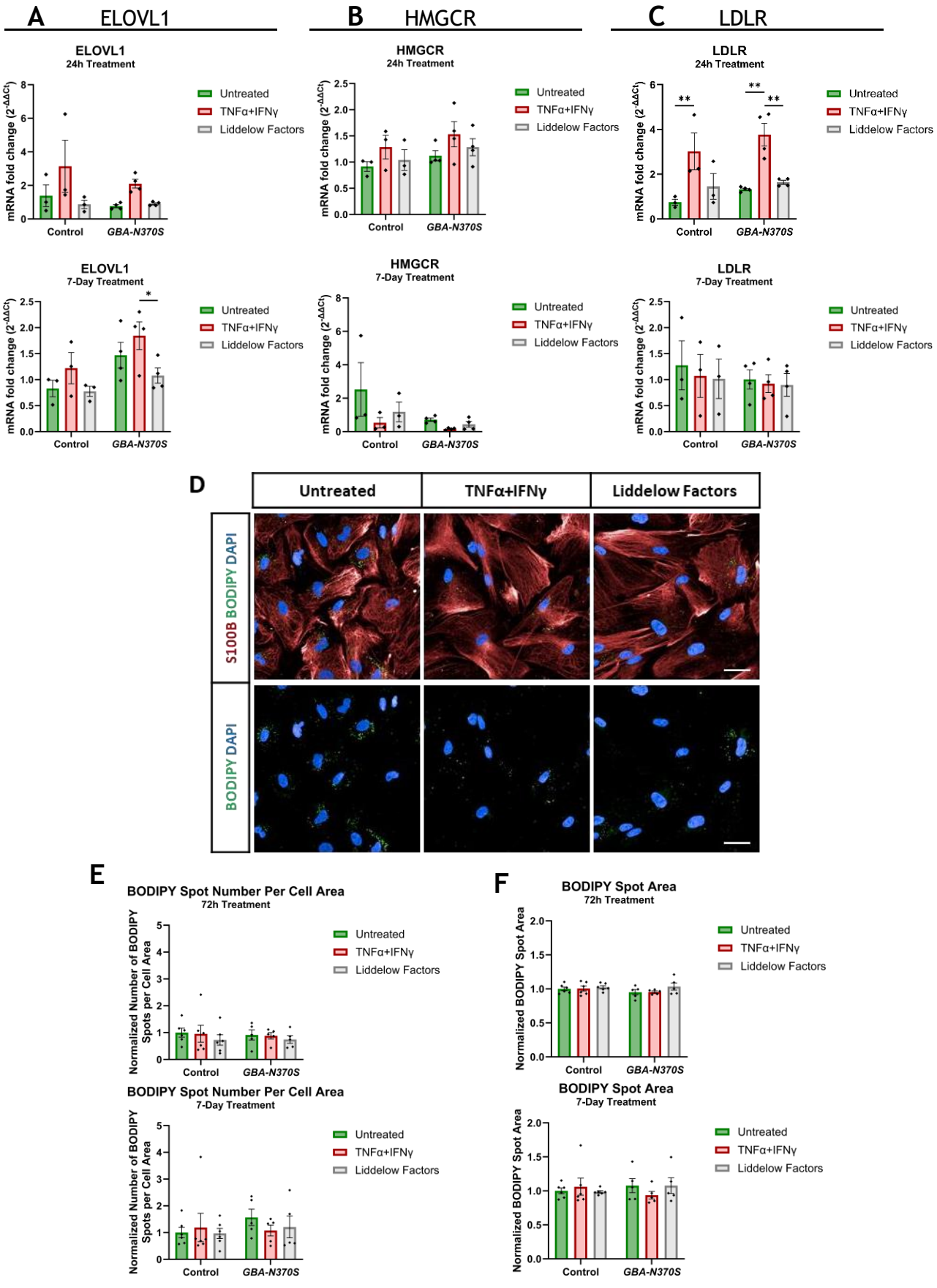

A
ELOVL1
B
HMGCR
C
LDLR
ELOVL1
24h Treatment
HMGCR
24h Treatment
LDLR
24h Treatment
ELOVL1
7-Day Treatment
HMGCR
7-Day Treatment
LDLR
7-Day Treatment
mRNA fold change (2-ΔΔCt)
Control
GBA-N370S
Untreated
TNFα+IFNγ
Liddelow Factors
D
Untreated
TNFα+IFNγ
Liddelow Factors
S100B BODIPY DAPI
BODIPY DAPI
E
BODIPY Spot Number Per Cell Area
72h Treatment
BODIPY Spot Number Per Cell Area
7-Day Treatment
Normalized Number of BODIPY Spots per Cell Area
F
BODIPY Spot Area
72h Treatment
BODIPY Spot Area
7-Day Treatment
Normalized BODIPY Spot Area

Figure 4.12. Control and *GBA-N370S* iASTROs present changes in the relative gene expression of some lipid metabolism related genes in response to TNFα+IFNγ, but this does not result in changes in the number or size of lipid droplets

(A-C) Relative gene expression analysis by RT-qPCR of (A) ELOVL1, (B) HMGCR and (C) LDLR in control and *GBA-N370S* iASTROs treated for 24h or 7 days with 30 ng/mL TNFα + 50 ng/mL IFNγ or the Liddelow factors (30 ng/mL TNFα + 3 ng/mL IL-1α + 400 ng/mL C1q)). In each differentiation, to calculate ΔΔCt for each gene, the ΔCt of one untreated control iASTRO line was subtracted to the ΔCt of all the lines (for the gene of interest). Each data point represents 1 iASTRO line averaged across differentiations. N = 3 control and 4 *GBA-N370S* lines, 1-4 differentiations. Mean ± SEM. The statistical analysis performed was two-way ANOVA with Tukey's multiple comparison test. *p<0.05, **p<0.01.

(D) Representative immunocytochemistry images of control iASTROs treated with 30 ng/mL TNFα + 50 ng/mL IFNγ or the Liddelow factors (30 ng/mL TNFα + 3 ng/mL IL-1α + 400 ng/mL C1q) for 72h, and stained for BODIPY 493/503 (green) and S100B (red). Scale bar: 50 μm. (E-F) Quantification of (E) the number of BODIPY spots per cell area and (F) the area of BODIPY spots in control and *GBA-N370S* iASTROs treated for 72h or 7 days with 30 ng/mL TNFα + 50 ng/mL IFNγ or the Liddelow factors (30 ng/mL TNFα + 3 ng/mL IL-1α + 400 ng/mL C1q)). For each differentiation, in each timepoint, values were normalized to the average of untreated control iASTROs. Each data point represents 1 iASTRO line averaged across differentiations. N = 6 control and 5 *GBA-N370S* lines, 1-4 differentiations. Mean ± SEM. The statistical analysis performed was two-way ANOVA with Tukey's multiple comparison test.

4.3.5. Relative gene expression of growth factors

As shown in Figure 4.7., *BDNF* expression was downregulated in iASTROs treated with TNFα+IFNγ and TNFα+IFNγ+PFFs but upregulated in cells treated with IFNγ alone, whereas TGFβ was slightly upregulated in those three treatments. On the contrary, genes encoding of other growth factors (*GDNF, MANF*, and *FGF2*) presented large line-to-line variability in the expression levels. To investigate if the expression of these growth factors changed at later timepoints, I analysed their relative gene expression in control and *GBA-N370S* iASTROs 24h and 7 days after treatment with 30 ng/mL TNFα + 50 ng/mL IFNγ or the Liddelow factors (30 ng/mL TNFα + 3 ng/mL IL-1α + 400 ng/mL C1q).

The expression patterns of *BDNF* in treated iASTROs differed from those observed in the RNAseq data (Figure 4.7). 24h after treatment, there was an increase in its expression in cells treated with the Liddelow factors compared to untreated and TNFα+IFNγ-treated cells, but this was only statistically significant in *GBA-N370S* iASTROs (Figure 4.13 Ai). On the other hand, 7 days after treatment there was an increase in the relative *BDNF* expression in iASTROs treated with TNFα+IFNγ, only statistically significant in *GBA-N370S* cells, but no differences in cells treated with the Liddelow factors (Figure 4.13 Aii). *GDNF* expression was more variable between the lines, and no significant differences were observed in either cell genotype with

any of the treatments in both timepoints, although 24h after treatment with TNFα+IFNγ its expression appeared to be decreased (Figure 4.13 B). Moreover, *FGF2* expression was significantly higher in control and *GBA-N370S* iASTROs treated with TNFα+IFNγ than in untreated cells, and this increase was more pronounced after 7 days (Figure 4.13 C). In iASTROs treated with the Liddelow factors for 24h, there was an increase in *FGF2* expression compared to untreated cells, which was abolished by 7 days (Figure 4.13 C). Expression of *MANF* did not vary significantly after either treatment, although there was a small increase after 24h but a decrease after 7 days of treatment with TNFα+IFNγ compared to untreated iASTROs (Figure 4.13 D). Lastly, *TGFβ1* expression did not change much in response to either treatment, but its expression was higher in *GBA-N370S* iASTROs than in control cells (Figure 4.13 E).

Moreover, I investigated how the expression of *BDNF* and *GDNF* differed between mature iDAn and iASTROs, because, despite its name, *GDNF* has been reported to be more highly expressed in neurons than in glial cells (Duarte Azevedo et al., 2020), and the evidence suggests that this is also true for *BDNF* (Esvald et al., 2023). Indeed, the relative expression of *BDNF* was significantly higher in both control and *GBA-N370S* iDAn than in iASTROs (Figure 4.13 Fi). On the other hand, expression of *GDNF* was higher in control iASTROs than in control iDAn, but no differences were observed between *GBA-N370S* iDAn and iASTROs (Figure 4.13 Fii). Moreover, expression in control iASTROs was higher than in *GBA-N370S* iASTROs, which was not observed in previous experiments (Figure 4.13 B). This discrepancy in the results could be for numerous reasons, namely the cells from different differentiations used in each experiment.

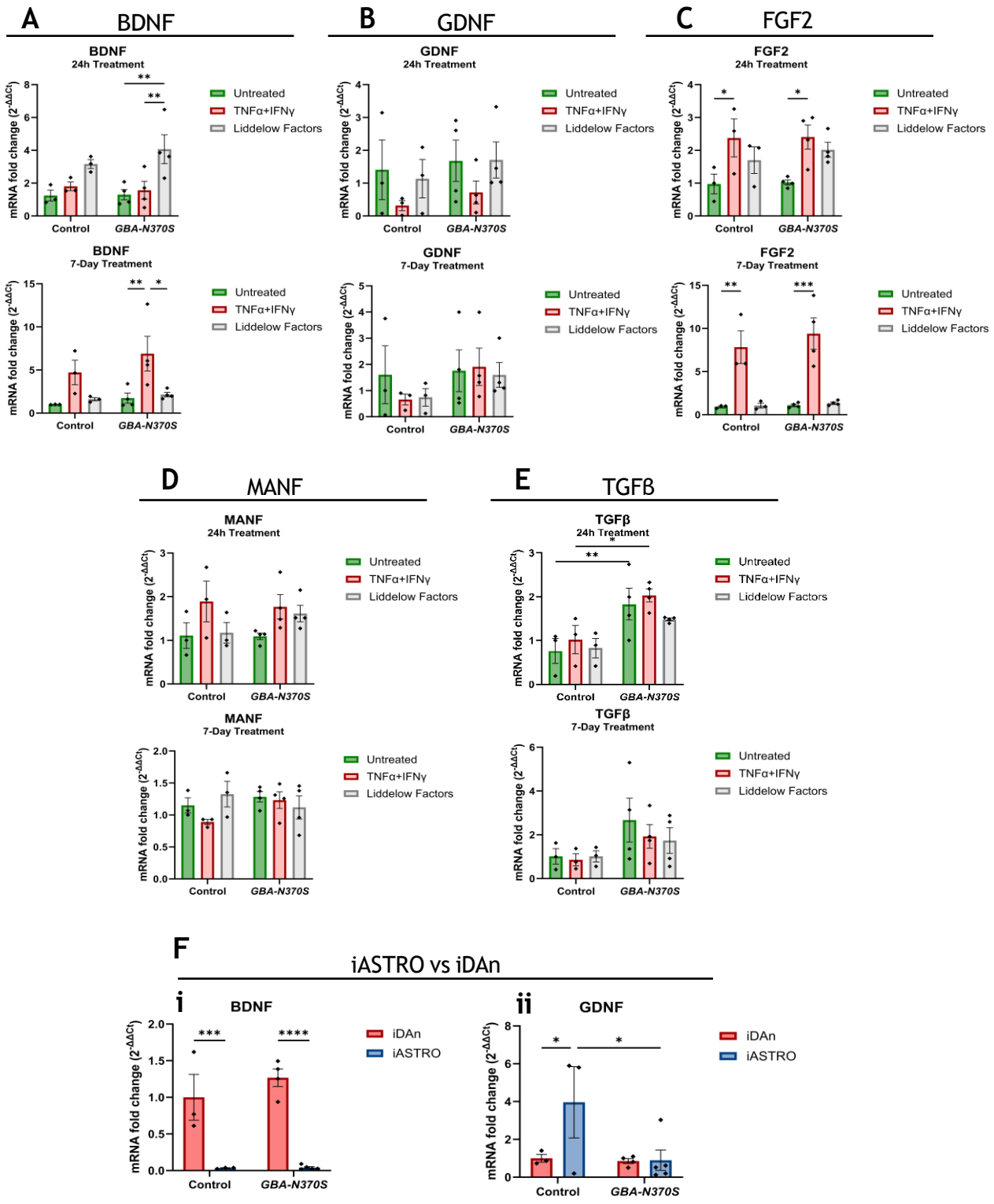


Figure 4.13. Relative gene expression of some growth factors is increased in control and *GBA-N370S* iASTROs in response to TNFα+IFNγ or the Liddelow factors

(A-E) Relative gene expression analysis by RT-qPCR of (A) BDNF, (B) GDNF, (C) FGF2, (D) MANF and (E) TGFβ in control and GBA-N370S iASTROs treated for 24h or 7 days with 30 ng/mL TNFα + 50 ng/mL IFNγ or the Liddelow factors (30 ng/mL TNFα + 3 ng/mL IL-1α + 400 ng/mL C1q). In each differentiation, to calculate ΔΔCt for each gene, the ΔCt of one untreated control iASTRO line was subtracted to the

ΔCt of all the lines (for the gene of interest). Each data point represents 1 iASTRO line averaged across differentiations. N = 3 control and 4 *GBA-N370S* lines, 1-4 differentiations. Mean ± SEM. The statistical analysis performed was two-way ANOVA with Tukey's multiple comparison test. *p<0.05, **p<0.01, ***p<0.001. (F) Relative gene expression analysis by RT-qPCR of (i) BDNF and (ii) GDNF in DIV35 control and *GBA-N370S* iDAn and DIV100 control and *GBA-N370S* iASTROs. To calculate ΔΔCt for each gene, the average ΔCt of control iDAn was subtracted to the ΔCt of all iDAn and iASTRO lines (for the gene of interest). Each data point represents 1 line averaged across differentiations. N = 3 control and 3 *GBA-N370S* lines for iDAn (2 differentiations), and 3 control and 5 *GBA-N370S* lines for iASTROs (1-2 differentiations). Mean ± SEM. The statistical analysis performed was two-way ANOVA with Fisher's LSD test. *p<0.05, **p<0.01, ***p<0.001, ****p<0.0001.

4.4. In vitro study of the inflammatory response of control and *GBA-N370S* iASTROs to α-synuclein PFFs, with or without TNFα+IFNγ

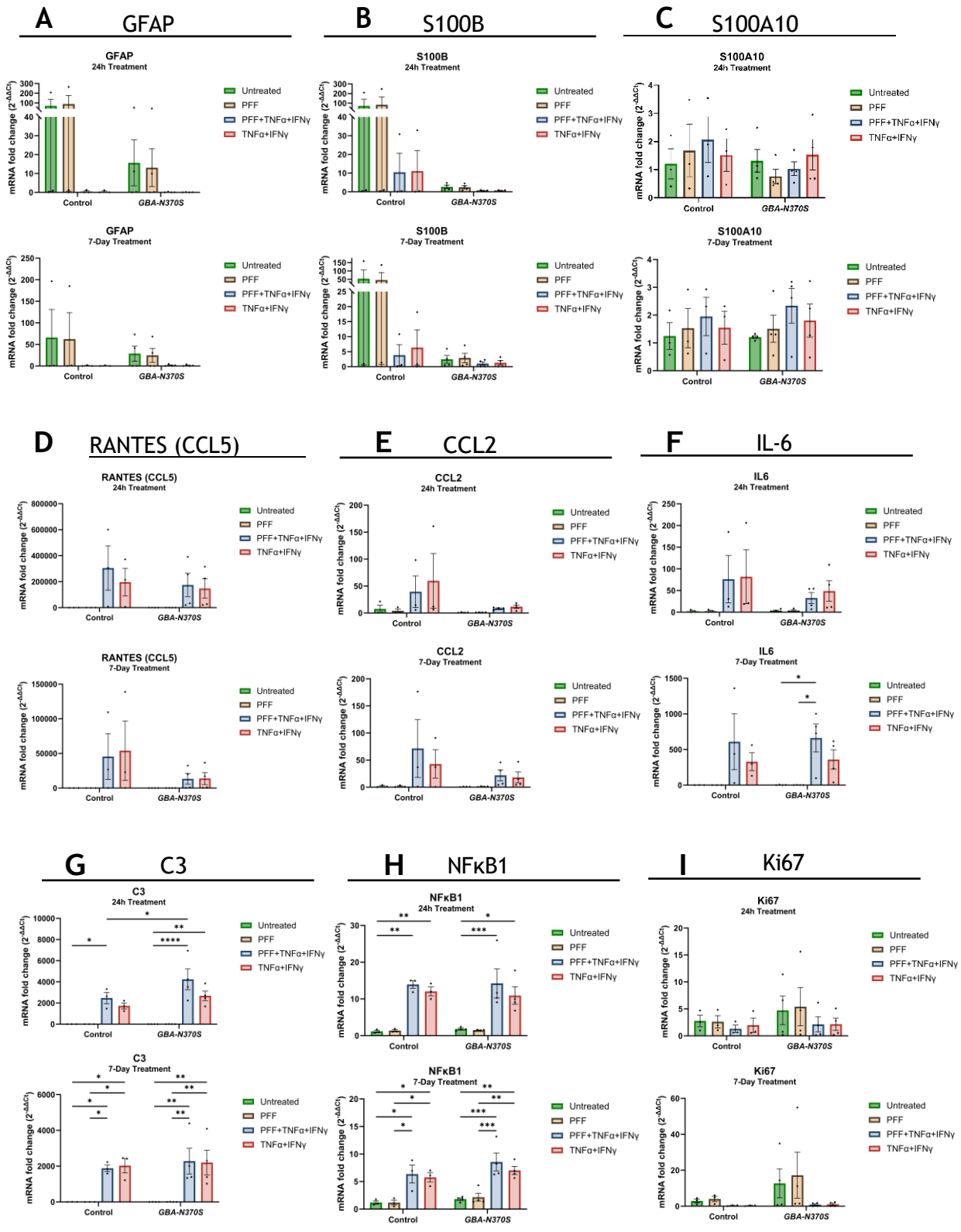
As discussed in section 4.2, 24h of exposure to α-synuclein PFFs alone did not cause major transcriptomic changes in control iASTROs, and the addition of α-synuclein PFFs to cells treated with TNFα+IFNγ did not cause additional transcriptomic changes either. However, since in the brain of PD patients astrocytes are exposed to excessive neuronal α-synuclein for years (Brash-Arias et al., 2024), longer exposure times might be required to induce cellular changes in astrocytes. Therefore, I carried out a similar in vitro characterization of iASTRO reactivity to the one presented in section 4.3., in this case treating the cells with α-synuclein PFFs, TNFα+IFNγ or a combination of both.

4.4.1. RT-qPCR analysis of relative gene expression

I first investigated the relative expression of the genes of interest described in Section 4.3.1. in control and *GBA-N370S* iASTROs treated for 24h or 7 days with α-synuclein PFFs (10 µg/mL), TNFα (30 ng/mL) + IFNγ (50 ng/mL) + α-synuclein PFFs (10 µg/mL), or TNFα (30 ng/mL) + IFNγ (50 ng/mL). The focus of this analysis was the effect of PFFs on the expression of these genes, and a more detailed description of the effect of TNFα+IFNγ and the *GBA-N370S* mutation in the expression of these genes is provided in Section 4.3.1. Overall, the trends in increase/decrease after treatment with TNFα+IFNγ were the same as in Figure 4.8, and, unless stated otherwise, cells treated with TNFα+IFNγ+PFFs followed a similar pattern.

No significant changes in the expression of *GFAP, S100B, S100A10, RANTES (CCL5*), *CCL2, IL-6, C3, NFκB1, Ki67* and *VCAM1* were detected after exposure to PFFs alone (Figure 4.14 A-J).

Overall, no major differences in the relative gene expression of these genes were observed between cells treated with TNFα+IFNγ+PFFs or TNFα+IFNγ, except a small and non-significant decrease in the expression of *IL-6* after 7 days, *C3* after 24h, and *NFκB1* at both timepoints in iASTROs treated with TNFα+IFNγ compared to TNFα+IFNγ+PFFs. Lastly, I investigated the expression of *HLA-DPB1* and *DLA-DRB1*, which were increased in iASTROs treated with TNFα+IFNγ (Figure 4.8 K-L), and a study showed that α-synuclein fibrils induced *HLA-DPB1* and *HLA-DRB1* expression in iPSC-derived astrocytes, which was abolished with the combined treatment with TNFα (Russ et al., 2021). However, there were no differences in *HLA-DPB1* and *HLA-DRB1* expression in iASTROs treated for 24h or 7 days with α-synuclein PFFs alone compared to untreated cells, or between iASTROs treated with TNFα+IFNγ and TNFα+IFNγ+PFFs (Figure 4.23 K-L). All in all, these results indicate that after 7 days of treatment α-synuclein PFFs do not induce changes in the expression of various gene related to inflammation and the immune response in control and *GBA-N370S* iASTROs.


A
GFAP
B
S100B
C
S100A10
GFAP
24h Treatment
S100B
24h Treatment
S100A10
24h Treatment
GFAP
7-Day Treatment
S100B
7-Day Treatment
S100A10
7-Day Treatment
mRNA fold change (2-ΔΔCt)
Control
GBA-N370S
Untreated
PFF
PFF+TNFα+IFNγ
TNFα+IFNγ
D
RANTES (CCL5)
E
CCL2
F
IL-6
RANTES (CCL5)
24h Treatment
CCL2
24h Treatment
IL6
24h Treatment
RANTES (CCL5)
7-Day Treatment
CCL2
7-Day Treatment
IL6
7-Day Treatment
G
C3
H
NFκB1
I
Ki67
C3
24h Treatment
NFκB1
24h Treatment
Ki67
24h Treatment
C3
7-Day Treatment
NFκB1
7-Day Treatment
Ki67
7-Day Treatment

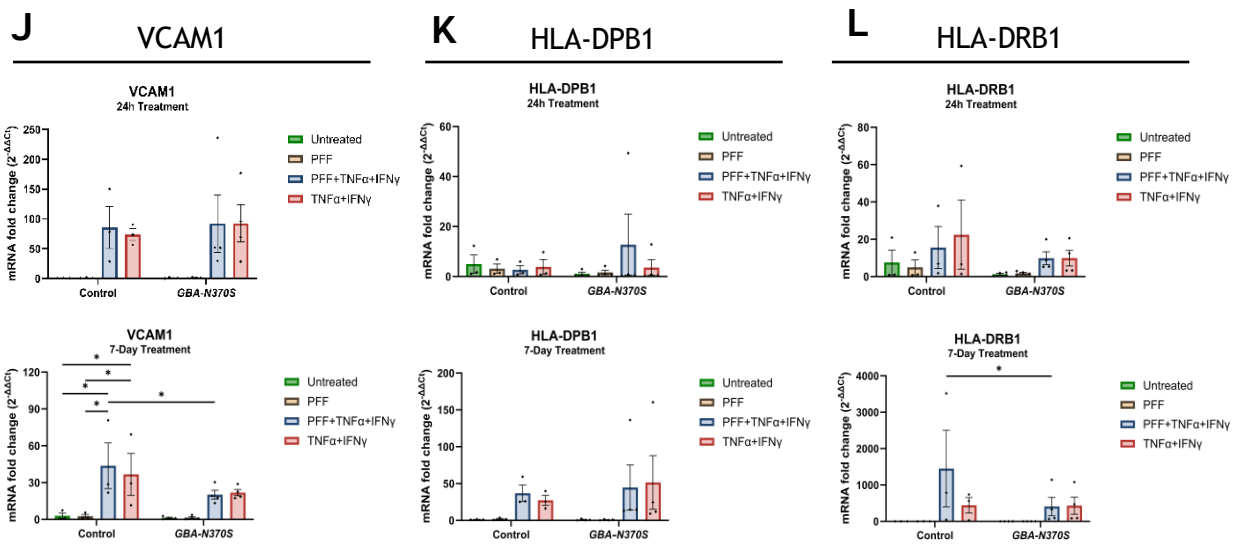


Figure 4.14. Relative gene expression analysis by RT-qPCR shows that iASTROs do not undergo an inflammatory response after 24h or 7-day treatment with α-synuclein PFFs

(A-L) Relative gene expression analysis by RT-qPCR of (A) GFAP, (B) S100B, (C) S100A10, (D) RANTES (CCL5), (E) CCL2, (F) IL-6, (G) C3, (H) NFκB1, (I) Ki67, (J) VCAM1, (K) HLA-DPB1, and (L) HLA-DRB1 in control and *GBA-N370S* iASTROs treated for 24h or 7 days with 10 µg/mL α-synuclein PFFs, 10 µg/mL α-synuclein PFFs + 30 ng/mL TNFα + 50 ng/mL IFNγ, or 30 ng/mL TNFα + 50 ng/mL IFNγ. In each differentiation, to calculate ΔΔCt for each gene, the ΔCt of one untreated control iASTRO line was subtracted to the ΔCt of all the lines (for the gene of interest). Each data point represents 1 iASTRO line averaged across differentiations. N = 3 control and 4 *GBA-N370S* lines, 1-4 differentiations. Mean ± SEM. The statistical analysis performed was two-way ANOVA with Tukey's multiple comparison test. *p<0.05, **p<0.01, ***p<0.001, ****p<0.0001.

4.4.2. Immunocytochemistry analysis of inflammatory markers and cellular morphology

Next, I used immunocytochemistry to analyse the morphology as well as the expression of a number of astrocytic and inflammatory markers in control and *GBA-N370S* iASTROs treated for 24h, 72h or 7 days with α-synuclein PFFs (10 µg/mL), TNFα (30 ng/mL) + IFNγ (50 ng/mL) + α-synuclein PFFs (10 µg/mL), or TNFα (30 ng/mL) + IFNγ (50 ng/mL) (Figure 4.15). As in section 4.4.1., the focus of this experiment was the effect of PFFs on iASTRO reactivity, and details on the effect of TNFα+IFNγ on these parameters are described in detail in section 4.3.2.

Overall, there were no differences in the total number of live cells due to the addition of PFFs to untreated or TNFα+IFNγ-treated cells (Figure 4.16 A). No changes in the cell area were detected either (Figure 4.16 B). Moreover, the cell roundness did not change between untreated or PFF-treated cells, but after 24h of treatment it was slightly higher in iASTROs

treated with TNFα+IFNγ compared to TNFα+IFNγ+PFFs. This observation is worth highlighting because, in some iASTRO lines, the morphology of iASTROs treated with TNFα+IFNγ was different when adding PFFs, as illustrated in the top panel of Figure 4.15, 3rd and 4th rows, but no differences were observed between untreated and PFF-treated cells. GFAP intensity was overall higher in *GBA-N370S* iASTROs (Figure 4.16 D), and, in all 3 timepoints, GFAP intensity was slightly increased (not statistically significant) in *GBA-N370S* iASTROs treated with PFFs alone compared to untreated cells, and in cells treated for 72h and 7 days with TNFα+IFNγ+PFFs compared to TNFα+IFNγ (Figure 4.16 D). The intensity of S100B and C3 did not differ due to the addition of PFFs to untreated or TNFα+IFNγ-treated cells (Figure 4.16 E-F). The cytoplasmic and nuclear intensity of NFκB, as well as the NFκB intensity ratio (intensity in the nucleus/intensity in the cytoplasm), did not significantly differ between untreated iASTROs or iASTROs treated with PFFs alone at any of the timepoints, there was only a small increase in the nuclear and cytoplasmic intensities after 72h and 7 days (Figure 4.16 G-H). On the other hand, the nuclear intensity of NFκB was higher in iASTROs treated with TNFα+IFNγ than with TNFα+IFNγ+PFFs after 72h and less so 7 days (Figure 4.16 H), but there were no differences between these two treatments in the intensity ratio (Figure 4.16 I).

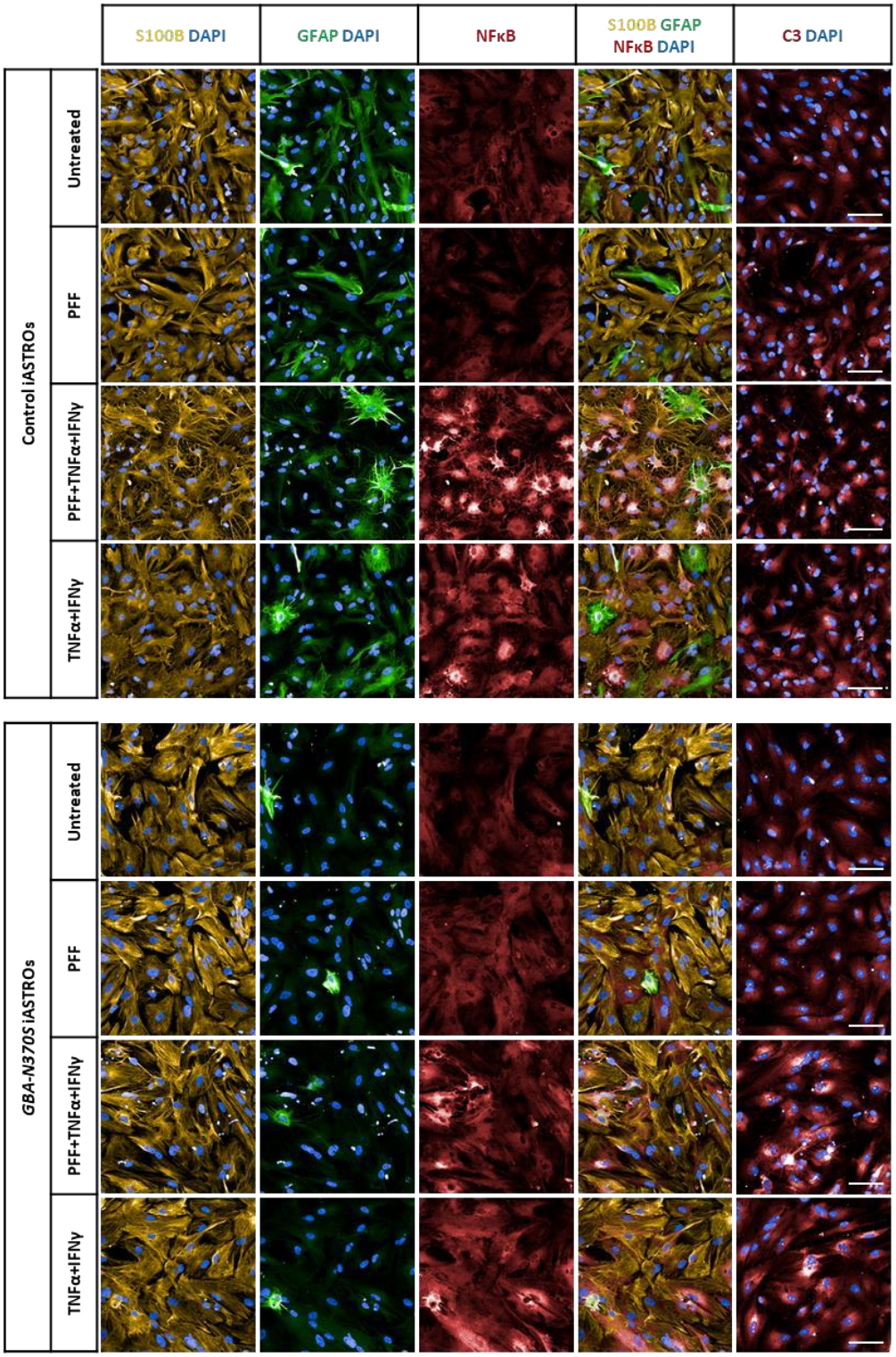
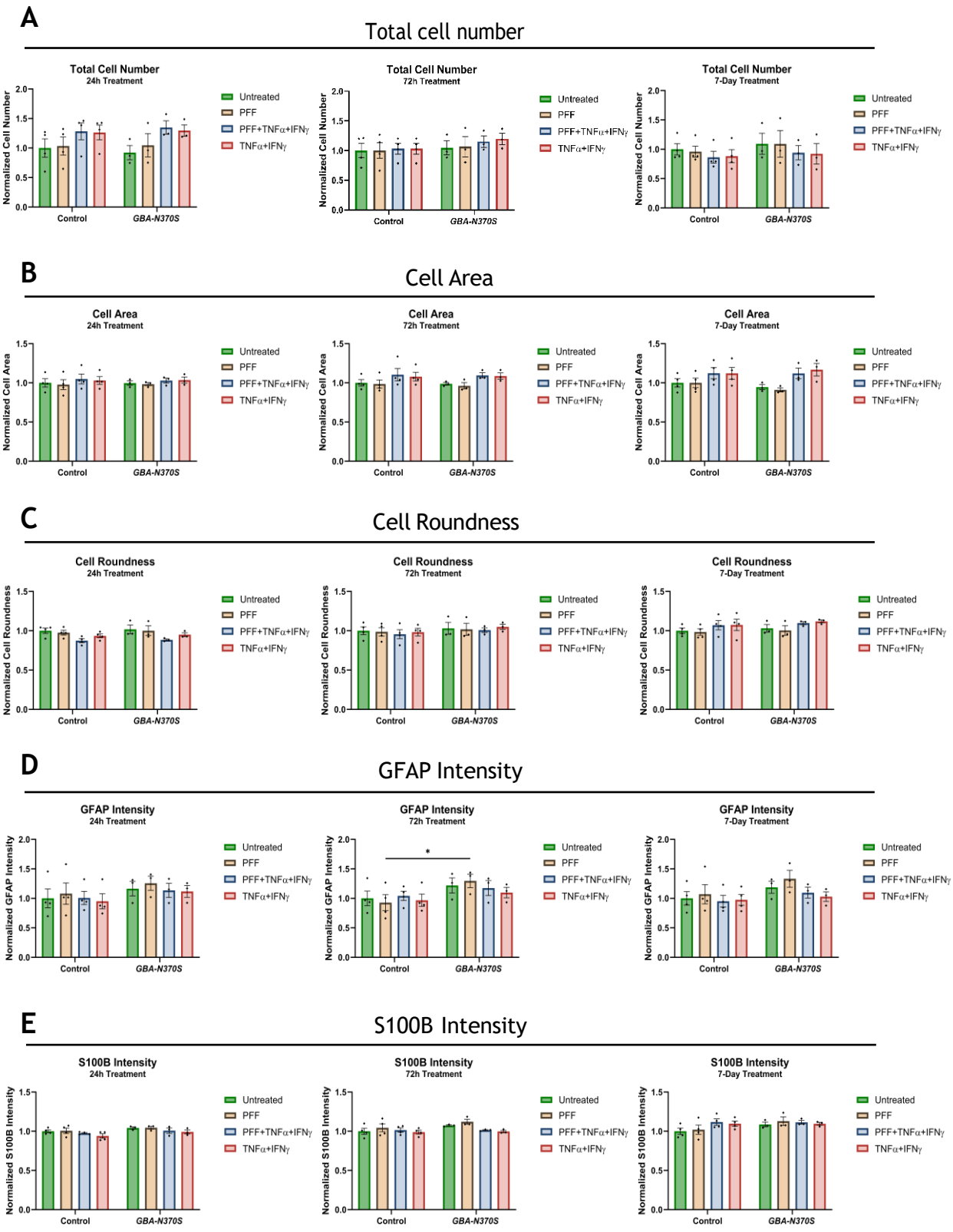


Figure 4.15. Representative immunocytochemistry images of control (top panel) and *GBA-N370S* (bottom panel) iASTROs treated with inflammatory cytokines and α-synuclein PFFs

α-synuclein PFFs (10 µg/mL), α-synuclein PFFs (10 µg/mL) + TNFα (30 ng/mL) + IFNγ (50 ng/mL), or TNFα (30 ng/mL) + IFNγ (50 ng/mL) for 72h. Cells are stained for S100B (yellow), GFAP (green), NFκB (red, third and fourth columns) and C3 (red, fifth column). Scale bar: 100 µm.


A
Total cell number
Total Cell Number
24h Treatment
Normalized Cell Number
Control
GBA-N370S
Untreated
PFF
PFF+TNFα+IFNγ
TNFα+IFNγ
Total Cell Number
72h Treatment
Total Cell Number
7-Day Treatment
B
Cell Area
Cell Area
24h Treatment
Normalized Cell Area
Cell Area
72h Treatment
Cell Area
7-Day Treatment
C
Cell Roundness
Cell Roundness
24h Treatment
Normalized Cell Roundness
Cell Roundness
72h Treatment
Cell Roundness
7-Day Treatment
D
GFAP Intensity
GFAP Intensity
24h Treatment
Normalized GFAP Intensity
*
GFAP Intensity
72h Treatment
GFAP Intensity
7-Day Treatment
E
S100B Intensity
S100B Intensity
24h Treatment
Normalized S100B Intensity
S100B Intensity
72h Treatment
S100B Intensity
7-Day Treatment

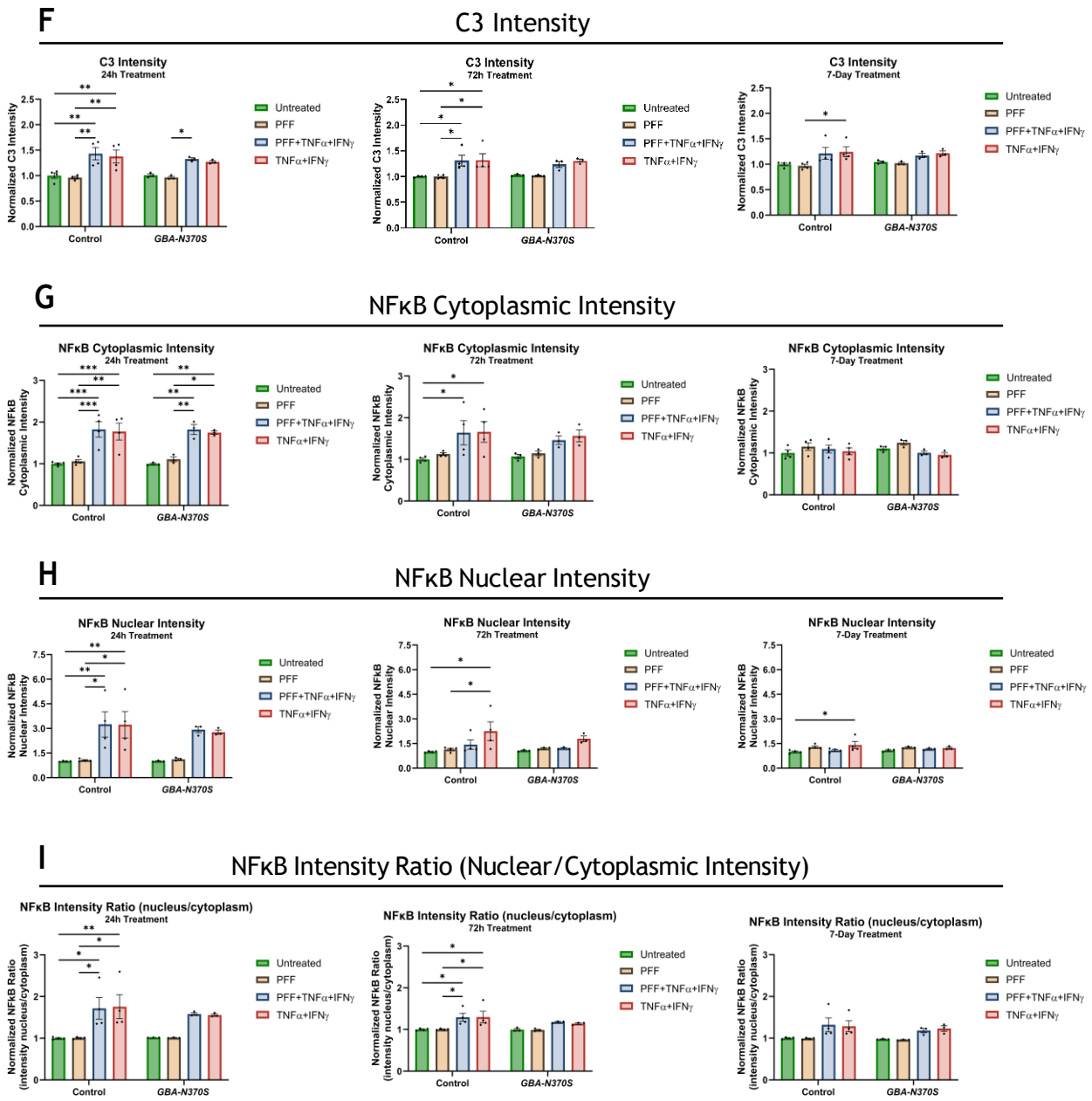


Figure 4.16. Control and *GBA-N370S* iASTROs do not undergo reactive astrogliosis in response to α-synuclein PFFs alone 24h, 72h and 7 days after treatment

(A-I) Quantification of (A) the total live cell number, (B) the cell area, (C) the cell roundness, (D) the cytoplasmic intensity of GFAP, (E) the cytoplasmic intensity of S100B, (F) the cytoplasmic intensity of C3, (G) the cytoplasmic intensity of NFκB, (H) the nuclear intensity of NFκB and (I) the NFκB intensity ratio (calculated by dividing the mean intensity in the nucleus by the mean intensity in the cytoplasm) in control and *GBA-N370S* iASTROs treated for 24h, 72h or 7 days with α-synuclein PFFs (10 µg/mL), α-synuclein PFFs (10 µg/mL) + TNFα (30 ng/mL) + IFNγ (50 ng/mL), or TNFα (30 ng/mL) + IFNγ (50 ng/mL). To obtain normalized values, in each timepoint, measured values were normalized to the average value of untreated control iASTROs. Each data point represents 1 iASTRO line averaged across differentiations. N = 3 control and 3 *GBA-N370S* lines, 3 differentiations. Mean ± SEM. The statistical analysis performed was two-way ANOVA with Tukey's multiple comparison test. *p<0.05, **p<0.01, ***p<0.001, ****p<0.0001.

4.4.3. Reactive oxygen species generation

As discussed in section 4.3.3., ROS levels were elevated in iASTROs 7 and 14 days after treatment with TNFα+IFNγ. Moreover, even if a number of PD-related mutations have been linked to increased ROS/RNS in astrocytes (Rizor et al., 2019), little is known about the effect α-synuclein has on astrocytic ROS/RNS production. To investigate this, I treated control and *GBA-N370S* iASTROs for 24h, 72h, 7 days and 14 days with α-synuclein PFFs (10 µg/mL), TNFα (30 ng/mL) + IFNγ (50 ng/mL) + α-synuclein PFFs (10 µg/mL), or TNFα (30 ng/mL) + IFNγ (50 ng/mL) and I quantified ROS production using the DCFDA/H_2DCFDA assay and normalizing to total cell count. Overall, no changes in ROS levels were observed at any timepoint in iASTROs treated with α-synuclein PFFs alone compared to untreated cells (Figure 4.26 A-D). On the other hand, after 7 days of treatment, ROS levels were higher in control and *GBA-N370S* iASTROs treated with TNFα+IFNγ compared to TNFα+IFNγ+PFFs (Figure 4.17 C), but this observation did not reach statistical significance.

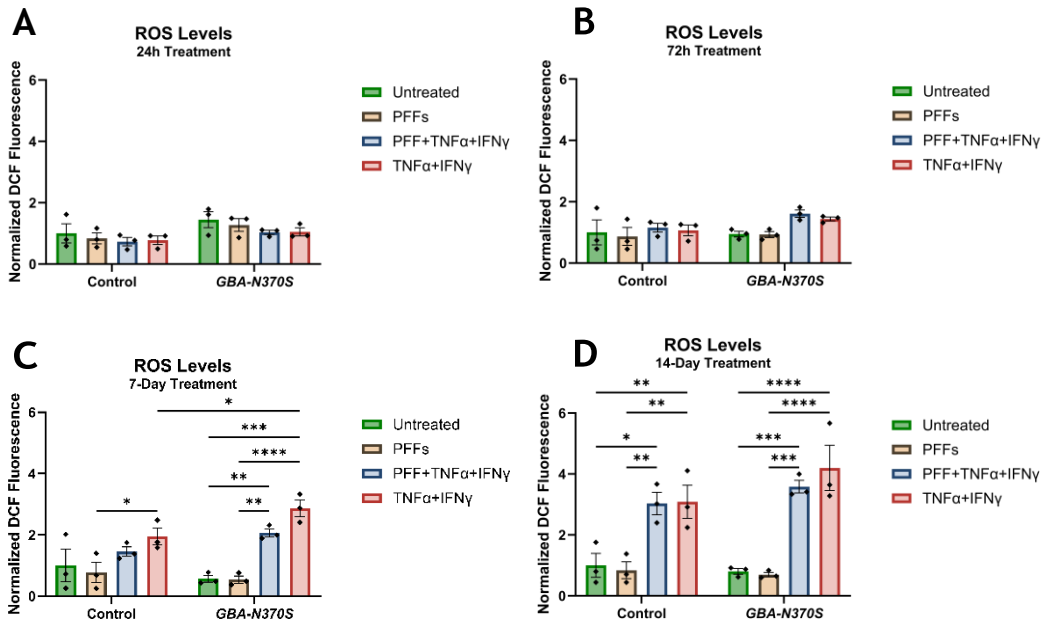


Figure 4.17. ROS levels are increased over time in control and *GBA-N370S* iASTROS in response to TNFα+IFNγ with or without α-synuclein PFFs, but not in cells treated with α-synuclein PFFs alone
(A-D) Quantification of the ROS levels in control and *GBA-N370S* iASTROs treated for (A) 24h, (B) 72h, (C) 7 days or (D) 14 days with α-synuclein PFFs (10 µg/mL), α-synuclein PFFs (10 µg/mL) + TNFα (30 ng/mL) + IFNγ (50 ng/mL), or TNFα (30 ng/mL) + IFNγ (50 ng/mL). The DCF fluorescence measured was normalized to the total number of nuclei, and afterwards, in each differentiation the values were normalized to the average of untreated control iASTROs. Each data point represents 1 iASTRO line averaged across differentiations. N = 3 control and 3 *GBA-N370S* lines, 3 differentiations. Mean ± SEM. The statistical analysis performed was: two-way ANOVA with Tukey's multiple comparison test. *p<0.05, **p<0.01, ***p<0.001, ****p<0.0001.

4.4.4. Lipid homeostasis and droplet formation

As discussed in section 4.2.4.2., most of the downregulated genes in PFF-treated iASTROs were related to lipid metabolism and homeostasis, such as *FAR1, LPCAT1, FASN, B4GALT5, DHCR24* and *ACACA* (Figure 4.3. Fi). Moreover, in the fgsea analysis, one of the main downregulated gene sets in PFF-treated iASTROs was "Cholesterol Homeostasis" (Figure 4.4. A). Therefore, I decided to investigate the expression of some genes of interest related to lipid homeostasis in iASTROs treated with PFFs, TNFα+IFNγ+PFFs and TNFα+IFNγ for 24h and 7 days. In *GBA-N370S* iASTROs, *FASN* expression was significantly downregulated after 24h of treatment with PFFs alone compared to untreated cells, and a decrease was also observed in cells treated with TNFα+IFNγ+PFFs for 24h compared to untreated cells or TNFα+IFNγ-treated cells (not statistically significant) (Figure 4.18 A). Similar expression patterns were observed after 24h of treatment in control iASTROs, but to a lesser magnitude (Figure 4.18). 7 days after treatment with TNFα+IFNγ+PFFs and TNFα+IFNγ, there was a decrease in *FASN* expression in both iASTRO populations (Figure 4.18 A). Moreover, *HMGCR* expression was lower in *GBA-N370S* iASTROs treated for 24h with PFFs alone compared to TNFα+IFNγ, and in control iASTROs expression was higher (but not statistically significant) in cells treated with TNFα+IFNγ+PFFs and TNFα+IFNγ compared to untreated cells (Figure 4.18 B). On the contrary, after 7 days, *HMGCR* expression was lower in control and *GBA-N370S* iASTROs treated with TNFα+IFNγ+PFFs and TNFα+IFNγ compared to untreated or PFF-treated cells, and *HMGCR* expression was lower in untreated *GBA-N370S* iASTROs than in untreated control iASTROs (Figure 4.18 Bii). Lastly, the expression of *LDLR* was higher in control and *GBA-N370S* iASTROs treated for 24h with TNFα+IFNγ+PFFs and TNFα+IFNγ than in untreated or PFF-treated cells, but the effect was abolished by 7 days (Figure 4.18 C). In addition, although not statistically significant, *LDLR* expression was lower in PFF-treated than in untreated *GBA-N370S* iASTROs at after 24h, and in control iASTROs treated for 7 days with PFFs compared to untreated iASTROs (Figure 4.18 C).

Next, I analysed the lipid droplet content of control and *GBA-N370S* iASTROs treated for 72h or 7 days with PFFs alone, TNFα+IFNγ+PFFs and TNFα+IFNγ (Figure 4.28 D), but there were no

differences in the number of BODIPY spots per cell area (Figure 4.18 E) or the area of BODIPY spots (Figure 4.18 F) at any timepoint in any conditions.

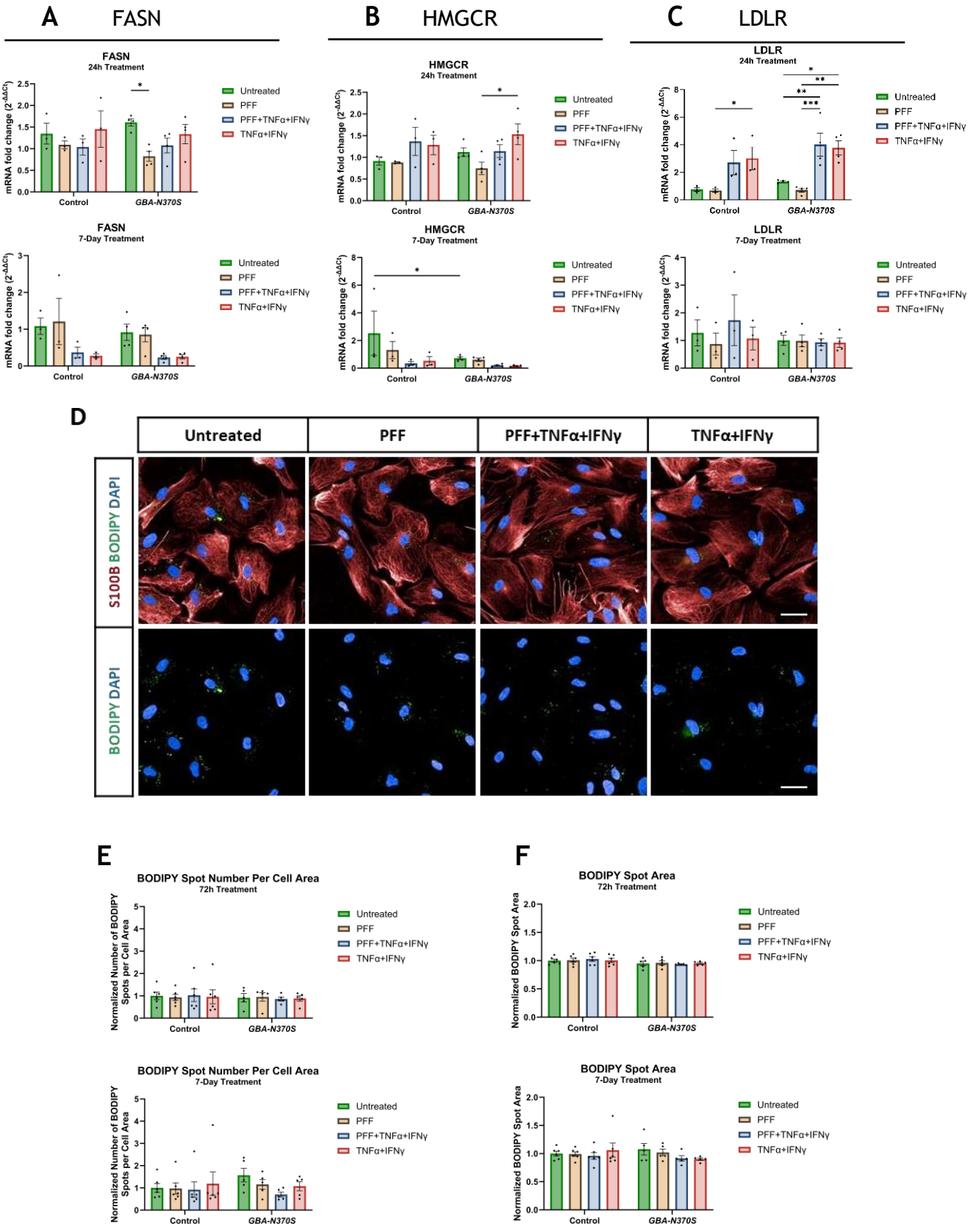


Figure 4.18. Control and *GBA-N370S* iASTROs present changes in the relative gene expression of some lipid metabolism related genes in response to α-synuclein PFFs and TNFα+IFNγ, but this does not result in changes in the number or size of lipid droplets

(A-C) Relative gene expression analysis by RT-qPCR of (A) FASN, (B) HMGCR and (C) LDLR in control and *GBA-N370S* iASTROs treated for 24h or 7 days with α-synuclein PFFs (10 µg/mL), α-synuclein PFFs (10 µg/mL) + TNFα (30 ng/mL) + IFNγ (50 ng/mL), or TNFα (30 ng/mL) + IFNγ (50 ng/mL). In each differentiation, to calculate ΔΔCt for each gene, the ΔCt of one untreated control iASTRO line was subtracted to the ΔCt of all the lines (for the gene of interest). Each data point represents 1 iASTRO line averaged across differentiations. N = 3 control and 4 *GBA-N370S* lines, 1-4 differentiations. Mean ± SEM. The statistical analysis performed was two-way ANOVA with Tukey's multiple comparison test. *p<0.05, **p<0.01, ***p<0.001. (D) Representative immunocytochemistry images of control iASTROs treated with α-synuclein PFFs (10 µg/mL), α-synuclein PFFs (10 µg/mL) + TNFα (30 ng/mL) + IFNγ (50 ng/mL), or TNFα (30 ng/mL) + IFNγ (50 ng/mL) for 72h, and stained for BODIPY 493/503 (green) and S100B (red). Scale bar: 50 µm. (E-F) Quantification of (E) the number of BODIPY spots per cell area and (F) the area of BODIPY spots in control and *GBA-N370S* iASTROs treated for 72h or 7 days with α-synuclein PFFs (10 µg/mL), α-synuclein PFFs (10 µg/mL) + TNFα (30 ng/mL) + IFNγ (50 ng/mL), or TNFα (30 ng/mL) + IFNγ (50 ng/mL). For each differentiation, in each timepoint, values were normalized to the average of untreated control iASTROs. Each data point represents 1 iASTRO line averaged across differentiations. N = 6 control and 5 *GBA-N370S* lines, 1-4 differentiations. Mean ± SEM. The statistical analysis performed was two-way ANOVA with Tukey's multiple comparison test.

4.5. Discussion

The main goal of this chapter was to investigate the inflammatory response of iASTROs to different inflammatory stimuli and α-synuclein PFFs, and to identify the cellular functions that might be altered due to these treatments. I also explored if the capacity of iASTROs to undergo astrogliosis was affected by the *GBA-N370S* mutation. This discussion section is divided into two parts: the first one (Section 4.5.1.) discusses the findings in iASTROs treated with inflammatory cytokines, and the second one (Section 4.5.2.) focuses on the response of iASTROs to α-synuclein PFFs.

4.5.1. Astrogliosis in iASTROs treated with inflammatory cytokines

First, the bulk RNAseq experiment in control iASTROs treated for 24h with different inflammatory cytokines provided very detailed information regarding the acute transcriptional changes iASTROs undergo upon acute inflammatory stimuli, and how this response varies depending on the cytokines cells are exposed to. The highest transcriptional

changes were induced by TNFα+IFNγ (over 8,000 DEGs), followed by IFNγ, the Liddelow factors and, lastly, the smallest changes were induced by TNFα alone.

One of the main outcomes of the RNAseq experiment was that TNFα and IFNγ act synergistically, which was apparent due to the higher number of DEGs and activated GO:BP terms in the TNFα+IFNγ vs TNFα and TNFα+IFNγ vs IFNγ comparisons than in the TNFα vs IFNγ comparison. Studies in other models (Barcia et al., 2011; Woznicki et al., 2021) and in iPSC-derived astrocytes (Spreng et al., 2022) have also shown that these two cytokines act synergistically. This synergistic action might be due to the different signalling pathways activated by each of these two cytokines; IFNγ mostly acts by activating the JAK-STAT signalling pathway (Ivashkiv, 2018), whereas TNFα activates the pro-survival NFκB and MAP kinase signalling pathways, and/or pathways leading to programmed cell death (Varfolomeev & Vucic, 2018). Therefore, these pathways might interact and potentiate the overall effect of TNFα and IFNγ.

On the contrary, very few transcriptomic changes were found between iASTROs treated with the Liddelow factors and TNFα, which suggests that most of the transcriptomic changes in cells treated with the Liddelow factors were driven by TNFα and not IL-1α or C1q. Subsequent immunocytochemistry experiments also showed that the changes occurring in iASTROs treated with TNFα alone or the Liddelow factors were very similar. Nonetheless, in the RNAseq data there were a few genes solely upregulated in iASTROs treated with the Liddelow factors, such as *CSF3, MMP12*, *CXCL1* and *CXCL2,* and *PTGS2*. Barbar and colleagues showed that there were not notable transcriptional differences between iPSC-derived astrocytes treated with the Liddelow factors or TNFα+IL-1β (Barbar et al., 2020), and since previous studies showed that IL-1β by itself does not trigger vast changes in iPSC-derived astrocytes (Perriot et al., 2018; Zhou et al., 2019), these findings support the notion that most of the transcriptional changes are driven by TNFα. However, there are other reports that claim that IL-1α alone induces changes in astrocytes (Bretheau et al., 2022) or that the response of astrocytes to TNFα+IL-1α is smaller than to the Liddelow factors (LaRocca et al., 2021). Therefore, further experiments are needed to elucidate if IL-1α, C1q, or a combination of both, induces any inflammatory changes in astrocytes, as the results obtained might indicate that the combination of TNFα+IL-1α+C1q, widely used in the literature, is not the most optimal to induce astrocyte reactivity.

The RNAseq experiment also revealed that GO:BP terms related to proliferation were enriched in iASTROs treated with TNFα and the Liddelow factors but suppressed in cells treated with TNFα+IFNγ. Similarly, GO:BP terms related to apoptosis and cell death were upregulated in reactive iASTROs after exposure to treatments that included TNFα, which was also observed in another study (Spreng et al., 2022). This is probably because one of the pathways activated by TNFα is programmed cell death (Varfolomeev & Vucic, 2018). Follow up immunocytochemistry experiments showed that the total number of live cells decreased slightly after 7 days of treatment with the Liddelow factors and TNFα+IFNγ, although Toxilight assays did not reveal any notable toxicity. Studies have described that different types of reactive astrocytes differ on their proliferative capacity; whereas some remain non-proliferative after exposure to insult, some enhance proliferation to surround the site of injury, and the latter are believed to be neuroprotective (Lawrence et al., 2023; Sofroniew, 2020). Other studies in reactive astrocytes have also described changes in proliferation and cytotoxicity. For instance, iPSC-derived astrocytes treated for 7 days with TNFα+IL-1β had increased proliferative capacity and cytotoxicity, which overall led to no changes in cell number (Hyvärinen et al., 2019).

Moreover, the transcriptomic data revealed a moderate dysregulation of some genes related to lipid homeostasis and metabolism in reactive iASTROs. Even if most genes were upregulated after treatments (e.g. *PTGES, FADS2/3, LSS, CYP7B1*), some were downregulated (e.g. *CYP46A1, FABP7, LPL*). Subsequent in vitro studies did not reveal any changes in lipid droplet number and size in iASTROs after treatment with TNFα+IFNγ or the Liddelow factors for 24h or 7 days, suggesting that the changes in the expression of enzymes related to lipid metabolism did not result in significant changes in the lipid storages of iASTROs. However, quantifying lipid droplet number and area is a very general and non-specific way to examine the lipid content of cells, and more sensitive and specific lipidomic studies are needed to explore the changes in the lipidome of reactive iASTROs.

Moreover, follow-up RT-qPCR experiments showed that *ELOVL1* expression was slightly upregulated in iASTROs treated with TNFα+IFNγ but not the Liddelow factors. This enzyme has recently gained significant interest because it has been postulated to be an important mediator in the neurotoxicity induced by reactive astrocytes after exposure to the Liddelow factors (Guttenplan et al., 2021). However, the authors of the original study did not check if

ELOVL1 expression was upregulated in reactive astrocytes, and another study by the same group showed that a 24h treatment with the Liddelow factors did not cause upregulation of *ELOVL1* in iPSC-derived astrocytes (Barbar et al., 2020). Other transcriptomic studies in iPSC-derived astrocytes showed a small upregulation in *ELOVL1* expression after treatment with the Liddelow factors (Leng et al., 2022) but no change after exposure to TNFα+IFNγ (Spreng et al., 2022). Therefore, the role of ELOVL1 in reactive astrocytes requires further study.

Finally, the data from the RNAseq experiment showed that various GO:BP terms related to calcium homeostasis and transport were upregulated in iASTROs treated with TNFα+IFNγ, and these GO:BP terms included the genes *CYP27B1* and *VDR*, which encode two crucial enzymes involved in vitamin D metabolism and signalling. Therefore, calcium signalling and vitamin D metabolism were chosen for further in vitro study in reactive iASTROs, which will be discussed in Chapter 5.

Follow-up RT-qPCR and immunocytochemistry studies in control and *GBA-N370S* iASTROs showed that, overall, the expression of inflammatory markers underwent a fast and big increase in expression during the first 24h after an acute inflammatory insult, and then decreased over time, although by 7 days the expression levels still remained high. On the contrary, changes in the cell area and morphology became more apparent with longer exposure times. As an exception, immunocytochemistry experiments did not reveal any morphological or intensity changes in iASTROs treated with only IFNγ, because, despite the vast transcriptional changes induced by this cytokine in the RNAseq experiment, IFNγ only caused minor increases in *NFκB1* and *C3* expression.

Contrary to other inflammatory genes, expression of *HLA-DPB1* and *HLA-DRB1* in iASTROs treated with TNFα+IFNγ was highest after 7 days, while no changes were observed in cells treated with the Liddelow factors. This is because the RNAseq data showed that GO:BP terms related to antigen processing and presentation were mostly upregulated in cells treated with IFNγ and TNFα+IFNγ, showing that this process is mostly driven by IFNγ. *HLA* genes have gained the interest of the PD-research community, since multiple GWAS studies and meta-analyses have shown an association between the *HLA* locus and PD (Hamza et al., 2010; Hill-Burns et al., 2011; Nalls et al., 2019). Even if microglia are considered the main antigen presenting cells (APCs) in the CNS (Sutter & Crocker, 2022), there is also evidence showing that

astrocytes act like APCs in PD. For instance, a study showed that MHC-II protein stains mostly co-localized with astrocytic markers in PD patients (Rostami et al., 2020). Nevertheless, *HLA* gene expression has not been widely studied in reactive astrocytes, and transcriptomic studies in iPSC-derived astrocytes have provided inconclusive results (Barbar et al., 2020; Leng et al., 2022).

Moreover, RT-qPCR experiments showed that *BDNF* and *FGF2* expression increased in iASTROs treated with TNFα+IFNγ, especially after 7 days of treatment, whereas expression of *GDNF*, *MANF* and *TGFβ* did not change significantly. Since the RNAseq experiment did not reveal a big dysregulation in growth factor expression after 24h treatments, the RT-qPCR results indicate that upregulation of some growth factors occurs at later timepoints. Indeed, the transcriptomic data published by Spreng and colleagues showed that increased *BDNF* expression in TNFα+IFNγ-treated cells could only be detected after 72h but not earlier, whereas elevated *FGF2* expression was detected after 8h (Spreng et al., 2022). Other studies in iPSC-derived astrocytes have shown an increase in *BDNF* expression in astrocytes treated with the Liddelow factors (Barbar et al., 2020; Leng et al., 2022), whereas another study using primary human astrocytes did not report any changes in BDNF production after 6 days of treatment with the Liddelow factors (Szpakowski et al., 2022).

The observation that iASTROs upregulate the expression of some growth factors days after the initial inflammatory insult requires further study, as this might indicate that over time reactive iASTROs acquire a more neurosupportive and neurotrophic phenotype. Future experiments should include more timepoints before and after 7 days, to determine when the peak in growth factor expression occurs. ELISA should also be done to investigate if the increase in the gene expression of growth factors is also accompanied by an increase in their synthesis and release. Nonetheless, the findings presented in this chapter offer new exciting therapeutic avenues, since low BDNF levels have been associated with various neurodegenerative diseases, including PD (Ali et al., 2024; Jin et al., 2023). Indeed, it has been postulated that in the early stages of astrogliosis, increased expression of BDNF might confer neuroprotection (Albini et al., 2023), as promoting astrocytic BDNF expression has been beneficial in different models of neurological diseases (de Pins et al., 2019; Giralt et al., 2010) and PD (Geng et al., 2023). FGF2 is also thought to be involved in PD (Liu et al., 2021), and this growth factor also exerts multiple neuroprotective functions (Li et al., 2006; Okada et al.,

2019). Thus, potentiating the expression of BDNF and FGF2 in reactive astrocytes may prevent or improve neuronal degeneration in PD.

Another interesting finding in iASTROs treated with TNFα+IFNγ was the increase in ROS production over time, which was higher in *GBA-N370S* iASTROs. The RNAseq data showed that there was an increase in the expression of genes encoding antioxidant enzymes, which might explain why after 24h and 72h of treatment with TNFα+IFNγ ROS levels remained unchanged. During the early stages after an acute inflammatory insult, astrocytes might increase the expression of antioxidant enzymes to combat oxidative stress and limit the damage to the surrounding cells. However, a sustained inflammatory stimulus and response might overexert the detoxifying capacity of astrocytes and result in increased ROS/RNS production and release, which can cause neuronal death. Furthermore, research shows that neuroinflammation and oxidative stress potentiate and sustain each other (He et al., 2020; Taylor et al., 2013), and there is ample evidence showing how reactive astrocytes release ROS (Murray et al., 2022). These observations have important implications for PD, as astrocytic oxidative and nitrosative stress are believed to be contributors to PD pathogenesis (Rizor et al., 2019), and DAn are more susceptible to oxidative stress than other neuronal populations (Guo et al., 2018). Therefore, future studies should seek to reduce the expression of ROS in reactive iASTROs as a potential therapeutic treatment.

On another note, in line with other studies (Barbar et al., 2020; Perriot et al., 2018), the results presented in this chapter oppose the hypothesis that activated astrocytes exist in either one of 2 reactive states, A1 (neurotoxic) or A2 (neuroprotective) (Liddelow et al., 2017; Zamanian et al., 2012). Instead, astrocytes acquire a context-specific reactive phenotype that is very dynamic and highly depends on the inflammatory stimulus, their regional identity, and their maturity, amongst other factors. According to the data from the bulk RNAseq experiment and subsequent in vitro assays, reactive iASTROs acquired both neurotoxic and neuroprotective or neurosupportive characteristics. For instance, the RNAseq experiment showed that there was an increase in GO:BP terms related to apoptosis and cell killing, but also upregulation of genes encoding antioxidant enzymes. Moreover, in vitro assays showed that, over time, iASTROs treated with TNFα+IFNγ produced higher levels of ROS but also elevated the expression of some growth factors. Further in vitro studies in co-cultures with iDAn were done to investigate if reactive iASTROs were neurotoxic or neuroprotective (Chapter 6).

Similarly, the data presented in this thesis adds on to the growing body of evidence (Barbar et al., 2020; Hyvärinen et al., 2019; Soubannier et al., 2020) that GFAP is not a marker of all reactive astrocytic states, as myself and others have reported that GFAP expression decreases after treatment with inflammatory cytokines (Barbar et al., 2020; Leng et al., 2022; Spreng et al., 2022). This is particularly important considering that, for multiple years, GFAP was used as the sole marker for astrocyte reactivity, and most immunohistochemical examinations in rodents and human patients solely relied on GFAP immunostaining to identify astrocytes and infer their reactive state (Ben Haim et al., 2015). For future studies, specific reactive astrocyte phenotypes should be defined using a combination of markers and functional assays (Escartin et al., 2021).

Overall, no significant changes in the inflammatory response of *GBA-N370S* iASTROs were observed compared to control cells, except a higher ROS production after treatment with TNFα+IFNγ. Not many studies have investigated the impact of *GBA1* mutations on astrocyte reactivity, but there is some evidence showing that primary mouse astrocytes carrying the *GBA1-D409V* mutation have reduced ability to release pro-inflammatory cytokines (Sanyal et al., 2020). On the contrary, iPSC-derived astrocytes carrying the *GBA-N370S* or *GBA-L444P* mutations released higher levels of some proinflammatory mediators (Aflaki et al., 2020). Therefore, more research is needed to investigate the effect of *GBA1* mutations on astrogliosis, especially their contributions to oxidative stress.

4.5.2. Effects of α-synuclein PFFs on iASTROs

The bulk RNAseq experiment revealed that α-synuclein PFFs, alone or in combination with TNFα+IFNγ, did not cause significant transcriptional changes in control iASTROs after 24h of treatment. This observation was further supported with subsequent in vitro experiments, which showed that, at least during the first 7 days after first exposure, PFFs did not induce big cellular changes in control or *GBA-N370S* iASTROs. Few studies have explored in detail how iPSC-derived astrocytes react to α-synuclein, and even less so PFFs. Moreover, there are no other transcriptomic datasets available of astrocytes treated with α-synuclein PFFs, as the only one available used monomers and fibrils (Russ et al., 2021). Thus, results presented in this chapter are novel and a direct contribution to a gap in this field.

First, the data from the bulk RNAseq experiment showed that there were only 17 DEGs between untreated and PFF-treated cells, and even fewer DEGs, 6, when comparing iASTROs treated with TNFα+IFNγ or TNFα+IFNγ+PFFs. Interestingly, most of the downregulated genes in PFF-treated iASTROs encoded proteins related to lipid metabolism and transport, and fgsea analysis showed that one of the gene sets with the lowest negative NES in PFF-treated cells was "Cholesterol Homeostasis". All these findings pointed towards a reduction in cholesterol and lipid homeostasis and metabolism in iASTROs after exposure to PFFs. However, in follow-up RT-qPCR experiments, out of the hit genes related to lipid homeostasis found in the RNAseq data, only *FASN* was significantly downregulated in *GBA-N370S*, but not control, iASTROs treated for 24h with PFFs. This might indicate that the *GBA-N370S* mutation makes astrocytes more prone to alterations in lipid metabolism after exposure to α-synuclein. No data is available on the relationship between α-synuclein and *FASN*, and the few studies exploring *FASN* expression in astrocytes showed conflicting results regarding whether *FASN* upregulation or inhibition is beneficial (Álvarez-Pérez et al., 2016; Wei et al., 2022). A recent GWAS meta-analysis study identified *FASN* as a new PD risk locus (J. J. Kim et al., 2024), as well as a potential genetic biomarker in prodromal PD patients (Badawy et al., 2024). Based on this, further studies should explore how α-synuclein PFFs might affect *FASN* expression in astrocytes, the effects of *FASN* downregulation in astrocyte function, and how *FASN* expression might be altered due to the *GBA-N370S* mutation.

Changes in the astrocyte lipidome after exposure to α-synuclein PFFs also require further study, because almost no research has been done to investigate α-synuclein-lipidome interactions in astrocytes. Studies in other models have shown that binding of α-synuclein to lipid membranes and the composition of these, impacts α-synuclein aggregation (Dasari et al., 2024; Dear et al., 2024), while the integrity of the lipid membrane might be disrupted after binding of different α-synuclein species (Gilmozzi et al., 2020). A study published in 2010 reported that human astrocytes treated with α-synuclein had reduced levels of cholesterol in the membrane (Koob et al., 2010), but since then, the research in this area has been scarce. Thus, further in-depth studies are needed to study lipidome changes in astrocytes exposed to α-synuclein, including the lipid content of extracellular vesicles (EVs) released by astrocytes.

In line with the RNAseq results, RT-qPCR and immunocytochemistry experiments did not reveal any major changes in the expression of various inflammatory markers or morphological

changes due to PFF exposure. On the contrary, Chavarría and colleagues showed that monomeric, oligomeric and fibrillar α-synuclein induced morphological changes and increases in GFAP intensity in rat cortical astrocytes (Chavarría et al., 2018), but the different cell models and α-synuclein species used could explain this disparity. Nevertheless, the immunohistochemistry images acquired showed that the morphology of iASTROs treated with TNFα+IFNγ+PFFs differed from those treated with TNFα+IFNγ. Unfortunately, it was not possible to fully examine and quantify these morphological changes, but this observation indicates that PFFs in combination with TNFα+IFNγ cause cellular changes in iASTROs. Further imaging experiments, ideally in conjunction with proteomic studies, should investigate what these changes are and the consequences they may have in iASTROs.

Additionally, no effects were detected in the generation of ROS in control or *GBA-N370S* iASTROs during the first 14 days of treatment with α-synuclein PFFs alone, nor did PFFs alter ROS production in iASTROs treated with TNFα+IFNγ. On the contrary, multiple studies have shown that α-synuclein induces ROS production and oxidative stress in neurons (Deas et al., 2016), microglia (Russo et al., 2019), and rodent astrocytes (Chavarría et al., 2018; Fellner et al., 2013). There is also evidence supporting the fact that oxidative stress promotes α-synuclein aggregation (Scudamore & Ciossek, 2018). Thus, ROS released by reactive astrocytes might promote the formation of α-synuclein aggregates, but further studies are needed to investigate the interplay between cytokine-induced inflammation, ROS production, and α-synuclein aggregation in astrocytes.

Even if the data presented in this chapter indicates that PFFs did not cause any significant cellular alterations in iASTROs, other studies have reported that α-synuclein induces changes in astrocytes. Indeed, in mice and primary astrocyte cultures, excessive α-synuclein uptake or expression of mutant *SNCA* in astrocytes impaired various cellular processes such as mitochondrial function and glutamate uptake (Gu et al., 2010; Lindström et al., 2017), as well as promoting astrogliosis (Chavarría et al., 2018; Diniz et al., 2019; Du et al., 2018; Fellner et al., 2013; Gu et al., 2010; Lee et al., 2010; Rannikko et al., 2015). Nonetheless, the data available on the effects of different α-synuclein species on human and iPSC-derived astrocytes is somewhat contradictory, as not all studies reported an α-synuclein-induced astrogliosis. For instance, a study claimed that 24h exposure to α-synuclein PFFs induced astrogliosis in human primary astrocytes, which also acquired neurotoxic properties towards SH-SY5Y cells (Chou et

al., 2021). On the other hand, Russ and colleagues showed that α-synuclein fibrillar polymorphs promoted the expression of various genes related to antigen presentation (Russ et al., 2021). This observation was not replicated in this thesis using PFFs or by Rostami and colleagues using PFFs and monomers (Rostami et al., 2020). Moreover, Russ and colleagues also reported that astrocytes carrying PD-related mutations released higher amounts of pro-inflammatory cytokines when stimulated with monomeric, but not fibrillar, α-synuclein (Russ et al., 2021).

Moreover, except differences in *FASN* expression, I did not observe any significant differences in the response of iASTROs to PFFs due to the *GBA-N370S* mutation. Similarly, Sanyal and colleagues found that the *GBA-D490V* mutation did not affect the ability of mouse primary astrocytes to uptake and degrade α-synuclein PFFs, and no astrogliosis after exposure to PFFs was reported (Sanyal et al., 2020). On the other hand, Gaucher's disease (GD) iPSC-derived astrocytes with *GBA* mutations were reported to release higher levels some pro-inflammatory cytokines after exposure to α-synuclein monomers and fibrils (Aflaki et al., 2020).

Some of the differences in the results of these studies and this thesis, especially the lack of astrogliosis in response to PFFs presented here, might be due to the different α-synuclein species used (monomers, oligomers, fibrils, PFFs), the different concentrations used, the use of fluorescently labelled α-synuclein, the cell model and species used, and the regional identity of astrocytes (Basurco et al., 2023). Additionally, when interpreting the results presented in this chapter and translating them to human patients, it is important to consider that, in the SNpc of PD patients, astrocytes, DAn, and other cells are exposed to α-synuclein aggregates, inflammatory cytokines, and other toxic molecules (e.g. ROS), for multiple years. Therefore, the experiments conducted in this thesis only represent the very early stages of the astrocytic response to acute α-synuclein and inflammogen exposure, and they do not fully recapitulate disease progression in the PD brain.

Finally, a limitation of this thesis was that the uptake and degradation of α-synuclein in iASTROs after exposure to PFFs, with or without TNFα+IFNγ, was not studied, and future experiments should address this to try to understand the mechanisms by which α-synuclein is taken up in iASTROs, as well as the mechanisms and timeframe by which it is degraded, and whether any of these pathways are altered with exposure to inflammatory cytokines. In

addition, it should also be investigated if there are any impairments in any of these processes due to the *GBA-N370S* mutation.

4.5.3. Concluding remarks

In summary, the results presented in this chapter show that control and *GBA-N370S* iASTROs are capable of undergoing astrogliosis in response to different inflammatory cytokines, but not α-synuclein PFFs. Reactive iASTROs underwent alterations in multiple cellular pathways and functions, including calcium signalling and vitamin D metabolism, which are investigated in Chapter 5. Since the data presented in this chapter does not fully elucidate whether reactive iASTROs are neurosupportive or neurotoxic, this will be further studied in Chapter 6.

Chapter 5 - Exploring calcium homeostasis and vitamin D metabolism in reactive iASTROs

5.1. Introduction and aims

The bulk RNAseq experiment presented in chapter 4 revealed that control iASTROs treated for 24h with TNFα+IFNγ upregulated genes associated with calcium transport and homeostasis, as well as *CYP27B1* and *VDR*, two enzymes essential in vitamin D metabolism and signalling. Moreover, in the RNAseq experiment, *CYP27B1* was one of the few genes upregulated in iASTROs treated with α-synuclein PFFs.

Calcium signalling in astrocytes is essential for their normal functioning, and, as a second messenger, calcium regulates multiple signalling pathways and intracellular processes, while also enabling to perceive extracellular signals (Verkhratsky & Zorec, 2019). Astrocytic calcium signalling undergoes changes after acute insults or during chronic diseases such as neurodegeneration, as well as when astrocytes acquire a reactive phenotype (Bancroft & Srinivasan, 2022). Nonetheless, even if there is some evidence showing how aberrant astrocytic calcium signalling can be detrimental to DAn (Ibáñez et al., 2019) and how different calcium pathways are altered in reactive astrocytes (Novakovic et al., 2023; Shigetomi et al., 2019), what this implies for neuroinflammation and DAn-astrocyte crosstalk in PD needs to be further investigated.

On the other hand, vitamin D has been associated with PD, as decreased levels have been reported in individuals with PD (Xia & Zhou, 2024), and because of the neuroprotective effects of this vitamin (Pignolo et al., 2022). Indeed, vitamin D activates the expression of various neurotrophic genes, such as *GDNF* and *BDNF* (Hafiz, 2024). In astrocytes, vitamin D was shown to partially prevent the negative effects of rotenone treatment, including cell death, ROS production and mitochondrial function (de Siqueira et al., 2023). Moreover, a recent study revealed that *CYP27B1* expression, the enzyme that catalyses the transformation of 25-hydroxyvitamin D3 into its active form 1α,25-dihydroxyvitamin D3 (calcitriol), was higher in astrocytes from PD patients than in astrocytes from healthy controls (Mazzetti et al., 2022). These CYP27B1-positive astrocytes were thought to be neuroprotective, as they contained α-synuclein oligomers that co-localized with LAMP1, and they were associated with neurons

without LBs, suggesting that they participated in the clearance of α-synuclein aggregates. However, very little research has been done to investigate the role of astrocytic vitamin D metabolism and signalling in the context of PD and how this may affect neuronal health and survival.

The aims of this chapter are:

- To investigate if and how ATP-induced ER-calcium release and store-operated calcium entry (SOCE) are altered in reactive iASTROs.
- To explore how vitamin D metabolism is altered in reactive iASTROs.
- To investigate if vitamin D supplementation affects iDAn survival.

5.2. Calcium homeostasis in reactive control and *GBA-N370S* iASTROs

As discussed in Section 4.2.4.5., GO:BP terms related with calcium transport and homeostasis were enriched in reactive iASTROs after treatment with TNFα+IFNγ. Therefore, I decided to further investigate how calcium homeostasis is altered in iASTROs after treatment with TNFα+IFNγ and the Liddelow factors at various timepoints after treatment.

5.2.1. Relative gene expression of calcium channels in reactive iASTROs

The expression of *ITPR3,* involved in ATP-induced calcium release, and *ORAI1*, involved in SOCE, were significantly upregulated in the RNAseq experiment in iASTROs treated with TNFα+IFNγ (Figures 4.6-4.7). Thus, I first analysed the relative gene expression of these two genes and some others involved in the same pathways in control and *GBA-N370S* iASTROs treated for 24h or 7 days with 30 ng/mL TNFα + 50 ng/mL IFNγ or the Liddelow factors (30 ng/mL TNFα + 3 ng/mL IL-1α + 400 ng/mL C1q).

As before, there was high line-to-line variability in the results. Expression of each of the *ITPR* genes showed different patterns in response to treatment (Figure 5.1 A-C). After 24h of treatment, expression of *ITPR1* did not change much with either treatment, although it

appeared a bit higher in cells treated with TNFα+IFNγ, but after 7 days of treatment the expression was significantly higher in iASTROs treated with TNFα+IFNγ and slightly lower in cells treated with the Liddelow factors (Figure 5.1 A). After treatment with TNFα+IFNγ, *ITPR1* expression was higher in control than in *GBA-N370S* iASTROs (not statistically significant). On the contrary, *ITPR2* expression was higher in *GBA-N370S* iASTROs in all conditions (Figure 5.1 B, albeit not statistically significant). 24h after treatment, *ITPR2* expression was slightly higher in treated cells, but by 7 days this small increase was only apparent in *GBA-N370S* iASTROs treated with TNFα+IFNγ (not statistically significant) (Figure 5.1 B). Finally, expression of *ITPR3* was higher in *GBA-N370S* iASTROs, and was slightly elevated after 24h of treatment with the Liddelow factors, and 7 days with TNFα+IFNγ and, in control iASTROs, with the Liddelow factors too (Figure 5.1 C, not statistically significant). Next, *ORAI1* and *STIM1* expression were investigated based on the data from the RNAseq experiment, which showed increased ORAI1 expression, and the importance of STIM1 in SOCE. Next, in line with the RNAseq results, expression of *ORAI1* was higher in both control and *GBA-N370S* iASTROs treated with TNFα+IFNγ at both timepoints (Figure 5.1 D). On the contrary, *STIM1* expression, the main homologue involved in astrocytic SOCE (Gao et al., 2016; Kwon et al., 2017), was lower after 24h of treatment with TNFα+IFNγ and 24h and 7 days of treatment with the Liddelow factors (Figure 5.1 E, not statistically significant).

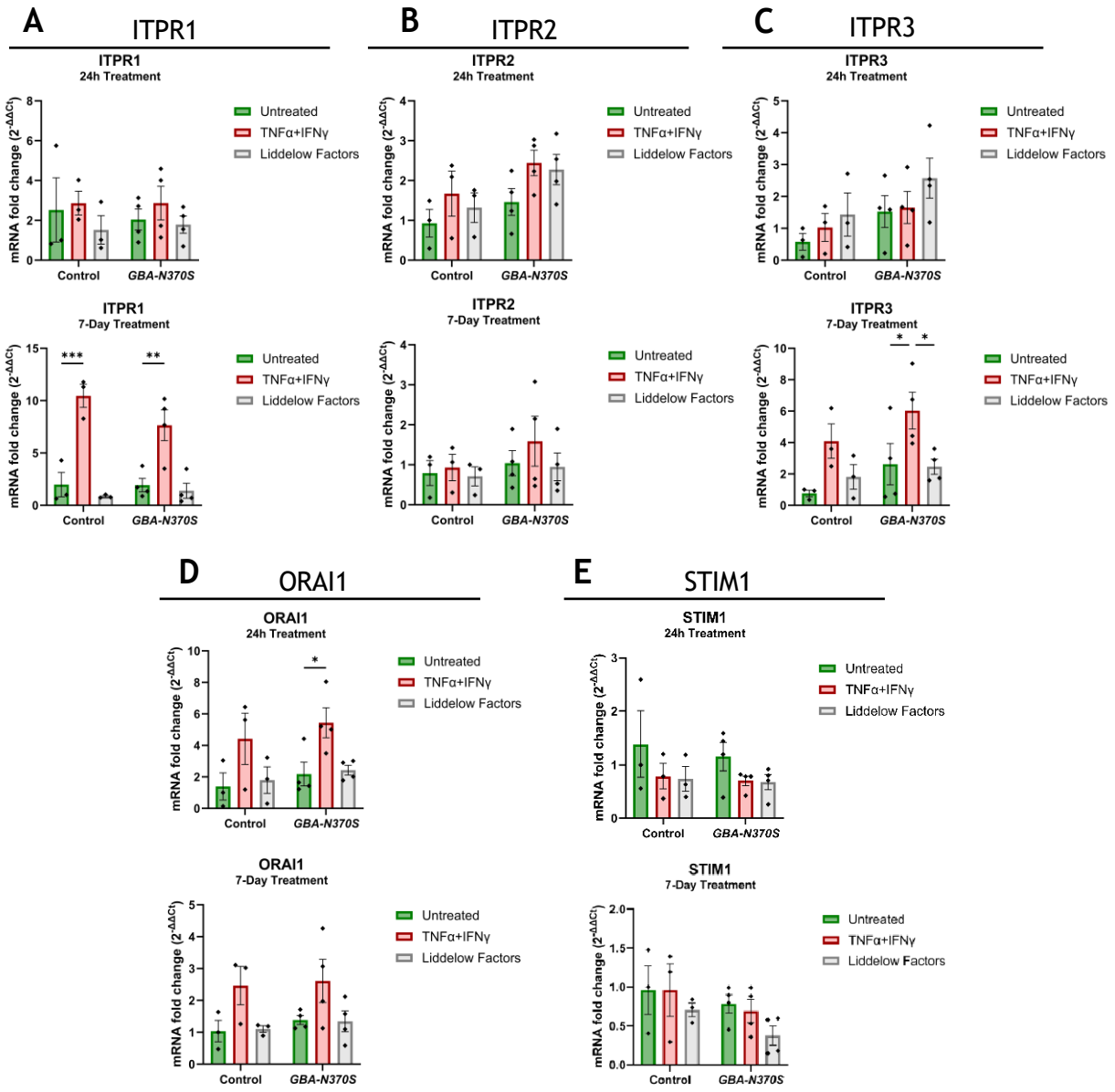


Figure 5.1. Relative gene expression of some calcium channels is increased in control and *GBA-N370S* iASTROs in response to TNFα+IFNγ, and to a lesser extent to the Liddelow factors

(A-E) Relative gene expression analysis by RT-qPCR of (A) ITPR1, (B) ITPR2, (C) ITPR3, (D) ORAI1 and (E) STIM1 in control and *GBA-N370S* iASTROs treated for 24h or 7 days with 30 ng/mL TNFα + 50 ng/mL IFNγ or the Liddelow factors (30 ng/mL TNFα + 3 ng/mL IL-1α + 400 ng/mL C1q). In each differentiation, to calculate ΔΔCt for each gene, the ΔCt of one untreated control iASTRO line was subtracted to the ΔCt of all the lines (for the gene of interest). Each data point represents 1 iASTRO line averaged across differentiations. N = 3 control and 4 *GBA-N370S* lines, 1-4 differentiations. Mean ± SEM. The statistical analysis performed was two-way ANOVA with Tukey's multiple comparison test. *p<0.05, **p<0.01, ***p<0.001.

5.2.2. Store Operated Calcium Entry in reactive iASTROs

Since iASTROs treated with TNFα+IFNγ had elevated expression of *ORAI1*, I studied SOCE in iASTROs treated for 24h, 72h or 7 days with 30 ng/mL TNFα + 50 ng/mL IFNγ or the Liddelow

factors (30 ng/mL TNFα + 3 ng/mL IL-1α + 400 ng/mL C1q). As discussed above, SOCE is a process that occurs when ER calcium levels are significantly reduced. Thus, to model this in vitro, iASTROs were incubated with a low dose of thapsigargin (100 nM) and 2.5 mM Fura-2 AM for 1.5h. This drug blocks the sarco-endoplasmic reticulum Ca^{2+}-ATPases (SERCA pumps), preventing calcium re-entry into the ER, and thus eventually depleting ER calcium stores, which then triggers SOCE (Bird et al., 2008). Next, iASTROs were washed three times with HBSS (without $CaCl_2$ and $MgCl_2$) to remove any calcium from the extracellular media, and at the time of imaging in the FlexStation, 2.5 mM $CaCl_2$ were added to the cells to include calcium entry into the cytoplasm through SOCE, which was measured as an increase in the Fura-2 AM 340/380 nm absorbance ratio. Because iASTROs treated with TNFα+IFNγ had higher expression of *ORAI1*, the hypothesis was that they would have higher and/or faster increases in cytoplasmic calcium after addition of $CaCl_2$.

In control iASTROs, there was a slightly bigger calcium entry in cells treated with TNFα+IFNγ for 24h and 72h compared to untreated cells, but by 7 days there were no differences (Figure 5.2 Ai). On the contrary, control iASTROs treated with the Liddelow factors only presented an increase in calcium release compared to untreated cells after 7 days of treatment (Figure 5.2 Ai). *GBA-N370S* iASTROs also displayed higher levels of calcium entry after 24h and 72h of treatment with TNFα+IFNγ, whereas treatment with the Liddelow factors for 24 and 72h caused a lower calcium entry compared to untreated cells (Figure 5.2 Aii). On average, after 7 days of treatment, *GBA-N370S* iASTROs did not have any differences in SOCE due to treatment. The changes in calcium entry due to the treatments differed between lines of the same genotype. For instance, the traces of the control 840 line (Figure 5.2 Bi) are similar to the average traces of control lines depicted in Figure 5.2 Ai, whereas those of the *GBA-N370S* line 82 (Figure 5.2 Bii) differ from the average traces in Figure 5.2 Aii, as after 7 days of treatment, calcium entry through SOCE was higher in 82 iASTROs treated with TNFα+IFNγ or the Liddelow factors compared to untreated cells.

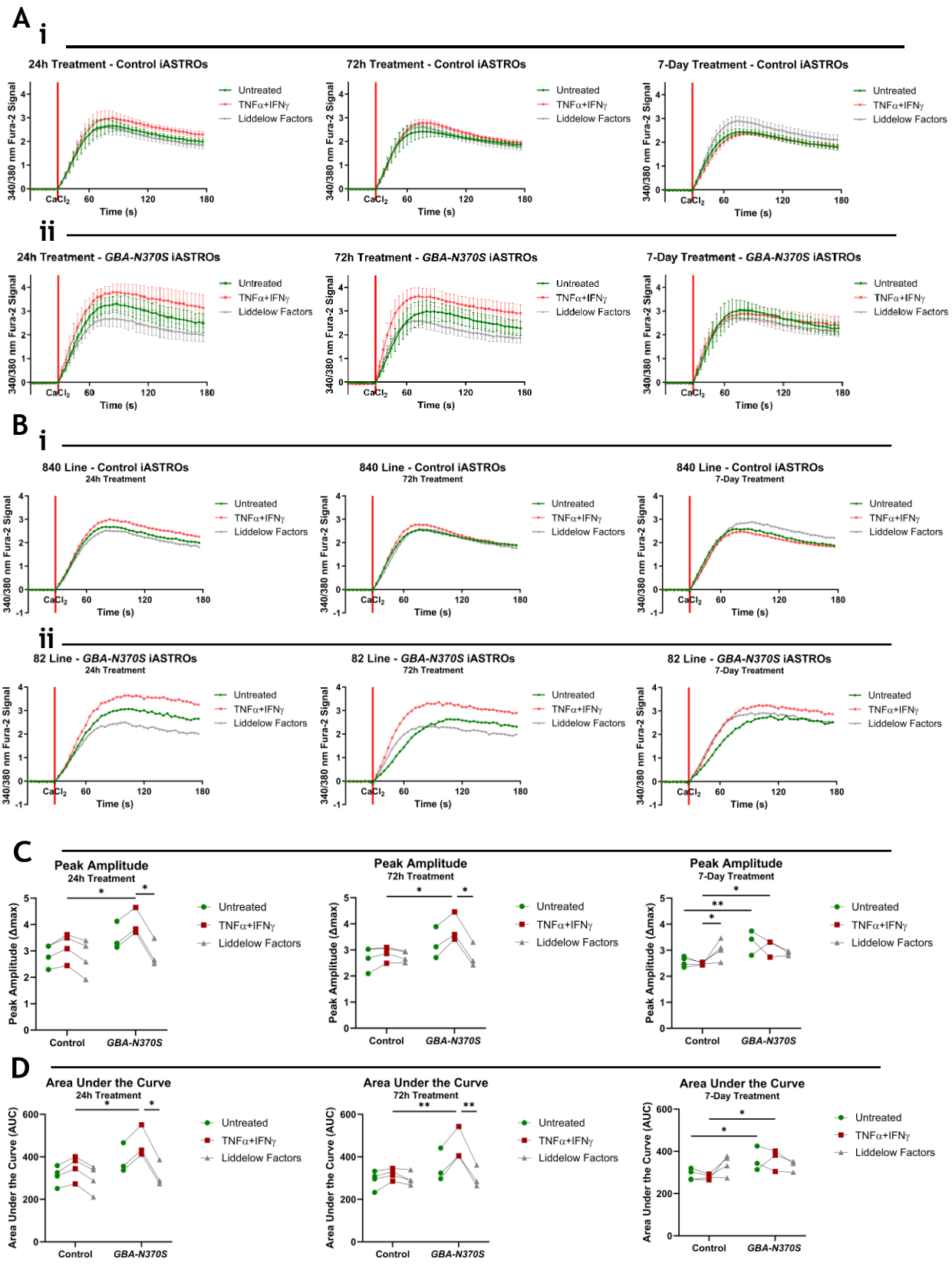


Figure 5.2. Store operated calcium entry (SOCE) is increased in iASTROs treated with TNFα+IFNγ, with bigger changes in *GBA-N370S* iASTROs

(A) Traces showing the average of the Fura-2 ratio in (i) control and (ii) *GBA-N370S* iASTROs treated with 30 ng/mL TNFα + 50 ng/mL IFNγ or the Liddelow factors (30 ng/mL TNFα + 3 ng/mL IL-1α + 400

ng/mL C1q)) for 24h, 72h or 7 days. The endoplasmic reticulum calcium stores were depleted with 1h incubation with 100 nM thapsigargin, and calcium entry into the cytoplasm was induced by addition of $CaCl_2$ (red vertical line in the graphs). Each line represents the average of all the lines of each genotype (4 control and 3 *GBA-N370S*), each line averaged across differentiations (1-3 differentiations per line). (B) Traces of the Fura-2 ratio in example (i) control and (ii) *GBA-N370S* lines, showing the averages across 3 differentiations. Same experimental design as in (A). (C-D) Quantification of (C) the peak amplitude and (D) the area under the curve (AUC) of the traces shown in (A). Each data point represents one line averaged across differentiations. N = 4 control and 3 *GBA-N370S* lines, 1-3 differentiations. Mean ± SEM. The statistical analysis performed was two-way ANOVA with Tukey's multiple comparison test. *p<0.05, **p<0.01.

Next, the peak amplitude (Figure 5.2 C) and the area under the curve (AUC) (Figure 5.2 D) were measured from the average traces of each line. At all timepoints, *GBA-N370S* iASTROs treated with TNFα+IFNγ had a higher peak amplitude and AUC than control iASTROs, especially after 24h and 72h. In untreated cells, the peak amplitude and AUC were also overall higher in *GBA-N370S* iASTROs than in control (not statistically significant). Lastly, after 7 days of treatment with the Liddelow factors, the peak amplitude in the traces of control iASTROs was significantly higher than in untreated or TNFα+IFNγ treated cells, but this was not observed in *GBA-N370S* iASTROs. Overall, this data shows that after 24h and 72h of treatment with TNFα+IFNγ, iASTROs presented higher calcium entry into the cytoplasm through SOCE than untreated cells, and this increase was bigger in *GBA-N370S* iASTROs. When comparing cells treated with the Liddelow factors with untreated cells, control iASTROs presented no differences after 24h and 72h of treatment, but and increase after 7 days, whereas *GBA-N370S* iASTROs presented a decrease after 24h and 72h and no clear changes after 7 days.

5.2.3. ATP-induced ER calcium release in reactive iASTROs

Next, based on the increase in *ITPR1* and *ITPR3* expression in iASTROs treated with TNFα+IFNγ, I investigated ATP-induced ER-calcium release in control and *GBA-N370S* iASTROs treated for 24h, 72h or 7 days with 30 ng/mL TNFα + 50 ng/mL IFNγ or the Liddelow factors (30 ng/mL TNFα + 3 ng/mL IL-1α + 400 ng/mL C1q). The initial hypothesis was that, if iASTROs treated with TNFα+IFNγ had higher expression of *ITPR1* and *ITPR3*, they would have higher and/or faster calcium release from the ER after stimulation with ATP. Figure 5.3 A shows the average Fura-2 traces of control (i) and *GBA-N370S* (ii) iASTROs.

Overall, after 24h, there were no differences in ER-calcium release due to any of the treatments. In control iASTROs, cells treated with TNFα+IFNγ for 72h or 7 days had a slightly bigger increase in ER-calcium release than untreated cells, and this increase was higher after treatment with the Liddelow factors (Figure 5.3 Ai). In *GBA-N370S* iASTROs, cells treated for 72h or 7 days with TNFα+IFNγ had a higher increase in calcium release than cells treated with the Liddelow factors, and both treatments resulted in higher calcium release than in untreated cells (Figure 5.3 Aii). Moreover, the kinetics of calcium release in *GBA-N370S* iASTROs were different depending on the treatment: in cells treated with the Liddelow factors, after an initial peak post ATP application the calcium levels fast decreased to the same level as in untreated cells, whereas in cells treated with TNFα+IFNγ calcium levels after ATP application remained higher throughout the entire measuring time.

Figure 5.3 B shows the traces of the same example control (i) and *GBA-N370S* (ii) line as in Figure 5.2 B, which differ from the average traces shown in Figure 5.3 B. The control 840 line had a significantly higher ER-calcium release after 72h and 7 days of treatment with TNFα+IFNγ or the Liddelow factors compared to untreated cells (Figure 5.3 Bi), differences that were not observed in the average traces. On the other hand, the *GBA-N370S* 82 line had a small increase after 72h of treatment with TNFα+IFNγ or the Liddelow factors compared to untreated cells, whereas after 7 days the increase in cells treated with the Liddelow factors was higher than the increase in iASTROs treated with TNFα+IFNγ (Figure 5.3 Bii).

The peak amplitude and AUC of the average traces of each line were quantified (Figure 5.3 C-D), which showed that each line responded differently to the treatments. For instance, after 72h of treatment with TNFα+IFNγ or the Liddelow factors, a control iASTRO line presented a high increase in the peak amplitude compared to untreated cells, whereas another line showed a big decrease (Figure 5.3 C). Moreover, after 7 days of treatment, some *GBA-N370S* iASTROs presented a higher increase in the peak amplitude after treatment with TNFα+IFNγ, whereas others had a higher increase with the Liddelow factors. Lastly, it is worth noting that, especially at the 24h timepoint, untreated control iASTROs had a higher peak amplitude than untreated *GBA-N370S* iASTROs, which correlates with the findings presented in Figure 3.6, where *GBA-N370S* iASTROs had an overall smaller ATP-induced calcium release from the ER.

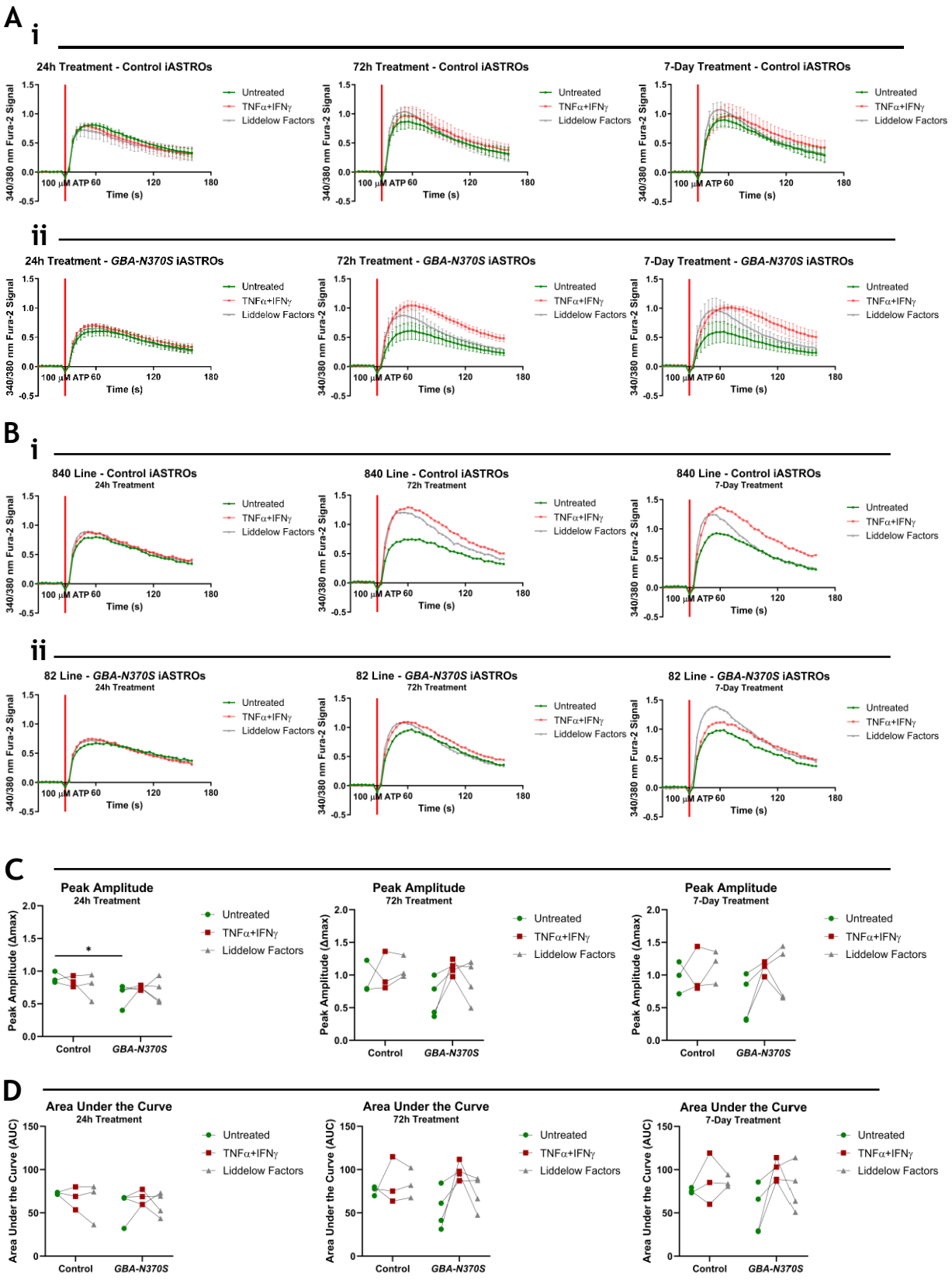


Figure 5.3. ATP-induced calcium release from the ER is increased over time in some, but not all, lines of control and *GBA-N370S* iASTROs treated with TNFα+IFNγ and the Liddelow factors

(A) Traces showing the average of the Fura-2 ratio in response to 100 µM ATP addition (vertical red line in the graphs) in (i) control and (ii) *GBA-N370S* iASTROs treated with 30 ng/mL TNFα + 50 ng/mL IFNγ or the Liddelow factors (30 ng/mL TNFα + 3 ng/mL IL-1α + 400 ng/mL C1q) for 24h, 72h or 7 days. Each line represents the average of all the lines of each genotype (3 control and 4 *GBA-N370S*), each line averaged across differentiations (1-4 differentiations per line). (B) Traces of the Fura-2 ratio in an example (i) control and (ii) *GBA-N370S* line, showing the averages across 3-4 differentiations. Same experimental design as in (A). (C-D) Quantification of (C) the peak amplitude and (D) the area under the curve (AUC) of the traces shown in (A). Each data point represents one line averaged across differentiations. N = 3 control and 4 *GBA-N370S* lines, 1-4 differentiations. Mean ± SEM. The statistical analysis performed was two-way ANOVA with Tukey's multiple comparison test. *p<0.05.

All in all, these results show that most control and *GBA-N370S* iASTRO lines had elevated ATP-induced ER calcium release after 72h or 7 days of treatment with TNFα+IFNγ or the Liddelow factors. However, the fact that not all the lines present the same phenotype after treatment highlights the importance of using multiple lines of the same genotype and presenting results in a way that allows to examine each line separately.

Subsequent experiments using the ITPR channel blocker 2-aminoethoxydiphenyl borate (2-APB) showed that partially blocking ER-calcium release with 2-APB does not affect the reactive response of iASTROs to TNFα+IFNγ (Appendix S.1).

5.3. Vitamin D metabolism in reactive iASTROs

As discussed in Section 4.2.4.2, the RNAseq data revealed that one of the few genes upregulated in iASTROs treated with α-synuclein PFFs was *CYP27B1,* and this gene, as well as *VDR* (encoding the receptor for vitamin D) were upregulated in all iASTROs treated with inflammatory cytokines, especially TNFα+IFNγ and PFFs+TNFα+IFNγ (Figure 4.7). Due to the association of low vitamin D levels with PD (Xia & Zhou, 2024) and the neuroprotective effects of this vitamin (Pignolo et al., 2022), I decided to explore how vitamin D metabolism is altered in reactive iASTROs, as well as whether vitamin D supplementation might affect iDAn.

5.3.1. *CYP27B1* and *VDR* expression in iASTROs after treatment with inflammatory cytokines and α-synuclein PFFs

I first analysed the expression of *CYP27B1* and *VDR* in control and *GBA-N370S* iASTROs treated for 24h or 7 days with 30 ng/mL TNFα + 50 ng/mL IFNγ or the Liddelow factors (30 ng/mL TNFα + 3 ng/mL IL-1α + 400 ng/mL C1q), to explore if their elevated expression changes with time and with the *GBA-N370S* mutation. In line with the results of the RNAseq experiment, expression of *CYP27B1* increased significantly in control and *GBA-N370S* iASTROs treated for 24h and 7 days with TNFα+IFNγ compared to untreated cells, although by 7 days the increase in treated cells was smaller (Figure 5.4 A). In cells treated with the Liddelow factors, there was a small increase in *CYP27B1* expression after 24h but not 7 days. *VDR* expression followed similar patterns, with a big increase in cells treated with TNFα+IFNγ for 24h, and less so for 7 days, and a much smaller increase in cells treated with the Liddelow factors (Figure 5.4 B). Expression of *VDR* was higher in *GBA-N370S* than in control iASTROs, especially after 24h treatment with TNFα+IFNγ.

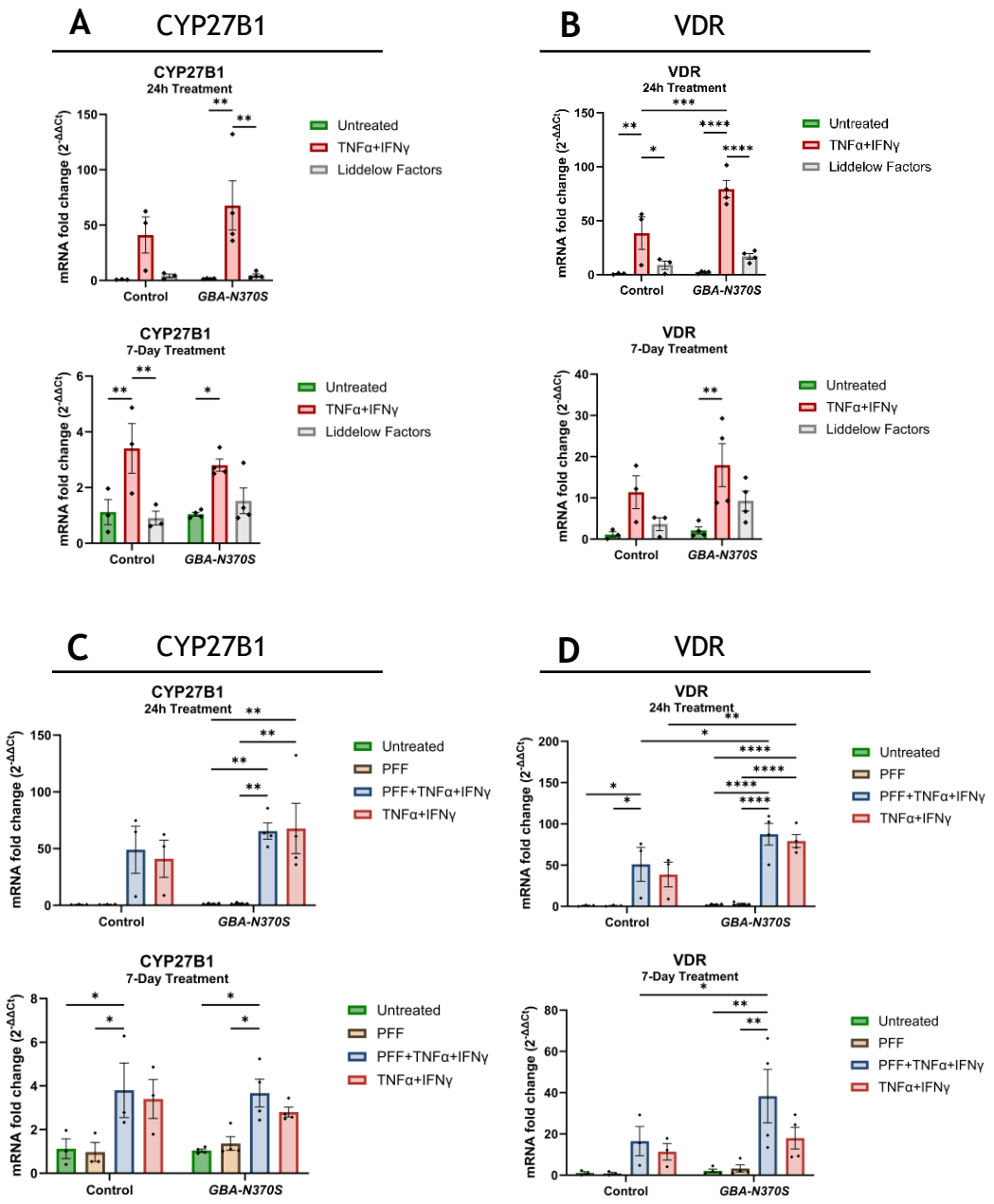


Figure 5.4. *CYP27B1* and *VDR* expression are increased in control and *GBA-N370S* iASTROs treated with TNFα+IFNγ but not α-synuclein PFFs alone, and the increase is bigger in *GBA-N370S* iASTROs

(A-B) Relative gene expression analysis by RT-qPCR of (A) CYP27B1 and (B) VDR in control and *GBA-N370S* iASTROs treated for 24h or 7 days with 30 ng/mL TNFα + 50 ng/mL IFNγ or the Liddelow factors (30 ng/mL TNFα + 3 ng/mL IL-1α + 400 ng/mL C1q). (C-D) Relative gene expression analysis by RT-qPCR of (C) CYP27B1 and (D) VDR in control and *GBA-N370S* iASTROs treated for 24h or 7 days with 10 µg/mL α-synuclein PFFs, 10 µg/mL α-synuclein PFFs + 30 ng/mL TNFα + 50 ng/mL IFNγ, or 30 ng/mL TNFα + 50 ng/mL IFNγ. In each differentiation, to calculate ΔΔCt for each gene, the ΔCt of one untreated control iASTRO line was subtracted to the ΔCt of each line (for the gene of interest). Each data point represents 1 iASTRO line averaged across differentiations. N = 3 control and 4 *GBA-N370S* lines, 1-4 differentiations. Mean ± SEM. The statistical analysis performed was two-way ANOVA with Tukey's multiple comparison test. *p<0.05, **p<0.01, ***p<0.001, ****p<0.0001.

Moreover, I explored the expression of *CYP27B1* and *VDR* in control and *GBA-N370S* iASTROs treated for 24h or 7 days with α-synuclein PFFs (10 µg/mL), α-synuclein PFFs (10 µg/mL) + TNFα (30 ng/mL) + IFNγ (50 ng/mL), or TNFα (30 ng/mL) + IFNγ (50 ng/mL). The expression pattern in cells treated with TNFα+IFNγ (+/- PFFs), was the same as described in Figure 5.4 A-B, except in *GBA-N370S* iASTROs treated for 7 days with PFFs+TNFα+IFNγ, where *VDR* expression was higher than after treatment with only TNFα+IFNγ (Figure 5.4 Dii). On the contrary, there were no differences in *CYP27B1* or *VDR* expression between untreated and PFF-treated cells (Figure 5.4 C-D), which does not corroborate the results from the RNAseq experiment. In conclusion, after 24h and 7 days of treatment, *CYP27B1* and *VDR* expression were elevated in reactive control and *GBA-N370S* iASTROs after treatment with TNFα+IFNγ, and much less so the Liddelow factors, but not with α-synuclein PFFs, and the increase in expression in reactive astrocytes diminished with time.

5.3.2. VDR nuclear translocation in reactive iASTROs

The active form of vitamin D, 1α,25-dihydroxyvitamin D3 (calcitriol), binds to VDR in the cytoplasm, which then translocates to the nucleus, where it regulates the expression of various genes (Rochel, 2022). Therefore, since *VDR* expression was upregulated in reactive iASTROs, I investigated whether this was accompanied by an increase in nuclear translocation of VDR. To this end, control and *GBA-N370S* iASTROs were treated for 24h, 72h and 7 days with 30 ng/mL TNFα + 50 ng/mL IFNγ or the Liddelow factors (30 ng/mL TNFα + 3 ng/mL IL-1α + 400 ng/mL C1q) and stained for GFAP and VDR (Figure 5.5 A). The cytoplasmic intensity of VDR did not change much upon treatment at any of the timepoints studied, whereas the nuclear intensity was higher in iASTROs treated with TNFα+IFNγ but not the Liddelow factors after 7 days (Figure 5.5 C). In line with this, after 7 days of treatment, the VDR intensity ratio (calculated as the intensity in the nucleus/intensity in the cytoplasm) was higher in iASTROs treated with TNFα+IFNγ (Figure 5.5 D). Moreover, although it was not significant, the nuclear VDR intensity and VDR intensity ratio after 7 days of treatment with TNFα+IFNγ were higher in *GBA-N370S* iASTROs, in line with the findings that these cells expressed more VDR than control cells after treatment with TNFα+IFNγ. Since no differences in the cytoplasmic intensity

were detected between both genotypes, this suggests that the newly synthetized VDR is quickly translocated into the nucleus.

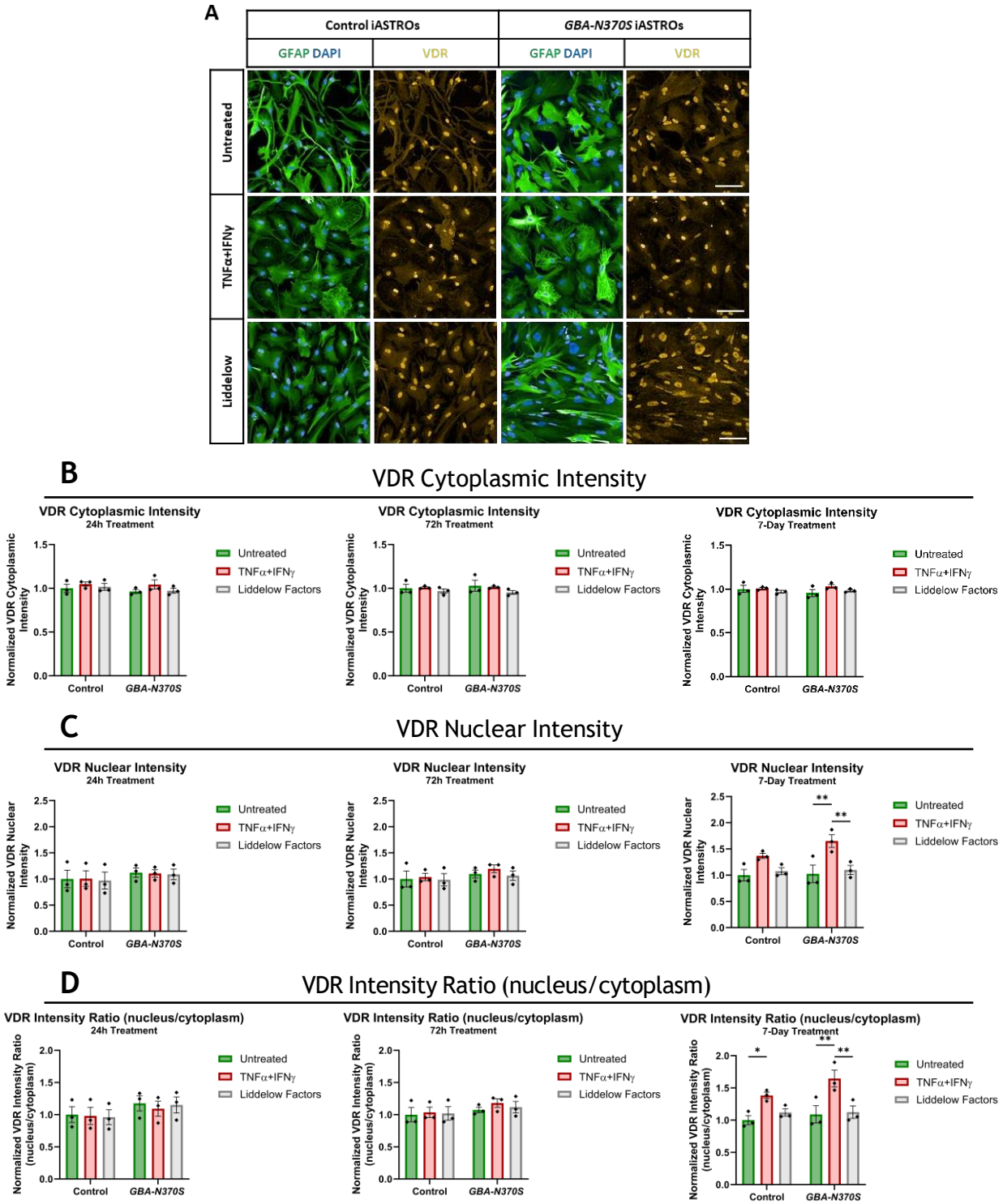


Figure 5.5. Control and *GBA-N370S* iASTROs have increased VDR nuclear translocation after 7-day treatment with TNFα+IFNγ but not the Liddelow factors

(A) Representative immunocytochemistry images of control and *GBA-N370S* iASTROs treated for 7 days with 30 ng/mL TNFα + 50 ng/mL IFNγ or the Liddelow factors (30 ng/mL TNFα + 3 ng/mL IL-1α + 400 ng/mL C1q) and stained for GFAP (green) and VDR (yellow). Scale bar: 100 µm. (B-D) Quantification of

(B) the cytoplasmic intensity of VDR, (C) the nuclear intensity of VDR, and (D) the VDR intensity ratio (calculated by dividing the mean VDR intensity in the nucleus by the mean VDR intensity in the cytoplasm) in control and *GBA-N370S* iASTROs treated for 24h, 72h or 7 days with 30 ng/mL TNFα + 50 ng/mL IFNγ or the Liddelow factors (30 ng/mL TNFα + 3 ng/mL IL-1α + 400 ng/mL C1q). To obtain normalized values, in each timepoint, measured values were normalized to the average value of untreated control iASTROs. Each data point represents 1 iASTRO line averaged across differentiations. N = 3 control and 3 *GBA-N370S* lines, 3 differentiations. Mean ± SEM. The statistical analysis performed was two-way ANOVA with Tukey's multiple comparison test. *p<0.05, **p<0.01.

5.3.3. Blockage of VDR nuclear translocation with MeTC7 and the effects on iASTRO reactivity

Next, I explored if blocking VDR translocation into the nucleus with the VDR antagonist MeTC7 (Khazan et al., 2022) affected iASTRO reactivity. I first validated the capacity of MeTC7 to partially block VDR translocation into the nucleus (Appendix S.2). Afterwards, control and *GBA-N370S* iASTROs were treated for 24h, 72h or 7 days with 30 ng/mL TNFα + 50 ng/mL IFNγ, 250 nM MeTC7, or 30 ng/mL TNFα + 50 ng/mL IFNγ + 250 nM MeTC7, and stained for S100B, GFAP and C3 (Figure 5.6). Two-way ANOVA and three-way ANOVA statistical analyses were done, to investigate the effect of each treatment and the overall effect of TNFα+IFNγ and MeTC7. Generally, the effect of TNFα+IFNγ on the measured parameters was the same as described previously (Figure 4.10 and Figure 4.16), so these changes will not be discussed here. The number of total live cells, the cell area, and S100B intensity did not change after treatment with MeTC7 (Figure 5.7 A-C). The cytoplasmic GFAP intensity was lower in control iASTROs treated for 72h with TNFα+IFNγ+MeTC7 compared to the other three conditions, and by 7 days there was a decrease in control and *GBA-N370S* iASTROs in both conditions with TNFα+IFNγ, but this decrease was bigger in cells treated with TNFα+IFNγ+MeTC7 (Figure 5.7 D). Lastly, C3 intensity appeared to be increased due to treatment with MeTC7 alone at all timepoints, and in control iASTROs treated with TNFα+IFNγ+MeTC7 compared to TNFα+IFNγ after 72h and 7 days (Figure 5.7 E). Indeed, three-way ANOVA analysis showed that, after 72h of treatment, there was almost a statistically significant increase in C3 intensity due to MeTC7 administration (p=0.0837).

All in all, except a small decrease in GFAP intensity in iASTROs treated with TNFα+IFNγ+MeTC7, and a small increase in C3 intensity in iASTROs treated with MeTC7 alone,

or in the case of control cells, TNFα+IFNγ+MeTC7, there was no big effect of MeTC7 on iASTROs reactivity.

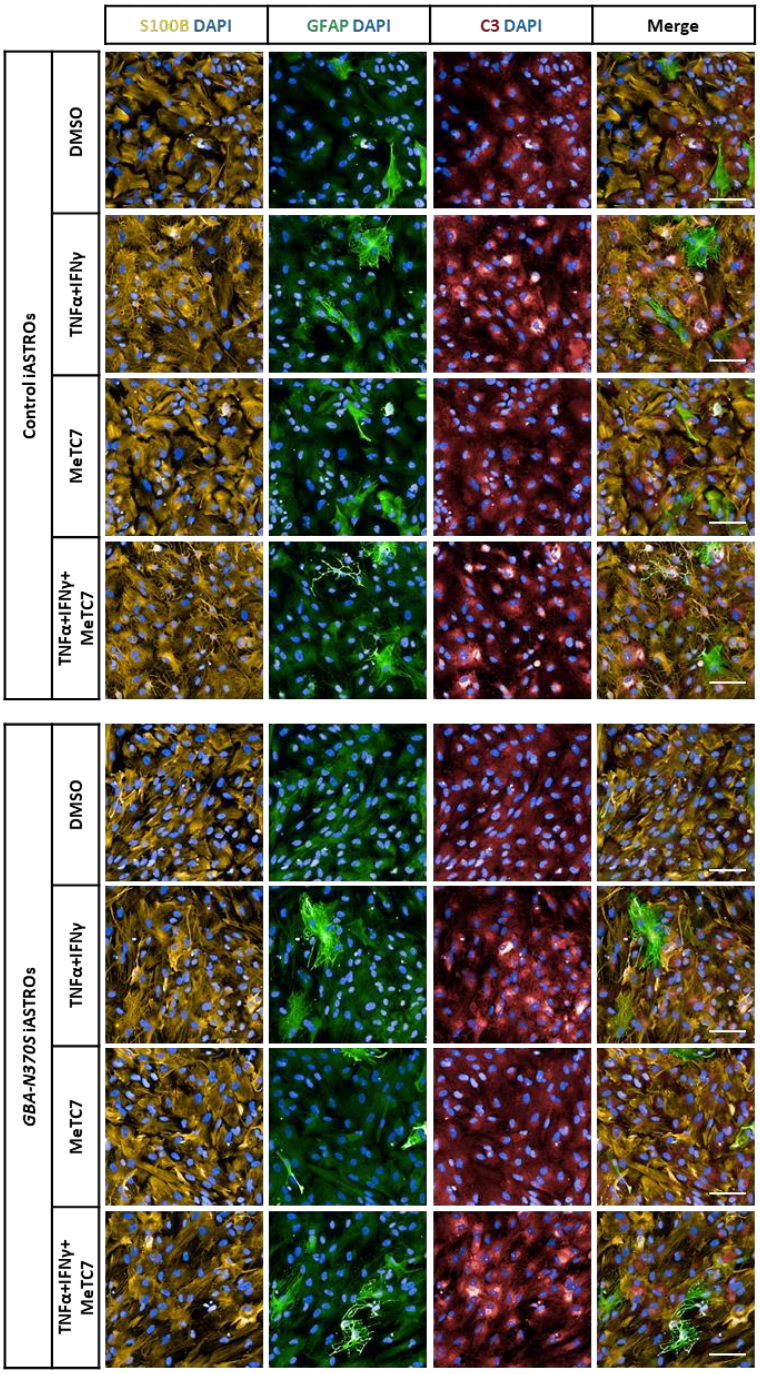


Figure 5.6. Representative immunocytochemistry images of control (top panel) and *GBA-N370S* (bottom panel) iASTROs treated for 72h with MeTC7 and TNFα+IFNγ

30 ng/mL TNFα + 50 ng/mL IFNγ, 100 nM MeTC7, or 30 ng/mL TNFα + 50 ng/mL IFNγ + 100 nM MeTC7, and stained for S100B (yellow), GFAP (green) and C3 (red). Scale bar: 100 µm.

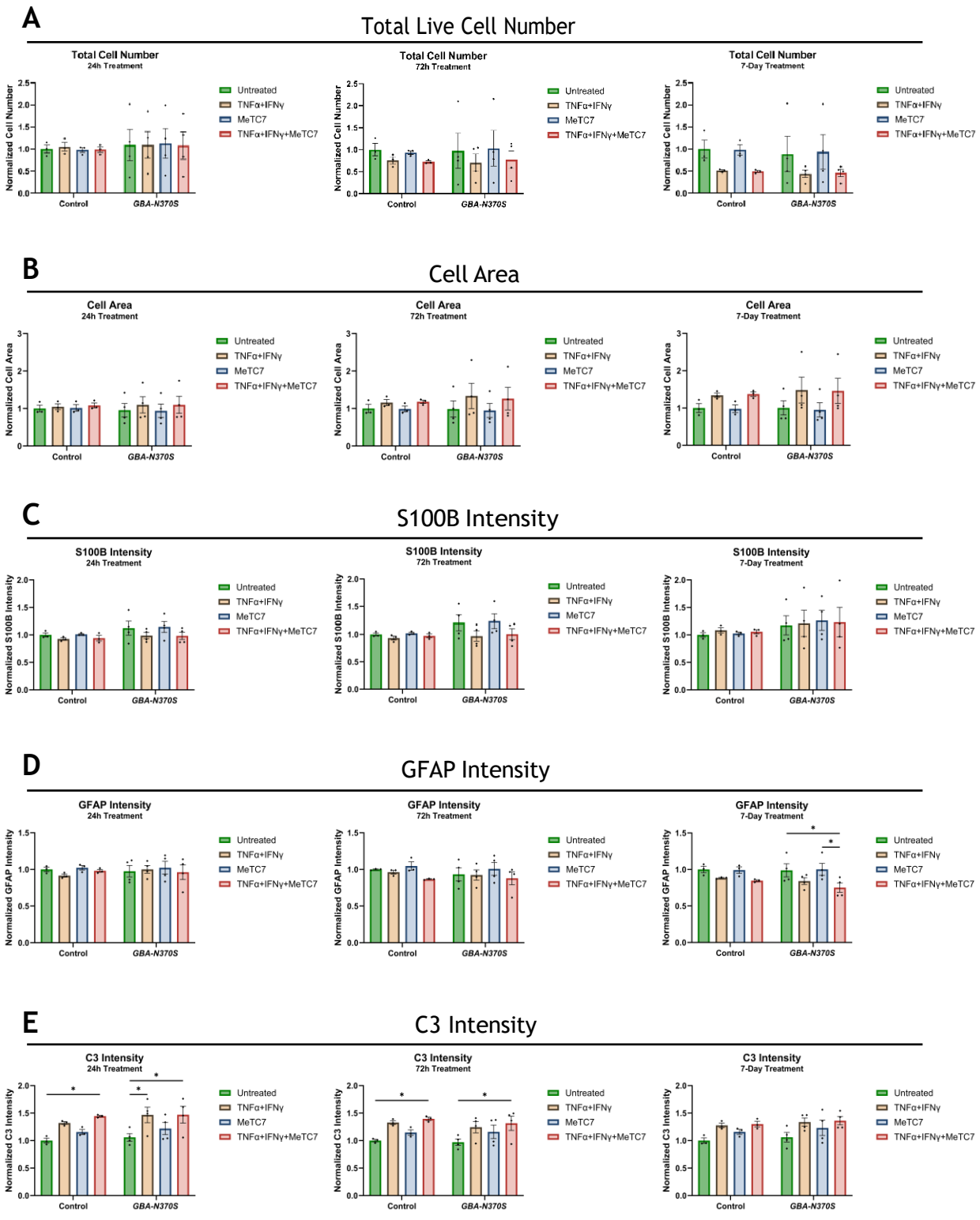


Figure 5.7. The VDR blocker MeTC7 does not affect the reactive response of iASTROs to TNFα+IFNγ
(A-E) Quantification of (A) the total live cell number, (B) the cell area, (C) the cytoplasmic S100B intensity, (D) the cytoplasmic GFAP intensity, and (E) the cytoplasmic C3 intensity of control and *GBA-N370S* iASTROs treated for 24h, 72h or 7 days with 30 ng/mL TNFα + 50 ng/mL IFNγ, 100 nM MeTC7, or 30 ng/mL TNFα + 50 ng/mL IFNγ + 100 nM MeTC7. To obtain normalized values, in each timepoint,

measured values were normalized to the average value of untreated control iASTROs. Each data point represents 1 iASTRO line averaged across differentiations. N = 3 control and 4 *GBA-N370S* lines, 1-3 differentiations. Mean ± SEM. The statistical analysis performed was two-way ANOVA with Tukey's multiple comparison test. *p<0.05, **p<0.01, ***p<0.001, ****p<0.0001. Three-way ANOVA was also performed to calculate the overall effect of MeTC7 or TNFα + IFNγ, and the esults of this statistical analysis are described in the text body.

5.3.4. Vitamin D supplementation in iDAn and its effects on cell survival

Lastly, based on the hypothesis that iASTROs increase vitamin D metabolism in response to inflammatory stimuli as a neuroprotective mechanism to neurons, I explored how direct administration of vitamin D in iDAn would affect their viability and survival. Thus, control and *GBA-N370S* iDAn in mono-cultures were treated for 24h, 7 or 14 days with 0, 10, 25, 50 and 100 nM of vitamin D, and stained for MAP2 and TH (Figure 5.8). Vitamin D was not a molecule included in the normal DAn maturation media, and in this experiment, it was added with every feed in the appropriate concentrations. There was no difference in the total number of live cells, the number of MAP2+ cells or the number of TH+ cells after vitamin D supplementation, regardless of the concentration and duration of treatment (Figure 5.9 A-C). The only differences observed were due to the genotype of the cells, as overall fewer live cells and MAP2+ cells were quantified with *GBA-N370S* iDAn compared to control cells, especially at the 24h and 7-day timepoints (Figure 5.9 A-B).

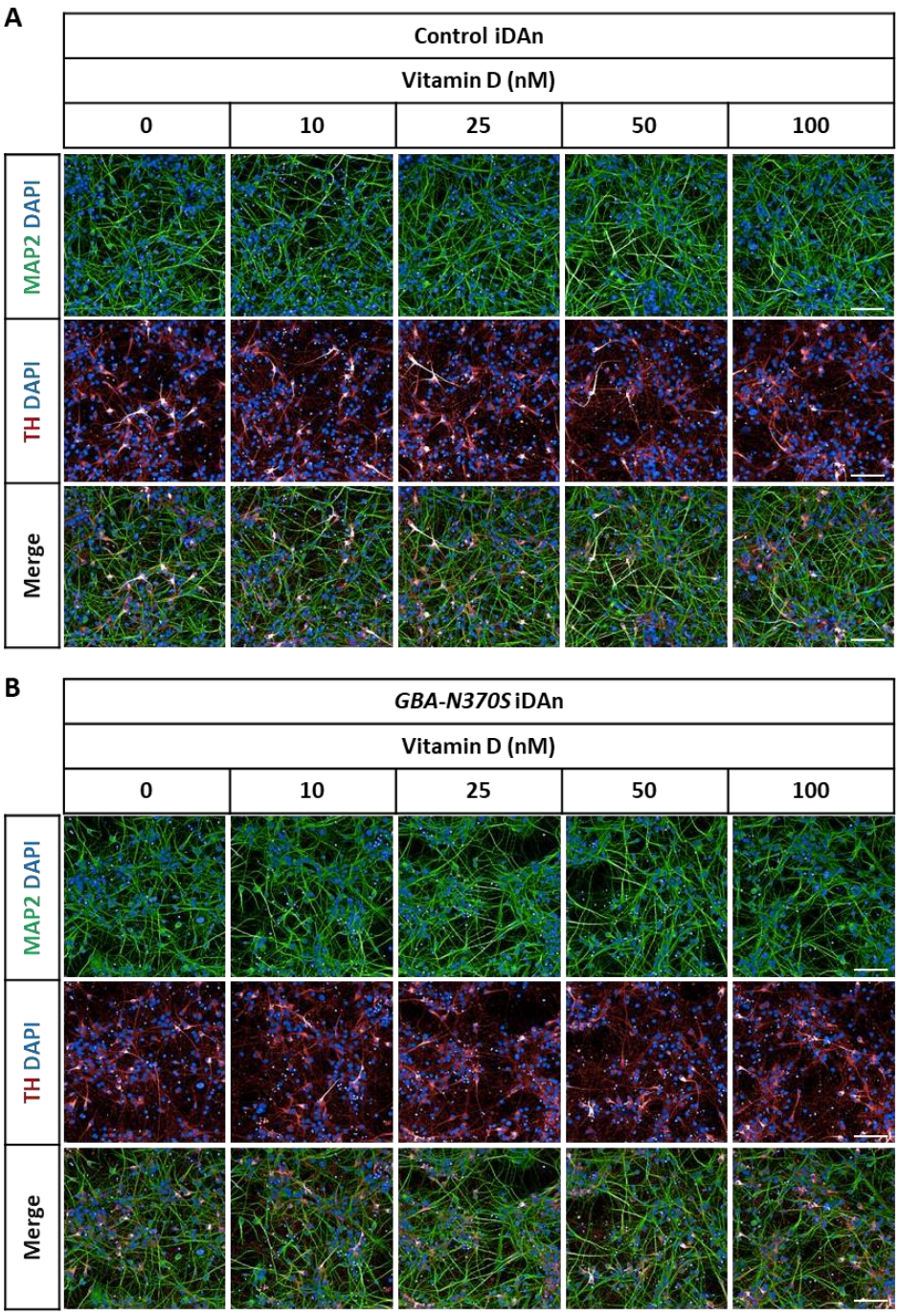


Figure 5.8. Representative immunocytochemistry images of (A) control and (B) *GBA-N370S* iDAn treated for 7 days with increasing concentrations of vitamin D

0, 10, 25, 50 and 100 nM of vitamin D were used, and iDAn were stained for MAP2 (green) and TH (red).

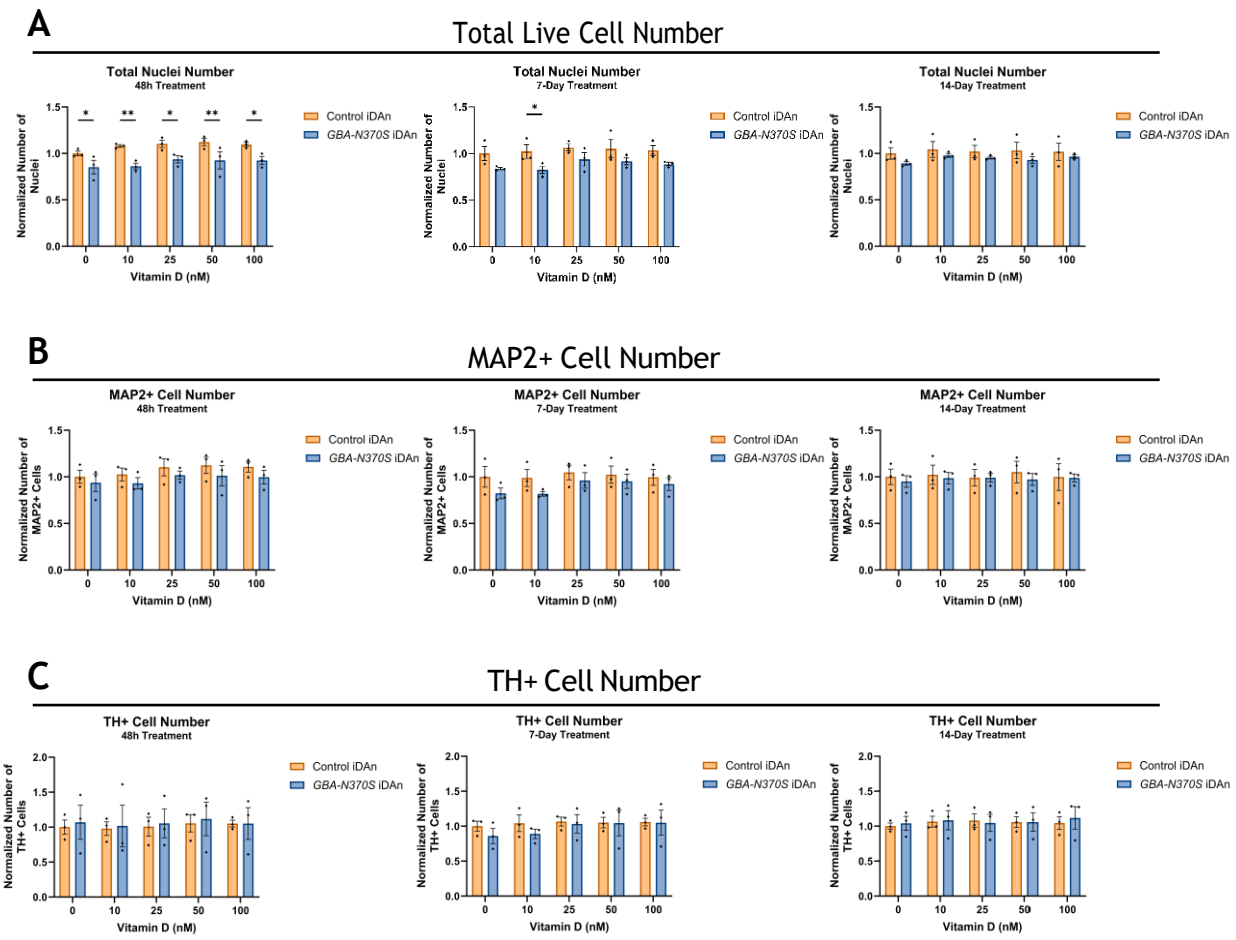


Figure 5.9. Vitamin D supplementation to iDAn does not affect their viability and survival
(A-C) Quantification of (A) the total number of live cells, (B) the number of MAP2+ cells and (C) the number of TH+ cells in control and *GBA-N370S* iDAn treated for 48h, 7 days of 14 days with 0, 10, 25, 50 or 100 nM Vitamin D. Each dot represents one line averaged across differentiations. N = 3 control and 3 *GBA-N370S* lines, 3 differentiations. Mean ± SEM. The statistical analysis performed was two-way ANOVA with Tukey's multiple comparison test. *p<0.05, **p<0.01.

5.4. Discussion

In this chapter, I followed up on two interesting findings made in the bulk RNAseq experiment. On the one hand, I explored SOCE and ATP-induced ER-calcium release in iASTROs treated with TNFα+IFNγ and the Liddelow factors, and how partially blocking the latter pathway might impact iASTRO reactivity. Moreover, I investigated some aspects of vitamin D metabolism and signalling in iASTROs treated with TNFα+IFNγ, the Liddelow factors, and α-synuclein PFFs, and the overall effect of vitamin D supplementation in DAn.

5.4.1. Calcium signalling and homeostasis in reactive iASTROs

First, RT-qPCR analysis of *ORAI1* expression showed an increase both in control and *GBA-N370S* iASTROs 24h and 7 days after treatment with TNFα+IFNγ. However, the Fura-2 traces showed a higher calcium entry in cells treated with TNFα+IFNγ for 24h and 72h but not 7 days, which indicates that an increased *ORAI1* expression, without changes in *STIM1* expression, is not sufficient to potentiate SOCE. Regarding iASTROs treated with the Liddelow factors, no changes in *ORAI1* and *STIM1* expression were observed after 24h and 7 days of treatment. On the contrary, control iASTROs had increased calcium entry through SOCE after 7 days of treatment and no changes at earlier timepoints, whereas *GBA-N370S* iASTROs treated for 24h and 72h had lower levels of calcium entry.

A reason for these conflicting observations between RT-qPCR and Fura-2 results might be that the other ORAI homologue channels expressed in iASTROs (ORAI2 and 3) are also mediators of SOCE. The data from the RNAseq experiment did not show any differences in the expression of *ORAI2/3* after 24h of treatment, but further studies should explore if *ORAI2/3* expression changes at later timepoints after treatment with inflammatory cytokines. Some studies in mice have claimed that ORAI1 is the main contributor to SOCE in astrocytes (Gao et al., 2016; Papanikolaou et al., 2017), but others have shown that ORAI3 also plays an important role (Kwon et al., 2017; Ronco et al., 2014). TRP channels can also participate in astrocytic SOCE (Verkhratsky & Parpura, 2014), and, therefore, changes in their expression levels could also lead to higher/lower calcium entry through SOCE. Furthermore, changes in the subcellular localization of the ER in reactive iASTROs could also cause changes in SOCE (Pivneva et al., 2008) without the change in the expression levels of ORAI1/2/3 and STIM1. Unfortunately, there was no time to further explore SOCE in reactive iASTROs and to manipulate this calcium pathway to investigate its role on iASTRO reactivity.

On the other hand, RT-qPCR analysis showed that iASTROs treated for 7 days with TNFα+IFNγ had increased expression of *ITPR1* and *ITPR3*, but not *ITPR2*, with overall very little changes in cells treated with the Liddelow factors. These results do not correlate with the findings in the bulk RNAseq experiment, which revealed that all *ITPR* genes had a higher expression after 24h treatment with TNFα+IFNγ, as well as the Liddelow factors in the case of *ITPR2* and *ITPR3*. There are multiple factors that could contribute to this discrepancy in results. For instance,

even if the efficiency of the primers used for RT-qPCR was tested and validated, they may not have detected all transcripts. Additionally, it may be due to differences between the lines and differentiations used in both sets of experiments.

Moreover, the functional analysis of ATP-induced ER-calcium release in reactive iASTROs revealed extensive line-to-line and differentiation-to-differentiation variability, and, as with SOCE, the results from the functional assay did not always correlate with the expression levels of the *ITPR* genes. The variability was most apparent in control iASTROs, where one line had decreased ER-calcium release at all timepoints after treatment with TNFα+IFNγ, another showed a big increase in ER-calcium release, and another showed little change, even if at the RNA level all lines showed an increase in *ITPR1* and *ITPR3* expression. *GBA-N370S* iASTROs had an overall elevated ER-calcium release after treatment with TNFα+IFNγ, but the magnitude of the increase was very different between the lines. As for cells treated with the Liddelow factors, most lines had an increase in ER-calcium release after the treatment, but this did not correlate with the RT-qPCR results that showed very little change in the expression of *ITPR* genes. Overall, these results point towards a higher ATP-induced ER-calcium release in iASTROs after treatment with the Liddelow factors and more so TNFα+IFNγ. However, the fact that this effect was not replicated in all lines and the results did not always correlate with the expression levels of *ITPR* genes, other pathways to mobilize calcium might also be altered in reactive iASTROs, and further experiments are needed to investigate this.

On the other hand, partially blocking ATP-induced ER-calcium release with 2-APB did not have any significant effects on the inflammatory response of iASTROs or the expression of neurotrophic factors (Appendix S.1). In the future, to successfully and specifically block ATP-induced ER-calcium release, *ITPR* genes should be knocked down or knocked out, either individually or in combination. After checking that lower *ITPR* expression does not affect cell viability, the effects on the inflammatory response of astrocytes should be studied.

Despite the line-to-line variability and the discrepancies between the functional calcium assays, the RT-qPCR results and the RNAseq data, it is evident that ATP-induced ER-calcium release and SOCE are dysregulated in iASTROs after treatment with TNFα+IFNγ, and less so, the Liddelow factors. In the literature, the first evidence that inflammatory cytokines increased intracellular calcium in astrocytes came over 3 decades ago (Holliday & Gruol,

1993). Since then, most studies have shown that reactive astrocytes mostly present calcium signals that are higher in amplitude, duration and frequency (Shigetomi et al., 2019). Nevertheless, there is still very little data available on the relationship between astrocytic calcium signalling, inflammation and neurological disease, and most studies have been done in rodent models and primary cultures.

Regarding the relationship between inflammation and SOCE, a recent study showed that, after stimulation with TNFα+IL-1α, mouse astrocytes express higher levels of *ORAI2*, although calcium entry through SOCE remained unchanged. Moreover, *ORAI2* expression was not related to inflammatory cytokine production (Nakajima et al., 2022). On the other hand, a few studies have reported that activation of SOCE with thapsigargin promoted production of TNFα, IL-6 and other inflammatory cytokines, and STIM1 and ORAI1 participated in LPS-induced production of these cytokines too (Birla et al., 2022; Gao et al., 2016; Novakovic et al., 2023). Furthermore, contrary to the results presented in this chapter, Ronco and colleagues reported that hippocampal astrocytes treated with TNFα had decreased expression levels of ITPR1, ITPR2 and ORAI3 but higher levels of ORAI2, although they did not mechanistically explore SOCE (Ronco et al., 2014). These differences could be due to the different cell model or concentration of TNFα used in that study and this thesis. Lastly, in human astroglioma U251 cells, 24h treatment with the Liddelow factors was shown to decrease calcium entry by SOCE (Poejo et al., 2023), which is in line with the findings presented in this chapter with *GBA-N370S* iASTROs but not control iASTROs. Based on all this evidence, in the iASTRO model used in this thesis, calcium mobilization through SOCE might participate in the production of inflammatory cytokines and the inflammatory response of iASTROs treated with TNFα+IFNγ.

On the other hand, fewer studies have focused on the role of ATP-induced ER-calcium release in inflammatory astrocytes. For instance, Barbar and colleagues also reported that iPSC-derived astrocytes, but not rat astrocytes, had increased ATP-induced ER-calcium release after 24h exposure to the Liddelow factors (Barbar et al., 2020), although in this thesis the effect of the Liddelow factors on ER-calcium release was more potent at later timepoints. Furthermore, some research suggests that TNFα triggers ATP release in astrocytes, which then induces ER-calcium release (Nikolic et al., 2018). This is another mechanism by which TNFα treatment results in increased ER-calcium release, regardless of the expression levels of ITRP channels.

All in all, the results presented in this chapter indicate that different calcium signalling pathways are altered in iASTROs treated with TNFα+IFNγ, and to a lesser extent, the Liddelow factors. However, due to the lack of specificity of most inhibitors used to block these pathways, such as 2-APB, further studies should focus on knocking down or knocking out the specific channels involved in ER-calcium release and SOCE, either alone or in combination, and then investigate how this impacts the release of pro-inflammatory cytokines and neurotrophic factors in astrocytes after an inflammatory stimulus.

On another note, the calcium experiments presented in this chapter revealed genotypic differences between control and *GBA-N370S* iASTROs. In chapter 3, during the characterization of mature iASTROs, reduced ER-calcium release after ATP application was observed in *GBA-N370S* cells, a finding that was replicated in the experiments presented in this chapter. However, the differences observed in the peak amplitude and AUC in this chapter between untreated control and *GBA-N370S* iASTROs were smaller than those observed in chapter 3. The most plausible explanation for this is that only mature and functional iASTROs that had passed QC were chosen for the experiments in this chapter, whereas all cells, even those that had not matured properly, were used for the characterization in chapter 3. On the contrary, *GBA-N370S* iASTROs had higher levels of calcium entry through SOCE than control iASTROs, especially after treatment with TNFα+IFNγ. A potential explanation for these two findings is that *GBA-N370S* iASTROs have less ER calcium stores than control cells, which results in a smaller ER-calcium release after ATP stimulation, but they have a more efficient SOCE system to compensate for the lower ER calcium stores. Further research is needed to validate this hypothesis. Additionally, the higher SOCE in *GBA-N370S* iASTROs treated with TNFα+IFNγ could also be related to the higher ROS production in these cells compared to control iASTROs, presented in Chapter 4, as there are studies reporting that redox modification of STIM1 and ORAI1 can result in increased SOCE activation (Johnson et al., 2022; Nunes & Demaurex, 2014).

Aflaki and colleagues reported that GD astrocytes homozygous for the *GBA-N370S* mutation had slightly lower ATP-induced ER-calcium release than controls, but this was not statistically significant (Aflaki et al., 2020). No other studies investigating calcium disturbances in *GBA* astrocytes could be found, although decreased ER-calcium release has been reported in *GBA-N370S* iDAn (Beccano-Kelly et al., 2023) and *LRRK2-G2019S* iPSC-derived astrocytes (Ramos-

Gonzalez et al., 2021; Sonninen et al., 2020). Nevertheless, more research should be done to study how different PD-related mutations affect astrocytic calcium homeostasis and the implications of aberrant calcium signalling in PD. Indeed, besides the involvement of calcium signalling in astrocyte-induced neuroinflammation, aberrant astrocytic calcium signalling has been postulated to promote PD pathogenesis through different mechanisms, such as changing the integrity of the BBB, promoting microglial activation, and causing DAn dysfunction (Bancroft & Srinivasan, 2022).

A big limitation of the calcium experiments presented in this chapter was the approach used to measure calcium in astrocytes. Indeed, using the Fura-2 AM organic dye and measuring the fluorescence emission ratios of an entire well of a 96-well plate in the FlexStation does not provide single cell resolution, which masks the differences in the response kinetics and amplitude of each cell. Moreover, Fura-2 does not enable to discern the calcium-level changes in different sub-cellular compartments and organelles, which are known to differ from one another (Semyanov et al., 2020). Thus, future studies should use more sensitive and precise techniques, such as genetically encoded calcium indicators (GECIs), which will provide much more in-depth information regarding the broad array of calcium responses in different populations of astrocytes and in different cellular compartments.

Lastly, it is worth mentioning that, even if a recent study claimed that 24h of exposure to α-synuclein aggregates caused upregulation of *STIM1* and *ORAI3* expression, as well as alterations in SOCE (Raj et al., 2023), and another study showed that mouse models of α-synucleinopathies presented aberrant astrocytic calcium signalling (Nanclares et al., 2023), no changes in any of these calcium pathways were observed in PFF-treated iASTROs in this thesis (data not shown).

5.4.2. Vitamin D metabolism and signalling in reactive iASTROs

RT-qPCR analysis revealed an increase in the expression of *CYP27B1* and *VDR* in iASTROs treated with TNFα+IFNγ, and to a much lesser extent the Liddelow factors. This increase was highest 24h after treatment and decreased over time. The elevated expression of *VDR* was accompanied by an increase in VDR nuclear translocation in iASTROs treated with TNFα+IFNγ.

However, partial blockage of VDR translocation with MeTC7 did not affect astrogliosis in cells treated with TNFα+IFNγ, as measured by cell morphology and C3 intensity. Nonetheless, the concentration of MeTC7 used in this thesis only resulted in partial blockage of VDR translocation, and maybe higher concentrations and more efficient VDR blockage are needed to alter VDR-regulated expression and astrogliosis.

The research exploring the relationship between astrocytic neuroinflammation and vitamin D is quite scarce, but there is some evidence showing how vitamin D ameliorates astrogliosis. For instance, vitamin D administration was shown to lower the LPS-induced expression of TNFα and other pro-inflammatory cytokines in rat astrocytes (Furman et al., 1996; Jiao et al., 2017), as well as reducing cellular alterations caused by rotenone in mouse astrocytes (de Siqueira et al., 2023). Moreover, in mice, 6-OHDA and MPTP-induced astrogliosis were reduced with vitamin D treatment (Calvello et al., 2017; Kim et al., 2020). Furthermore, vitamin D and VDR activation promote the expression of neurotrophic factors in astrocytes, such as GDNF, as well as γ-glutamyl transpeptidase (Garcion et al., 1999), which participates in the metabolism of glutathione, an essential antioxidant.

Therefore, increasing vitamin D metabolism and VDR activation might be a neuroprotective mechanism in astrocytes after acute inflammatory insult, with the goal of decreasing the neuroinflammatory response whilst increasing their antioxidant properties. However, *CYP27B1* and *VDR* expression in reactive iASTROs decreased over time, which might indicate that this is a short-term neuroprotective mechanism. Potential future experiments to investigate the relationship between neuroinflammation and vitamin D should include treating astrocytes with both inflammatory cytokines and vitamin D to investigate if the latter ameliorates the production of pro-inflammatory cytokines and ROS. Another option is to knock down *CYP27B1* and *VDR* and explore how this affects the inflammatory response after exposure to inflammatory cytokines. Furthermore, it would be interesting to study how the expression of VDR-target genes changes in response to inflammatory insults, VDR blockage, VDR activation with vitamin D, or a combination of these.

Another potential beneficial effect of increased vitamin D production in astrocytes could be the effects vitamin D has on neurons. Indeed, research has indicated that vitamin D promotes the proliferation and differentiation of DAn (Pertile et al., 2023). In the experiments presented

in this chapter, no differences were observed in the total number of live cells, MAP2+ and TH+ cells in iDAn mono-cultures after vitamin D supplementation, indicating that vitamin D did not potentiate neuronal survival. However, the iDAn cultures consisted of mature and non-proliferating cells, and they were in normal basal conditions. Therefore, potentially a pathological or toxic trigger is needed to evoke the neuroprotective effects of vitamin D on iDAn. For instance, studies in rodents have shown that 6-OHDA administration results in lower VDR expression, whereas vitamin D administration prevents 6-OHDA-induced DAn loss, ROS production, mitochondrial dysfunction, and behavioural deficits (Araújo de Lima et al., 2022; Kim et al., 2020; Lima et al., 2018). Similar beneficial effects of vitamin D supplementation have been observed in rotenone-induced rat models (Magdy et al., 2022). Thus, future experiments should investigate the neuroprotective effects of vitamin D in iDAn cultures treated with a pathological insult such as MPP^+, 6-OHDA or rotenone. Furthermore, the elevated *CYP27B1* and *VDR* expression in reactive iASTROs may only act in a cell-autonomous manner to lower astrogliosis and promote the expression of neurotrophic factors and antioxidant enzymes in astrocytes, which would then exert their neuroprotective effects on neurons.

Despite the beneficial effects of vitamin D supplementation observed PD rodent models, the few trials that have been done in PD patients have yielded inconclusive or contradictory results. While some studies have reported positive effects of vitamin D on functional tests such as timed up-and-go (TUG), others have claimed that there were no improvements after vitamin D administration (Detopoulou et al., 2023). However, since vitamin D deficiency has been widely reported in PD patients and it has been linked to disease severity (Xia & Zhou, 2024), further clinical studies in patients are needed to investigate the effects of vitamin D administration in different aspects of the disease.

On the other hand, even if the bulk RNAseq experiment discussed in chapter 4 showed that iASTROs treated with α-synuclein PFFs alone had upregulated expression of *CYP27B1*, the subsequent RT-qPCR experiments presented in this chapter did not corroborate that finding, as neither control nor *GBA-N370S* iASTROs exhibited altered *CYP27B1*, or *VDR*, expression after exposure to PFFs. Unfortunately, there is very little data available regarding the effects of α-synuclein on vitamin D metabolism and signalling, just some reports indicating than PFF injection in mice expressing human α-synuclein results in lower VDR expression (Kim et al.,

2020). Furthermore, another link between vitamin D and α-synuclein is the activation of autophagy and α-synuclein degradation. Even if a study claimed that VDR inhibition activated autophagy and prevented α-synuclein oligomerization in SH-SY5Y cells (Ding et al., 2021), most research shows that calcitriol administration and VDR activation leads to an increase in autophagy in neurotoxin-induced PD models (Li et al., 2015; Magdy et al., 2022), and in SH-SY5Y cells, the vitamin D-mediated increase in autophagy prevented α-synuclein aggregation (Rcom-H'cheo-Gauthier et al., 2017; Zhang et al., 2022).

Lastly, Mazzetti and colleagues reported that *CYP27B1* expression was higher in astrocytes from PD patients compared to control cases (Mazzetti et al., 2022). These CYP27B1-positive astrocytes contained intracellular α-synuclein oligomers that colocalized with LAMP1 and were in contact with DAn lacking LBs. Thus, the authors hypothesized that CYP27B1-positive astrocytes are neuroprotective and participate in autophagy-mediated α-synuclein uptake and degradation (Mazzetti et al., 2022). Based on all these findings, increased vitamin D metabolism and signalling in astrocytes in PD might be beneficial in numerous ways: by increasing autophagy-mediated α-synuclein degradation, decreasing neuroinflammation, increasing antioxidant activities, and increasing vitamin D availability for DAn.

To conclude, since one of the main functions of vitamin D is calcium homeostasis in the body (Fleet, 2017), the changes in vitamin D metabolism and calcium signalling occurring in reactive iASTROs are probably interrelated, as vitamin D, acting through VDR, regulates the expression of genes involved in calcium homeostasis and transport.

Overall, the results presented in this chapter show that acute treatment with TNFα+IFNγ and the Liddelow factors caused calcium dysregulation in control and *GBA-N370S* iASTROs, namely changes in SOCE and ATP-induced ER-calcium release. Moreover, *GBA-N370S* iASTROs displayed higher increases in cytoplasmic calcium through SOCE but lower ER-calcium release after ATP application compared to control iASTROs. On the other hand, the data outlined in this chapter indicates that reactive control and *GBA-N370S* iASTROs had increased expression of *CYP27B1* and *VDR*, as well as VDR translocation into the nucleus, although partial blockage of VDR translocation did not affect iASTRO reactivity, nor did vitamin D supplementation enhance iDAn viability.

Chapter 6 - Investigating the effect of reactive iASTROs on iDAn

6.1. Introduction and aims

In Chapter 4, I performed an in-depth exploration of the response of iASTROs to different inflammatory cytokines and α-synuclein PFFs in mono-culture, including a detailed analysis of the transcriptomic changes occurring in control iASTROs after 24h of treatment and subsequent in vitro RT-qPCR, immunocytochemistry and ROS assays. All these assays showed that iASTROs undergo vast changes after exposure to inflammatory cytokines but not α-synuclein PFFs, and the biggest changes were induced with the combined treatment of TNFα+IFNγ. However, the information obtained in these assays did not specify if iASTROs acquired a neurotoxic or neuroprotective phenotype in response to each of treatments, as some evidence pointed towards a neurotoxic phenotype (enriched GO:BP terms related to cell killing and apoptosis, release of pro-inflammatory cytokines, increased ROS production over time), whereas other results suggested that cells acquire a neuroprotective phenotype (increased expression of antioxidant enzymes, increased expression of some growth factors, increased vitamin D metabolism).

On the other hand, in the brain, astrocytes do not exist in isolation, they are surrounded by neurons and other glial cells. Astrocytes are in continuous contact and interaction with all these cells, and the specific signals they receive from different cell populations, especially microglia and neurons, shapes their function, including their inflammatory response. In the context of PD, because DAn are the most affected cell population, and they are known to be surrounded by reactive astrocytes, it is important to understand the contribution of these astrocytes to DAn neurodegeneration, as they might be harmful to DAn or, in turn, they might try to counteract the neurodegenerative process. To add on to this puzzle, it is likely that the reactive phenotype of astrocytes fluctuates throughout the disease progression, shifting from a more neuroprotective phenotype to a more neurotoxic one, or vice versa.

Not many studies have explored the direct effect of inflammatory astrocytes on neurons, or whether the inflammatory response of astrocytes changes when in direct contact with neurons. Moreover, some of the studies available lack appropriate controls to demonstrate that the treatments used do not directly act on neurons, and often, very short treatment and

co-culture durations were explored. Nevertheless, most studies observed a neurotoxic action of astrocytes on neurons after treatment with inflammatory cytokines, although there are also reports claiming that upon inflammatory cytokine stimulation, reactive astrocytes are neuroprotective to neurons.

The aims of this chapter are:

- To study the effect of reactive control and *GBA-N370S* iASTROs on iDAn when treating iASTROs with TNFα+IFNγ before the co-cultures.
- To study the effect of reactive control and *GBA-N370S* iASTROs on iDAn when treating the co-cultures directly with a range of different inflammatory cytokines.
- To investigate the effect of α-synuclein PFFs, with or without TNFα+IFNγ, on iDAn neuron survival and iASTRO reactivity in direct co-culture.

6.2. Effect of pre-treated reactive control and *GBA-N370S* iASTROs on iDAn

To investigate the effect of reactive iASTROs on iDAn, I used two different co-culture and treatment strategies: one where iASTROs were treated in mono-culture with TNFα+IFNγ and then added to iDAn, and another where the co-cultures were directly treated with different inflammatory cytokines.

In the first approach, I treated control and *GBA-N370S* iASTROs for 24h in mono-culture with 30 ng/mL TNFα + 50 ng/mL IFNγ, and then added them to control and *GBA-N370S* iDAn (Figure 6.1 A). Untreated iASTROs were used in parallel to compare the effect of pre-treated and untreated iASTROs on iDAn, and a condition of iDAn in mono-culture was also added as a control. Inspection of iASTROs in the brightfield microscope right before adding them to iDAn showed that after 24h of treatment with TNFα+IFNγ iASTROs had undergone morphological changes characteristic of astrogliosis (Figure 6.1 B), proving that iASTROs had responded to the treatment. The co-cultures were maintained for 48h, 5 and 10 days, and then stained for the DAn markers TH and MAP2, and the astrocyte and reactive astrocyte markers C3, S100B and NFκB (Figure 6.1. C-D).

I first analysed neuronal survival in the co-cultures. As expected, the total number of live cells was higher in the co-cultures with untreated and pre-treated iASTROs than in iDAn mono-cultures, with no notable difference due to the pre-treatment of iASTROs, the genotype of iASTROs, or the time in co-culture (Figure 6.2 A). The number of MAP2+ cells was also higher in the co-cultures with untreated and pre-treated iASTROs than in iDAn mono-cultures, although this observation was only statistically significant 5 and 10 days after co-culture (Figure 6.2 B). In co-cultures with control iASTROs, after 5 days the number of MAP2+ was higher in control than in *GBA-N370S* iDAn, but by day 10 similar levels were observed (Figure 6.2 Bi), whereas in co-cultures with *GBA-N370S* iASTROs no differences in MAP2+ cell number were observed between iDAn genotypes (Figure 6.2 Bii). Moreover, in co-cultures with control iASTROs, the number of TH+ cells was higher in co-cultures with pre-treated or untreated iASTROs compared to iDAn mono-cultures at all timepoints, even if not all observations were statistically significant, and the overall TH+ cell number was lower in *GBA-N370S* iDAn than in control iDAn, in all conditions (Figure 6.2 Ci). With *GBA-N370S* iASTROs, there was also an increase in TH+ cell number in co-cultures, regardless of whether the iASTROs had been previously treated or not, and an overall decrease in *GBA-N370S* iDAn, but these observations were mostly not significant (Figure 6.2 Cii). Lastly, in co-cultures with control iASTROs, the dead cell ratio (measured as the number of dead cells divided by the total number of cells) was higher in all conditions with *GBA-N370S* iDAn at all timepoints (Figure 6.2 Di). Moreover, in *GBA-N370S* iDAn, the dead cell ratio was lower with untreated than with pre-treated control iASTROs (Figure 6.2 Di). On the other hand, with *GBA-N370S* iASTROs, the dead cell ratio was slightly higher in *GBA-N370S* iDAn, but the difference with control iDAn was not as big as in the co-cultures with control iASTROs, and it only reached statistical significance after 10 days (Figure 4.15 Dii). Furthermore, after 48h and 10 days in co-culture, the dead cell ratio appeared to be smaller with untreated than with pre-treated *GBA-N370S* iASTROs (Figure 6.2 Dii).

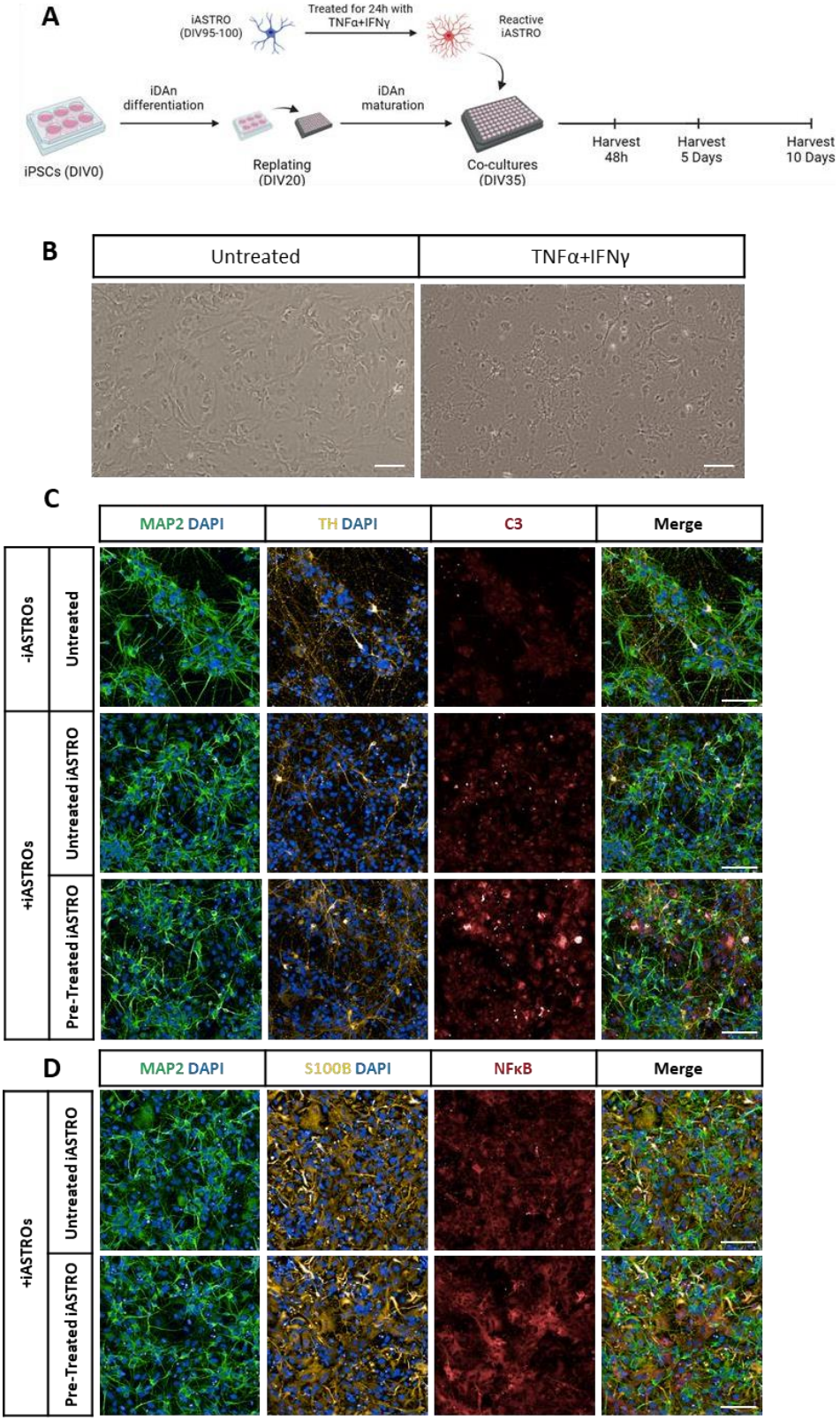
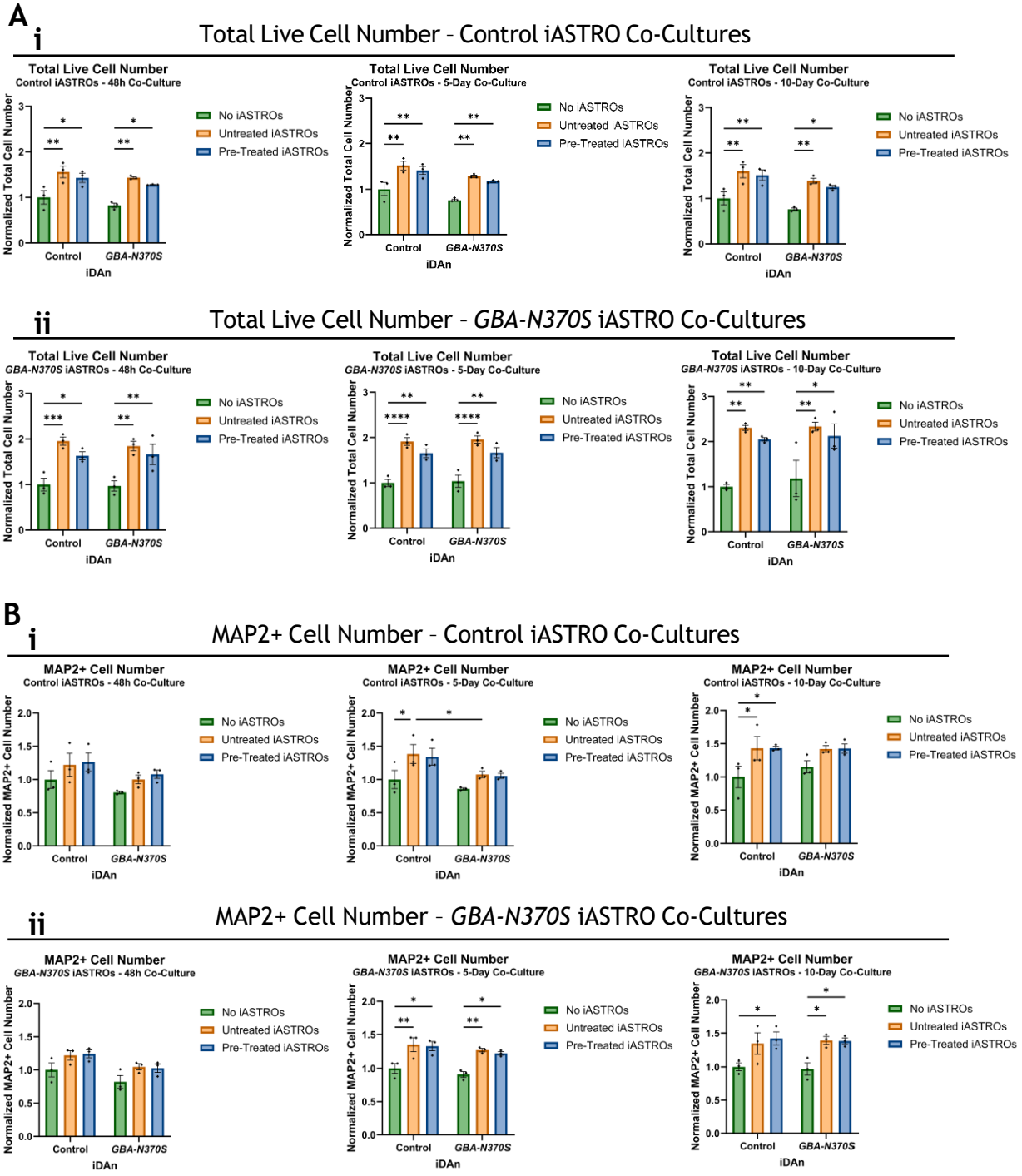


Figure 6.1. Experimental design and immunocytochemistry images of iDAn co-cultured with iASTROs treated for 24h with TNFα+IFNγ prior to the co-culture

(A) Diagram of the experimental design. (B) Brightfield images of live control iASTROs untreated or treated for 24h with 30 ng/mL TNFα + 50 ng/mL IFNγ. Scale bar: 100 µm. (C) Representative immunocytochemistry images of control iDAn in mono-culture or in co-culture for 48h with untreated

control iASTROs or control iASTROs treated for 24h with 30 ng/mL TNFα + 50 ng/mL IFNγ, stained for MAP2 (green), TH (yellow) and C3 (red). Scale bar: 100 µm. (D) Representative immunocytochemistry images of control iDAn in co-culture for 48h with untreated control iASTROs or control iASTROs treated for 24h with 30 ng/mL TNFα + 50 ng/mL IFNγ, stained for MAP2 (green), S100B (yellow) and NFκB (red). Scale bar: 100 µm.



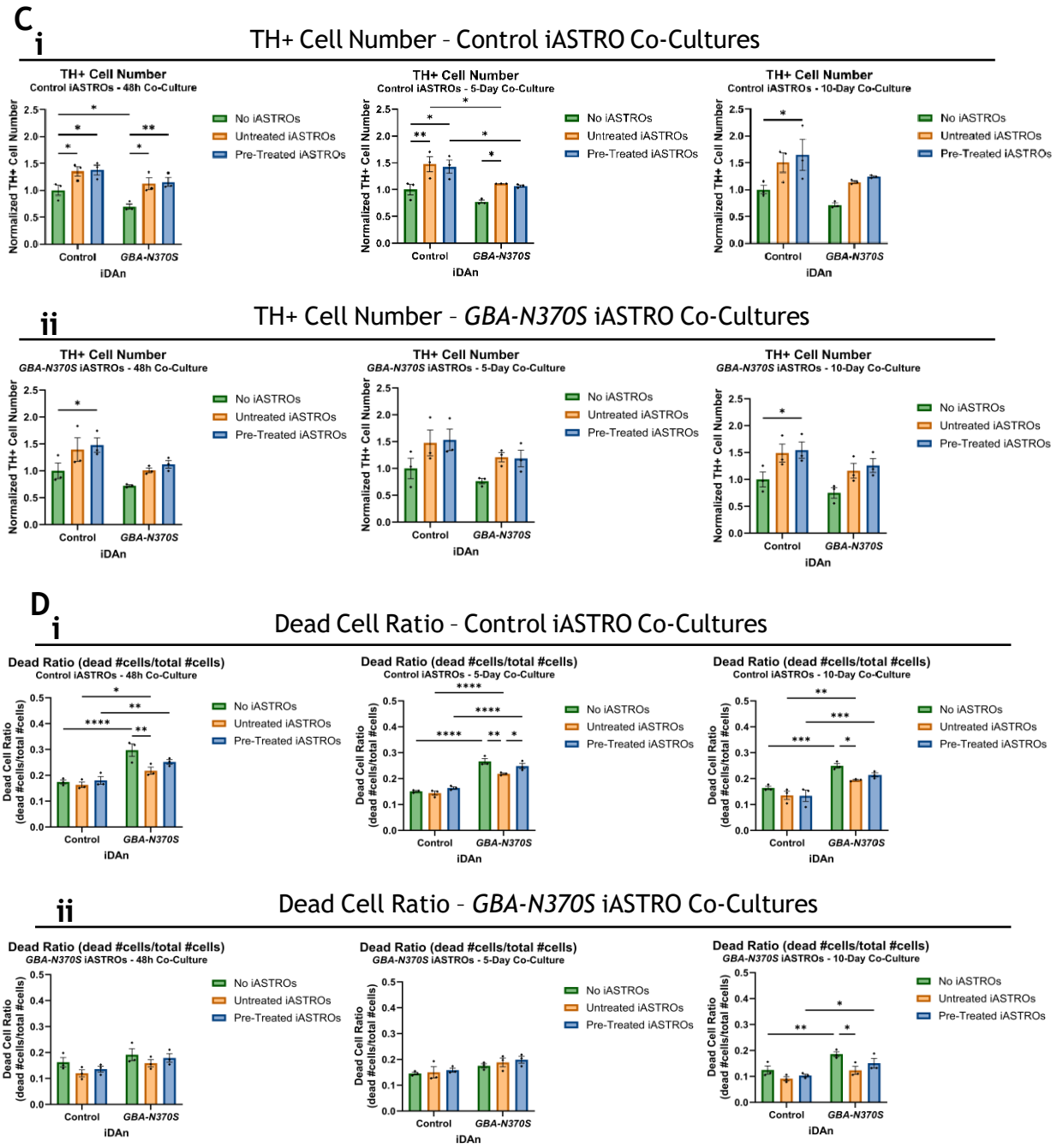


Figure 6.2. 24h treatment of iASTROs with TNFα+IFNγ prior to the co-culture does not affect their ability to support iDAn

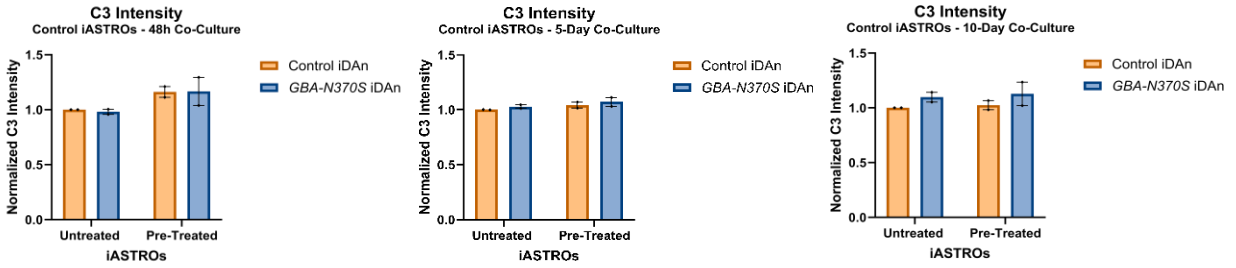
(A-D) Quantification of (A) the total number of live cells, (B) the number of MAP2+ cells, (C) the number of TH+ cells and (D) the ratio of dead cells (calculated by dividing the number of dead cells by the total number of cells) in control and *GBA-N370S* iDAn in mono-culture or co-cultured with untreated iASTROs or iASTROs treated for 24h with 30 ng/mL TNFα + 50 ng/mL IFNγ prior to the co-cultures. Results are shown for co-cultures with both (i) control iASTROs and (ii) *GBA-N370S* iASTROs, 48h, 5 days and 10 days after the establishment of the co-cultures. Each data point represents 1 iDAn line averaged across differentiations. For each differentiation, values were normalized to the average of untreated control iDAn in mono-culture. N = 3 control and 3 *GBA-N370S* lines for iDAn (3 differentiations), and N = 2 control and 3 *GBA-N370S* lines for iASTROs (2-3 differentiations). Mean ±

SEM. The statistical analysis performed was two-way ANOVA with Tukey's multiple comparison test. *p<0.05, **p<0.01, ***p<0.001, ****p<0.0001.

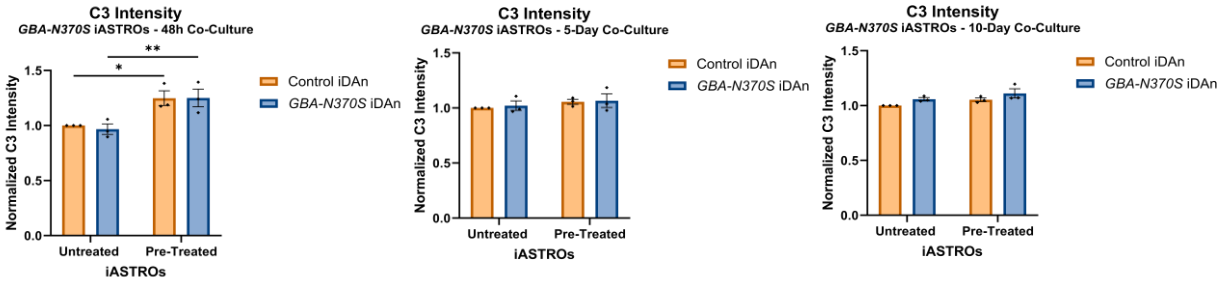
Furthermore, I studied different markers of astrocyte reactivity in the co-cultures discussed above, to investigate how the reactivity of the cells changed throughout time when no cytokines were added to the co-cultures. After 48h in the co-cultures, the cytoplasmic intensity of C3 was higher in pre-treated iASTROs, regardless of the genotype of iDAn, but after 5 days in co-culture the intensity reverted to basal levels (Figure 6.3 Ai). In addition, after 5 days in co-culture with control iDAn, the S100B intensity was modestly lower in pre-treated than in untreated *GBA-N370S* iASTROs (Figure 6.3 Bii). In addition, no differences were observed in the NFκB intensity ratio (measured as the intensity in the nucleus divided by the intensity in the cytoplasm) at any timepoint in any of the conditions and genotypes (Figure 6.3 D). Lastly, in control iASTROs, the cell area was higher in co-cultures with *GBA-N370S* as opposed to control iDAn, but this observation was only statistically significant after 10 days in co-culture in pre-treated iASTROs (Figure 6.3 Di). Moreover, after 10 days in co-culture with *GBA-N370S* iDAn, the cell area was higher in pre-treated than in untreated control iASTROs (Figure 6.3 Di). In *GBA-N370S* iASTROs, after 48h and 5 days in co-culture the cell area was higher in pre-treated cells than in untreated cells, but this was lost by 10 days (Figure 6.3 Dii). The area was also bigger when co-cultured for 5 and 10 days with *GBA-N370S* iDAn (Figure 6.3 Dii).

Overall, these results suggest that the neurosupportive capacity of control and *GBA-N370S* iASTROs explored in Chapter 3 was not significantly affected by a 24h pre-treatment with TNFα+IFNγ, although there seemed to be a small increase in the dead cell ratio with pre-treated iASTROs. However, the increase in cell death could be due to the death of undifferentiated cells, as the overall number of TH+ and MAP2+ cells did not differ. Moreover, pre-treated iASTROs maintained their reactive phenotype during the first few days in co-culture but reverted back to a non-reactive phenotype afterwards. The bigger iASTRO cell area and S100B intensity observed in co-cultures with *GBA-N370S* iDAn discussed in Chapter 3 was replicated in this experiment, further proving that iASTROs respond differently when in co-culture with *GBA-N370S* iDAn.

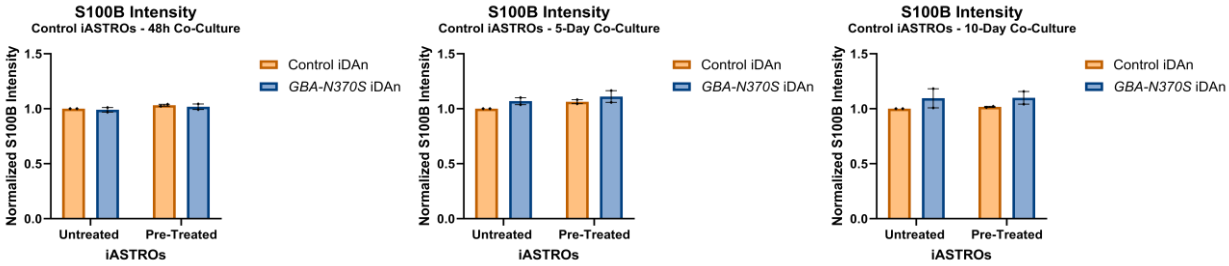
A i C3 Intensity – Control iASTRO Co-Cultures



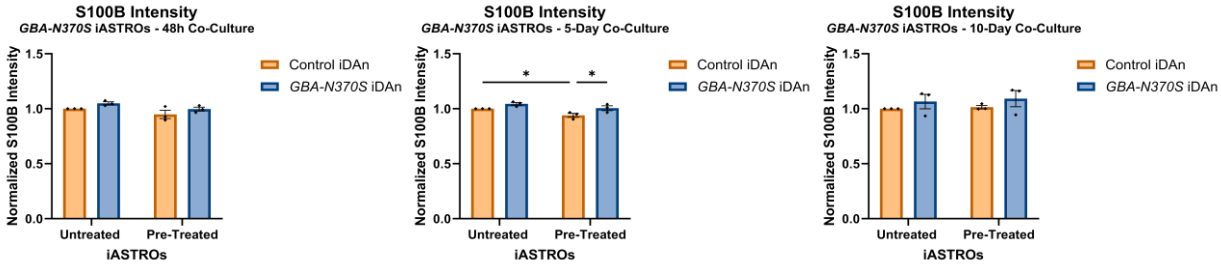
ii C3 Intensity – *GBA-N370S* iASTRO Co-Cultures



B i S100B Intensity – Control iASTRO Co-Cultures



ii S100B Intensity – *GBA-N370S* iASTRO Co-Cultures



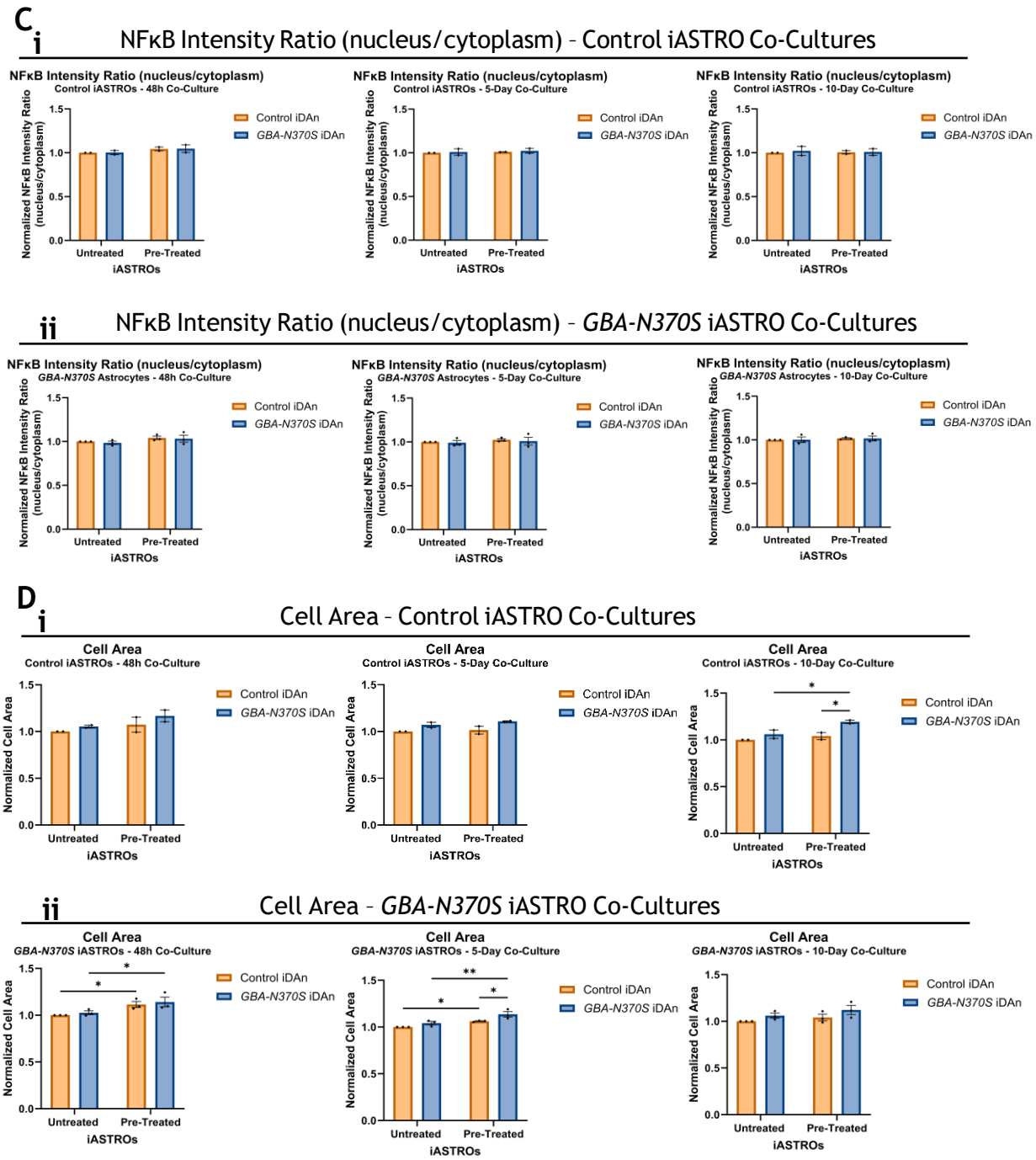


Figure 6.3. iASTROs treated for 24h with TNFα+IFNγ maintain their reactivity after co-culture establishment with iDAn, but the reactivity decreases over time in the co-cultures

(A-D) Quantification of (A) the cytoplasmic C3 intensity, (B) the cytoplasmic S100B intensity, (C) the NFκB intensity ratio (calculated by dividing the mean intensity in the nucleus by the mean intensity in the cytoplasm), and (D) the cell area in untreated or pre-treated (for 24h with 30 ng/mL TNFα + 50 ng/mL IFNγ prior to the co-cultures) (i) control and (ii) *GBA-N370S* iASTROs after 48h, 5 days and 10 days in co-culture with control or *GBA-N370S* iDAn. For each differentiation, in each timepoint, values were normalized to the average of untreated iASTROs co-cultured with control iDAn. Each data point represents 1 iASTRO line averaged across differentiations. N = 2 control and 3 *GBA-N370S* lines for iASTROs (2-3 differentiations), and N = 3 control and 3 *GBA-N370S* lines for iDAn (3 differentiations).

Mean ± SEM. The statistical analysis performed was two-way ANOVA with Fisher's LSD test. *p<0.05, **p<0.01.

6.3. Effect of inflammatory iASTROs on iDAn when treating the co-cultures directly

6.3.1. Co-cultures with control iASTROs – batch #1 of experiments

After seeing that pre-treating iASTROs with TNFα+IFNγ did not greatly affect their neurosupportive capacity, I wanted to investigate how reactive iASTROs would affect iDAn when the co-cultures were directly treated with inflammatory cytokines and were constantly kept in an inflammatory environment. Initially (referred to as batch #1), this experiment was only conducted with control iASTROs due to the high number of plates required. The treatments were separated into 2 plates, each one containing 6 iDAn lines (3 control, 3 *GBA-N370S*), 1 line of iASTROs, and the following conditions:

- Plate format 1: untreated iDAn mono-cultures, iDAn mono-cultures treated with the Liddelow factors (30 ng/mL TNFα + 3 ng/mL IL-1α + 400 ng/mL C1q), untreated co-cultures, co-cultures treated with TNFα (30 ng/mL) and co-cultures treated with the Liddelow factors (Figures 6.4-6.5)

- Plate format 2: untreated iDAn mono-cultures, iDAn mono-cultures treated with TNFα (30 ng/mL) + IFNγ (50 ng/mL), untreated co-cultures, co-cultures treated with IFNγ (50 ng/mL) and co-cultures treated with TNFα+IFNγ (Figures 6.6-6.7).

iDAn mono-cultures were treated with the strongest treatment (Liddelow factors and TNFα+IFNγ) to ensure that the treatments did not positively/negatively affect iDAn directly, and any changes observed in iDAn cell number and morphology were due to the action of reactive iASTROs. In both plate formats, after the initial 48h treatment, the cytokines were added in the appropriate concentrations with every feed. Cells were harvested 7 and 14 days after the first treatment, and stained for MAP2, TH and C3 (Figure 6.4 and 6.6). As a side note, in Figures 6.5 and 6.7 A-D, the lines and asterisks showing the statistical significance of the comparisons between iDAn mono-cultures and co-cultures are not shown due to the high number of stars, which complicated the interpretation of the graphs. I had previously shown

that there was a higher number of MAP2+ and TH+ cells in co-cultures with iASTROs, so the goal of these experiments was to focus on the effect of the treatments in the co-cultures.

6.3.1.1. Treatment with TNFα and the Liddelow factors

First, in the plates treated with TNFα and the Liddelow factors, the total number of live cells was a bit higher in the co-cultures with treatment than in the untreated co-cultures, especially after 14 days (Figure 6.5 A), whereas the dead cell ratio in the co-cultures did not change due to treatment (Figure 6.5 B). The number of MAP2+ cells was higher in co-cultures treated with TNFα alone or the Liddelow factors, and this observation was more evident in the co-cultures with *GBA-N370S* iDAn, which in all conditions had less MAP2+ cells than control iDAn (Figure 6.5 C). Moreover, the number of TH+ cells was higher in the co-cultures treated with TNFα and more so the Liddelow factors compared to untreated co-cultures, especially after 14 days (Figure 6.5 D). When analysing the morphology of TH+ cells, which is indicative of cellular health, there were no changes in the cell area at any timepoint in any of the mono-culture or co-culture conditions (Figure 6.5 E). On the other hand, the TH+ cell roundness was smaller in the co-cultures, and even more so in the co-cultures treated with TNFα or the Liddelow factors, although the decrease was small and not statistically significant (Figure 6.5 F). Overall, no significant differences were observed in any of these parameters in the iDAn mono-cultures due to treatment with the Liddelow factors, suggesting that the changes observed in the treated co-cultures were due to the action of reactive iASTROs. Lastly, I checked the intensity of C3 in iASTROs in the co-cultures to verify that iASTROs were becoming reactive in the treated co-cultures. The C3 intensity was higher in the co-cultures treated with TNFα, and more so in the Liddelow factors, than in the untreated co-cultures (Figure 6.5 G). Overall, this data suggests that in co-cultures treated with TNFα and the Liddelow factors, reactive control iASTROs are more neurosupportive to iDAn.

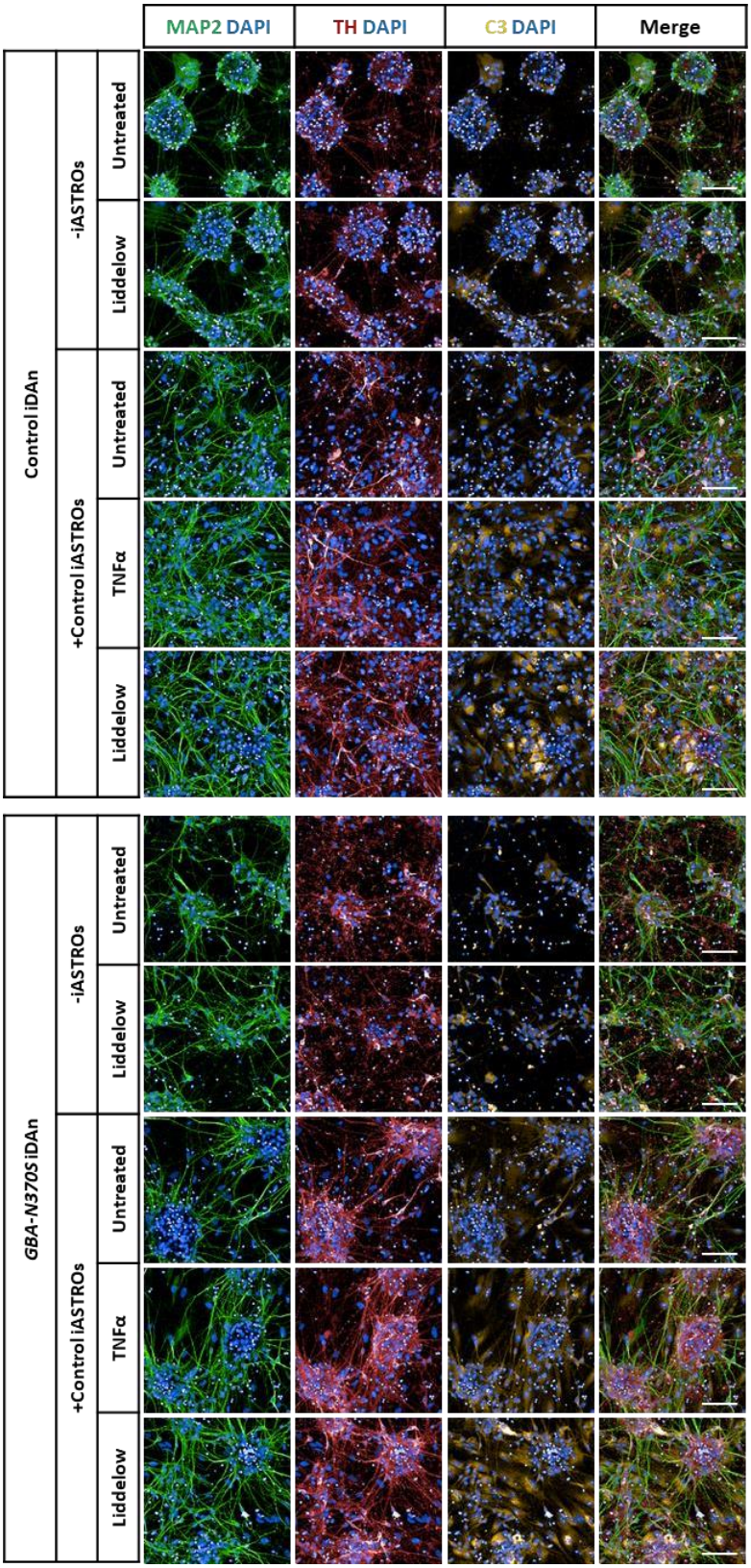


Figure 6.4. Representative immunocytochemistry images of control (top panel) and *GBA-N370S* (bottom panel) iDAn in mono-culture or in co-culture with control iASTROs, untreated or treated for 14 days with TNFα or the Liddelow factors

Treatments: 30 ng/mL TNFα or the Liddelow factors (30 ng/mL TNFα + 3 ng/mL IL-1α + 400 ng/mL C1q). Cells were stained for MAP2 (green), TH (red) and C3 (yellow). Scale bar: 100 µm

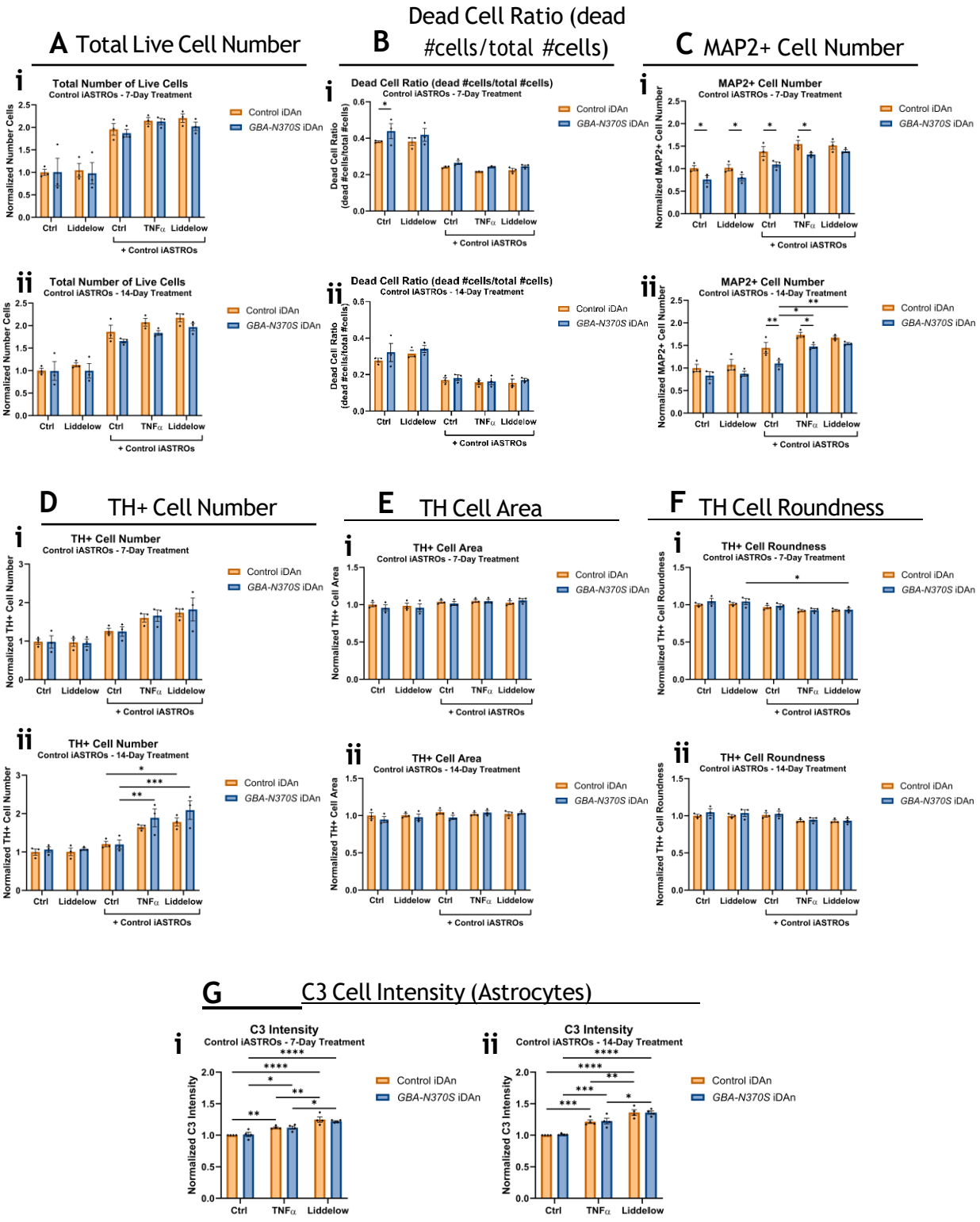


Figure 6.5. In direct co-culture, control iASTROs treated with Liddelow factors or TNFα alone become more neurosupportive to iDAn

(A-F) Quantification of (A) the total number of live cells, (B) the dead cell ratio (calculated by dividing the number of dead cells by the total number of cells), (C) the number of MAP2+ cells, (D) the number of TH+ cells, (E) the cell area of TH+ cell, and (F) the cell roundness of TH+ cells in control and *GBA-N370S* iDAn, in mono-culture or in co-culture with control or iASTROs, untreated or treated with 30 ng/mL TNFα or the Liddelow factors (30 ng/mL TNFα + 3 ng/mL IL-1α + 400 ng/mL C1q) for 7 or 14

days. Each data point represents 1 iDAn line, averaged in each differentiation to all the conditions either in mono-culture or co-cultured with 1-3 lines of iASTROs, and then averaged across differentiations. For each differentiation, values were normalized to the average of untreated (ctrl) control iDAn in mono-culture. N = 3 control and 3 *GBA-N370S* lines for iDAn (3 differentiations), and N = 3 control lines for iASTROs (1-3 differentiations per line). Mean ± SEM. The statistical analysis performed was two-way ANOVA with Tukey's multiple comparison test. *p<0.05, **p<0.01, ***p<0.001, ****p<0.0001. Not all statistically significant comparisons are shown in the graphs, due to the large number of comparisons with p values below 0.05. (G) Quantification of the C3 intensity in control iASTROs in co-culture with control and *GBA-N370S* iDAn, untreated or treated with 30 ng/mL TNFα or the Liddelow factors (30 ng/mL TNFα + 3 ng/mL IL-1α + 400 ng/mL C1q) for 7 or 14 days. For each differentiation, in each timepoint, values were normalized to the average of untreated iASTROs co-cultured with control iDAn. Each data point represents 1 iASTRO line averaged across differentiations. N = 3 control and 3 *GBA-N370S* lines for iDAn (3 differentiations), and N = 3 control lines for iASTROs (1-3 differentiations per line). Mean ± SEM. The statistical analysis performed was two-way ANOVA with Tukey's multiple comparison test. *p<0.05, **p<0.01, ***p<0.001, ****p<0.0001.

6.3.1.2. Treatment with IFNγ and TNFα+IFNγ

Next, the same analysis was performed in the plates treated with IFNγ alone and TNFα+IFNγ (Figure 6.7). In this case, in both timepoints, the total number of live cells was lower in the co-cultures treated with TNFα+IFNγ than in the untreated or IFNγ-treated co-cultures (Figure 6.7 A). Similarly, the ratio of dead cells was higher in the co-cultures treated with TNFα+IFNγ than in the untreated or IFNγ-treated co-cultures, and it was also slightly higher in IFNγ-treated compared to untreated co-cultures (Figure 6.7 B). Moreover, as in Figure 6.5 B, after 7 days the dead ratio in *GBA-N370S* iDAn mono-cultures was higher than in control iDAn mono-cultures (Figure 6.7 B). Of note, the dead ratio in iDAn mono-cultures treated with TNFα+IFNγ was slightly higher than in untreated mono-cultures, but this was not statistically significant, and the magnitude of the increase was much smaller than when comparing untreated co-cultures with co-cultures treated with TNFα+IFNγ. On the other hand, after 7 days there were no changes in the MAP2+ cell number in the co-cultures due to treatment, whereas after 14 days there was a higher number of MAP2+ cells in the co-cultures treated with IFNγ alone and TNFα+IFNγ (Figure 6.7 C). As in Figure 6.5, the number of MAP2+ cells was lower in *GBA-N370S* iDAn cultures compared to control iDAn, especially after 14 days of co-culture (Figure 6.7 C). Similar results were obtained when quantifying the number of TH+ cells; after 14 days the number of TH+ cells was higher in co-cultures treated with IFNγ alone and TNFα+IFNγ than in untreated co-cultures, but this increase was smaller in co-cultures with *GBA-N370S* iDAn

(Figure 6.7 Dii). On the contrary, the area of TH+ cells was smaller in the treated co-cultures than in the untreated co-cultures, especially after 14 days (Figure 6.7 E). The TH+ cell roundness also appeared to be smaller in the treated co-cultures, but this decrease was not statistically significant (Figure 6.7 F). As in Figure 6.5, no significant differences were observed in any of these parameters in the iDAn mono-cultures due to treatment with TNFα+IFNγ, except a very small increase in the dead cell ratio, suggesting that almost all changes observed in the treated co-cultures were due to the action of reactive iASTROs. Finally, the C3 intensity of iASTROs was higher in the co-cultures treated with TNFα+IFNγ but not IFNγ when compared to untreated co-cultures (Figure 6.7 G), which is in line with my previous findings (Figure 4.10 F). This suggests that in response to IFNγ iASTROs acquire a reactive phenotype that does not involve increases in C3 intensity.

All in all, these results suggest that, in direct co-culture, when treating cells with TNFα+IFNγ control iASTROs acquire a reactive phenotype that results in cell toxicity but an increase in MAP2+ and TH+ cell number. The discrepancy between these two findings will be further discussed in the discussion, section 6.5. Moreover, the small changes in TH+ cell area and roundness observed indicate that the health of TH+ cells might be compromised when co-cultured with reactive iASTROs.

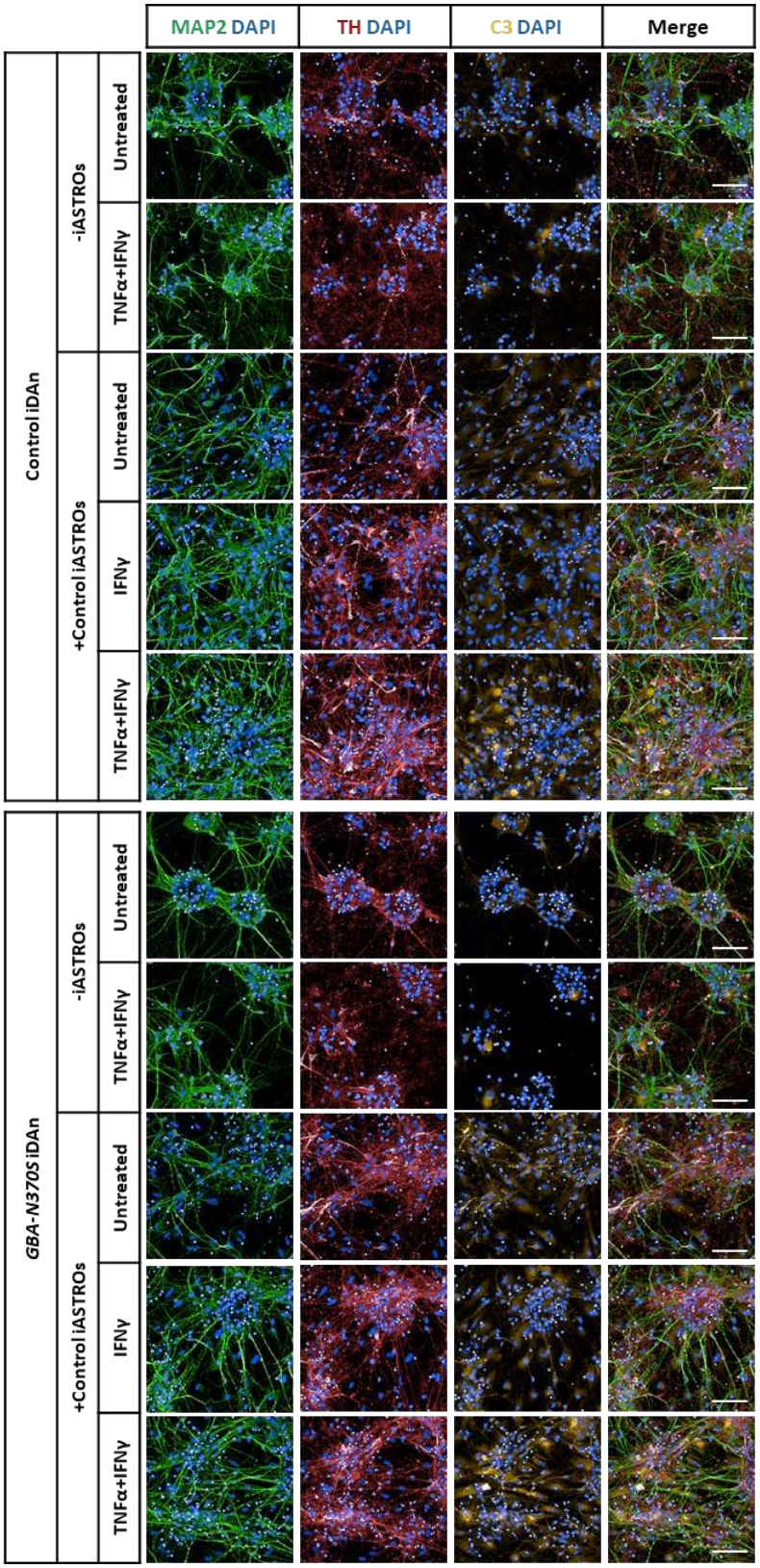


Figure 6.6. Representative immunocytochemistry images of control (top panel) and *GBA-N370S* (bottom panel) iDAn in mono-culture or in co-culture with control iASTROs, untreated or treated for 14 days with IFNγ or TNFα+IFNγ

Treatments: 50 ng/mL IFNγ or 30 ng/mL TNFα + 50 ng/mL IFNγ. Cells were stained for MAP2 (green), TH (red) and C3 (yellow). Scale bar: 100 µm

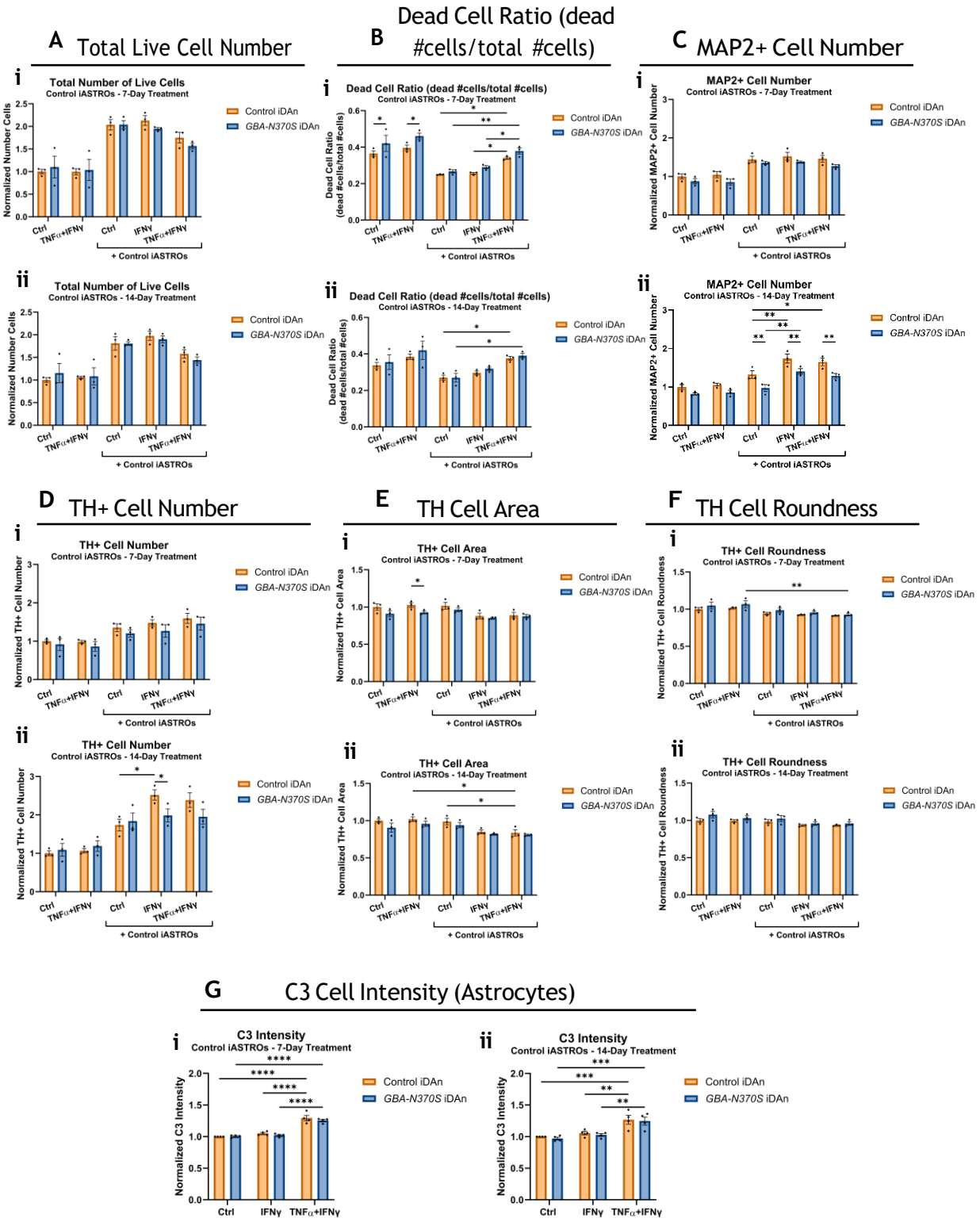


Figure 6.7. In direct co-culture, control iASTROs treated with IFNγ alone or TNFα+IFNγ become more neurosupportive to iDAn but this is accompanied with increased death of non-iDAn cells

(A-F) Quantification of (A) the total number of live cells, (B) the dead cell ratio (calculated by dividing the number of dead cells by the total number of cells), (C) the number of MAP2+ cells, (D) the number of TH+ cells, (E) the cell area of TH+ cell, and (F) the cell roundness of TH+ cells in control and *GBA-N370S* iDAn, in mono-culture or in co-culture with control or iASTROs, untreated or treated with 50 ng/mL IFNγ or 30 ng/mL TNFα + 50 ng/mL IFNγ for 7 or 14 days. Each data point represents 1 iDAn

line, averaged in each differentiation to all the conditions either in mono-culture or co-cultured with 1-3 lines of iASTROs, and then averaged across differentiations. For each differentiation, values were normalized to the average of untreated (ctrl) control iDAn in mono-culture. N = 3 control and 3 *GBA-N370S* lines for iDAn (3 differentiations), and N = 3 control lines for iASTROs (1-3 differentiations per line). Mean ± SEM. The statistical analysis performed was two-way ANOVA with Tukey's multiple comparison test. *p<0.05, **p<0.01, ***p<0.001, ****p<0.0001. Not all statistically significant comparisons are shown in the graphs, due to the large number of comparisons with p values below 0.05. (G) Quantification of the C3 intensity in control iASTROs in co-culture with control and *GBA-N370S* iDAn, untreated or treated with 50 ng/mL IFNγ or 30 ng/mL TNFα + 50 ng/mL IFNγ for 7 or 14 days. For each differentiation, in each timepoint, values were normalized to the average of untreated iASTROs co-cultured with control iDAn. Each data point represents 1 iASTRO line averaged across differentiations. N = 3 control and 3 *GBA-N370S* lines for iDAn (3 differentiations), and N = 3 control lines for iASTROs (1-3 differentiations per line). Mean ± SEM. The statistical analysis performed was two-way ANOVA with Tukey's multiple comparison test. *p<0.05, **p<0.01, ***p<0.001, ****p<0.0001.

6.3.1. Co-cultures with control and *GBA-N370S* iASTROs – batch #2 of experiments

The results presented in the previous section were very promising, and suggested that in direct co-culture, iASTROs acquired a reactive phenotype in response to different inflammatory cytokines, especially TNFα+IFNγ and the Liddelow factors, which was accompanied by a higher number of MAP2+ and TH+ cells, suggesting an enhanced neurosupportive activity of reactive iASTROs. However, after treatment with TNFα+IFNγ there was increased cell toxicity in the co-cultures, which was surprisingly still accompanied by a higher number of MAP2+ and TH+ cells. To try to understand better how iASTROs treated with different inflammatory cytokines in direct co-culture might affect neuronal viability, I decided to repeat the same experiments but also including *GBA-N370S* iASTROS, to see if the PD mutation would affect the neurosupportive or neurotoxic activity of reactive iASTROs. Moreover, the co-cultures were maintained in an inflammatory environment for longer, 21 days. The experimental design was otherwise the same as described above.

6.3.2.1. Treatment with TNFα and the Liddelow factors

First, co-cultures of control or *GBA-N370S* iDAn with control or *GBA-N370S* iASTROs were treated for 7, 14 or 21 days with TNFα (30 ng/mL) or the Liddelow factors (30 ng/mL TNFα + 3 ng/mL IL-1α + 400 ng/mL C1q), and stained for MAP2, TH and C3 (Figure 6.8). iDAn mono-cultures were also treated with the Liddelow factors. Of note, most of the observations discussed are not statistically significant, mostly due to line-to-line differences, but the trends

in increase/decrease are apparent. After 14 and more so 21 days, there was a small decline in the total number of live cells in the treated co-cultures compared to the untreated co-cultures (Figure 6.9 A). Similarly, starting from 7 days of treatments, there was a slightly elevated dead ratio in the co-cultures treated with the Liddelow factors and even more with TNFα alone compared to untreated co-cultures, and this increase was more apparent in co-cultures with *GBA-N370S* iASTROs after 14 and 21 days (Figure 6.9 B). In line with this, there were less MAP2+ cells in the co-cultures treated with TNFα or the Liddelow factors than in untreated co-cultures (Figure 6.9 C). The morphology of TH+ cells (cell area and roundness), did not seem to differ in the co-cultures as a result of treatment with TNFα or the Liddelow factors, but the area was higher and the roundness smaller in the co-cultures compared to iDAn mono-cultures (Figure 6.9 D-E). None of these parameters varied between untreated iDAn mono-cultures and the mono-cultures treated with the Liddelow factors, demonstrating that the reduced cell viability and number of MAP2+ cells observed in the treated co-cultures was through the action of reactive iASTROs on iDAn. Lastly, the C3 intensity of iASTROs was higher in the co-cultures upon TNFα treatment compared to the untreated condition, and even higher after treatment with the Liddelow factors (Figure 6.9 F). The magnitude of the increase was higher in control iASTROs, which, contrary to what I saw before (Figure 6.3 Ai), had lower C3 intensity in the presence of *GBA-N370S* iDAn compared to control iDAn. Therefore, these results indicate that in direct iDAn-iASTRO co-cultures treated with TNFα alone or the Liddelow factors, control and *GBA-N370S* iASTROs acquire a reactive phenotype and small neurotoxic properties. These findings do not correlate with those presented in Figure 6.5., and the potential reasons for this discrepancy will be further discussed in the discussion section (6.5). Overall, no major differences between control and *GBA-N370S* iASTROs were observed.

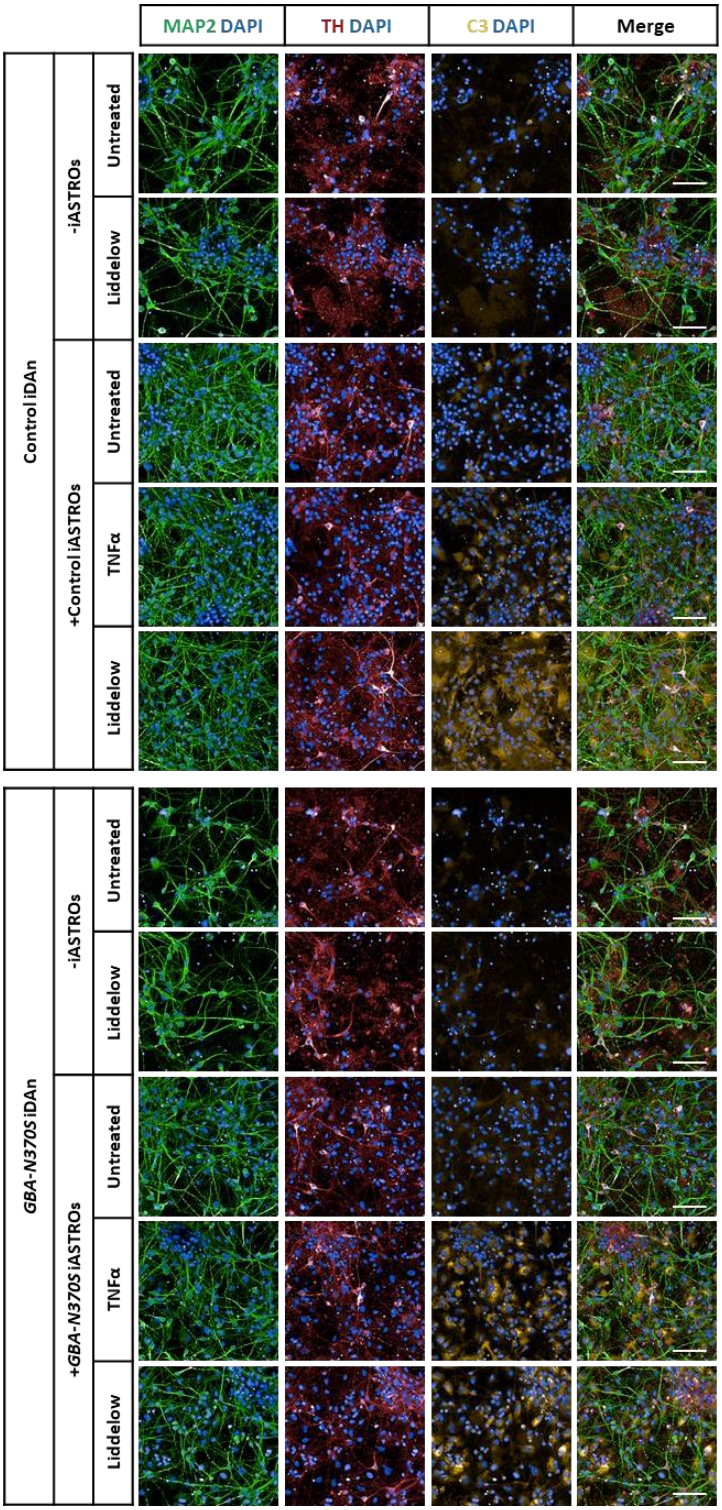
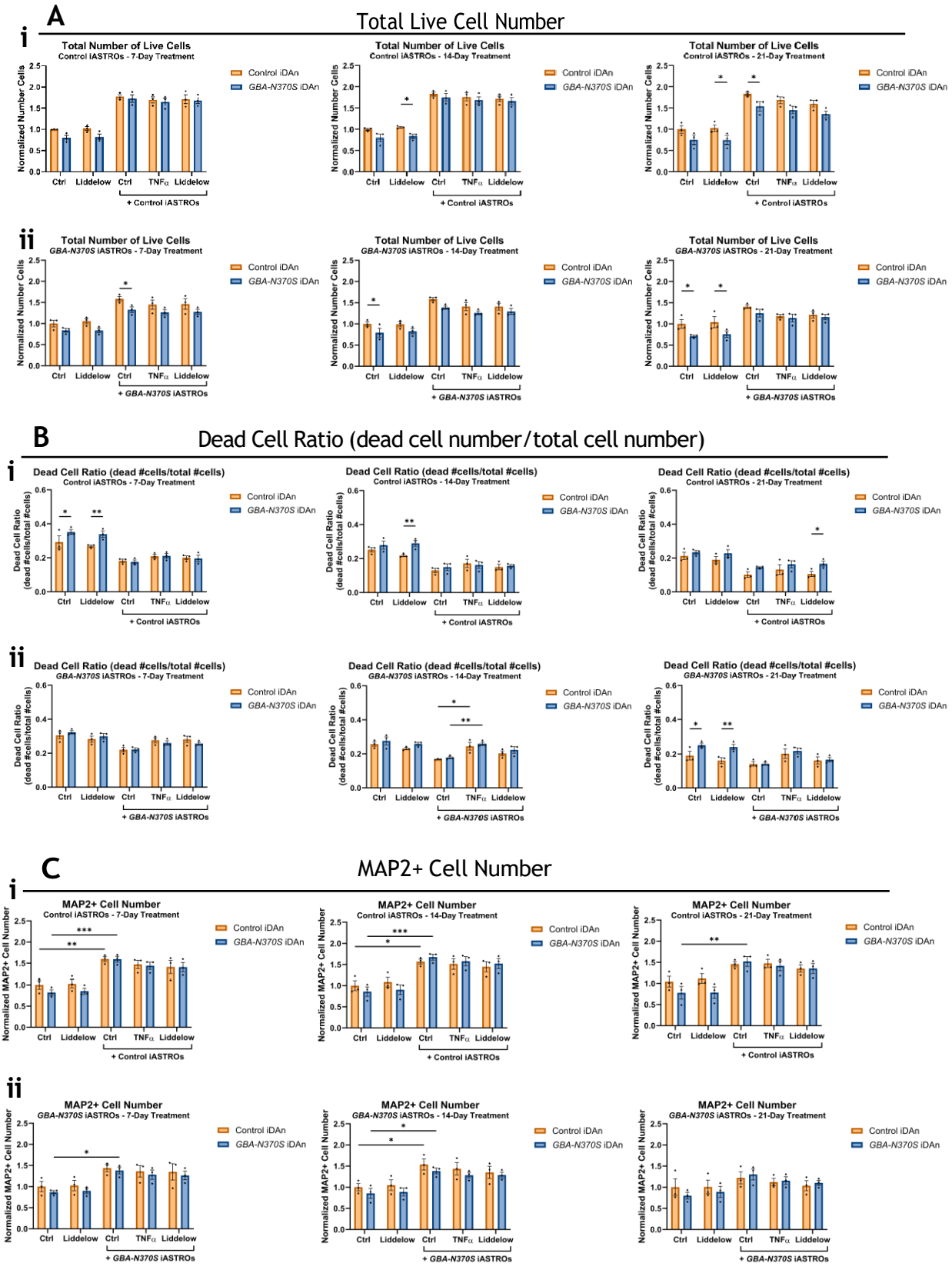


Figure 6.8. Representative immunocytochemistry images of control (top panel) and *GBA-N370S* (bottom panel) iDAn in mono-culture or in co-culture with control (top panel) or *GBA-N370S* (bottom panel) iASTROs, untreated or treated for 21 days with TNFα or the Liddelow

Treatments: 30 ng/mL TNFα or the Liddelow factors (30 ng/mL TNFα + 3 ng/mL IL-1α + 400 ng/mL C1q). Cells were stained for MAP2 (green), TH (red) and C3 (yellow). Scale bar: 100 µm


A
Total Live Cell Number
i
Total Number of Live Cells
Control iASTROs - 7-Day Treatment
Total Number of Live Cells
Control iASTROs - 14-Day Treatment
Total Number of Live Cells
Control iASTROs - 21-Day Treatment
ii
Total Number of Live Cells
GBA-N370S iASTROs - 7-Day Treatment
Total Number of Live Cells
GBA-N370S iASTROs - 14-Day Treatment
Total Number of Live Cells
GBA-N370S iASTROs - 21-Day Treatment
Normalized Number Cells
Control iDAn
GBA-N370S iDAn
Ctrl
Liddelow
TNFα
+ Control iASTROs
+ GBA-N370S iASTROs
B
Dead Cell Ratio (dead cell number/total cell number)
Dead Cell Ratio (dead #cells/total #cells)
Control iASTROs - 7-Day Treatment
Dead Cell Ratio (dead #cells/total #cells)
Control iASTROs - 14-Day Treatment
Dead Cell Ratio (dead #cells/total #cells)
Control iASTROs - 21-Day Treatment
Dead Cell Ratio (dead #cells/total #cells)
GBA-N370S iASTROs - 7-Day Treatment
Dead Cell Ratio (dead #cells/total #cells)
GBA-N370S iASTROs - 14-Day Treatment
Dead Cell Ratio (dead #cells/total #cells)
GBA-N370S iASTROs - 21-Day Treatment
C
MAP2+ Cell Number
MAP2+ Cell Number
Control iASTROs - 7-Day Treatment
MAP2+ Cell Number
Control iASTROs - 14-Day Treatment
MAP2+ Cell Number
Control iASTROs - 21-Day Treatment
MAP2+ Cell Number
GBA-N370S iASTROs - 7-Day Treatment
MAP2+ Cell Number
GBA-N370S iASTROs - 14-Day Treatment
MAP2+ Cell Number
GBA-N370S iASTROs - 21-Day Treatment
Normalized MAP2+ Cell Number

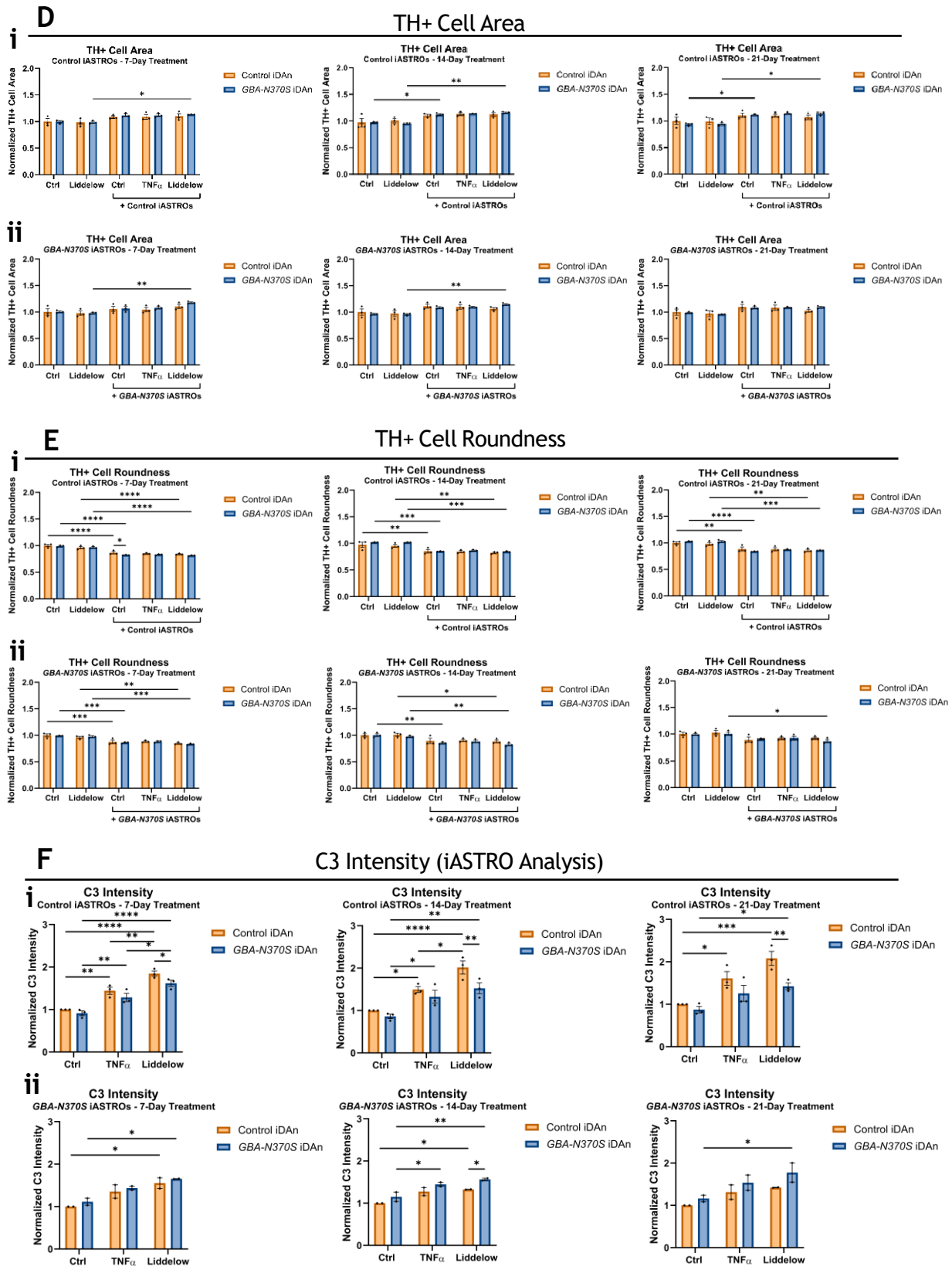


Figure 6.9. In direct co-culture, reactive control and *GBA-N370S* iASTROs treated with the Liddelow factors or TNFα alone lose their neurosupportive capacities to iDAn

(A-E) Quantification of (A) the total number of live cells, (B) the dead cell ratio (calculated by dividing the number of dead cells by the total number of cells), (C) the number of MAP2+ cells, (D) the cell area

of TH+ cell, and (E) the cell roundness of TH+ cells in control and *GBA-N370S* iDAn, in mono-culture or in co-culture with (i) control or (ii) *GBA-N370S* iASTROs, untreated or treated with 30 ng/mL TNFα or the Liddelow factors (30 ng/mL TNFα + 3 ng/mL IL-1α + 400 ng/mL C1q) for 7, 14 or 21 days. Each data point represents 1 iDAn line, averaged in each differentiation to all the conditions either in mono-culture or co-cultured with 1-2 lines of iASTROs of each genotype, and then averaged across differentiations. For each differentiation, values were normalized to the average of untreated (ctrl) control iDAn in mono-culture. N = 3 control and 3 *GBA-N370S* lines for iDAn (3 differentiations), and N = 3 control and 2 *GBA-N370S* lines for iASTROs (1-2 differentiations per line). Mean ± SEM. The statistical analysis performed was two-way ANOVA with Tukey's multiple comparison test. *p<0.05, **p<0.01, ***p<0.001, ****p<0.0001. Not all statistically significant comparisons are shown in the graphs, due to the large number of comparisons with p values below 0.05. (F) Quantification of the C3 intensity in (i) control and (ii) *GBA-N370S* iASTROs in co-culture with control and *GBA-N370S* iDAn, untreated or treated with 30 ng/mL TNFα or the Liddelow factors (30 ng/mL TNFα + 3 ng/mL IL-1α + 400 ng/mL C1q) for 7, 14 or 21 days. For each differentiation, in each timepoint, values were normalized to the average of untreated iASTROs co-cultured with control iDAn. Each data point represents 1 iASTRO line averaged across differentiations. N = 3 control and 3 *GBA-N370S* lines for iDAn (3 differentiations), and N = 3 control and 2 *GBA-N370S* lines for iASTROs (1-2 differentiations per line). Mean ± SEM. The statistical analysis performed was two-way ANOVA with Tukey's multiple comparison test. *p<0.05, **p<0.01, ***p<0.001, ****p<0.0001.

6.3.2.2. Treatment with IFNγ and TNFα+IFNγ

Co-cultures of control or *GBA-N370S* iDAn with control or *GBA-N370S* iASTROs were treated for 7, 14 or 21 days with IFNγ (50 ng/mL) or TNFα (30 ng/mL) + IFNγ (50 ng/mL), and stained for MAP2, TH and C3 (Figure 6.10). In co-culture, the total number of live cells decreased significantly after treatment with IFNγ and even more with TNFα+IFNγ, and the difference between untreated and treated co-cultures became higher with longer treatment periods (Figure 6.11 A). After 21 days of treatment, the number of total live cells in co-cultures treated with TNFα+IFNγ was almost the same as in iDAn mono-cultures. Likewise, the dead cell ratio was significantly higher in the co-cultures treated with IFNγ and even higher in those treated with TNFα+IFNγ than in the untreated co-cultures, regardless of the iASTRO genotype, and the difference increased with time (Figure 6.11 B). Furthermore, the number of MAP2+ cells in the co-cultures declined after treatment with IFNγ and more so TNFα+IFNγ, and this was most significant after 14 days of treatment (Figure 6.11 C). In iDAn mono-cultures, no differences in the number of MAP2+ cells were observed after treatment, whereas the dead cell ratio was higher after treatment with TNFα+IFNγ. Nonetheless, this increase was much smaller than in the treated co-cultures, which indicates that most of the toxicity came from the action of reactive iASTROs on iDAn. Next, the area of TH+ cells was higher in the untreated

co-cultures than in iDAn mono-cultures, but became smaller in the treated co-cultures over time (Figure 6.11 D). On the contrary, the TH+ cell roundness increased in the co-cultures treated with IFNγ and TNFα+IFNγ compared to the untreated co-cultures, and the increase was higher with longer treatment times (Figure 6.11 E). After 14 and 21 days of treatment with TNFα+IFNγ, the TH+ cell area and roundness in mono-culture were slightly smaller and higher, respectively, than in untreated mono-cultures, but the magnitude of changes was smaller than the differences observed in the co-cultures. Lastly, there was a small increase in C3 intensity in both iASTRO genotypes after IFNγ treatment that became higher with time, whereas a much bigger increase was observed after TNFα+IFNγ treatment from day 7 (Figure 6.11 F). In conclusion, these findings clearly indicate that in co-cultures treated with IFNγ and TNFα+IFNγ, control and *GBA-N370S* iASTROs become neurotoxic and lose their neuroprotective capacities. This detrimental effect of reactive iASTROs on iDAn was much more drastic in this batch of experiments than in those presented in Figure 6.6-6.7, and the possible explanations for this will be discussed in Section 6.5.

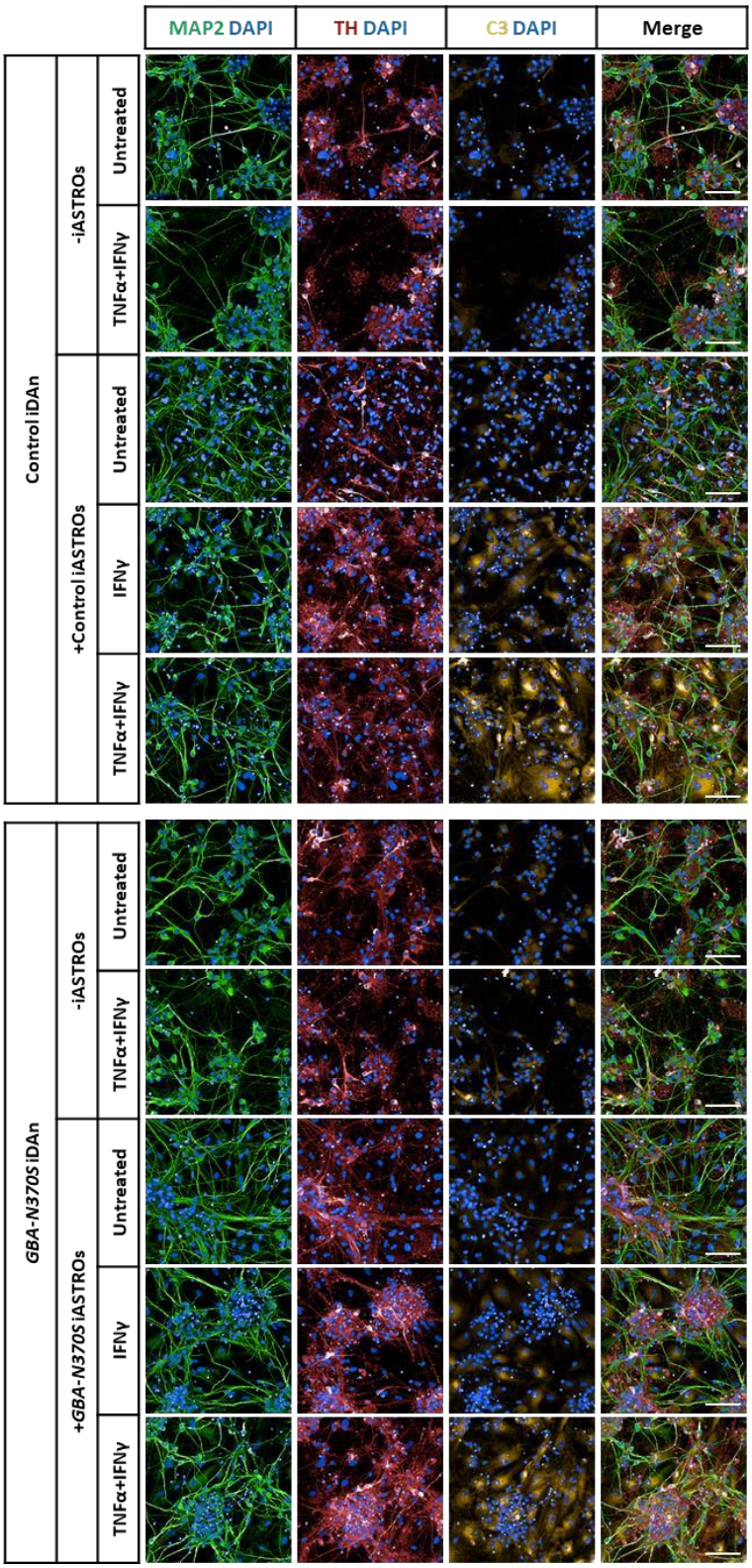
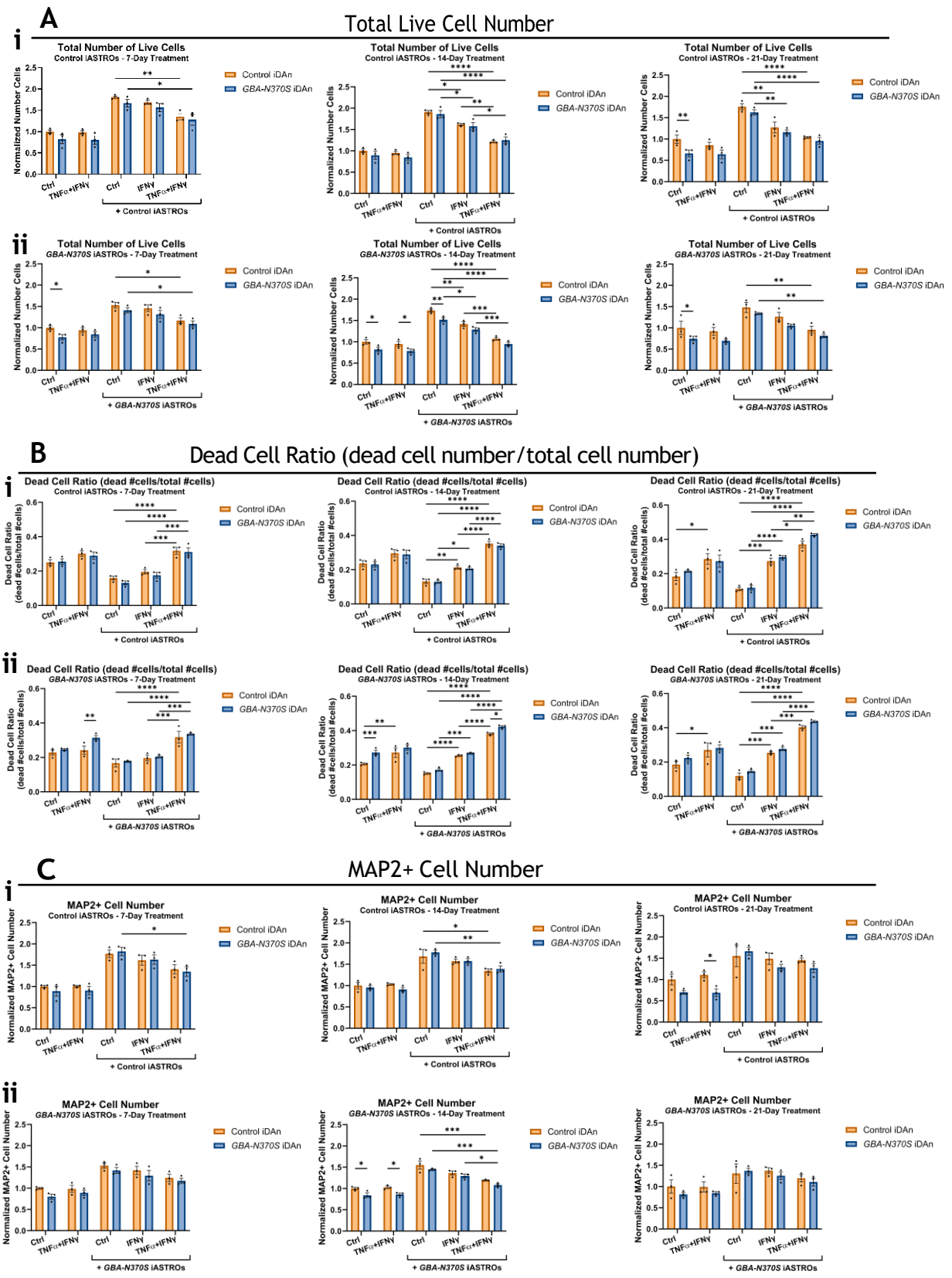


Figure 6.10. Representative immunocytochemistry images of control and *GBA-N370S* iDAn in mono-culture or in co-culture with control or *GBA-N370S* iASTROs, untreated or treated for 21 days with IFNγ or TNFα+ IFNγ

Treatments: 50 ng/mL IFNγ or 30 ng/mL TNFα + 50 ng/mL IFNγ. Cells were stained for MAP2 (green), TH (red) and C3 (yellow). Scale bar: 100 µm


A
Total Live Cell Number
i
Total Number of Live Cells
Control iASTROs - 7-Day Treatment
Total Number of Live Cells
Control iASTROs - 14-Day Treatment
Total Number of Live Cells
Control iASTROs - 21-Day Treatment
ii
Total Number of Live Cells
GBA-N370S iASTROs - 7-Day Treatment
Total Number of Live Cells
GBA-N370S iASTROs - 14-Day Treatment
Total Number of Live Cells
GBA-N370S iASTROs - 21-Day Treatment
Normalized Number Cells
Control iDAn
GBA-N370S iDAn
Ctrl
TNFα+IFNγ
IFNγ
+ Control iASTROs
+ GBA-N370S iASTROs
B
Dead Cell Ratio (dead cell number/total cell number)
Dead Cell Ratio (dead #cells/total #cells)
Control iASTROs - 7-Day Treatment
Dead Cell Ratio (dead #cells/total #cells)
Control iASTROs - 14-Day Treatment
Dead Cell Ratio (dead #cells/total #cells)
Control iASTROs - 21-Day Treatment
Dead Cell Ratio (dead #cells/total #cells)
GBA-N370S iASTROs - 7-Day Treatment
Dead Cell Ratio (dead #cells/total #cells)
GBA-N370S iASTROs - 14-Day Treatment
Dead Cell Ratio (dead #cells/total #cells)
GBA-N370S iASTROs - 21-Day Treatment
C
MAP2+ Cell Number
Control iASTROs - 7-Day Treatment
MAP2+ Cell Number
Control iASTROs - 14-Day Treatment
MAP2+ Cell Number
Control iASTROs - 21-Day Treatment
MAP2+ Cell Number
GBA-N370S iASTROs - 7-Day Treatment
MAP2+ Cell Number
GBA-N370S iASTROs - 14-Day Treatment
MAP2+ Cell Number
GBA-N370S iASTROs - 21-Day Treatment
Normalized MAP2+ Cell Number

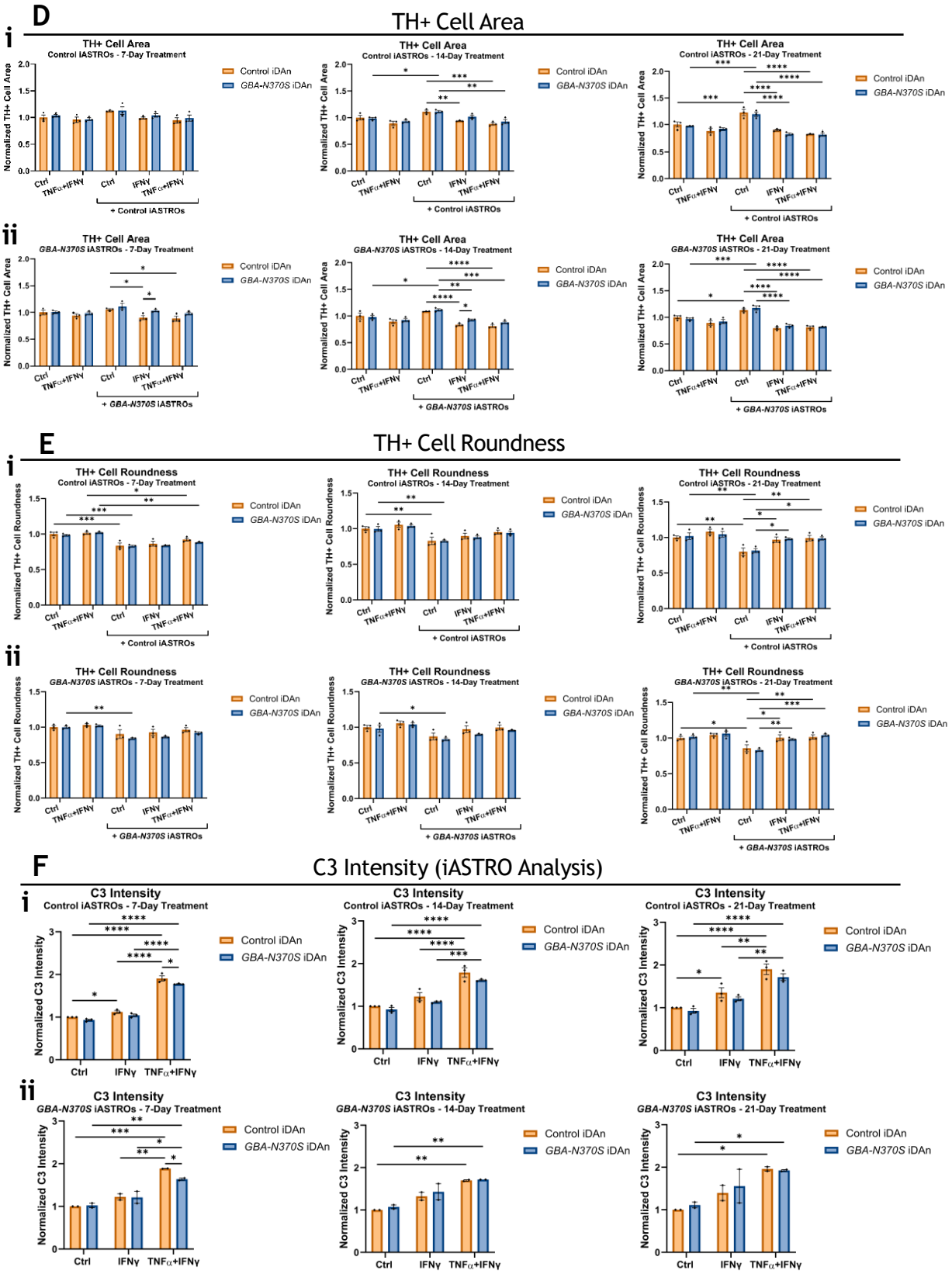


Figure 6.11. In direct co-cultures, reactive control and *GBA-N370S* iASTROs treated with IFNγ alone or TNFα+IFNγ lose their neurosupportive functions and become neurotoxic to iDAn

(A-E) Quantification of (A) the total number of live cells, (B) the dead cell ratio (calculated by dividing the number of dead cells by the total number of cells), (C) the number of MAP2+ cells, (D) the cell area

of TH+ cell, and (E) the cell roundness of TH+ cells in control and *GBA-N370S* iDAn, in mono-culture or in co-culture with (i) control or (ii) *GBA-N370S* iASTROs, untreated or treated with 50 ng/mL IFNγ or 30 ng/mL TNFα + 50 ng/mL IFNγ for 7, 14 or 21 days. Each data point represents 1 iDAn line, averaged in each differentiation to all the conditions either in mono-culture or co-cultured with 1-2 lines of iASTROs of each genotype, and then averaged across differentiations. For each differentiation, values were normalized to the average of untreated (ctrl) control iDAn in mono-culture. N = 3 control and 3 *GBA-N370S* lines for iDAn (3 differentiations), and N = 3 control and 2 *GBA-N370S* lines for iASTROs (1-2 differentiations per line). Mean ± SEM. The statistical analysis performed was two-way ANOVA with Tukey's multiple comparison test. *p<0.05, **p<0.01, ***p<0.001, ****p<0.0001. Not all statistically significant comparisons are shown in the graphs, due to the large number of comparisons with p values below 0.05. (F) Quantification of the cytoplasmic C3 intensity in (i) control and (ii) *GBA-N370S* iASTROs in co-culture with control and *GBA-N370S* iDAn, untreated or treated with 50 ng/mL IFNγ or 30 ng/mL TNFα + 50 ng/mL IFNγ for 7, 14 or 21 days. For each differentiation, in each timepoint, values were normalized to the average of untreated iASTROs co-cultured with control iDAn. Each data point represents 1 iASTRO line averaged across differentiations. N = 3 control and 3 *GBA-N370S* lines for iDAn (3 differentiations), and N = 3 control and 2 *GBA-N370S* lines for iASTROs (1-2 differentiations per line). Mean ± SEM. The statistical analysis performed was two-way ANOVA with Tukey's multiple comparison test. *p<0.05, **p<0.01, ***p<0.001, ****p<0.0001.

6.4. Exploration of the effects of α-synuclein PFF treatment, alone or in combination with TNFα+IFNγ, in direct iDAn-iASTRO co-cultures

As discussed in Chapter 4, in the RNAseq experiment and the follow up in vitro experiments no significant effect of α-synuclein PFFs on iASTRO reactivity was observed. However, morphologically, iASTROs treated with TNFα+IFNγ+PFFs had more abundant and more complex processes than iASTROs treated with TNFα+IFNγ, suggesting an effect of PFFs on iASTRO reactivity when the cells are in an inflammatory state. Moreover, in the PD brain, cells are exposed to both inflammatory cytokines and α-synuclein. Therefore, I explored the effects of PFF addition in iDAn-iASTRO co-cultures, with or without TNFα+IFNγ, to investigate: a) if PFFs by themselves altered cell viability in iDAn mono-cultures or iDAn-iASTRO co-cultures, b) if the neurotoxic action of iASTROs in co-cultures treated with TNFα+IFNγ was potentiated with PFF addition, c) if the capacity to degrade PFFs was higher in co-cultures than in iDAn mono-cultures and whether this was impacted by combined treatment with TNFα+IFNγ in the co-cultures.

To this end, control and *GBA-N370S* iDAn were co-cultured with control or *GBA-N370S* iASTROs and treated with 10 μg/mL α-synuclein PFFs alone or in combination with TNFα (30

ng/mL) + IFNγ (50 ng/mL). PFFs were only added once, but TNFα and IFNγ were added with every feed in the appropriate concentration. iDAn mono-cultures were also treated with 10 µg/mL α-synuclein PFFs. Cells were harvested 7, 14 or 21 days after the initial PFF treatment, and stained for MAP2, α-synuclein, C3 and TH (Figure 6.12). As early as 7 days after treatment, the total number of live cells in co-cultures treated with TNFα+IFNγ+PFFs was significantly lower than in untreated co-cultures or co-cultures treated with PFFs alone, reaching numbers similar to iDAn mono-cultures, regardless of the iASTRO or iDAn genotype (Figure 6.13 A). In line with this, the dead cell ratio was much higher in co-cultures exposed to TNFα+IFNγ+PFFs than in the untreated or PFF-treated co-cultures or iDAn mono-cultures, and the differences were bigger with longer treatment times (Figure 6.13 B). These results were evident from the immunocytochemistry images (Figure 6.12), where a much lower number of cells could be detected in the co-cultures treated with TNFα+IFNγ+PFFs than in the other co-cultures.

Additionally, the number of MAP2+ cells in co-cultures was significantly lower after treatment with TNFα+IFNγ+PFFs, but not PFFs alone, compared to the untreated condition, starting from 7 days after treatment (Figure 6.13 C). This decrease in co-cultures treated with TNFα+IFNγ+PFFs was bigger in *GBA-N370S* iDAn than in control iDAn, especially in co-cultures with *GBA-N370S* iASTROs. Similarly, the area of TH+ cells was lower in co-cultures exposed to TNFα+IFNγ+PFFs than in the untreated and PFF-treated co-cultures, and the difference became bigger with longer treatment times (Figure 6.13 D). No differences in any of these parameters were observed between untreated and PFF-treated iDAn mono-cultures or between untreated and PFF-treated iDAn-iASTRO co-cultures in any of the genotypes, suggesting that the PFFs by themselves to dot exert any toxic effects on either cell type at the timepoints studied.

Next, I analysed the area of α-synuclein spots (including aggregates), to see if the capacity to degrade PFFs was bigger in the co-cultures than in mono-cultures, and whether this was impaired in inflammatory conditions. At all timepoints and in all genotypes, the area of α-synuclein spots was bigger in the mono-culture and co-cultures where PFFs were added. However, over time, the area decreased, although not to baseline levels, suggesting that the cells partially degraded PFFs (Figure 6.13 E). No differences in the size of α-synuclein spots were observed between mono-culture and co-cultures treated with PFFs alone, except after 7 days in co-culture with control iASTROs, where the area was smaller than in mono-cultures

(Figure 6.13 E). In addition, the α-synuclein spot area was bigger in co-cultures treated with TNFα+IFNγ+PFFs than in co-cultures treated with PFFs alone, especially after 14 and 21 days, regardless of the genotype (Figure 6.13 E). Finally, the C3 intensity of iASTROs was significantly higher when treated with TNFα+IFNγ+PFFs compared to untreated co-cultures, but in line with previous observations (Figure 4.15-4.16), no changes were observed in co-cultures treated with PFFs alone, which indicates that even when co-cultured with iDAn and being exposed to PFFs for 21 days, iASTROs do not become reactive (Figure 6.13 F).

In conclusion, these results suggest that α-synuclein PFFs alone are not neurotoxic to control or *GBA-N370S* iDAn in mono-culture or in co-culture with iASTROs, and they do not induce a reactive response in iASTROs in the co-cultures. However, the combined treatment of α-synuclein PFFs with TNFα+IFNγ potentiates the neurotoxic effect of reactive iASTROs described in Figure 6.11, as the magnitude of the decrease in cell number and the increase in cell death was higher than in the co-cultures only treated with TNFα+IFNγ.

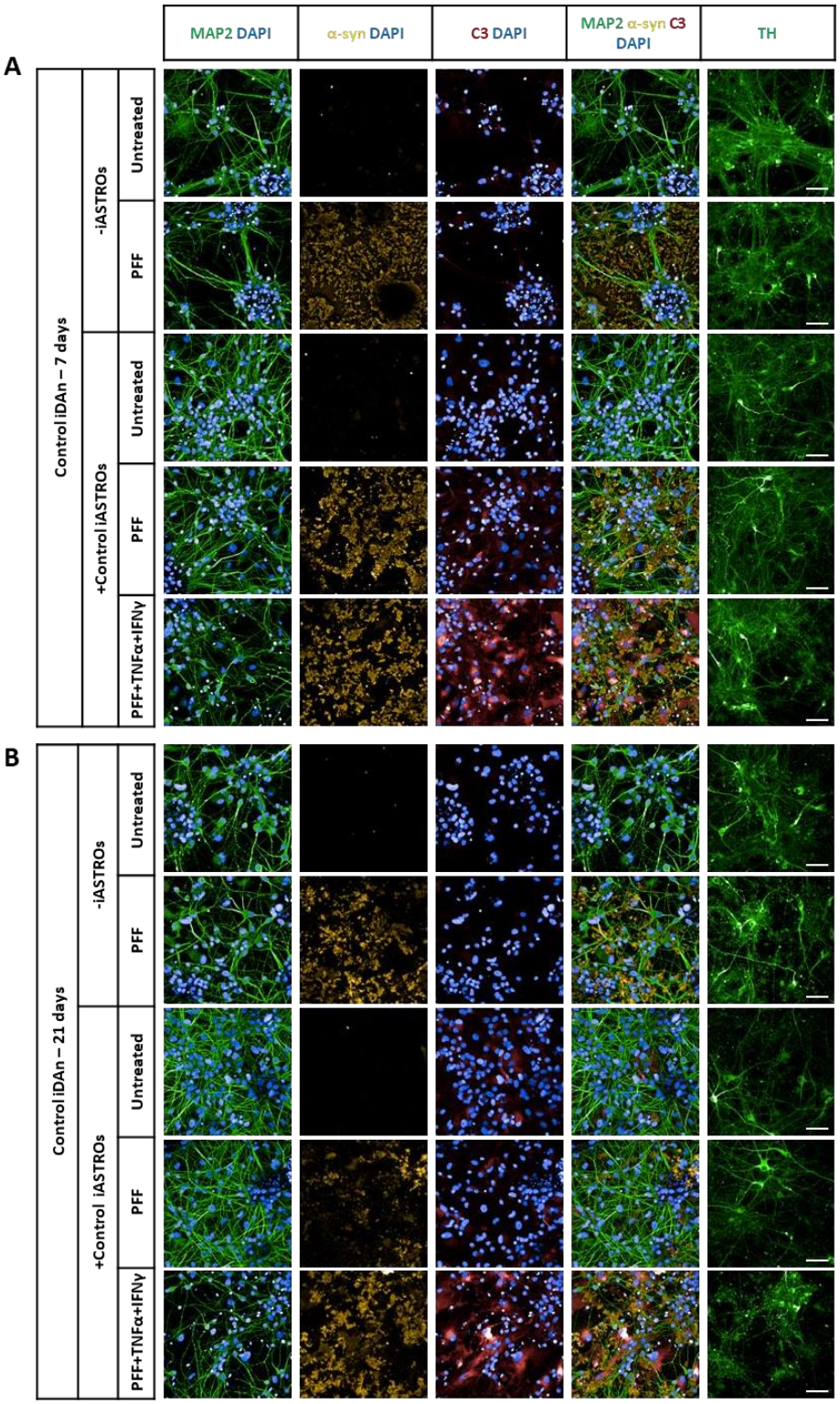
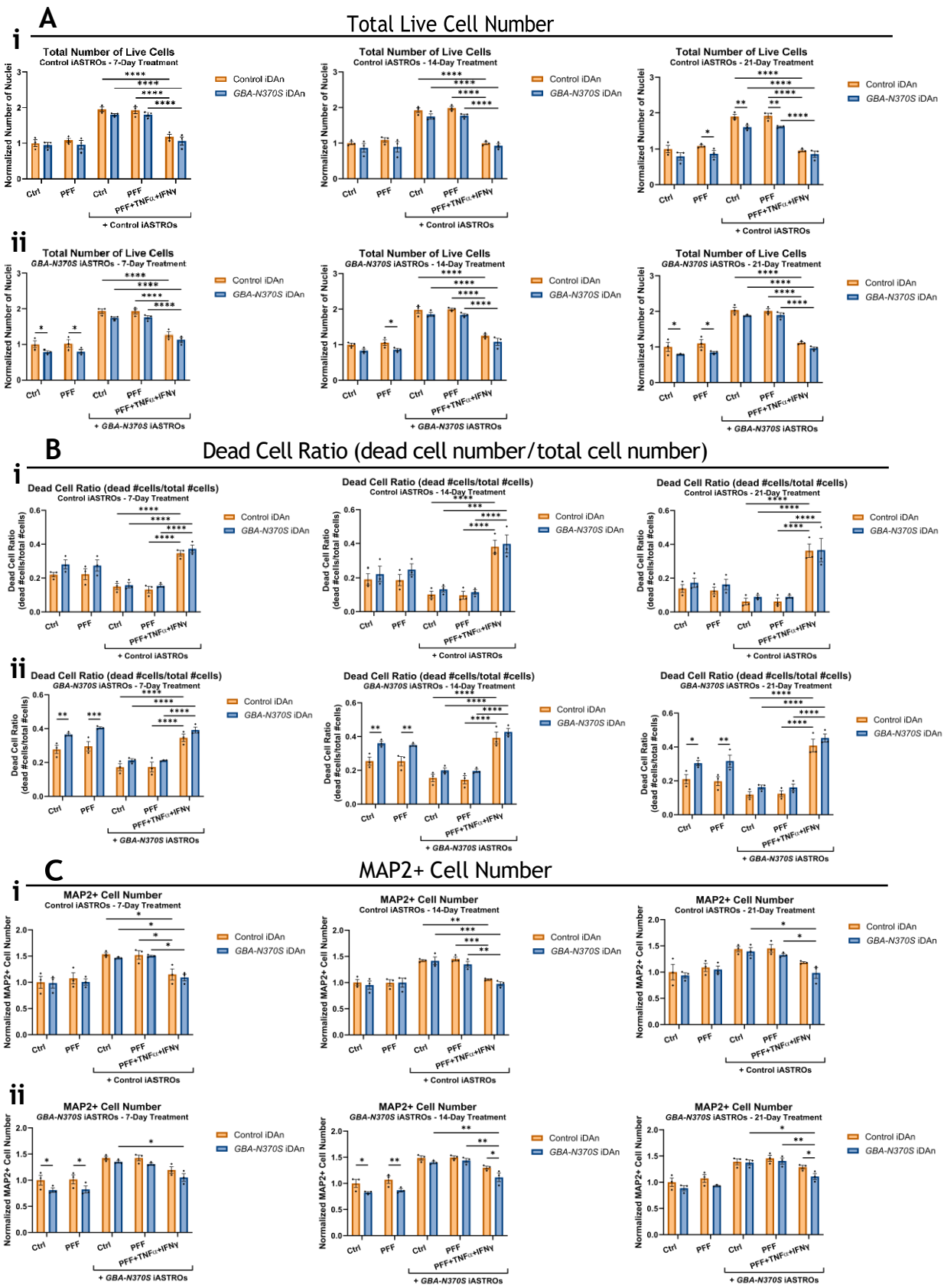


Figure 6.12. Representative immunocytochemistry images of control iDAn in mono-culture or in co-culture with control iASTROs, untreated or treated for (A) 7 days or (B) 21 days with α-synuclein PFFs with or without TNFα+IFNγ

Treatments: α-synuclein PFFs (10 µg/mL) or α-synuclein PFFs (10 µg/mL) + TNFα (30 ng/mL) + IFNγ (50 ng/mL). Cells were stained for MAP2 (green, first and fourth columns), TH (green, fifth column), α-synuclein (yellow) and C3 (red). Scale bar: 50 µm


A
Total Live Cell Number
i
Total Number of Live Cells
Control iASTROs - 7-Day Treatment
Total Number of Live Cells
Control iASTROs - 14-Day Treatment
Total Number of Live Cells
Control iASTROs - 21-Day Treatment
ii
Total Number of Live Cells
GBA-N370S iASTROs - 7-Day Treatment
Total Number of Live Cells
GBA-N370S iASTROs - 14-Day Treatment
Total Number of Live Cells
GBA-N370S iASTROs - 21-Day Treatment
Normalized Number of Nuclei
Control iDAn
GBA-N370S iDAn
Ctrl
PFF
PFF+TNFα+IFNγ
+ Control iASTROs
+ GBA-N370S iASTROs
B
Dead Cell Ratio (dead cell number/total cell number)
i
Dead Cell Ratio (dead #cells/total #cells)
Control iASTROs - 7-Day Treatment
Dead Cell Ratio (dead #cells/total #cells)
Control iASTROs - 14-Day Treatment
Dead Cell Ratio (dead #cells/total #cells)
Control iASTROs - 21-Day Treatment
ii
Dead Cell Ratio (dead #cells/total #cells)
GBA-N370S iASTROs - 7-Day Treatment
Dead Cell Ratio (dead #cells/total #cells)
GBA-N370S iASTROs - 14-Day Treatment
Dead Cell Ratio (dead #cells/total #cells)
GBA-N370S iASTROs - 21-Day Treatment
C
MAP2+ Cell Number
i
MAP2+ Cell Number
Control iASTROs - 7-Day Treatment
MAP2+ Cell Number
Control iASTROs - 14-Day Treatment
MAP2+ Cell Number
Control iASTROs - 21-Day Treatment
ii
MAP2+ Cell Number
GBA-N370S iASTROs - 7-Day Treatment
MAP2+ Cell Number
GBA-N370S iASTROs - 14-Day Treatment
MAP2+ Cell Number
GBA-N370S iASTROs - 21-Day Treatment

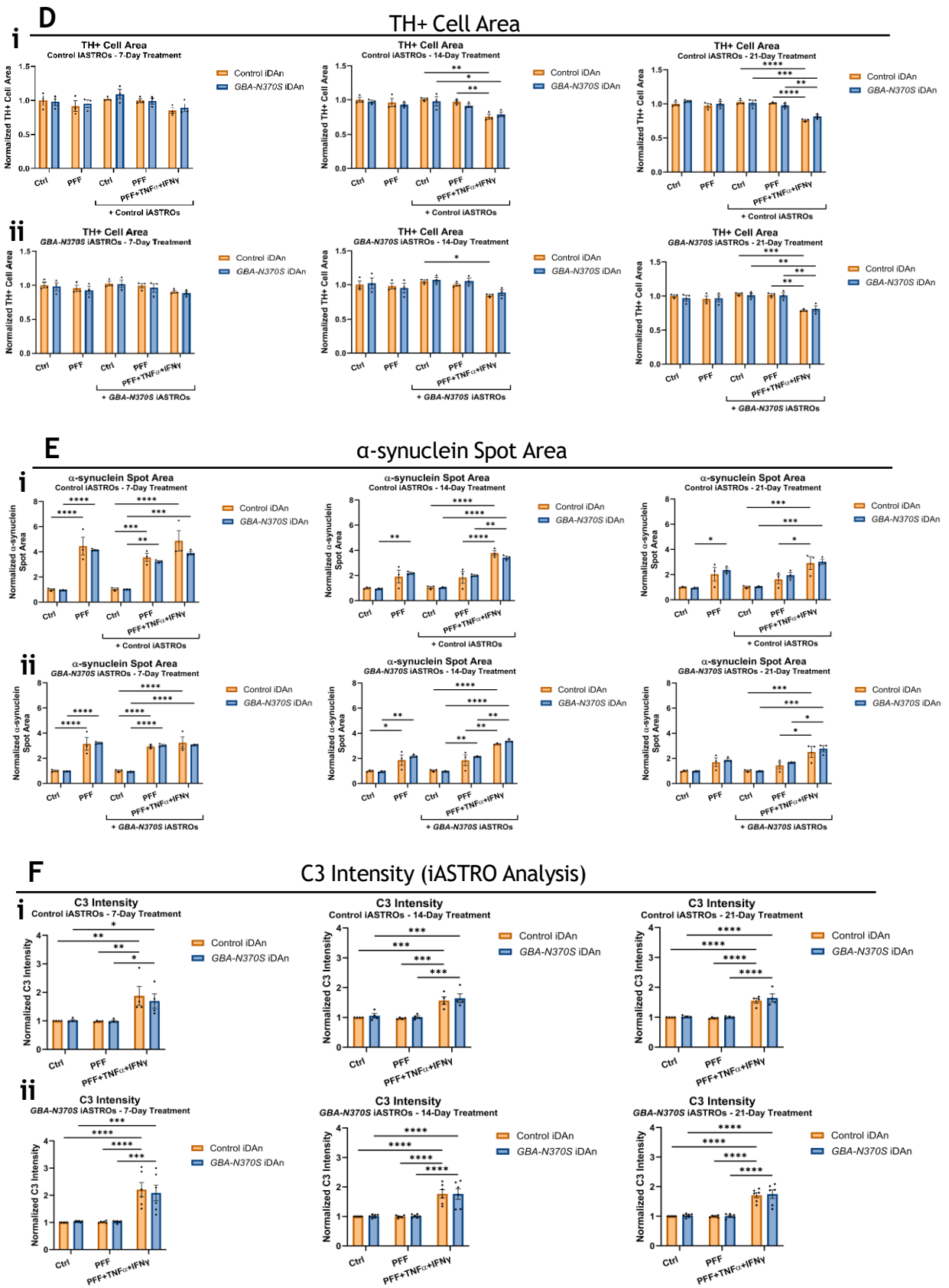


Figure 6.13. In control and *GBA-N370S* iDAn mono-cultures or in co-cultures with control and *GBA-N370S* iASTROs, α-synuclein PFFs alone do not affect the viability of either cell type, but when combining them with TNFα+IFNγ, iASTROs become reactive and neurotoxic

(A-E) Quantification of (A) the total number of live cells, (B) the dead cell ratio (calculated by dividing the number of dead cells by the total number of cells), (C) the number of MAP2+ cells, (D) the cell area of TH+ cells, and (E) the area of α-synuclein spots in control and *GBA-N370S* iDAn, in mono-culture or in co-culture with (i) control or (ii) *GBA-N370S* iASTROs, untreated or treated with α-synuclein PFFs (10 μg/mL) or α-synuclein PFFs (10 μg/mL) + TNFα (30 ng/mL) + IFNγ (50 ng/mL) for 7, 14 or 21 days. Each data point represents 1 iDAn line averaged across differentiations. For each differentiation, values were normalized to the average of untreated (ctrl) control iDAn in mono-culture. N = 3 control and 3 *GBA-N370S* lines for iDAn (4-5 differentiations), and N = 3 control and 4 *GBA-N370S* lines for iASTROs (1-2 differentiations per line). Mean ± SEM. The statistical analysis performed was two-way ANOVA with Tukey's multiple comparison test. *p<0.05, **p<0.01, ***p<0.001, ****p<0.0001. Not all statistically significant comparisons are shown in the graphs, due to the large number of comparisons with p values below 0.05. (F) Quantification of the cytoplasmic C3 intensity in (i) control and (ii) *GBA-N370S* iASTROs in co-culture with control and *GBA-N370S* iDAn, untreated or treated with α-synuclein PFFs (10 μg/mL) or α-synuclein PFFs (10 μg/mL) + TNFα (30 ng/mL) + IFNγ (50 ng/mL) for 7, 14 or 21 days. For each differentiation, in each timepoint, values were normalized to the average of untreated iASTROs co-cultured with control iDAn. Each data point represents 1 iASTRO line averaged across differentiations. N = 3 control and 3 *GBA-N370S* lines for iDAn (4-5 differentiations), and N = 3 control and 4 *GBA-N370S* lines for iASTROs (1-2 differentiations per line). Mean ± SEM. The statistical analysis performed was two-way ANOVA with Tukey's multiple comparison test. *p<0.05, **p<0.01, ***p<0.001, ****p<0.0001.

6.5. Discussion

In this chapter, I explored the impact of reactive iASTROs on iDAn using two experimental designs: treating iASTROs with TNFα+IFNγ in mono-culture and then adding them to iDAn, or treating the co-cultures directly with a range of different inflammatory cytokines and maintaining them in an inflammatory environment. I also investigated the effects of α-synuclein PFFs on cellular viability in iDAn mono-cultures and iDAn-iASTRO co-cultures, and whether PFFs potentiated the neurotoxic effects of reactive iASTROs in co-culture. Not many studies have explored the direct effects of reactive astrocytes on neurons in vitro, and there is even less data available using human iPSC-derived models. Moreover, to my best knowledge, there are no studies exploring the combined effects of inflammatory cytokines and α-synuclein in neuron-astrocyte co-cultures. Consequently, most of the studies discussed in this discussion section are not fully comparable to the experiments presented in this chapter or with the other published studies, as they differ on the cell models used (species, brain region, etc), the cytokines and concentrations used, the treatment durations, and the co-culture method.

First of all, I did not observe any changes in the number of MAP2+ and TH+ cells between co-cultures with untreated iASTROs or iASTROs pre-treated with TNFα+IFNγ before the co-cultures. Moreover, the reactivity of pre-treated iASTROs was still apparent after 48h in co-culture, but decreased significantly over time. Therefore, this indicates that iASTROs that become reactive after an acute inflammatory insult and then are put in direct contact with iDAn are not neurotoxic and lose their inflammatory phenotype in a few days. On the contrary, a study showed that mouse ESC-derived brainstem astrocytes pre-treated for 24h with TNFα or TNFα+IL-1α were neurotoxic to mouse ESC-derived motor neurons in direct co-culture (Lindblad et al., 2023). However, the motor neurons were plated on top of the pre-treated astrocytes without changing the astrocyte media containing the inflammatory cytokines, whereas in this thesis iASTROs were plated on top of iDAn in fresh media. Another study using this treatment approach saw that iPSC-derived astrocytes pre-treated with IL-1β for 5h were neurotoxic to iPSC-derived neurons after 48h in co-culture (Santos et al., 2022), but due to the different treatment used, the results are not comparable.

In addition, these experiments with pre-treated iASTROs showed that the S100B intensity and cell area, as well as the C3 intensity, were higher in control and *GBA-N370S* iASTROs when co-cultured with *GBA-N370S* iDAn as opposed to control iDAn. These results are in line with those presented in Chapter 3, and possible explanations for this are further explained in the discussion of Chapter 3.

On the other hand, when treating the iASTRO-iDAn co-cultures with a range of different inflammatory cytokines, different results were obtained depending on the differentiation and the treatment. On a first set of experiments, which included 3 independent neuronal differentiations co-cultured with control iASTROs, co-cultures treated with TNFα or the Liddelow factors had a higher number of total, MAP2+ and TH+ positive cells, and a higher astrocytic reactivity, than untreated co-cultures. On the contrary, in the second set of experiments, which included co-cultures with control and *GBA-N370S* iASTROs, there was a decrease in the number of total and MAP2+ cells in the treated co-cultures compared to the untreated co-cultures. The TH+ cell morphology remained mostly unchanged after treatment in both sets of experiments.

Furthermore, a higher variability between both batches of experiments was observed in the co-cultures treated with IFNγ alone or TNFα+IFNγ. In the first set of experiments, a higher

number of TH+ and MAP2+ cells were quantified in the co-cultures treated with IFNγ alone or TNFα+IFNγ, although there was a decrease in the total cell number and an increase in the dead cell ratio in the treated co-cultures. Moreover, the TH+ cell area was also lower in treated than in untreated co-cultures. The discrepancy between the results regarding the total number of live cells and the number of MAP2+ and TH+ cells could be due to 2 main reasons. First of all, non-neuronal and undifferentiated cells in the culture could be dying in the treated co-cultures, whereas reactive iASTROs confer neuroprotection to MAP2+ and TH+ neurons. Additionally, there might have been an issue with the image analysis software, in which stressed neurons in the treated co-cultures were easier to detect and quantify than healthy neurons in the untreated co-cultures. Indeed, the fact that the TH+ cell area was lower in the treated co-cultures suggests that iDAn are stressed. In the second batch of experiments, the decrease in the total number of live cells, and the increase in the dead cell ratio in the co-cultures treated with IFNγ and TNFα+IFNγ, compared to untreated co-cultures was much bigger than in the previous set of experiments. In this case, this was accompanied by a decrease in the number of MAP2+ cells, a decrease in the TH+ cell area, and an increase in the TH+ cell roundness in treated co-cultures. All these effects were more pronounced in the conditions with TNFα+IFNγ. These results suggest that, in the first set of experiments, reactive iASTROs were more neurosupportive to iDAn when the co-cultures were maintained in a constant inflammatory state. However, in the second set of experiments, iASTROs lost their neurosupportive capacity and became neurotoxic. The degree of neurotoxicity depended on the treatment, as iASTROs treated with TNFα alone or the Liddelow factors appeared to be less neurotoxic than those treated with IFNγ or TNFα+IFNγ. Moreover, the longer the cells were kept in an inflammatory milieu, the bigger the impact of reactive iASTROs on iDAn.

There are multiple factors that could explain the differences in the neurotoxic/neuroprotective effects of reactive iASTROs observed in both sets of experiments. Each batch of experiments consisted of 3 independent neuronal differentiations, and 1-3 independent astrocyte differentiations per line, and these experiments were conducted over 1 year apart. Consequently, the inflammatory cytokines used in each batch came from different lots, and there may have been differences in the effectiveness of one or more cytokines between the lots. Moreover, based on the iDAn morphologies, there were differences between both batches. For instance, in the first batch, the TH+ cell area and

roundness were the same between untreated iDAn mono-cultures and untreated iDAn-iASTRO co-cultures, whereas in the second batch the TH+ cell area was bigger, and the cell roundness smaller, in untreated co-cultures than in mono-cultures. With this information, it is not easy to make any conclusions regarding which differentiations had the most mature cells, which benefitted more by addition of iASTROs, and so on, but it does indicate that there were inherent differences in the iDAn populations.

On the other hand, there were differences in the magnitude of the increase in iASTRO C3 intensity in treated compared to untreated co-cultures. In the second batch, the increase in iASTRO C3 intensity in all treated conditions was higher than in the first batch. Moreover, while in the first batch there was no increase in C3 intensity in co-cultures treated with IFNγ compared to untreated co-cultures, in the second batch there was an increase that became higher with time. Therefore, the inflammatory response of iASTROs in the second batch seemed to be more pronounced than in the first batch, and this may explain why the neurotoxic and neuroprotective/neurotrophic capacity of the reactive cells in both batches were different: the more reactive the cell, the less neurosupportive and the more neurotoxic. Additionally, this change in the degree of inflammatory response could also be due to the different lots of cytokines used or the maturity of iASTROs.

Following on from the last point, Gatto and colleagues used a direct conversion method to differentiate astrocytes from fibroblasts obtained from either young or old donors, and they showed that “old” astrocytes underwent a much more pronounced inflammatory response to IL-1β than “young” astrocytes, and whereas “old” reactive astrocytes were neurotoxic to iPSC-derived motor neurons, “young” astrocytes were not (Gatto et al., 2021). Barbar and colleagues also demonstrated that the ability of iPSC-derived astrocytes to undergo astrogliosis highly depends on their maturity (Barbar et al., 2020). Therefore, it is plausible to argue that in the first set of experiments iASTROs were less mature and underwent a less pronounced inflammatory response, which was accompanied by a gain in their neuroprotective and neurosupportive capacity, whereas in the second batch they became more inflammatory, which resulted in a gain of neurotoxic function. Furthermore, this could be related to the hypothesis that an early inflammatory response after an acute stimulus or a repeated subthreshold stimulus can be neuroprotective (Sochocka et al., 2017), as this could indicate that in the first batch of experiments, especially in cells treated with TNFα, IFNγ or

the Liddelow factors, the inflammatory stimulus was low enough to keep iASTROs in the subthreshold state of reactivity and thus maintain their neurosupportive functions.

All this said, further experiments are needed to understand if reactive iASTROs become more neuroprotective or if in turn lose their neurosupportive capacity and become neurotoxic. Furthermore, how different inflammatory cytokines, concentrations, and treatment times affect any of these phenotypes on reactive iASTROs should also be explored further. A simple way to do this would be to repeat the experiments presented in this chapter, but using different cell lines and treatments.

Overall, no differences were detected due to the genotype of iASTROs in any of the parameters measured in the second set of experiments, which indicates that the neurotoxic effect observed in reactive iASTROs was not affected by the *GBA-N370S* mutation. In the case of iDAn, in some conditions less neurons were observed in mono- and co-cultures with *GBA-N370S* iDAn, which is in line with the observations in Chapter 3.

As mentioned above, there is not much information in the literature regarding the direct effects of reactive astrocytes on neurons in vitro, and the studies vary greatly on the cell models, treatments, etc. used. This further emphasizes the need of more experiments to understand the effect of reactive astrocytes on neurons. A very important finding in the field was the study by Liddelow and colleagues, which showed that conditioned media of mouse astrocytes treated with the Liddelow factors for 24h was toxic to human ESC-derived dopaminergic neurons after 5 days (Liddelow et al., 2017). Later, Barbar and colleagues showed a less mature firing pattern in iPSC-derived neuron-astrocyte co-cultures treated with the Liddelow factors for 18 days than in untreated co-cultures (Barbar et al., 2020). Moreover, conditioned media from astrocytes treated with the Liddelow factors was reported to be neurotoxic to neurons after 3 days of treatment. Similarly, Leng and colleagues showed that in direct iPSC-derived neuron-astrocyte co-cultures, treatment with the Liddelow factors for 3 days lead to neuronal toxicity and less neuronal calcium activity (Leng et al., 2022). However, these last two studies were not done in midbrain-specific neural cells, and as discussed in chapter 3, the regional differences in both cell types might greatly affect the neuronal susceptibility and inflammatory response of astrocytes (Asanuma et al., 2019; Clarke et al., 2020; Lee et al., 2022). Lastly, in co-cultures of LUHMES-derived human neurons and mouse astrocytes, TNFα induced neurotoxicity whereas IFNγ did not (Efremova et al., 2017).

On the other hand, there is evidence in the literature showing that reactive astrocytes can have neuroprotective or neurosupportive functions. For instance, using a microfluidics system, a study showed that iPSC-derived astrocytes exposed to TNFα+IL-1β were more neurosupportive (using axonal density as a measuring factor) than untreated cells (Hyvärinen et al., 2019). However, in this system, the axonal density was higher in untreated neuron mono-cultures than in untreated co-cultures, which is not indicative of a biologically representative model. In a multiple sclerosis (MS) model, iPSC-derived astrocytes obtained from benign MS patients protected iPSC-derived neurons from TNFα+IL-17-induced neurite damage, whereas iPSC-derived astrocytes obtained from progressive MS patients did not (Kerkering et al., 2023). In mouse neurons, conditioned media of mouse astrocytes treated with IFNγ was neuroprotective against oxidative stress, and conditioned media of astrocytes treated with 10 ng/mL IFNγ was more neuroprotective than those treated with 100 ng/mL IFNγ, whereas direct treatment of neurons with IFNγ also led to apoptosis (Garg et al., 2009). Similarly, in direct co-culture with astrocytes, low doses of LPS were neurosupportive whereas higher doses induced neuronal death, and both these effects were mediated by astrocyte-released IL-6 (Li et al., 2009). As a side note, there are different reports in the literature regarding the neurotoxic (Pons-Espinal et al., 2024) or neuroprotective (Sun et al., 2017) effect of astrocytic IL-6 on neurons.

In the experiments where co-cultures were directly treated with inflammatory cytokines, iDAn mono-cultures were also treated with the Liddelow factors or TNFα+IFNγ to ensure that any effects observed in the treated co-cultures where through the action of reactive iASTROs and not the impact of cytokines on iDA. In iDAn treated with the Liddelow factors, I did not see any changes in cell number, death ratio, or TH morphology, but TNFα+IFNγ exerted a bit of toxicity on iDAn mono-cultures, which was more apparent in the second batch of experiments. Nevertheless, any of the changes observed in iDAn mono-cultures after treatment with TNFα+IFNγ were much smaller than those observed in co-cultures treated with TNFα+IFNγ. Therefore, this indicates that most of the effects of inflammatory cytokines on iDAn cell viability and health in the co-cultures happened indirectly through the action of reactive iASTROs on iDAn.

Similar to the observations in this thesis, others have also claimed that direct treatment with the Liddelow factors does not induce hESC/iPSC-derived DAn neurotoxicity (Barbar et al.,

2020; Liddelow et al., 2017). Regarding TNFα and IFNγ, there is discrepancy between different studies, as some claim that there is no effect, whereas others report that there is. Nevertheless, these studies vary on the concentrations and treatment durations, as well as the cell model, which makes the results less comparable. For instance, in a mixed population of iPSC-derived dopaminergic and serotonergic/GABAergic neurons, 24h treatment with TNFα and IFNγ alone had small effects on neurite integrity, whereas the effect was milder with combined treatment of TNFα+IFNγ (Meyer-Arndt et al., 2023). There are additional reports claiming that IFNγ induces apoptosis in mouse neurons (Garg et al., 2009), but there is also data claiming that IFNγ does not induce any changes in LUHMES human neurons (Efremova et al., 2017). Similarly, some studies observed that TNFα promotes the differentiation of NSCs into DAn (Schmidt et al., 2021), or induces necroptosis in SH-SY5Y cells and mouse primary cortical neurons (Xu et al., 2021), as well as senescence in SH-SY5Y cells (Bae et al., 2022). An important conclusion that can be drawn from all these studies is that one should not solely rely on the results from previous independent studies to make conclusions regarding the effect, or lack thereof, of inflammatory cytokines on neurons, and experiments that involve treating neuron-astrocyte co-cultures with inflammatory cytokines should include the appropriate control of treated neuron mono-cultures. Lastly, as a future experiment, it would be interesting to check the expression of the receptors for these cytokines in iDAn, as was done by Meyer-Arndt and colleagues (Meyer-Arndt et al., 2023), and also compare the expression levels with those of iASTROs, to see if any of these cytokines could potentially activate signalling pathways in the iDAn model.

To conclude this chapter and this thesis, I explored the effects of adding α-synuclein PFFs to iDAn mono-cultures and iDAn-iASTRO co-cultures, and whether PFFs modulated the neurotoxic effect of iASTROs treated with TNFα+IFNγ I had observed in the second batch of experiments, which were conducted simultaneously. First, in iDAn mono-cultures, treatment with α-synuclein PFFs did not impact the cellular viability or caused any changes in neuronal morphology, even after 21 days of treatment. In addition, although the size of α-synuclein aggregates decreased over time, by 21 days aggregates were still present in the cultures, which suggests that iDAn were unable to fully degrade the α-synuclein PFFs in the first 21 days. On the other hand, several studies have shown that α-synuclein PFFs induce neuronal toxicity and cellular dysfunction in various models such as primary mouse neurons (Volpicelli-

Daley et al., 2011) and SH-SY5Y cells (Arcos et al., 2023), although other reports claim that PFFs do not induce neuronal toxicity in vitro (Gao et al., 2019). In studies using rodent models of α-synuclein PFFs injection, the degree of neurodegeneration and the subsequent motor deficits are quite variable between studies too (Björklund et al., 2022; Polinski, 2021). There is little data available on the impact of α-synuclein PFFs in iPSC-derived iDAn, with or without PD-related mutations, because most studies have focused on other α-synuclein species, overexpression of α-synuclein, or endogenous expression of α-synuclein mutants. Therefore, further studies are needed to explore the effects of PFFs on iDAn cellular function and toxicity, focusing on different intracellular pathways such as lysosomal degradation and mitochondrial function.

Moreover, in co-cultures treated with α-synuclein PFFs alone, no astroglial reactivity was observed at any timepoint. This is in line with the results presented in Chapter 4 showing that, in iASTRO mono-cultures, PFFs alone do not induce an inflammatory response in astrocytes. Similarly, it indicates that the action of PFFs on iDAn does not result in cellular alterations or release of factors that are then detected by iASTROs and induce an inflammatory response. However, as mentioned in the discussion in Chapter 4, other studies have shown that α-synuclein PFFs cause astrogliosis (Aflaki et al., 2020), accompanied by neurotoxic properties towards SH-SY5Y cells (Chou et al., 2021). Another study showed that rat astrocytes pre-treated for 16h with α-synuclein monomers, oligomers or fibrils became reactive and were neurotoxic to hippocampal rat neurons after 72h in direct co-culture (Chavarría et al., 2018), and similar observations were made in primary mouse cultures using a transwell co-culture system (Li et al., 2024). However, because I did not observe any astrogliosis in iASTRO mono-cultures treated with PFFs, it is not surprising that these non-reactive iASTROs were not neurotoxic to iDAn. Moreover, by 21 days, the area of α-synuclein aggregates appeared to be smaller in co-cultures treated with PFFs than in mono-cultures with PFFs, although the difference was not significant. This suggests that, even in the presence of both iASTROs and iDAn, PFFs cannot be degraded completely. Multiple reports have claimed that astrocytes are better scavengers of α-synuclein than neurons (Loria et al., 2017; Tsunemi et al., 2020), and also how fibrils are better degraded in neuron-astrocyte co-cultures than in neuronal mono-cultures (Loria et al., 2017). Further studies in iDAn and iASTRO mono-cultures treated with PFFs will be needed to test that hypothesis in this model.

Lastly, in co-cultures treated with TNFα+IFNγ and PFFs, there was a very big decrease in total and MAP2+ cell number, and a big increase in dead cell ratio, as well as a significant decrease in the TH+ cell area. The magnitude of these changes was much bigger than when treating co-cultures with TNFα+IFNγ without PFFs, which suggests that PFFs potentiate the neurotoxic effects of reactive iASTROs in an inflammatory environment. In Chapter 4, I described that a difference in iASTRO morphology could be observed between cells treated with TNFα+IFNγ+PFFs or TNFα+IFNγ, which I hypothesized indicated that PFFs do modulate the inflammatory response of iASTROs to inflammatory cytokines. This effect could be potentiated in iDAn-iASTRO co-cultures, where the addition of PFFs to an inflammatory system that is already less neurosupportive surpasses the capacity of the cells to handle PFFs and any neuroprotective mechanism that might be working to counteract the effect of the inflammatory cytokines and PFFs. All this results in a cellular environment that is highly toxic to iDAn. Additionally, the size of α-synuclein aggregates was bigger in co-cultures treated with TNFα+IFNγ+PFFs than in co-cultures exposed to PFFs alone, which indicates that the overall capacity of iDAn and/or iASTROs to degrade PFFs is impaired when iASTROs are reactive. However, this could also be due to the lower number of cells in the culture, as the smaller the number of cells, the less PFFs that will be degraded.

In summary, the data presented in this chapter indicates that iASTROs pre-treated with TNFα+IFNγ are as neurosupportive as untreated iASTROs to iDAn. On the other hand, conflicting results were obtained regarding the neuroprotective or neurotoxic effect of iASTROs on iDAn when direct co-cultures were kept in an inflammatory environment, although the differences observed in iDAn morphologies and the magnitude in the reactive response of iASTROs, quantified by C3 intensity, might explain the different effects. Lastly, the reduced neurosupportive capacity and increased neurotoxicity of reactive iASTROs was aggravated with combined treatment with PFFs in direct co-culture.

To my best knowledge, this is the first study exploring the direct effect of the combined treatment of inflammatory cytokines and α-synuclein PFFs, and more studies are needed to investigate in detail the cellular processes driving the neurotoxicity of PFF and TNFα+IFNγ. Ultimately, both neuroinflammation and α-synuclein aggregates are found in the brains of PD patients, and thus, both of them should be studied in conjunction to fully understand what

their impact is on neurons and astrocytes in the context of PD. Moreover, this might open new avenues for therapy, as new therapeutic targets and strategies could be discovered.

Chapter 7 – Discussion

The work presented in this thesis makes multiple contributions to the field of astrocyte research in Parkinson's disease and neuroinflammatory astrocytes. First, a robust, representative human model of iPSC-derived midbrain-specific astrocytes was extensively characterized and used to study potential cell autonomous alterations in *GBA-N370S* astrocytes. Moreover, a direct iPSC-derived DAn-astrocyte co-culture was stablished and optimized. This platform enabled to study the direct interaction between both cell types, the effect of the *GBA-N370S* mutation in their homeostasis, and the consequences of exposure to inflammatory cytokines and α-synuclein PFFs. In addition, this thesis provides extensive data regarding the inflammatory response of control and *GBA-N370S* iASTROs to different inflammatory cytokines and α-synuclein PFFs in mono-culture. Finally, the results presented in this thesis open multiple new research and therapeutic avenues worth pursuing further.

7.1. Main findings and discussion

7.1.1. Control and *GBA-N370S* iASTROs are a representative human model of midbrain astrocytes, capable of supporting DAn

The extensive characterization of control and *GBA-N370S* iPSC-derived midbrain astrocytes (iASTROs) conducted in this thesis demonstrates that iASTROs are a representative human model of midbrain astrocytes, and thus, they can be used to study the potential involvement of astrocytes in PD. Most studies using iPSC-derived astrocytes only include a basic characterization of the cells (e.g. expression of a few astrocytic markers) at the end stage of the protocol, and do not include a comprehensive transcriptomic analysis or comparison with other datasets to verify their cellular identity (Aflaki et al., 2020; Hyvärinen et al., 2019; Ramos-Gonzalez et al., 2021; Sonninen et al., 2020; Yarkova et al., 2023). Furthermore, most of these studies are based on different differentiation protocols, which, together with the lack of appropriate characterization and quality control standards, results in significant study-to-study variability on the results reported. Similarly, the majority of studies on iPSC-derived astrocytes have used cells without any regional specification (Aflaki et al., 2020; Cheng et al., 2020; di Domenico et al., 2019; Nonaka et al., 2024; Ramos-Gonzalez et al., 2021), even

though it is known that human astrocytes present vast regional and sub-regional differences (B. E. Clarke et al., 2020; J. Lee et al., 2022). In the case of PD, due to the increased susceptibility of SNpc DAn (Gonzalez-Rodriguez et al., 2020; Surmeier et al., 2017) and the higher neuroprotective capacities of midbrain astrocytes (Nam et al., 2024), midbrain-specific astrocytes should be used to study their interactions with DAn and contributions to PD pathogenesis. Based on the characterization of iASTROs conducted in this thesis, the differentiation protocol used, developed by Crompton and colleagues (Crompton et al., 2021), generates a robust and representative human midbrain-specific astrocyte model, albeit with some degree of line-to-line and differentiation-to-differentiation variability.

Furthermore, a direct co-culture system for iPSC-derived DAn (iDAn) and iASTROs was established and optimized, where a media composed of 50% iDAn maturation media and 50% iASTRO maturation media was the most optimal for the maintenance of both cell types. The co-culture media optimization step conducted in this thesis has not been done by others, as other studies on direct iPSC-derived neuron-astrocyte co-cultures have used relatively basic culture medias (de Rus Jacquet, 2019; di Domenico et al., 2019) or DAn maturation media (Barbar et al., 2020; Cheng et al., 2020), without including any data regarding a co-culture media optimization step. Moreover, using this co-culture system, I showed that both control and *GBA-N370S* iASTROs promoted iDAn survival and synaptogenesis in a similar way, which validates the physiological relevance of the model used, as well as suggesting that the *GBA-N370S* mutation that does not significantly compromise the neurosupportive capacity of iASTROs, at least during the first 30 days in co-culture. On the contrary, *LRRK2-G2019S* have been shown to be less neurosupportive to DAn and induce neurodegeneration in non-PD DAn (di Domenico et al., 2019). Nonetheless, the increased S100B expression in iASTROs co-cultured with *GBA-N370S* iDAn compared to control iDAn found suggests that iDAn carrying the *GBA-N370S* mutation induce different cellular responses in iASTROs. This effect might be due to the numerous cellular alterations described in *GBA-N370S* DAn by others (Beccano-Kelly et al., 2023; Bogetofte et al., 2023; Fernandes et al., 2016; Grigor'eva et al., 2023; Schöndorf et al., 2014), but to determine exactly the mechanism by which this response is elicited, further research is needed. Overall, the co-culture system developed in this thesis enable to study the effect of different disease-associated mutations in neuron-astrocyte interactions, and, as will be discussed later, it can also be used to model neuroinflammation.

7.1.2. The *GBA-N370S* mutation has a very small impact on iASTRO function

The evidence provided in this thesis suggests that the *GBA-N370S* mutation does not cause significant alterations in iASTROs in terms of their morphology and astrocytic identity, inflammatory response, and neurosupportive activity. Nonetheless, iASTROs carrying the *GBA-N370S* mutation presented calcium dysregulation, as shown by increased calcium entry through SOCE but decreased ATP-induced ER-calcium release, as well as higher ROS production. There is little data available regarding the effects of *GBA1* mutations on human astrocytes, as most studies in iPSC-derived models have been conducted in cells carrying the *LRRK2-G2019S* mutation, which have shown that this mutation causes multiple cellular alterations in astrocytes (Booth et al., 2019; de Rus Jacquet et al., 2021, 2023; di Domenico et al., 2019; Ramos-Gonzalez et al., 2021; Streubel-Gallasch et al., 2021). The most extensive study that has explored the effect of the *GBA-N370S* mutation in human iPSC-derived astrocytes found some alterations in α-synuclein accumulation and increases in reactivity, as well as significant reduction in GCase activity (Aflaki et al., 2020). However, the cells used in this study were derived from Gaucher's disease patients and were homozygous for *GBA-N370S*, whereas the cells used in this study were heterozygous. On the other hand, as mentioned, multiple reports have shown the cellular dysfunctions caused by the *GBA-N370S* mutation in iPSC-derived dopaminergic neurons (Beccano-Kelly et al., 2023; Bogetofte et al., 2023; Fernandes et al., 2016; Grigor'eva et al., 2023; Schöndorf et al., 2014). Therefore, it is plausible to hypothesize that, in the context of PD, the *GBA-N370S* mutation has a more detrimental impact in DAn than in astrocytes.

7.1.3. Control and *GBA-N370S* iASTROs undergo vast transcriptional and cellular changes in response to inflammatory cytokines but not α-synuclein PFFs

Neuroinflammation is one of the main hallmarks of PD, but it is not understood yet whether it is a cause or consequence of PD. Furthermore, the role of inflammatory astrocytes in PD has not been fully elucidated yet, nor how different PD-associated mutations might alter astrogliosis.

The field has discarded the viewpoint that reactive astrocytes are either neurotoxic or neuroprotective in favour of the hypothesis that there is a continuum of dynamic reactive astrocytic phenotypes, although these phenotypes and how different factors affect them have not been determined yet. The evidence provided in this thesis shows that, upon stimulus with different inflammatory cytokines, reactive iASTROs present characteristics of both neurotoxicity (e.g. increased ROS production) and neuroprotection (e.g. increased expression of growth factors), and this was most evident in cells treated with TNFα+IFNγ. Nonetheless, due to the vast transcriptional changes undergone by astrocytes upon inflammatory stimulus, it was very challenging to exactly determine their degree of neuroprotective and/or neurotoxic activity. Subsequent iDAn-iASTRO co-culture experiments, discussed in section 7.1.5., were conducted to explore this.

Although there are multiple published transcriptomic datasets that have explored the reactive response of iPSC-derived astrocytes to inflammatory cytokines (Barbar et al., 2020; Leng et al., 2022; Perriot et al., 2018; M. D. Smith et al., 2022; Spreng et al., 2022), to my best knowledge, the bulk RNAseq dataset presented in this thesis is the most extensive one regarding the number of independent biological replicates used and the different treatment conditions tested. This experiment revealed vast transcriptomic changes (thousands of DEGs and hundreds of GO:BP terms) in response to all treatments that included inflammatory cytokines, but, due to time constraints, it was not possible to explore all of them. Nonetheless, the dataset obtained, and the preliminary findings discussed in this thesis, open multiple new research avenues to investigate the intracellular pathways that are altered during astrogliosis, such as changes in lipid metabolism and homeostasis, changes in the proliferative capacity of the cells, and the modulation and interaction with the extracellular matrix, amongst others.

Furthermore, the different cytokines and their combination used in the experiments presented in this thesis enabled to study how the transcriptomic changes in iASTROs highly varied depending on the individual cytokine used, as different cytokines activate different pathways. Moreover, the combination of cytokines showed how some of them have an additive effect whereas others, such as TNFα+IFNγ, act synergistically, an effect also described by others (Barcia et al., 2011; Spreng et al., 2022; Woznicki et al., 2021). The use of different cytokine combinations also revealed that most of the transcriptional changes induced by the Liddelow factors were driven by TNFα. Moreover, iASTROs underwent less cellular and

transcriptomic changes after exposure to the Liddelow factors compared to TNFα+IFNγ. These results imply that the combination of TNFα+IL-1α+C1q is not the most optimal to induce astrocyte reactivity and investigate different reactive responses in our iASTRO model. This finding has important implications to multiple other studies that have solely used this combination of cytokines to induce and study astrocyte reactivity (Barbar et al., 2020; Guttenplan et al., 2021; Labib et al., 2022; LaRocca et al., 2021; Leng et al., 2022; Szpakowski et al., 2022). All things considered, future studies investigating astrocyte reactivity should consider using different combinations of inflammatory cytokines, or use the cytokines that are most relevant to the disease condition of interest, as has been done by others (Perriot et al., 2018).

Although the RNAseq experiment presented in this thesis only captured the transcriptomic changes in iASTROs 24h after the initial insult, subsequent in vitro experiments provided more insight into the changes happening in the first 7 days. Overall, the results indicate that a single inflammatory insult induces a rapid, but sustained, inflammatory response in iASTROs, with some changes becoming more apparent and significant with time, such as the expression of *HLA* genes and the production of ROS. Most studies exploring astrogliosis in iPSC-derived models have only focused on the first 24h-72h after treatment (Barbar et al., 2020; Labib et al., 2022; Leng et al., 2022; Spreng et al., 2022), which, based on the observations made in this thesis, is not sufficient to capture all the changes occurring during astrogliosis. Similarly, the fact that the bulk RNAseq was only conducted at one timepoint after the inflammatory insult is one of the major drawbacks of this experiment. Spreng and colleagues showed how the transcriptomic changes during astrogliosis occur rapidly and dynamically in the first 72h after an inflammatory stimulus (Spreng et al., 2022), and the data provided in this thesis shows that some changes occur after 72h. Thus, future transcriptomic studies should investigate multiple timepoints before and after the 24h mark, as this will be essential to fully decipher the changes occurring during astrogliosis, the time at which each of these changes happen, and how they evolve over time.

One of the changes occurring in reactive iASTROs after being exposed to TNFα+IFNγ for a few days was an increase in the expression of *BDNF* and *FGF2*, which suggests that reactive iASTROs acquired some neurosupportive characteristics over time. Furthermore, since both BDNF and FGF2 have been associated with increased neuroprotection in PD (Geng et al., 2023;

Liu et al., 2021; Palasz et al., 2020), promoting their expression in astrocytes might offer a new therapeutic approach for PD. In the case of BDNF, most therapeutic strategies explored have used small molecules that modulate its signalling pathway through TrkB, albeit with varying success (Ali et al., 2024). Therefore, promoting BDNF production in astrocytes might be another possible therapeutic avenue to investigate. On the other hand, iASTROs also elevated ROS production days after exposure to TNFα+IFNγ, which is a potential sign of neurotoxicity, as has been described by others (Murray et al., 2022). Since DAn of the midbrain are more susceptible to oxidative stress than other neural populations (Guo et al., 2018), lowering ROS production in reactive midbrain astrocytes could also be a new potential therapeutic strategy to prevent DAn loss in PD. All in all, these two findings suggest that astrocytes enhance both neurotoxic and neuroprotective functions over time. However, since all experiments were conducted at the population level and not at single cell resolution, it cannot be determined whether the same cell may acquire these two characteristics or whether different cells in the culture shift towards a more neuroprotective or a more neurotoxic phenotype. Future experiments at the single-cell level should be able to elucidate this.

On another note, the data currently available regarding the response of human astrocytes to α-synuclein is inconclusive and highly variable depending on the study and the α-synuclein species used. The work presented here indicates that control and *GBA-N370S* iASTROs do not undergo any major cellular changes after exposure to α-synuclein PFFs for one week. On the other hand, other studies, mostly conducted in primary cells and rodent models, have claimed that exposure to α-synuclein and expression of mutant α-synuclein in astrocytes causes multiple cellular alterations and astrogliosis (Chavarría et al., 2018; Diniz et al., 2019; Du et al., 2018; Fellner et al., 2013; Gu et al., 2010; Lee et al., 2010; Lindström et al., 2017; Rannikko et al., 2015). Data on human astrocytes, however, is much scarcer and more inconclusive, with some studies claiming that iPSC-derived astrocytes become reactive after exposure to PFFs (Chou et al., 2021), whereas others did not observe extensive astrogliosis in response to fibrils and monomers (Russ et al., 2021). A big source of variability in all these studies is the α-synuclein species used, as well as the source, modification (e.g. addition of a fluorescent tag) and preparation of α-synuclein, because endotoxin traces might induce reactive responses in astrocytes. Studies do not commonly mention whether the α-synuclein used contains endotoxin or not, and in many instances, a QC of the fibrils, oligomers or PFFs is not shown

either. On the contrary, the PFFs used in this thesis passed stringent QC and were endotoxin free. Thus, based on the observations made in this thesis and the literature available, it is not possible to conclude whether human astrocytes undergo astrogliosis in response to α-synuclein or not. To minimize the study-to-study variability and to obtain more conclusive and reproducible results, standardized α-synuclein species preparations should be used, and the most representative approach would be to use Lewy Body extracts obtained from PD patients, as done by others (Cavaliere et al., 2017).

Furthermore, no significant genotypic differences were observed in the response of iASTROs to PFFs due to the *GBA-N370S* mutation, except a more significant decrease in *FASN* expression, a finding that requires further investigation due to the association of *FASN* with PD (Badawy et al., 2024; Kim et al., 2024). On the other hand, there are reports indicating that mutations in *GBA1* (Aflaki et al., 2020), *LRRK2* (di Domenico et al., 2019; He et al., 2023; Streubel-Gallasch et al., 2021), and *PARK2* (Russ et al., 2021) negatively affect the response of human astrocytes to α-synuclein and their capacity to handle and degrade this protein. Since the bulk RNAseq experiment presented in this thesis was only conducted using control iASTROs, future transcriptomic analysis in *GBA-N370S* iASTROs might reveal other genotypic differences after PFF exposure besides changes in *FASN* expression.

Moreover, an important factor to consider when interpreting the data presented in this thesis and other studies is that, in the PD brain, both inflammatory molecules and α-synuclein aggregates are present. However, barely any studies have investigated the effects of the combined treatment of both on astrocytes. Therefore, the results presented in this thesis provide novel information regarding the response of astrocytes to PFFs in combination with TNFα+IFNγ. Although PFF addition did not significantly alter the response of iASTROs to TNFα+IFNγ, changes in the cellular morphology were detected between iASTROs treated with TNFα+IFNγ and TNFα+IFNγ+PFFs, suggesting that PFFs somehow modulate the inflammatory response of iASTROs, a hypothesis that was supported by experiments in iDAn-iASTRO co-cultures, discussed below. More comprehensive transcriptomic, proteomic and imaging assays spanning a longer time period will be needed to further investigate how PFFs alter the response of iASTROs to inflammatory cytokines, and whether any of these changes are affected by PD-associated mutations or by the presence of DAn.

7.1.4. Calcium signalling pathways and vitamin D metabolism and signalling at altered in reactive control and *GBA-N370S* iASTROs

Out of the multiple cellular pathways upregulated in iASTROs treated with TNFα+IFNγ, two, calcium signalling and vitamin D metabolism, were chosen for further in vitro study, as these two pathways have been associated with PD.

Indeed, calcium dysregulation has been extensively investigated in the context of PD, although most studies have focused on neurons (Kaur et al., 2023). However, in recent years, calcium signalling in astrocytes has gained significant attention, and there is increased evidence showing astrocytic calcium dysregulation in PD (Bancroft & Srinivasan, 2022). The findings presented in this thesis offer evidence for different factors that result in changes in astrocytic calcium signalling. On the one hand, iASTROs carrying the *GBA-N370S* mutation displayed reduced ATP-induced ER-calcium release but elevated calcium entry through SOCE, and the latter might be linked to the increased ROS production in these cells (Johnson et al., 2022; Nunes & Demaurex, 2014). Even if aberrant calcium signalling in *GBA-N370S* astrocytes has not been previously reported, there is evidence showing that this mutation affects calcium handling in DAn (Beccano-Kelly et al., 2023; Schöndorf et al., 2014). Therefore, considering that differences in calcium homeostasis were one of the very few genotypic differences observed between control and *GBA-N370S* iASTROs, this finding should be followed up with further experiments, including co-culture experiments with iDAn to investigate how changes in calcium signalling in *GBA-N370S* iASTROs and/or iDAn impacts calcium homeostasis in the other cell type and their interaction.

Moreover, ATP-induced ER-calcium release and SOCE were also altered (mostly elevated) in iASTROs after treatment with TNFα+IFNγ and, less so, the Liddelow factors. Even if higher calcium levels in reactive astrocytes have been reported for many years (Holliday & Gruol, 1993), its specific function in modulating astrogliosis and subsequent cellular alterations are not fully understood yet. To shed light on this, in this thesis I partially blocked ATP-induced ER-calcium release using 2-APB, but no changes in the inflammatory response were observed as a result. However, considering that calcium is one of the most pleiotropic second messengers, further research using more sensitive tools to study intracellular calcium activity (e.g. GECIs) and more specific modulation of different calcium signalling pathways will be needed to

understand the consequences of elevated cytoplasmic calcium in reactive astrocytes. Modulating calcium signalling in astrocytes might be a potential strategy to modulate the inflammatory response of astrocytes and the subsequent changes to their function.

On another note, the work presented in this thesis shows that iASTROs treated with TNFα+IFNγ increased the expression of *CYP27B1* and *VDR*, which encode two essential enzymes involved in vitamin D metabolism and signalling. This finding has important implications for PD, since vitamin D deficiency has been widely reported in PD patients (Knekt et al., 2010; Xia & Zhou, 2024). Additionally, vitamin D exerts multiple neuroprotective functions in the CNS, such as regulating the expression of growth factors (Hafiz, 2024), promoting DAn differentiation and maturation (Cui et al., 2010), and preventing mitochondrial dysfunction and ROS production (Berridge, 2017). Therefore, elevating *CYP27B1* and *VDR* expression after an inflammatory insult might be a neuroprotective and/or compensatory mechanism in astrocytes, similar to the increase in growth factor expression discussed above. Indeed, vitamin D promotes the expression of various neurotrophic factors, and thus, these two observations might be directly linked. Future studies at single cell resolution should investigate if the expression levels of *CYP27B1* and *VDR* positively correlate with the expression and release of growth factors, and whether there are any notable differences within cells of the same population. Although there is very little data available regarding the role of vitamin D metabolism in PD astrocytes, the current findings point towards a neuroprotective effect of CYP27B1-positive astrocytes in PD (Mazzetti et al., 2022). Therefore, based on the mixed results from clinical trials that have investigated the benefits of vitamin D supplementation to manage PD (Detopoulou et al., 2023), elevating vitamin D metabolism in midbrain astrocytes might be an alternative approach to increase its availability to DAn, while also increasing growth factor production on astrocytes.

7.1.5. In direct co-culture, reactive control and *GBA-N370S* iASTROs may lose neurosupportive properties and become neurotoxic, and this effect is potentiated in the presence of α-synuclein PFFs

Investigating the inflammatory response of astrocytes in mono-culture, such as in the experiments presented in this thesis and most studies, can provide extensive information

regarding the cell autonomous changes occurring during astrogliosis. However, astrocytes in isolation are not the most physiologically relevant model to study the response and effect of inflammatory astrocytes in their environment and surrounding cells, as other cells present in the culture might modulate their response by direct or indirect signals. Thus, to investigate the impact of reactive astrocytes in neurological conditions such as PD, co-culture platforms including the cell populations of interest are needed, as was done in this thesis using iDAn-iASTRO co-cultures.

The work presented here suggests that pre-treatment of iASTROs with TNFα+IFNγ does not affect their neurosupportive activity or induce the acquisition of neurotoxic properties, although studies in other models, using different cytokines for the stimulation of astrocytes, have claimed that pre-treated astrocytes can be neurotoxic to neurons (Lindblad et al., 2023; Santos et al., 2022). Nonetheless, this model is not the most physiologically relevant to study the impact of inflammatory astrocytes on neurons, as, in neurological conditions, both cell types are exposed to inflammatory cytokines and other potentially toxic molecules for prolonged time periods.

Therefore, a different approach was used, in which direct iDAn-iASTRO co-cultures were treated with inflammatory cytokines and maintained in these conditions, a method also used by others (Leng et al., 2022) but still not widely utilized. With this model, an effect of reactive iASTROs on iDAn was observed, demonstrating that direct co-cultures are a better experimental platform to explore the impact of reactive astrocytes on neurons. Nonetheless, the outcomes from these experiments differed between different batches, as in some cases a neuroprotective effect of reactive iASTROs on iDAn was observed, especially after treatment with the Liddelow factors, whereas in other cases reactive iASTROs were neurotoxic to iDAn, particularly in co-cultures exposed to TNFα+IFNγ.

In the literature, there is evidence for both a neurotoxic/less neurosupportive effect (Barbar et al., 2020; Leng et al., 2022) and a neuroprotective effect (Hyvärinen et al., 2019; Kerkering et al., 2023) of reactive astrocytes on neurons. However, if inconsistent and opposing results were obtained in this thesis, where the same protocols and cell lines were used, it is not surprising that published studies are also inconsistent. Based on the observations made in this thesis, some of the factors that might alter the impact of reactive astrocytes on neurons are the degree of astrogliosis undergone by the astrocytes, which could be linked to the

differentiation efficiency or maturity, the different types and batches of cytokines used, and the maturity of the neurons. Consequently, even if the data presented in this thesis points towards a neurotoxic effect of reactive iASTROs on iDAn, further research is needed to validate this observation and to understand the mechanisms by which reactive iASTROs lose their neurosupportive characteristics and how they mediate neurotoxicity, which could happened through a number of mechanisms, such as by the release of saturated lipids (Guttenplan et al., 2021).

A drawback of the direct co-cultures used in this thesis is that conclusions were drawn for the whole cell population, without distinguishing the contributions of each cell to the main effect. Thus, one should not exclude the possibility that, even if the overall effect of the reactive astrocyte population is increased neurotoxicity, there might be individual cells in the population that are working to compensate for this effect by acquiring neuroprotective characteristics. This hypothesis should be further studied, because, if it is indeed true, specifically promoting the neurosupportive population and/or suppressing the neurotoxic one might be a potential therapeutic strategy.

To conclude, this is the first study that has provided a comprehensive exploration of the inflammatory response of *GBA-N370S* astrocytes and their effect of DAn, and, in line with the observations made throughout this thesis, no significant genotypic differences were observed. This adds on to the hypothesis proposed above that, in PD, the *GBA-N370S* mutation has more detrimental effects on DAn than on astrocytes. Others have claimed that mutations in *GBA1* alter the inflammatory response of astrocytes, but both a decrease (Sanyal et al., 2020) and an increase (Aflaki et al., 2020) in pro-inflammatory cytokine release have been reported, differences that could be explained by the mutations investigated and the copy number of the mutation explored.

On another note, the work of this thesis indicates that, the neurotoxic effect of iASTROs treated with TNFα+IFNγ was potentiated with the addition of PFFs, which was accompanied by a reduction in the capacity to degrade PFFs. Together with the morphological differences observed between iASTROs treated with TNFα+IFNγ and TNFα+IFNγ+PFFs, these results indicate that PFFs modulate the inflammatory response of iASTROs and potentiate their neurotoxic action on iDAn. Research on this area is lacking, and therefore, follow-up experiments based on the findings of this thesis should be conducted.

On the contrary, PFFs alone did not compromise iDAn survival in mono-culture or in co-culture with iASTROs, demonstrating that the PFFs used in this thesis were not toxic to iDAn. Others have also claimed that PFFs do not cause neuronal death (Gao et al., 2019), whereas in other studies neuronal toxicity was reported (Arcos et al., 2023; Volpicelli-Daley et al., 2011), but these inconsistencies could be explained by the different cell models used. Furthermore, the results from these co-culture experiments showed that the PFFs used in this thesis did not induce a reactive response in iASTROs in the presence of iDAn, which suggests that iDAn exposed to PFFs did not undergo cellular changes or release factors that might induce astrogliosis in this model.

7.2. Conclusions

In summary, the work presented in this thesis shows that iASTROs are a representative in vitro model of human midbrain astrocytes. Similarly, the direct iDAn-iASTRO co-culture system established and used throughout this thesis enables to study the interaction between these two cell types, including the effects of PD mutations in each cell population, and the addition of inflammatory cytokines and α-synuclein. Moreover, even if *GBA-N370S* iASTROs mostly had similar cell-autonomous and non-cell autonomous properties and functions as control iASTROs, they displayed alterations in calcium signalling and ROS generation upon inflammatory stimuli. In addition, this thesis provides a large body of data regarding the response of iASTROs to inflammatory cytokines, with more in-depth exploration of the changes in calcium signalling and vitamin D metabolism. Evidence is also provided showing an almost lack of response of iASTROs to α-synuclein PFFs, although PFFs seemed to modulate the response of iASTROs exposed to TNFα+IFNγ. Lastly, some of the data suggests that, in direct co-cultures, reactive iASTROs are neurotoxic to iDAn, and in the case of cells treated with TNFα+IFNγ, this effect is potentiated in the presence of PFFs.

S. Appendix

S.1. Effects of partially blocking ATP-induced ER calcium release with 2-APB in reactive iASTROs

After observing that, overall, iASTROs treated with TNFα+IFNγ had an increased expression of *ITPR1* and *ITPR3*, which was accompanied by a higher calcium release from the ER after ATP application (Chapter 5), I investigated how partially blocking the calcium release from the ER may affect iASTRO reactivity. To this end, I used the ITPR channel blocker 2-aminoethoxydiphenyl borate (2-APB) (Maruyama et al., 1997).

First, to verify that 2-APB was successful at partially blocking ER calcium release, I explored ATP-induced ER calcium release using Fura-2 AM in control and *GBA-N370S* iASTROs treated for 24h, 72h or 7 days with 30 ng/mL TNFα + 50 ng/mL IFNγ, 25 µM 2-APB, or 30 ng/mL TNFα + 50 ng/mL IFNγ + 25 µM 2-APB. This concentration of 2-APB was chosen based on the literature and a pilot dose-response study conducted in this project (data not shown). The goal was to partially block ER calcium release, as calcium is an essential second messenger in iASTROs, and higher dosages of 2-APB caused cell death (data not shown). The average calcium traces displayed in Figure S.1 A show that, overall, the calcium release in iASTROs treated with 2-APB was lower than in untreated cells, and it was also lower in iASTROs treated with TNFα+IFNγ+2-APB compared to TNFα+IFNγ. To view this effect more clearly, Figure S.1 B shows the traces of an example control (i) and *GBA-N370S* (ii) iASTRO lines. Lastly, quantification of the peak amplitude and AUC of the traces shown in Figure S.1 A (Figure S.1 C-D) also shows that cells treated with 2-APB displayed lower peak amplitudes and AUC. In conclusion, 25 µM of 2-APB were sufficient to partially block ATP-induced ER-calcium release.

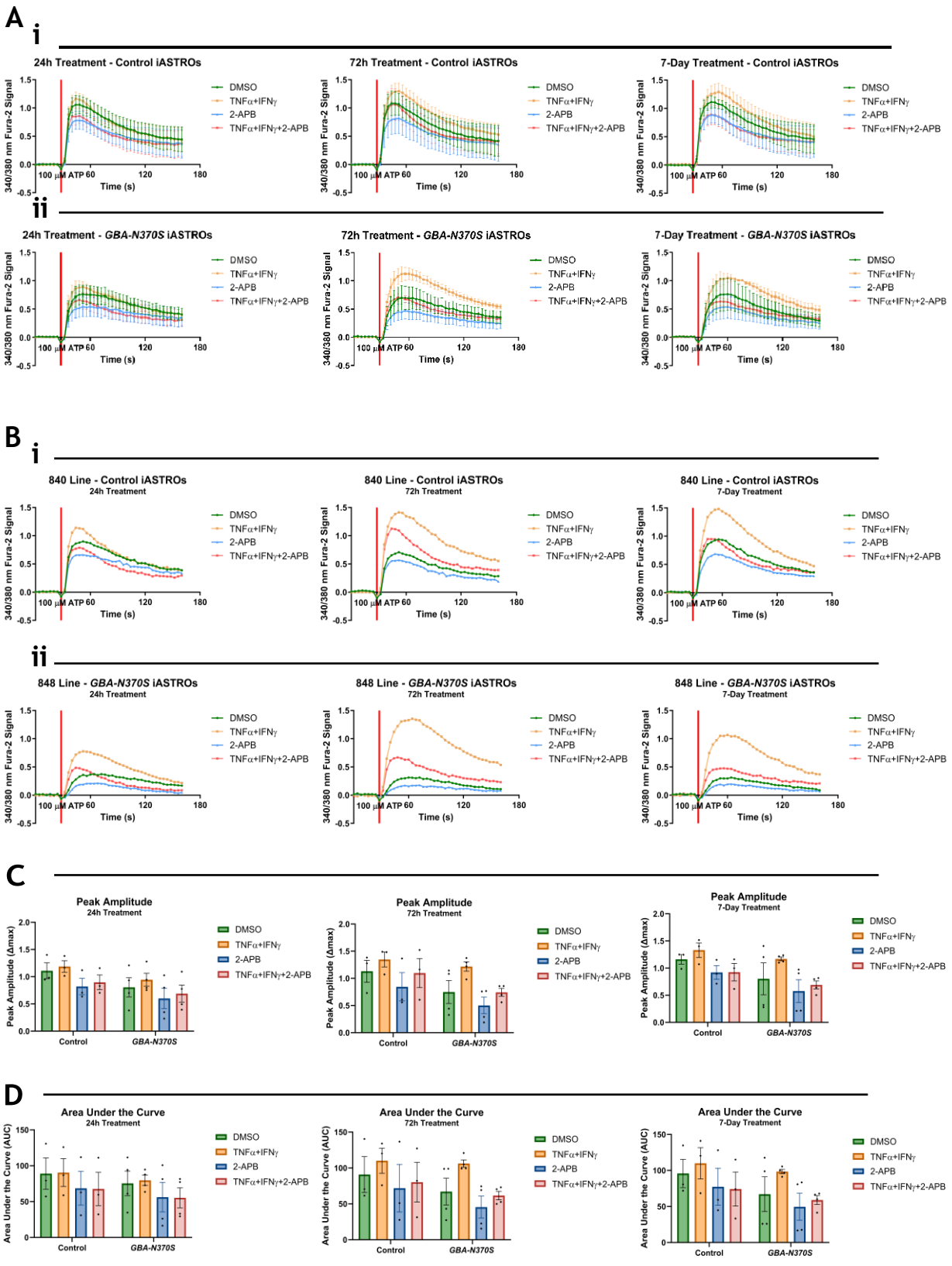


Figure S.1. The ITPR blocker 2-APB reduces the amount of calcium released from the ER in response to ATP in iASTROs

(A) Traces showing the average of the Fura-2 ratio in response to 100 µM ATP (red vertical line in the graphs) in (i) control and (ii) *GBA-N370S* iASTROs treated with 25 µM 2-APB, 30 ng/mL TNFα + 50 ng/mL IFNγ or 25 µM 2-APB + 30 ng/mL TNFα + 50 ng/mL IFNγ for 24h, 72h or 7 days. Each line represents the average of multiple lines (3 control and 4 *GBA-N370S*), each line averaged across differentiations

(1-3 differentiations per line). (B) Traces of the Fura-2 ratio in example (i) control and (ii) *GBA-N370S* lines, showing the averages across 3 differentiations. Same experimental design as in (A). (C-D) Quantification of (C) the peak amplitude and (D) the area under the curve (AUC) of the traces shown in (A). Each data point represents one line averaged across differentiations. N = 3 control and 4 *GBA-N370S* lines, 1-3 differentiations. Mean ± SEM. The statistical analysis performed was two-way ANOVA with Tukey's multiple comparison test.

S.1.1. Relative gene expression of calcium channels in reactive iASTROs after treatment with 2-APB

Next, I investigated if the expression of *ITPR1/2/3*, *ORAI1* and *STIM1*, was affected by 2-APB, as iASTROs might alter their expression to compensate for any calcium dysregulation caused by 2-APB. Therefore, control and *GBA-N370S* iASTROs were treated for 72h or 7 days with 30 ng/mL TNFα + 50 ng/mL IFNγ, 25 µM 2-APB, or 30 ng/mL TNFα + 50 ng/mL IFNγ + 25 µM 2-APB. In the conditions without 2-APB, DMSO was added in equal percentage as 2-APB in the other conditions, to correct for any effects the DMSO 2-APB was dissolved in may have had. The 72h hour timepoint was chosen instead of 24h because a bigger increase in ATP-induced ER-calcium release was measured after 72h treatment with TNFα+IFNγ. Moreover, in this experiment and in those discussed in the next section, two different statistical analyses were performed:

- Two-way ANOVA to compare all conditions with each other in each genotype, and both genotypes in each condition.
- Three-way ANOVA to compare the overall effect of TNFα+IFNγ or 2-APB.

Overall, the expression of these genes after treatment with TNFα+IFNγ followed the same pattern as that presented in Figure 5.1, and it was statistically analysed using three-way ANOVA. However, the goal of this experiment was to focus on the effect of 2-APB, so only this will be discussed in detail in this section. No major effects of 2-APB treatment were observed in untreated or TNFα+IFNγ-treated cells in the expression of either of the genes analysed at 72h and 7 days, there were only some small, not statistically significant effects. After 72h, *ITPR1* expression was slightly lower in *GBA-N370S* iASTROs treated with TNFα+IFNγ+2-APB compared to TNFα+IFNγ (Figure S.2 A). Expression of *ITPR3* was lower in *GBA-N370S* iASTROs after 72h treatment with TNFα+IFNγ+2-APB compared to TNFα+IFNγ, whereas by 7 days it was higher in both iASTRO populations treated with TNFα+IFNγ+2-APB compared to

TNFα+IFNγ (Figure S.2 C). In *GBA-N370S* iASTROs, after 72h, *ORAI1* expression was lower in TNFα+IFNγ+2-APB treated cells compared to TNFα+IFNγ, whereas by 7 days this pattern was reversed (Figure S.2 D). Lastly, *STIM1* expression levels were slightly lower in *GBA-N370S* iASTROs treated for 72h with TNFα+IFNγ+2-APB compared to 2-APB or TNFα+IFNγ (Figure S.2 E).

All in all, these results show that, at 25 µM, 2-APB by itself does not significantly alter the expression of *ITPR1/2/3, ORAI1* or *STIM1*, as the small differences observed in some cases between cells treated with TNFα+IFNγ+2-APB vs TNFα+IFNγ are not statistically significant.

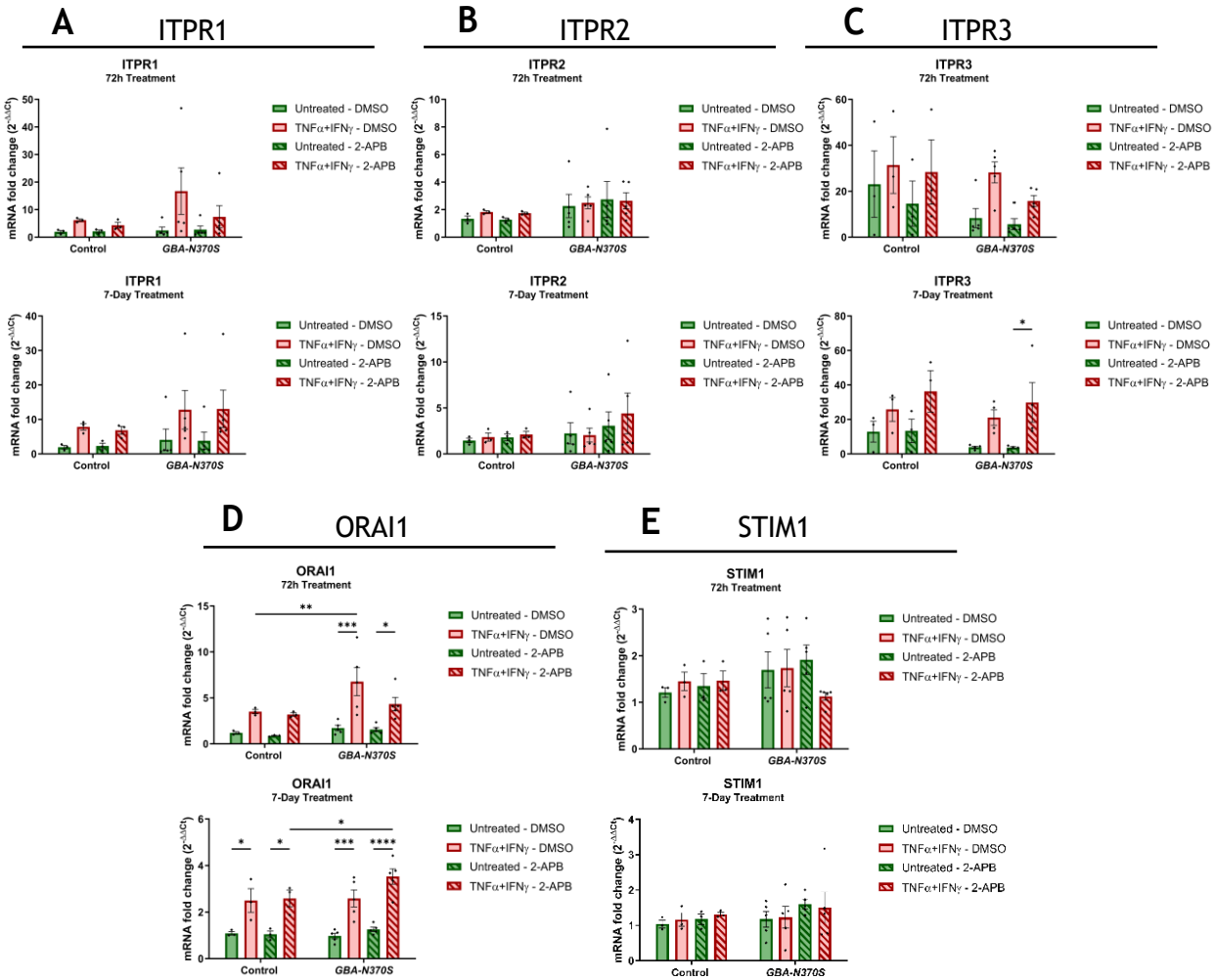


Figure S.2. The ITPR blocker 2-APB does not alter the expression changes of various calcium channels in iASTROs, with or without combined treatment with TNFα+IFNγ

(A-E) Relative gene expression analysis by RT-qPCR of (A) ITPR1, (B) ITPR2, (C) ITPR3, (D) ORAI1, and (E) STIM1 in control and *GBA-N370S* iASTROs treated for 24h or 7 days with 25 µM 2-APB, 30 ng/mL TNFα + 50 ng/mL IFNγ, or 25 µM 2-APB+30 ng/mL TNFα + 50 ng/mL IFNγ. In each differentiation, to calculate ΔΔCt for each gene, the ΔCt of one untreated control iASTRO line was subtracted to the ΔCt of each line (for the gene of interest). Each data point represents 1 iASTRO line averaged across differentiations. N = 3 control and 5 *GBA-N370S* lines, 2-3 differentiations. Mean ± SEM. The statistical

analysis performed was two-way ANOVA with Tukey's multiple comparison test. *p<0.05, **p<0.01, ***p<0.001, ****p<0.0001. Three-way ANOVA was also performed to calculate the overall effect of 2-APB or TNFα + IFNγ, and results of this statistical analysis are described in the text body.

S.1.2. Effects of 2-APB treatment on iASTRO reactivity

I then explored how partially blocking ER-calcium release with 2-APB might affect iASTRO reactivity, focusing on the immunocytochemical parameters and genes known to be altered in iASTROs treated with TNFα+IFNγ (chapter 4). First, control and *GBA-N370S* iASTROs were treated for 24h, 72h or 7 days with 30 ng/mL TNFα + 50 ng/mL IFNγ, 25 µM 2-APB, or 30 ng/mL TNFα + 50 ng/mL IFNγ + 25 µM 2-APB and stained for S100B, GFAP, C3 and NFκB (Figure S.3). DMSO was added to the conditions without 2-APB as a control.

Overall, very minor effects were observed in any of the measured parameters after treatment with 2-APB, as measured by three-way ANOVA. For instance, GFAP intensity was higher after 24h with 2-APB (three-way ANOVA effect of 2-APB: p=0.01) (Figure S.4 D), and the same was observed in S100B intensity after 24h with 2-APB (three-way ANOVA analysis of the effect of 2-APB: p=0.0182) (Figure S.4 E). Interestingly, even if TNFα+IFNγ treatment induced similar changes in all these parameters as those presented in Figures 4.10 and 4.16, a higher GFAP and S100B intensity were observed in *GBA-N370S* iASTROs compared to control iASTROs, especially at the 24h and 72h treatment, and this effect was not observed in the previous experiments. Therefore, the fact that the only changes due to 2-APB treatment were also detected in GFAP and S100B intensities might indicate that these differences are technical rather than phenotypic. On another note, elevated cytoplasmic and nuclear NFκB intensities were observed in control iASTROs compared to *GBA-N370S* iASTROs, but there were no changes due to 2-APB treatment (Figure S.4 G-H).

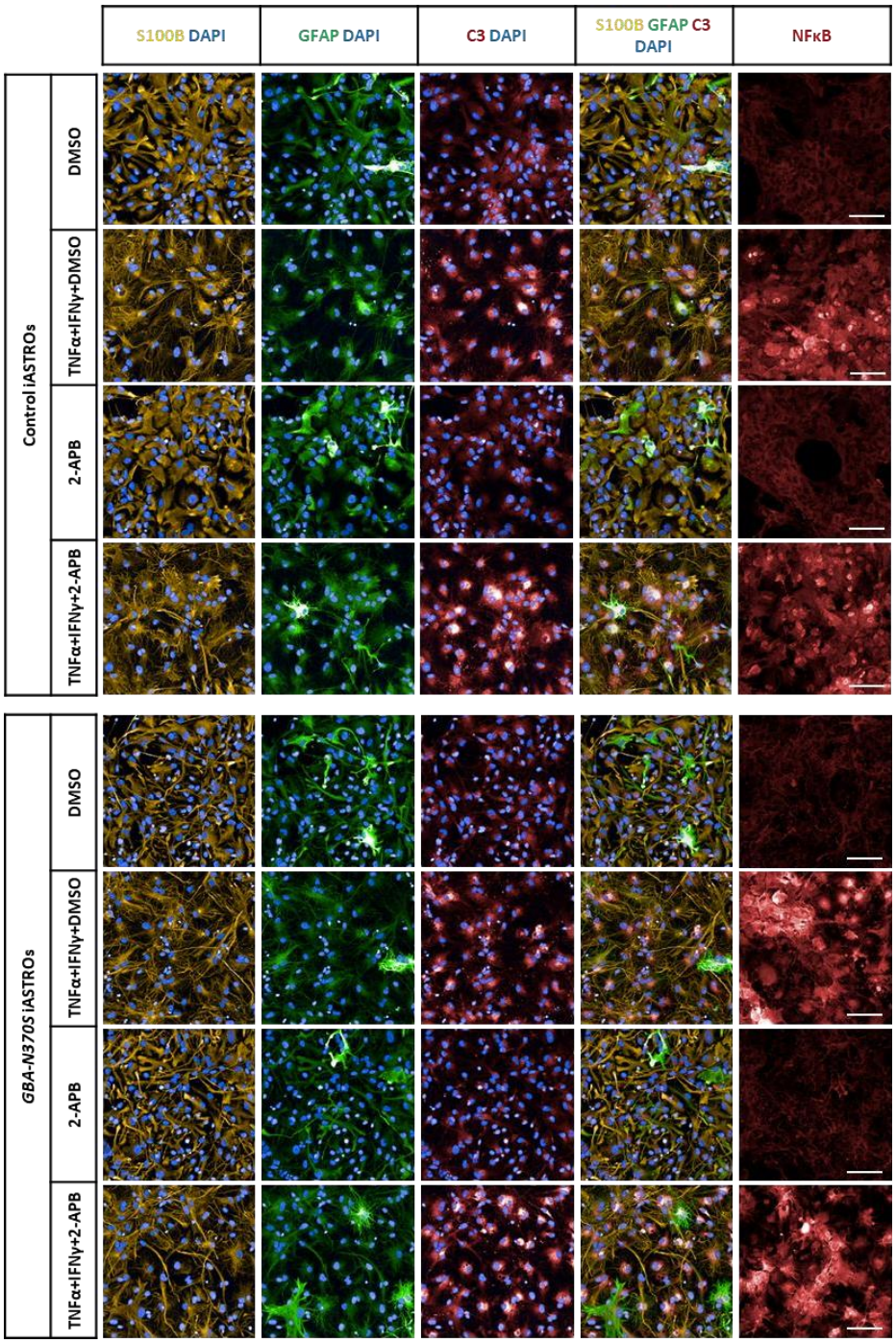
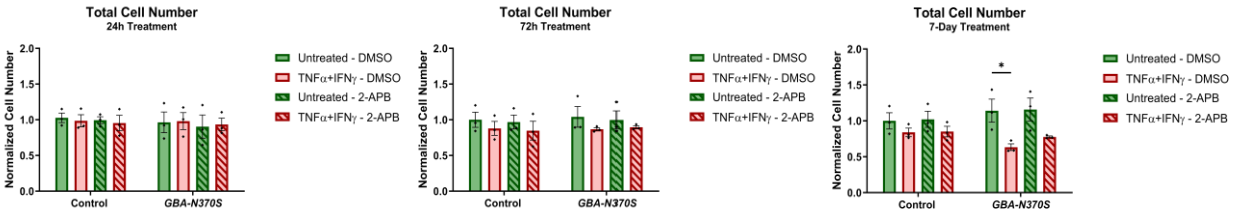


Figure S.3. Representative immunocytochemistry images of control (top panel) and *GBA-N370S* (bottom panel) iASTROs treated for 72h with different cytokines

25 µM 2-APB, 30 ng/mL TNFα + 50 ng/mL IFNγ or 25 µM 2-APB + 30 ng/mL TNFα + 50 ng/mL IFNγ, and stained for S100B (yellow), GFAP (green), NFκB (red, third and fourth columns) and C3 (red, fifth column). Scale bar: 100 µm.

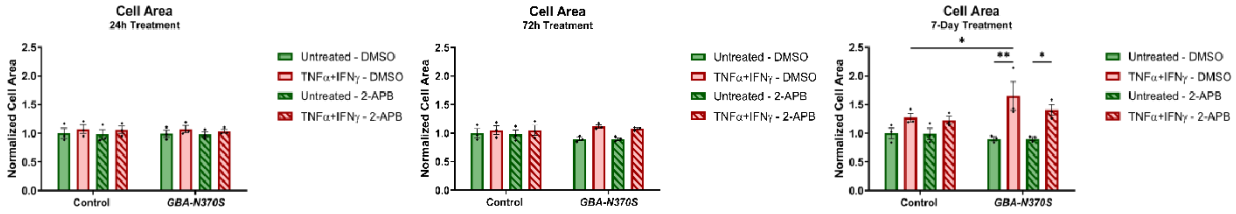
A

Total cell number



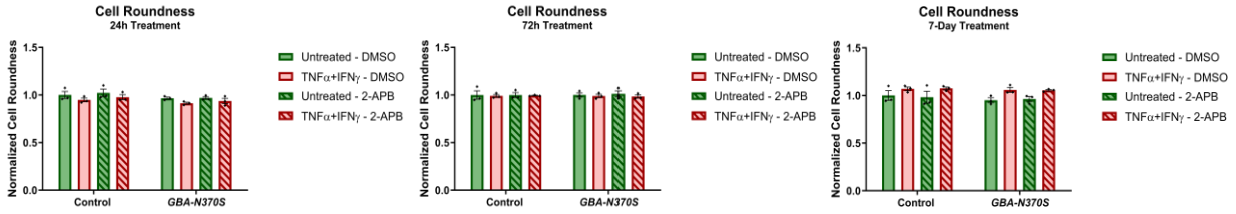
B

Cell Area



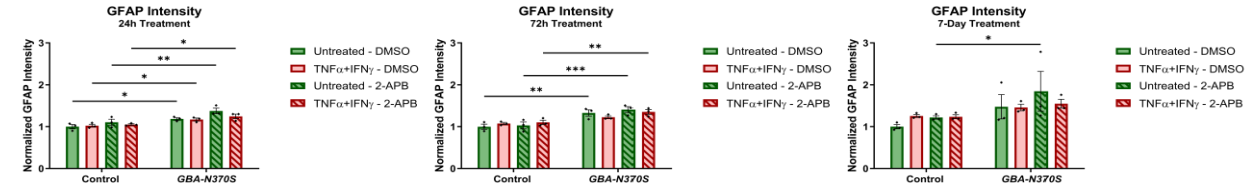
C

Cell Roundness



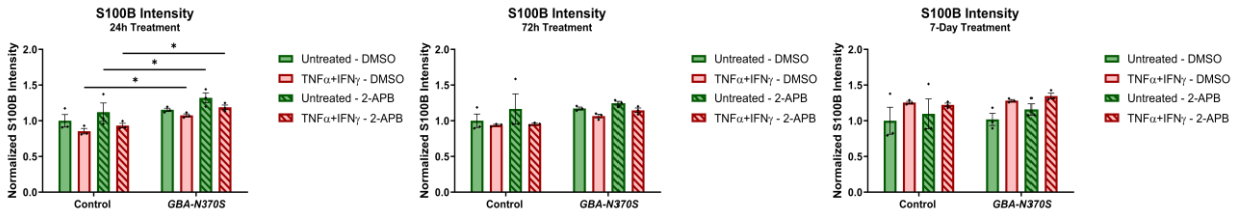
D

GFAP Intensity



E

S100B Intensity



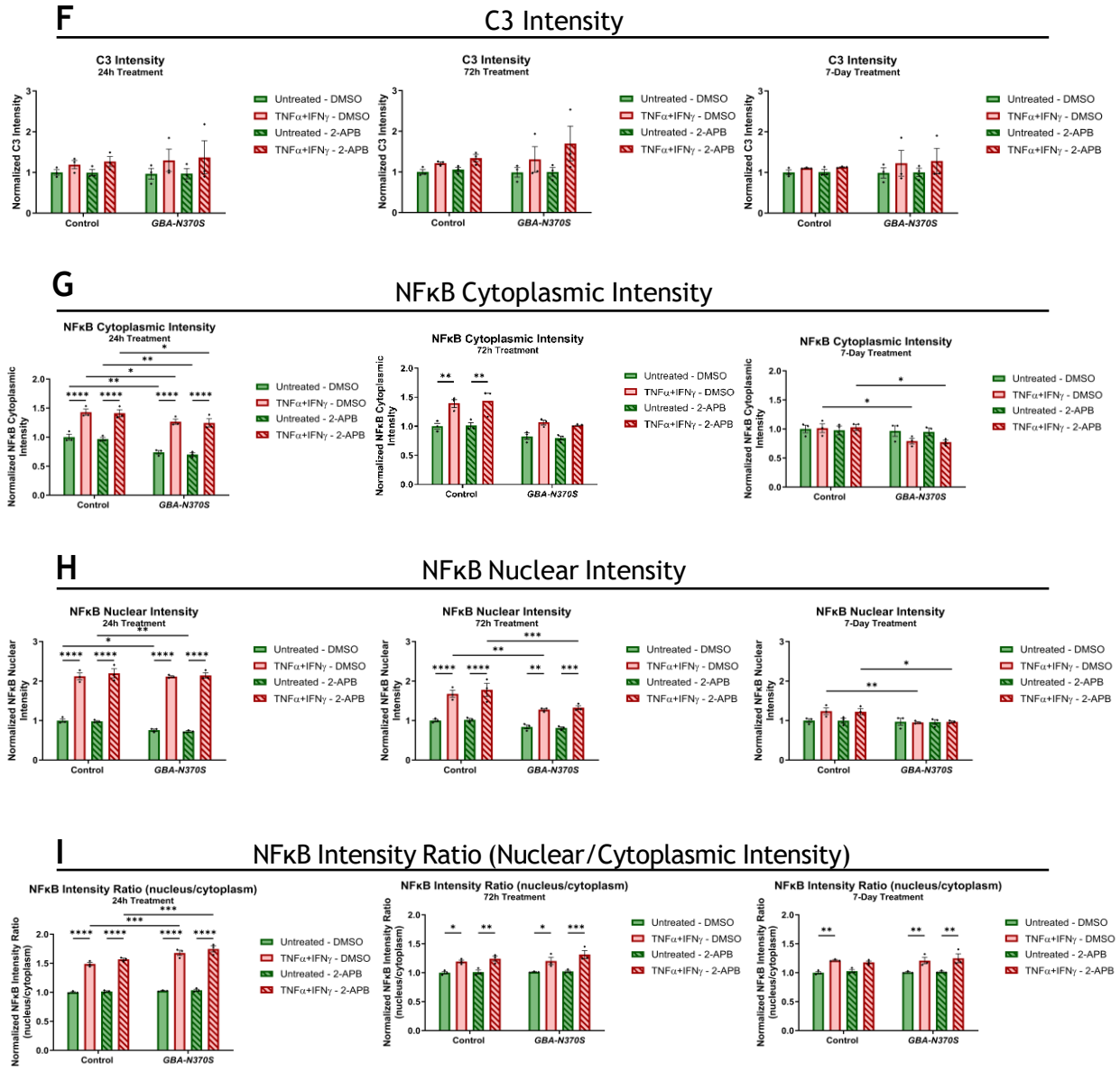


Figure S.4. The ITPR blocker 2-APB does not affect the reactive response of iASTROs to TNFα+IFNγ

(A-I) Quantification of (A) the total live cell number, (B) the cell area, (C) the cell roundness, (D) the cytoplasmic intensity of GFAP, (E) the cytoplasmic intensity of S100B, (F) the cytoplasmic intensity of C3, (G) the cytoplasmic intensity of NFκB, (H) the nuclear intensity of NFκB and (I) the NFκB intensity ratio (calculated by dividing the mean intensity in the nucleus by the mean intensity in the cytoplasm) in control and *GBA-N370S* iASTROs treated for 24h, 72h or 7 days with 25 µM 2-APB, 30 ng/mL TNFα + 50 ng/mL IFNγ, or 25 µM 2-APB+30 ng/mL TNFα + 50 ng/mL IFNγ. To obtain normalized values, in each timepoint, measured values were normalized to the average value of untreated control iASTROs. Each data point represents 1 iASTRO line averaged across differentiations. N = 3 control and 3 *GBA-N370S* lines, 3 differentiations. Mean ± SEM. The statistical analysis performed was two-way ANOVA with Tukey's multiple comparison test. *p<0.05, **p<0.01, ***p<0.001, ****p<0.0001. Three-way ANOVA was also performed to calculate the overall effect of 2-APB or TNFα + IFNγ, and the results of this statistical analysis are described in the text body.

Next, I explored the expression of genes previously found to be altered in iASTROs treated with TNFα+IFNγ in control and *GBA-N370S* iASTROs treated for 72h or 7 days with 30 ng/mL TNFα + 50 ng/mL IFNγ, 25 µM 2-APB, or 30 ng/mL TNFα + 50 ng/mL IFNγ + 25 µM 2-APB. Two- and three-way ANOVA analyses were performed. Overall, the expression of these genes followed the same pattern observed previously after treatment with TNFα+IFNγ (Figure 4.8 and Figure 4.14), and thus only potential effects due to 2-APB will be discussed here. Of note, three-way ANOVA analysis showed statistically significant effects of TNFα+IFNγ on the expression of all these genes at all timepoints, except for *GDNF*. Overall, no differences in the expression of any of the genes were observed after the addition of 2-APB alone compared to untreated cells (Figure S.5), and three-way ANOVA analysis showed that there were no significant effects due to 2-APB addition.

Collectively, these results show that partially blocking ER-calcium release with 2-APB does not affect the reactive response of iASTROs to TNFα+IFNγ.

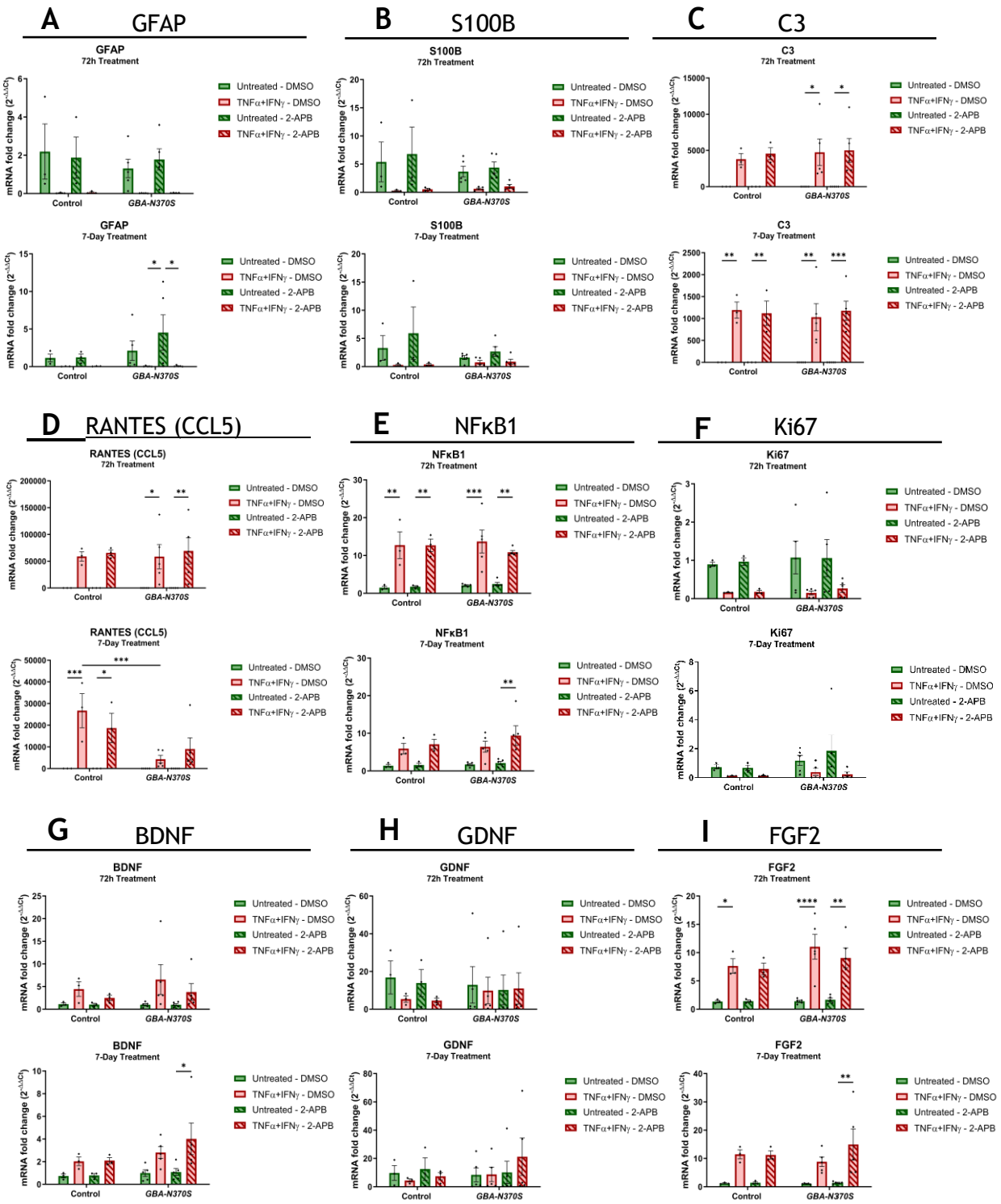


Figure S.5. The ITPR blocker 2-APB does not alter the gene expression changes of iASTROs, with or without combined treatment with TNFα+IFNγ

(A-I) Relative gene expression analysis by RT-qPCR of (A) GFAP, (B) S100B, (C) C3, (D) RANTES (CCL5), (E) NFκB1, (F) Ki67, (G) BDNF, (H) GDNF and (I) FGF2 in control and *GBA-N370S* iASTROs treated for 24h or 7 days with 25 µM 2-APB, 30 ng/mL TNFα + 50 ng/mL IFNγ, or 25 µM 2-APB+30 ng/mL TNFα + 50 ng/mL IFNγ. In each differentiation, to calculate ΔΔCt for each gene, the ΔCt of one untreated control iASTRO line was subtracted to the ΔCt of each line (for the gene of interest). Each data point represents 1 iASTRO line averaged across differentiations. N = 3 control and 5 *GBA-N370S* lines, 2-3

differentiations. Mean ± SEM. The statistical analysis performed was two-way ANOVA with Tukey's multiple comparison test. *p<0.05, **p<0.01, ***p<0.001, ****p<0.0001. Three-way ANOVA was also performed to calculate the overall effect of 2-APB or TNFα + IFNγ, and the results of this statistical analysis are described in the text body.

S.2. Studying the potential of MeTC7 to act as a blocker of VDR nuclear translocation

First, I treated iASTROs with vitamin D (100 nM), MeTC7 (250 nM), or both, for 24h, 72h and 7 days to ensure that MeTC7 successfully blocked nuclear translocation of VDR. After the initial treatment, vitamin D and MeTC7 were replenished every 2-3 days to ensure constant availability in the cells. These concentrations were chosen based on the literature and on a pilot dose-response experiment (data not shown). Two different statistical analyses were performed with the results: two-way ANOVA to compare all conditions with each other in each genotype and both genotypes in each condition, and three-way ANOVA to compare the overall effect of MeTC7 and VitD addition. The total number of live cells in the culture was not affected by any of the treatments (Figure S.6 A), suggesting that neither vitamin D nor MeTC7 affected iASTRO viability or induced proliferation. Moreover, VDR intensity in the cytoplasm was slightly increased after vitamin D treatment, and this was noticeable in *GBA-N370S* iASTROs after 24h, and in both cell populations after 72h and 7 days (three-way ANOVA of the effect of vitamin D: p=0.0213 after 72h, p=0.0093 after 7 days), whereas no effects were observed with MeTC7 administration (Figure S.6 B). The increase in nuclear VDR intensity after vitamin D administration was more apparent starting at 24h, as indicated by three-way ANOVA analysis of the effect of vitamin D on nuclear VDR intensity (p=0.0642 after 24h, p=0.0028 after 72h, p=0.0035 after 7 days) (Figure S.6 C). After 72h and 7 days of treatment with MeTC7 alone, the nuclear intensity of VDR was also higher in both iASTRO genotypes, but in cells treated with both MeTC7+vitamin D the intensity was slightly lower than in cells treated with vitamin D alone (Figure S.6 C). A similar pattern was observed in the increase in the intensity ratio of VDR, where vitamin D treatment alone caused the biggest increase, followed by vitamin D+MeTC7 and, lastly, the smallest increase with MeTC7 alone (Figure S.6 D). Three-way ANOVA analysis showed an effect of vitamin D on VDR ratio at all timepoints (p=0.0526 after 24h, p=0.0002 after 72h, p=0.015 after 7 days), but no effect of MeTC7. In summary, the increase in VDR nuclear intensity and VDR intensity ratio was higher when comparing cell

treated with vitamin D with untreated cells, than when comparing cells treated with vitamin D+MeTC7 with MeTC7-treated cells, thus indicating that MeTC7 partially blocks VDR translocation into the nucleus.

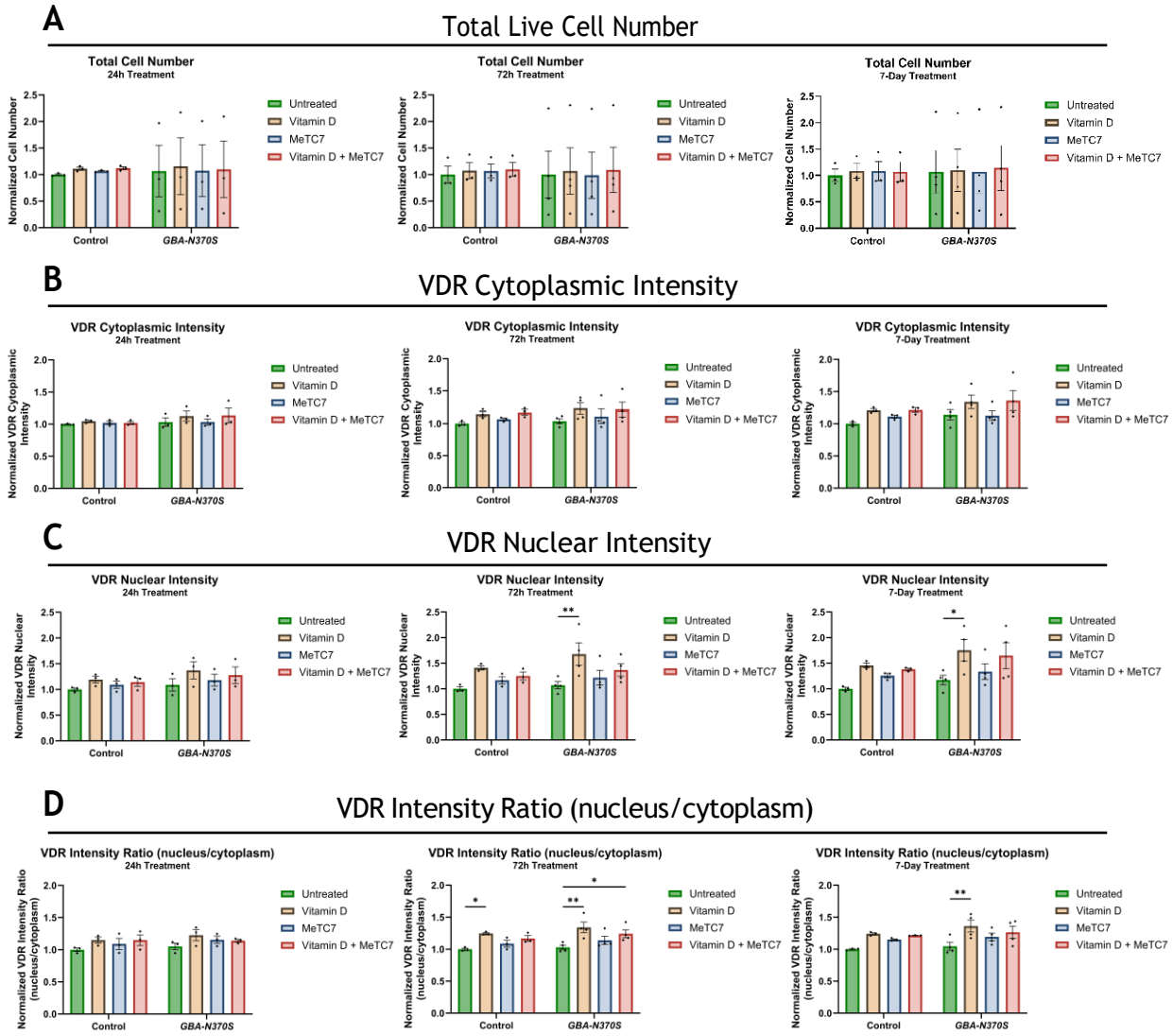


Figure S.6. Addition of vitamin D to iASTROs increases the nuclear translocation of VDR, and this is partially blocked with MeTC7, without affecting the cellular viability

(A-D) Quantification of (A) the total live cell number, (B) the cytoplasmic intensity of VDR, (C) the nuclear intensity of VDR, and (D) the VDR intensity ratio (calculated by dividing the mean VDR intensity in the nucleus by the mean VDR intensity in the cytoplasm) in control and *GBA-N370S* iASTROs treated for 24h, 72h or 7 days with 50 nM vitamin D, 100 nM MeTC7, or 50 nM vitamin D + 100 nM MeTC7. To obtain normalized values, in each timepoint, measured values were normalized to the average value of untreated control iASTROs. Each data point represents 1 iASTRO line averaged across differentiations. N = 3 control and 4 *GBA-N370S* lines, 1-3 differentiations. Mean ± SEM. The statistical analysis performed was two-way ANOVA with Tukey's multiple comparison test. *p<0.05, **p<0.01, ***p<0.001, ****p<0.0001. Three-way ANOVA was also performed to calculate the overall effect of MeTC7 or vitamin D, and the results of this statistical analysis are described in the text body.

References

Aflaki, E., Stubblefield, B. K., McGlinchey, R. P., McMahon, B., Ory, D. S., & Sidransky, E. (2020). A characterization of Gaucher iPS-derived astrocytes: Potential implications for Parkinson's disease. *Neurobiology of Disease*, *134*, 104647. https://doi.org/10.1016/j.nbd.2019.104647

Ahrens, M. B., Khakh, B. S., & Poskanzer, K. E. (2024a). Astrocyte Calcium Signaling. *Cold Spring Harbor Perspectives in Biology*, a041353. https://doi.org/10.1101/cshperspect.a041353

Ahrens, M. B., Khakh, B. S., & Poskanzer, K. E. (2024b). Astrocyte Calcium Signaling. *Cold Spring Harbor Perspectives in Biology*, a041353. https://doi.org/10.1101/cshperspect.a041353

Albini, M., Krawczun-Rygmaczewska, A., & Cesca, F. (2023). Astrocytes and brain-derived neurotrophic factor (BDNF). *Neuroscience Research*, *197*, 42–51. https://doi.org/10.1016/j.neures.2023.02.001

Alcalay, R. N., Levy, O. A., Waters, C. H., Fahn, S., Ford, B., Kuo, S.-H., Mazzoni, P., Pauciulo, M. W., Nichols, W. C., Gan-Or, Z., Rouleau, G. A., Chung, W. K., Wolf, P., Oliva, P., Keutzer, J., Marder, K., & Zhang, X. (2015). Glucocerebrosidase activity in Parkinson's disease with and without *GBA* mutations. *Brain*, *138*(9), 2648–2658. https://doi.org/10.1093/brain/awv179

Ali, N. H., Al-Kuraishy, H. M., Al-Gareeb, A. I., Alexiou, A., Papadakis, M., AlAseeri, A. A., Alruwaili, M., Saad, H. M., & Batiha, G. E. (2024). BDNF/TrkB activators in Parkinson's disease: A new therapeutic strategy. *Journal of Cellular and Molecular Medicine*, *28*(10). https://doi.org/10.1111/jcmm.18368

Alizadeh, S. D., Jalalifar, M.-R., Ghodsi, Z., Sadeghi-Naini, M., Malekzadeh, H., Rahimi, G., Mojtabavi, K., Shool, S., Eskandari, Z., Masoomi, R., Kiani, S., Harrop, J., & Rahimi-Movaghar, V. (2024). Reprogramming of astrocytes to neuronal-like cells in spinal cord injury: a systematic review. *Spinal Cord*, *62*(4), 133–142. https://doi.org/10.1038/s41393-024-00969-8

Alrouji, M., Al-Kuraishy, H. M., Al-Mahammadawy, A. A. A., Al-Gareeb, A. I., Saad, H. M., & Batiha, G. E.-S. (2023). The potential role of cholesterol in Parkinson's disease neuropathology: perpetrator or victim. *Neurological Sciences*, *44*(11), 3781–3794. https://doi.org/10.1007/s10072-023-06926-2

Álvarez-Pérez, B., Homs, J., Bosch-Mola, M., Puig, T., Reina, F., Verdú, E., & Boadas-Vaello, P. (2016). Epigallocatechin-3-gallate treatment reduces thermal hyperalgesia after spinal cord injury by down-regulating RhoA expression in mice. *European Journal of Pain*, *20*(3), 341–352. https://doi.org/10.1002/ejp.722

Anderson, J. P., Walker, D. E., Goldstein, J. M., de Laat, R., Banducci, K., Caccavello, R. J., Barbour, R., Huang, J., Kling, K., Lee, M., Diep, L., Keim, P. S., Shen, X., Chataway, T., Schlossmacher, M. G., Seubert, P., Schenk, D., Sinha, S., Gai, W. P., & Chilcote, T. J. (2006). Phosphorylation of Ser-129 Is the Dominant Pathological Modification of α-Synuclein in Familial and Sporadic Lewy Body Disease. *Journal of Biological Chemistry*, *281*(40), 29739–29752. https://doi.org/10.1074/jbc.M600933200

Araújo de Lima, L., Oliveira Cunha, P. L., Felicio Calou, I. B., Tavares Neves, K. R., Facundo, H. T., & Socorro de Barros Viana, G. (2022). Effects of vitamin D (VD3) supplementation on the brain mitochondrial function of male rats, in the 6-OHDA-induced model of Parkinson's disease. *Neurochemistry International*, *154*, 105280. https://doi.org/10.1016/j.neuint.2022.105280

Arcos, J., Grunenwald, F., Sepulveda, D., Jerez, C., Urbina, V., Huerta, T., Troncoso-Escudero, P., Tirado, D., Perez, A., Diaz-Espinoza, R., Nova, E., Kubitscheck, U., Rodriguez-Gatica, J. E., Hetz, C., Toledo, J., Ahumada, P., Rojas-Rivera, D., Martín-Montañez, E., Garcia-Fernandez, M., & Vidal, R. L. (2023). IGF2 prevents dopaminergic neuronal loss and decreases intracellular alpha-synuclein accumulation in Parkinson's disease models. *Cell Death Discovery*, *9*(1), 438. https://doi.org/10.1038/s41420-023-01734-1

Argaw, A. T., Asp, L., Zhang, J., Navrazhina, K., Pham, T., Mariani, J. N., Mahase, S., Dutta, D. J., Seto, J., Kramer, E. G., Ferrara, N., Sofroniew, M. V., & John, G. R. (2012). Astrocyte-derived VEGF-A drives blood-brain barrier disruption in CNS inflammatory disease. *Journal of Clinical Investigation*, *122*(7), 2454–2468. https://doi.org/10.1172/JCI60842

Asanuma, M., Okumura-Torigoe, N., Miyazaki, I., Murakami, S., Kitamura, Y., & Sendo, T. (2019). Region-Specific Neuroprotective Features of Astrocytes against Oxidative Stress Induced by 6-Hydroxydopamine. *International Journal of Molecular Sciences*, *20*(3), 598. https://doi.org/10.3390/ijms20030598

Ascherio, A., & Schwarzschild, M. A. (2016). The epidemiology of Parkinson's disease: risk factors and prevention. *The Lancet Neurology*, *15*(12), 1257–1272. https://doi.org/10.1016/S1474-4422(16)30230-7

Ásgrímsdóttir, E. S., & Arenas, E. (2020). Midbrain Dopaminergic Neuron Development at the Single Cell Level: In vivo and in Stem Cells. *Frontiers in Cell and Developmental Biology*, *8*. https://doi.org/10.3389/fcell.2020.00463

Badawy, M. T., Salama, A. A., & Salama, M. (2024). Novel Variants Linked to the Prodromal Stage of Parkinson's Disease (PD) Patients. *Diagnostics*, *14*(9), 929. https://doi.org/10.3390/diagnostics14090929

Bae, E.-J., Choi, M., Kim, J. T., Kim, D.-K., Jung, M. K., Kim, C., Kim, T.-K., Lee, J. S., Jung, B. C., Shin, S. J., Rhee, K. H., & Lee, S.-J. (2022). TNF-α promotes α-synuclein propagation through stimulation of senescence-associated lysosomal exocytosis. *Experimental & Molecular Medicine*, *54*(6), 788–800. https://doi.org/10.1038/s12276-022-00789-x

Baird, J. K., Bourdette, D., Meshul, C. K., & Quinn, J. F. (2019). The key role of T cells in Parkinson's disease pathogenesis and therapy. *Parkinsonism & Related Disorders*, *60*, 25–31. https://doi.org/10.1016/j.parkreldis.2018.10.029

Bancroft, E. A., & Srinivasan, R. (2022). Emerging Roles for Aberrant Astrocytic Calcium Signals in Parkinson's Disease. *Frontiers in Physiology*, *12*. https://doi.org/10.3389/fphys.2021.812212

Barbar, L., Jain, T., Zimmer, M., Kruglikov, I., Sadick, J. S., Wang, M., Kalpana, K., Rose, I. V. L., Burstein, S. R., Rusielewicz, T., Nijsure, M., Guttenplan, K. A., di Domenico, A., Croft, G., Zhang, B., Nobuta, H., Hébert, J. M., Liddelow, S. A., & Fossati, V. (2020). CD49f Is a Novel Marker of Functional and Reactive Human iPSC-Derived Astrocytes. *Neuron*, *107*(3), 436–453.e12. https://doi.org/10.1016/j.neuron.2020.05.014

Barcia, C., Ros, C. M., Annese, V., Gómez, A., Ros-Bernal, F., Aguado-Llera, D., Martínez-Pagán, M. E., de Pablos, V., Fernandez-Villalba, E., & Herrero, M. T. (2011). IFN-γ signaling, with the synergistic contribution of TNF-α, mediates cell specific microglial and astroglial activation in experimental models of Parkinson's disease. *Cell Death & Disease*, *2*(4), e142–e142. https://doi.org/10.1038/cddis.2011.17

Bardien, S., Lesage, S., Brice, A., & Carr, J. (2011). Genetic characteristics of leucine-rich repeat kinase 2 (LRRK2) associated Parkinson's disease. *Parkinsonism & Related Disorders*, *17*(7), 501–508. https://doi.org/10.1016/j.parkreldis.2010.11.008

Bartels, T., Choi, J. G., & Selkoe, D. J. (2011). α-Synuclein occurs physiologically as a helically folded tetramer that resists aggregation. *Nature*, *477*(7362), 107–110. https://doi.org/10.1038/nature10324

Basurco, L., Abellanas, M. A., Ayerra, L., Conde, E., Vinueza-Gavilanes, R., Luquin, E., Vales, A., Vilas, A., Martin-Uriz, P. S., Tamayo, I., Alonso, M. M., Hernaez, M., Gonzalez-Aseguinolaza, G., Clavero, P., Mengual, E., Arrasate, M., Hervás-Stubbs, S., & Aymerich, M. S. (2023). Microglia and astrocyte activation is region-dependent in the α-synuclein mouse model of Parkinson's disease. *Glia*, *71*(3), 571–587. https://doi.org/10.1002/glia.24295

Bayati, A., Banks, E., Han, C., Luo, W., Reintsch, W. E., Zorca, C. E., Shlaifer, I., Del Cid Pellitero, E., Vanderperre, B., McBride, H. M., Fon, E. A., Durcan, T. M., & McPherson, P. S. (2022). Rapid macropinocytic transfer of α-synuclein to lysosomes. *Cell Reports*, *40*(3), 111102. https://doi.org/10.1016/j.celrep.2022.111102

Beccano-Kelly, D. A., Cherubini, M., Mousba, Y., Cramb, K. M. L., Giussani, S., Caiazza, M. C., Rai, P., Vingill, S., Bengoa-Vergniory, N., Ng, B., Corda, G., Banerjee, A., Vowles, J., Cowley, S., & Wade-Martins, R. (2023). Calcium dysregulation combined with mitochondrial failure and electrophysiological maturity converge in Parkinson's iPSC-dopamine neurons. *IScience*, *26*(7), 107044. https://doi.org/10.1016/j.isci.2023.107044

Ben Haim, L., Carrillo-de Sauvage, M.-A., CeyzÃ©riat, K., & Escartin, C. (2015). Elusive roles for reactive astrocytes in neurodegenerative diseases. *Frontiers in Cellular Neuroscience*, *9*. https://doi.org/10.3389/fncel.2015.00278

Bengoa-Vergniory, N., Roberts, R. F., Wade-Martins, R., & Alegre-Abarrategui, J. (2017). Alpha-synuclein oligomers: a new hope. *Acta Neuropathologica*, *134*(6), 819–838. https://doi.org/10.1007/s00401-017-1755-1

Ben-Shlomo, Y., Darweesh, S., Llibre-Guerra, J., Marras, C., San Luciano, M., & Tanner, C. (2024). The epidemiology of Parkinson's disease. *The Lancet*, *403*(10423), 283–292. https://doi.org/10.1016/S0140-6736(23)01419-8

Berridge, M. J. (2017). Vitamin D deficiency accelerates ageing and age-related diseases: a novel hypothesis. *The Journal of Physiology*, *595*(22), 6825–6836. https://doi.org/10.1113/JP274887

Bird, G. S., DeHaven, W. I., Smyth, J. T., & Putney, J. W. (2008). Methods for studying store-operated calcium entry. *Methods*, *46*(3), 204–212. https://doi.org/10.1016/j.ymeth.2008.09.009

Birla, H., Xia, J., Gao, X., Zhao, H., Wang, F., Patel, S., Amponsah, A., Bekker, A., Tao, Y.-X., & Hu, H. (2022). Toll-like receptor 4 activation enhances Orai1-mediated calcium signal promoting cytokine production in spinal astrocytes. *Cell Calcium*, *105*, 102619. https://doi.org/10.1016/j.ceca.2022.102619

Björklund, A., Nilsson, F., Mattsson, B., Hoban, D. B., & Parmar, M. (2022). A Combined α-Synuclein/Fibril (SynFib) Model of Parkinson-Like Synucleinopathy Targeting the Nigrostriatal Dopamine System. *Journal of Parkinson's Disease*, *12*(8), 2307–2320. https://doi.org/10.3233/JPD-223452

Bo, R.-X., Li, Y.-Y., Zhou, T.-T., Chen, N.-H., & Yuan, Y.-H. (2022). The neuroinflammatory role of glucocerebrosidase in Parkinson's disease. *Neuropharmacology*, *207*, 108964. https://doi.org/10.1016/j.neuropharm.2022.108964

Bogetofte, H., Ryan, B. J., Jensen, P., Schmidt, S. I., Vergoossen, D. L. E., Barnkob, M. B., Kiani, L. N., Chughtai, U., Heon-Roberts, R., Caiazza, M. C., McGuinness, W., Márquez-Gómez, R., Vowles, J., Bunn, F. S., Brandes, J., Kilfeather, P., Connor, J. P., Fernandes, H. J. R., Caffrey, T. M., … Wade-Martins, R. (2023). Post-translational proteomics platform identifies neurite outgrowth impairments in Parkinson's disease GBA-N370S dopamine neurons. *Cell Reports*, *42*(3), 112180. https://doi.org/10.1016/j.celrep.2023.112180

Bolam, J. P., & Pissadaki, E. K. (2012). Living on the edge with too many mouths to feed: Why dopamine neurons die. *Movement Disorders*, *27*(12), 1478–1483. https://doi.org/10.1002/mds.25135

Booth, H. D. E., Hirst, W. D., & Wade-Martins, R. (2017). The Role of Astrocyte Dysfunction in Parkinson's Disease Pathogenesis. *Trends in Neurosciences*, *40*(6), 358–370. https://doi.org/10.1016/j.tins.2017.04.001

Booth, H. D. E., Wessely, F., Connor-Robson, N., Rinaldi, F., Vowles, J., Browne, C., Evetts, S. G., Hu, M. T., Cowley, S. A., Webber, C., & Wade-Martins, R. (2019). RNA sequencing reveals MMP2 and TGFB1 downregulation in LRRK2 G2019S Parkinson's iPSC-derived astrocytes. *Neurobiology of Disease*, *129*, 56–66. https://doi.org/10.1016/j.nbd.2019.05.006

Braak, H., & Del Tredici, K. (2004). Poor and protracted myelination as a contributory factor to neurodegenerative disorders. *Neurobiology of Aging*, *25*(1), 19–23. https://doi.org/10.1016/j.neurobiolaging.2003.04.001

Braak, H., Sastre, M., & Del Tredici, K. (2007). Development of α-synuclein immunoreactive astrocytes in the forebrain parallels stages of intraneuronal pathology in sporadic Parkinson's disease. *Acta Neuropathologica*, *114*(3), 231–241. https://doi.org/10.1007/s00401-007-0244-3

Braak, H., Tredici, K. Del, Rüb, U., de Vos, R. A. I., Jansen Steur, E. N. H., & Braak, E. (2003). Staging of brain pathology related to sporadic Parkinson's disease. *Neurobiology of Aging*, *24*(2), 197–211. https://doi.org/10.1016/S0197-4580(02)00065-9

Bradley, R. A., Shireman, J., McFalls, C., Choi, J., Canfield, S. G., Dong, Y., Liu, K., Lisota, B., Jones, J. R., Petersen, A., Bhattacharyya, A., Palecek, S. P., Shusta, E. V., Kendziorski, C., & Zhang, S.-C. (2019). Regionally specified human pluripotent stem cell-derived astrocytes exhibit different molecular signatures and functional properties. *Development*. https://doi.org/10.1242/dev.170910

Braidy, N., Gai, W.-P., Xu, Y. H., Sachdev, P., Guillemin, G. J., Jiang, X.-M., Ballard, J. W. O., Horan, M. P., Fang, Z. M., Chong, B. H., & Chan, D. Y. (2013). Uptake and mitochondrial dysfunction of alpha-synuclein in human astrocytes, cortical neurons and fibroblasts. *Translational Neurodegeneration*, *2*(1), 20. https://doi.org/10.1186/2047-9158-2-20

Brash-Arias, D., García, L. I., Pérez-Estudillo, C. A., Rojas-Durán, F., Aranda-Abreu, G. E., Herrera-Covarrubias, D., & Chi-Castañeda, D. (2024). The Role of Astrocytes and Alpha-Synuclein in Parkinson's Disease: A Review. *NeuroSci*, *5*(1), 71–86. https://doi.org/10.3390/neurosci5010005

Brekk, O. R., Honey, J. R., Lee, S., Hallett, P. J., & Isacson, O. (2020). Cell type-specific lipid storage changes in Parkinson's disease patient brains are recapitulated by experimental glycolipid disturbance. *Proceedings of the National Academy of Sciences*, *117*(44), 27646–27654. https://doi.org/10.1073/pnas.2003021117

Bretheau, F., Castellanos-Molina, A., Bélanger, D., Kusik, M., Mailhot, B., Boisvert, A., Vallières, N., Lessard, M., Gunzer, M., Liu, X., Boilard, É., Quan, N., & Lacroix, S. (2022). The alarmin interleukin-1α triggers secondary degeneration through reactive astrocytes and endothelium after spinal cord injury. *Nature Communications*, *13*(1), 5786. https://doi.org/10.1038/s41467-022-33463-x

Brockmann, K., Srulijes, K., Hauser, A.-K., Schulte, C., Csoti, I., Gasser, T., & Berg, D. (2011). GBA-associated PD presents with nonmotor characteristics. *Neurology*, *77*(3), 276–280. https://doi.org/10.1212/WNL.0b013e318225ab77

Brown, E. G., & Goldman, S. M. (2020). Modulation of the Microbiome in Parkinson's Disease: Diet, Drug, Stool Transplant, and Beyond. *Neurotherapeutics*, *17*(4), 1406–1417. https://doi.org/10.1007/s13311-020-00942-2

Burbulla, L. F., Song, P., Mazzulli, J. R., Zampese, E., Wong, Y. C., Jeon, S., Santos, D. P., Blanz, J., Obermaier, C. D., Strojny, C., Savas, J. N., Kiskinis, E., Zhuang, X., Krüger, R., Surmeier, D. J., & Krainc, D. (2017). Dopamine oxidation mediates mitochondrial and lysosomal dysfunction in Parkinson's disease. *Science*, *357*(6357), 1255–1261. https://doi.org/10.1126/science.aam9080

Bushong, E. A., Martone, M. E., Jones, Y. Z., & Ellisman, M. H. (2002). Protoplasmic Astrocytes in CA1 Stratum Radiatum Occupy Separate Anatomical Domains. *The Journal of Neuroscience*, *22*(1), 183–192. https://doi.org/10.1523/JNEUROSCI.22-01-00183.2002

Caiazza, M. C., Lang, C., & Wade-Martins, R. (2020). *What we can learn from iPSC-derived cellular models of Parkinson's disease* (pp. 3–25). https://doi.org/10.1016/bs.pbr.2019.11.002

Calvello, R., Cianciulli, A., Nicolardi, G., De Nuccio, F., Giannotti, L., Salvatore, R., Porro, C., Trotta, T., Panaro, M. A., & Lofrumento, D. D. (2017). Vitamin D Treatment Attenuates Neuroinflammation and Dopaminergic Neurodegeneration in an Animal Model of Parkinson's Disease, Shifting M1 to M2 Microglia Responses. *Journal of Neuroimmune Pharmacology*, *12*(2), 327–339. https://doi.org/10.1007/s11481-016-9720-7

Canals, I., Ginisty, A., Quist, E., Timmerman, R., Fritze, J., Miskinyte, G., Monni, E., Hansen, M. G., Hidalgo, I., Bryder, D., Bengzon, J., & Ahlenius, H. (2018). Rapid and efficient induction of functional astrocytes from human pluripotent stem cells. *Nature Methods*, *15*(9), 693–696. https://doi.org/10.1038/s41592-018-0103-2

Cavaliere, F., Cerf, L., Dehay, B., Ramos-Gonzalez, P., De Giorgi, F., Bourdenx, M., Bessede, A., Obeso, J. A., Matute, C., Ichas, F., & Bezard, E. (2017). In vitro α-synuclein neurotoxicity and spreading among neurons and astrocytes using Lewy body extracts from Parkinson disease brains. *Neurobiology of Disease*, *103*, 101–112. https://doi.org/10.1016/j.nbd.2017.04.011

Chambers, S. M., Fasano, C. A., Papapetrou, E. P., Tomishima, M., Sadelain, M., & Studer, L. (2009). Highly efficient neural conversion of human ES and iPS cells by dual inhibition of SMAD signaling. *Nature Biotechnology*, *27*(3), 275–280. https://doi.org/10.1038/nbt.1529

Chaudhary, H., Iyer, A., Subramaniam, V., & Claessens, M. M. A. E. (2016). α-Synuclein Oligomers Stabilize Pre-Existing Defects in Supported Bilayers and Propagate Membrane Damage in a Fractal-Like Pattern. *Langmuir*, *32*(45), 11827–11836. https://doi.org/10.1021/acs.langmuir.6b02572

Chavarría, C., Rodríguez-Bottero, S., Quijano, C., Cassina, P., & Souza, J. M. (2018). Impact of monomeric, oligomeric and fibrillar alpha-synuclein on astrocyte reactivity and toxicity to neurons. *Biochemical Journal*, *475*(19), 3153–3169. https://doi.org/10.1042/BCJ20180297

Chen, L., Xie, Z., Turkson, S., & Zhuang, X. (2015). A53T Human α-Synuclein Overexpression in Transgenic Mice Induces Pervasive Mitochondria Macroautophagy Defects Preceding Dopamine Neuron Degeneration. *The Journal of Neuroscience*, *35*(3), 890–905. https://doi.org/10.1523/JNEUROSCI.0089-14.2015

Chen, R., Gu, X., & Wang, X. (2022). α-Synuclein in Parkinson's disease and advances in detection. *Clinica Chimica Acta*, *529*, 76–86. https://doi.org/10.1016/j.cca.2022.02.006

Cheng, X.-Y., Biswas, S., Li, J., Mao, C.-J., Chechneva, O., Chen, J., Li, K., Li, J., Zhang, J.-R., Liu, C.-F., & Deng, W.-B. (2020). Human iPSCs derived astrocytes rescue rotenone-induced mitochondrial dysfunction and dopaminergic neurodegeneration in vitro by donating functional mitochondria. *Translational Neurodegeneration*, *9*(1), 13. https://doi.org/10.1186/s40035-020-00190-6

Chia, S. J., Tan, E.-K., & Chao, Y.-X. (2020). Historical Perspective: Models of Parkinson's Disease. *International Journal of Molecular Sciences*, *21*(7), 2464. https://doi.org/10.3390/ijms21072464

Choe, Y., Jo, M. G., Kim, B. G., Lee, S., Lee, B., Kim, S.-H., Seong, H., Yoo, W.-S., Kim, M., Lee, D.-K., Kim, S. J., Yun, S. P., & Kim, M. (2024). The autoimmune response induced by α-synuclein peptides drives neuronal cell death and glial cell activation. *Journal of Autoimmunity*, *147*, 103256. https://doi.org/10.1016/j.jaut.2024.103256

Choi, B.-K., Choi, M.-G., Kim, J.-Y., Yang, Y., Lai, Y., Kweon, D.-H., Lee, N. K., & Shin, Y.-K. (2013). Large α-synuclein oligomers inhibit neuronal SNARE-mediated vesicle docking. *Proceedings of the National Academy of Sciences*, *110*(10), 4087–4092. https://doi.org/10.1073/pnas.1218424110

Choi, Y. R., Kang, S.-J., Kim, J.-M., Lee, S.-J., Jou, I., Joe, E.-H., & Park, S. M. (2015). FcγRIIB mediates the inhibitory effect of aggregated α-synuclein on microglial phagocytosis. *Neurobiology of Disease*, *83*, 90–99. https://doi.org/10.1016/j.nbd.2015.08.025

Chou, T.-W., Chang, N. P., Krishnagiri, M., Patel, A. P., Lindman, M., Angel, J. P., Kung, P.-L., Atkins, C., & Daniels, B. P. (2021). Fibrillar α-synuclein induces neurotoxic astrocyte activation via RIP kinase signaling and NF-κB. *Cell Death & Disease*, *12*(8), 756. https://doi.org/10.1038/s41419-021-04049-0

Clarke, B. E., Taha, D. M., Ziff, O. J., Alam, A., Thelin, E. P., García, N. M., Helmy, A., & Patani, R. (2020). Human stem cell-derived astrocytes exhibit region-specific heterogeneity in their secretory profiles. *Brain*, *143*(10), e85–e85. https://doi.org/10.1093/brain/awaa258

Clarke, L. E., Liddelow, S. A., Chakraborty, C., Münch, A. E., Heiman, M., & Barres, B. A. (2018). Normal aging induces A1-like astrocyte reactivity. *Proceedings of the National Academy of Sciences*, *115*(8). https://doi.org/10.1073/pnas.1800165115

Cleeter, M. W. J., Chau, K.-Y., Gluck, C., Mehta, A., Hughes, D. A., Duchen, M., Wood, N. W., Hardy, J., Mark Cooper, J., & Schapira, A. H. (2013). Glucocerebrosidase inhibition causes mitochondrial dysfunction and free radical damage. *Neurochemistry International*, *62*(1), 1–7. https://doi.org/10.1016/j.neuint.2012.10.010

Colla, E., Jensen, P. H., Pletnikova, O., Troncoso, J. C., Glabe, C., & Lee, M. K. (2012). Accumulation of Toxic α-Synuclein Oligomer within Endoplasmic Reticulum Occurs in α-Synucleinopathy *In Vivo*. *The Journal of Neuroscience*, *32*(10), 3301–3305. https://doi.org/10.1523/JNEUROSCI.5368-11.2012

Connolly, B. S., & Lang, A. E. (2014). Pharmacological Treatment of Parkinson Disease. *JAMA*, *311*(16), 1670. https://doi.org/10.1001/jama.2014.3654

Contaldi, E., Magistrelli, L., & Comi, C. (2022). T Lymphocytes in Parkinson's Disease. *Journal of Parkinson's Disease*, *12*(s1), S65–S74. https://doi.org/10.3233/JPD-223152

Conway, K. A., Harper, J. D., & Lansbury, P. T. (2000). Fibrils Formed in Vitro from α-Synuclein and Two Mutant Forms Linked to Parkinson's Disease are Typical Amyloid. *Biochemistry*, *39*(10), 2552–2563. https://doi.org/10.1021/bi991447r

Crompton, L. A., McComish, S. F., Stathakos, P., Cordero-Llana, O., Lane, J. D., & Caldwell, M. A. (2021). Efficient and Scalable Generation of Human Ventral Midbrain Astrocytes from Human-Induced Pluripotent Stem Cells. *Journal of Visualized Experiments*, *176*. https://doi.org/10.3791/62095

Crompton, L. A., McComish, S. F., Steward, T. G. J., Whitcomb, D. J., Lane, J. D., & Caldwell, M. A. (2023). Human stem cell-derived ventral midbrain astrocytes exhibit a region-specific secretory profile. *Brain Communications*, *5*(2). https://doi.org/10.1093/braincomms/fcad114

Cui, X., Pelekanos, M., Burne, T. H. J., McGrath, J. J., & Eyles, D. W. (2010). Maternal vitamin D deficiency alters the expression of genes involved in dopamine specification in the developing rat mesencephalon. *Neuroscience Letters*, *486*(3), 220–223. https://doi.org/10.1016/j.neulet.2010.09.057

Dagan, E., Schlesinger, I., Ayoub, M., Mory, A., Nassar, M., Kurolap, A., Peretz-Aharon, J., & Gershoni-Baruch, R. (2015). The contribution of Niemann-Pick SMPD1 mutations to Parkinson disease in Ashkenazi Jews. *Parkinsonism & Related Disorders*, *21*(9), 1067–1071. https://doi.org/10.1016/j.parkreldis.2015.06.016

Daniele, S. G., Béraud, D., Davenport, C., Cheng, K., Yin, H., & Maguire-Zeiss, K. A. (2015). Activation of MyD88-dependent TLR1/2 signaling by misfolded α-synuclein, a protein linked to neurodegenerative disorders. *Science Signaling*, *8*(376). https://doi.org/10.1126/scisignal.2005965

Dasari, A. K. R., Sengupta, U., Viverette, E., Borgnia, M. J., Kayed, R., & Lim, K. H. (2024). Characterization of α-synuclein oligomers formed in the presence of lipid vesicles. *Biochemistry and Biophysics Reports*, *38*, 101687. https://doi.org/10.1016/j.bbrep.2024.101687

Dawson, T. M., Golde, T. E., & Lagier-Tourenne, C. (2018). Animal models of neurodegenerative diseases. *Nature Neuroscience*, *21*(10), 1370–1379. https://doi.org/10.1038/s41593-018-0236-8

Day, J. O., & Mullin, S. (2021). The Genetics of Parkinson's Disease and Implications for Clinical Practice. *Genes*, *12*(7), 1006. https://doi.org/10.3390/genes12071006

de Pins, B., Cifuentes-Díaz, C., Thamila Farah, A., López-Molina, L., Montalban, E., Sancho-Balsells, A., López, A., Ginés, S., Delgado-García, J. M., Alberch, J., Gruart, A., Girault, J.-A., & Giralt, A. (2019). Conditional BDNF delivery from astrocytes rescues memory deficits, spine density and synaptic properties in the 5xFAD mouse model of Alzheimer disease. *The Journal of Neuroscience*, 2121–18. https://doi.org/10.1523/JNEUROSCI.2121-18.2019

de Rus Jacquet, A. (2019). Preparation and Co-Culture of iPSC-Derived Dopaminergic Neurons and Astrocytes. *Current Protocols in Cell Biology*, *85*(1). https://doi.org/10.1002/cpcb.98

de Rus Jacquet, A., Alpaugh, M., Denis, H. L., Tancredi, J. L., Boutin, M., Decaestecker, J., Beauparlant, C., Herrmann, L., Saint-Pierre, M., Parent, M., Droit, A., Breton, S., & Cicchetti, F. (2023). The

contribution of inflammatory astrocytes to BBB impairments in a brain-chip model of Parkinson's disease. *Nature Communications*, *14*(1), 3651. https://doi.org/10.1038/s41467-023-39038-8

de Rus Jacquet, A., Tancredi, J. L., Lemire, A. L., DeSantis, M. C., Li, W.-P., & O'Shea, E. K. (2021). The LRRK2 G2019S mutation alters astrocyte-to-neuron communication via extracellular vesicles and induces neuron atrophy in a human iPSC-derived model of Parkinson's disease. *ELife*, *10*. https://doi.org/10.7554/eLife.73062

de Siqueira, E. A., Magalhães, E. P., de Menezes, R. R. P. P. B., Sampaio, T. L., Lima, D. B., da Silva Martins, C., Neves, K. R. T., de Castro Brito, G. A., Martins, A. M. C., & de Barros Viana, G. S. (2023). Vitamin D3 actions on astrocyte cells: A target for therapeutic strategy in Parkinson's disease? *Neuroscience Letters*, *793*, 136997. https://doi.org/10.1016/j.neulet.2022.136997

Dear, A. J., Teng, X., Ball, S. R., Lewin, J., Horne, R. I., Clow, D., Stevenson, A., Harper, N., Yahya, K., Yang, X., Brewerton, S. C., Thomson, J., Michaels, T. C. T., Linse, S., Knowles, T. P. J., Habchi, J., & Meisl, G. (2024). Molecular mechanism of α-synuclein aggregation on lipid membranes revealed. *Chemical Science*, *15*(19), 7229–7242. https://doi.org/10.1039/D3SC05661A

Deas, E., Cremades, N., Angelova, P. R., Ludtmann, M. H. R., Yao, Z., Chen, S., Horrocks, M. H., Banushi, B., Little, D., Devine, M. J., Gissen, P., Klenerman, D., Dobson, C. M., Wood, N. W., Gandhi, S., & Abramov, A. Y. (2016). Alpha-Synuclein Oligomers Interact with Metal Ions to Induce Oxidative Stress and Neuronal Death in Parkinson's Disease. *Antioxidants & Redox Signaling*, *24*(7), 376–391. https://doi.org/10.1089/ars.2015.6343

Delamarre, A., & Meissner, W. G. (2017). Epidemiology, environmental risk factors and genetics of Parkinson's disease. *La Presse Médicale*, *46*(2), 175–181. https://doi.org/10.1016/j.lpm.2017.01.001

Detopoulou, P., Voulgaridou, G., Saridaki, A., Pylarinou, I., Argyris, E.-M., Dedes, V., Giaginis, C., Panoutsopoulos, G. I., & Papadopoulou, S. K. (2023). Vitamin D in Parkinson's disease: A systematic review of randomized controlled trials. *Clinical Nutrition Open Science*, *52*, 1–13. https://doi.org/10.1016/j.nutos.2023.09.005

di Domenico, A., Carola, G., Calatayud, C., Pons-Espinal, M., Muñoz, J. P., Richaud-Patin, Y., Fernandez-Carasa, I., Gut, M., Faella, A., Parameswaran, J., Soriano, J., Ferrer, I., Tolosa, E., Zorzano, A., Cuervo, A. M., Raya, A., & Consiglio, A. (2019). Patient-Specific iPSC-Derived Astrocytes Contribute to Non-Cell-Autonomous Neurodegeneration in Parkinson's Disease. *Stem Cell Reports*, *12*(2), 213–229. https://doi.org/10.1016/j.stemcr.2018.12.011

Di Maio, R., Barrett, P. J., Hoffman, E. K., Barrett, C. W., Zharikov, A., Borah, A., Hu, X., McCoy, J., Chu, C. T., Burton, E. A., Hastings, T. G., & Greenamyre, J. T. (2016). α-Synuclein binds to TOM20 and inhibits mitochondrial protein import in Parkinson's disease. *Science Translational Medicine*, *8*(342). https://doi.org/10.1126/scitranslmed.aaf3634

Ding, M.-Y., Peng, Y., Li, F., Li, Z.-Q., Wang, D., Zhou, G.-C., & Wang, Y. (2021). Andrographolide derivative as antagonist of vitamin D receptor to induce lipidation of microtubule associate protein 1 light chain 3 (LC3). *Bioorganic & Medicinal Chemistry*, *51*, 116505. https://doi.org/10.1016/j.bmc.2021.116505

Ding, Z.-B., Song, L.-J., Wang, Q., Kumar, G., Yan, Y.-Q., & Ma, C.-G. (2021). Astrocytes: a double-edged sword in neurodegenerative diseases. *Neural Regeneration Research*, *16*(9), 1702. https://doi.org/10.4103/1673-5374.306064

Diniz, L. P., Matias, I., Araujo, A. P. B., Garcia, M. N., Barros-Aragão, F. G. Q., Alves-Leon, S. V., de Souza, J. M., Foguel, D., Figueiredo, C. P., Braga, C., Romão, L., & Gomes, F. C. A. (2019). α-synuclein oligomers enhance astrocyte-induced synapse formation through TGF-β1 signaling in a Parkinson's disease model. *Journal of Neurochemistry*, *150*(2), 138–157. https://doi.org/10.1111/jnc.14710

Dodel, R., Tinelli, M., Deuschl, G., Petersen, G., Oertel, W., & Ahmerkamp-Böhme, J. (2021). The economic benefit of timely, adequate, and adherence to Parkinson's disease treatment: the Value of Treatment Project 2. *European Journal of Neurology*, *28*(2), 707–716. https://doi.org/10.1111/ene.14584

Dolatshahi, M., Ranjbar Hameghavandi, M. H., Sabahi, M., & Rostamkhani, S. (2021). Nuclear factor-kappa B (NF-κB) in pathophysiology of Parkinson disease: Diverse patterns and mechanisms contributing to neurodegeneration. *European Journal of Neuroscience*, *54*(1), 4101–4123. https://doi.org/10.1111/ejn.15242

Dong, Y., Fischer, R., Naudé, P. J. W., Maier, O., Nyakas, C., Duffey, M., Van der Zee, E. A., Dekens, D., Douwenga, W., Herrmann, A., Guenzi, E., Kontermann, R. E., Pfizenmaier, K., & Eisel, U. L. M. (2016). Essential protective role of tumor necrosis factor receptor 2 in neurodegeneration. *Proceedings of the National Academy of Sciences*, *113*(43), 12304–12309. https://doi.org/10.1073/pnas.1605195113

Doorn, K. J., Moors, T., Drukarch, B., van de Berg, W. D., Lucassen, P. J., & van Dam, A.-M. (2014). Microglial phenotypes and toll-like receptor 2 in the substantia nigra and hippocampus of incidental Lewy body disease cases and Parkinson's disease patients. *Acta Neuropathologica Communications*, *2*(1), 90. https://doi.org/10.1186/s40478-014-0090-1

Dorsey, E. R., Sherer, T., Okun, M. S., & Bloem, B. R. (2018). The Emerging Evidence of the Parkinson Pandemic. *Journal of Parkinson's Disease*, *8*(s1), S3–S8. https://doi.org/10.3233/JPD-181474

Du, F., Yu, Q., Chen, A., Chen, D., & Yan, S. S. (2018). Astrocytes Attenuate Mitochondrial Dysfunctions in Human Dopaminergic Neurons Derived from iPSC. *Stem Cell Reports*, *10*(2), 366–374. https://doi.org/10.1016/j.stemcr.2017.12.021

Du, R.-H., Zhou, Y., Xia, M.-L., Lu, M., Ding, J.-H., & Hu, G. (2018). α-Synuclein disrupts the anti-inflammatory role of Drd2 via interfering β-arrestin2-TAB1 interaction in astrocytes. *Journal of Neuroinflammation*, *15*(1), 258. https://doi.org/10.1186/s12974-018-1302-6

Duarte Azevedo, M., Sander, S., & Tenenbaum, L. (2020). GDNF, A Neuron-Derived Factor Upregulated in Glial Cells during Disease. *Journal of Clinical Medicine*, *9*(2), 456. https://doi.org/10.3390/jcm9020456

Efremova, L., Chovancova, P., Adam, M., Gutbier, S., Schildknecht, S., & Leist, M. (2017). Switching from astrocytic neuroprotection to neurodegeneration by cytokine stimulation. *Archives of Toxicology*, *91*(1), 231–246. https://doi.org/10.1007/s00204-016-1702-2

Eidson, L. N., Kannarkat, G. T., Barnum, C. J., Chang, J., Chung, J., Caspell-Garcia, C., Taylor, P., Mollenhauer, B., Schlossmacher, M. G., Ereshefsky, L., Yen, M., Kopil, C., Frasier, M., Marek, K., Hertzberg, V. S., & Tansey, M. G. (2017). Candidate inflammatory biomarkers display unique relationships with alpha-synuclein and correlate with measures of disease severity in subjects with Parkinson's disease. *Journal of Neuroinflammation*, *14*(1), 164. https://doi.org/10.1186/s12974-017-0935-1

Elsworth, J. D. (2020). Parkinson's disease treatment: past, present, and future. *Journal of Neural Transmission*, *127*(5), 785–791. https://doi.org/10.1007/s00702-020-02167-1

Escartin, C., Galea, E., Lakatos, A., O'Callaghan, J. P., Petzold, G. C., Serrano-Pozo, A., Steinhäuser, C., Volterra, A., Carmignoto, G., Agarwal, A., Allen, N. J., Araque, A., Barbeito, L., Barzilai, A., Bergles, D. E., Bonvento, G., Butt, A. M., Chen, W.-T., Cohen-Salmon, M., … Verkhratsky, A. (2021). Reactive astrocyte nomenclature, definitions, and future directions. *Nature Neuroscience*, *24*(3), 312–325. https://doi.org/10.1038/s41593-020-00783-4

Esvald, E.-E., Tuvikene, J., Kiir, C. S., Avarlaid, A., Tamberg, L., Sirp, A., Shubina, A., Cabrera-Cabrera, F., Pihlak, A., Koppel, I., Palm, K., & Timmusk, T. (2023). Revisiting the expression of BDNF and its receptors in mammalian development. *Frontiers in Molecular Neuroscience*, *16*. https://doi.org/10.3389/fnmol.2023.1182499

Eyles, D. W., Smith, S., Kinobe, R., Hewison, M., & McGrath, J. J. (2005). Distribution of the Vitamin D receptor and 1α-hydroxylase in human brain. *Journal of Chemical Neuroanatomy*, *29*(1), 21–30. https://doi.org/10.1016/j.jchemneu.2004.08.006

Fanning, S., Selkoe, D., & Dettmer, U. (2020). Parkinson's disease: proteinopathy or lipidopathy? *Npj Parkinson's Disease*, *6*(1), 3. https://doi.org/10.1038/s41531-019-0103-7

Fares, M. B., Jagannath, S., & Lashuel, H. A. (2021). Reverse engineering Lewy bodies: how far have we come and how far can we go? *Nature Reviews Neuroscience*, *22*(2), 111–131. https://doi.org/10.1038/s41583-020-00416-6

Farfel-Becker, T., Vitner, E. B., Kelly, S. L., Bame, J. R., Duan, J., Shinder, V., Merrill, A. H., Dobrenis, K., & Futerman, A. H. (2014). Neuronal accumulation of glucosylceramide in a mouse model of neuronopathic Gaucher disease leads to neurodegeneration. *Human Molecular Genetics*, *23*(4), 843–854. https://doi.org/10.1093/hmg/ddt468

Farooqui, A. A. (2022). Contribution of neuroinflammation, resolution, and neuroprotection in neurodegenerative diseases. In *Neuroinflammation, Resolution, and Neuroprotection in the Brain* (pp. 121–160). Elsevier. https://doi.org/10.1016/B978-0-323-88460-0.00010-2

Fearnley, J. M., & Lees, A. J. (1991). Ageing and Parkinson's disease: substantia nigra regional selectivity. *Brain*, *114*(5), 2283–2301. https://doi.org/10.1093/brain/114.5.2283

Fecchio, C., De Franceschi, G., Relini, A., Greggio, E., Dalla Serra, M., Bubacco, L., & Polverino de Laureto, P. (2013). α-Synuclein Oligomers Induced by Docosahexaenoic Acid Affect Membrane Integrity. *PLoS ONE*, *8*(11), e82732. https://doi.org/10.1371/journal.pone.0082732

Fedele, S., Collo, G., Behr, K., Bischofberger, J., Müller, S., Kunath, T., Christensen, K., Gündner, A. L., Graf, M., Jagasia, R., & Taylor, V. (2017). Expansion of human midbrain floor plate progenitors from induced pluripotent stem cells increases dopaminergic neuron differentiation potential. *Scientific Reports*, *7*(1), 6036. https://doi.org/10.1038/s41598-017-05633-1

Fellner, L., Irschick, R., Schanda, K., Reindl, M., Klimaschewski, L., Poewe, W., Wenning, G. K., & Stefanova, N. (2013). Toll-like receptor 4 is required for α-synuclein dependent activation of microglia and astroglia. *Glia*, *61*(3), 349–360. https://doi.org/10.1002/glia.22437

Fernandes, H. J. R., Hartfield, E. M., Christian, H. C., Emmanoulidou, E., Zheng, Y., Booth, H., Bogetofte, H., Lang, C., Ryan, B. J., Sardi, S. P., Badger, J., Vowles, J., Evetts, S., Tofaris, G. K., Vekrellis, K., Talbot, K., Hu, M. T., James, W., Cowley, S. A., & Wade-Martins, R. (2016). ER Stress and

Autophagic Perturbations Lead to Elevated Extracellular α-Synuclein in GBA-N370S Parkinson's iPSC-Derived Dopamine Neurons. *Stem Cell Reports*, *6*(3), 342–356. https://doi.org/10.1016/j.stemcr.2016.01.013

Filippini, A., Mutti, V., Faustini, G., Longhena, F., Ramazzina, I., Rizzi, F., Kaganovich, A., Roosen, D. A., Landeck, N., Duffy, M., Tessari, I., Bono, F., Fiorentini, C., Greggio, E., Bubacco, L., Bellucci, A., Missale, M., Cookson, M. R., Gennarelli, M., & Russo, I. (2021). Extracellular clusterin limits the uptake of α-synuclein fibrils by murine and human astrocytes. *Glia*, *69*(3), 681–696. https://doi.org/10.1002/glia.23920

Fiore, N. J., Ganat, Y. M., Devkota, K., Batorsky, R., Lei, M., Lee, K., Cowen, L. J., Croft, G., Noggle, S. A., Nieland, T. J. F., & Kaplan, D. L. (2022). Bioengineered models of Parkinson's disease using patient-derived dopaminergic neurons exhibit distinct biological profiles in a 3D microenvironment. *Cellular and Molecular Life Sciences*, *79*(2), 78. https://doi.org/10.1007/s00018-021-04047-7

Fleet, J. C. (2017). The role of vitamin D in the endocrinology controlling calcium homeostasis. *Molecular and Cellular Endocrinology*, *453*, 36–45. https://doi.org/10.1016/j.mce.2017.04.008

Foehring, R. C., Zhang, X. F., Lee, J. C. F., & Callaway, J. C. (2009). Endogenous Calcium Buffering Capacity of Substantia Nigral Dopamine Neurons. *Journal of Neurophysiology*, *102*(4), 2326–2333. https://doi.org/10.1152/jn.00038.2009

Forno, L. S., DeLanney, L. E., Irwin, I., Monte, D. Di, & Langston, J. W. (1992). *Chapter 36: Astrocytes and Parkinson's disease* (pp. 429–436). https://doi.org/10.1016/S0079-6123(08)61770-7

Friederich, A., Flinspach, A., Suenkel, U., Eschweiler, G. W., Greulich, K., Maetzler, W., Berg, D., & Heinzel, S. (2019). Prodromal features of Parkinson's disease: Self-reported symptoms versus clinically assessed signs. *Movement Disorders*, *34*(1), 144–146. https://doi.org/10.1002/mds.27539

Fujita, K., Peng, S., Ma, Y., Tang, C. C., Hellman, M., Feigin, A., Eidelberg, D., & Dhawan, V. (2021). Blood–brain barrier permeability in Parkinson's disease patients with and without dyskinesia. *Journal of Neurology*, *268*(6), 2246–2255. https://doi.org/10.1007/s00415-021-10411-1

Furman, I., Baudet, C., & Brachet, P. (1996). Differential expression of M-CSF, LIF, and TNF-? genes in normal and malignant rat glial cells: Regulation by lipopolysaccharide and vitamin D. *Journal of Neuroscience Research*, *46*(3), 360–366. https://doi.org/10.1002/(SICI)1097-4547(19961101)46:3<360::AID-JNR9>3.0.CO;2-I

Galiano-Landeira, J., Torra, A., Vila, M., & Bové, J. (2020). CD8 T cell nigral infiltration precedes synucleinopathy in early stages of Parkinson's disease. *Brain*, *143*(12), 3717–3733. https://doi.org/10.1093/brain/awaa269

Galper, J., Dean, N. J., Pickford, R., Lewis, S. J. G., Halliday, G. M., Kim, W. S., & Dzamko, N. (2022). Lipid pathway dysfunction is prevalent in patients with Parkinson's disease. *Brain*, *145*(10), 3472–3487. https://doi.org/10.1093/brain/awac176

Ganguly, U., Singh, S., Pal, S., Prasad, S., Agrawal, B. K., Saini, R. V., & Chakrabarti, S. (2021). Alpha-Synuclein as a Biomarker of Parkinson's Disease: Good, but Not Good Enough. *Frontiers in Aging Neuroscience*, *13*. https://doi.org/10.3389/fnagi.2021.702639

Gao, J., Perera, G., Bhadbhade, M., Halliday, G. M., & Dzamko, N. (2019). Autophagy activation promotes clearance of α-synuclein inclusions in fibril-seeded human neural cells. *Journal of Biological Chemistry*, *294*(39), 14241–14256. https://doi.org/10.1074/jbc.RA119.008733

Gao, X., Xia, J., Munoz, F. M., Manners, M. T., Pan, R., Meucci, O., Dai, Y., & Hu, H. (2016). STIMs and Orai1 regulate cytokine production in spinal astrocytes. *Journal of Neuroinflammation*, *13*(1), 126. https://doi.org/10.1186/s12974-016-0594-7

Garcia-Abreu, J., Neto, V. M., Carvalho, S. L., & Cavalcante, L. A. (1995). Regionally specific properties of midbrain glia: I. Interactions with midbrain neurons. *Journal of Neuroscience Research*, *40*(4), 471–477. https://doi.org/10.1002/jnr.490400406

Garcion, E., Sindji, L., Leblondel, G., Brachet, P., & Darcy, F. (1999). 1,25-Dihydroxyvitamin D3 Regulates the Synthesis of γ-Glutamyl Transpeptidase and Glutathione Levels in Rat Primary Astrocytes. *Journal of Neurochemistry*, *73*(2), 859–866. https://doi.org/10.1046/j.1471-4159.1999.0730859.x

Garg, S. K., Kipnis, J., & Banerjee, R. (2009). IFN-γ and IL-4 differentially shape metabolic responses and neuroprotective phenotype of astrocytes. *Journal of Neurochemistry*, *108*(5), 1155–1166. https://doi.org/10.1111/j.1471-4159.2009.05872.x

Gate, D., Tapp, E., Leventhal, O., Shahid, M., Nonninger, T. J., Yang, A. C., Strempfl, K., Unger, M. S., Fehlmann, T., Oh, H., Channappa, D., Henderson, V. W., Keller, A., Aigner, L., Galasko, D. R., Davis, M. M., Poston, K. L., & Wyss-Coray, T. (2021). CD4 + T cells contribute to neurodegeneration in Lewy body dementia. *Science*, *374*(6569), 868–874. https://doi.org/10.1126/science.abf7266

Gatto, N., Dos Santos Souza, C., Shaw, A. C., Bell, S. M., Myszczynska, M. A., Powers, S., Meyer, K., Castelli, L. M., Karyka, E., Mortiboys, H., Azzouz, M., Hautbergue, G. M., Márkus, N. M., Shaw, P. J., & Ferraiuolo, L. (2021). Directly converted astrocytes retain the ageing features of the donor fibroblasts and elucidate the astrocytic contribution to human CNS health and disease. *Aging Cell*, *20*(1). https://doi.org/10.1111/acel.13281

Gegg, M. E., Burke, D., Heales, S. J. R., Cooper, J. M., Hardy, J., Wood, N. W., & Schapira, A. H. V. (2012). Glucocerebrosidase deficiency in substantia nigra of parkinson disease brains. *Annals of Neurology*, *72*(3), 455–463. https://doi.org/10.1002/ana.23614

Gegg, M. E., Menozzi, E., & Schapira, A. H. V. (2022). Glucocerebrosidase-associated Parkinson disease: Pathogenic mechanisms and potential drug treatments. *Neurobiology of Disease*, *166*, 105663. https://doi.org/10.1016/j.nbd.2022.105663

Geng, X., Zou, Y., Li, J., Li, S., Qi, R., Yu, H., & Zhong, L. (2023). BDNF alleviates Parkinson's disease by promoting STAT3 phosphorylation and regulating neuronal autophagy. *Cell and Tissue Research*, *393*(3), 455–470. https://doi.org/10.1007/s00441-023-03806-1

Gerhard, A., Pavese, N., Hotton, G., Turkheimer, F., Es, M., Hammers, A., Eggert, K., Oertel, W., Banati, R. B., & Brooks, D. J. (2006). In vivo imaging of microglial activation with [11C](R)-PK11195 PET in idiopathic Parkinson's disease. *Neurobiology of Disease*, *21*(2), 404–412. https://doi.org/10.1016/j.nbd.2005.08.002

Giasson, B. I., Murray, I. V. J., Trojanowski, J. Q., & Lee, V. M.-Y. (2001). A Hydrophobic Stretch of 12 Amino Acid Residues in the Middle of α-Synuclein Is Essential for Filament Assembly. *Journal of Biological Chemistry*, *276*(4), 2380–2386. https://doi.org/10.1074/jbc.M008919200

Gilmozzi, V., Gentile, G., Castelo Rueda, M. P., Hicks, A. A., Pramstaller, P. P., Zanon, A., Lévesque, M., & Pichler, I. (2020). Interaction of Alpha-Synuclein With Lipids: Mitochondrial Cardiolipin as a Critical Player in the Pathogenesis of Parkinson's Disease. *Frontiers in Neuroscience*, *14*. https://doi.org/10.3389/fnins.2020.578993

Giordano, A. M. S., Abou Alezz, M., Merelli, I., & Kajaste-Rudnitski, A. (2023). Protocol to differentiate monolayer human induced pluripotent stem cells into inflammatory responsive astrocytes. *STAR Protocols*, *4*(1), 102142. https://doi.org/10.1016/j.xpro.2023.102142

Giralt, A., Friedman, H. C., Caneda-Ferrón, B., Urbán, N., Moreno, E., Rubio, N., Blanco, J., Peterson, A., Canals, J. M., & Alberch, J. (2010). BDNF regulation under GFAP promoter provides engineered astrocytes as a new approach for long-term protection in Huntington's disease. *Gene Therapy*, *17*(10), 1294–1308. https://doi.org/10.1038/gt.2010.71

Golovko, M. Y., Rosenberger, T. A., Feddersen, S., Færgeman, N. J., & Murphy, E. J. (2007). α-Synuclein gene ablation increases docosahexaenoic acid incorporation and turnover in brain phospholipids. *Journal of Neurochemistry*, *101*(1), 201–211. https://doi.org/10.1111/j.1471-4159.2006.04357.x

Gonzalez-Rodriguez, P., Zampese, E., & Surmeier, D. J. (2020). *Selective neuronal vulnerability in Parkinson's disease* (pp. 61–89). https://doi.org/10.1016/bs.pbr.2020.02.005

Graves, S. M., Xie, Z., Stout, K. A., Zampese, E., Burbulla, L. F., Shih, J. C., Kondapalli, J., Patriarchi, T., Tian, L., Brichta, L., Greengard, P., Krainc, D., Schumacker, P. T., & Surmeier, D. J. (2020). Dopamine metabolism by a monoamine oxidase mitochondrial shuttle activates the electron transport chain. *Nature Neuroscience*, *23*(1), 15–20. https://doi.org/10.1038/s41593-019-0556-3

Grigor'eva, E. V., Kopytova, A. E., Yarkova, E. S., Pavlova, S. V., Sorogina, D. A., Malakhova, A. A., Malankhanova, T. B., Baydakova, G. V., Zakharova, E. Y., Medvedev, S. P., Pchelina, S. N., & Zakian, S. M. (2023). Biochemical Characteristics of iPSC-Derived Dopaminergic Neurons from N370S GBA Variant Carriers with and without Parkinson's Disease. *International Journal of Molecular Sciences*, *24*(5), 4437. https://doi.org/10.3390/ijms24054437

Grosch, J., Winkler, J., & Kohl, Z. (2016). Early Degeneration of Both Dopaminergic and Serotonergic Axons – A Common Mechanism in Parkinson's Disease. *Frontiers in Cellular Neuroscience*, *10*. https://doi.org/10.3389/fncel.2016.00293

Gu, R., Pan, J., Awan, M. U. N., Sun, X., Yan, F., Bai, L., & Bai, J. (2024). The major histocompatibility complex participates in Parkinson's disease. *Pharmacological Research*, *203*, 107168. https://doi.org/10.1016/j.phrs.2024.107168

Gu, X.-L., Long, C.-X., Sun, L., Xie, C., Lin, X., & Cai, H. (2010). Astrocytic expression of Parkinson's disease-related A53T α-synuclein causes neurodegeneration in mice. *Molecular Brain*, *3*(1), 12. https://doi.org/10.1186/1756-6606-3-12

Guedes, L. C., Chan, R. B., Gomes, M. A., Conceição, V. A., Machado, R. B., Soares, T., Xu, Y., Gaspar, P., Carriço, J. A., Alcalay, R. N., Ferreira, J. J., Outeiro, T. F., & Miltenberger-Miltenyi, G. (2017). Serum lipid alterations in GBA-associated Parkinson's disease. *Parkinsonism & Related Disorders*, *44*, 58–65. https://doi.org/10.1016/j.parkreldis.2017.08.026

Guo, J., Zhao, X., Li, Y., Li, G., & Liu, X. (2018). Damage to dopaminergic neurons by oxidative stress in Parkinson's disease (Review). *International Journal of Molecular Medicine*. https://doi.org/10.3892/ijmm.2018.3406

Gustavsson, A., Svensson, M., Jacobi, F., Allgulander, C., Alonso, J., Beghi, E., Dodel, R., Ekman, M., Faravelli, C., Fratiglioni, L., Gannon, B., Jones, D. H., Jennum, P., Jordanova, A., Jönsson, L., Karampampa, K., Knapp, M., Kobelt, G., Kurth, T., … Olesen, J. (2011). Cost of disorders of the brain in Europe 2010. *European Neuropsychopharmacology*, *21*(10), 718–779. https://doi.org/10.1016/j.euroneuro.2011.08.008

Guttenplan, K. A., Weigel, M. K., Prakash, P., Wijewardhane, P. R., Hasel, P., Rufen-Blanchette, U., Münch, A. E., Blum, J. A., Fine, J., Neal, M. C., Bruce, K. D., Gitler, A. D., Chopra, G., Liddelow, S. A., & Barres, B. A. (2021). Neurotoxic reactive astrocytes induce cell death via saturated lipids. *Nature*, *599*(7883), 102–107. https://doi.org/10.1038/s41586-021-03960-y

Guzman, J. N., Ilijic, E., Yang, B., Sanchez-Padilla, J., Wokosin, D., Galtieri, D., Kondapalli, J., Schumacker, P. T., & Surmeier, D. J. (2018). Systemic isradipine treatment diminishes calcium-dependent mitochondrial oxidant stress. *Journal of Clinical Investigation*, *128*(6), 2266–2280. https://doi.org/10.1172/JCI95898

Guzman, J. N., Sánchez-Padilla, J., Chan, C. S., & Surmeier, D. J. (2009). Robust Pacemaking in Substantia Nigra Dopaminergic Neurons. *The Journal of Neuroscience*, *29*(35), 11011–11019. https://doi.org/10.1523/JNEUROSCI.2519-09.2009

Haenseler, W., Zambon, F., Lee, H., Vowles, J., Rinaldi, F., Duggal, G., Houlden, H., Gwinn, K., Wray, S., Luk, K. C., Wade-Martins, R., James, W. S., & Cowley, S. A. (2017). Excess α-synuclein compromises phagocytosis in iPSC-derived macrophages. *Scientific Reports*, *7*(1), 9003. https://doi.org/10.1038/s41598-017-09362-3

Hafiz, A. A. (2024). The neuroprotective effect of vitamin D in Parkinson's disease: association or causation. *Nutritional Neuroscience*, *27*(8), 870–886. https://doi.org/10.1080/1028415X.2023.2259680

Hamza, T. H., Zabetian, C. P., Tenesa, A., Laederach, A., Montimurro, J., Yearout, D., Kay, D. M., Doheny, K. F., Paschall, J., Pugh, E., Kusel, V. I., Collura, R., Roberts, J., Griffith, A., Samii, A., Scott, W. K., Nutt, J., Factor, S. A., & Payami, H. (2010). Common genetic variation in the HLA region is associated with late-onset sporadic Parkinson's disease. *Nature Genetics*, *42*(9), 781–785. https://doi.org/10.1038/ng.642

Hanisch, U.-K., & Kettenmann, H. (2007). Microglia: active sensor and versatile effector cells in the normal and pathologic brain. *Nature Neuroscience*, *10*(11), 1387–1394. https://doi.org/10.1038/nn1997

Harms, A. S., Cao, S., Rowse, A. L., Thome, A. D., Li, X., Mangieri, L. R., Cron, R. Q., Shacka, J. J., Raman, C., & Standaert, D. G. (2013). MHCII Is Required for -Synuclein-Induced Activation of Microglia, CD4 T Cell Proliferation, and Dopaminergic Neurodegeneration. *Journal of Neuroscience*, *33*(23), 9592–9600. https://doi.org/10.1523/JNEUROSCI.5610-12.2013

Hasel, P., Aisenberg, W. H., Bennett, F. C., & Liddelow, S. A. (2023). Molecular and metabolic heterogeneity of astrocytes and microglia. *Cell Metabolism*, *35*(4), 555–570. https://doi.org/10.1016/j.cmet.2023.03.006

Hasel, P., Dando, O., Jiwaji, Z., Baxter, P., Todd, A. C., Heron, S., Márkus, N. M., McQueen, J., Hampton, D. W., Torvell, M., Tiwari, S. S., McKay, S., Eraso-Pichot, A., Zorzano, A., Masgrau, R., Galea, E., Chandran, S., Wyllie, D. J. A., Simpson, T. I., & Hardingham, G. E. (2017). Neurons and neuronal

activity control gene expression in astrocytes to regulate their development and metabolism. *Nature Communications*, *8*(1), 15132. https://doi.org/10.1038/ncomms15132

Hawkes, C. H., Del Tredici, K., & Braak, H. (2007). Parkinson's disease: a dual-hit hypothesis. *Neuropathology and Applied Neurobiology*, *33*(6), 599–614. https://doi.org/10.1111/j.1365-2990.2007.00874.x

Hayes, M. T. (2019). Parkinson's Disease and Parkinsonism. *The American Journal of Medicine*, *132*(7), 802–807. https://doi.org/10.1016/j.amjmed.2019.03.001

He, C., & Duan, S. (2023). Novel Insight into Glial Biology and Diseases. *Neuroscience Bulletin*, *39*(3), 365–367. https://doi.org/10.1007/s12264-023-01039-4

He, J., Zhu, G., Wang, G., & Zhang, F. (2020). Oxidative Stress and Neuroinflammation Potentiate Each Other to Promote Progression of Dopamine Neurodegeneration. *Oxidative Medicine and Cellular Longevity*, *2020*, 1–12. https://doi.org/10.1155/2020/6137521

He, K.-J., Zhang, J.-B., Liu, J.-Y., Zhao, F.-L., Yao, X.-Y., Tang, Y.-T., Zhang, J.-R., Cheng, X.-Y., Hu, L.-F., Wang, F., & Liu, C.-F. (2023). LRRK2 G2019S promotes astrocytic inflammation induced by oligomeric α-synuclein through NF-κB pathway. *IScience*, *26*(11), 108130. https://doi.org/10.1016/j.isci.2023.108130

Hill-Burns, E. M., Factor, S. A., Zabetian, C. P., Thomson, G., & Payami, H. (2011). Evidence for More than One Parkinson's Disease-Associated Variant within the HLA Region. *PLoS ONE*, *6*(11), e27109. https://doi.org/10.1371/journal.pone.0027109

Ho, M. S. (2019). *Microglia in Parkinson's Disease* (pp. 335–353). https://doi.org/10.1007/978-981-13-9913-8_13

Holliday, J., & Gruol, D. L. (1993). Cytokine stimulation increases intracellular calcium and alters the response to quisqualate in cultured cortical astrocytes. *Brain Research*, *621*(2), 233–241. https://doi.org/10.1016/0006-8993(93)90111-Y

Huang, S., Chen, Z., Fan, B., Chen, Y., Zhou, L., Jiang, B., Long, H., Zhong, W., Li, X., & Li, Y. (2021). A selective NLRP3 inflammasome inhibitor attenuates behavioral deficits and neuroinflammation in a mouse model of Parkinson's disease. *Journal of Neuroimmunology*, *354*, 577543. https://doi.org/10.1016/j.jneuroim.2021.577543

Hughes, C. D., Choi, M. L., Ryten, M., Hopkins, L., Drews, A., Botía, J. A., Iljina, M., Rodrigues, M., Gagliano, S. A., Gandhi, S., Bryant, C., & Klenerman, D. (2019). Picomolar concentrations of oligomeric alpha-synuclein sensitizes TLR4 to play an initiating role in Parkinson's disease pathogenesis. *Acta Neuropathologica*, *137*(1), 103–120. https://doi.org/10.1007/s00401-018-1907-y

Hyvärinen, T., Hagman, S., Ristola, M., Sukki, L., Veijula, K., Kreutzer, J., Kallio, P., & Narkilahti, S. (2019). Co-stimulation with IL-1β and TNF-α induces an inflammatory reactive astrocyte phenotype with neurosupportive characteristics in a human pluripotent stem cell model system. *Scientific Reports*, *9*(1), 16944. https://doi.org/10.1038/s41598-019-53414-9

Ibáñez, I., Bartolomé-Martín, D., Piniella, D., Giménez, C., & Zafra, F. (2019). Activity dependent internalization of the glutamate transporter GLT-1 requires calcium entry through the NCX sodium/calcium exchanger. *Neurochemistry International*, *123*, 125–132. https://doi.org/10.1016/j.neuint.2018.03.012

Ibáñez, P., Bonnet, A.-M., Débarges, B., Lohmann, E., Tison, F., Agid, Y., Dürr, A., Brice, A., & Pollak, P. (2004). Causal relation between α-synuclein locus duplication as a cause of familial Parkinson's disease. *The Lancet*, *364*(9440), 1169–1171. https://doi.org/10.1016/S0140-6736(04)17104-3

Ikuno, M., Yamakado, H., Akiyama, H., Parajuli, L. K., Taguchi, K., Hara, J., Uemura, N., Hatanaka, Y., Higaki, K., Ohno, K., Tanaka, M., Koike, M., Hirabayashi, Y., & Takahashi, R. (2019). GBA haploinsufficiency accelerates alpha-synuclein pathology with altered lipid metabolism in a prodromal model of Parkinson's disease. *Human Molecular Genetics*, *28*(11), 1894–1904. https://doi.org/10.1093/hmg/ddz030

Ivashkiv, L. B. (2018). IFNγ: signalling, epigenetics and roles in immunity, metabolism, disease and cancer immunotherapy. *Nature Reviews Immunology*, *18*(9), 545–558. https://doi.org/10.1038/s41577-018-0029-z

Jiang, L.-Y., Jiang, W., Tian, N., Xiong, Y.-N., Liu, J., Wei, J., Wu, K.-Y., Luo, J., Shi, X.-J., & Song, B.-L. (2018). Ring finger protein 145 (RNF145) is a ubiquitin ligase for sterol-induced degradation of HMG-CoA reductase. *Journal of Biological Chemistry*, *293*(11), 4047–4055. https://doi.org/10.1074/jbc.RA117.001260

Jiao, K.-P., Li, S.-M., Lv, W.-Y., Jv, M.-L., & He, H.-Y. (2017). Vitamin D3 repressed astrocyte activation following lipopolysaccharide stimulation in vitro and in neonatal rats. *NeuroReport*, *28*(9), 492–497. https://doi.org/10.1097/WNR.0000000000000782

Jin, H., Shen, H., Liu, C., Wang, L., Mao, C., Chen, J., Liu, C., & Zhang, Y. (2023). Decreased serum BDNF contributes to the onset of REM sleep behavior disorder in Parkinson's disease patients. *Neuroscience Letters*, *812*, 137380. https://doi.org/10.1016/j.neulet.2023.137380

Jiwaji, Z., & Hardingham, G. E. (2022). Good, bad, and neglectful: Astrocyte changes in neurodegenerative disease. *Free Radical Biology and Medicine*, *182*, 93–99. https://doi.org/10.1016/j.freeradbiomed.2022.02.020

Johnson, J., Blackman, R., Gross, S., & Soboloff, J. (2022). Control of STIM and Orai function by post-translational modifications. *Cell Calcium*, *103*, 102544. https://doi.org/10.1016/j.ceca.2022.102544

Jurcau, A., Andronie-Cioara, F. L., Nistor-Cseppento, D. C., Pascalau, N., Rus, M., Vasca, E., & Jurcau, M. C. (2023). The Involvement of Neuroinflammation in the Onset and Progression of Parkinson's Disease. *International Journal of Molecular Sciences*, *24*(19), 14582. https://doi.org/10.3390/ijms241914582

Kakita, A., Takahashi, H., Homma, Y., & Ikuta, F. (1994). Lewy bodies in the cerebellar dentate nucleus of a patient with Parkinson's disease. *Pathology International*, *44*(12), 878–880. https://doi.org/10.1111/j.1440-1827.1994.tb01688.x

Kalaitzakis, M. E., Graeber, M. B., Gentleman, S. M., & Pearce, R. K. B. (2008). The dorsal motor nucleus of the vagus is not an obligatory trigger site of Parkinson's disease: a critical analysis of α-synuclein staging. *Neuropathology and Applied Neurobiology*, *34*(3), 284–295. https://doi.org/10.1111/j.1365-2990.2007.00923.x

Kalia, L. V, & Lang, A. E. (2015). Parkinson's disease. *The Lancet*, *386*(9996), 896–912. https://doi.org/10.1016/S0140-6736(14)61393-3

Karikari, A. A., McFleder, R. L., Ribechini, E., Blum, R., Bruttel, V., Knorr, S., Gehmeyr, M., Volkmann, J., Brotchie, J. M., Ahsan, F., Haack, B., Monoranu, C.-M., Keber, U., Yeghiazaryan, R., Pagenstecher, A., Heckel, T., Bischler, T., Wischhusen, J., Koprich, J. B., … Ip, C. W. (2022). Neurodegeneration by α-synuclein-specific T cells in AAV-A53T-α-synuclein Parkinson's disease mice. *Brain, Behavior, and Immunity*, *101*, 194–210. https://doi.org/10.1016/j.bbi.2022.01.007

Kaur, S., Sehrawat, A., Mastana, S. S., Kandimalla, R., Sharma, P. K., Bhatti, G. K., & Bhatti, J. S. (2023). Targeting calcium homeostasis and impaired inter-organelle crosstalk as a potential therapeutic approach in Parkinson's disease. *Life Sciences*, *330*, 121995. https://doi.org/10.1016/j.lfs.2023.121995

Kerkering, J., Muinjonov, B., Rosiewicz, K. S., Diecke, S., Biese, C., Schiweck, J., Chien, C., Zocholl, D., Conrad, T., Paul, F., Alisch, M., & Siffrin, V. (2023). iPSC-derived reactive astrocytes from patients with multiple sclerosis protect cocultured neurons in inflammatory conditions. *Journal of Clinical Investigation*, *133*(13). https://doi.org/10.1172/JCI164637

Khazan, N., Kim, K. K., Hansen, J. N., Singh, N. A., Moore, T., Snyder, C. W. A., Pandita, R., Strawderman, M., Fujihara, M., Takamura, Y., Jian, Y., Battaglia, N., Yano, N., Teramoto, Y., Arnold, L. A., Hopson, R., Kishor, K., Nayak, S., Ojha, D., … Moore, R. G. (2022). Identification of a Vitamin-D Receptor Antagonist, MeTC7, which Inhibits the Growth of Xenograft and Transgenic Tumors *In Vivo*. *Journal of Medicinal Chemistry*, *65*(8), 6039–6055. https://doi.org/10.1021/acs.jmedchem.1c01878

Khor, S. L. Q., Ng, K. Y., Koh, R. Y., & Chye, S. M. (2024). Blood-brain Barrier and Neurovascular Unit Dysfunction in Parkinson's Disease: From Clinical Insights to Pathogenic Mechanisms and Novel Therapeutic Approaches. *CNS & Neurological Disorders - Drug Targets*, *23*(3), 315–330. https://doi.org/10.2174/1871527322666230330093829

Kim, C., Ho, D.-H., Suk, J.-E., You, S., Michael, S., Kang, J., Joong Lee, S., Masliah, E., Hwang, D., Lee, H.-J., & Lee, S.-J. (2013). Neuron-released oligomeric α-synuclein is an endogenous agonist of TLR2 for paracrine activation of microglia. *Nature Communications*, *4*(1), 1562. https://doi.org/10.1038/ncomms2534

Kim, C., Spencer, B., Rockenstein, E., Yamakado, H., Mante, M., Adame, A., Fields, J. A., Masliah, D., Iba, M., Lee, H.-J., Rissman, R. A., Lee, S.-J., & Masliah, E. (2018). Immunotherapy targeting toll-like receptor 2 alleviates neurodegeneration in models of synucleinopathy by modulating α-synuclein transmission and neuroinflammation. *Molecular Neurodegeneration*, *13*(1), 43. https://doi.org/10.1186/s13024-018-0276-2

Kim, H., Shin, J.-Y., Lee, Y.-S., Yun, S. P., Maeng, H.-J., & Lee, Y. (2020). Brain Endothelial P-Glycoprotein Level Is Reduced in Parkinson's Disease via a Vitamin D Receptor-Dependent Pathway. *International Journal of Molecular Sciences*, *21*(22), 8538. https://doi.org/10.3390/ijms21228538

Kim, J. J., Vitale, D., Otani, D. V., Lian, M. M., Heilbron, K., Aslibekyan, S., Auton, A., Babalola, E., Bell, R. K., Bielenberg, J., Bryc, K., Bullis, E., Cannon, P., Coker, D., Partida, G. C., Dhamija, D., Das, S., Elson, S. L., Eriksson, N., … Mata, I. (2024). Multi-ancestry genome-wide association meta-analysis of Parkinson's disease. *Nature Genetics*, *56*(1), 27–36. https://doi.org/10.1038/s41588-023-01584-8

Knekt, P., Kilkkinen, A., Rissanen, H., Marniemi, J., Sääksjärvi, K., & Heliövaara, M. (2010). Serum Vitamin D and the Risk of Parkinson Disease. *Archives of Neurology*, *67*(7). https://doi.org/10.1001/archneurol.2010.120

Koob, A. O., Paulino, A. D., & Masliah, E. (2010). GFAP reactivity, apolipoprotein E redistribution and cholesterol reduction in human astrocytes treated with α-synuclein. *Neuroscience Letters*, *469*(1), 11–14. https://doi.org/10.1016/j.neulet.2009.11.034

Kostuk, E. W., Cai, J., & Iacovitti, L. (2019). Subregional differences in astrocytes underlie selective neurodegeneration or protection in Parkinson's disease models in culture. *Glia*, *67*(8), 1542–1557. https://doi.org/10.1002/glia.23627

Krencik, R., & Zhang, S.-C. (2011). Directed differentiation of functional astroglial subtypes from human pluripotent stem cells. *Nature Protocols*, *6*(11), 1710–1717. https://doi.org/10.1038/nprot.2011.405

Kriks, S., Shim, J.-W., Piao, J., Ganat, Y. M., Wakeman, D. R., Xie, Z., Carrillo-Reid, L., Auyeung, G., Antonacci, C., Buch, A., Yang, L., Beal, M. F., Surmeier, D. J., Kordower, J. H., Tabar, V., & Studer, L. (2011). Dopamine neurons derived from human ES cells efficiently engraft in animal models of Parkinson's disease. *Nature*, *480*(7378), 547–551. https://doi.org/10.1038/nature10648

Kuter, K. Z., Cenci, M. A., & Carta, A. R. (2020). *The role of glia in Parkinson's disease: Emerging concepts and therapeutic applications* (pp. 131–168). https://doi.org/10.1016/bs.pbr.2020.02.004

Kuusisto, E., Parkkinen, L., & Alafuzoff, I. (2003). Morphogenesis of Lewy Bodies: Dissimilar Incorporation of α-Synuclein, Ubiquitin, and p62. *Journal of Neuropathology & Experimental Neurology*, *62*(12), 1241–1253. https://doi.org/10.1093/jnen/62.12.1241

Kwon, J., An, H., Sa, M., Won, J., Shin, J. I., & Lee, C. J. (2017). Orai1 and Orai3 in Combination with Stim1 Mediate the Majority of Store-operated Calcium Entry in Astrocytes. *Experimental Neurobiology*, *26*(1), 42–54. https://doi.org/10.5607/en.2017.26.1.42

Labib, D., Wang, Z., Prakash, P., Zimmer, M., Smith, M. D., Frazel, P. W., Barbar, L., Sapar, M. L., Calabresi, P. A., Peng, J., Liddelow, S. A., & Fossati, V. (2022). Proteomic Alterations and Novel Markers of Neurotoxic Reactive Astrocytes in Human Induced Pluripotent Stem Cell Models. *Frontiers in Molecular Neuroscience*, *15*. https://doi.org/10.3389/fnmol.2022.870085

Lai, T. T., Kim, Y. J., Ma, H., & Kim, Y. E. (2022). Evidence of Inflammation in Parkinson's Disease and Its Contribution to Synucleinopathy. *Journal of Movement Disorders*, *15*(1), 1–14. https://doi.org/10.14802/jmd.21078

Langston, J. W., Ballard, P., Tetrud, J. W., & Irwin, I. (1983). Chronic Parkinsonism in Humans Due to a Product of Meperidine-Analog Synthesis. *Science*, *219*(4587), 979–980. https://doi.org/10.1126/science.6823561

LaRocca, T. J., Cavalier, A. N., Roberts, C. M., Lemieux, M. R., Ramesh, P., Garcia, M. A., & Link, C. D. (2021). Amyloid beta acts synergistically as a pro-inflammatory cytokine. *Neurobiology of Disease*, *159*, 105493. https://doi.org/10.1016/j.nbd.2021.105493

Larsen, N. J., Ambrosi, G., Mullett, S. J., Berman, S. B., & Hinkle, D. A. (2011). DJ-1 knock-down impairs astrocyte mitochondrial function. *Neuroscience*, *196*, 251–264. https://doi.org/10.1016/j.neuroscience.2011.08.016

Lawrence, J. M., Schardien, K., Wigdahl, B., & Nonnemacher, M. R. (2023). Roles of neuropathology-associated reactive astrocytes: a systematic review. *Acta Neuropathologica Communications*, *11*(1), 42. https://doi.org/10.1186/s40478-023-01526-9

Le, W., Wu, J., & Tang, Y. (2016). Protective Microglia and Their Regulation in Parkinson's Disease. *Frontiers in Molecular Neuroscience*, *9*. https://doi.org/10.3389/fnmol.2016.00089

Lee, H.-J., Suk, J.-E., Patrick, C., Bae, E.-J., Cho, J.-H., Rho, S., Hwang, D., Masliah, E., & Lee, S.-J. (2010). Direct Transfer of α-Synuclein from Neuron to Astroglia Causes Inflammatory Responses in Synucleinopathies. *Journal of Biological Chemistry*, *285*(12), 9262–9272. https://doi.org/10.1074/jbc.M109.081125

Lee, J., Kim, S. W., & Kim, K.-T. (2022). Region-Specific Characteristics of Astrocytes and Microglia: A Possible Involvement in Aging and Diseases. *Cells*, *11*(12), 1902. https://doi.org/10.3390/cells11121902

Leng, K., Rose, I. V. L., Kim, H., Xia, W., Romero-Fernandez, W., Rooney, B., Koontz, M., Li, E., Ao, Y., Wang, S., Krawczyk, M., TCW, J., Goate, A., Zhang, Y., Ullian, E. M., Sofroniew, M. V., Fancy, S. P. J., Schrag, M. S., Lippmann, E. S., & Kampmann, M. (2022). CRISPRi screens in human iPSC-derived astrocytes elucidate regulators of distinct inflammatory reactive states. *Nature Neuroscience*, *25*(11), 1528–1542. https://doi.org/10.1038/s41593-022-01180-9

Lev, N., Barhum, Y., Ben-Zur, T., Melamed, E., Steiner, I., & Offen, D. (2013). Knocking Out DJ-1 Attenuates Astrocytes Neuroprotection Against 6-Hydroxydopamine Toxicity. *Journal of Molecular Neuroscience*, *50*(3), 542–550. https://doi.org/10.1007/s12031-013-9984-9

Leventoux, N., Morimoto, S., Imaizumi, K., Sato, Y., Takahashi, S., Mashima, K., Ishikawa, M., Sonn, I., Kondo, T., Watanabe, H., & Okano, H. (2020). Human Astrocytes Model Derived from Induced Pluripotent Stem Cells. *Cells*, *9*(12), 2680. https://doi.org/10.3390/cells9122680

Li, A., Guo, H., Luo, X., Sheng, J., Yang, S., Yin, Y., Zhou, J., Zhou, J., Li, A., Guo, H., Luo, X., Sheng, J., Yang, S., Yin, Y., Zhou, J., & Zhou, J. (2006). Apomorphine-induced activation of dopamine receptors modulates FGF-2 expression in astrocytic cultures and promotes survival of dopaminergic neurons. *The FASEB Journal*, *20*(8), 1263–1265. https://doi.org/10.1096/ɳ.05-5510ɳe

Li, H., Jang, W., Kim, H. J., Jo, K. D., Lee, M. K., Song, S. H., & Yang, H. O. (2015). Biochemical protective effect of 1,25-dihydroxyvitamin D3 through autophagy induction in the MPTP mouse model of Parkinson's disease. *NeuroReport*, *26*(12), 669–674. https://doi.org/10.1097/WNR.0000000000000401

Li, J.-Y., Englund, E., Holton, J. L., Soulet, D., Hagell, P., Lees, A. J., Lashley, T., Quinn, N. P., Rehncrona, S., Björklund, A., Widner, H., Revesz, T., Lindvall, O., & Brundin, P. (2008). Lewy bodies in grafted neurons in subjects with Parkinson's disease suggest host-to-graft disease propagation. *Nature Medicine*, *14*(5), 501–503. https://doi.org/10.1038/nm1746

Li, K., Ling, H., Huang, W., Luo, W., Gu, C., Tao, B., Xie, Q., & Qiu, P. (2024). Single-cell RNA-sequencing analysis reveals α-syn induced astrocyte-neuron crosstalk-mediated neurotoxicity. *International Immunopharmacology*, *139*, 112676. https://doi.org/10.1016/j.intimp.2024.112676

Li, X., Bai, L., Yang, Y., Luo, W., Hu, W., Chen, J., Mao, C., & Liu, C. (2009). Effects of IL-6 secreted from astrocytes on the survival of dopaminergic neurons in lipopolysaccharide-induced inflammation. *Neuroscience Research*, *65*(3), 252–258. https://doi.org/10.1016/j.neures.2009.07.007

Li, X., Tao, Y., Bradley, R., Du, Z., Tao, Y., Kong, L., Dong, Y., Jones, J., Yan, Y., Harder, C. R. K., Friedman, L. M., Bilal, M., Hoffmann, B., & Zhang, S.-C. (2018). Fast Generation of Functional Subtype Astrocytes from Human Pluripotent Stem Cells. *Stem Cell Reports*, *11*(4), 998–1008. https://doi.org/10.1016/j.stemcr.2018.08.019

Liberzon, A., Birger, C., Thorvaldsdóttir, H., Ghandi, M., Mesirov, J. P., & Tamayo, P. (2015). The Molecular Signatures Database Hallmark Gene Set Collection. *Cell Systems*, *1*(6), 417–425. https://doi.org/10.1016/j.cels.2015.12.004

Liddelow, S. A., Guttenplan, K. A., Clarke, L. E., Bennett, F. C., Bohlen, C. J., Schirmer, L., Bennett, M. L., Münch, A. E., Chung, W.-S., Peterson, T. C., Wilton, D. K., Frouin, A., Napier, B. A., Panicker, N., Kumar, M., Buckwalter, M. S., Rowitch, D. H., Dawson, V. L., Dawson, T. M., … Barres, B. A. (2017). Neurotoxic reactive astrocytes are induced by activated microglia. *Nature*, *541*(7638), 481–487. https://doi.org/10.1038/nature21029

Lim, D., Semyanov, A., Genazzani, A., & Verkhratsky, A. (2021a). *Calcium signaling in neuroglia* (pp. 1–53). https://doi.org/10.1016/bs.ircmb.2021.01.003

Lim, D., Semyanov, A., Genazzani, A., & Verkhratsky, A. (2021b). *Calcium signaling in neuroglia* (pp. 1–53). https://doi.org/10.1016/bs.ircmb.2021.01.003

Lima, L. A. R., Lopes, M. J. P., Costa, R. O., Lima, F. A. V, Neves, K. R. T., Calou, I. B. F., Andrade, G. M., & Viana, G. S. B. (2018). Vitamin D protects dopaminergic neurons against neuroinflammation and oxidative stress in hemiparkinsonian rats. *Journal of Neuroinflammation*, *15*(1), 249. https://doi.org/10.1186/s12974-018-1266-6

Lindblad, C., Neumann, S., Kolbeinsdóttir, S., Zachariadis, V., Thelin, E. P., Enge, M., Thams, S., Brundin, L., & Svensson, M. (2023). Stem cell-derived brainstem mouse astrocytes obtain a neurotoxic phenotype in vitro upon neuroinflammation. *Journal of Inflammation*, *20*(1), 22. https://doi.org/10.1186/s12950-023-00349-8

Lindestam Arlehamn, C. S., Dhanwani, R., Pham, J., Kuan, R., Frazier, A., Rezende Dutra, J., Phillips, E., Mallal, S., Roederer, M., Marder, K. S., Amara, A. W., Standaert, D. G., Goldman, J. G., Litvan, I., Peters, B., Sulzer, D., & Sette, A. (2020). α-Synuclein-specific T cell reactivity is associated with preclinical and early Parkinson's disease. *Nature Communications*, *11*(1), 1875. https://doi.org/10.1038/s41467-020-15626-w

Lindström, V., Gustafsson, G., Sanders, L. H., Howlett, E. H., Sigvardson, J., Kasrayan, A., Ingelsson, M., Bergström, J., & Erlandsson, A. (2017). Extensive uptake of α-synuclein oligomers in astrocytes results in sustained intracellular deposits and mitochondrial damage. *Molecular and Cellular Neuroscience*, *82*, 143–156. https://doi.org/10.1016/j.mcn.2017.04.009

Liu, N., Wang, A., Xue, M., Zhu, X., Liu, Y., & Chen, M. (2024). FOXA1 and FOXA2: the regulatory mechanisms and therapeutic implications in cancer. *Cell Death Discovery*, *10*(1), 172. https://doi.org/10.1038/s41420-024-01936-1

Liu, Y., Deng, J., Liu, Y., Li, W., & Nie, X. (2021). FGF, Mechanism of Action, Role in Parkinson's Disease, and Therapeutics. *Frontiers in Pharmacology*, *12*. https://doi.org/10.3389/fphar.2021.675725

Livak, K. J., & Schmittgen, T. D. (2001). Analysis of Relative Gene Expression Data Using Real-Time Quantitative PCR and the 2−ΔΔCT Method. *Methods*, *25*(4), 402–408. https://doi.org/10.1006/meth.2001.1262

Loria, F., Vargas, J. Y., Bousset, L., Syan, S., Salles, A., Melki, R., & Zurzolo, C. (2017). α-Synuclein transfer between neurons and astrocytes indicates that astrocytes play a role in degradation rather than in spreading. *Acta Neuropathologica*, *134*(5), 789–808. https://doi.org/10.1007/s00401-017-1746-2

Love, M. I., Huber, W., & Anders, S. (2014). Moderated estimation of fold change and dispersion for RNA-seq data with DESeq2. *Genome Biology*, *15*(12), 550. https://doi.org/10.1186/s13059-014-0550-8

Love, M. I., Soneson, C., Hickey, P. F., Johnson, L. K., Pierce, N. T., Shepherd, L., Morgan, M., & Patro, R. (2020). Tximeta: Reference sequence checksums for provenance identification in RNA-seq. *PLOS Computational Biology*, *16*(2), e1007664. https://doi.org/10.1371/journal.pcbi.1007664

Luthra, N. S., Kim, S., Zhang, Y., & Christine, C. W. (2018). Characterization of vitamin D supplementation and clinical outcomes in a large cohort of early Parkinson's disease. *Journal of Clinical Movement Disorders*, *5*(1), 7. https://doi.org/10.1186/s40734-018-0074-6

Ma, H., Zhou, Y., Li, Z., Zhu, L., Li, H., Zhang, G., Wang, J., Gong, H., Xu, D., Hua, W., Liu, P., Zhang, X., Zhang, Y., Zhang, L., Hong, B., Zhou, W., Yang, P., & Liu, J. (2022). Single-Cell RNA-Sequencing Analyses Revealed Heterogeneity and Dynamic Changes of Metabolic Pathways in Astrocytes at the Acute Phase of Ischemic Stroke. *Oxidative Medicine and Cellular Longevity*, *2022*, 1–22. https://doi.org/10.1155/2022/1817721

Ma, Röytt, Collan, & Rinne. (1999). Unbiased morphometrical measurements show loss of pigmented nigral neurones with ageing. *Neuropathology and Applied Neurobiology*, *25*(5), 394–399. https://doi.org/10.1046/j.1365-2990.1999.00202.x

Macías-García, D., Periñán, M. T., Muñoz-Delgado, L., Jimenez-Jaraba, M. V., Labrador-Espinosa, M. Á., Jesús, S., Buiza-Rueda, D., Méndez-Del Barrio, C., Adarmes-Gómez, A., Gómez-Garre, P., & Mir, P. (2021). Serum lipid profile among sporadic and familial forms of Parkinson's disease. *Npj Parkinson's Disease*, *7*(1), 59. https://doi.org/10.1038/s41531-021-00206-6

Magdy, A., Farrag, E. A. E., Hamed, S. M., Abdallah, Z., El Nashar, E. M., Alghamdi, M. A., Ali, A. A. H., & Abd El-kader, M. (2022). Neuroprotective and therapeutic effects of calcitriol in rotenone-induced Parkinson's disease rat model. *Frontiers in Cellular Neuroscience*, *16*. https://doi.org/10.3389/fncel.2022.967813

Mahmoud, S., Gharagozloo, M., Simard, C., & Gris, D. (2019). Astrocytes Maintain Glutamate Homeostasis in the CNS by Controlling the Balance between Glutamate Uptake and Release. *Cells*, *8*(2), 184. https://doi.org/10.3390/cells8020184

Malek, N. (2019). Deep Brain Stimulation in Parkinson's Disease. *Neurology India*, *67*(4), 968. https://doi.org/10.4103/0028-3886.266268

Markey, K. M., Saunders, J. C., Smuts, J., von Reyn, C. R., & Garcia, A. D. R. (2023). Astrocyte development—More questions than answers. *Frontiers in Cell and Developmental Biology*, *11*. https://doi.org/10.3389/fcell.2023.1063843

Martinez-Vicente, M., Talloczy, Z., Kaushik, S., Massey, A. C., Mazzulli, J., Mosharov, E. V., Hodara, R., Fredenburg, R., Wu, D.-C., Follenzi, A., Dauer, W., Przedborski, S., Ischiropoulos, H., Lansbury, P. T., Sulzer, D., & Cuervo, A. M. (2008). Dopamine-modified α-synuclein blocks chaperone-mediated autophagy. *Journal of Clinical Investigation*. https://doi.org/10.1172/JCI32806

Maruyama, T., Kanaji, T., Nakade, S., Kanno, T., & Mikoshiba, K. (1997). 2APB, 2-Aminoethoxydiphenyl Borate, a Membrane-Penetrable Modulator of Ins(1,4,5)P3-Induced Ca2+ Release. *Journal of Biochemistry*, *122*(3), 498–505. https://doi.org/10.1093/oxfordjournals.jbchem.a021780

Mazzetti, S., Barichella, M., Giampietro, F., Giana, A., Calogero, A. M., Amadeo, A., Palazzi, N., Comincini, A., Giaccone, G., Bramerio, M., Caronni, S., Cereda, V., Cereda, E., Cappelletti, G., Rolando, C., & Pezzoli, G. (2022). Astrocytes expressing Vitamin D-activating enzyme identify Parkinson's disease. *CNS Neuroscience & Therapeutics*, *28*(5), 703–713. https://doi.org/10.1111/cns.13801

Mazzulli, J. R., Xu, Y.-H., Sun, Y., Knight, A. L., McLean, P. J., Caldwell, G. A., Sidransky, E., Grabowski, G. A., & Krainc, D. (2011). Gaucher Disease Glucocerebrosidase and α-Synuclein Form a Bidirectional Pathogenic Loop in Synucleinopathies. *Cell*, *146*(1), 37–52. https://doi.org/10.1016/j.cell.2011.06.001

McGeer, P. L., Itagaki, S., Boyes, B. E., & McGeer, E. G. (1988). Reactive microglia are positive for HLA-DR in the substantia nigra of Parkinson's and Alzheimer's disease brains. *Neurology*, *38*(8), 1285–1285. https://doi.org/10.1212/WNL.38.8.1285

McNeill, J., Rudyk, C., Hildebrand, M. E., & Salmaso, N. (2021). Ion Channels and Electrophysiological Properties of Astrocytes: Implications for Emergent Stimulation Technologies. *Frontiers in Cellular Neuroscience*, *15*. https://doi.org/10.3389/fncel.2021.644126

Mehra, S., Sahay, S., & Maji, S. K. (2019). α-Synuclein misfolding and aggregation: Implications in Parkinson's disease pathogenesis. *Biochimica et Biophysica Acta (BBA) - Proteins and Proteomics*, *1867*(10), 890–908. https://doi.org/10.1016/j.bbapap.2019.03.001

Meng, Y., Ding, J., Li, C., Fan, H., He, Y., & Qiu, P. (2020). Transfer of pathological α-synuclein from neurons to astrocytes via exosomes causes inflammatory responses after METH exposure. *Toxicology Letters*, *331*, 188–199. https://doi.org/10.1016/j.toxlet.2020.06.016

Messing, A., & Brenner, M. (2020). GFAP at 50. *ASN Neuro*, *12*, 175909142094968. https://doi.org/10.1177/1759091420949680

Meyer-Arndt, L., Kerkering, J., Kuehl, T., Infante, A. G., Paul, F., Rosiewicz, K. S., Siffrin, V., & Alisch, M. (2023). Inflammatory Cytokines Associated with Multiple Sclerosis Directly Induce Alterations of Neuronal Cytoarchitecture in Human Neurons. *Journal of Neuroimmune Pharmacology*, *18*(1–2), 145–159. https://doi.org/10.1007/s11481-023-10059-w

Misgeld, T., & Schwarz, T. L. (2017). Mitostasis in Neurons: Maintaining Mitochondria in an Extended Cellular Architecture. *Neuron*, *96*(3), 651–666. https://doi.org/10.1016/j.neuron.2017.09.055

Miyazaki, I., & Asanuma, M. (2020). Neuron-Astrocyte Interactions in Parkinson's Disease. *Cells*, *9*(12), 2623. https://doi.org/10.3390/cells9122623

Miyazaki, I., Asanuma, M., Kikkawa, Y., Takeshima, M., Murakami, S., Miyoshi, K., Sogawa, N., & Kita, T. (2011). Astrocyte-derived metallothionein protects dopaminergic neurons from dopamine quinone toxicity. *Glia*, *59*(3), 435–451. https://doi.org/10.1002/glia.21112

Mogi, M., Harada, M., Riederer, P., Narabayashi, H., Fujita, K., & Nagatsu, T. (1994). Tumor necrosis factor-α (TNF-α) increases both in the brain and in the cerebrospinal fluid from parkinsonian patients. *Neuroscience Letters*, *165*(1–2), 208–210. https://doi.org/10.1016/0304-3940(94)90746-3

Mogi, M., Kondo, T., Mizuno, Y., & Nagatsu, T. (2007). p53 protein, interferon-γ, and NF-κB levels are elevated in the parkinsonian brain. *Neuroscience Letters*, *414*(1), 94–97. https://doi.org/10.1016/j.neulet.2006.12.003

Mori, A., Imai, Y., & Hattori, N. (2020). Lipids: Key Players That Modulate α-Synuclein Toxicity and Neurodegeneration in Parkinson's Disease. *International Journal of Molecular Sciences*, *21*(9), 3301. https://doi.org/10.3390/ijms21093301

Murray, T. E., Richards, C. M., Robert-Gostlin, V. N., Bernath, A. K., Lindhout, I. A., & Klegeris, A. (2022). Potential neurotoxic activity of diverse molecules released by astrocytes. *Brain Research Bulletin*, *189*, 80–101. https://doi.org/10.1016/j.brainresbull.2022.08.015

Nakajima, H., Fujita, S., Kakae, M., Nagayasu, K., Oh-hora, M., Shirakawa, H., & Kaneko, S. (2022). Orai2 channel regulates prostaglandin E2 production in TNFα/IL1α-stimulated astrocytes. *Glia*, *70*(9), 1666–1680. https://doi.org/10.1002/glia.24188

Nakamura, T., Sugeno, N., Hasegawa, T., Ikeda, K., Yoshida, S., Ishiyama, S., Sato, K., Takeda, A., & Aoki, M. (2024). Alpha-synuclein promotes PRMT5-mediated H4R3me2s histone methylation by interacting with the BAF complex. *The FEBS Journal*, *291*(9), 1892–1908. https://doi.org/10.1111/febs.17037

Nalls, M. A., Blauwendraat, C., Vallerga, C. L., Heilbron, K., Bandres-Ciga, S., Chang, D., Tan, M., Kia, D. A., Noyce, A. J., Xue, A., Bras, J., Young, E., von Coelln, R., Simón-Sánchez, J., Schulte, C., Sharma, M., Krohn, L., Pihlstrøm, L., Siitonen, A., … Zhang, F. (2019). Identification of novel risk loci, causal insights, and heritable risk for Parkinson's disease: a meta-analysis of genome-wide association studies. *The Lancet Neurology*, *18*(12), 1091–1102. https://doi.org/10.1016/S1474-4422(19)30320-5

Nam, Y. R., Kang, M., Kim, M., Seok, M. J., Yang, Y., Han, Y. E., Oh, S.-J., Kim, D. G., Son, H., Chang, M.-Y., & Lee, S.-H. (2024). Preparation of human astrocytes with potent therapeutic functions from human pluripotent stem cells using ventral midbrain patterning. *Journal of Advanced Research*. https://doi.org/10.1016/j.jare.2024.03.012

Nanclares, C., Poynter, J., Martell-Martinez, H. A., Vermilyea, S., Araque, A., Kofuji, P., Lee, M. K., & Covelo, A. (2023). Dysregulation of astrocytic Ca2+ signaling and gliotransmitter release in mouse models of α-synucleinopathies. *Acta Neuropathologica*. https://doi.org/10.1007/s00401-023-02547-3

Neudorfer, O., Giladi, N., Elstein, D., Abrahamov, A., Turezkite, T., Aghai, E., Reches, A., Bembi, B., & Zimran, A. (1996). Occurrence of Parkinson's syndrome in type 1 Gaucher disease. *QJM*, *89*(9), 691–694. https://doi.org/10.1093/qjmed/89.9.691

Nikolic, L., Shen, W., Nobili, P., Virenque, A., Ulmann, L., & Audinat, E. (2018). Blocking TNFα-driven astrocyte purinergic signaling restores normal synaptic activity during epileptogenesis. *Glia*, *66*(12), 2673–2683. https://doi.org/10.1002/glia.23519

Nonaka, H., Kondo, T., Suga, M., Yamanaka, R., Sagara, Y., Tsukita, K., Mitsutomi, N., Homma, K., Saito, R., Miyoshi, F., Ohzeki, H., Okuyama, M., & Inoue, H. (2024). Induced pluripotent stem cell-based assays recapture multiple properties of human astrocytes. *Journal of Cellular and Molecular Medicine*, *28*(7). https://doi.org/10.1111/jcmm.18214

Novakovic, M. M., Korshunov, K. S., Grant, R. A., Martin, M. E., Valencia, H. A., Budinger, G. R. S., Radulovic, J., & Prakriya, M. (2023). Astrocyte reactivity and inflammation-induced depression-

like behaviors are regulated by Orai1 calcium channels. *Nature Communications*, *14*(1), 5500. https://doi.org/10.1038/s41467-023-40968-6

Noyce, A. J., Bestwick, J. P., Silveira-Moriyama, L., Hawkes, C. H., Giovannoni, G., Lees, A. J., & Schrag, A. (2012). Meta-analysis of early nonmotor features and risk factors for Parkinson disease. *Annals of Neurology*, *72*(6), 893–901. https://doi.org/10.1002/ana.23687

Nunes, P., & Demaurex, N. (2014). Redox Regulation of Store-Operated Ca2+ Entry. *Antioxidants & Redox Signaling*, *21*(6), 915–932. https://doi.org/10.1089/ars.2013.5615

Oberheim, N. A., Takano, T., Han, X., He, W., Lin, J. H. C., Wang, F., Xu, Q., Wyatt, J. D., Pilcher, W., Ojemann, J. G., Ransom, B. R., Goldman, S. A., & Nedergaard, M. (2009). Uniquely Hominid Features of Adult Human Astrocytes. *The Journal of Neuroscience*, *29*(10), 3276–3287. https://doi.org/10.1523/JNEUROSCI.4707-08.2009

Ohta, K., Kuno, S., Inoue, S., Ikeda, E., Fujinami, A., & Ohta, M. (2010). The effect of dopamine agonists: The expression of GDNF, NGF, and BDNF in cultured mouse astrocytes. *Journal of the Neurological Sciences*, *291*(1–2), 12–16. https://doi.org/10.1016/j.jns.2010.01.013

Okada, T., Enkhjargal, B., Travis, Z. D., Ocak, U., Tang, J., Suzuki, H., & Zhang, J. H. (2019). FGF-2 Attenuates Neuronal Apoptosis via FGFR3/PI3k/Akt Signaling Pathway After Subarachnoid Hemorrhage. *Molecular Neurobiology*, *56*(12), 8203–8219. https://doi.org/10.1007/s12035-019-01668-9

Olzmann, J. A., & Carvalho, P. (2019). Dynamics and functions of lipid droplets. *Nature Reviews Molecular Cell Biology*, *20*(3), 137–155. https://doi.org/10.1038/s41580-018-0085-z

Ou, Z., Pan, J., Tang, S., Duan, D., Yu, D., Nong, H., & Wang, Z. (2021). Global Trends in the Incidence, Prevalence, and Years Lived With Disability of Parkinson's Disease in 204 Countries/Territories From 1990 to 2019. *Frontiers in Public Health*, *9*. https://doi.org/10.3389/fpubh.2021.776847

Oueslati, A., Fournier, M., & Lashuel, H. A. (2010). *Role of post-translational modifications in modulating the structure, function and toxicity of α-synuclein* (pp. 115–145). https://doi.org/10.1016/S0079-6123(10)83007-9

Palasz, E., Wysocka, A., Gasiorowska, A., Chalimoniuk, M., Niewiadomski, W., & Niewiadomska, G. (2020). BDNF as a Promising Therapeutic Agent in Parkinson's Disease. *International Journal of Molecular Sciences*, *21*(3), 1170. https://doi.org/10.3390/ijms21031170

Palmer, A. L., & Ousman, S. S. (2018). Astrocytes and Aging. *Frontiers in Aging Neuroscience*, *10*. https://doi.org/10.3389/fnagi.2018.00337

Pang, S. Y.-Y., Ho, P. W.-L., Liu, H.-F., Leung, C.-T., Li, L., Chang, E. E. S., Ramsden, D. B., & Ho, S.-L. (2019). The interplay of aging, genetics and environmental factors in the pathogenesis of Parkinson's disease. *Translational Neurodegeneration*, *8*(1), 23. https://doi.org/10.1186/s40035-019-0165-9

Papadopoulos, V. E., Nikolopoulou, G., Antoniadou, I., Karachaliou, A., Arianoglou, G., Emmanouilidou, E., Sardi, S. P., Stefanis, L., & Vekrellis, K. (2018). Modulation of β-glucocerebrosidase increases α-synuclein secretion and exosome release in mouse models of Parkinson's disease. *Human Molecular Genetics*. https://doi.org/10.1093/hmg/ddy075

Papanikolaou, M., Lewis, A., & Butt, A. M. (2017). Store-operated calcium entry is essential for glial calcium signalling in CNS white matter. *Brain Structure and Function*, *222*(7), 2993–3005. https://doi.org/10.1007/s00429-017-1380-8

Park, S.-Y., Yang, H., Kim, S., Yang, J., Go, H., & Bae, H. (2023). Alpha-Synuclein-Specific Regulatory T Cells Ameliorate Parkinson's Disease Progression in Mice. *International Journal of Molecular Sciences*, *24*(20), 15237. https://doi.org/10.3390/ijms242015237

Parkinson, J. (2002). An Essay on the Shaking Palsy. *The Journal of Neuropsychiatry and Clinical Neurosciences*, *14*(2), 223–236. https://doi.org/10.1176/jnp.14.2.223

Parkkinen, L., Neumann, J., O'Sullivan, S. S., Holton, J. L., Revesz, T., Hardy, J., & Lees, A. J. (2011). Glucocerebrosidase mutations do not cause increased Lewy body pathology in Parkinson's disease. *Molecular Genetics and Metabolism*, *103*(4), 410–412. https://doi.org/10.1016/j.ymgme.2011.04.015

Parpura, V., & Verkhratsky, A. (2012). Astrocytes revisited: concise historic outlook on glutamate homeostasis and signaling. *Croatian Medical Journal*, *53*(6), 518–528. https://doi.org/10.3325/cmj.2012.53.518

Patro, R., Duggal, G., Love, M. I., Irizarry, R. A., & Kingsford, C. (2017). Salmon provides fast and bias-aware quantification of transcript expression. *Nature Methods*, *14*(4), 417–419. https://doi.org/10.1038/nmeth.4197

Perriot, S., Mathias, A., Perriard, G., Canales, M., Jonkmans, N., Merienne, N., Meunier, C., El Kassar, L., Perrier, A. L., Laplaud, D.-A., Schluep, M., Déglon, N., & Du Pasquier, R. (2018). Human Induced Pluripotent Stem Cell-Derived Astrocytes Are Differentially Activated by Multiple Sclerosis-Associated Cytokines. *Stem Cell Reports*, *11*(5), 1199–1210. https://doi.org/10.1016/j.stemcr.2018.09.015

Pertile, R. A. N., Brigden, R., Raman, V., Cui, X., Du, Z., & Eyles, D. (2023). Vitamin D: A potent regulator of dopaminergic neuron differentiation and function. *Journal of Neurochemistry*, *166*(5), 779–789. https://doi.org/10.1111/jnc.15829

Peteri, U.-K., Pitkonen, J., Utami, K. H., Paavola, J., Roybon, L., Pouladi, M. A., & Castrén, M. L. (2021). Generation of the Human Pluripotent Stem-Cell-Derived Astrocyte Model with Forebrain Identity. *Brain Sciences*, *11*(2), 209. https://doi.org/10.3390/brainsci11020209

Pignolo, A., Mastrilli, S., Davì, C., Arnao, V., Aridon, P., dos Santos Mendes, F. A., Gagliardo, C., & D'Amelio, M. (2022). Vitamin D and Parkinson's Disease. *Nutrients*, *14*(6), 1220. https://doi.org/10.3390/nu14061220

Pike, A. F., Varanita, T., Herrebout, M. A. C., Plug, B. C., Kole, J., Musters, R. J. P., Teunissen, C. E., Hoozemans, J. J. M., Bubacco, L., & Veerhuis, R. (2021). <scp>α-Synuclein</scp> evokes <scp>NLRP3</scp> inflammasome-mediated <scp>IL</scp> -1β secretion from primary human microglia. *Glia*, *69*(6), 1413–1428. https://doi.org/10.1002/glia.23970

Pivneva, T., Haas, B., Reyes-Haro, D., Laube, G., Veh, R. W., Nolte, C., Skibo, G., & Kettenmann, H. (2008). Store-operated Ca2+ entry in astrocytes: Different spatial arrangement of endoplasmic reticulum explains functional diversity in vitro and in situ. *Cell Calcium*, *43*(6), 591–601. https://doi.org/10.1016/j.ceca.2007.10.004

Plotegher, N., Gratton, E., & Bubacco, L. (2014). Number and Brightness analysis of alpha-synuclein oligomerization and the associated mitochondrial morphology alterations in live cells. *Biochimica et Biophysica Acta (BBA) - General Subjects*, *1840*(6), 2014–2024. https://doi.org/10.1016/j.bbagen.2014.02.013

Poejo, J., Berrocal, M., Saez, L., Gutierrez-Merino, C., & Mata, A. M. (2023). Store-Operated Calcium Entry Inhibition and Plasma Membrane Calcium Pump Upregulation Contribute to the Maintenance of Resting Cytosolic Calcium Concentration in A1-like Astrocytes. *Molecules*, *28*(14), 5363. https://doi.org/10.3390/molecules28145363

Poewe, W., Stankovic, I., Halliday, G., Meissner, W. G., Wenning, G. K., Pellecchia, M. T., Seppi, K., Palma, J.-A., & Kaufmann, H. (2022). Multiple system atrophy. *Nature Reviews Disease Primers*, *8*(1), 56. https://doi.org/10.1038/s41572-022-00382-6

Polinski, N. K. (2021). A Summary of Phenotypes Observed in the In Vivo Rodent Alpha-Synuclein Preformed Fibril Model. *Journal of Parkinson's Disease*, *11*(4), 1555–1567. https://doi.org/10.3233/JPD-212847

Polinski, N. K., Martinez, T. N., Gorodinsky, A., Gareus, R., Sasner, M., Herberth, M., Switzer, R., Ahmad, S. O., Cosden, M., Kandebo, M., Drolet, R. E., Buckett, P. D., Shan, W., Chen, Y., Pellegrino, L. J., Ellsworth, G. D., Dungan, L. B., Hirst, W. D., Clark, S. W., & Dave, K. D. (2021). Decreased glucocerebrosidase activity and substrate accumulation of glycosphingolipids in a novel GBA1 D409V knock-in mouse model. *PLOS ONE*, *16*(6), e0252325. https://doi.org/10.1371/journal.pone.0252325

Polymeropoulos, M. H., Lavedan, C., Leroy, E., Ide, S. E., Dehejia, A., Dutra, A., Pike, B., Root, H., Rubenstein, J., Boyer, R., Stenroos, E. S., Chandrasekharappa, S., Athanassiadou, A., Papapetropoulos, T., Johnson, W. G., Lazzarini, A. M., Duvoisin, R. C., Di Iorio, G., Golbe, L. I., & Nussbaum, R. L. (1997). Mutation in the α-Synuclein Gene Identified in Families with Parkinson's Disease. *Science*, *276*(5321), 2045–2047. https://doi.org/10.1126/science.276.5321.2045

Pons-Espinal, M., Blasco-Agell, L., Fernandez-Carasa, I., Andrés-Benito, P., di Domenico, A., Richaud-Patin, Y., Baruffi, V., Marruecos, L., Espinosa, L., Garrido, A., Tolosa, E., Edel, M. J., Otero, M. J., Mosquera, J. L., Ferrer, I., Raya, A., & Consiglio, A. (2024). Blocking IL-6 signaling prevents astrocyte-induced neurodegeneration in an iPSC-based model of Parkinson's disease. *JCI Insight*, *9*(3). https://doi.org/10.1172/jci.insight.163359

Postuma, R. B., & Berg, D. (2019). Prodromal Parkinson's Disease: The Decade Past, the Decade to Come. *Movement Disorders*, *34*(5), 665–675. https://doi.org/10.1002/mds.27670

Postuma, R. B., Berg, D., Stern, M., Poewe, W., Olanow, C. W., Oertel, W., Obeso, J., Marek, K., Litvan, I., Lang, A. E., Halliday, G., Goetz, C. G., Gasser, T., Dubois, B., Chan, P., Bloem, B. R., Adler, C. H., & Deuschl, G. (2015). MDS clinical diagnostic criteria for Parkinson's disease. *Movement Disorders*, *30*(12), 1591–1601. https://doi.org/10.1002/mds.26424

Potokar, M., Morita, M., Wiche, G., & Jorgačevski, J. (2020). The Diversity of Intermediate Filaments in Astrocytes. *Cells*, *9*(7), 1604. https://doi.org/10.3390/cells9071604

Pringsheim, T., Jette, N., Frolkis, A., & Steeves, T. D. L. (2014). The prevalence of Parkinson's disease: A systematic review and meta-analysis. *Movement Disorders*, *29*(13), 1583–1590. https://doi.org/10.1002/mds.25945

Prunell, G., & Olivera-Bravo, S. (2022). A Focus on Astrocyte Contribution to Parkinson's Disease Etiology. *Biomolecules*, *12*(12), 1745. https://doi.org/10.3390/biom12121745

Qian, D., Li, L., Rong, Y., Liu, W., Wang, Q., Zhou, Z., Gu, C., Huang, Y., Zhao, X., Chen, J., Fan, J., & Yin, G. (2019). Blocking Notch signal pathway suppresses the activation of neurotoxic A1 astrocytes

after spinal cord injury. *Cell Cycle*, *18*(21), 3010–3029. https://doi.org/10.1080/15384101.2019.1667189

Raj, A., Banerjee, R., Santhoshkumar, R., Sagar, C., & Datta, I. (2023). Presence of Extracellular Alpha-Synuclein Aggregates Trigger Astrocytic Degeneration Through Enhanced Membrane Rigidity and Deregulation of Store-Operated Calcium Entry (SOCE) into the Endoplasmic Reticulum. *Molecular Neurobiology*, *60*(9), 5309–5329. https://doi.org/10.1007/s12035-023-03400-0

Ramos-Gonzalez, P., Mato, S., Chara, J. C., Verkhratsky, A., Matute, C., & Cavaliere, F. (2021). Astrocytic atrophy as a pathological feature of Parkinson's disease with LRRK2 mutation. *Npj Parkinson's Disease*, *7*(1), 31. https://doi.org/10.1038/s41531-021-00175-w

Rangasamy, S. B., Soderstrom, K., Bakay, R. A. E., & Kordower, J. H. (2010). *Neurotrophic factor therapy for Parkinson's disease* (pp. 237–264). https://doi.org/10.1016/S0079-6123(10)84013-0

Rannikko, E. H., Weber, S. S., & Kahle, P. J. (2015). Exogenous α-synuclein induces toll-like receptor 4 dependent inflammatory responses in astrocytes. *BMC Neuroscience*, *16*(1), 57. https://doi.org/10.1186/s12868-015-0192-0

Rcom-H'cheo-Gauthier, A. N., Meedeniya, A. C. B., & Pountney, D. L. (2017). Calcipotriol inhibits α-synuclein aggregation in <scp>SH</scp> - <scp>SY</scp> 5Y neuroblastoma cells by a Calbindin-D28k-dependent mechanism. *Journal of Neurochemistry*, *141*(2), 263–274. https://doi.org/10.1111/jnc.13971

Rees, K., Stowe, R., Patel, S., Ives, N., Breen, K., Clarke, C. E., & Ben-Shlomo, Y. (2011). Non-steroidal anti-inflammatory drugs as disease-modifying agents for Parkinson's disease: evidence from observational studies. *Cochrane Database of Systematic Reviews*. https://doi.org/10.1002/14651858.CD008454.pub2

Reeve, A., Simcox, E., & Turnbull, D. (2014). Ageing and Parkinson's disease: Why is advancing age the biggest risk factor? *Ageing Research Reviews*, *14*, 19–30. https://doi.org/10.1016/j.arr.2014.01.004

Rizor, A., Pajarillo, E., Johnson, J., Aschner, M., & Lee, E. (2019). Astrocytic Oxidative/Nitrosative Stress Contributes to Parkinson's Disease Pathogenesis: The Dual Role of Reactive Astrocytes. *Antioxidants*, *8*(8), 265. https://doi.org/10.3390/antiox8080265

Rocha, E. M., De Miranda, B., & Sanders, L. H. (2018). Alpha-synuclein: Pathology, mitochondrial dysfunction and neuroinflammation in Parkinson's disease. *Neurobiology of Disease*, *109*, 249–257. https://doi.org/10.1016/j.nbd.2017.04.004

Rocha, E. M., Smith, G. A., Park, E., Cao, H., Graham, A.-R., Brown, E., McLean, J. R., Hayes, M. A., Beagan, J., Izen, S. C., Perez-Torres, E., Hallett, P. J., & Isacson, O. (2015). Sustained Systemic Glucocerebrosidase Inhibition Induces Brain α-Synuclein Aggregation, Microglia and Complement C1q Activation in Mice. *Antioxidants & Redox Signaling*, *23*(6), 550–564. https://doi.org/10.1089/ars.2015.6307

Rochel, N. (2022). Vitamin D and Its Receptor from a Structural Perspective. *Nutrients*, *14*(14), 2847. https://doi.org/10.3390/nu14142847

Ronco, V., Grolla, A. A., Glasnov, T. N., Canonico, P. L., Verkhratsky, A., Genazzani, A. A., & Lim, D. (2014). Differential deregulation of astrocytic calcium signalling by amyloid-β, TNFα, IL-1β and LPS. *Cell Calcium*, *55*(4), 219–229. https://doi.org/10.1016/j.ceca.2014.02.016

Rosety, I., Zagare, A., Saraiva, C., Nickels, S., Antony, P., Almeida, C., Glaab, E., Halder, R., Velychko, S., Rauen, T., Schöler, H. R., Bolognin, S., Sauter, T., Jarazo, J., Krüger, R., & Schwamborn, J. C. (2023). Impaired neuron differentiation in GBA-associated Parkinson's disease is linked to cell cycle defects in organoids. *Npj Parkinson's Disease*, *9*(1), 166. https://doi.org/10.1038/s41531-023-00616-8

Rossi, A., Pizzo, P., & Filadi, R. (2019). Calcium, mitochondria and cell metabolism: A functional triangle in bioenergetics. *Biochimica et Biophysica Acta (BBA) - Molecular Cell Research*, *1866*(7), 1068–1078. https://doi.org/10.1016/j.bbamcr.2018.10.016

Rostami, J., Fotaki, G., Sirois, J., Mzezewa, R., Bergström, J., Essand, M., Healy, L., & Erlandsson, A. (2020). Astrocytes have the capacity to act as antigen-presenting cells in the Parkinson's disease brain. *Journal of Neuroinflammation*, *17*(1), 119. https://doi.org/10.1186/s12974-020-01776-7

Rostami, J., Holmqvist, S., Lindström, V., Sigvardson, J., Westermark, G. T., Ingelsson, M., Bergström, J., Roybon, L., & Erlandsson, A. (2017). Human Astrocytes Transfer Aggregated Alpha-Synuclein via Tunneling Nanotubes. *The Journal of Neuroscience*, *37*(49), 11835–11853. https://doi.org/10.1523/JNEUROSCI.0983-17.2017

Russ, K., Teku, G., Bousset, L., Redeker, V., Piel, S., Savchenko, E., Pomeshchik, Y., Savistchenko, J., Stummann, T. C., Azevedo, C., Collin, A., Goldwurm, S., Fog, K., Elmer, E., Vihinen, M., Melki, R., & Roybon, L. (2021). TNF-α and α-synuclein fibrils differently regulate human astrocyte immune reactivity and impair mitochondrial respiration. *Cell Reports*, *34*(12), 108895. https://doi.org/10.1016/j.celrep.2021.108895

Russo, I., Kaganovich, A., Ding, J., Landeck, N., Mamais, A., Varanita, T., Biosa, A., Tessari, I., Bubacco, L., Greggio, E., & Cookson, M. R. (2019). Transcriptome analysis of LRRK2 knock-out microglia cells reveals alterations of inflammatory- and oxidative stress-related pathways upon treatment with α-synuclein fibrils. *Neurobiology of Disease*, *129*, 67–78. https://doi.org/10.1016/j.nbd.2019.05.012

Samet, J. M. (2013). Tobacco Smoking. *Thoracic Surgery Clinics*, *23*(2), 103–112. https://doi.org/10.1016/j.thorsurg.2013.01.009

Sanchez, A., Morales, I., Rodriguez-Sabate, C., Sole-Sabater, M., & Rodriguez, M. (2021). Astrocytes, a Promising Opportunity to Control the Progress of Parkinson's Disease. *Biomedicines*, *9*(10), 1341. https://doi.org/10.3390/biomedicines9101341

Sánchez Campos, S., Alza, N. P., & Salvador, G. A. (2018). Lipid metabolism alterations in the neuronal response to A53T α-synuclein and Fe-induced injury. *Archives of Biochemistry and Biophysics*, *655*, 43–54. https://doi.org/10.1016/j.abb.2018.08.007

Sanchez-Martinez, A., Beavan, M., Gegg, M. E., Chau, K.-Y., Whitworth, A. J., & Schapira, A. H. V. (2016). Parkinson disease-linked GBA mutation effects reversed by molecular chaperones in human cell and fly models. *Scientific Reports*, *6*(1), 31380. https://doi.org/10.1038/srep31380

Santos, R., Mei, A., & Marchetto, M. C. (2022). Generation of inflammation-responsive astrocytes from glial progenitors derived from human pluripotent stem cells. *STAR Protocols*, *3*(2), 101261. https://doi.org/10.1016/j.xpro.2022.101261

Sanyal, A., DeAndrade, M. P., Novis, H. S., Lin, S., Chang, J., Lengacher, N., Tomlinson, J. J., Tansey, M. G., & LaVoie, M. J. (2020). Lysosome and Inflammatory Defects in GBA1-Mutant Astrocytes Are

Normalized by LRRK2 Inhibition. *Movement Disorders*, *35*(5), 760–773. https://doi.org/10.1002/mds.27994

Sassone, J., Reale, C., Dati, G., Regoni, M., Pellecchia, M. T., & Garavaglia, B. (2021). The Role of VPS35 in the Pathobiology of Parkinson's Disease. *Cellular and Molecular Neurobiology*, *41*(2), 199–227. https://doi.org/10.1007/s10571-020-00849-8

Schaser, A. J., Osterberg, V. R., Dent, S. E., Stackhouse, T. L., Wakeham, C. M., Boutros, S. W., Weston, L. J., Owen, N., Weissman, T. A., Luna, E., Raber, J., Luk, K. C., McCullough, A. K., Woltjer, R. L., & Unni, V. K. (2019). Alpha-synuclein is a DNA binding protein that modulates DNA repair with implications for Lewy body disorders. *Scientific Reports*, *9*(1), 10919. https://doi.org/10.1038/s41598-019-47227-z

Schmidt, S. I., Bogetofte, H., Ritter, L., Agergaard, J. B., Hammerich, D., Kabiljagic, A. A., Wlodarczyk, A., Lopez, S. G., Sørensen, M. D., Jørgensen, M. L., Okarmus, J., Serrano, A. M., Kristensen, B. W., Freude, K., Owens, T., & Meyer, M. (2021). Microglia-Secreted Factors Enhance Dopaminergic Differentiation of Tissue- and iPSC-Derived Human Neural Stem Cells. *Stem Cell Reports*, *16*(2), 281–294. https://doi.org/10.1016/j.stemcr.2020.12.011

Schöndorf, D. C., Aureli, M., McAllister, F. E., Hindley, C. J., Mayer, F., Schmid, B., Sardi, S. P., Valsecchi, M., Hoffmann, S., Schwarz, L. K., Hedrich, U., Berg, D., Shihabuddin, L. S., Hu, J., Pruszak, J., Gygi, S. P., Sonnino, S., Gasser, T., & Deleidi, M. (2014). iPSC-derived neurons from GBA1-associated Parkinson's disease patients show autophagic defects and impaired calcium homeostasis. *Nature Communications*, *5*(1), 4028. https://doi.org/10.1038/ncomms5028

Scudamore, O., & Ciossek, T. (2018). Increased Oxidative Stress Exacerbates α-Synuclein Aggregation In Vivo. *Journal of Neuropathology & Experimental Neurology*, *77*(6), 443–453. https://doi.org/10.1093/jnen/nly024

Semyanov, A., Henneberger, C., & Agarwal, A. (2020). Making sense of astrocytic calcium signals — from acquisition to interpretation. *Nature Reviews Neuroscience*, *21*(10), 551–564. https://doi.org/10.1038/s41583-020-0361-8

Sengoku, R., Saito, Y., Ikemura, M., Hatsuta, H., Sakiyama, Y., Kanemaru, K., Arai, T., Sawabe, M., Tanaka, N., Mochizuki, H., Inoue, K., & Murayama, S. (2008). Incidence and Extent of Lewy Body-Related α-Synucleinopathy in Aging Human Olfactory Bulb. *Journal of Neuropathology & Experimental Neurology*, *67*(11), 1072–1083. https://doi.org/10.1097/NEN.0b013e31818b4126

Sezgin, M., Bilgic, B., Tinaz, S., & Emre, M. (2019). Parkinson's Disease Dementia and Lewy Body Disease. *Seminars in Neurology*, *39*(02), 274–282. https://doi.org/10.1055/s-0039-1678579

Shahmoradian, S. H., Lewis, A. J., Genoud, C., Hench, J., Moors, T. E., Navarro, P. P., Castaño-Díez, D., Schweighauser, G., Graff-Meyer, A., Goldie, K. N., Sütterlin, R., Huisman, E., Ingrassia, A., Gier, Y. de, Rozemuller, A. J. M., Wang, J., Paepe, A. De, Erny, J., Staempfli, A., … Lauer, M. E. (2019). Lewy pathology in Parkinson's disease consists of crowded organelles and lipid membranes. *Nature Neuroscience*, *22*(7), 1099–1109. https://doi.org/10.1038/s41593-019-0423-2

Sharma, M., & Burré, J. (2023). α-Synuclein in synaptic function and dysfunction. *Trends in Neurosciences*, *46*(2), 153–166. https://doi.org/10.1016/j.tins.2022.11.007

Shigetomi, E., Saito, K., Sano, F., & Koizumi, S. (2019). Aberrant Calcium Signals in Reactive Astrocytes: A Key Process in Neurological Disorders. *International Journal of Molecular Sciences*, *20*(4), 996. https://doi.org/10.3390/ijms20040996

Siderowf, A., Jennings, D., Eberly, S., Oakes, D., Hawkins, K. A., Ascherio, A., Stern, M. B., & Marek, K. (2012). Impaired olfaction and other prodromal features in the Parkinson At-Risk Syndrome study. *Movement Disorders*, *27*(3), 406–412. https://doi.org/10.1002/mds.24892

Sina, F., Shojaee, S., Elahi, E., & Paisán-Ruiz, C. (2009). R632W mutation in *PLA2G6* segregates with dystonia-parkinsonism in a consanguineous Iranian family. *European Journal of Neurology*, *16*(1), 101–104. https://doi.org/10.1111/j.1468-1331.2008.02356.x

Sinclair, E., Trivedi, D. K., Sarkar, D., Walton-Doyle, C., Milne, J., Kunath, T., Rijs, A. M., de Bie, R. M. A., Goodacre, R., Silverdale, M., & Barran, P. (2021). Metabolomics of sebum reveals lipid dysregulation in Parkinson's disease. *Nature Communications*, *12*(1), 1592. https://doi.org/10.1038/s41467-021-21669-4

Singh, A., Tripathi, P., & Singh, S. (2021). Neuroinflammatory responses in Parkinson's disease: relevance of Ibuprofen in therapeutics. *Inflammopharmacology*, *29*(1), 5–14. https://doi.org/10.1007/s10787-020-00764-w

Singh, K., Han, K., Tilve, S., Wu, K., Geller, H. M., & Sack, M. N. (2018). Parkin targets NOD2 to regulate astrocyte endoplasmic reticulum stress and inflammation. *Glia*, *66*(11), 2427–2437. https://doi.org/10.1002/glia.23482

Smajić, S., Prada-Medina, C. A., Landoulsi, Z., Ghelfi, J., Delcambre, S., Dietrich, C., Jarazo, J., Henck, J., Balachandran, S., Pachchek, S., Morris, C. M., Antony, P., Timmermann, B., Sauer, S., Pereira, S. L., Schwamborn, J. C., May, P., Grünewald, A., & Spielmann, M. (2022). Single-cell sequencing of human midbrain reveals glial activation and a Parkinson-specific neuronal state. *Brain*, *145*(3), 964–978. https://doi.org/10.1093/brain/awab446

Smeyne, R. J., Breckenridge, C. B., Beck, M., Jiao, Y., Butt, M. T., Wolf, J. C., Zadory, D., Minnema, D. J., Sturgess, N. C., Travis, K. Z., Cook, A. R., Smith, L. L., & Botham, P. A. (2016). Assessment of the Effects of MPTP and Paraquat on Dopaminergic Neurons and Microglia in the Substantia Nigra Pars Compacta of C57BL/6 Mice. *PLOS ONE*, *11*(10), e0164094. https://doi.org/10.1371/journal.pone.0164094

Smith, L., & Schapira, A. H. V. (2022a). GBA Variants and Parkinson Disease: Mechanisms and Treatments. *Cells*, *11*(8), 1261. https://doi.org/10.3390/cells11081261

Smith, L., & Schapira, A. H. V. (2022b). GBA Variants and Parkinson Disease: Mechanisms and Treatments. *Cells*, *11*(8), 1261. https://doi.org/10.3390/cells11081261

Smith, M. D., Chamling, X., Gill, A. J., Martinez, H., Li, W., Fitzgerald, K. C., Sotirchos, E. S., Moroziewicz, D., Bauer, L., Paull, D., Gharagozloo, M., Bhargava, P., Zack, D. J., Fossati, V., & Calabresi, P. A. (2022). Reactive Astrocytes Derived From Human Induced Pluripotent Stem Cells Suppress Oligodendrocyte Precursor Cell Differentiation. *Frontiers in Molecular Neuroscience*, *15*. https://doi.org/10.3389/fnmol.2022.874299

Sochocka, M., Diniz, B. S., & Leszek, J. (2017). Inflammatory Response in the CNS: Friend or Foe? *Molecular Neurobiology*, *54*(10), 8071–8089. https://doi.org/10.1007/s12035-016-0297-1

Sofroniew, M. V. (2020). Astrocyte Reactivity: Subtypes, States, and Functions in CNS Innate Immunity. *Trends in Immunology*, *41*(9), 758–770. https://doi.org/10.1016/j.it.2020.07.004

Soneson, C., Love, M. I., & Robinson, M. D. (2016). Differential analyses for RNA-seq: transcript-level estimates improve gene-level inferences. *F1000Research*, *4*, 1521. https://doi.org/10.12688/f1000research.7563.2

Sonninen, T.-M., Hämäläinen, R. H., Koskuvi, M., Oksanen, M., Shakirzyanova, A., Wojciechowski, S., Puttonen, K., Naumenko, N., Goldsteins, G., Laham-Karam, N., Lehtonen, M., Tavi, P., Koistinaho, J., & Lehtonen, Š. (2020). Metabolic alterations in Parkinson's disease astrocytes. *Scientific Reports*, *10*(1), 14474. https://doi.org/10.1038/s41598-020-71329-8

Soubannier, V., Maussion, G., Chaineau, M., Sigutova, V., Rouleau, G., Durcan, T. M., & Stifani, S. (2020). Characterization of human iPSC-derived astrocytes with potential for disease modeling and drug discovery. *Neuroscience Letters*, *731*, 135028. https://doi.org/10.1016/j.neulet.2020.135028

Spillantini, M. G., Schmidt, M. L., Lee, V. M.-Y., Trojanowski, J. Q., Jakes, R., & Goedert, M. (1997). α-Synuclein in Lewy bodies. *Nature*, *388*(6645), 839–840. https://doi.org/10.1038/42166

Spreng, A.-S., Brüll, M., Leisner, H., Suciu, I., & Leist, M. (2022). Distinct and Dynamic Transcriptome Adaptations of iPSC-Generated Astrocytes after Cytokine Stimulation. *Cells*, *11*(17), 2644. https://doi.org/10.3390/cells11172644

Stefanova, N., Fellner, L., Reindl, M., Masliah, E., Poewe, W., & Wenning, G. K. (2011). Toll-Like Receptor 4 Promotes α-Synuclein Clearance and Survival of Nigral Dopaminergic Neurons. *The American Journal of Pathology*, *179*(2), 954–963. https://doi.org/10.1016/j.ajpath.2011.04.013

Stoll, A. C., & Sortwell, C. E. (2022). Leveraging the preformed fibril model to distinguish between alpha-synuclein inclusion- and nigrostriatal degeneration-associated immunogenicity. *Neurobiology of Disease*, *171*, 105804. https://doi.org/10.1016/j.nbd.2022.105804

Streubel-Gallasch, L., Giusti, V., Sandre, M., Tessari, I., Plotegher, N., Giusto, E., Masato, A., Iovino, L., Battisti, I., Arrigoni, G., Shimshek, D., Greggio, E., Tremblay, M.-E., Bubacco, L., Erlandsson, A., & Civiero, L. (2021). Parkinson's Disease–Associated LRRK2 Interferes with Astrocyte-Mediated Alpha-Synuclein Clearance. *Molecular Neurobiology*, *58*(7), 3119–3140. https://doi.org/10.1007/s12035-021-02327-8

Su, X., Maguire-Zeiss, K. A., Giuliano, R., Prifti, L., Venkatesh, K., & Federoff, H. J. (2008). Synuclein activates microglia in a model of Parkinson's disease. *Neurobiology of Aging*, *29*(11), 1690–1701. https://doi.org/10.1016/j.neurobiolaging.2007.04.006

Sulzer, D., Alcalay, R. N., Garretti, F., Cote, L., Kanter, E., Agin-Liebes, J., Liong, C., McMurtrey, C., Hildebrand, W. H., Mao, X., Dawson, V. L., Dawson, T. M., Oseroff, C., Pham, J., Sidney, J., Dillon, M. B., Carpenter, C., Weiskopf, D., Phillips, E., … Sette, A. (2017). T cells from patients with Parkinson's disease recognize α-synuclein peptides. *Nature*, *546*(7660), 656–661. https://doi.org/10.1038/nature22815

Sun, L., Li, Y., Jia, X., Wang, Q., Li, Y., Hu, M., Tian, L., Yang, J., Xing, W., Zhang, W., Wang, J., Xu, H., Wang, L., Zhang, D., & Ren, H. (2017). Neuroprotection by IFN-γ *via* astrocyte-secreted IL-6 in acute neuroinflammation. *Oncotarget*, *8*(25), 40065–40078. https://doi.org/10.18632/oncotarget.16990

Supakul, S., Murakami, R., Oyama, C., Shindo, T., Hatakeyama, Y., Itsuno, M., Bannai, H., Shibata, S., Maeda, S., & Okano, H. (2024). Mutual interaction of neurons and astrocytes derived from iPSCs with APP V717L mutation developed the astrocytic phenotypes of Alzheimer's disease. *Inflammation and Regeneration*, *44*(1), 8. https://doi.org/10.1186/s41232-023-00310-5

Surmeier, D. J., Obeso, J. A., & Halliday, G. M. (2017). Selective neuronal vulnerability in Parkinson disease. *Nature Reviews Neuroscience*, *18*(2), 101–113. https://doi.org/10.1038/nrn.2016.178

Sutter, P. A., & Crocker, S. J. (2022). Glia as antigen-presenting cells in the central nervous system. *Current Opinion in Neurobiology*, *77*, 102646. https://doi.org/10.1016/j.conb.2022.102646

Suzuki, M., Yoshioka, M., Hashimoto, M., Murakami, M., Noya, M., Takahashi, D., & Urashima, M. (2013). Randomized, double-blind, placebo-controlled trial of vitamin D supplementation in Parkinson disease. *The American Journal of Clinical Nutrition*, *97*(5), 1004–1013. https://doi.org/10.3945/ajcn.112.051664

Szpakowski, P., Ksiazek-Winiarek, D., Turniak-Kusy, M., Pacan, I., & Glabinski, A. (2022). Human Primary Astrocytes Differently Respond to Pro- and Anti-Inflammatory Stimuli. *Biomedicines*, *10*(8), 1769. https://doi.org/10.3390/biomedicines10081769

Taguchi, Y. V., Liu, J., Ruan, J., Pacheco, J., Zhang, X., Abbasi, J., Keutzer, J., Mistry, P. K., & Chandra, S. S. (2017). Glucosylsphingosine Promotes α-Synuclein Pathology in Mutant GBA-Associated Parkinson's Disease. *The Journal of Neuroscience*, *37*(40), 9617–9631. https://doi.org/10.1523/JNEUROSCI.1525-17.2017

Takahashi, K., Tanabe, K., Ohnuki, M., Narita, M., Ichisaka, T., Tomoda, K., & Yamanaka, S. (2007). Induction of Pluripotent Stem Cells from Adult Human Fibroblasts by Defined Factors. *Cell*, *131*(5), 861–872. https://doi.org/10.1016/j.cell.2007.11.019

Takouda, J., Katada, S., & Nakashima, K. (2017). Emerging mechanisms underlying astrogenesis in the developing mammalian brain. *Proceedings of the Japan Academy, Series B*, *93*(6), 386–398. https://doi.org/10.2183/pjab.93.024

Tan, C. X., Burrus Lane, C. J., & Eroglu, C. (2021). *Role of astrocytes in synapse formation and maturation* (pp. 371–407). https://doi.org/10.1016/bs.ctdb.2020.12.010

Tan, M. M. X., Lawton, M. A., Pollard, M. I., Brown, E., Real, R., Carrasco, A. M., Bekadar, S., Jabbari, E., Reynolds, R. H., Iwaki, H., Blauwendraat, C., Kanavou, S., Hubbard, L., Malek, N., Grosset, K. A., Bajaj, N., Barker, R. A., Burn, D. J., Bresner, C., … Morris, H. R. (2024). Genome-wide determinants of mortality and motor progression in Parkinson's disease. *Npj Parkinson's Disease*, *10*(1), 113. https://doi.org/10.1038/s41531-024-00729-8

Tan, Z., Qin, S., Yuan, Y., Hu, X., Huang, X., Liu, H., Pu, Y., He, C., & Su, Z. (2022). NOTCH1 signaling regulates the latent neurogenic program in adult reactive astrocytes after spinal cord injury. *Theranostics*, *12*(10), 4548–4563. https://doi.org/10.7150/thno.71378

Tanik, S. A., Schultheiss, C. E., Volpicelli-Daley, L. A., Brunden, K. R., & Lee, V. M. Y. (2013). Lewy Body-like α-Synuclein Aggregates Resist Degradation and Impair Macroautophagy. *Journal of Biological Chemistry*, *288*(21), 15194–15210. https://doi.org/10.1074/jbc.M113.457408

Tanner, C. M., Kamel, F., Ross, G. W., Hoppin, J. A., Goldman, S. M., Korell, M., Marras, C., Bhudhikanok, G. S., Kasten, M., Chade, A. R., Comyns, K., Richards, M. B., Meng, C., Priestley, B., Fernandez, H. H., Cambi, F., Umbach, D. M., Blair, A., Sandler, D. P., & Langston, J. W. (2011). Rotenone, Paraquat, and Parkinson's Disease. *Environmental Health Perspectives*, *119*(6), 866–872. https://doi.org/10.1289/ehp.1002839

Tanner, C. M., Ross, G. W., Jewell, S. A., Hauser, R. A., Jankovic, J., Factor, S. A., Bressman, S., Deligtisch, A., Marras, C., Lyons, K. E., Bhudhikanok, G. S., Roucoux, D. F., Meng, C., Abbott, R. D., & Langston,

J. W. (2009). Occupation and Risk of Parkinsonism. *Archives of Neurology*, *66*(9). https://doi.org/10.1001/archneurol.2009.195

Tansey, M. G., Wallings, R. L., Houser, M. C., Herrick, M. K., Keating, C. E., & Joers, V. (2022). Inflammation and immune dysfunction in Parkinson disease. *Nature Reviews Immunology*, *22*(11), 657–673. https://doi.org/10.1038/s41577-022-00684-6

Taylor, J. M., Main, B. S., & Crack, P. J. (2013a). Neuroinflammation and oxidative stress: Co-conspirators in the pathology of Parkinson's disease. *Neurochemistry International*, *62*(5), 803–819. https://doi.org/10.1016/j.neuint.2012.12.016

Taylor, J. M., Main, B. S., & Crack, P. J. (2013b). Neuroinflammation and oxidative stress: Co-conspirators in the pathology of Parkinson's disease. *Neurochemistry International*, *62*(5), 803–819. https://doi.org/10.1016/j.neuint.2012.12.016

Taylor, M., & Alessi, D. R. (2020). Advances in elucidating the function of leucine-rich repeat protein kinase-2 in normal cells and Parkinson's disease. *Current Opinion in Cell Biology*, *63*, 102–113. https://doi.org/10.1016/j.ceb.2020.01.001

TCW, J., Wang, M., Pimenova, A. A., Bowles, K. R., Hartley, B. J., Lacin, E., Machlovi, S. I., Abdelaal, R., Karch, C. M., Phatnani, H., Slesinger, P. A., Zhang, B., Goate, A. M., & Brennand, K. J. (2017). An Efficient Platform for Astrocyte Differentiation from Human Induced Pluripotent Stem Cells. *Stem Cell Reports*, *9*(2), 600–614. https://doi.org/10.1016/j.stemcr.2017.06.018

Teismann, P., & Ferger, B. (2001). Inhibition of the cyclooxygenase isoenzymes COX-1 and COX-2 provide neuroprotection in the MPTP-mouse model of Parkinson's disease. *Synapse*, *39*(2), 167–174. https://doi.org/10.1002/1098-2396(200102)39:2<167::AID-SYN8>3.0.CO;2-U

Thion, M. S., Ginhoux, F., & Garel, S. (2018). Microglia and early brain development: An intimate journey. *Science*, *362*(6411), 185–189. https://doi.org/10.1126/science.aat0474

Tolosa, E., Garrido, A., Scholz, S. W., & Poewe, W. (2021). Challenges in the diagnosis of Parkinson's disease. *The Lancet Neurology*, *20*(5), 385–397. https://doi.org/10.1016/S1474-4422(21)00030-2

Tong, J., Ang, L.-C., Williams, B., Furukawa, Y., Fitzmaurice, P., Guttman, M., Boileau, I., Hornykiewicz, O., & Kish, S. J. (2015). Low levels of astroglial markers in Parkinson's disease: relationship to α-synuclein accumulation. *Neurobiology of Disease*, *82*, 243–253. https://doi.org/10.1016/j.nbd.2015.06.010

Tönges, L., Buhmann, C., Klebe, S., Klucken, J., Kwon, E. H., Müller, T., Pedrosa, D. J., Schröter, N., Riederer, P., & Lingor, P. (2022). Blood-based biomarker in Parkinson's disease: potential for future applications in clinical research and practice. *Journal of Neural Transmission*, *129*(9), 1201–1217. https://doi.org/10.1007/s00702-022-02498-1

Trist, B. G., Hare, D. J., & Double, K. L. (2019). Oxidative stress in the aging substantia nigra and the etiology of Parkinson's disease. *Aging Cell*, *18*(6). https://doi.org/10.1111/acel.13031

Tsunemi, T., Ishiguro, Y., Yoroisaka, A., Valdez, C., Miyamoto, K., Ishikawa, K., Saiki, S., Akamatsu, W., Hattori, N., & Krainc, D. (2020). Astrocytes Protect Human Dopaminergic Neurons from α-Synuclein Accumulation and Propagation. *The Journal of Neuroscience*, *40*(45), 8618–8628. https://doi.org/10.1523/JNEUROSCI.0954-20.2020

Tysnes, O.-B., & Storstein, A. (2017). Epidemiology of Parkinson's disease. *Journal of Neural Transmission*, *124*(8), 901–905. https://doi.org/10.1007/s00702-017-1686-y

Varfolomeev, E., & Vucic, D. (2018). Intracellular regulation of TNF activity in health and disease. *Cytokine*, *101*, 26–32. https://doi.org/10.1016/j.cyto.2016.08.035

Verkhratsky, A., & Parpura, V. (2014). Store-operated calcium entry in neuroglia. *Neuroscience Bulletin*, *30*(1), 125–133. https://doi.org/10.1007/s12264-013-1343-x

Verkhratsky, A., Parpura, V., Vardjan, N., & Zorec, R. (2019). *Physiology of Astroglia* (pp. 45–91). https://doi.org/10.1007/978-981-13-9913-8_3

Verkhratsky, A., & Zorec, R. (2019). Astroglial signalling in health and disease. *Neuroscience Letters*, *689*, 1–4. https://doi.org/10.1016/j.neulet.2018.07.026

Volpicelli-Daley, L. A., Luk, K. C., Patel, T. P., Tanik, S. A., Riddle, D. M., Stieber, A., Meaney, D. F., Trojanowski, J. Q., & Lee, V. M.-Y. (2011). Exogenous α-Synuclein Fibrils Induce Lewy Body Pathology Leading to Synaptic Dysfunction and Neuron Death. *Neuron*, *72*(1), 57–71. https://doi.org/10.1016/j.neuron.2011.08.033

von Bartheld, C. S., Bahney, J., & Herculano-Houzel, S. (2016). The search for true numbers of neurons and glial cells in the human brain: A review of 150 years of cell counting. *Journal of Comparative Neurology*, *524*(18), 3865–3895. https://doi.org/10.1002/cne.24040

Voulgaris, D., Nikolakopoulou, P., & Herland, A. (2022). Generation of Human iPSC-Derived Astrocytes with a mature star-shaped phenotype for CNS modeling. *Stem Cell Reviews and Reports*, *18*(7), 2494–2512. https://doi.org/10.1007/s12015-022-10376-2

Wakabayashi, K., Hayashi, S., Yoshimoto, M., Kudo, H., & Takahashi, H. (2000). NACP/α-synuclein-positive filamentous inclusions in astrocytes and oligodendrocytes of Parkinson's disease brains. *Acta Neuropathologica*, *99*(1), 14–20. https://doi.org/10.1007/PL00007400

Wakabayashi, K., Tanji, K., Odagiri, S., Miki, Y., Mori, F., & Takahashi, H. (2013). The Lewy Body in Parkinson's Disease and Related Neurodegenerative Disorders. *Molecular Neurobiology*, *47*(2), 495–508. https://doi.org/10.1007/s12035-012-8280-y

Wardman, P. (2023). Factors Important in the Use of Fluorescent or Luminescent Probes and Other Chemical Reagents to Measure Oxidative and Radical Stress. *Biomolecules*, *13*(7), 1041. https://doi.org/10.3390/biom13071041

Wei, H., Zhen, L., Wang, S., Zhang, Y., Wang, K., Jia, P., Zhang, Y., Wu, Z., Yang, Q., Hou, W., Lv, J., & Zhang, P. (2022). De novo Lipogenesis in Astrocytes Promotes the Repair of Blood–Brain Barrier after Transient Cerebral Ischemia Through Interleukin-33. *Neuroscience*, *481*, 85–98. https://doi.org/10.1016/j.neuroscience.2021.11.026

Whitehouse, C. A., He, Y., Brownlees, J., & Corbett, N. (2023). Three-Dimensional Bioprinting of Human iPSC-Derived Neuron-Astrocyte Cocultures for Screening Applications. *Journal of Visualized Experiments*, *199*. https://doi.org/10.3791/65856

Williams, G. P., Schonhoff, A. M., Jurkuvenaite, A., Gallups, N. J., Standaert, D. G., & Harms, A. S. (2021). CD4 T cells mediate brain inflammation and neurodegeneration in a mouse model of Parkinson's disease. *Brain*, *144*(7), 2047–2059. https://doi.org/10.1093/brain/awab103

Willis, A. W., Roberts, E., Beck, J. C., Fiske, B., Ross, W., Savica, R., Van Den Eeden, S. K., Tanner, C. M., Marras, C., Alcalay, R., Schwarzschild, M., Racette, B., Chen, H., Church, T., Wilson, B., & Doria, J. M. (2022). Incidence of Parkinson disease in North America. *Npj Parkinson's Disease*, *8*(1), 170. https://doi.org/10.1038/s41531-022-00410-y

Witte, M. D., Kallemeijn, W. W., Aten, J., Li, K.-Y., Strijland, A., Donker-Koopman, W. E., van den Nieuwendijk, A. M. C. H., Bleijlevens, B., Kramer, G., Florea, B. I., Hooibrink, B., Hollak, C. E. M., Ottenhoff, R., Boot, R. G., van der Marel, G. A., Overkleeft, H. S., & Aerts, J. M. F. G. (2010). Ultrasensitive in situ visualization of active glucocerebrosidase molecules. *Nature Chemical Biology*, *6*(12), 907–913. https://doi.org/10.1038/nchembio.466

Woodard, C. M., Campos, B. A., Kuo, S.-H., Nirenberg, M. J., Nestor, M. W., Zimmer, M., Mosharov, E. V., Sulzer, D., Zhou, H., Paull, D., Clark, L., Schadt, E. E., Sardi, S. P., Rubin, L., Eggan, K., Brock, M., Lipnick, S., Rao, M., Chang, S., … Noggle, S. A. (2014). iPSC-Derived Dopamine Neurons Reveal Differences between Monozygotic Twins Discordant for Parkinson's Disease. *Cell Reports*, *9*(4), 1173–1182. https://doi.org/10.1016/j.celrep.2014.10.023

Woznicki, J. A., Saini, N., Flood, P., Rajaram, S., Lee, C. M., Stamou, P., Skowyra, A., Bustamante-Garrido, M., Regazzoni, K., Crawford, N., McDade, S. S., Longley, D. B., Aza-Blanc, P., Shanahan, F., Zulquernain, S. A., McCarthy, J., Melgar, S., McRae, B. L., & Nally, K. (2021). TNF-α synergises with IFN-γ to induce caspase-8-JAK1/2-STAT1-dependent death of intestinal epithelial cells. *Cell Death & Disease*, *12*(10), 864. https://doi.org/10.1038/s41419-021-04151-3

Wright Willis, A., Evanoff, B. A., Lian, M., Criswell, S. R., & Racette, B. A. (2010). Geographic and Ethnic Variation in Parkinson Disease: A Population-Based Study of US Medicare Beneficiaries. *Neuroepidemiology*, *34*(3), 143–151. https://doi.org/10.1159/000275491

Wu, T., Hu, E., Xu, S., Chen, M., Guo, P., Dai, Z., Feng, T., Zhou, L., Tang, W., Zhan, L., Fu, X., Liu, S., Bo, X., & Yu, G. (2021). clusterProfiler 4.0: A universal enrichment tool for interpreting omics data. *The Innovation*, *2*(3), 100141. https://doi.org/10.1016/j.xinn.2021.100141

Xia, M., & Zhou, Q. (2024). Correlation between 25-hydroxy-vitamin D and Parkinson's disease. *IBRO Neuroscience Reports*, *16*, 162–167. https://doi.org/10.1016/j.ibneur.2023.02.006

Xicoy, H., Wieringa, B., & Martens, G. J. M. (2019). The Role of Lipids in Parkinson's Disease. *Cells*, *8*(1), 27. https://doi.org/10.3390/cells8010027

Xin, W., Schuebel, K. E., Jair, K., Cimbro, R., De Biase, L. M., Goldman, D., & Bonci, A. (2019). Ventral midbrain astrocytes display unique physiological features and sensitivity to dopamine D2 receptor signaling. *Neuropsychopharmacology*, *44*(2), 344–355. https://doi.org/10.1038/s41386-018-0151-4

Xiong, H., Wang, D., Chen, L., Choo, Y. S., Ma, H., Tang, C., Xia, K., Jiang, W., Ronai, Z., Zhuang, X., & Zhang, Z. (2009). Parkin, PINK1, and DJ-1 form a ubiquitin E3 ligase complex promoting unfolded protein degradation. *Journal of Clinical Investigation*, *119*(3), 650–660. https://doi.org/10.1172/JCI37617

X.-Q. Chen, C., Deneault, E., Abdian, N., You, Z., Sirois, J., Nicouleau, M., Shlaifer, I., Villegas, L., Boivin, M.-N., Gaborieau, L., Karamchandani, J., Beitel, L. K., Fon, E. A., & Durcan, T. M. (2022). Generation of patient-derived pluripotent stem cell-lines and CRISPR modified isogenic controls with mutations in the Parkinson's associated GBA gene. *Stem Cell Research*, *64*, 102919. https://doi.org/10.1016/j.scr.2022.102919

Xu, C., Wu, J., Wu, Y., Ren, Z., Yao, Y., Chen, G., Fang, E. F., Noh, J. H., Liu, Y. U., Wei, L., Chen, X., & Sima, J. (2021). TNF-α-dependent neuronal necroptosis regulated in Alzheimer's disease by coordination of RIPK1-p62 complex with autophagic UVRAG. *Theranostics*, *11*(19), 9452–9469. https://doi.org/10.7150/thno.62376

Xu, Y., Li, Y., Wang, C., Han, T., Liu, H., Sun, L., Hong, J., Hashimoto, M., & Wei, J. (2023). The reciprocal interactions between microglia and T cells in Parkinson's disease: a double-edged sword. *Journal of Neuroinflammation*, *20*(1), 33. https://doi.org/10.1186/s12974-023-02723-y

Yang, L., Mao, K., Yu, H., & Chen, J. (2020). Neuroinflammatory Responses and Parkinson' Disease: Pathogenic Mechanisms and Therapeutic Targets. *Journal of Neuroimmune Pharmacology*, *15*(4), 830–837. https://doi.org/10.1007/s11481-020-09926-7

Yarkova, E. S., Grigor'eva, E. V., Medvedev, S. P., Pavlova, S. V., Zakian, S. M., & Malakhova, A. A. (2023). IPSC-Derived Astrocytes Contribute to In Vitro Modeling of Parkinson's Disease Caused by the GBA1 N370S Mutation. *International Journal of Molecular Sciences*, *25*(1), 327. https://doi.org/10.3390/ijms25010327

Yeon, G.-B., Jeon, B.-M., Yoo, S. H., Kim, D., Oh, S. S., Park, S., Shin, W.-H., Kim, H. W., Na, D., Kim, D.-W., & Kim, D.-S. (2023). Differentiation of astrocytes with characteristics of ventral midbrain from human embryonic stem cells. *Stem Cell Reviews and Reports*, *19*(6), 1890–1906. https://doi.org/10.1007/s12015-023-10536-y

Yu, E., Ambati, A., Andersen, M. S., Krohn, L., Estiar, M. A., Saini, P., Senkevich, K., Sosero, Y. L., Sreelatha, A. A. K., Ruskey, J. A., Asayesh, F., Spiegelman, D., Toft, M., Viken, M. K., Sharma, M., Blauwendraat, C., Pihlstrøm, L., Mignot, E., & Gan-Or, Z. (2021). Fine mapping of the HLA locus in Parkinson's disease in Europeans. *Npj Parkinson's Disease*, *7*(1), 84. https://doi.org/10.1038/s41531-021-00231-5

Yu, G., Wang, L.-G., Han, Y., & He, Q.-Y. (2012). clusterProfiler: an R Package for Comparing Biological Themes Among Gene Clusters. *OMICS: A Journal of Integrative Biology*, *16*(5), 284–287. https://doi.org/10.1089/omi.2011.0118

Yu, J., Vodyanik, M. A., Smuga-Otto, K., Antosiewicz-Bourget, J., Frane, J. L., Tian, S., Nie, J., Jonsdottir, G. A., Ruotti, V., Stewart, R., Slukvin, I. I., & Thomson, J. A. (2007). Induced Pluripotent Stem Cell Lines Derived from Human Somatic Cells. *Science*, *318*(5858), 1917–1920. https://doi.org/10.1126/science.1151526

Zali, A., Hajyani, S., Salari, M., Tajabadi-Ebrahimi, M., Mortazavian, A. M., & Pakpour, B. (2024). Co-administration of probiotics and vitamin D reduced disease severity and complications in patients with Parkinson's disease: a randomized controlled clinical trial. *Psychopharmacology*. https://doi.org/10.1007/s00213-024-06606-9

Zamanian, J. L., Xu, L., Foo, L. C., Nouri, N., Zhou, L., Giffard, R. G., & Barres, B. A. (2012). Genomic Analysis of Reactive Astrogliosis. *The Journal of Neuroscience*, *32*(18), 6391–6410. https://doi.org/10.1523/JNEUROSCI.6221-11.2012

Zhang, Y., He, K., Wang, F., Li, X., & Liu, D. (2015). Notch-1 signaling regulates astrocytic proliferation and activation after hypoxia exposure. *Neuroscience Letters*, *603*, 12–18. https://doi.org/10.1016/j.neulet.2015.07.009

Zhang, Y., Ji, W., Zhang, S., Gao, N., Xu, T., Wang, X., & Zhang, M. (2022). Vitamin D Inhibits the Early Aggregation of α-Synuclein and Modulates Exocytosis Revealed by Electrochemical

Measurements. *Angewandte Chemie International Edition*, *61*(1). https://doi.org/10.1002/anie.202111853

Zhang, Y., Sloan, S. A., Clarke, L. E., Caneda, C., Plaza, C. A., Blumenthal, P. D., Vogel, H., Steinberg, G. K., Edwards, M. S. B., Li, G., Duncan, J. A., Cheshier, S. H., Shuer, L. M., Chang, E. F., Grant, G. A., Gephart, M. G. H., & Barres, B. A. (2016). Purification and Characterization of Progenitor and Mature Human Astrocytes Reveals Transcriptional and Functional Differences with Mouse. *Neuron*, *89*(1), 37–53. https://doi.org/10.1016/j.neuron.2015.11.013

Zhang, Y., Sun, Q., Zhao, Y., Shu, L., Guo, J., Xu, Q., Yan, X., & Tang, B. (2015). Effect of *GBA* Mutations on Phenotype of Parkinson's Disease: A Study on Chinese Population and a *Meta-Analysis*. *Parkinson's Disease*, *2015*, 1–10. https://doi.org/10.1155/2015/916971

Zhang, Y., Tan, F., Xu, P., & Qu, S. (2016). Recent Advance in the Relationship between Excitatory Amino Acid Transporters and Parkinson's Disease. *Neural Plasticity*, *2016*, 1–8. https://doi.org/10.1155/2016/8941327

Zheng, W., & Fan, D. (2022). Glucocerebrosidase Mutations Cause Mitochondrial and Lysosomal Dysfunction in Parkinson's Disease: Pathogenesis and Therapeutic Implications. *Frontiers in Aging Neuroscience*, *14*. https://doi.org/10.3389/fnagi.2022.851135

Zhou, Q., Viollet, C., Efthymiou, A., Khayrullina, G., Moritz, K. E., Wilkerson, M. D., Sukumar, G., Dalgard, C. L., & Doughty, M. L. (2019). Neuroinflammatory astrocytes generated from cord blood-derived human induced pluripotent stem cells. *Journal of Neuroinflammation*, *16*(1), 164. https://doi.org/10.1186/s12974-019-1553-x